



NATIONAL AND KAPODISTRIAN UNIVERSITY OF ATHENS

Health Sciences School
Faculty of Pharmacy

Doctoral Dissertation

**Molecular basis of inhibition and resistance of the influenza M2
ion channel by aminoadamantane drugs and discovery of novel
resistance-breaking inhibitors targeting the mutant M2 proton
channel**

Tzitzoglaki N. Christina

Athens July 2018



ΕΘΝΙΚΟ ΚΑΙ ΚΑΠΟΔΙΣΤΡΙΑΚΟ ΠΑΝΕΠΙΣΤΗΜΙΟ ΑΘΗΝΩΝ

Σχολή Επιστημών Υγείας
Τμήμα Φαρμακευτικής

Διδακτορική Διατριβή

Μοριακή βάση αναστολής και ανθεκτικότητας του ιοντικού διαύλου Influenza M2 από τα αμινοαδαμαντανικά φάρμακα και ανακάλυψη καινοτόμων αναστολέων των μεταλλαγμένων M2 πρωτεϊνών των ανθεκτικών στελεχών του ιού.

Τζιτζογλάκη Ν Χριστίνα

Αθήνα Ιούλιος 2018

ΔΙΔΑΚΤΟΡΙΚΗ ΔΙΑΤΡΙΒΗ

Τζιτζογλάκη Ν Χριστίνα

**ΕΠΙΒΛΕΠΩΝ ΚΑΘΗΓΗΤΗΣ: Αναπληρωτής καθηγητής Κολοκούρης Αντώνιος,
Τμήμα Φαρμακευτικής, ΕΚΠΑ**

ΤΡΙΜΕΛΗΣ ΕΠΙΤΡΟΠΗ ΠΑΡΑΚΟΛΟΥΘΗΣΗΣ:

**Αναπληρωτής καθηγητής Κολοκούρης Αντώνιος, Τμήμα Φαρμακευτικής, ΕΚΠΑ
Καθηγητής Τσοτίνης Ανδρέας, Τμήμα Φαρμακευτικής, ΕΚΠΑ
Καθηγητής Μαράκος Παναγιώτης, Τμήμα Φαρμακευτικής, ΕΚΠΑ**

ΕΠΤΑΜΕΛΗΣ ΕΞΕΤΑΣΤΙΚΗ ΕΠΙΤΡΟΠΗ

**Κολοκούρης Αντώνιος
Αναπλ. Καθηγητής Τμήμα Φαρμακευτικής,
ΕΚΠΑ**

**Τσοτίνης Ανδρέας
Καθηγητής Τμήμα Φαρμακευτικής
ΕΚΠΑ**

**Μαράκος Παναγιώτης
Καθηγητής Τμήμα Φαρμακευτικής,
ΕΚΠΑ**

**Μικρός Εμμανουήλ,
Καθηγητής Τμήμα Φαρμακευτικής,
ΕΚΠΑ**

**Παπαναστασίου Ιωάννης,
Επίκουρος Καθηγητής , Τμήμα
Φαρμακευτικής, ΕΚΠΑ**

**Μαυρομούστακος Θωμάς,
Καθηγητής Τμήμα Χημείας,
ΕΚΠΑ**

**Busath David,
Καθηγητής Department of Physiology
and Biophysics , Brigham Young
University, USA**

Ημερομηνία εξέτασης 19/07/2018

PhD THESIS

Tzitzoglaki N Christina

**SUPERVISOR: Kolocouris Antonios, Assoc. Professor , Department of Pharmacy,
UOA**

THREE-MEMBER ADVISORY COMMITTEE:

Assoc. Prof. A. Kolocouris, Department of Pharmacy, UOA

Professor Andrew Tsotinis, Department of Pharmacy, UOA

Professor Panagiotis Marakos, Department of Pharmacy, UOA

SEVEN-MEMBER EXAMINATION COMMITTEE

**Assoc. Prof. A. Kolocouris
Department of Pharmacy, UOA**

**Prof. Andrew Tsotinis
Department of Pharmacy, UOA**

**Prof. Panagiotis Marakos
Department of Pharmacy, UOA**

**Prof. Emmanuel Mikros
Department of Pharmacy, UOA**

**Asst. Prof. Ioannis Papanastasiou
Department of Pharmacy, UOA**

**Prof. Thomas Mavromoustakos
Department of Chemistry, UOA**

**Καθηγητής Busath David,
Department of Physiology and
Biophysics , Brigham Young University,
USA**

Examination Date 19/07/2018

I would like to dedicate this thesis to my mother

Εκτενής Περίληψη

Περιγραφή Ερευνητικής Εργασίας

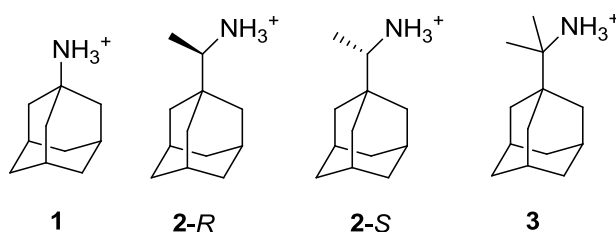
Εισαγωγή: Η αμανταδίνη (*Amt* (1)) και η ριμανταδίνη (*Rim* (2)) είναι αναστολείς της μεταφοράς πρωτονίων διαμέσου του ιοντικού διαύλου της πρωτεΐνης M2 του ιού influenza A, ^{1,2} και αποτέλεσαν εγκεκριμένα μέσα πρόληψης και θεραπείας έναντι των ιών της γρίπης A άγριου τύπου (WT). Ωστόσο, από το 2005, η μετάλλαξη του αμινοξέος σερίνη σε ασπαραγίνη στη θέση 31 (S31N) στην M2 πρωτεΐνη, δημιούργησε ένα στέλεχος ανθεκτικό στην *Amt* το οποίο έχει κυριαρχήσει παγκοσμίως, καταργώντας την κλινική χρησιμότητα της αμανταδίνης ^{3,4} και πιθανότατα και άλλων προαναφερθέντων, στη διεθνή βιβλιογραφία, αναστολέων της M2. Επομένως, είναι απαραίτητη η ανάπτυξη νέων μορίων για την καταπολέμηση των ανθεκτικών στελεχών της γρίπης.

Η κύρια θέση πρόσδεσης της *Amt* (1) και της *Rim* (2) είναι η διαμεμβρανική περιοχή (transmembrane domain, TM) των αμινοξέων 22-46 του συμπλέγματος των τεσσάρων α -ελίκων της M2 που σχηματίζει τον δίαυλο μεταφοράς πρωτονίων. Σύμφωνα με δομές υψηλής διαχωριστικότητας που προέκυψαν από πειράματα κρυσταλλογραφίας ακτίνων-Χ και φασματοσκοπίας πυρηνικού μαγνητικού συντονισμού στερεάς κατάστασης (solid state NMR, ssNMR) και δημοσιεύτηκαν μεταξύ 2008-2011 από τους ερευνητές και καθηγητές Tim Cross, William DeGrado και Mei Hong στα πιο έγκριτα περιοδικά όπως Nature, JACS κλπ, η *Amt* (1) και η *Rim* (2) δρουν φράσσοντας τον πόρο του διαύλου M2TM. ^{5,6,7,8,9,10,11} Ο κλωβός του αδαμαντανίου των ενώσεων αυτών περικλείεται από τις τέσσερις πλευρικές αλυσίδες των V27 και της A30 του τετραμερούς M2TM προκαλώντας τον στερεοχημικό αποκλεισμό της μεταφοράς πρωτονίων ^{6,7,8,9} και αποτρέποντας την συνέχεια του κύκλου ζωής του ιού. Τα αποτελέσματα ssNMR έδειξαν επίσης ότι η ομάδα αμμωνίου αυτών των φαρμάκων έχει προσανατολισμό προς τα τέσσερα αμινοξέα της His37 δηλαδή προς το C-τελικό άκρο. ⁹ Αυτός ο προσανατολισμός σταθεροποιείται μέσω ενός δικτύου δεσμών υδρογόνου μεταξύ προσδέτη και (α) μορίων νερού εντός του πόρου του ιοντικού διαύλου, που βρίσκονται μεταξύ ιμιδαζολίου της H37 και προσδέτη, και, ενδεχομένως, (β) με το καρβονύλιο της A30 σύμφωνα με πειραματικά αποτελέσματα και προσομοιώσεις μοριακής δυναμικής (MD). ^{9,12,13,14,15,16,17,18,19} Δεδομένου ότι η M2TM αποτελεί το απλούστερο μοντέλο πρόσδεσης της *Amt* (1) και *Rim* (2) για την M2, οι προηγούμενες πειραματικές δομές υψηλής ανάλυσης μπορούν να χρησιμοποιηθούν για το σχεδιασμό και ανάπτυξη νέων αναστολέων που να συνδέονται αποτελεσματικότερα με τον πόρο M2TM, μέσω προσομοιώσεων μοριακής δυναμικής (MD) ¹⁹ ή ακριβέστερα με υπολογισμούς ελεύθερης ενέργειας. ^{20,21,22}

Στόχοι της διδακτορικής διατριβής: Στόχοι της παρούσας εργασίας είναι να διερευνηθούν πως μικρές αλλαγές: (α) στη δομή της αμανταδίνης έχουν ως αποτέλεσμα την αύξηση ή τη μείωση της συγγένειας σύνδεσης έναντι του πόρου M2TM διαφόρων στελεχών του ιού influenza, και (β) στη δομή της M2TM που

προκαλείται από μία μόνο μετάλλαξη, όπως η S31N), προκαλούν ανθεκτικότητα του ιού της γρίπης Α καταργώντας έτσι την κλινική αποτελεσματικότητα των φαρμάκων της τάξης των αμινοαδαμαντανικών παραγώγων. Η κατανόηση του μηχανισμού ανθεκτικότητας του ιού σε μοριακή βάση μέσω βιοφυσικών και υπολογιστικών μεθόδων, θα χρησιμοποιηθεί για τον ορθολογικό σχεδιασμό και την ανάπτυξη καινοτόμων αναστολέων έναντι πανδημικών στελεχών της γρίπης Α που προκαλούν ασθένεια. Το κεφάλαιο 1 θα επικεντρωθεί στο (α) ενώ τα Κεφάλαια 2-5 στο (β).

Ανάλυση κεφαλαίων: Στο Κεφάλαιο 1 η συγγένεια σύνδεσης των εναντιομερών της ριμανταδίνης (Σχήμα 1) αναθεωρήθηκε χρησιμοποιώντας βιοφυσικές μεθόδους και αλχημικούς υπολογισμούς ελεύθερης ενέργειας σύνδεσης.



M2TM WT: SSDPLVVAASIIGILHLILWILDRL

Σχήμα 1. Δομές των αμινοαδαμαντανικών παραγώγων που μελετήθηκαν, αμανταδίνης (**1**), εναντιομερών ριμανταδίνης, **2-R** και **2-S**, και του ανάλογου της ριμανταδίνης **3**. Η ένωση **3** και η αλληλουχία αμινοξέων του πεπτιδίου M2TM WT συντέθηκαν για τους σκοπούς αυτής της μελέτης.

Πρόσφατα, εφαρμόσαμε υπολογισμούς σύνδεσης MM-PBSA, δηλαδή υπολογισμών πρόσδεσης μοριακής μηχανικής (MM) και της ενέργειας επιδιάλυτωσης με τη μέθοδο Poisson-Boltzmann (MM-PBSA), για να ερμηνευθούν τα θερμοδυναμικά προφίλ σύνδεσης αμινοαδαμαντανικών παραγώγων με την αλληλουχία που προσβάλλει θηλαστικά M2TM_{Weybridge}, τα οποία μετρήθηκαν χρησιμοποιώντας ισοθερμική θερμιδομετρία τιτλοδότησης (isothermal titration calorimetry, ITC). Η μέθοδος χρησιμοποιήθηκε για την ορθή κατάταξη της δραστηριότητας ενός συνόλου αμινοαδαμαντανικών παραγώγων και τον επιτυχή σχεδιασμό δραστικών αναλόγων.²² Εφαρμόσαμε επίσης ακριβείς υπολογισμούς ελεύθερης σύνδεσης χρησιμοποιώντας τη μέθοδο Bennett acceptance ratio (BAR), ώστε να επιτρέπουν τον ακριβή υπολογισμό της σχετικής ελεύθερης ενέργειας σύνδεσης αμινοαδαμαντανικών παραγώγων με τη διαμεμβρανική περιοχή M2TM_{WT} ή M2TM_{Weybridge} των οποίων οι πειραματικές τιμές μετρήθηκαν αντίστοιχα με ITC ή με φασματοσκοπικές μεθόδους.^{20,21} Ωστόσο, η συγγένεια σύνδεσης των εναντιομερών της ριμανταδίνης με την πρωτεΐνη M2 δεν έχει διερευνηθεί ποτέ λεπτομερώς. Τα αποτελέσματα από μελέτες ssNMR που δημοσιεύθηκαν από την ομάδα Cross το 2016 προτείνουν ότι τα εναντιομερή της ριμανταδίνης συνδέονται

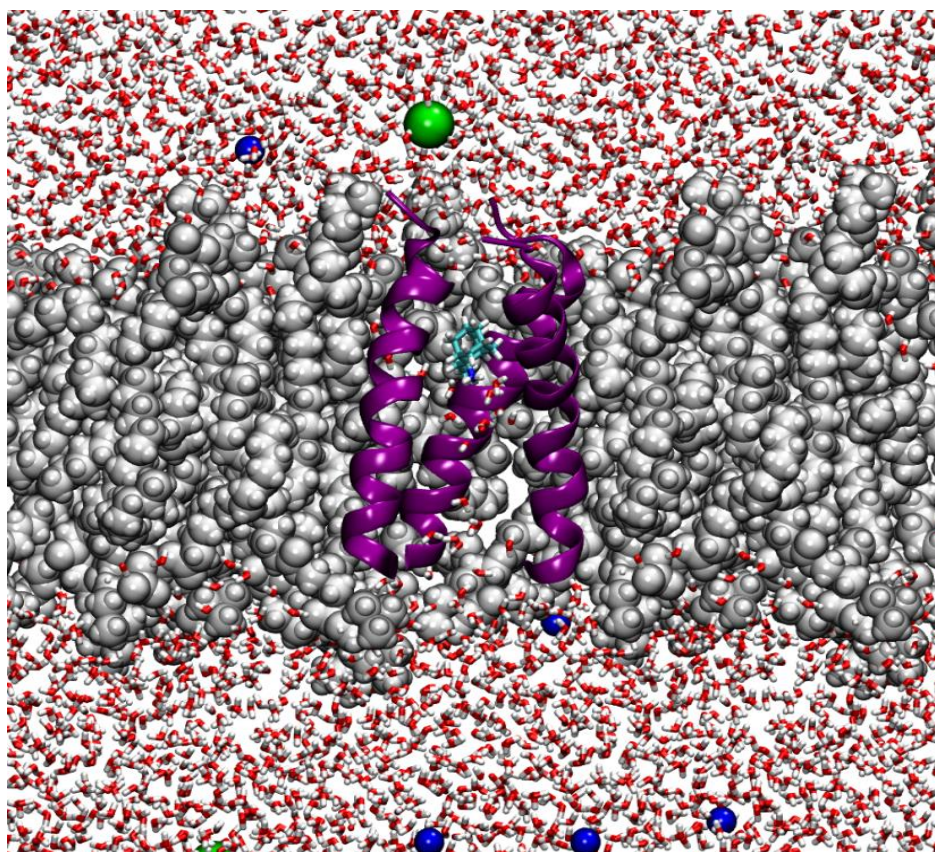
με τη M2 με διαφορετική συγγένεια όπως αναμένεται με βάση την αλληλεπίδραση των εναντιομερών με ένα χειρόμορφο βιοπολυμερές. Συγκεκριμένα, η ομάδα του Cross πρότεινε ότι το (R)-εναντιομερές της ριμανταδίνης συνδέεται με την M2 πρωτεΐνη με υψηλότερη συγγένεια σύνδεσης συγκριτικά το (S)-εναντιομερές.¹⁰ Αυτή ήταν η πρώτη μελέτη ssNMR της πλήρους πρωτεΐνης M2, αλλά το συμπέρασμα ενώ ήταν παράδοξο, διότι: (α) Είχε αποδειχθεί προηγουμένως ότι τα εναντιομερή της ριμανταδίνης είχαν παρόμοια *in vivo* αντιϊκή δραστηριότητα στην προστασία ποντικών από τη θανατηφόρο γρίπη, και β) Η ριμανταδίνη έχει εγκριθεί ως εμπορικό φάρμακο στις ΗΠΑ το 1993 και περιείχε και τα δύο εναντιομερή. Τα αποτελέσματα αυτά κέντρισαν το ενδιαφέρον του εργαστηρίου μας και σε συνεργασία με άλλα εργαστήρια εφαρμόστηκαν πειράματα αντιϊκής δραστηριότητας *in vitro* και ηλεκτροφυσιολογίας (Electrophysiology, EP), για να αξιολογηθεί η συγγένεια σύνδεσης των εναντιομερών της ριμανταδίνης με την πρωτεΐνη M2. Επιπλέον, οι σταθερές σύνδεσης των εναντιομερών της ριμανταδίνης έναντι του M2TM_{WT} μετρήθηκαν για πρώτη φορά χρησιμοποιώντας ITC και βρέθηκαν να είναι ίσες (βλέπε Πίνακα 1). Για τον σκοπό αυτό: (α) συντέθηκε το M2TM WT πεπτιδίο, που αντιστοιχεί στα αμινοξέα 22-46 της αλληλουχίας άγριου Udorn/72 της M2 με άμιδο τερματική ομάδα του C-τελικού άκρου (CONH₂) που περιλαμβάνει την αλληλουχία SSDPLVVAASIIIGILHLILWILDRL, με Fmoc πεπτιδική σύνθεση στερεάς φάσης χρησιμοποιώντας ρητίνη αμινομεθυλοπολυστυρενίου (AMPS) συζευγμένη με τον αμιδικό συνδέτη, (β) καθαρίστηκε με HPLC αντίστροφης φάσης και, (γ) χαρακτηρίστηκε με φασματοσκοπία μάζας.

Πίνακας 1. Σύνοψη των μετρήσεων των εναντιομερών της ριμανταδίνης στην πρωτεΐνη A/M2.²³

Rim-R	Rim-S
KdM2TM _{Udorn} (ITC) = 0.32 μM	KdM2TM _{Udorn} (ITC) = 0.34 μM
%blocktoM2 _{Udorn} (TEVC) = 95%	%blocktoM2 _{Udorn} (TEVC) = 96%
%blocktoM2 _{WSN/33-N31S} (TEVC) = 90%	%blocktoM2 _{WSN/33-N31S} (TEVC) = 92%
IC ₅₀ (Udorn/72, CPE) = 0.05 μM	IC ₅₀ (Udorn/72, CPE) = 0.06 μM
IC ₅₀ (WSN/33-M2-N31S, CPE) = 0.05 μM	IC ₅₀ (WSN/33-M2-N31S, CPE) = 0.03 μM
3 → Rim-R, ΔΔG _{FEP} =0.62 ± 0.14, ΔΔG _{exp} =0.33 ± 0.50	3 → Rim-S, ΔΔG _{FEP} =0.68 ± 0.15, ΔΔG _{exp} =0.42 ± 0.48

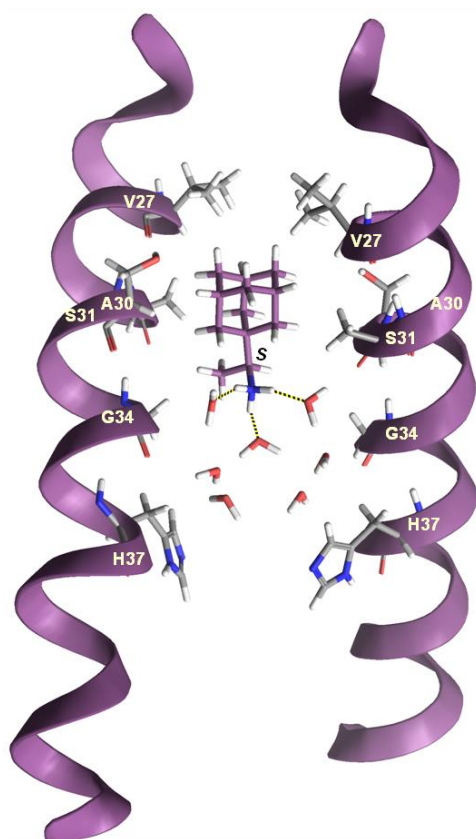
Τα πειραματικά μας δεδομένα βασισμένα στην λειτουργία της πλήρους πρωτεΐνης M2 επιβεβαιώθηκαν περαιτέρω με προσομοιώσεις MD (Εικόνα 1 και 2). Εφαρμόστηκαν αλχημικοί υπολογισμοί ελεύθερης ενέργειας με τη μέθοδο Bennett (BAR) για να υπολογιστεί η σχετική συγγένεια σύνδεσης των εναντιομερών της ριμανταδίνης σε σύγκριση με την ένωση **3**, που συντέθηκε και μετρήθηκε γι' αυτή τη σύγκριση, έναντι της M2TM στην κλειστή μορφή σε pH 8 εντός 1,2-διμυριστοϋλο-sn-γλυκερο-3-φωσφοχολίνης (1,2-

dimyristoyl-*sn*-glycero-3-phosphocholine, DMPC) για τη μίμηση του περιβάλλοντος της μεμβράνης. Δεν βρέθηκε σημαντική διαφορά μεταξύ των δύο εναντιομερών. Και τα δύο εναντιομερή παρουσιάζουν τον ίδιο βαθμό αποκλεισμού του διαλύου, και έχουν την ίδια συγγένεια σύνδεσης και αντιϊκή δράση (Σχήμα 1, Πίνακας 1). Η μελέτη αυτή δημοσιεύθηκε στο *ACSMed. Chem. Lett.* **2017**, 27, 145-150, και μέρος της εργασίας αυτής στο *ACSJ. Chem. Info. Model.* **2016**, 56, 862-76 (βλ. αναφ. 23 και 21 στον κατάλογον βιβλιογραφικών αναφορών αντίστοιχα).

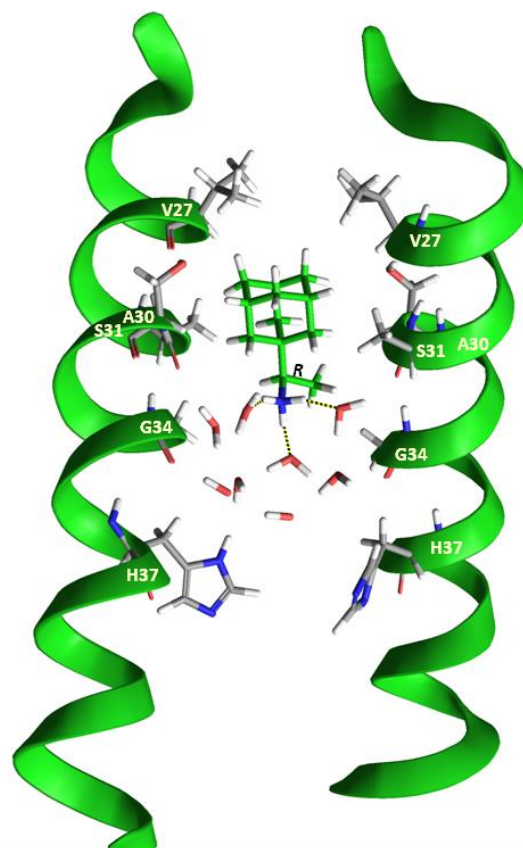


Εικόνα 1. Αντιπροσωπευτική εικόνα από τους υπολογισμούς FEP/MD συστήματος: Προσδέτης **3** εντός του πόρου του ιοντικού διαύλου M2TM WT σε ενυδατωμένη λιπιδική μεμβράνη DMPC. Απεικονίζεται όλο το σύστημα.

(α)



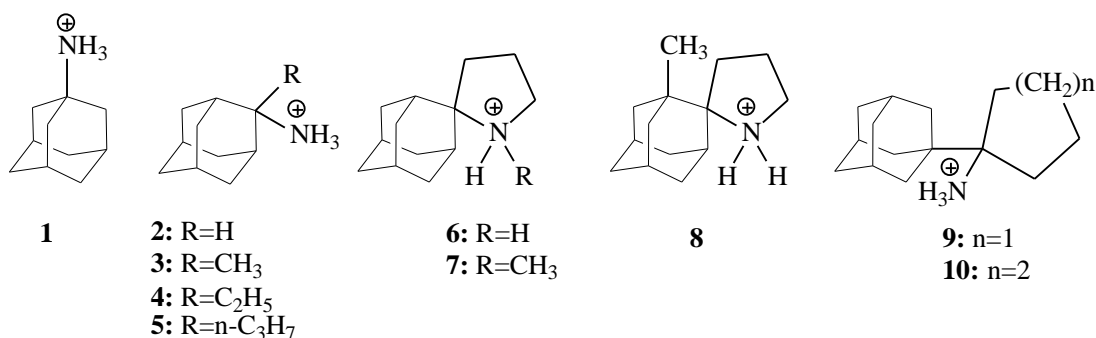
(β)



C-τελικό άκρο

Εικόνα 2. (α) Προσδέτης 2-S, ή (β) Προσδέτης 2-Rεντός του πόρου M2TM WT. Απεικονίζονται επτά και οκτώ μόρια νερού μεταξύ του προσδέτη 2-S ή 2-R και του αμινοξέος H37, αντίστοιχα. Απεικονίζονται επίσης τρεις δεσμοί υδρογόνου μεταξύ της ομάδας αμμωνίου της ριμανταδίνης και τριών μορίων νερού. Αυτοί οι δεσμοί υδρογόνου μαζί με τις αλληλεπιδράσεις Van der Waals του αδαμαντανικού σκελετού με τα αμινοξέα V27 και A30 σταθεροποιούν το μόριο εντός του πόρου με κατεύθυνση της αμινομάδας προς το C-τελικό άκρο.

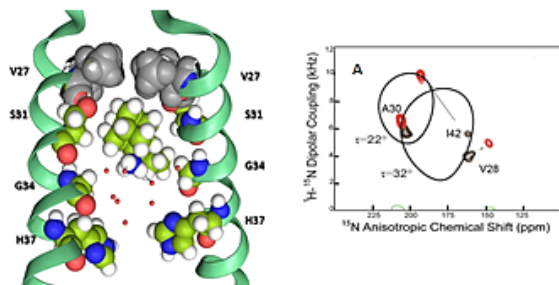
Στο Κεφάλαιο 2 διερευνάται η μοριακή βάση του μηχανισμού ανθεκτικότητας της πρωτεΐνης M2 WT στα αμινοαδαμαντανικά παράγωγα. Ενώ τα αμινοαδαμαντάνια είναι καθιερωμένοι αναστολείς του ιοντικού δίαυλου του ιού influenza A M2, οι μηχανισμοί με τους οποίους τα παράγωγα καθίστανται αναποτελεσματικά έναντι του M2_{S31N} είναι ασαφείς. Οι διαφορές στη σύνδεση αλλά και στον αποκλεισμό των πρωτονίων από τα παράγωγα αμανταδίνης για τις πρωτεΐνες M2_{WT} και M2_{S31N} εξηγούνται μέσω χρήσης ssNMR και προσομοιώσεων MD. Για το σκοπό αυτό: (α) συντέθηκε πεπτίδιο M2TM S31N, που αντιστοιχεί στα αμινοξέα 22-46 της Udorn/72 αλλά περιλαμβάνει τη μετάλλαξη Ser31Asn στη M2 με άμιδο τερματική ομάδα του C-τελικού άκρου (CONH₂) που περιλαμβάνει την αλληλουχία SSDPLVVAANIIGILHLILWILDRL, με Fmoc πεπτιδική σύνθεση στερεάς φάσης χρησιμοποιώντας ρητίνη AMPS συζευγμένη με τον αμιδικό συνδέτη, (β) καθαρίστηκε με HPLC αντίστροφης φάσης και, (γ) χαρακτηρίστηκε με φασματοσκοπία μάζας. Επανασυντέθηκαν οι ενώσεις **3-7**, **9** και συντέθηκαν δύο νέες ενώσεις δηλ. **8**, **10** με μικρές αλλαγές στη δομή σε σύγκριση με το σπειροπυρρολιδινό[2,2'] αδαμαντάνιο **6** (Σχήμα 2) προκειμένου να διερευνηθεί ο τρόπος με τον οποίο επηρεάζουν αυτές οι δομικές τροποποιήσεις τα αποτελέσματα του ssNMR.



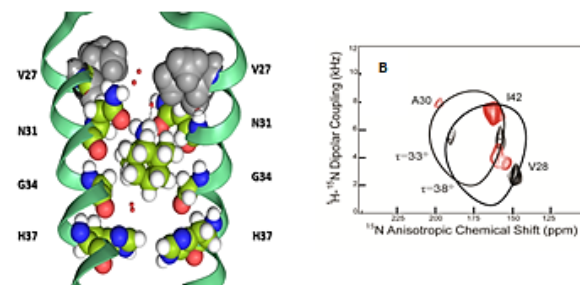
M2TM S31N: SSDPLVVAANIIGILHLILWILDRL

Σχήμα 2. Ενώσεις που συντέθηκαν για την μελέτη. Το πεπτίδιο M2TM S31N συντέθηκε επίσης για τους σκοπούς αυτής της μελέτης.

A Σταθερό σύμπλοκο M2TM_{WT}-5; ισχυρός προσανατολισμός προς το C-τελικό άκρο, σχηματισμός λιπόφιλης θήκης V27, γωνίωση της έλικας στο ήμισυ του C-τελικού άκρου κατά 10^o



B Ασταθές σύμπλοκο M2TM_{S31N}-5; τάση προσανατολισμού στο N-τελικό άκρο, απώλεια της λιπόφιλης κοιλότητας V27, ευθύγραμμη άξονας α-έλικας

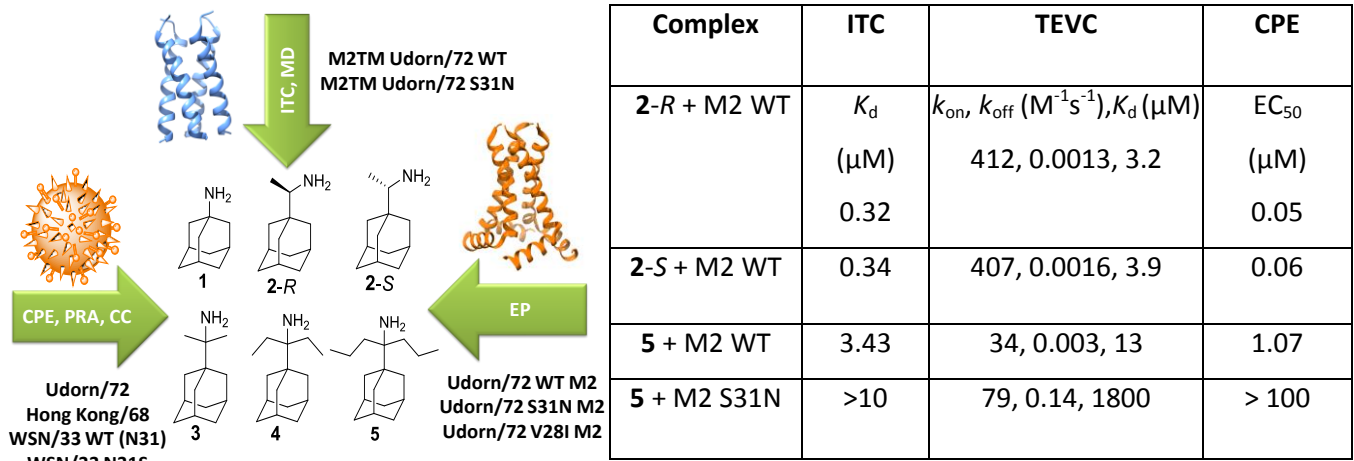


Εικόνα 3. Περιγραφή των πιο σημαντικών συνεπειών της πρόσδεσης των αμινοαδαμαντανικών παραγώγων στην διαμεμβρανική περιοχή του M2TM_{WT} και M2TM_{S31N}.²⁵

Πειράματα ssNMR, ITC, EP, αντιϊκές δοκιμασίες και προσομοιώσεις MD έδειξαν ισχυρότερες αλληλεπιδράσεις πρόσδεσης μεταξύ αμινοαδαμαντανικών παραγώγων και M2_{WT} σε σύγκριση με την αμελητέα ή ασθενή πρόσδεση τους με τη M2_{S31N}. Αιτία φαίνεται να είναι η ανακατάταξη του πόρου του ιοντικού διαύλου M2TM λόγω μετάλλαξης του αμινοξέος S31 από το N31, με συνέπεια: Α) Την απώλεια της λιπόφιλης κοιλότητας που δημιουργείται από τις πλευρικές αλυσίδες των αμινοξέων V27 για τον αδαμαντανικό κλωβό και στην τάση προσανατολισμού της ομάδας αμμωνίου του προσδέτη προς το N-τελικό άκρο. Η μετάλλαξη S31N του M2TM οδηγεί σε μετατόπιση του υδρόφοβου αδαμαντανικού δακτυλίου προς το C-τελικό άκρο κοντά στο αμινοξύ G34, λόγω της άπωσης του υδρόφοβου αδαμαντανίου από τις αμιδικές πλευρικές αλυσίδες του αμινοξέος N31. Το πεπτίδιο M2TM S31N στην περιοχή των αμινοξέων G34 έχει τη μεγαλύτερη διάμετρο και το αδαμαντάνιο δεν μπορεί να προσδεθεί σταθερά. Ως συνέπεια οι υδρόφοβες αλληλεπιδράσεις των ομάδων ισοπροπυλίου των αμινοξέων V27 με το αδαμαντάνιο που υπάρχουν στο M2TM WT δεν υφίστανται στο M2TM S31N. Επιπλέον, ο προσδέτης περιστρέφεται προς το N-τελικό άκρο για να σχηματίσει δεσμό υδρογόνου με το αμινοξύ N31 χωρίς να υπάρχουν πλέον αλληλεπιδράσεις Van der Waals που να σταθεροποιούν τον προσδέτη μέσα στον πόρο. Β) Την έλλειψη της γωνίωσης (κλίση κατά 10^o ως προς τον άξονα z) του άξονα της α-έλικας κατά τη σύνδεση του προσδέτη στον πόρο M2TMS31N. Η γωνίωση αυτή, η οποία μειώνει την γωνία μεταξύ της C-τελικής ελικοειδούς περιοχής και κάθετου άξονα στη μεμβράνη, περιλαμβάνει την πύλη αγωγιμότητας πρωτονίων W41 της M2 και επομένως μπορεί να εμποδίσει το άνοιγμα της πύλης αυτής. Η πρόταση αυτή αποτελεί ένα

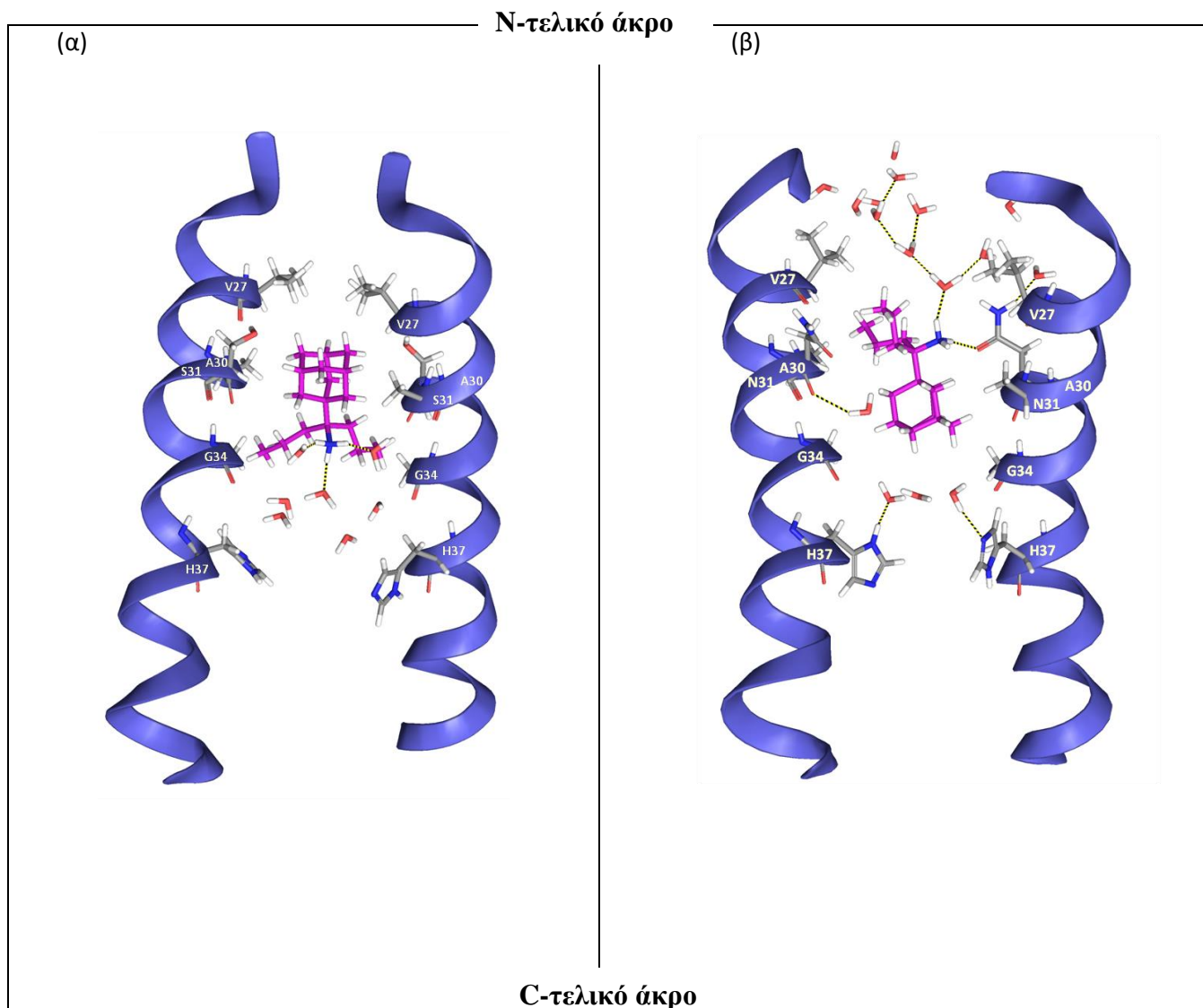
εναλλακτικό τρόπο για το πώς αυτές οι ενώσεις εμποδίζουν την αγωγιμότητα των πρωτονίων στη M2TM WT, δηλαδή μέσω σύγκρισης της γωνίωσης που προκαλούν οι προσδέτες στη M2TMWT με αυτή που προκαλούν στην M2TM S31N (Εικόνα 3). Τα αποτελέσματα της μελέτης αυτής δημοσιεύτηκαν στο *J. Med. Chem.* **2014**, *57*, 4629-4639 και στο *J. Med. Chem.* **2017**, *60*, 1716-1733 (βλέπε αναφ. 24 and 25 αντίστοιχα στον βιβλιογραφικό κατάλογο της εκτενούς περίληψης).

Στο Κεφάλαιο 3 διευκρινίζεται περαιτέρω η μοριακή βάση πρόσδεσης των ενώσεων, ο αποκλεισμός πρωτονίων και η αναστολή της influenza A WT και S31N από ανάλογα ριμανταδίνης χρησιμοποιώντας κινητικές μελέτες σύνδεσης μέσω πειραμάτων ηλεκτροφυσιολογίας EP, βιοφυσικών μεθόδων στην κατάσταση ισορροπίας όπως ITC, πειραμάτων αντιϊκής δραστηριότητας και MD προσομοιώσεις. Πρόσφατα, η κινητική της αλληλεπίδρασης προσδέτη-υποδοχέα, δηλαδή η διάρκεια παραμονής του φαρμακομορίου εντός του υποδοχέα θεωρείται όλο και πιο σημαντική για την αποτελεσματικότητα του φαρμάκου. Στο κεφάλαιο εξετάζονται αυτές οι έννοιες για να εξηγηθεί η πρόσδεση και ο αποκλεισμός πρωτονίων του ιοντικού διαλύου influenza A M2 WT και M2 S31N, από τα ανάλογα της ριμανταδίνης που περιλαμβάνουν αλκύλια συστηματικά αυξανόμενου μεγέθους. Αποδείχτηκε με τη βοήθεια των μετρήσεων EP ότι η ανθεκτικότητα της M2 S31N, έναντι της M2 WT, στα ανάλογα της ριμανταδίνης οφείλεται στις μεγαλύτερες ταχύτητες k_{off} συγκριτικά με τις σταθερές σύνδεσης k_{on} (βλ. Εικόνα 4). Αυτό οφείλεται στο γεγονός ότι, στη M2 S31N, η απώλεια της λιπόφιλης κοιλότητας για τον αδαμαντανικό σκελετό που σχηματίζεται από τις V27 προκάλεσε τον μικρό χρόνο παραμονής μέσα στον πόρο M2 (βλ. Εικόνες 2, 4). Αμφότερα τα εναντιομερή της ριμανταδίνης έχουν παρόμοιες τιμές k_{on} και k_{off} έναντι της M2 WT. Στη εργασία αυτή επίσης αποδείχτηκε ότι μια μικρή αλλαγή στην αλληλουχία της M2 δηλαδή η αντικατάσταση ενός αμινοξέος στη θέση 28 της M2 WT, παρότι δεν έχει πλευρική αλυσίδα με κατεύθυνση εντός του πόρου, επηρεάζει σημαντικά τη σύνδεση και τον φραγμό της M2 WT από έναν προσδέτη. Η μελέτη αυτή δημοσιεύθηκε στο *ACS Med. Chem. Lett.* **2018**, *29*, 198-203 (βλ. αναφ. 26 στον κατάλογο της βιβλιογραφίας).



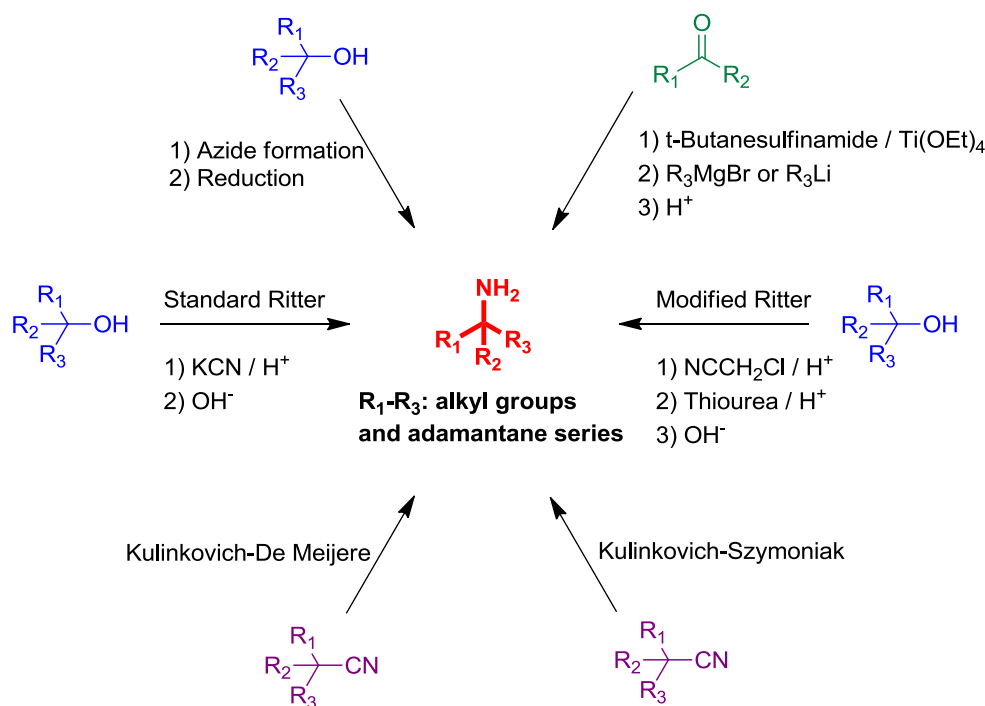
Εικόνα 4. Περιγραφή των πιο σημαντικών συνεπειών της πρόσδεσης των παραγώγων ριμανταδίνης στις πρωτεΐνες M2TM_{WT} και M2TM_{S31N}.²⁶

Με βάση την παρατήρηση ότι τα αμινοαδαμαντανικά παράγωγα προσανατολίζονται προς το N-τελικό άκρο στη S31N M2 έγινε προσπάθεια σχεδιασμού νέων ενώσεων που να αναστέλλουν τη M2 S31N επιδιώκοντας την (α) Αύξηση της συγγένειας σύνδεσης με το N-άκρο της M2 S31N συνδέοντας την αμινομάδα των αμινοαδαμαντανικών παραγώγων με πολικές ομάδες, προς σχηματισμό υβριδικών ενώσεων αμινοαδαμαντανίων-πολικών ομάδων, που μπορούν να σχηματίσουν δεσμούς υδρογόνου και αλληλεπιδράσεις van der Waals με το N-τελικό άκρο και, (β) Αύξηση του όγκου του λιπόφιλου κλωβού των υβριδικών ενώσεων αμινοαδαμαντανίων-πολικών ομάδων για την επίτευξη ισχυρότερων αλληλεπιδράσεων van der Waals στην ευρεία περιοχή γύρω από το αμινοξύ G34 των δύο ελικών, όπου δεν μπορεί να προσαρμοστεί σταθερά το αδαμαντάνιο. Μεγαλύτεροι σε όγκο λιπόφιλοι σκελετοί από το αδαμαντάνιο μπορούν να παρασκευαστούν με σύνθεση άλκυλο υποκατεστημένων αμινοαδαμαντανών, αμινοδιαδαμαντανίων, αμινοτριαδαμαντανίων. Πράγματι, μετρήσεις ITC έδειξαν ότι αυτά τα ογκωδέστερα ανάλογα μπορούν να προσδεθούν εντός του πόρου M2TM WT. Επιπλέον, συντέθηκαν ανάλογα ανοικτής αλυσίδας του αδαμαντανίου, όπως οι πρωτοταγείς *tert*-αλκυλαμίνες με σχετικά μεγάλες αλυσίδες αλκυλίου. Αυτές οι αμίνες επίσης περιέχουν μια πολική ομάδα με στόχο να προσαρμόζονται ικανοποιητικά στο εσωτερικό του M2TM S31N όπως θα συζητηθεί στο κεφάλαιο 5.



Εικόνα 5. Αντιπροσωπευτικά αντίγραφα από την προσομοίωση μοριακής δυναμικής του προσδέτη **5** (α) συνδεδεμένου εντός του M2TM WT. Επτά μόρια νερού απεικονίζονται μεταξύ του προσδέτη και του αμινοξέος H37 των δύο ελικών. Τρεις δεσμοί υδρογόνου μεταξύ της ομάδας αμμωνίου του προσδέτη και τριών μορίων νερού απεικονίζονται. Οι δεσμοί υδρογόνου με μόρια νερού και οι αλληλεπιδράσεις van der Waals του αδαμαντανικού κλωβού με τις πλευρικές αλυσίδες V27 και A30 σταθεροποιούν τον προσδέτη μέσα στον πόρο με την ομάδα αμμωνίου να είναι προσανατολισμένη προς το C-τελικό άκρο του διαύλου. (β) συνδεδεμένου εντός του M2TMS31N. Απεικονίζονται τρία μόρια νερού μεταξύ του προσδέτη και των αμινοξέων H37 και δώδεκα μόρια νερού μεταξύ του N31 και του N-άκρου του πόρου. Η ομάδα αμμωνίου του προσδέτη προσανατολίζεται προς το N-τελικό άκρο, όπου σχηματίζει δεσμούς υδρογόνου με μόρια νερού ή με την καρβονυλομάδα του αμιδίου της πλευρικής αλυσίδας του αμινοξέος N31. Η απώλεια της λιπόφιλης κοιλότητας των αμινοξέων V27 για τον αδαμαντανικό κλωβό είναι υπεύθυνη για την ασθενή σύνδεση των αμινοαδαμαντανίων μέσα στον πόρο.

Το κεφάλαιο 4 μελετά τρόπους σύνθεσης των πρωτοταγών *tert*-αλκυλαμινών ως δομικών τμημάτων ενώσεων της φαρμακοχημείας. Το περιεχόμενο του κεφαλαίου αφορά τη συνθετική χημεία και τις δυναμικές μελέτες NMR αυτής της κατηγορίας ενώσεων και των πρόδρομων τους ενώσεων. Μελετήθηκαν πέντε διαφορετικές πορείες σύνθεσης πρωτοταγών *tert*-αλκυλαμινών αλειφατικής δομής που περιλαμβάνουν επίσης τμήματα αδαμαντανίου (βλέπε Σχήμα 4).

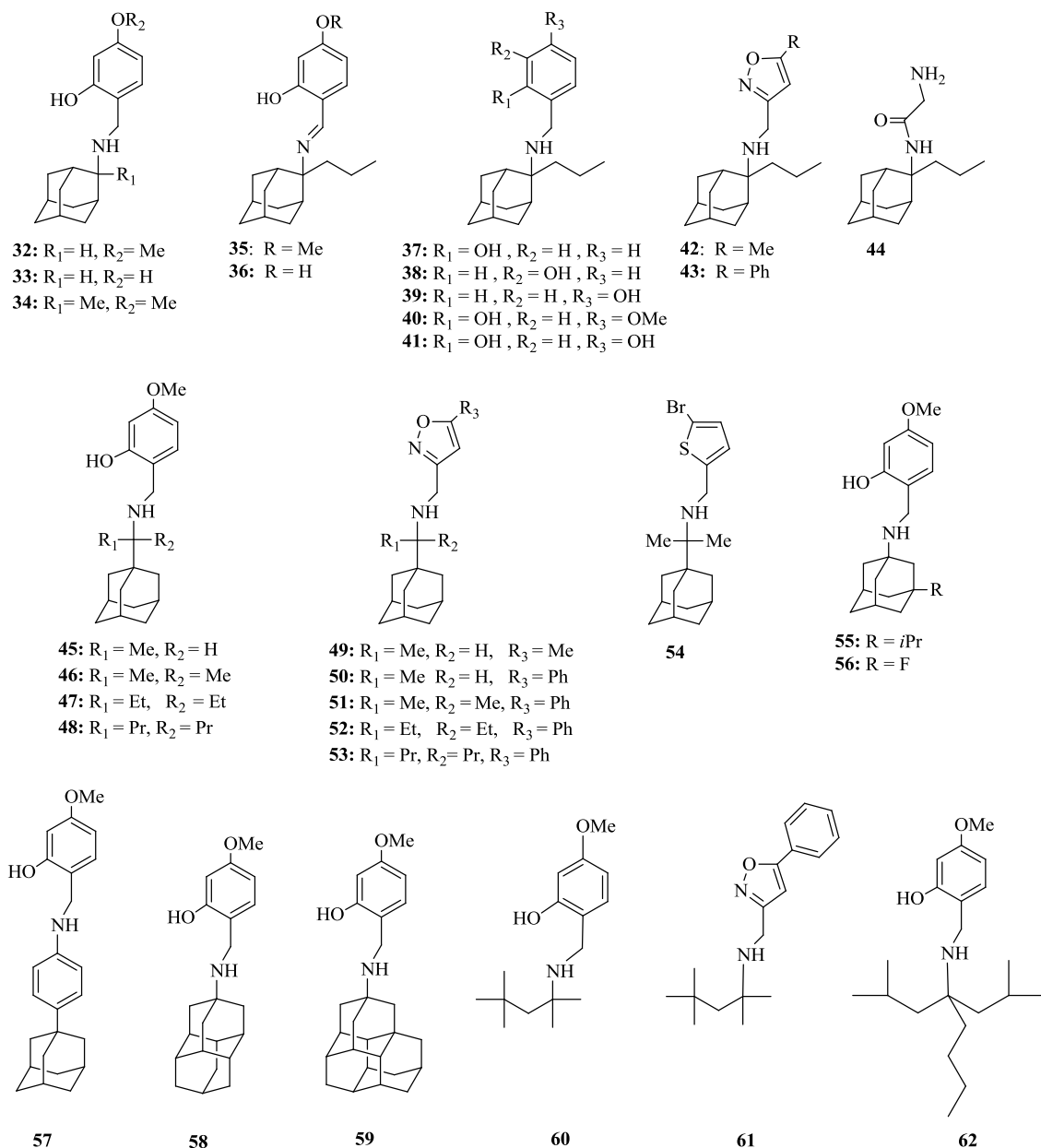


Σχήμα 4. Πορείες σύνθεσης πρωτοταγών *tert*-αλκυλαμινών ως δομικών τμημάτων ενώσεων της φαρμακοχημείας.

Οι αμίνες που συντέθηκαν είναι ανάλογα της αμανταδίνης που περιλαμβάνεται σε ενώσεις που δρουν σε διάφορους βιολογικούς στόχους. Στην πρώτη πορεία μελετήθηκε ο σχηματισμός και η αναγωγή των *tert*-αλκυλαζιδίων (πορεία A), όπου η απόδοση εξαρτάται από την επιλογή του διαλύτη για τον σχηματισμό του αζιδίου και το αντιδραστήριο που χρησιμοποιείται, καθώς και από τις συνθήκες που εφαρμόζονται στην αντίδραση αναγωγής. Το διχλωρομεθάνιο ή το 1,2-διχλωροαιθάνιο και το LiAlH_4 βρέθηκαν να είναι οι βέλτιστες επιλογές. Οι αποδόσεις της *tert*-αλκυλαμίνης μειώθηκαν όταν το *tert*-αλκυλικό υπόστρωμα περιείχε μεγαλύτερες ομάδες αλκυλίου από το Pr_3 . Αυτή η συνήθης πορεία σύνθεσης βρέθηκε να είναι η πιο γενική, συγκριτικά με τις υπόλοιπες τέσσερις που θα περιγραφούν παρακάτω, καλύπτοντας το ευρύτερο φάσμα υποστρωμάτων συμπεριλαμβανομένων και των ογκωδών υποκαταστατών αδαμαντανίου. Η αντίδραση Ritter (πορεία B) δεν ήταν αποδοτική. Παρόλα αυτά η τροποποιημένη αντίδραση Ritter (πορεία C), η οποία βαίνει μέσω ενός *tert*-άλκυλο χλωροακεταμίδιου, οδηγεί στο σχηματισμό των *tert*-

αλκυλαμινών με ικανοποιητικές αποδόσεις ακόμα και σε ενώσεις που περιλαμβάνουν μακριές αλκυλικές αλυσίδες. Η πορεία αυτή δεν ήταν αποδοτική όταν το υπόστρωμα περιελάμβανε αδαμαντάνιο. Η πορεία D, που περιλαμβάνει την προσθήκη οργανομεταλλικών αντιδραστηρίων σε *N-tert*-βουτυλο-σουλφινυλοκετιμίνες παρουσιάζει επίσης τους ίδιους περιορισμούς. Η σύνθεση πρωτοταγών *tert*-αλκυλαμινών από νιτρίλια με τη χρήση οργανομεταλλικών αντιδραστηρίων και $Ti(i-PrO)_4$ είναι μια συνθετική πορεία «μίας φιάλης» (μέθοδος E) που αποδείχθηκε πετυχημένη. Θέλοντας να διερευνήσουμε την επίδραση του αδαμαντανίου στη δραστικότητα και τη διαμορφωτική δυσκαμψία, η περιστροφή της 1-αδαμαντυλομάδας μελετήθηκε χρησιμοποιώντας δυναμικό NMR (dynamic NMR, DNMR) στις ενώσεις Ad-C(Et₂)OH και Ad-C(Et₂)Cl. Στα φάσματα NMR παρατηρήθηκε σχάση των σημάτων των ανθράκων 2', 8', 9'-C και 4', 6', 10'-C μειώνοντας την θερμοκρασία στους -100 °C. Η ελεύθερη ενέργεια για περιστροφή δεσμού υπολογίστηκε ότι είναι $\Delta G^\ddagger = 8.7 \pm 0.2 \text{ kcal mol}^{-1}$ για το δεσμό Αδαμαντίου-C στην ένωση Ad-C(Et₂)OH και $10.0 \pm 0.4 \text{ kcal mol}^{-1}$ στην ένωση Ad-C(Et₂)Cl συγκριτικά με $9.3 \text{ kcal mol}^{-1}$ στην ένωση Ad-C(Me₂)Cl ή $10.6 \text{ kcal mol}^{-1}$ στην ένωση Ad-CMe(t-Bu)Cl.

Στο Κεφάλαιο 5 περιγράφεται ο σχεδιασμός και η ανάπτυξη αναστολέων που στοχεύουν τον διάυλο πρωτονίων M2 ανθεκτικών στελεχών του ιού influenza A. Οι λοιμώξεις από τον ιό influenza οδηγούν σε πολυάριθμους θανάτους και σε εκατομμύρια νοσηλείες κάθε χρόνο. Μια πρόκληση που αντιμετωπίζει η ανάπτυξη φαρμάκων κατά του ιού influenza είναι η ετερογένεια των διαφόρων υποτύπων του ιού που είναι εξαπλωμένοι, και περιλαμβάνουν πολλά στελέχη με διαφορετική ευαισθησία στα αντιικά φάρμακα. Για παράδειγμα οι ιοί influenza A WT, όπως είναι αυτός που προκαλεί την εποχική επιδημία H1N1, είναι ευαίσθητοι στα αντιικά φάρμακα αμανταδίνη και ριμανταδίνη. Αντίθετα οι μεταλλαγμένοι ιοί S31N, όπως είναι αυτοί που προκάλεσαν την πανδημία 2009 H1N1 (H1N1pdm09) και είναι υπεύθυνοι για την εποχική επιδημία H3N2, και οι ιοί L26F, V27A, A30T, G34E παρουσιάζουν ανθεκτικότητα σε αυτή την κατηγορία φαρμάκων. Αναφέρουμε στην εργασία αυτή ενώσεις-οδηγούς που αντιστοιχούν σε αναστολείς των μεταλλαγμένων ιών που παρουσίασαν σημαντική αντιϊκή δράση έναντι των ιών WT, S31N, L26F και μέτριες δραστικότητες έναντι των ιών V27A, A30T, G34E. Οι ενώσεις αυτές περιλαμβάνουν την αμανταδίνη ή ένα υποκατεστημένο αμινοαδαμαντάνιο, στη θέση 1 ή 2 του αδαμαντανίου (αλκυλομάδα, φθόριο κτλ) ή αμινοδιαδαμαντάνιο, αμινοτριαδαμαντάνιο ή πρωτοταγή *tert*-αλκυλαμίνη όπου η αμινομάδα συνδέεται με μια πολική ομάδα, πολική κεφαλή, μέσω μιας γέφυρας μεθυλενίου²⁷⁻²⁹ (Σχήμα 5). Συγκεκριμένα, οι ενώσεις **45**, **46**, **57** και **58** ήταν οι πιο σημαντικές παρουσιάζοντας ανασταλτική δράση έναντι πολλαπλών στελεχών, δηλαδή, των ιών S31 (που αντιστοιχεί σε WT), S31N, V27A, L26F, A30T και G34E. Οι ιοί αυτοί σχηματίστηκαν με εφαρμογή μεθόδων αντίστροφης γενετικής.

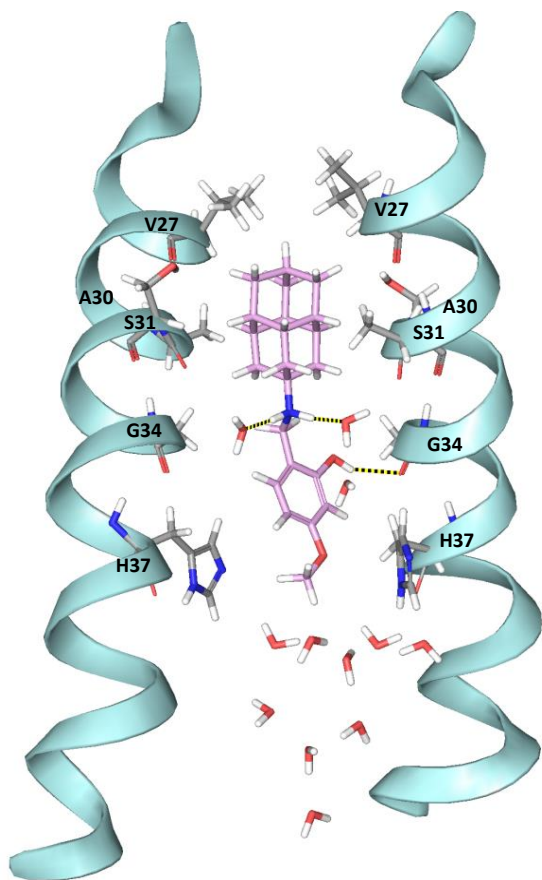


Σχήμα 5. Χημικές δομές υβριδικών μορίων αμινοαδαμαντανικών παραγώγων συζευγμένων με πολικές ομάδες, που συντέθηκαν στην παρούσα εργασία.

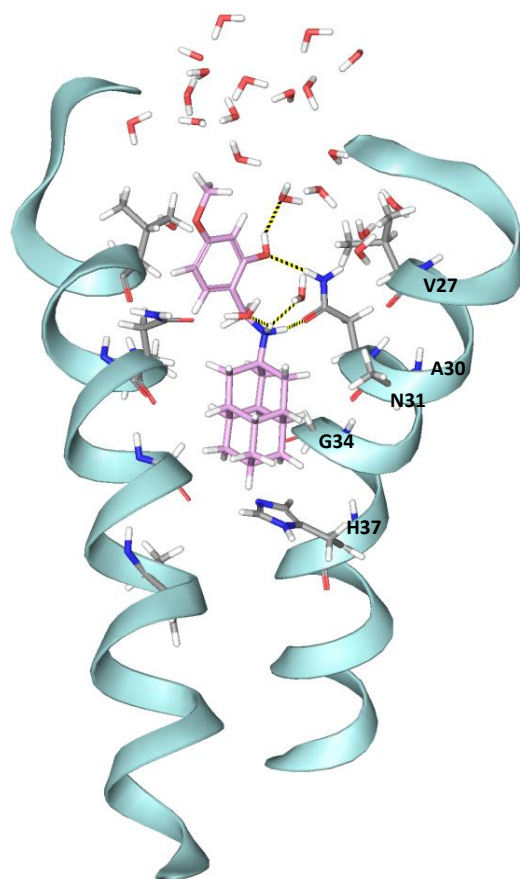
Η έρευνα και διεκρίνιση της πρόσδεσης του προσδέτη στη M2 μεταξύ πρωτεΐνης επιτεύχθηκε χρησιμοποιώντας πειράματα EP και προσομοιώσεις MD. Έτσι, τα αποτελέσματα της EP έδειξαν τον φραγμό της ροής των πρωτονίων εντός του πόρου των ιών M2 WT και S31N M2 από τις δραστικές ενώσεις. Οι προσομοιώσεις MD των αλληλεπιδράσεων του συμπλόκου υποδοχέα M2-προσδέτη έδειξαν ότι ένας αναστολέας διπλής δράσης στους ιούς WT και S31N προσδένεται στον διάυλο WT M2 με την αρωματική ομάδα της πολικής κεφαλής στραμμένη προς το C-τελικό άκρο, ενώ η ίδια ένωση προσδένεται στο διάυλο S31N M2 με την αρωματική του ομάδα να είναι στραμμένη προς το N-τελικό άκρο (βλ. Εικόνα 6).²⁸

(α)

N-τελικό άκρο



(β)



C-τελικό άκρο

Εικόνα 6. (α) Αντιπροσωπευτικές εικόνες από την προσομοίωση MD του προσδέτη **58** στο M2TMWT με την ομάδα αμμωνίου προσανατολισμένη στο N-τελικό άκρο του διαύλου. Απεικονίζονται δυο δεσμοί υδρογόνου μεταξύ της ομάδας αμμωνίου της ένωσης και δύο μορίων νερού και μεταξύ της ομάδας 4-MeO-2-OH-φαινυλίου του προσδέτη και δύο μορίων νερού. (β) Αντιπροσωπευτικά αντίγραφα από την προσομοίωση MD του προσδέτη **58** στο M2TMS31N με την ομάδα αμμωνίου προσανατολισμένη προς το C-τελικό άκρο του διαύλου. Η ομάδα αμμωνίου του προσδέτη σχηματίζει δύο δεσμούς υδρογόνου, ένα με ένα μόριο νερού και ένα με την καρβόνυλο ομάδα της πλευρικής αλυσίδας του αμινοξέος N31. Η ομάδα MeO-2-OH-φαινυλίου του προσδέτη σχηματίζει δύο δεσμούς υδρογόνου, ένα με ένα μόριο νερού και ένα με την αμινομάδα της πλευρικής αλυσίδας του αμινοξέος N31. Οι αλληλεπιδράσεις Van der Waals μεταξύ του προσδέτη και της περιοχής του πόρου M2TM μεταξύ V27 και H37 σταθεροποιούν το μόριο εντός του διαύλου.

Extensive Summary

Research Project Description

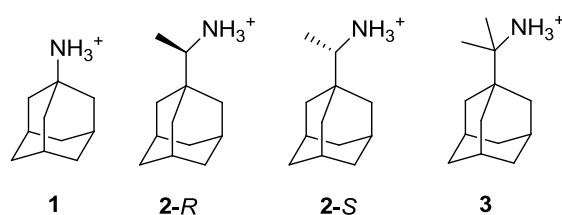
Introduction:

Amantadine (*Amt* (1)) and rimantadine (*Rim* (2)) are blockers of proton transport by influenza A virus M2 ion channel protein,^{1,2} and approved as prophylactics and therapeutics against influenza A wild type (WT) viruses. However, since 2005, the amantadine-insensitive Ser-to-Asn mutation at position 31 (S31N) in M2 protein has become globally prevalent, abrogating the clinical usefulness of amantadine^{3,4} and possibly other previously reported M2 inhibitors. Thus, new agents are needed to combat drug-resistant strains of influenza.

The primary binding site of amantadine and rimantadine is the transmembrane domain lumen (TM, amino acids 22-46) in the four-helix bundle of tetrameric M2 WT, that forms the proton transport path. According to high resolution structures from X-ray and solid state NMR (ssNMR) experiments published between 2008-2011 by Tim Cross, William DeGrado, and Mei Hong in the highest impact factor Journals i.e., Nature, JACS etc, the M2TM protein channel is blocked by amantadine and rimantadine via a pore-binding mechanism.^{5,6,7,8,9,10,11} The adamantyl cage in these molecules is tightly contacted on all sides by V27 and A30 side chains, producing a steric occlusion of proton transport^{6,7,8,9} and thereby preventing the continuation of the viral life cycle. The ssNMR results also demonstrated that the ammonium group of these drugs is pointing towards the four H37 residues at the C-end.⁹ This orientation can be stabilized only through hydrogen bonds between the ligand and (a) with water molecules in the channel lumen between the imidazoles of H37 and the ligand and (b) possibly with A30 carbonyls in the vicinity, according to experimental and molecular dynamics (MD) simulations data.^{9,12,13,14,15,16,17,18,19} Provided that M2TM is a minimal model for M2 binding, these experimental high resolution structures can be used for the prediction of new ligands binding more effectively to the M2TM pore for example through MD simulations¹⁹ or more precisely by binding free energy calculations.^{20,21,22}

Aims of the PhD thesis: We aim to investigate how subtle changes: (a) in amantadine structure are related with the binding affinity against M2TM pore variants resulting in increase or reduce of binding affinity, and (b) in M2TM structure caused by a single mutation, i.e.. S31N cause resistance of influenza A virus abrogating the clinical effectiveness of amantadine based drugs. The understanding of the molecular basis of resistance through biophysical and computational methods will be used for the rational drug design and synthesis of novel molecules to combat pandemic mutant influenza A viruses causing disease. Chapter 1 will focus on (a) while Chapters 2-5 on (b).

Chapter analysis: In Chapter 1 affinity of rimantadine enantiomers (Scheme 1) was revisited using biophysical methods and alchemical binding free energy calculations.



M2TM WT: SSDPLVVAASIIGILHLILWILDRL

Scheme 1. Structures of studied aminoadamantane derivatives amantadine (**1**), rimantadine enantiomers, **2-R** and **2-S**, and rimantadine analogue **3**. Compound **3** and amino acid sequence of M2TM WT peptide were synthesized for the purposes of this study.

We previously used molecular mechanics (MM) Poisson-Boltzmann surface area (MM/PBSA) to interpret thermodynamic profiles measured using (a) isothermal titration calorimetry (ITC) for aminoadamantanes binding to the avian M2TM_{Weybridge} in order to successfully prioritize aminoadamantane derivatives.²² We also applied rigorous relative free energy binding calculations by the Bennett acceptance ratio (BAR) approach to accurately predict experimental relative binding affinities of aminoadamantane derivatives towards M2TM_{WT} or M2TM_{Weybridge} measured respectively by ITC or spectroscopic methods.^{20,21} However, the affinity of rimantadine enantiomers to the M2 protein channel has never been investigated in detail. Findings from ssNMR studies published by Cross group in 2016 suggested that enantiomers bind to M2 with different affinity as expected based on the interaction of enantiomers with a chiral guest biopolymer. In particular, Cross group suggested that the (*R*)-enantiomer of rimantadine binds to the full M2 protein with higher affinity than the (*S*)-enantiomer.¹⁰ This was the first state of the art ssNMR study of the full M2 protein but the conclusion, although made sense, seemed to be puzzling as it has been shown before that: (a) Rimantadine enantiomers have similar in vivo antiviral activity in protecting mice from lethal influenza; (b) Rimantadine was approved as commercial drug in the US in 1993 containing both enantiomers. Intrigued by these findings, we applied in collaboration functional assays, such as antiviral assay and electrophysiology (EP), to evaluate the binding affinity of rimantadine enantiomers to the M2 protein channel. Additionally the binding constants of rimantadine enantiomers against M2TM_{WT} were measured for the first time using ITC and found to be equal (see Table 1). For this purpose: (a) M2TM WT peptide, corresponding to residues 22-46 of Udorn/72 wild type sequence of M2, was synthesized as C-terminally amidated M2TM_{Udorn/72}, including the sequence SSDPLVVAASIIGILHLILWILDRL, by standard Fmoc solid phase peptide synthesis using an aminomethyl polystyrene resin loaded with the amide linker, (b) purified by reverse phase HPLC and, (c) characterized by mass spectroscopy.

Table 1. Synopsis of rimantadine enantiomers to influenza A/M2 protein.²³

Rim-R	Rim-S
Kd M2TM _{Udorn} (ITC) = 0.32 μ M	Kd M2TM _{Udorn} (ITC) = 0.34 μ M
%block to M2 _{Udorn} (TEVC) = 95%	%block to M2 _{Udorn} (TEVC) = 96%
%block to M2 _{WSN/33-N31S} (TEVC) = 90%	%block to M2 _{WSN/33-N31S} (TEVC) = 92%
IC ₅₀ (Udorn/72, CPE) = 0.05 μ M	IC ₅₀ (Udorn/72, CPE) = 0.06 μ M
IC ₅₀ (WSN/33-M2-N31S, CPE) = 0.05 μ M	IC ₅₀ (WSN/33-M2-N31S, CPE) = 0.03 μ M
3 \rightarrow Rim-R, $\Delta\Delta G_{\text{FEP}}=0.62 \pm 0.14$, $\Delta\Delta G_{\text{exp}}=0.33 \pm 0.50$	3 \rightarrow Rim-S, $\Delta\Delta G_{\text{FEP}}=0.68 \pm 0.15$, $\Delta\Delta G_{\text{exp}}=0.42 \pm 0.48$

Our experimental data based on the full M2 protein function, were further supported by MD simulations (Figure 1 and 2). Alchemical free energy calculations using the Bennett acceptance ratio (BAR) method were performed to calculate the relative binding affinity of rimantadine enantiomers compared to **3**, synthesized and measured for this comparison, against M2TM in its closed form at pH 8 in 1,2-dimyristoyl-*sn*-glycero-3-phosphocholine (DMPC) lipids to mimic the membrane environment. No significant difference was found between the two enantiomers Both enantiomers have similar channel blockage, affinity and antiviral potency (Figure 1, Table 1). The work was published in *ACS Med. Chem. Lett.* **2017**, 27, 145-150, and part of the work in *ACS J. Chem. Info. Model.* **2016**, 56, 862-76 i.e., see ref. 23 and 21 respectively in References list of the extended summary.

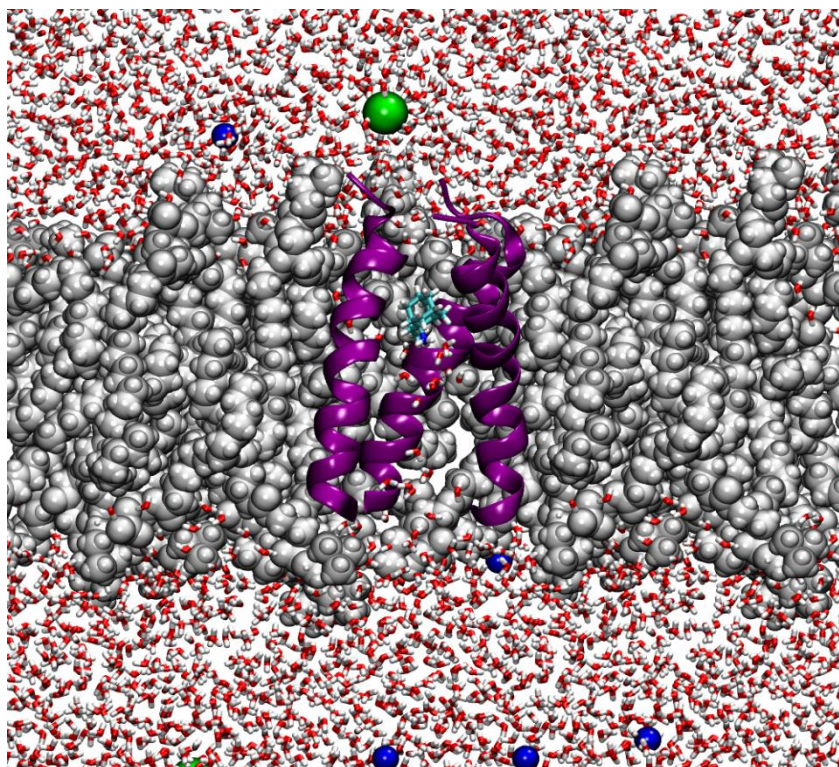
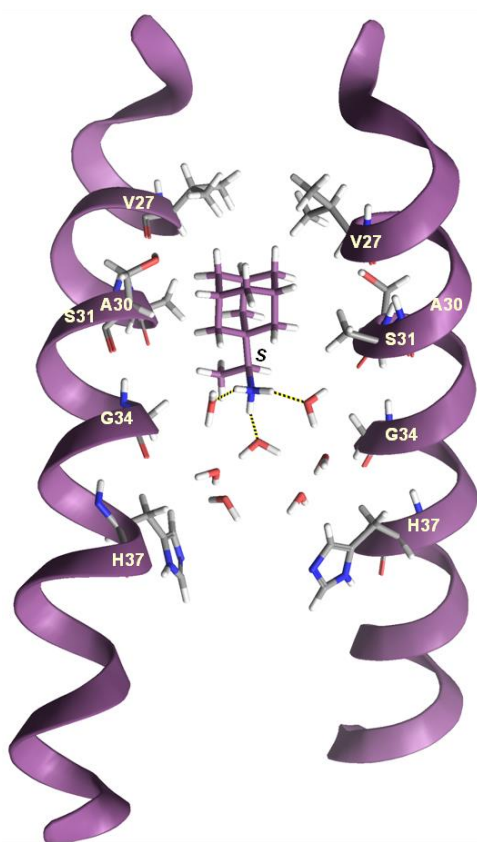


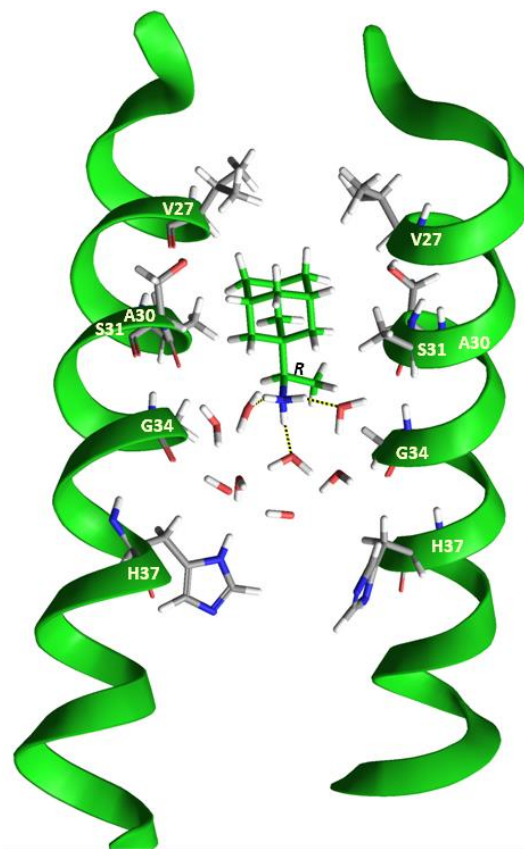
Figure 1. Representative replicas from FEP/MD simulations: Ligand **3** bound inside M2TM WT ion channel pore in hydrated DMPC bilayer. The full system is shown.

N-terminus

(a)



(b)

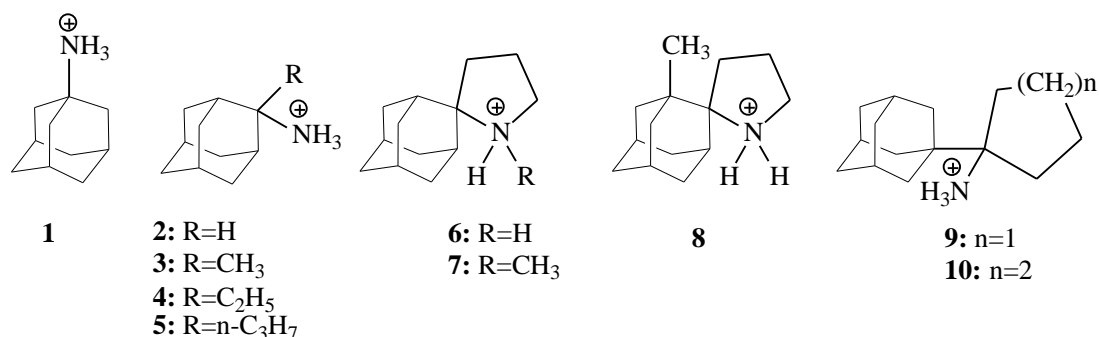


C-terminus

Figure 2. (a) Ligand **2-S** or (b) of **2-R** bound to M2TM. Seven and eight waters are shown between the ligand and H37 residues respectively. Three hydrogen bonds between the ammonium group of the ligand and three water molecules are shown. These hydrogen bonding together with van der Waals interactions of the adamantane core with V27 and A30 stabilize the ligand inside the pore with its ammonium group oriented towards the C-terminus.

In Chapter 2 the molecular basis of resistance of M2 WT protein to amantadine based drugs is investigated. While aminoadamantanes are well-established inhibitors of the influenza A M2 proton channel, the mechanisms by which they are rendered ineffective against M2_{S31N} are unclear. The differences in binding and proton blockage by amantadine variants of the influenza M2_{WT} and M2_{S31N} is explained using ssNMR and MD simulations. For this purpose M2TM S31N peptide corresponding to residues 22-46 of Udorn/72 but including the mutation Ser31-to-Asn (C-terminally amidated M2TMS31N: SSDPLVVAANIIGILHLILWILDRL) was synthesized by standard Fmoc solid phase peptide synthesis using an aminomethyl polystyrene resin loaded with the amide linker and purified by reverse phase HPLC and

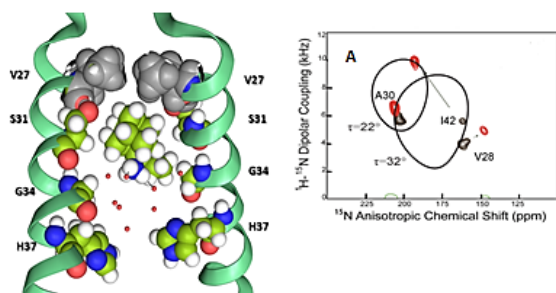
characterized by mass spectroscopy. Ligands **2-7, 9** were re-synthesized and two new ligands i.e., **8, 10** were synthesized with subtle changes in structure compared to spiropyrrolidine[2,2']adamantane **6** (Scheme 2) in order to investigate how these structural modifications affect ssNMR signals.



M2TM S31N: SSDPLVVAANIIGILHLILWILDRL

Scheme 2. Ligands synthesized for the studies. M2TM S31N peptide was also synthesized for the purposes of this study.

A Tight M2TM_{WT}-5 complex; strong C-terminus direction, V27 lipophilic pocket, 10° kink in C-terminus half



B Weak M2TM_{S31N}-5 complex; propensity for N-terminus direction, loss of V27 lipophilic pocket, uniform helical tilt

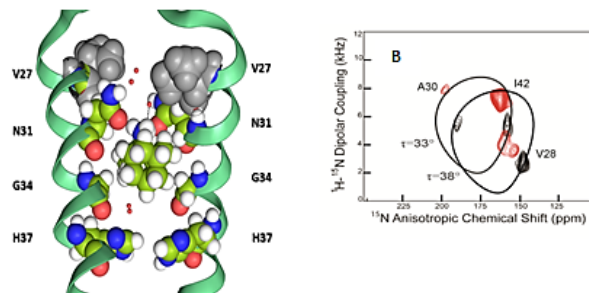


Figure 3. Summary of the most important binding consequences by amantadine variants to the influenza M2TM_{WT} and M2TM_{S31N}.²⁵

ssNMR, ITC, EP, anti-viral assays and MD simulations suggested stronger binding interactions for aminoadamantanes to M2_{WT} compared to negligible or weak binding to M2_{S31N}. This is due to reshaping of the M2pore when N31 is present which in contrast to wild type (WT), leads: A) To the loss of the V27 pocket for the adamantyl cage and to a predominant orientation of the ligand's ammonium group toward the N-terminus. S31N mutation of M2TM results in a shift of the hydrophobic adamantyl ring towards the C-terminus close to G34, due to the repulsive forces of N31 amide side chains to adamantyl ring. In G34 M2TM has the highest diameter and adamantane can't be tightly accommodated. As a consequence the stabilizing hydrophobic interactions of the V27 isopropyl groups with the adamantyl ring that are present in the M2TM WT are lost in M2TM S31N. Additionally ligand is rotated towards the N-terminus to form H-bond with Asn31 without having stabilizing van der Waals contacts. B) To the lack of a helical kink upon ligand binding to M2TM S31N. The kink, which reduces the tilt of the C-terminal helical domain relative to the bilayer normal includes the W41 primary gate for proton conductance and may prevent the gate from opening. This represents an alternative view for how these drugs prevent proton conductance i.e., through comparison of the kink caused by the ligands to M2TM WT compared to M2TM S31N (see also Figure 3). The work was published in *J. Med. Chem.* **2014**, *57*, 4629-4639 and *J. Med. Chem.* **2017**, *60*, 1716-1733 i.e., see ref. 24 and 25 in References list respectively of the extended summary.

In Chapter 3 the unraveling of the binding, proton blockage and inhibition of the influenza M2 WT and S31N by rimantadine variants is further pursued using binding kinetics by means of EP, and biophysical methods and assays in the equilibrium state like ITC, antiviral assays and MD simulations. Recently, the binding kinetics of a ligand-target interaction, such as the residence time of a small molecule on its protein target, are seen as increasingly important for drug efficacy. Here we investigate these concepts to explain binding and proton blockage of synthetic rimantadine variants bearing progressively larger alkyl group size to influenza A virus M2 WT and M2 S31N protein proton channel. We showed that resistance of M2 S31N to rimantadine analogues compared to M2 WT resulted from their higher k_{off} rates compared to the k_{on} rates according to EP measurements (see Figure 4). This is due to the fact that, in M2 S31N, the loss of the V27 pocket for the adamantyl cage resulted in low residence time inside the M2 pore (see Figure 2, 4). Both rimantadine enantiomers have similar channel blockage and binding k_{on} and k_{off} against M2 WT. It was also shown that a small change in an amino acid at site 28 of M2 WT, which does not line the pore, seriously affects M2 WT blockage efficiency. The work was published in *ACS Med. Chem. Lett.* **2018**, *29*, 198-203 i.e., see ref. 26 in References list.

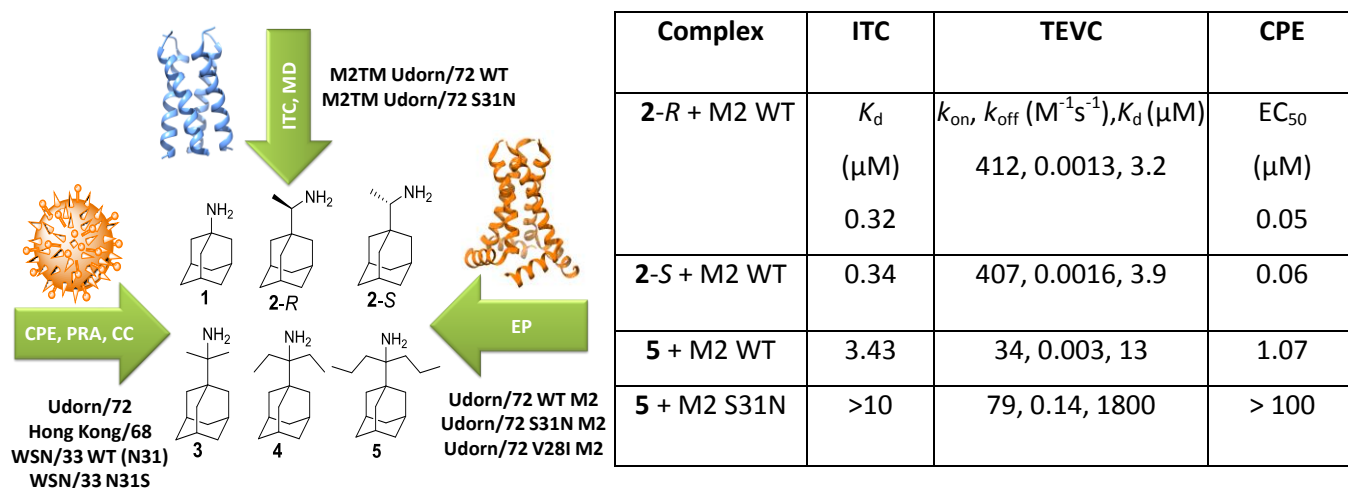


Figure 4. Summary of the most important binding consequences by amantadine variants to the influenza M2TM_{WT} and M2TM_{S31N}.²⁶

Based on the observation that aminoadamantane drugs oriented towards the N-end in S31N M2 we then seek to design novel compounds targeting M2 S31N by (a) Increasing binding strength with the N-end of M2 S31N after connecting the amine group of the aminoadamantane derivatives with polar heads, resulting to aminoadamantane-polar head conjugates that can form H-bonds and van der Waals interactions with M2TM N-end and, (b) Increasing lipophilic cage volume in the aminoadamantane-polar head conjugates in order to effect stronger van der Waals interactions in the broad area around G34, where adamantane can't be tightly accommodated. Larger adducts can be made by synthesizing alkyl substituted aminoadamantanes, aminodiadamantanes, aminotriadamantanes. Indeed these bigger adduct analogues were found to bind to M2TM WT using ITC and thus they can fit inside the M2TM pore. Additionally adamantane open chain analogues like primary *tert*-alkyl amines with relatively long alkyl chains will be synthesized. These amines were also connected with a polar head to fit favorably inside M2TM S31N as will be discussed in Chapter 5.

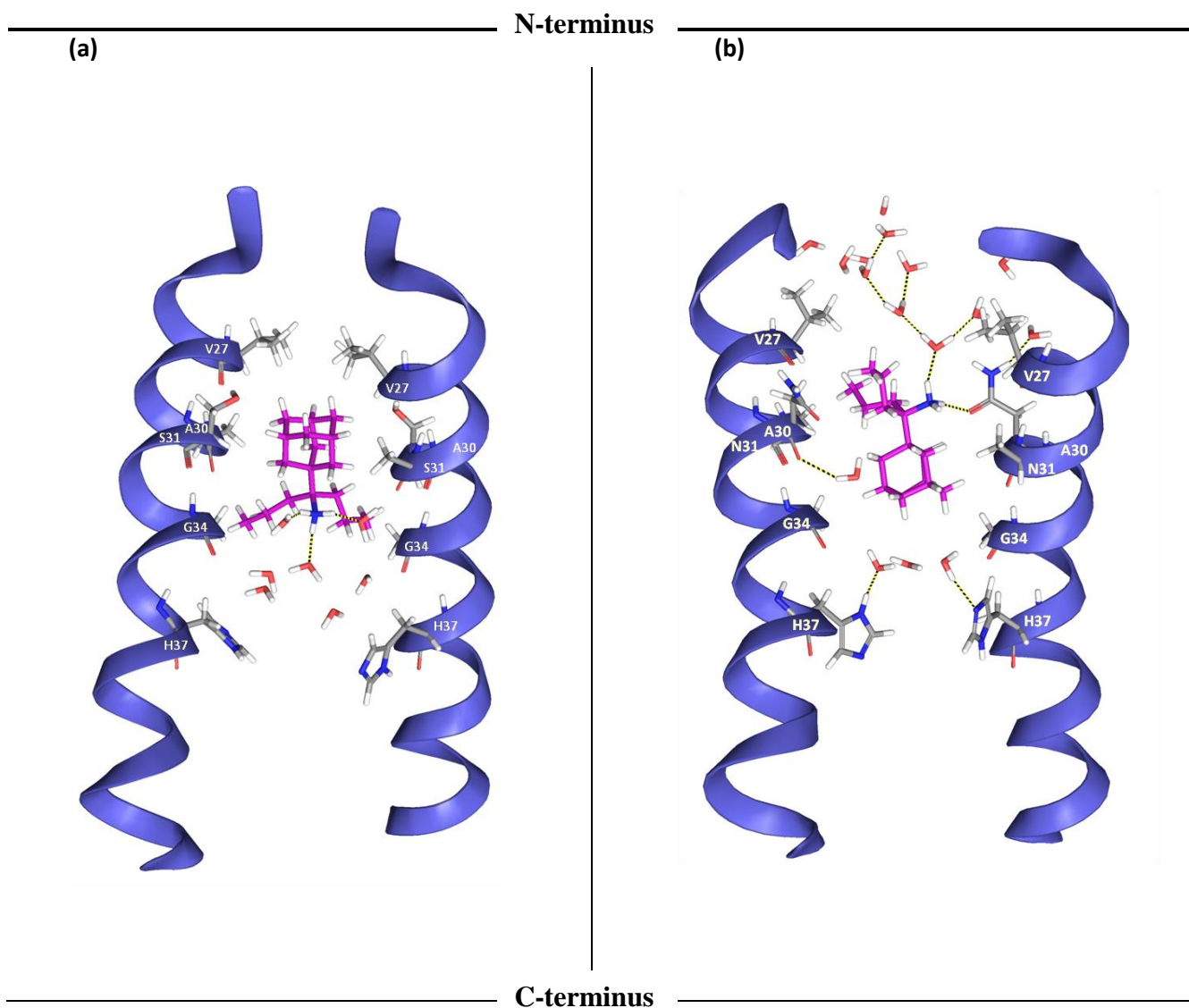
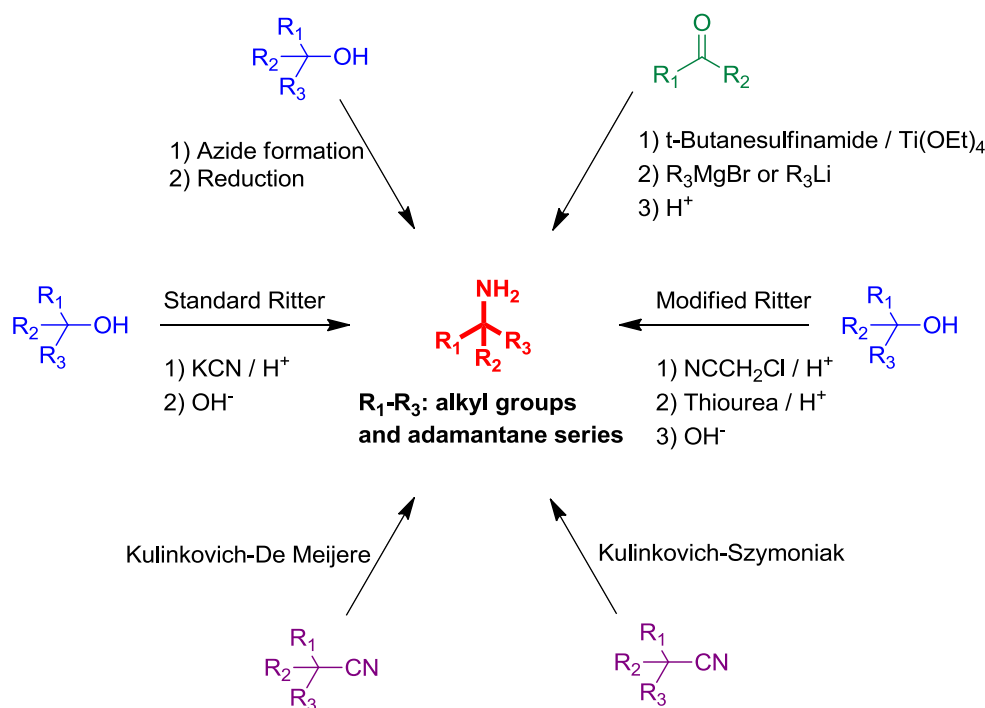


Figure 5. Representative replicas from the simulation of ligand **5** (a) bound to M2TM WT. Seven water molecules are shown between the ligand and H37 residues. Three hydrogen bonds between the ammonium group of the ligand and three water molecules are shown. Hydrogen bonding with water molecules and van der Waals interactions of the adamantane core with V27 and A30 side chains stabilize the ligand inside the pore with its ammonium group oriented towards the C-terminus of the channel; (b) bound to M2TMS31N. Three water molecules are shown between ligand and the H37 residues and twelve water molecules between N31 and the mouth of the pore. The ammonium group of the ligand is oriented towards the N-terminus, where it forms hydrogen bonds with water molecules or the carbonyl group of the N31 amide side chain. The loss of the V27 pocket for the adamantyl cage would be expected to lead to weak binding of aminoadamantane ligands.

Chapter 4 is dealing with approaches to the synthesis of primary *tert*-alkyl amines as medicinal chemistry building blocks. The content is towards synthetic chemistry and dynamic NMR studies of this class of molecules and their precursors. Five procedures were tested for the synthesis of primary *tert*-alkyl primary amines in aliphatic series including also adamantane adducts (see Scheme 4).

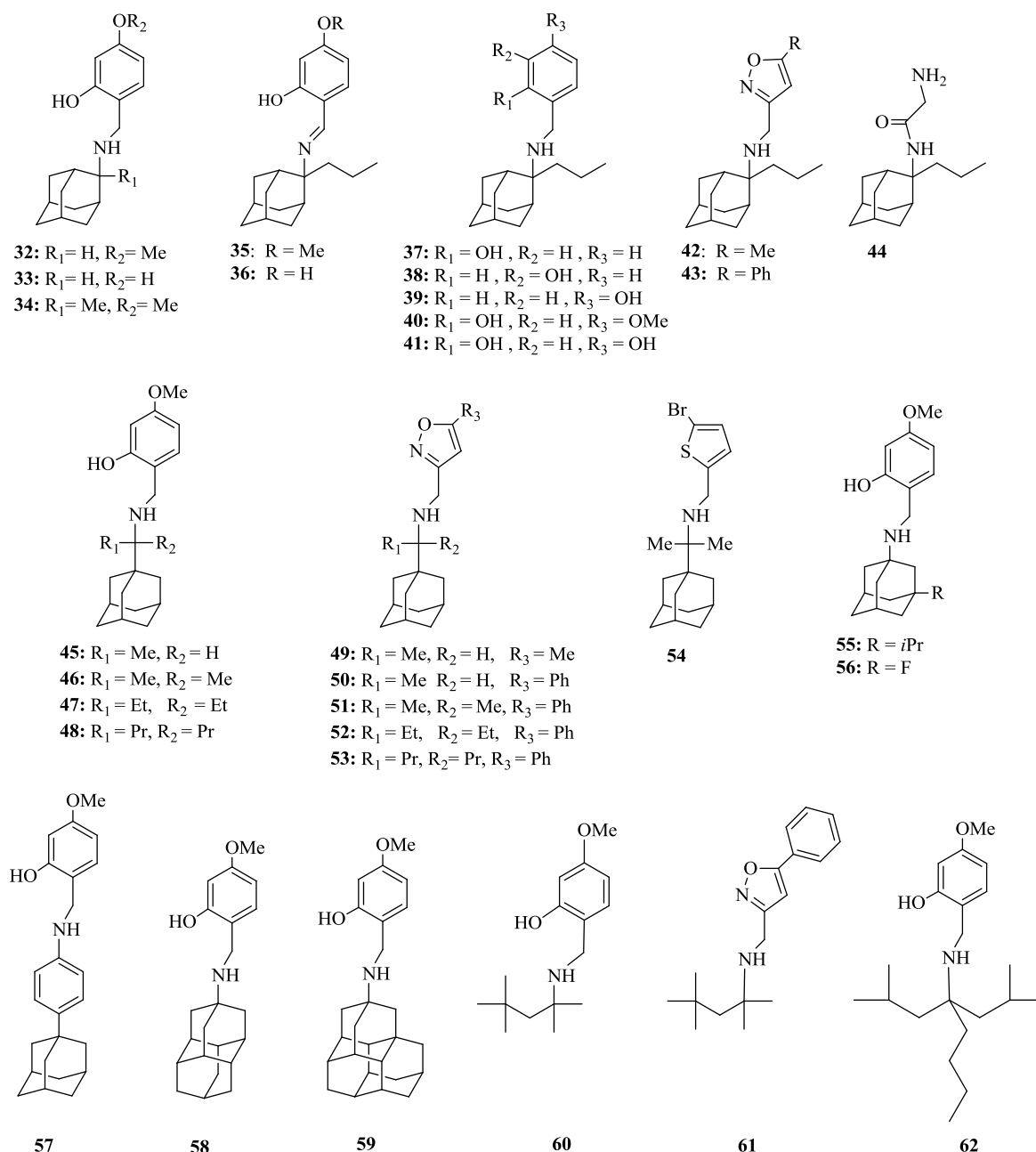


Scheme 4. Approaches to primary *tert*-alkyl amines as medicinal chemistry building blocks.

The synthesized amines are analogues of amantadine which is included in compounds acting against various biological targets. The first procedure included the formation and reduction of *tert*-alkyl azides (procedure A), where yield depends from the selection of solvent for azide formation and the reagent and conditions for its reduction. Dichloromethane or 1,2-dichloroethane and LiAlH_4 were found to be optimal choices. The yields of the amine products were diminished when the *tert*-alkyl substrate includes longer alkyl groups than Pr_3 . This common procedure was the most general compared with the next four described below covering a broader range of substrates including also bulky adamantane adducts. Standard Ritter reaction (procedure B) was not affordable. A modified Ritter scheme (procedure C), which proceeds through a *tert*-alkyl chloroacetamide produced *tert*-alkyl amines with good yields also for long alkyl groups. The procedure failed when the substrate included an adamantane adduct. Procedure D included the addition of organometallic reagents to *N-tert*-butyl sulfinylketimines and had also the same limitations. The synthesis of primary *tert*-alkyl amines from nitriles using organometallic reagents and $\text{Ti}(\text{i-PrO})_4$ was a useful one-flask transformation (procedure E). Triggered by the effects of the adamantane adduct in reactivity and

conformational strain the rotation of the 1-adamantyl group was investigated using dynamic NMR (DNMR) in the synthesized Ad-C(Et₂)OH and Ad-C(Et₂)Cl. Their NMR spectra resulted in decalescence for carbons 2', 8', 9'-C and 4', 6', 10'-C signals at temperatures as low as -100 °C. The free energy for bond rotation was calculated to be $\Delta G^\ddagger = 8.7 \pm 0.2 \text{ kcal mol}^{-1}$ for adamantyl-C bond in Ad-C(Et₂)OH and $10.0 \pm 0.4 \text{ kcal mol}^{-1}$ in Ad-C(Et₂)Cl compared to $9.3 \text{ kcal mol}^{-1}$ in Ad-C(Me₂)Cl or $10.6 \text{ kcal mol}^{-1}$ in Ad-CMe(t-Bu)Cl.

In Chapter 5 the design and development of resistance-breaking inhibitors targeting the M2 proton channel of influenza A viruses is described. Influenza virus infections lead to numerous deaths and millions of hospitalizations each year. One challenge facing anti-influenza drug development is the heterogeneity of the circulating influenza viruses, which comprise several strains with variable susceptibility to antiviral drugs. For example, the WT influenza A viruses, such as the seasonal H1N1, tend to be sensitive to antiviral drugs amantadine and rimantadine. In contrast, the S31N mutant viruses, such as the pandemic 2009 H1N1 (H1N1pdm09) and seasonal H3N2, as well as L26F, V27A, A30T, G34E are resistant to this class of drugs. We report here lead compounds that represent resistance-breaking inhibitors with fair antiviral potencies against WT, S31N, L26F and moderate potencies against V27A, A30T, G34E. The inhibitors included amantadine or a substituted aminoadamantane, at 1, or 2- adamantane position (alkyl group, fluoro group etc) or aminodiadamantane, aminotriadamantane or primary *tert*-alkyl amine compound, linked to amino group with a polar head through a methylene bridge²⁷⁻²⁹ (Scheme 5). In particular compounds **45**, **46**, **57** and **58** were the most interesting being multi-strain inhibitors i.e., exhibiting potency against S31 (corresponding to WT), S31N, V27A, L26F, A30T and G34E viruses. These viruses were generate through reverse-genetics methods.



Scheme 5. Chemical structures of synthesized aminoadamantane-polar heads conjugates.

Target M2 protein-ligand binding investigation was achieved using EP and MD simulations. Thus, EP supported the blockage of protons flow by the compounds inside M2 WT and S31N M2. MD simulations of drug-M2 interactions showed that a dual WT, S31N inhibitor binds in the WT M2 channel with an aromatic group facing down toward the C-terminus, while the same drug binds in the S31N M2 channel with its aromatic group facing up toward the N-terminus (see Figure 6).²⁸

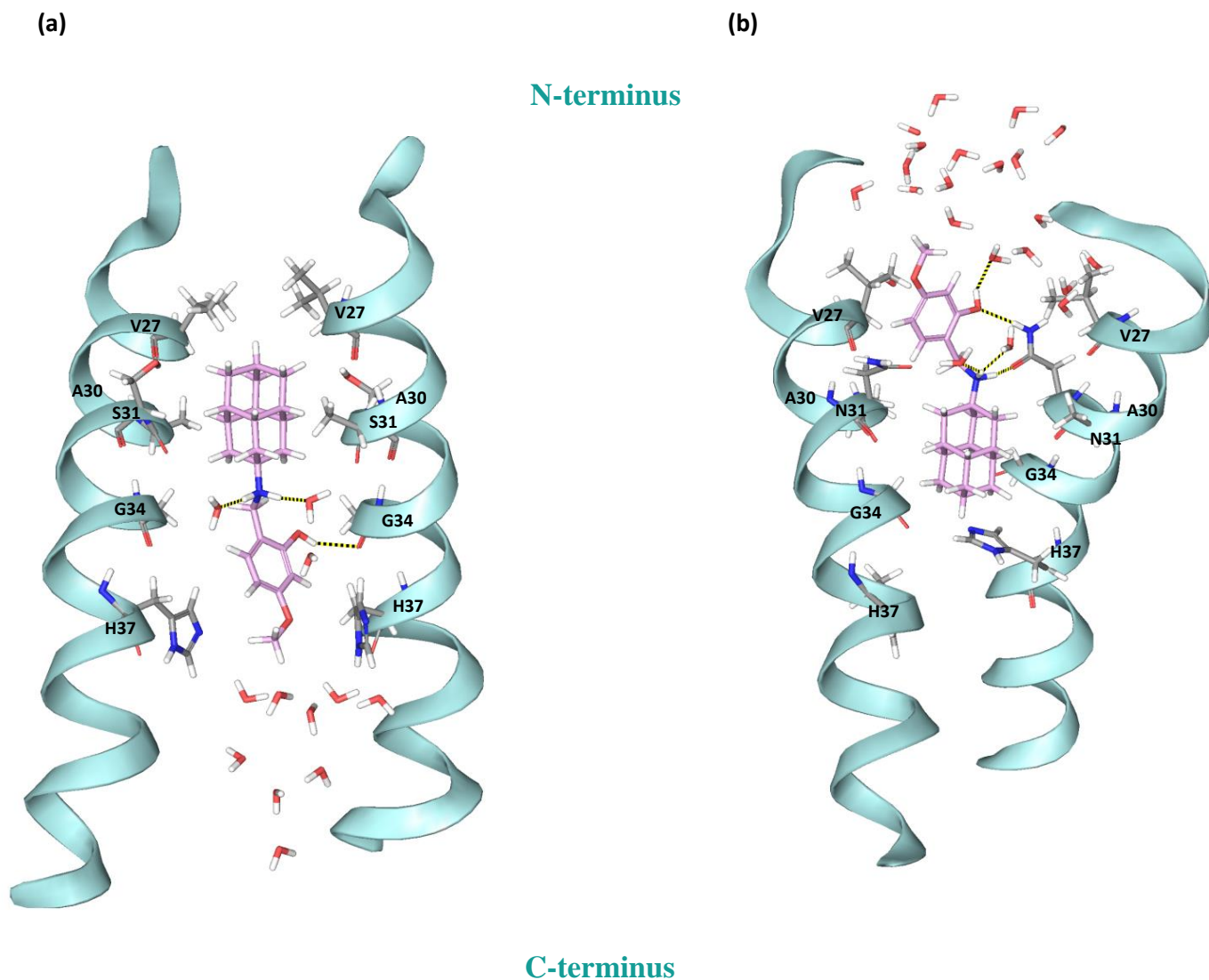


Figure 6. (a) Representative replica from the MD simulation of ligand **58** bound to M2TM WT with its ammonium group oriented towards the C-terminus of the channel. Two hydrogen bonds between the ammonium group of the ligand and two water molecules and between 4-MeO-2-OH phenyl group of the ligand and two water molecules are shown. (b) Representative replica from the MD simulation of ligand **58** bound to M2TMS31N with its ammonium group oriented towards the N-terminus of the channel. The ammonium group of the ligand forms two hydrogen bonds – one with water molecule and one with N31 side chain carbonyl group. The 4-MeO-2-OH phenyl group of the ligand forms one hydrogen bond with one water molecule and another one with N31 side chain NH₂ group. Van der Waals interactions between the ligand and the M2TM pore walls between V27 and H37 stabilize the ligand inside the pore.

Acknowledgements

First of all I would like to express my deepest gratitude for my supervisor, Associate Professor Antonios Kolokouris, who provided me the opportunity to work on that project, for trusting me, guiding and for all the scientific support during this time of research and writing this thesis. He was always trying to encourage me and to solve any arising problem. I would also like to thank him for his support in gaining the chance to join the drug synthesis group in RnD center, of Pharmaceutical company Chiesi, as intern.

Then, I would like to acknowledge the following people whose contribution was crucial for the successful completion of my PhD project:

Dr Michaela Schmidke and Anja Hoffmann from the department of Virology and Antiviral Therapy (IVAT) of University of Jena in Germany, for the antiviral testing of the final compounds and the reverse genetics experiments.

Dr David Busath and Kelly Mcguire from Brigham Young *University* (BYU) of Utah, USA for their contribution in biophysics by performing electrophysiology experiments they did and the strong collaboration with our group for more than 8 years.

Prof Timothy Cross (Professor and Program Director at the National High Magnetic Field Lab) and Dr Anna Wright from Institute of Molecular Biophysics and Department of Chemistry and Biochemistry of the Florida State University (FSU), USA performing ssNMR experiments.

Dr David Fedida, Chunlong Ma and Jun Wang from the department of anesthesiology pharmacology and therapeutics of University of British Columbia of Canada (UBC) for the extra electrophysiology testing.

Prof Günter Gauglitz , Dr Kathrin Freudenberger and Dr Johanna Hutterer, from the Institute of Physical and Theoretical Chemistry of University of Tübingen for the ITC measurements.

Dr Christos Zigos and Dr Christos Liolios from the *National Center* for Scientific Research Demokritos for their help in peptide synthesis which was performed in NKUA.

Ast Prof Ioannis Papanastasiou for sharing his knowledge and experience in the synthesis of an intermediate aminoadamantane scaffold.

Prof Panagiotis Marakos and Prof Tsotinis Andrew which are members of my three member committee, for their useful remarks and suggestions during the writing of my PhD.

Prof Thomas Mavromoustakos for his valuable remarks in the text and Prof Emmanuel Mikros for his advice and the insightful comments.

Ast Prof Evaggelos Gikas for his assistance in high resolution mass spectrometry.

Also I would like to thank Chiesi Hellas for the financial support provides me throughout my PhD thesis.

Many thanks to EFMC association for the fellowship to attend Urbino, EFMC school and IKYDA for the one month fellowship to visit Professor's Gohlke lab, Pharmaceutical Chemistry, University of Dusseldorf for running calculation with AMBER in M2-aminoadamantane complex.

My partners in lab Panagiotis Lagarias and Athina Konstantinidi for creating a friendly atmosphere in the lab.

Last but not the least, I would like to thank my family: my mother and my brothers and sisters for supporting me spiritually throughout all these years of my PhD studies.

References and Notes

- (1) Wang, C.; Takeuchi, K.; Pinto, L. H.; Lamb, R. a. IonChannelActivityofInfluenzaAVirusM2 Protein: CharacterizationoftheAmantadineBlock. *J. Virol.* **1993**, *67*, 5585–5594.
- (2) Chizhnikov, I. V.; Geraghty, F. M.; Ogden, D. C.; Hayhurst, A.; Antoniou, M.; Hay, A. J. SelectiveProtonPermeabilityandpHRegulation of the Influenza Virus M2 Channel Expressed in Mouse Erythroleukaemia Cells. *J. Physiol.* **1996**, *494*, 329–336.
- (3) Furuse, Y.; Suzuki, A.; Oshitani, H. Large-Scale Sequence Analysis of M Gene of Influenza A Viruses from Different Species: Mechanisms for Emergence and Spread of Amantadine Resistance. *Antimicrob. Agents Chemother.* **2009**, *53*, 4457–4463.
- (4) Dong, G.; Peng, C.; Luo, J.; Wang, C.; Han, L.; Wu, B.; Ji, G.; He, H. Adamantane-Resistant Influenza a Viruses in the World (1902-2013): Frequency and Distribution of M2 Gene Mutations. *PLoS One* **2015**, *10*, 1–20.
- (5) Hu, J.; Asbury, T.; Achuthan, S.; Li, C.; Bertram, R.; Quine, J. R.; Fu, R.; Cross, T. a. Backbone Structure of the Amantadine-Blocked Trans-Membrane Domain M2 Proton Channel from Influenza A Virus. *Biophys. J.* **2007**, *92*, 4335–4343.
- (6) Stouffer, A. L.; Acharya, R.; Salom, D.; Levine, A. S.; Di Costanzo, L.; Soto, C. S.; Tereshko, V.; Nanda, V.; Stayrook, S.; DeGrado, W. F. Structural Basis for the Function and Inhibition of an Influenza Virus Proton Channel. *Nature* **2008**, *451*, 596–599.
- (7) Cady, S. D.; Schmidt-Rohr, K.; Wang, J.; Soto, C. S.; DeGrado, W. F.; Hong, M. Structure of the Amantadine Binding Site of Influenza M2 Proton Channels in Lipid Bilayers. *Nature* **2010**, *463*, 689–U127.
- (8) Pielak, R. M.; Oxenoid, K.; Chou, J. J. Structural Investigation of Rimantadine Inhibition of the AM2-BM2 Chimera Channel of Influenza Viruses. *Structure* **2011**, *19*, 1655–1663.
- (9) Cady, S. D.; Wang, J.; Wu, Y.; Degrado, W. F.; Hong, M. Specific Binding of Adamantane Drugs and Direction of Their Polar Amines in the Pore of the Influenza M2 Transmembrane Domain in Lipid

Bilayers and Dodecylphosphocholine Micelles Determined by NMR Spectroscopy. *J. Am. Chem. Soc.* **2011**, *133*, 4274–4284.

- (10) Wright, A. K.; Batsomboon, P.; Dai, J.; Hung, I.; Zhou, H. X.; Dudley, G. B.; Cross, T. A. Differential Binding of Rimantadine Enantiomers to Influenza A M2 Proton Channel. *J. Am. Chem. Soc.* **2016**, *138*, 1506–1509.
- (11) Ma, C.; Polishchuk, a L.; Ohigashi, Y.; Stouffer, a L.; Schon, a; Magavern, E.; Jing, X.; Lear, J. D.; Freire, E.; Lamb, R. a; DeGrado, W. F.; Pinto, L. H. Identification of the Functional Core of the Influenza A Virus A/M2 Proton-Selective Ion Channel. *Proc Natl Acad Sci U S A* **2009**, *106*, 12283–12288.
- (12) Luo, W.; Hong, M. Conformational Changes of an Ion Channel Detected through Water-Protein Interactions Using Solid-State NMR Spectroscopy. *J Am Chem Soc* **2010**, *132*, 2378–2384.
- (13) Gianti, E.; Carnevale, V.; Degrado, W. F.; Klein, M. L.; Fiorin, G. Hydrogen-Bonded Water Molecules in the m2 Channel of the Influenza a Virus Guide the Binding Preferences of Ammonium-Based Inhibitors. *J. Phys. Chem. B* **2015**, *119*, 1173–1183.
- (14) Gleed, M. L.; Ioannidis, H.; Kolocouris, A.; Busath, D. D. Resistance-Mutation (N31) Effects on Drug Orientation and Channel Hydration in Amantadine-Bound Influenza A M2. *J. Phys. Chem. B* **2015**, *119*, 11548–11559.
- (15) Leonov, H.; Astrahan, P.; Krugliak, M.; Arkin, I. T. How Do Aminoadamantanes Block the Influenza M2 Channel, and How Does Resistance Develop? *J. Am. Chem. Soc.* **2011**, *133*, 9903–9911.
- (16) Yi, M.; Cross, T. a; Zhou, H.-X. Conformational Heterogeneity of the M2 Proton Channel and a Structural Model for Channel Activation. *Proc. Natl. Acad. Sci. U. S. A.* **2009**, *106*, 13311–13316.
- (17) Intharathep, P.; Laohpongspaisan, C.; Rungrotmongkol, T.; Loiruangsinsin, A.; Malaisree, M.; Decha, P.; Aruksakunwong, O.; Chuenpennit, K.; Kaiyawet, N.; Sompornpisut, P.; Pianwanit, S.; Hannongbua, S. How Amantadine and Rimantadine Inhibit Proton Transport in the M2 Protein Channel. *J. Mol. Graph. Model.* **2008**, *27*, 342–348.
- (18) Khurana, E.; Devane, R. H.; Dal Peraro, M.; Klein, M. L. Computational Study of Drug Binding to the

Membrane-Bound Tetrameric M2 Peptide Bundle from Influenza A Virus. *Biochim. Biophys. Acta - Biomembr.* **2011**, *1808*, 530–537.

- (19) Wang, J.; Ma, C.; Fiorin, G.; Carnevale, V.; Wang, T.; Hu, F.; Lamb, R. A.; Pinto, L. H.; Hong, M.; Klein, M. L.; DeGrado, W. F. Molecular Dynamics Simulation Directed Rational Design of Inhibitors Targeting Drug-Resistant Mutants of Influenza A Virus M2. *J. Am. Chem. Soc.* **2011**, *133*, 12834–12841.
- (20) Gkeka, P.; Eleftheratos, S.; Kolocouris, A.; Cournia, Z. Free Energy Calculations Reveal the Origin of Binding Preference for Aminoadamantane Blockers of Influenza A/M2TM Pore. *J. Chem. Theory Comput.* **2013**, *9*, 1272–1281.
- (21) Ioannidis, H.; Drakopoulos, A.; Tzitzoglaki, C.; Homeyer, N.; Kolarov, F.; Gkeka, P.; Freudenberger, K.; Liolios, C.; Gauglitz, G.; Cournia, Z.; Gohlke, H.; Kolocouris, A. Alchemical Free Energy Calculations and Isothermal Titration Calorimetry Measurements of Aminoadamantanes Bound to the Closed State of Influenza A/M2TM. *J. Chem. Inf. Model.* **2016**, *56*, 862–876.
- (22) Homeyer, N.; Stoll, F.; Hillisch, A.; Gohlke, H. Binding Free Energy Calculations for Lead Optimization: Assessment of Their Accuracy in an Industrial Drug Design Context. *J. Chem. Theory Comput.* **2014**, *10*, 3331–3344.
- (23) Drakopoulos, A.; Tzitzoglaki, C.; Ma, C.; Freudenberger, K.; Hoffmann, A.; Hu, Y.; Gauglitz, G.; Schmidtke, M.; Wang, J.; Kolocouris, A. Affinity of Rimantadine Enantiomers against Influenza A/M2 Protein Revisited. *ACS Med. Chem. Lett.* **2017**, *8*.
- (24) Kolocouris, A.; Tzitzoglaki, C.; Johnson, F. B.; Zell, R.; Wright, A. K.; Cross, T. A.; Tietjen, I.; Fedida, D.; Busath, D. D. Aminoadamantanes with Persistent in Vitro Efficacy against H1N1 (2009) Influenza A. *J. Med. Chem.* **2014**, *57*, 4629–4639.
- (25) Tzitzoglaki, C.; Wright, A.; Freudenberger, K.; Hoffmann, A.; Tietjen, I.; Stylianakis, I.; Kolarov, F.; Fedida, D.; Schmidtke, M.; Gauglitz, G.; Cross, T. A.; Kolocouris, A. Binding and Proton Blockage by Amantadine Variants of the Influenza M2WT and M2S31N Explained. *J. Med. Chem.* **2017**, *60*, 1716–1733.
- (26) Drakopoulos, A.; Tzitzoglaki, C.; McGuire, K.; Hoffmann, A.; Konstantinidi, A.; Kolocouris, D.; Ma, C.;

Freudenberger, K.; Hutterer, J.; Gauglitz, G.; Wang, J.; Schmidtke, M.; Busath, D. D.; Kolocouris, A. Unraveling the Binding, Proton Blockage, and Inhibition of Influenza M2 WT and S31N by Rimantadine Variants. *ACS Med. Chem. Lett.* **2018**, *9*.

- (27) Wang, J.; Ma, C.; Wang, J.; Jo, H.; Canturk, B.; Fiorin, G.; Pinto, L. H.; Lamb, R. A.; Klein, M. L.; DeGrado, W. F. Discovery of Novel Dual Inhibitors of the Wild-Type and the Most Prevalent Drug-Resistant Mutant, S31N, of the M2 Proton Channel from Influenza A Virus. *J. Med. Chem.* **2013**, *56*, 2804–2812.
- (28) Wu, Y.; Canturk, B.; Jo, H.; Ma, C.; Gianti, E.; Klein, M. L.; Pinto, L. H.; Lamb, R. A.; Fiorin, G.; Wang, J.; DeGrado, W. F. Flipping in the Pore: Discovery of Dual Inhibitors That Bind in Different Orientations to the Wild-Type versus the Amantadine-Resistant s31n Mutant of the Influenza a Virus m2 Proton Channel. *J. Am. Chem. Soc.* **2014**, *136*, 17987–17995.
- (29) Wang, J. J.; Wu, Y.; Ma, C.; Fiorin, G.; Pinto, L. H.; Lamb, R. a.; Klein, M. L.; DeGrado, W. F.; Wang, J. J.; Pinto, L. H.; Lamb, R. a.; Klein, M. L.; DeGrado, W. F. Structure and Inhibition of the Drug-Resistant S31N Mutant of the M2 Ion Channel of Influenza A Virus. *Proc Natl Acad Sci U S A* **2013**, *110*, 1315–1320.

Εκτενής Περίληψη	iv
Extensive Summary	xviii
Chapter 1	
Affinity of rimantadine enantiomers against Influenza A/M2 protein Revisited	1
1.1 Abstract	2
1.2 Introduction	3
1.3 Results and Discussion	7
1.3.1 Ligands Synthesis.....	7
1.3.2 ITC measurements	7
1.3.3 FEP/MD simulations	10
1.3.4 Analysis of trajectories	12
1.3.5 Electrophysiology experiments	15
1.3.6 Anti-viral assays.....	16
1.4 Conclusions	18
1.5 Experimental Work	19
1.5.1 Ligands.....	19
1.5.2 Peptide synthesis.....	21
1.5.2.1 General.....	21
1.5.2.2 Sequence of peptide.....	22
1.5.2.3 Reagents	22
1.5.2.4 Steps of the M2TM _{Udorn} peptide synthesis.....	24
1.5.3 ITC measurements	30
1.5.4 Free energy calculations using the BAR method of M2TM-amantadine complexes in lipids bilayers (FEP/MD Simulations)	32
1.5.4.1 Docking calculations.....	32
1.5.4.2 FEP/MD simulations.....	32
1.5.5 Two-Electrode Voltage Clamp (TEVC) Assay	35
1.5.6 Anti-viral assays.....	36
1.5.6.1 Cells and viruses.....	36
1.5.6.2 CPE inhibition activity.....	36
1.5.6.3 Evaluation of inhibition activity using Plaque Reduction Assay	36
1.6 Supporting information	37
1.6.1 Scheme and Figure captions.....	37
1.6.2 NMR Spectra of aminoadamantane compound 3 and Synthetic intermediates 3a-3c.....	39
1.6.2.1 ¹ H NMR spectra	39
1.6.2.2 ¹³ C NMR spectra	42
1.7 References	45

Chapter 2

Binding and Proton Blockage by Amantadine Variants of the Influenza M2_{WT} and M2_{S31N} Explained	58
2.1 Abstract	59
2.2 Introduction	60
2.3 Results	64
2.3.1 Chemistry	64
2.3.2 Binding affinities of aminoadamantanes to M2TM by ITC.....	67
2.3.3 Solid state NMR of M2TM - aminoadamantanes complexes	69
2.3.3.1 OS ssNMR spectra	69

2.3.4 MAS spectra	74
2.3.5 MD simulations of M2TM - aminoadamantanes complexes	76
2.3.5.1 Starting structure of protein ligand-complex	76
2.3.5.2 Complexes of ligands with M2TM _{WT}	76
2.3.5.3 Complexes of ligands with M2TM _{S31N}	80
2.3.5.4 Additional MD simulations runs	86
2.3.6 Electrophysiology results of aminoadamantanes blockage using full-length M2.....	88
2.3.7 In vitro testing of aminoadamantanes against influenza A virus	89
2.4 Discussion	90
2.4.1 Unraveling the binding differences for aminoadamantanes to M2TM _{S31N} and M2TM _{WT}	90
2.4.2 Changes in C-terminus structure-function of M2TM _{S31N} and M2TM _{WT} induced by V27 interactions with the adamantyl cage of amantadine variants	92
2.5 Conclusions	93
2.6 Experimental Work	95
2.6.1 Ligands synthesis	95
2.6.2 M2TM peptide synthesis	100
2.6.3 ITC measurements of aminoadamantane ligands binding to M2TM	102
2.6.4 Solid state NMR	103
2.6.4.1 Sample preparation for solid state NMR	103
2.6.4.2.1 OS ssNMR spectra	103
2.6.4.2.2 NCA MAS spectra	104
2.6.5 MD simulations of M2TM-aminoadamantane complexes	104
2.6.5.1 Docking calculations.....	104
2.6.5.2 MD simulations	104
2.6.6 Electrophysiology experiments of M2 blockage by aminoadamantanes	106
2.6.7 Anti-viral assays.....	107
2.6.7.1 Cells and viruses.....	107
2.6.7.2 CPE inhibition assay of influenza A viruses by aminoadamantanes	107
2.8 Supporting information	108
2.8.1 Synthetic Schemes for the preparation of compounds 2, 6,7.....	108
2.8.1.1 Few representative RMSD plots from the MD simulations of M2TM _{WT} ligand and M2TM _{S31N} ligand complexes in DMPC bilayer (M2TM C α -carbons with respect to the initial structure of the production period	109
2.8.1.2 Nuclear Magnetic Resonance (NMR) Spectra of aminoadamantane compounds 8, 9 and 10 and intermediate derivatives 3a, 3b and 3c.	121
2.8.1.2.1 ¹ H NMR spectra	121
2.8.1.2.2 ¹³ C NMR spectra	123
2.9 References	124

Chapter 3

Unraveling the Binding, Proton Blockage and Inhibition of influenza M2 WT and S31N by Rimantadine variants

3.1 Abstract	134
3.2 Introduction	135
3.3 Results	138
3.3.1 Compound synthesis.....	138
3.3.2 ITC measurements	140
3.3.3 In vitro testing against Influenza A Virus	142
3.3.4 Electrophysiology measurements.....	143

3.3.5 MD simulations	143
3.3.6 Compound prioritization against M2 WT	154
3.4 Conclusions	155
3.5 Experimental Part	157
3.5.1 Synthesis of the ligands.....	157
3.5.2 Peptide synthesis and ITC measurements.....	159
3.5.3 Two-electrode voltage clamp assay	159
3.5.4 Cells and viruses.....	160
3.5.5 Evaluation of cytotoxicity and CPE inhibition activity	160
3.5.6 Evaluation of inhibition activity using Plaque Reduction Assay	160
3.6 Supporting information	162
3.6.1 Nuclear Magnetic Resonance (NMR) Spectra of aminoadamantane compounds 4 and 5 and the intermediate derivatives 7b, 7c and 8.....	162
3.6.1.1 ¹ H NMR spectra	162
3.6.1.2 ¹³ C NMR spectra	165
3.7 References	168

Chapter 4

Approaches to primary <i>tert</i>-alkyl amines as medicinal chemistry building blocks	173
4.1 Abstract	174
4.2 Introduction	175
4.3 Results and Discussion	178
4.3.1 Synthetic studies	178
4.3.3.1 From <i>tert</i> -alkyl alcohols through <i>tert</i> -alkyl azides reduction (Procedure A).....	178
4.3.3.2 From <i>tert</i> -alkyl alcohols using Ritter reaction (Procedure B)	182
4.3.3.4 Examples for the preparation of primary <i>tert</i> -alkyl amines in adamantane series (Procedures A-D).....	185
4.3.3.5 From the addition of organometallic reagents to nitriles (Procedure E).....	189
4.3.3.6 Examples for the preparation of primary <i>tert</i> -alkyl amines in adamantane series (Procedure E).....	191
4.3.2 Dynamic NMR spectroscopy.....	195
4.4 Conclusions	200
4.5 Experimental Part	202
4.5.1 Chemistry	202
4.5.1.1 Procedure A.....	202
4.5.1.2 Procedure B.....	210
4.5.1.3 Procedure C.....	211
4.5.1.4 Procedure D	212
4.5.1.5 Procedure E	213
4.5.2 Computational chemistry details	217
4.5.3 Dynamic NMR Spectroscopy	218
4.6 References	219
4.7 Experimental Part	224

Chapter 5

Discovery of resistance-breaking inhibitors targeting the M2 proton channel of influenza A viruses	247
5.1 Abstract	248
5.2 Introduction	249

5.3 Results and Discussion	255
5.3.1 Synthesis of aminoadamantane derivatives and other lipophilic amine analogues 15-31	255
5.3.2 Binding of lipophilic amines to M2TM WT	258
5.3.3 Synthesis of aminoadamantanes-polar head conjugates 32-62	259
5.3.4 In vitro testing against Influenza Virus A	264
5.3.5 TEVC experiments.....	268
5.3.6 MD simulations.....	269
5.4 Conclusions	274
5.5 Experimental Part	274
5.5.1 Synthesis of aminoadamantane fragments and derivatives	275
5.5.2 Synthesis of aminoadamantane polar head conjugates.....	280
5.5.2.1 General Procedures of Reductive Amination	280
5.5.2.2 Aminoadamantane polar head conjugates	281
5.5.3 Cells and viruses.....	293
5.5.4 CPE assay	294
5.5.5 MD simulations of M2TM-aminoadamantyl Complexes	294
5.5.5.1 Docking calculations	294
5.5.5.2 MD simulations.....	295
5.6 References	297
5.7 Supporting Information	304
Chapter 6	
Publications	312

Abbreviations

ssNMR	solid state NMR
MAS	Magic Angle Spinning
OS	Oriented Sample
M2TM	M2 Transmembrane Domain
MD	Molecular Dynamics
CPE	Cytopathic Effect
DMPC	1,2-dimyristoyl-sn-glycero-3-phosphocholine
DPhPC	1,2-diphytanoyl-sn-glycero-3-phosphocholine
ITC	Isothermal Titration Calorimetry
EP	Electrophysiology
WT	Wild-Type
MM/PBSA	Molecular Mechanics Poisson-Boltzmann Surface Area
BAR	Bennett acceptance ratio
HEK	Human Embryonic Kidney
PMF	Potential of Mean Force.
RMSD	Root-Mean-Square Deviation
PDB	Protein data bank
PME	Particle Mesh Ewald method
RESPA	Reversible multiple time scale molecular dynamics.

CHAPTER 1

Affinity of rimantadine enantiomers against Influenza A/M2 protein Revisited

1.1 Abstract

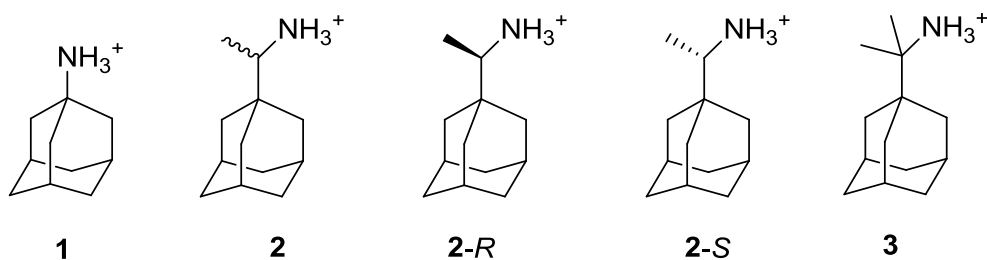
Recent findings from solid state NMR (ssNMR) and molecular dynamics (MD) simulations studies suggested that the (*R*)-enantiomer of rimantadine binds to the M2 channel with higher affinity than the (*S*)-enantiomer. Intrigued by these findings, we applied functional assays, such as antiviral assay and electrophysiology (EP), to evaluate the binding affinity of rimantadine enantiomers to the M2 protein channel. Unexpectedly, no significant difference was found between the two enantiomers. Our experimental data based on the full M2 protein function, were further supported by alchemical free energy calculations and Isothermal Titration Calorimetry (ITC) allowing an evaluation of the binding affinity of rimantadine enantiomers to the M2TM pore. Both enantiomers have similar channel blockage, affinity and antiviral potency.

1.2 Introduction

Amantadine (*Amt*, **1**) and rimantadine (**2**) (Scheme 1) are blockers of proton transport in the wildtype (WT) influenza A M2 proton channel^{1,2} and have been effective prophylactics and therapeutics against influenza A virus.³ The M2 protein of the influenza A virus has a short 97-residue sequence. It forms tetramers, and its transmembrane domain (A/M2TM, residues 22-46) comprises the pore of a proton channel that is activated by low pH in the viral endosome; the open state of the channel results when the imidazole rings of the four His37 residues, which line the inner part of the pore, are protonated.⁴ Its activation ultimately leads to the unpacking of the influenza viral genome and to pathogenesis.⁵ The TM domain of the M2 protein, which contains the proton-conducting residue, His37,⁴ and the channel-gating residue, Trp41^{6,7} reproduces most of the electrophysiological, pharmacological, and biophysical features of the full-length M2 protein, such as low-pH activated proton conductivity, **1**-dependent sensitivity of the proton current, and tetramerization of the protein.^{8,9, 10,34} Starting at the exterior of the virus, the N-terminal half of the M2TM sequence forms a water-filled pore lined by Val27, Ala30, Ser31, and Gly34. These sites are frequently mutated in **1**-resistant mutants.^{11,12} The pore is interrupted by His37 and Trp41, which project towards the center of the channel, while Asp44 defines its C-terminal end.¹⁰

Although **1** and **2** have been used as antivirals for decades, it was only after 2008 that high resolution structures from x-ray and solid state NMR (ssNMR) experiments have been unveiled of the high resolution structures of M2TM in complex with **1** or **2**^{13,14,15,16,17}. According to these findings the M2TM protein channel is blocked by **1** and **2** via a pore-binding mechanism.^{14,15,16,17,9} The adamantane cage in **1** and **2** and aminoadamantane analogues^{18,19,20} is tightly contacted on all sides by V27 and A30 side chains, producing a steric occlusion of proton transport^{14,15,16,17} and thereby preventing the viral replication. The ssNMR results for **2** also demonstrated that the ammonium group of the drug is pointing towards the four H37 residues at the C-end (Figure 1).¹⁷ This orientation can be stabilized either through hydrogen bonds with water molecules in the channel lumen between the imidazoles of H37 and the ligand and/or possibly with A30 carbonyls²¹ in the vicinity according to experimental and molecular dynamics (MD) simulations data.^{17,21,22,23,24,25,26,27,28,29} This is consistent with a lowering of the pK_a of the proton-sensing His37 by ~ three log units compared with the first pK_a of histidine in **1** free M2TM. Thus, upon drug binding to M2TM, the pK_a of His37 drops from 8.2 to 5.4.^{30,31}

Provided that M2TM is a minimal model for M2 binding,⁹ these high resolution structures can be used for the prediction of new ligands binding more effectively to the M2TM pore.



Scheme 1. Structures of studied aminoadamantane derivatives adamantane (**1**), rimantadine (**2**) (**2-R** and **2-S**) and rimantadine analogue **3**.

The effect of ligand's chirality in its binding with a chiral receptor is of outstanding significance and the characterization of protein-ligand interactions for each enantiomer separately may identify potential stereospecific binding interactions to the receptor. While rimantadine analogues are known antiviral drugs for more than four decades, the relative potency of rimantadine enantiomers has not been studied at the molecular level. Binding affinity of each enantiomer results from chiral interactions with the binding area inside the four-fold symmetric M2 protein. Based on differences in isotropic chemical shift changes measured using ssNMR and MD simulations results, it has been recently suggested that **2-R** and **2-S** have a strong but differential binding to full length M2, i.e., that **2-R** binds more tightly than **2-S**.²⁹ This was the first state of the art ssNMR study of the full M2 protein and analysis of the rimantadine enantiomers binding, but this conclusion appears to be puzzling as it has been shown before that: (1) **2-R** and **2-S** have similar in vivo antiviral activity in protecting mice from lethal influenza³²; (2) Rimantadine was developed prior to the 1992 FDA guidance on the development of stereoisomers. It was approved as commercial drug in the US in 1993 containing both enantiomers.

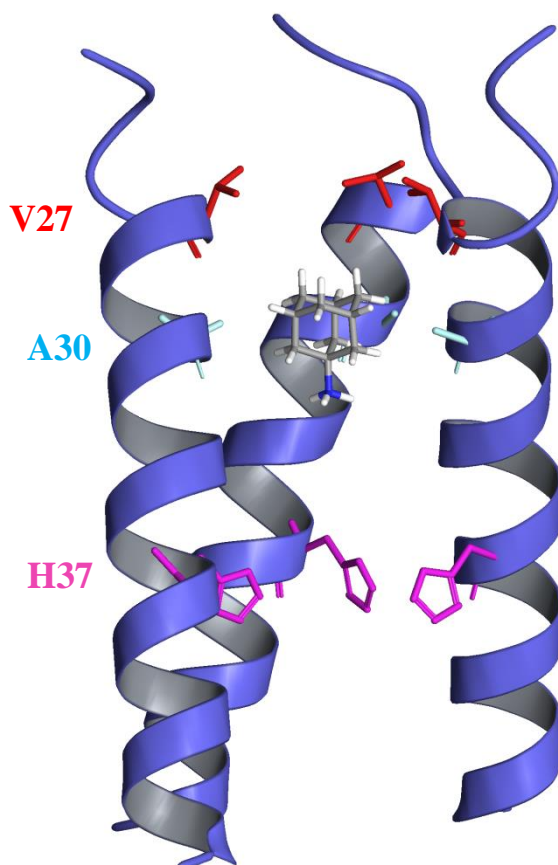


Figure 1. Structure and amino acid sequence of M2TM_{Udorn/72}. Cartoon representation of M2TM (PDB entry: 2KQT13'15) with critical residues for binding: V27 (red), A30 (light blue), His37 (pink) depicted as sticks. Side view of M2TM_{Udorn/72}; one monomer of the tetramer was removed for visualization purposes; the N-terminal end is at the top. Amino acid sequence of M2TM_{Udorn/72} corresponding to 2KQT: SSDPLVVAASIIGILHLILWILDRL.

Using ssNMR analysis and molecular dynamics simulations it has just been recently suggested that **2-R** and **2-S** have a strong but differential binding to full length M2 as it was showed that they affect different significant isotropic chemical shift changes at S31 and G34 when bound to the M2 protein as measured using ssNMR.²⁹ This was the first state-of-the-art ssNMR study of the full M2 protein but this conclusion appears to be puzzling as it has been shown before that: (a) **2-R** and **2-S** has similar in vivo antiviral activity in protecting mice from influenza virus infection induced death³²; (b) Rimantadine (**2**) was approved and used as a racemic mixture.

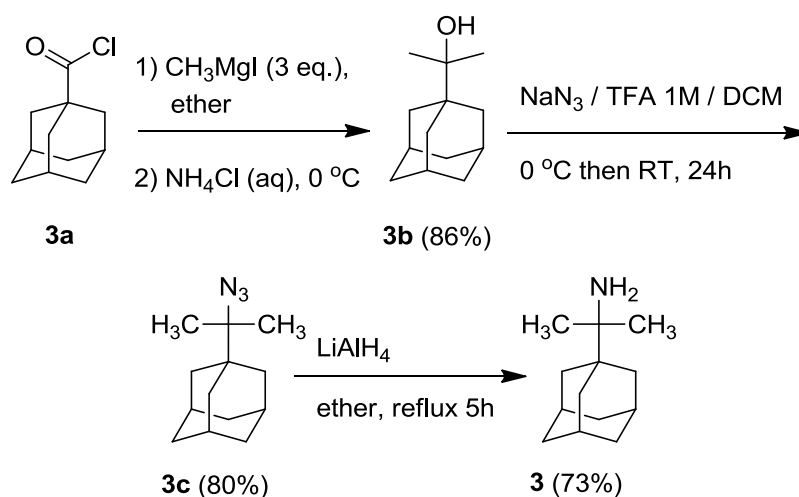
To solve the controversy between in vitro binding assay (ssNMR) results and the in vivo efficacy results, we hereby characterize the binding affinity of two rimantadine enantiomers and their antiviral

efficacy using a consortium of in vitro and cellular assays. Collectively our results demonstrate that rimantadine enantiomers (**2-R** and **2-S**) have equal potency. More specifically we first measured the ITC binding affinities of **2-R**, **2-S**, and **3** against the M2TM_{Udorn/72} in its closed form at pH 8. Compound **3** is a non-chiral dimethyl analogue of rimantadine and it was designed and synthesized as a probe to independently validate the assay results from **2-R** and **2-S**. We then applied a free energy perturbation coupled with MD simulations (FEP/MD) alchemical calculation scheme to calculate the relative free energies of binding between rimantadine enantiomers (**2-R** and **2-S**) as well as compound **3**. In particular, we calculated the relative free energies of binding for the alchemical transformations **3** to **2-R** and **3** to **2-S**. Following up, the blocking effect of **2-R**, **2-S** and **3** against full length A/Udorn/72 M2 protein (M2_{Udorn/72}) and A/WSN/33-M2-N31S conductance was estimated using electrophysiology (EP). Finally, the antiviral potency of these compounds was measured against amantadine-sensitive A/Udorn/72 and A/WSN/33-M2-N31S viruses.

1.3 Results and Discussion

1.3.1 Ligands Synthesis

For the synthesis of primary *tert*-alkyl amine **3** (AdCMe₂NH₂) the *tert*-alkyl alcohol **3b** was prepared according to Scheme 2 from the reaction between 1-adamantane carbonyl chloride **3a** and methylmagnesium iodide. Treatment of *tert*-alkyl alcohol **3b** with NaN₃/TFA in dichloromethane afforded azide **3c** in high yield which was further subjected to reduction through LiAlH₄ to form *tert*-alkyl amine **3** in a good yield.



Scheme 2. Synthetic scheme for the preparation of corresponding *tert*-alkyl amine **3**.

1.3.2 ITC measurements

Table 1 includes thermodynamic parameters of binding against M2TM_{Udorn/72}. Binding affinities were determined by ITC^{33f} for M2TM-ligand systems in dodecylphosphocholine (DPC) micelles at pH 8, where M2TM fragments form stable tetramers.³⁴ ITC measurements yield the enthalpy of binding (ΔH) as well as the dissociation constant (K_d). From K_d , the binding free energy (ΔG) is calculated (Table 1). The estimation of the binding entropy is based on the difference between ΔG and ΔH . Binding constants of **1**, **2-R**, **2-S** and its racemate **2** measured in a previous work¹⁹ were included in Table 2. Enantiomers may have a different enthalpy of binding against a protein since the two complexes formed are diastereomers.³⁵ It has been suggested through *in silico* prediction that enantiomers of compound **2** bind with different affinity to the M2 protein.³⁶ As depicted in Table 1 enantiomers **2-R** and **2-S** have the same K_d s against M2TM_{Udorn/72} ($K_d = 0.34$

and 0.32 μM respectively). Racemic **2** has a $K_d = 0.51 \mu\text{M}$ which is close to the K_d 's of the enantiomers considering the experimental errors and the lower chemical purity of the commercial enantiomers (90% for **2-R** and 95% for **2-S**) compared to racemic **2**. An effect from the impurities on the ITC results of **2-R** and **2-S** cannot be excluded. However, we do not expect large changes in the measured K_d values for **2-R** and **2-S**, given also the very similar/identical affinity results of the two enantiomers from Two Electrode Voltage Clamp (TEVC) and antiviral assays.**3**, having two methyl groups instead of one methyl group in **2**, has the smallest K_d (0.13 μM), i.e., the highest binding affinity of all studied aminoadamantane compounds suggesting that polar and lipophilic characteristics are well balanced in its structure. All three compounds (**2-R**, **2-S**, and **3**) were more potent than amantadine (**1**).

Table 1. Binding constant, free energy, enthalpy, and entropy of binding derived from ITC measurements for M2TM_{Udorn/72}.

Ligand ¹	K_d ²	ΔG ^{3,4}	ΔH ^{3,5}	$-T\Delta S$ ^{3,6}
1	2.17 ± 0.52	-7.77 ± 0.14	-6.66 ± 0.50	-1.11 ± 0.52
2-R	0.32 ± 0.16	-8.97 ± 0.26	-7.54 ± 0.34	-1.42 ± 0.43
2-S	0.34 ± 0.12	-8.88 ± 0.21	-7.73 ± 0.28	-1.15 ± 0.35
2	0.51 ± 0.26	-8.64 ± 0.30	-7.60 ± 0.28	-1.04 ± 0.41
3	0.13 ± 0.12	-9.30 ± 0.43	-4.19 ± 0.28	-5.12 ± 0.51

¹See Scheme 1.

²Binding constant K_d in μM calculated from measured K_a in M^{-1} by $K_d = 1/K_a \times 10^{-6}$ and error in K_d in μM determined by $K_{d, \text{error}} = (K_{a, \text{error}}/K_a^2) \times 10^{-6}$ ITC measurements were performed in triplicate for each ligand to calculate means and standard deviations).

³In kcal mol^{-1} .

⁴Free energy of binding computed from K_d by $\Delta G = -RT \ln(K_d^{\text{ref}}/K_d)$ with $K_d^{\text{ref}} = 1 \text{ M}$ and $T = 300 \text{ K}$ and

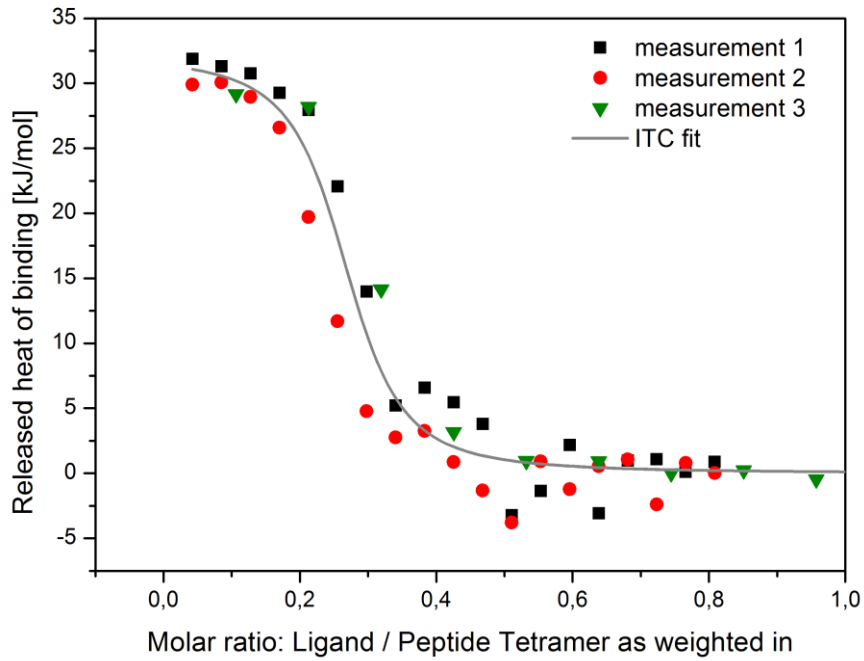
$$\text{error in } \Delta G \text{ determined according to } \Delta G_{\text{error}} = \sqrt{\left(\frac{RT K_{d, \text{error}}}{K_d}\right)^2} \text{ with } T = 300 \text{ K.}$$

⁵Enthalpy of binding and error in the enthalpy of binding calculated from measured binding enthalpy and measured error by $\Delta H = \Delta H_{\text{measured}}(T/T_{\text{measured}})$ with $T = 300 \text{ K}$ and the temperature at which the ITC measurements were performed $T_{\text{measured}} = 293.15 \text{ K}$.

⁶Entropy of binding calculated by $\Delta S = (-\Delta G + \Delta H)/T$ and error in ΔS computed by the equation

$$\Delta S_{\text{error}} = \sqrt{\Delta G_{\text{error}}^2 + \Delta H_{\text{error}}^2}$$

A



B

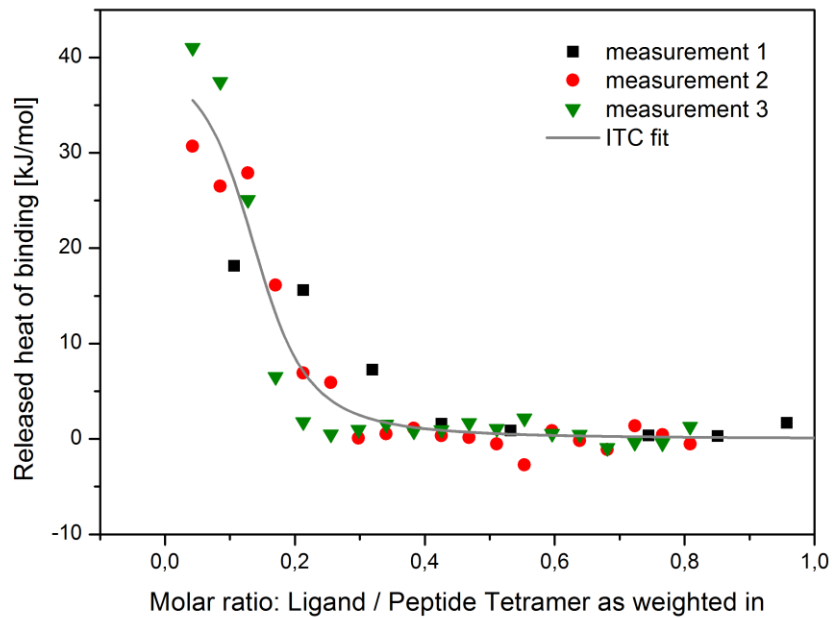


Figure 2. ITC thermograms for titration of: **A.** *R*-Rim with M2TM peptide and **B.** *S*-Rim with M2TM peptide.

1.3.3 FEP/MD simulations

We then analyzed the binding properties of 2-*R* and 2-*S* by alchemical free energy calculations^{19,37} with the Bennett Acceptance Ratio (BAR) method^{37, 67}. The calculations for the alchemical transformations **3** → 2-*R*, **3** → 2-*S* were run and the results of the FEP/MD predictions (Table 2) were compared with binding affinities measured by ITC (Table 1). The computational predictions were set by employing a protocol successfully benchmarked by our group in order to match experimental conditions as closely as possible.¹⁹ M2TM_{Udorn/72} structure was simulated in the closed conformation found at high pH and assigning a neutral form for all H37. M2TM_{Udorn/72}-ligand complexes were simulated in DMPC bilayers which represent a better membrane mimetic system for retaining proper M2TM structure compared to other glycerophospholipids.³⁸ We used an experimental structure (PDB ID 2KQT13:15) (Figure 3).

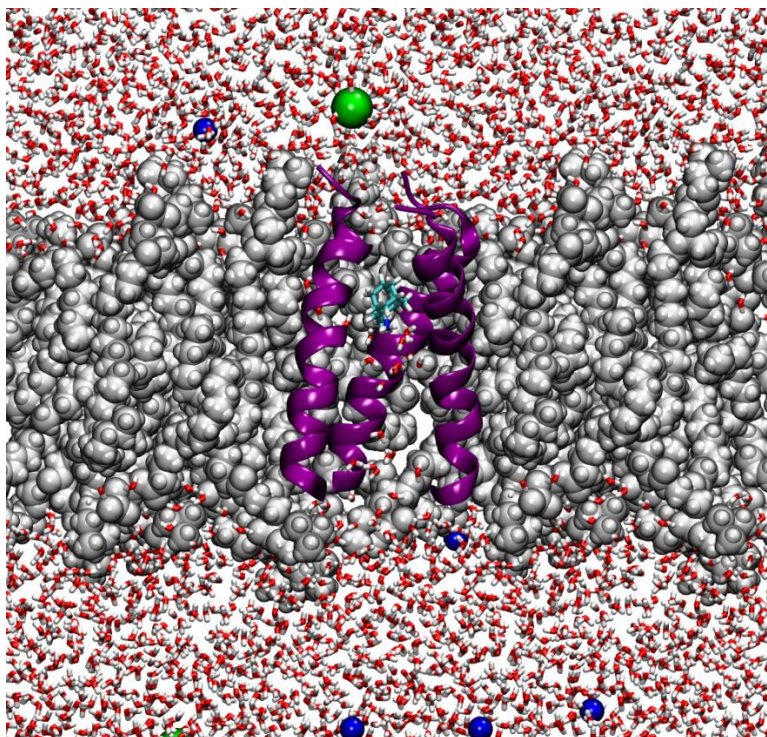


Figure 3. System setup used both in Molecular Dynamics (MD) and Free Energy Calculations (FEP). The M2TM_{Udorn/72} domain of Influenza A virus (PDB entry: 2KQT13:15 (*purple*)) embedded in a DPPC lipid bilayer (lipids: *water*, waters: *red – white*). Sodium ions are colored with *blue* and chloride ions with *green*, whereas amantadine is bound at the N-terminal end of the M2TM pore (*cyan*).

We chose this structure because it was determined at pH 7.5 and in DMPC vesicles,¹⁵ i.e., under conditions that closely resemble the conditions we applied in our simulations to model high pH and DMPC bilayer system. Consequently, this M2TM structure should already be adapted to these environmental conditions, such that no large structural changes are to be expected during MD simulations, and only a short equilibration phase should be required. This M2TM_{U_{dorn}/72} structure is already adapted to these environmental conditions and only a short equilibration phase is required. The experimental relative binding free energy values ($\Delta\Delta G_{\text{exp}}$) for the transformations **3** \rightarrow **2-R** and **3** \rightarrow **2-S** were 0.33 and 0.42 kcal mol⁻¹ (Table 2), favoring **3**, thus suggesting that the addition of an extra methyl group is a successful substitution for increasing affinity. The experimental relative binding free energy values were quite close to calculated values ($\Delta\Delta G_{\text{FEP}}$) of 0.62 and 0.68 kcal mol⁻¹ respectively. Thus, the calculations also predict the experimental finding by ITC that **2-R** and **2-S** have the same binding affinity against M2TM_{U_{dorn}/72} (Table 1), which is consistent with the results from afore-mentioned antiviral and electrophysiology assays performed using full M2 protein (Tables 1 and 2). Thus using the functional core of M2 (transmembrane domain) for binding studies are appropriate. (Table 2).

Table 2. Relative binding free energies for pairs of compounds computed by the BAR method for M2TM embedded in a DMPC bilayer or derived from experimental binding affinity data in Table 1.

Transformation	$\Delta\Delta G_{\text{FEP}}^{1,2}$	$\Delta\Delta G_{\text{exp}}^{1,3}$
3 \rightarrow 2-R	0.62 \pm 0.14	0.33 \pm 0.50
3 \rightarrow 2-S	0.68 \pm 0.15	0.42 \pm 0.48

¹In kcal mol⁻¹.

²Propagation error calculated according to the bootstrap method.²⁸

³Difference in binding free energy calculated from experimentally determined K_d values by $\Delta\Delta G = -RT \ln (K_d^A / K_d^B)$ with $T = 300$ K and error calculated from individual experimental errors by

$$\text{error}_{\Delta\Delta G} = \sqrt{(\text{error}_{\Delta G, A}^2 + \text{error}_{\Delta G, B}^2)}$$

1.3.4 Analysis of trajectories

The simulated complexes of M2TM_{Udorn/72} with **2-R** and **2-S** showed that the height of the ligands inside the pore differed only slightly, that is, less than 0.3 Å towards the N- relatively to **1** (Table 3) and their orientation in the pore are similar in accordance to the similar frequencies for S31 and G34 found for the *R*- and *S*-enantiomer by Cross group ssNMD data.²⁹

Table 3. Structural and dynamic measures from FEP/MD trajectories of M2TM_{Udorn/72}-ligand complexes in DMPC bilayer.

Ligand ¹	RMSD(Ca) ²	Angle C-N vector ³	Angle C-C vector ⁴	V27-Ad ⁵	A30-Ad ⁵	G34-Ad ⁶	G34 Ca-lig.CH ₃ ⁷	G34-CH ₃ -lig.CH ₃ ⁸	H-bonds with water ⁹	RMSF ligand ¹⁰
1	1.5 ± 0.1	11.2 ± 5.9	-	4.2 ± 0.3	1.1 ± 0.3	7.0 ± 1.5	-	-	2.7 ± 0.5	0.1
2-R	1.5 ± 0.2	44.7 ± 7.6	13.7 ± 6.1	3.9 ± 0.3	1.4 ± 0.3	5.7 ± 0.3	2.9 ± 0.4	3.9 ± 0.3	2.6 ± 0.6	0.3
2-S	1.1 ± 0.2	55.7 ± 6.1	13.9 ± 7.0	4.2 ± 0.3	1.0 ± 0.3	4.8 ± 0.3	3.2 ± 0.3	3.5 ± 0.3	2.8 ± 0.4	0.3
3	1.4 ± 0.2	51.5 ± 4.9	5.3 ± 6.6	4.4 ± 0.3	0.8 ± 0.3	5.0 ± 0.4	2.2 ± 0.3	3.8 ± 0.3	2.9 ± 0.3	0.2

¹See Scheme 1; values taken from ref. ⁷⁶ of the draft; measures for **1** were added for comparison reasons.

²Maximum root-mean-square deviation (RMSD) for Ca atoms of M2TM relative to the initial structure (PDB entry: 2KQT) after root-mean-square fitting of Ca atoms of M2TM; in Å.

³Angle between the vector along the bond from the carbon atom of the adamantane core to the ligand nitrogen atom and the normal of the membrane; in degree.

⁴Angle between the vector along the bond from the carbon atom of the adamantane core to the carbon bridge of rimantadine analogue; in degree.

⁵Mean distance between center of mass of A30 and centers of mass of adamantane calculated using Gromacs tools; in Å.

⁶Mean distance between center of mass of G34 and centers of mass of adamantane calculated using Gromacs tools; in Å.

⁷Mean distance between center of mass of rimantadine methyl and G34 Ca calculated using Gromacs tools; in Å.

⁸Mean distance between center of mass of rimantadine methyl and A30 methyl calculated using Gromacs tools; in Å.

⁹Mean number of H-bonds between ligand's ammonium group and waters.

¹⁰Root-mean-square fluctuation of a ligand after fitting of the ligand to the average structure considering all ligand atoms; in Å.

The simulated complexes of M2TM_{Udorn/72} with **2-R** and **2-S** and **3** showed that the height of the ligands inside the pore differed only slightly, that is, less than 0.3 Å towards the N-end relatively to **1** (Table S1) and their orientation in the pore are similar in accordance to the similar frequencies for S31 and G34 found for the two enantiomers **2-R**- and **2-S** in the recent ssNMR study.²⁹ The center of mass between V27 and the adamantane core of the ligand varies between 4.0-4.5 Å on average (Table 2). For **2-R**, **2-S** the average tilt angle was measured ~ 14° in accordance to experimental ssNMR values¹⁷ and for **3** the average tilt angle was measured ~ 5°. The angle between the pore axis or the normal of the membrane and C-N bond vector was ~

11° for **1** and close to 50° for **2-R**, **2-S** and **3**. These angle values suggest that the ammonium group of all aminoadamantane compounds oriented towards the C-end in consistency with previous experimental findings^{15,17} and observations¹⁴ (Table 2). The distance Ad-A30 for 1-3 was measured $\sim 1 \text{ \AA}$, and the distance CH₃(lig.)-G34Ca for **2-R**, **2-S** and **3** was $\sim 3 \text{ \AA}$ and 2 \AA respectively in accordance to the REDOR measurements.²⁹ The adamantane was embraced by V27 and A30 side chains which defined the binding site of the ligands. **1**, **2-R**, **2-S** and **3** form hydrogen bonds through the ammonium group with neighboring water molecules (average 3 hydrogen bonds) found C-ward between the ligand and H37 residues. In the area located below the adamantane core towards the N-end no waters were found^{19,28,39,40} which is consistent with the proton blocking effect of **1** and other aminoadamantane derivatives^{18,41}. A close-up of a snapshot from the simulation of ligands **2-R** and **2-S** is depicted in Figure 4. The CHCH₃ fragment which includes the chiral carbon of **2-R**, **2-S** fits into the cleft between G34 and A30 which is a chiral amino acid than can differentiate binding interactions with enantiomers. However, the distance CH₃(lig.)-A30CH₃ which is similar for both enantiomers (3.9 ± 0.3 and $3.5 \pm 0.3 \text{ \AA}$) suggesting no difference in their binding interactions. Taken together hydrogen bonding interactions for **2-R**, **2-S** and geometric measures which reflect van der Waals contacts were found to be similar for both enantiomers (see Table 3). These measures are consistent with the calculated relative binding affinities which are in accordance to the ITC data and functional assays included here and will be presented into the next paragraphs. These measures are consistent with the calculated relative binding affinities which are in accordance to the ITC data and functional assays described previously.

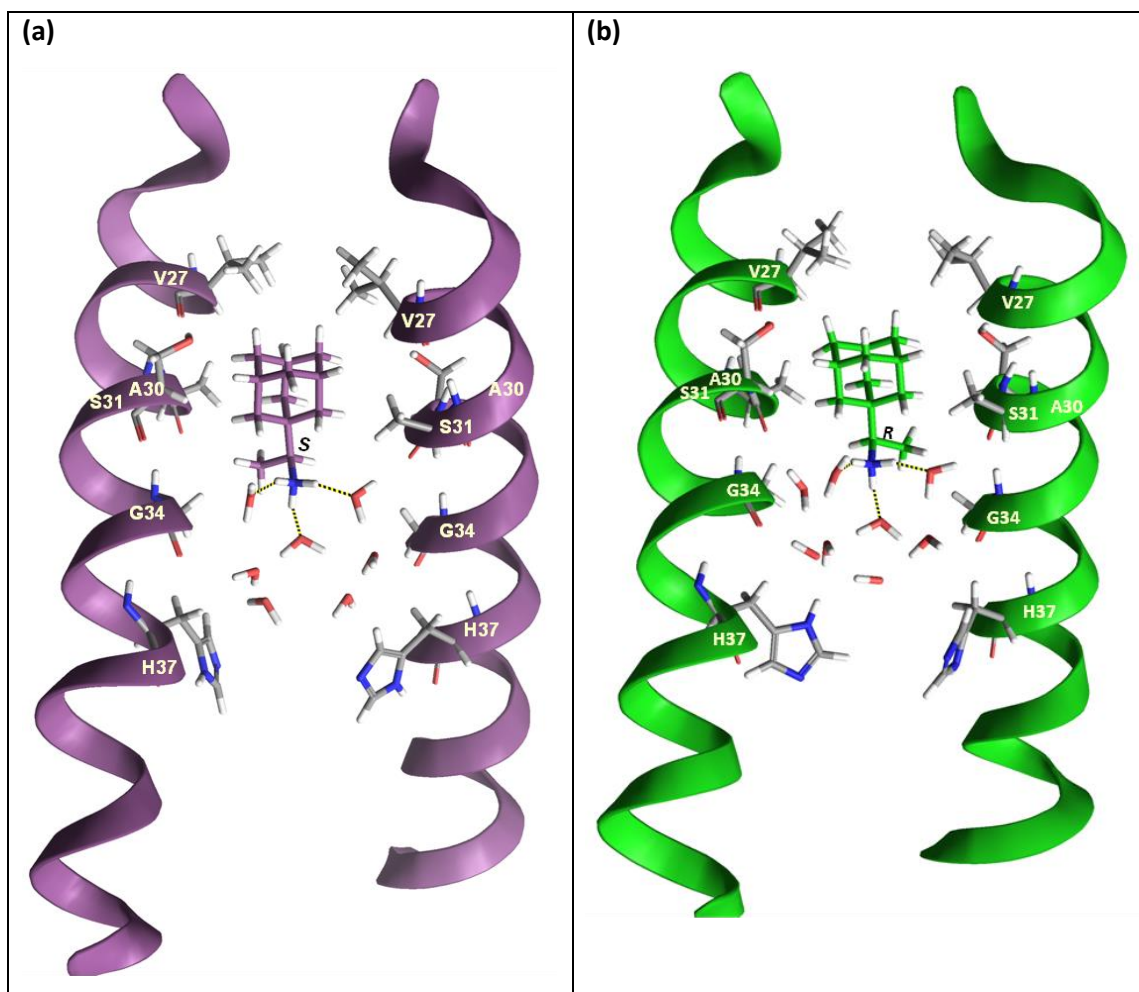


Figure 4. Representative snapshots from the simulation: (a) of **2-S** and (b) of **2-R** bound to M2TM_{Udorn/72}. Seven and nine waters are shown between the ligand and H37 residues respectively. Three hydrogen bonds between the ammonium group of the ligand and three water molecules are shown. Hydrogen bonding together with van der Waals interactions of the adamantane core with V27 and A30 stabilize the ligand inside the pore with its ammonium group oriented towards the C-end.

1.3.5 Electrophysiology experiments

The inhibitors were tested via a TEVC assay using *X. laevis* frog oocytes microinjected with RNA expressing the M2 protein as in a previous report.³⁷ The blocking effect of the aminoadamantane derivatives against M2 was investigated with electrophysiology experiments using M2_{Udorn/72} (Table 4, figure 5). The potency of the inhibitors was expressed as the inhibition percentage of the A/M2 current observed after 2 min and 5 min of incubation with 100 μ M of compound. The electrophysiology experiments against M2_{Udorn/72} showed that **2-R** and **2-S** block this channel equally to amantadine (about 90%) at a concentration of 100 μ M. In addition, we also tested these adamantane analogs in inhibiting another amantadine-sensitive M2 channel, A/WSN/33-M2-N31S (M2_{WSN/33-N31S}) which includes the V28I mutation in M2TM sequence, in electrophysiology assay. Again, no significant channel blockage difference was found among **2-R** and **2-S**, and **3**.

Table 4. Block of full-length M2-dependent current by adamantane analogs.¹

Compound	M2 _{Udorn/72}		M2 _{WSN/33-N31S}	
	% Block after 2m	% Block after 5m	% Block after 2m	% Block after 5m
1	90 \pm 2% (100 μ M; 3)	95 \pm 1% (100 μ M; 3)	-----	-----
2	96 \pm 1% (100 μ M; 3)	96 \pm 1% (100 μ M; 3)	84 \pm 1% (100 μ M; 3)	93 \pm 0% (100 μ M; 3)
2-R	93 \pm 1% (100 μ M; 3)	95 \pm 1% (100 μ M; 3)	71 \pm 1% (100 μ M; 3)	90 \pm 1% (100 μ M; 3)
2-S	95 \pm 1% (100 μ M; 3)	96 \pm 1% (100 μ M; 3)	78 \pm 1% (100 μ M; 4)	92 \pm 0% (100 μ M; 4)
3	90 \pm 2% (100 μ M; 3)	96 \pm 1% (100 μ M; 4)	56 \pm 3% (100 μ M; 3)	80 \pm 2% (100 μ M; 3)

¹For each compound, percent block of pH-dependent M2 current at listed concentrations (+/- s.e.m.).

Parenthesis show number of replicates.

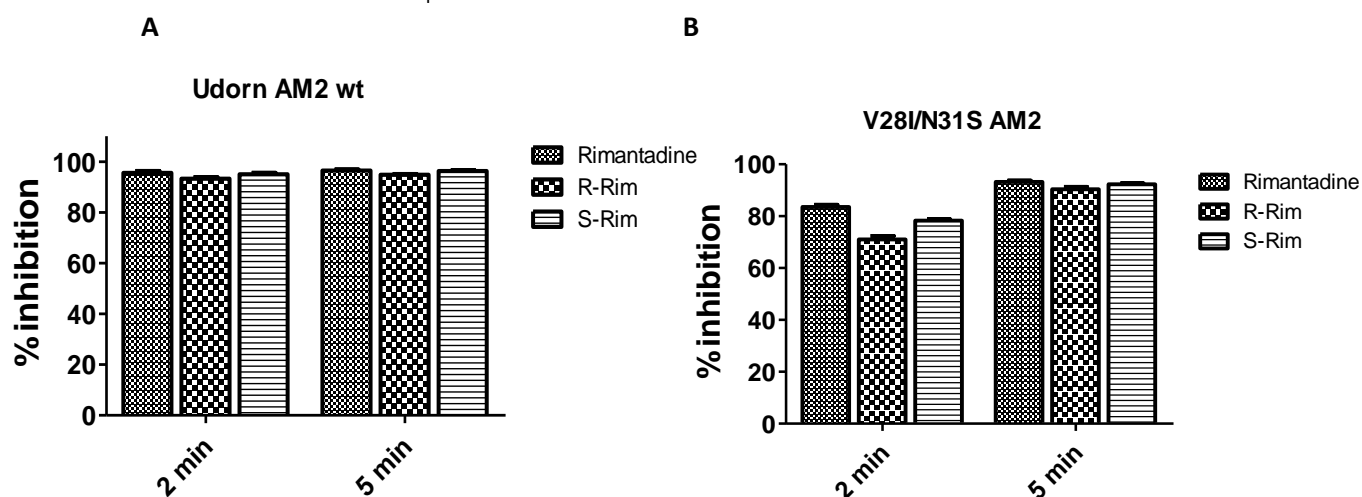


Figure 5. Electrophysiology assay of *R*-Rim, *S*-Rim and racemic mixture with **A**) Udorn M2 and **B**) A/WSN/33-N31S.

1.3.6 Anti-viral assays

Finally, antiviral assay was used^{86,87} to compare the antiviral activity of **1**, **2**, **2-R**, **2-S** and **3** against two amantadine-sensitive influenza A strains, A/Udorn/72 (H3N2) and A/WSN/33-M2-N31S⁴² (H1N1) in MDCK cells. All compounds showed sub-micromolar EC₅₀ values against both influenza strains and there is no significant difference between the two rimantadine enantiomers (**2-R** and **2-S**) (Table 5), which is consistent with results from afore-mentioned FEP/MD, ITC, and electrophysiology assays.

Table 5. Antiviral activity of compounds **1–3** against influenza virus A/Udorn (H3N2) and A/WSN/33-M2-N31S (H1N1) in Madin-Darby canine kidney cells.

Compound	IC ₅₀ (μM) ^{1,2} (A/Udorn/72)	IC ₅₀ (μM) ^{1,3} (A/WSN/33-M2-N31S)
1	0.33±0.04	0.52±0.35
2	0.05±0.02	0.04±0.01
2-R	0.05±0.01	0.05±0.01
2-S	0.06±0.02	0.03±0.01
3	0.04±0.01	0.02±0.01

¹ Mean and standard deviations of the 50% inhibitory concentration (IC₅₀) of at least three independent measures.

² determined using plaque reduction assay.

³ determined using CPE assay.

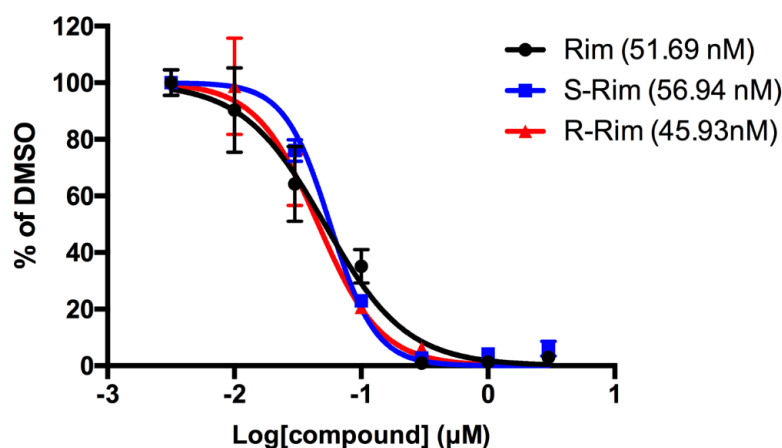


Figure 6. IC₅₀ curves for racemic mixture of Rim, S-Rim (in red) and R-Rim (in blue) against influenza virus A/Udorn/72 (H3N2).

Our results demonstrated no difference in the binding affinity between the two enantiomers in contrast to the recent ssNMR and MD simulations study²⁹ in which it was suggested that **2-R** was a stronger binder than **2-S**.

In ref. ²⁹, in the presence of **2-R** or **2-S** a new resonance (i.e. one that was not recorded in the spectrum of the apo-M2 protein) was observed for S31 at 120/64 ppm in the ¹⁵N/¹³Ca spectrum which had strong intensity for both enantiomers. The G34 resonance had also a stronger intensity for both enantiomers compared to the spectrum of the apo-M2. The Ser31 and Gly34 resonance frequencies were similar for both **2-R** and **2-S**. These results suggest that both enantiomers bind strongly and the binding site and orientation of the drug in the pore are similar for the two enantiomers and this was also mentioned in ref. ²⁹. The authors reported the appearance of an additional resonance of medium intensity for the **2-S** enantiomer at 115/63 ppm close to the frequencies of the S31 resonance of the unbound M2 state at ~ 114/62 ppm which may suggest a weaker binding of **2-S** and a quantitative binding for **2-R**. This resonance was also reported to be potentially in exchange with the bound state but there was no exchange correlation experimental evidence for this suggestion. However, for **2-R** two broader resonances of lower intensity are observed at 114 and 110 ppm which may correspond to the resonances at 115 and 111 ppm for **2-S**; the unequal intensities resulted from differences in the relaxation of the relevant nuclear spins for the diastereomeric complexes. The lower intensity of these peaks might result to a lower resolution of the extracted slices in this region of the ¹⁵N/¹³Ca spectrum for **2-R** complex. This might result to a lower resolution of the extracted slices in this region of the ¹⁵N/¹³Ca spectrum for **2-R** complex. The authors also led to suggest a different binding strength for the two enantiomers against M2 based on the position restrained MD simulations. Position restrained MD simulations may cause a biased sampling of the conformational space for each enantiomer bound to M2 for the limited duration of the trajectories. In particular, the authors observed in the MD trajectories much stronger H-bonding interactions and higher binding site occupancy for **2-R** than **2-S**. However, the significant and almost equal enhancement of the S31 spectral intensity suggest tight binding for both enantiomers.

1.4 Conclusions

In conclusion, rimantadine enantiomers (**2-R** and **2-S**) bind equally well to the M2 proton channel and have equal channel blockage and antiviral activity against amantadine-sensitive M2 channels. This conclusion was supported by a consortium of techniques including antiviral assays, electrophysiology ITC and FEP/MD (Table 6).

Table 6. Synopsis of rimantadine enantiomers to influenza A/M2 protein.

Rim-R	Rim-S
Kd M2TM _{Udorn} (ITC) = 0.32 μ M	Kd M2TM _{Udorn} (ITC) = 0.34 μ M
%block to M2 _{Udorn} (TEVC) = 95%	%block to M2 _{Udorn} (TEVC) = 96%
%block to M2 _{WSN/33-N31S} (TEVC) = 90%	%block to M2 _{WSN/33-N31S} (TEVC) = 92%
IC ₅₀ (Udorn/72, CPE) = 0.05 μ M	IC ₅₀ (Udorn/72, CPE) = 0.06 μ M
IC ₅₀ (WSN/33-M2-N31S, CPE) = 0.05 μ M	IC ₅₀ (WSN/33-M2-N31S, CPE) = 0.03 μ M
3 \rightarrow Rim-R, $\Delta\Delta G_{\text{FEP}}=0.62 \pm 0.14$,	3 \rightarrow Rim-S, $\Delta\Delta G_{\text{FEP}}=0.68 \pm 0.15$,
$\Delta\Delta G_{\text{exp}}=0.33 \pm 0.50$	$\Delta\Delta G_{\text{exp}}=0.42 \pm 0.48$

Our non clinical results support the previous use of rimantadine as a racemic mixture as a drug for the prevention and treatment of influenza virus infection. Further correlation of these results with the pharmacokinetic and pharmacodynamic properties for each enantiomer in humans would confirm these findings. For example, although there are no significant differences in the concentration-time profiles and disposition of **2-R** and **2-S** and of the 3-hydroxyrimantadine metabolites, large stereospecific differences in the disposition of their 4-hydroxyrimantadine metabolites are observed.⁴³ However, it should be that 3- and 4-hydroxy metabolites, both of which are found in rimantadine-treated patients, showed only modest inhibitory activity against influenza A virus i.e. they are modestly active metabolites.⁴⁴

1.5 Experimental Work

1.5.1 Ligands

1 was purchased from Merck and **2** from Alfa chemicals (> 99 % purity). Enantiomers of **2** were purchased from Enamine; **2-S** has 95% chemical purity and **2-R** has 90% chemical purity and the enantiomeric excess of each enantiomer sample is 99%. Details for the synthesis of compounds **5-8** and **9, 10** can be found in ref. ¹⁸ and ⁴⁵, respectively. The synthesis of compounds **4** and **11** will be described in chapters 5 and 3 respectively.

2-(Tricyclo[3.3.1.1^{3,7}]dec-1-yl)-2-propanol (AdMe₂C-OH) 3b. Methylmagnesium iodide was prepared from magnesium turnings (1.99 g, 83.1mmol) and methyl iodide (10.7 g, 75.6mmol) in 40 mL of dry diethyl ether. A solution of 1-adamantanecarbonyl chloride **3a** (2.5 g, 12.6 mmol) in 60 mL of dry diethyl ether was added dropwise under Ar atmosphere and stirring. The reaction mixture was heated at gentle reflux for 4h under stirring and Ar atmosphere. The mixture was treated with an equal volume of saturated solution of ammonium chloride under ice-cooling. The organic layer was separated and the aqueous phase was extracted with diethyl ether 2 times. The combined organic phases were washed with water and brine, dried (Na₂SO₄) and evaporated under vacuum to yield a white colored solid residue of 2-(1-adamantyl)-propan-2-ol **3b**. Yield 2.09 g (85.5%); IR (Nujol): $\nu(\text{OH})$ 3400 (br s, O-H) cm⁻¹; ¹H-NMR (400MHz, CDCl₃) δ (ppm) 1.12 (s, 6H, 2xCH₃), 1.62-1.69 (m, 12H, 2,4,6,8,9,10-H, adamantane H), 1.99 (br s, 3H, 3,5,7-H, adamantane H); ¹³C-NMR (200 MHz, CDCl₃) δ (ppm) 24.34 (CH₃), 28.74 (3,5,7-C, adamantane C), 36.35 (2,8,9-C, adamantane C), 37.22 (4,6,10-C, adamantane C), 38.84 (1-C, adamantane C), 74.88 (C-OH).

2-(Tricyclo[3.3.1.1^{3,7}]dec-1-yl)-2-azido-propane (AdMe₂C-N₃) 3c. The oily 2-(1-adamantyl)-2-azido-propane **3c** was prepared by treatment of the tertiary alcohol **3b** with CH₂Cl₂/NaN₃/TFA. To a stirring mixture of sodium azide (503 mg, 7.74 mmol) and dry dichloromethane (15 mL), trifluoroacetic acid (2.94 g, 25.8mmol) was added at 0 °C. The resulting mixture was stirred for 10 min at 0 °C and a solution of 2-(1-adamantyl)-propan-2-ol **3b** (500 mg, 2.58mmol) in 15mL of dry dichloromethane was added dropwise under ice-cooling. The mixture was stirred vigorously at 0-5 °C for 4 h and additional 24 h at ambient temperature. The mixture was made alkaline by adding NH₃ 12 % (40 mL) and the organic phase was separated and washed with 30 mL of water two times. The aqueous phase was extracted two times with dichloromethane (30 mL) and the combined organic phases were washed with water, brine and dried (Na₂SO₄). Solvent was evaporated in vacuo to afford 2-(1-adamantyl)-propan-2-azide **3c**. Yield: 80%; IR (Nujol): $\nu(\text{N}_3)$ 2098 cm⁻¹ (s); ¹H-NMR (400MHz, CDCl₃) δ (ppm) 1.23 (s, 6H, 2xCH₃), 1.60-1.71 (m, 12H, 2,4,6,8,9,10-H, adamantane H), 2.0 (br s, 3H,

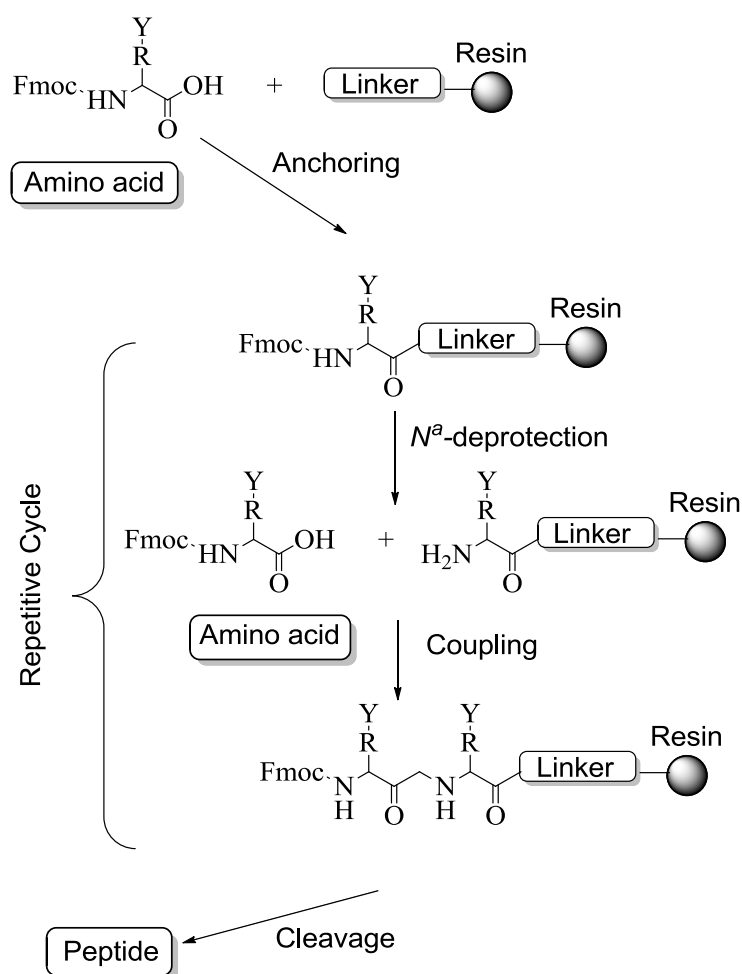
3,5,7-H, adamantane H); ^{13}C -NMR (200 MHz, CDCl_3) δ (ppm) 20.79 (CH_3), 28.66 (3,5,7-C, adamantane C), 36.56 (2,8,9-C, adamantane C), 37.07 (4,6,10-C, adamantane C), 39.10 (1-C, adamantane C), 67.57 (C-N).

2-(Tricyclo[3.3.1.1^{3,7}]dec-1-yl)-propan-2-amine (AdMe₂C-NH₂) 3. A solution of 2-azido-2(1-adamantyl)propane **3c** (250 mg, 1.14 mmol) in 10 mL of dry diethyl ether was added dropwise to a solution of lithium aluminum hydride (173 mg, 4.56 mmol) in 10 mL of dry diethyl ether under ice-cooling. The mixture was heated at reflux for 5 h under stirring. Then the mixture was hydrolyzed with a dropwise addition of 2 mL water, 2 mL of sodium hydroxide 10% w/v solution and 6 mL water under stirring and ice-cooling. The mixture was filtered under vacuum and the residue was washed 2 times with diethyl ether. Another 30 mL of diethyl ether was added to the ethereal filtrate and the solution was extracted with 60 mL (2×30 mL) of hydrochloric acid 6% w/v. The aqueous phase was separated and made alkaline through addition of an excess solid sodium carbonate under ice-cooling. The aqueous phase was extracted two times with 30 mL of dichloromethane. The combined organic extracts were dried (Na_2SO_4) and evaporated under vacuum, to yield a light yellow colored solid residue of 2-(1-adamantyl)-propan-2-amine **3**. Yield: 73%; IR (Film): $\nu(\text{NH}_2)$ 3373 cm^{-1} (s); ^1H -NMR (400 MHz, CDCl_3) δ (ppm) 0.99 (s, 6H, 2x CH_3), 1.60-1.68 (m, 12H, 2,4,6,8,9,10-H, adamantane H), 1.99 (br s, 3H, 3,5,7-H, adamantane H); ^{13}C -NMR (200MHz, CDCl_3) δ (ppm) 25.30 (CH_3), 28.87 (3,5,7-C, adamantane C), 36.23 (2,8,9-C, adamantane C), 37.26 (4,6,10-C, adamantane C), 38.12 (1-C, adamantane C), 53.68 (C-N). Anal. Hydrochloride ($\text{C}_{13}\text{H}_{24}\text{NCl}$) (EtOH-Ether).

1.5.2 Peptide synthesis

1.5.2.1 General

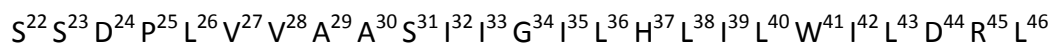
M2TM peptides corresponding to residues 22-46 of Udorn/72 wild type sequence of M2 (C-terminally amidated M2TM_{Udorn/72}: SSDPLVVAASIIGILHLILWILDRL) were synthesized by standard Fmoc solid phase peptide synthesis using an aminomethyl polystyrene resin loaded with the amide linker and purified by reverse phase HPLC as described in detail below.



Scheme 5. General procedure for Fmoc solid phase peptide synthesis using an aminomethyl polystyrene resin loaded with the amide linker.

1.5.2.2 Sequence of peptide

The peptide synthesis was performed using the Fmoc strategy. The peptide synthesis, Udm sequencing was performed according to the following sequence:



Scheme 6. Amino acid residues sequence of M2TM_{Udm} (22-46).

1.5.2.3 Reagents

- Commercial resin GAMP 0305075020 (see Scheme 7), 300 mg with capacity 0.5 mmol / g.
- Rink-Amide (linker) ([4-[(R,S)-[1-(9H-fluoren-9-yl)methoxycarbonylamino]-[2,4-dimethoxybenzyl]phenoxyacetic acid)] (M_w 539.6) 324 mg (0.3 g x 0.5 mmol/g x 4 = 0.6 mmol).
- N,N'-Diisopropylcarbodiimide (DIC) (M_w 126.2) 75 mg or 94 μL (0.6 mmol).
- Ethyl-2-cyano-2-(hydroxyimino)acetate (Oxyma) (M_w 145.7) 87 mg (0.6 mmol)
- Piperidine 20% in DMF 3 mL / 300 mg resin
- Amino acids 4 x 0.5 x 0.3 mmol (see Table 11).

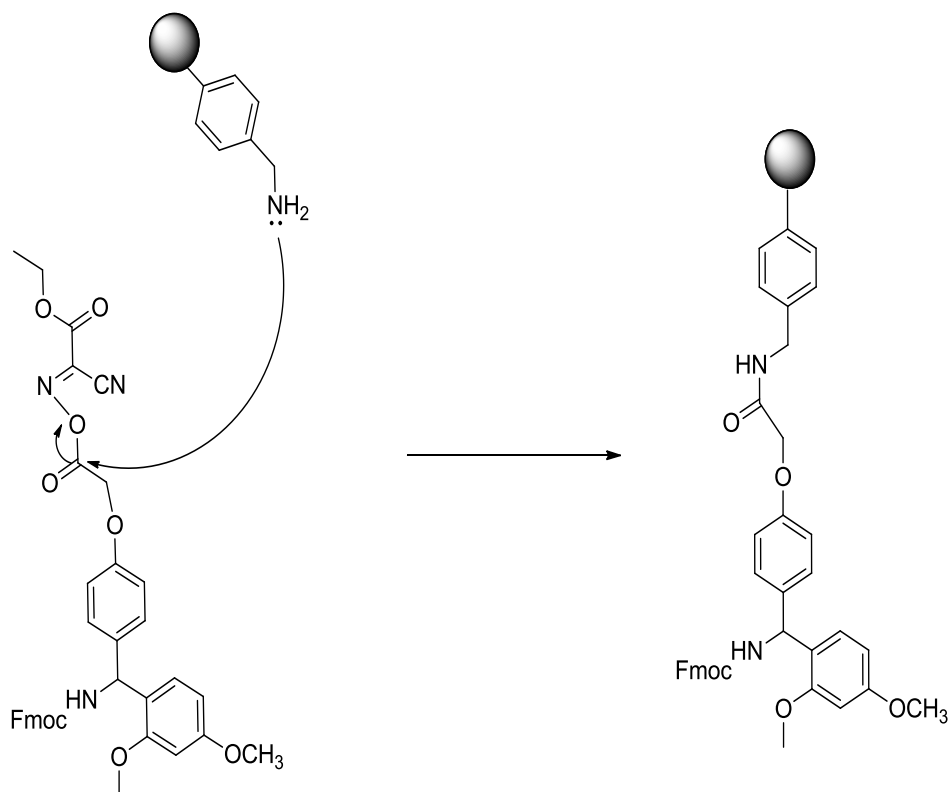
Table 11. Required amounts of Fmoc amino protected amino acids for the synthesis of the 25-peptide M2TM_{Udown} sequence (22-46) of M2 protein. Amounts corresponding to about 4 eq amino acid for resin capacity 0.5 mmol / g.

Aminoacids	Quantity
Fmoc-Leu-OH	236 mg
Fmoc-Arg-(Pbf)-OH	433 mg
Fmoc-Asp(^t Bu)-OH	275 mg
Fmoc-Ile-OH	236 mg
Fmoc-Trp-OH	284 mg
Fmoc-His(Trt)-OH	412 mg
Fmoc-Gly-OH	198 mg
Fmoc-Ser(^t Bu)-OH	255 mg
Fmoc-Ala-OH	219 mg
Fmoc-Val-OH	226 mg
Fmoc-Pro-OH	283 mg

1.5.2.4 Steps of the M2TM_{Udorn} peptide synthesis

Step 1. Binding of the ligand (linker) in aminomethyl polystyrene resin

300 mg of resin was placed in a plastic tube for solid phase peptide synthesis reactions. The resin was washed with DMF (5 x 1min) and the solvent remained in the tube for 30 min, in order to expand the resin. Then, the solvent was filtered and the process was repeated twice. The necessary quantities of Rink-Amide linker (324 mg, 0.6 mmol), of Oxyma (87 mg, 0.6 mmol) and of DIC (75 mg, 0.6 mmol) were dissolved in DMF (5 mL) and were added to the container composition. The mixture was incubated for 24 h at 4 °C to form an amide bond between the carboxyl group of the binding molecule (Rink-Amide Linker) and the amino group of the resin GAMP (Scheme 7). After the resin was washed 4 times with DMF (1 mL) reaction completion was checked using the Kaiser test (ninhydrin test) which informed about the presence or not of free amino groups.



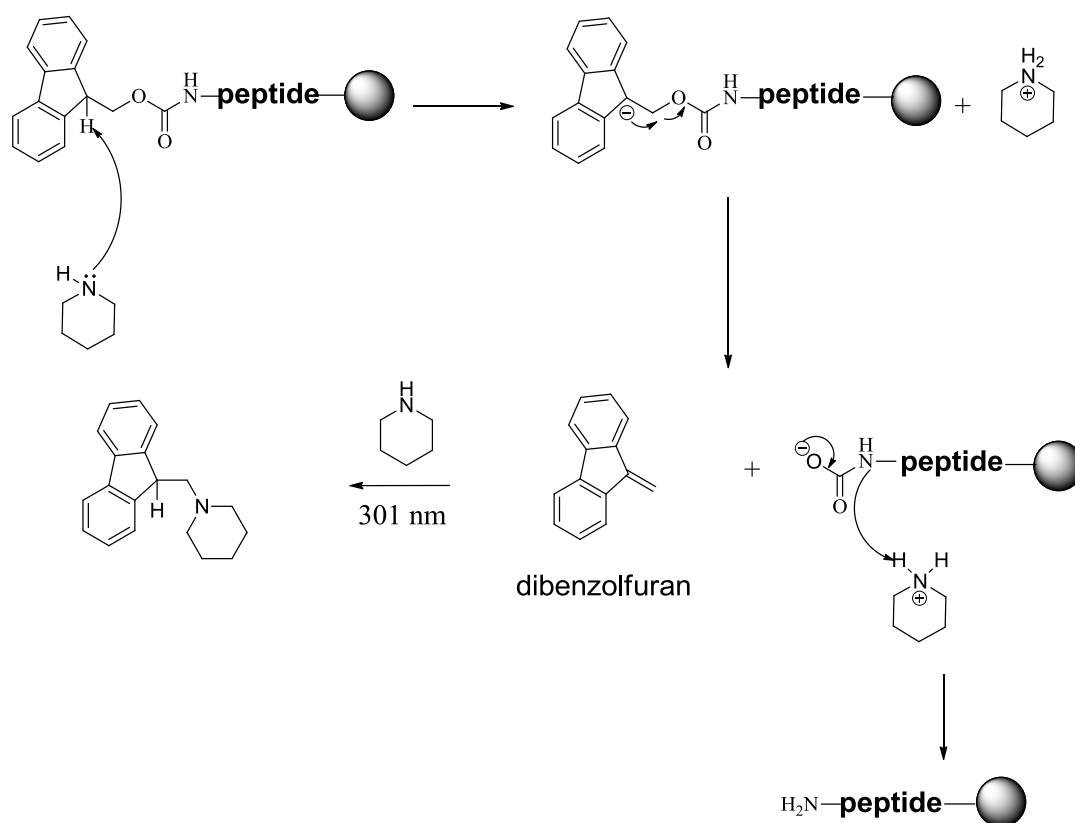
Scheme 7. Coupling of the activated linker molecule (with DIC/Oxyma, see next Scheme 8) to the resin.

For the Kaiser three solutions were used: A. 500 mg of pure ninhydrin in 10 mL of absolute ethanol; B. 80 mg of pure phenol in 20 mL of absolute ethanol; C. 2 mL of aqueous 0.001 M solution of KCN in 98 mL of distilled pyridine. First, a few resin granules are placed into an empty tube. Then 2 drops of reagent A are

added, 4 drops of reagent B and 2 drops of reagent C. The mixture is heated for 5 min at 100 °C in a sand bath. The coloring of the grains of peptide resin (blue or brown) indicates the presence of free amino groups (positive test). The non-coloring of the grains is an indication that all the amino groups of the peptide resin are blocked (negative test). In this case, the test result is negative, which means that the covalent binding reaction of Rink Amide resin in GAMP proceeded quantitatively.

Step 2. N-Fmoc deprotection of the Linker

Deprotection of the Fmoc group from the α -amino group was carried out by treating the peptide resin with 20% v/v piperidine in DMF for 10 min, so that the first amino acid could be then coupled (control of the deprotection may be realized using a lamp spectrophotometer at 301 nm in which length Fmoc group absorbs, see scheme 8).

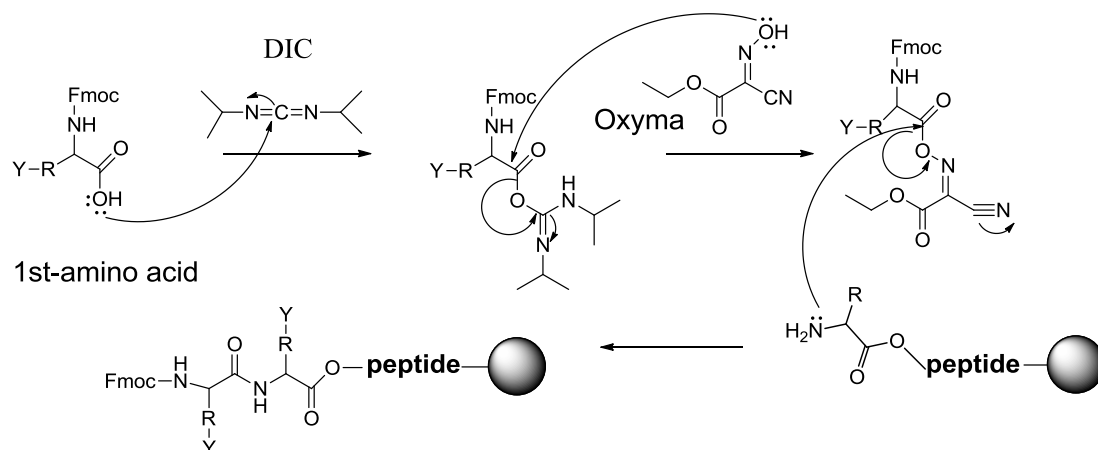


Scheme 8. Schematic representation of the step of deprotection of the amino group of the amino acid.

Step 3. Addition of first amino acid acid

Oxyma (87 mg, 0.6 mmol) was dissolved in 1 mL DMF in a plastic tube. Amino acid was added and the solution was left for 30 min at 4 °C. After the solution reach room temperature, DIC (75 mg or 94 μ L, 0.6 mmol) was added and the resulting solution was placed in the reaction tube. The mixture was stirred at

regular intervals and left for 2 h to complete the coupling reaction (see Scheme 9). Then four washes with DMF were made and Kaiser test was performed to check for the completion of coupling. In case of a negative result so all amino groups were blocked, deprotection of the α -amino group from the Fmoc group was carried out using 20% piperidine in DMF so that the next amino acid in the sequence could be coupled.



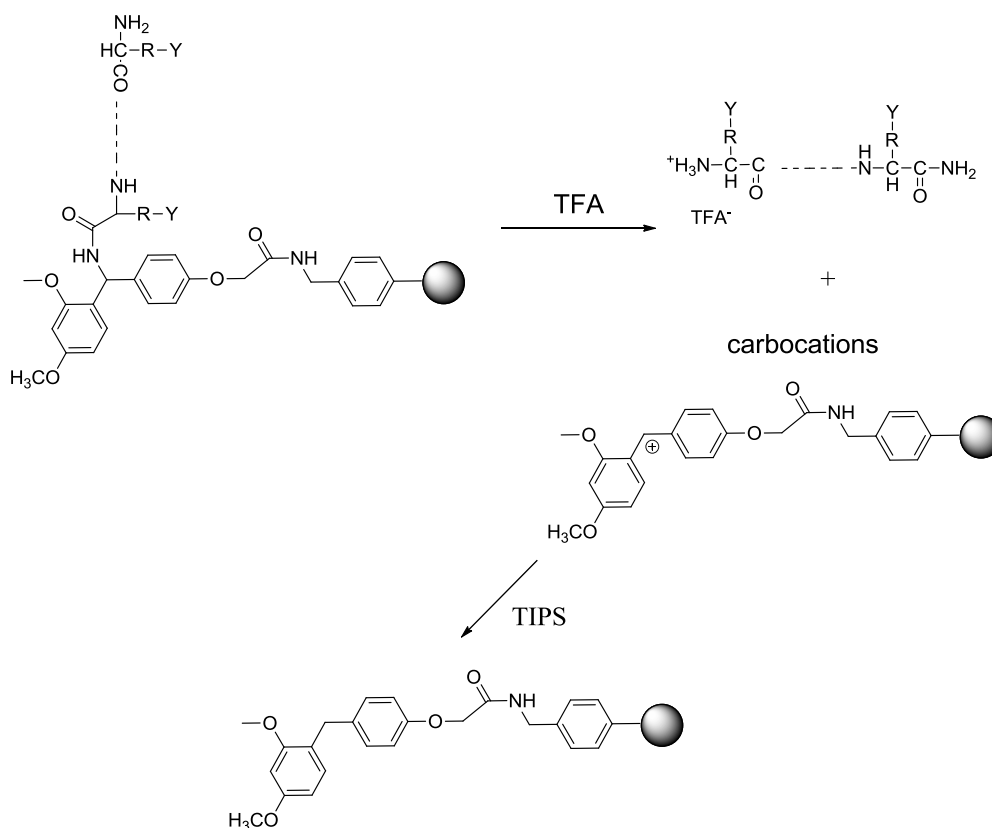
Scheme 9. Amino acid activation combined DIC / Oxyma and coupling with hypothetical peptide.

Step 4. Addition of the rest amino acid residues

For the addition of each amino acid equimolar quantity of activation reagents Oxyma and DIC was used, 87 mg and 94 μ L, respectively. The process is repeated for all the remaining amino acids of the peptide sequence up to the completion of the synthesis.

Step 5. Cleavage of peptide from resin

The peptide resin was treated with a solution of TFA/ H_2O , ethane-1,2-dithiol (EDT), triisopropylmethylsilane (TIPS) (TFA/ H_2O /EDT/TIPS) in a ratio of 95:2.5:2.5:2 (% v/v/v/v) for 2 h to cleave the peptide from the resin (C-end amide, see Scheme 10). The reaction mixture was filtrated and washed with 500 μ L TFA. The filtrate was collected in spherical flask and evaporated. Then the solid residue centrifugated for 12.5 min with Et_2O (3x15mL) and lyophilized to afford crude peptide: Yield; 370 mg (80%, crude).



Scheme 10. Cleavage of peptide from the resin.

Step 6. Peptide purification

Thus, a purification procedure previously described⁴⁶ and modified was used⁴⁷ as described below.

The solvent system used for the purification of the crude peptide was determined by analytical reverse phase HPLC (RP-HPLC) on a 7 10 Nucleosil C18 [(12.7×250) mm ID column, Macherey – Nagel].

- Elution solvents: **A**: H₂O (0,05% TFA), **B**: 90:10 CH₃CN:(A).

- Flow: 3 mL / min

- Solvent elution system: for a period of 30 min in a **A/B** gradient from 75:25 to 60:40 (the above solvent system was chosen as the most suitable among those tested).

The isolation of the pure peptide was realized by reverse phase semi-preparative HPLC (RP-HPLC).

on Symmetry 300 RP C4 [5 μm, (4.6×250) mm ID] column.

- Elution solvents: **A**: H₂O (0,05% TFA), **B**: 90:10 CH₃CN:(A).

- Flow: 1 mL/min

- Solvent elution system: for a period of 40 min in a CH₃CN/H₂O gradient from 80:20 to 20:80.

(In both cases (analytical HPLC and semipreparative HPLC) the column was washed with MeOH of purity 99.99% (Fischer Scientific) for a period of 20 min and then with water (double distilled, HPLC, grade) for a period of 15 to 20 min).

Figure 10 illustrates the analytical spectrum obtained by RP-HPLC, while Figure 11 shows the mass spectrum obtained after purification and lyophilization of the fractions containing the pure peptide. The retention time was $R_f = 26.37$ min and the purity was $\sim 98\%$.

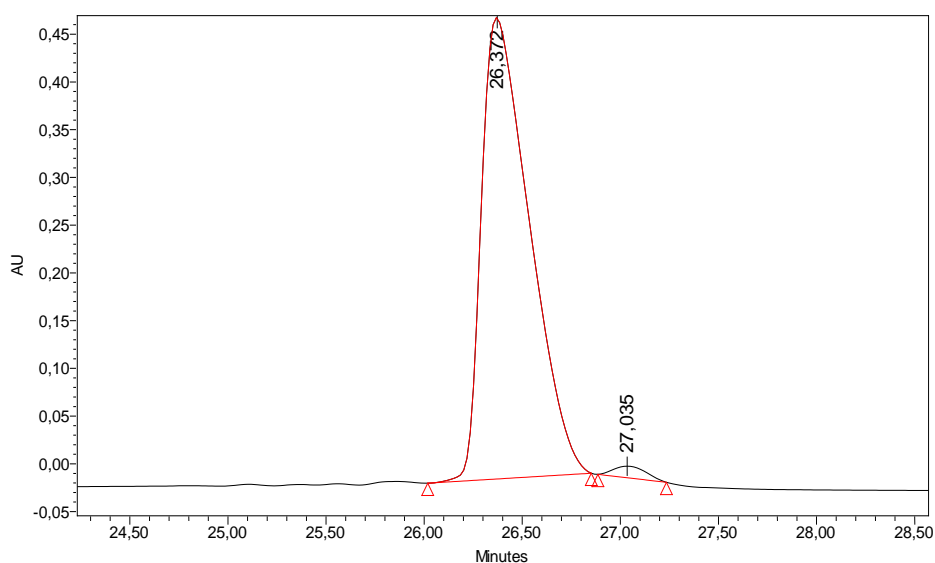


Figure 10. Analytical RP-HPLC chromatograph of Udorn peptide sequence after purification. The retention time is noted.

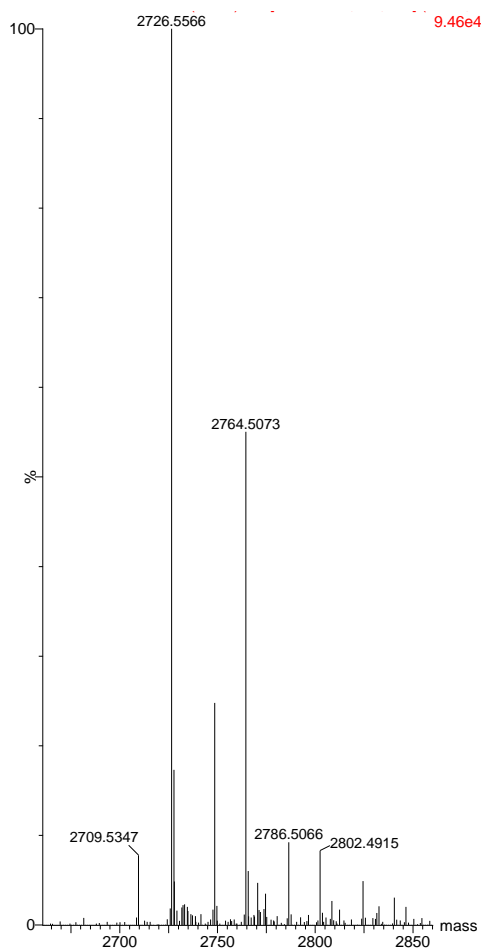


Figure 11. ESI-MS spectrum of Udorn peptide after purification. Mass spectra were obtained on ESI Navigator Finnigan spectrometer and the analysis was performed with an ionization mass spectrometer through (ESI-MS) Finnigan AQA Thermoquest at the Institute "Radioisotopes & Radiodiagnostic Derivatives" of NCSR "Democritus".

1.5.3 ITC measurements

ITC is a widely used method in drug discovery, especially in quantitative structure-activity-relationship studies.^{33,48} However, there are some inherent limitations with respect to the overall applicability of this method. Since warmth released or consumed by an interaction is detected, the method fails measuring interactions that are almost exclusively driven by entropy. The bigger the change of enthalpy during an interaction, the easier this interaction can be measured with ITC. A further limitation is set by the affinity of the interaction. The product of dissociation constant and receptor concentration (called Wiseman constant) determines the slope of the resulting titration curve and should be optimally between 10 and 100.⁴⁹ For very high affinity interactions, one needs to dilute the system. For low affinity interactions (i.e., K_d values in the range of 10 μ M) a very high quantity of the receptor is needed, and this is accompanied with difficulties due to limitations such as availability, costs, solubility, or stability.

Binding affinities of aminoadamantane derivatives (see Scheme 1 in the main text) for M2TM_{Udorn/72} were determined by ITC experiments for M2TM-ligand systems in DPC micelles at pH 8. Furthermore, experimental data indicate that **1** binds with higher affinity at alkaline pH to M2TM, where the pore of the M2 channel is in the closed state, than at low pH, where the open state of M2TM is prevalent.^{34,50}

All measurements were performed in triplicate with a TAM 2277 (TA instrument) at pH 8 and 20 °C in a buffer of 50 mM NaH₂PO₄ and 100 mM NaCl. The peptide and the aminoadamantane derivative were dissolved in a freshly prepared DPC solution with a concentration of 13 mmol L⁻¹. Measurements were conducted using 2 mL of 125 μ M peptide (corresponding to 31.25 μ M M2TM tetramer). A concentration of 1.1 mM of the ligand was used for the titrant, of which 7.6 μ L (equivalent to 8.4 nmol) were dispensed in the peptide/DPC solution with each injection. The time interval between two injections was set to at least 6 minutes. The time interval between two injections was set to at least 6 minutes. First injection wasn't used due to dilution effects.

Synthetic M2TM (residues 22-46) was reconstituted at a 1:57 monomer/lipid ratio - which guarantees the quantitative formation of M2TM tetramers (see ref. 13, 14 of the draft) - in DPC micelles at pH 8 by dissolving and sonicating 225 nmol of M2TM with the 57 fold amount of DPC in the aforementioned buffer system. Solutions of ligands **1**, **2-R**, **2-S**, **3** in the buffer were titrated into the calorimetric cell at 20°C. The heat evolved was obtained from the integral of the calorimetric signal. The heat associated with the binding of the ligand to M2TM was obtained by subtracting the heat of dilution from the heat of reaction.^{51,52}

Describing in more detail, to determine the heat of dilution ligand as well as receptor (M2TM) were dissolved in buffer containing DPC. Two reference experiments were carried out, i.e., (a) ligand was titrated into the buffer containing DPC and (b) receptor was titrated into buffer containing DPC. The obtained signals showed, that the released heat of each injection is very small and stays constant during the experiment. No

interaction is detected between ligand and DPC containing buffer or receptor and DPC containing buffer, respectively. The released heat is the heat of dilution, which occurs when the two solutions are mixed. The heat of dilution was estimated for each titration experiment individually. At the end of each measurement, the receptor is titrated with the ligand being in an excess (the ratio for ligand/receptor after 19 injections is 2:1). If all binding sites are saturated, ligand can't bind to the receptor anymore. The released heat is then equivalent to the heat of dilution. As mentioned the heat of dilution is calculated as an average from the last five titration steps, when the heat is constant. This heat is taken into account as Q correction. It is subtracted from all titration steps in this measurement. Data evaluation was carried out with Digitam for Windows v4.1.

Affinity constants were calculated by non-linear regression of the measured heat per injection using Origin 8.0⁵³ and are included in Table 1. For the calculation, the concentration of the peptide was kept variable because the M2TM tetramer formation is not complete. Data of three independent measurements was used, whereby all measurements were performed with the same experimental conditions using one stock solution.

The fit function involves three parameters. One of them is a factor for the correction of the peptide concentration (the difference between the concentration, which has been weighted in, and the active concentration). The cell volume is fixed at 2 mL. The concentration of the ligand in the solution is known, because pure substance was weighted in and the stoichiometry of the binding of ligand to receptor was assumed to be 1:1. If these quantities are set, the concentration of active receptor is obtained by fitting the measured data points. From the calculations, it can be seen, that the concentration of active receptor is lower than the concentration of receptor that has been weighted in.

Data evaluation was done by plotting the measured heat per amount of substance against the molar ratio of titrant to peptide tetramer. The resulting titration curve was fitted using a global fit including the data of three independent measurements.

The measured binding affinity of **1** was $2.17 \pm 0.52 \mu\text{M}$ and is comparable with the value of $12 \mu\text{M}$ measured using analytical ultracentrifugation⁵⁴ and the value of $9 \pm 2 \mu\text{M}$ derived based on kinetic studies in electrophysiological experiments. For the M2TM peptide investigated in this study, the solubility in the DPC micelles limits the possible concentration. Consequently, affinity constants of low affinity binders (e.g., ligand **3**) possess relatively large errors.

1.5.4 Free energy calculations using the BAR method of M2TM-amantadine complexes in lipids bilayers (FEP/MD Simulations)

1.5.4.1 Docking calculations

The M2TM_{Udorn}-**1** complex structure (PDB ID 2KQT^{13,15}) served as a model structure for the docking calculations of M2TM_{Udorn} complexes with ligands **1-3** (Scheme 1). N- and C-termini of the M2TM model systems were capped by acetyl and methylamino groups after applying the protein preparation module of Maestro. The structures of the protein and **1** were saved separately and were used for the subsequent docking calculations.

The ligands in their ammonium forms were built by means of Maestro 8.5 were then minimized by means of Macromodel 9.6 and the MMFF94 force field^{55,56} implemented with Macromodel 9.6 using the conjugate gradient (CG) method and a distance-dependent dielectric constant of 4.0 until a convergence value of 0.0001 kJ Å⁻¹ mol⁻¹ was reached. Docking poses of aminoadamantane derivatives in the M2TM bound state were generated by docking the prepared compound structures into the pore binding site of the M2TM. Docking was performed with GOLD 5.2^{57,58} using the CHEMPLP or ASP scoring function^{59,60}, after deletion of **1**, and considering six water molecules located within the M2TM pore-binding site between the ligand and His37. The option “toggle” was used to let the algorithm decide whether taking into account a water molecule or neglecting it based on an empirical desolvation penalty. The region of interest used by GOLD was defined to contain the atoms that were within ~15 Å of the ligand binding site in the receptor structure. The “allow early termination” command was deactivated. For all the other parameters, GOLD default values were used. Ligands were submitted to 30 genetic algorithm runs. Ten docking poses were produced for each ligand and were visually inspected using the UCSF Chimera package.⁶¹ The pose with the best score was used in FEP/MD simulations.

1.5.4.2 FEP/MD simulations

The M2TM_{Udorn}-**1** complex structure (PDB ID 2KQT^{13,15}) served as a model structure for the simulations of M2TM_{Udorn} complexes with ligands **2-R**, **2-S** and rimantadine analogue **3** (Scheme 1) in DMPC. We chose this structure because it was determined at pH 7.5 and in DMPC vesicles,^{13,15} i.e., under conditions that closely resemble the conditions we applied in our simulations to model high pH and a DMPC or DPPC bilayer system. Consequently, this M2TM structure should already be adapted to these environmental conditions, such that no large structural changes are to be expected during MD simulations, and only a short equilibration phase should be required. It has been also shown that the stability of the binding region for **1** in the M2TM tetramer is increased considerably when using DMPC compared to other lipids.^{38,62,63,64,65,66} In addition, 2KQT should be considered as the best structure of the amantadine bound state of M2TM since it

utilized both isotropic chemical shift restraints and all of the orientational restraints of an earlier structure characterized by Cross and coworkers (see ref. 13).

Relative binding free energies for aminoadamantane derivatives (Scheme 3) bound to M2TM_{Udorn} were computed following the BAR approach⁶⁷ and applying a thermodynamic cycle (Scheme 11). Alchemical free energy calculations were carried out for M2TM-ligand complexes under periodic boundary conditions with Desmond^{68,69,70} using the settings and the simulation protocol described below and also in³⁹ and¹⁹.

The M2TM complexes were embedded in a DMPC lipid bilayer extending 10 Å beyond the solutes. Complex and ligand systems were solvated using the TIP3P⁷¹ water model. Na⁺ and Cl⁻ ions were placed in the water phase to neutralize the systems and to reach the experimental salt concentration of 0.150 M NaCl. Membrane creation and system solvation were conducted with the “System Builder” utility of Desmond (Figure 3).^{47,46,51} The OPLS 2005 force field^{72,73,74,75} was used to model all protein and ligand interactions, and the TIP3P model⁷² was used for water. The particle mesh Ewald method (PME)^{76,77} was employed to calculate long-range electrostatic interactions with a grid spacing of 0.8 Å. Van der Waals and short range electrostatic interactions were smoothly truncated at 9.0 Å. The Nosé-Hoover thermostat⁷⁸ was utilized to maintain a constant temperature in all simulations, and the Martyna-Tobias-Klein method⁷⁹ was used to control the pressure. The equations of motion were integrated using the multistep RESPA integrator⁷⁸ with an inner time step of 2 fs for bonded interactions and non-bonded interactions within a cutoff of 9 Å. An outer time step of 6.0 fs was used for non-bonded interactions beyond the cut-off. Periodic boundary conditions were applied.

Each system was equilibrated in MD simulations with a modification of the default protocol provided in Desmond, which consists of a series of restrained minimizations and molecular dynamics simulations designed to relax the system, while not deviating substantially from the initial coordinates. First, two rounds of steepest descent minimization were performed with a maximum of 2000 steps with harmonic restraints of 50 kcal mol⁻¹ Å⁻² applied on all solute 2500, followed by 10,000 steps of minimization without restraints. A series of four MD simulations was performed. The first simulation was run for 12 ps at a temperature of 10 K in the NVT (constant number of particles, volume, and temperature) ensemble with solute heavy atoms restrained with a force constant of 50 kcal mol⁻¹ Å⁻², followed by an identical simulation in the NPT ensemble. The temperature was then raised during a 25 ps simulation to 310 K in the NPT ensemble with the force constant retained. The temperature of 310 K was used in the MD simulations in order to ensure that the membrane state is above the melting temperature state of 297 K for DMPC lipids.⁸⁰ Then an unrestrained NPT production simulation at 310 K⁸⁰ followed saving snapshots in intervals of 4 ps.

Production simulations at each λ value were run for 4 ns or 6 ns for compounds without and with a cyclic group, respectively. A λ schedule comprising 12 windows was used (see Table S1 in ref. ³⁹). The complex systems were stable in the alchemical free energy simulations as indicated by an RMSD of the protein heavy atoms ≤ 1.5 Å such that the sampled structures could be used for computing relative binding

free energies. Free energy differences ΔG were calculated by the BAR method⁶⁷ and checked for convergence by computing ΔG based on increasing time intervals of the alchemical free energy simulations (Table S1 in sup. ref.³⁹). Errors in the computed relative binding free energies were estimated using block bootstrapping as described in Supporting Information in ref.³⁹. With the definition of the variable coupling lambda staging can be achieved by applying the following combinatorial potential (eq.1).

$$V(\lambda) = V_0 + \lambda\Delta V = V_0 + \lambda(V_1 - V_0) \quad (1)$$

$$\Delta V(\lambda) = V(\lambda) - V_A = \lambda(V_B - V_A) \quad (2)$$

According to the free-energy perturbation method, the free energy difference for going from state **A** to state **B** is obtained from the following equation, known as the *Zwanzig* equation (eq.3).

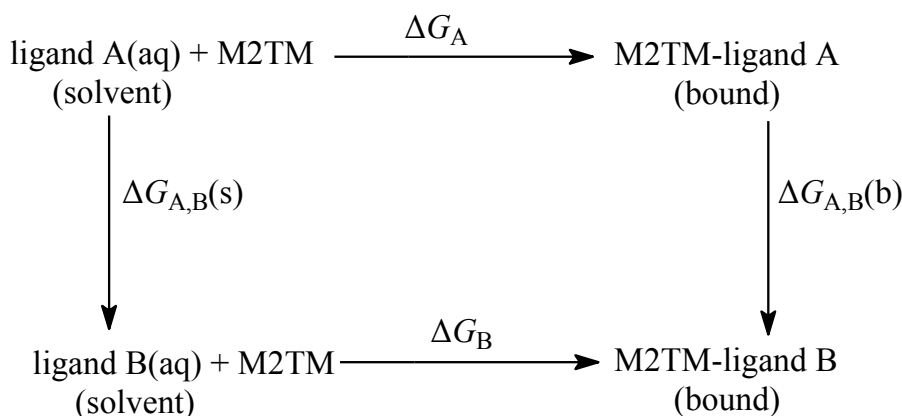
$$\Delta G_{A,B} = \langle G \rangle_B - \langle G \rangle_A = -k_B T \ln \left\langle e^{-(V_B - V_A)/k_B T} \right\rangle_A \quad (3)$$

The difference of ΔG between two λ values is according eq. 4

$$\langle G \rangle_{\lambda+d\lambda} - \langle G \rangle_{\lambda} = k_B T \ln \left\langle e^{(V_{\lambda+d\lambda} - V_{\lambda})/k_B T} \right\rangle_{\lambda} \quad (4)$$

Relative binding free energies between pairs of ligands $\Delta\Delta G_{\text{ligand A} \rightarrow \text{B}}$ were calculated according to eq. 5 based on ΔG obtained for the transformations of the ligands in the bound and the solvated state, respectively, $\Delta G_{A,B}(\text{b})$ and $\Delta G_{A,B}(\text{s})$ (see thermodynamic cycle in Scheme 11)

$$\Delta\Delta G_{\text{ligand A} \rightarrow \text{B}} = \Delta G_A - \Delta G_B = \Delta G_{A,B}(\text{b}) - \Delta G_{A,B}(\text{s}) \quad (5)$$



Scheme 11. Thermodynamic cycle for the calculation of relative free energies of binding applied to alchemical transformations of aminoadamantane derivatives **1**, **2-R**, **2-S** and **3** (Scheme 1). ΔG_A , ΔG_B are the free energies of transfer of A and B from the aqueous phase (unbound state) to the bound state, respectively. $\Delta G_{A,B}(s)$ and $\Delta G_{A,B}(b)$ are the free energy differences of the mutation of A into B in aqueous solution, and bound to the protein respectively.

For structural analyses, snapshots of the different systems were created with VMD⁸¹ or Maestro.⁷⁰ Trajectories were analyzed with Maestro,⁷⁰ Gromacs^{82,83} and VMD.⁸¹ For the calculation of hydrogen bonds, a cut-off angle of 30° deviation from 180° between the donor-hydrogen-acceptor atoms and a cut-off distance of 3.5 Å between the donor and acceptor atoms were applied.

1.5.5 Two-Electrode Voltage Clamp (TEVC) Assay

The inhibitors were tested via a TEVC assay using *X. laevis* frog oocytes microinjected with RNA expressing the M2 protein as in a previous report.⁸⁴ The blocking effect of the aminoadamantane derivatives against M2 was investigated with electrophysiology experiments using M2_{Udorn}. Because WSN/33-M2-N31S which will be used to compare antiviral potencies using a whole cell assay, M2_{WSN-N31S} was generated and studied in parallel. The potency of the inhibitors was expressed as the inhibition percentage of the A/M2 current observed after 2 min and 5 min of incubation with 100 μM of compound.

1.5.6 Anti-viral assays

1.5.6.1 Cells and viruses

Madin-Darby canine kidney (MDCK) cells (Cat.no. RIE 328, Friedrich-Loeffler Institute, Riems, Germany) were propagated as monolayer in Eagle's minimum essential medium (EMEM) supplemented with 10% fetal bovine serum, 1% non-essential amino acids (NEAA), 1 mM sodium pyruvate and 2 mM L-glutamine. Amantadine-sensitive Udorn, and WSN/33-M2-N31S⁴² were used in this study. For the generation of WSN/33-M2-N31S⁴² the plasmid pHW187-M2-N31 was altered by site-directed mutagenesis PCR and afterwards used as part of a plasmid set for virus recovery.⁸⁵ Both WSN/33-variants were propagated on MDCK cells in serum-free EMEM supplemented with 2 mM L-glutamine, 2 µg/mL trypsin, and 0.1% sodium bicarbonate (test medium). Virus containing supernatant was harvested after about 48 h of incubation at 37 °C when cytopathic effect became microscopically visible. Aliquots were stored at -80 °C until use. The M2 gene identity was verified by sequencing.

1.5.6.2 CPE inhibition activity

CPE inhibition studies were performed on two-day-old confluent monolayers of MDCK cells grown in 96-well plates as published.⁸⁶ In CPE inhibition assay, 50 µl of at least six serial half-log dilutions of compound in test medium and a constant multiplicity of infection of test virus (0.03 for WSN/33-M2-N31S) in a volume of 50 µL of the test medium were added to cells. Then, plates were incubated at 37 °C with 5% CO₂ for 48 h. Crystal violet staining or neutral red staining and optical density determination were performed as described before.^{86,87} After log transformation of compound concentrations, linear regression was used to determine the 50% inhibitory concentration (IC₅₀). At least three independent assays were conducted to calculate the mean IC₅₀ and their standard deviations.

1.5.6.3 Evaluation of inhibition activity using Plaque Reduction Assay

Confluent monolayers of MDCK cells were incubated with the Udorn virus [~ 100 plaque-forming units (pfu) per well] in a DMEM/1% bovine serum albumin mixture for 30 min at 4 °C, then 1 h at 37 °C. The inoculums were removed, and the cells were washed with phosphate-buffered saline (PBS). The cells were then overlaid with DMEM-containing 1.2% Avicel microcrystalline cellulose (FMC BioPolymer, Philadelphia, PA) and NAT (1.0 µg/mL). To examine the effect of compounds on plaque

formation, the compounds, at various concentrations, were included in the Avicel overlay solution. Two days after infection, the monolayers were fixed and stained with a naphthalene black dye solution (0.1% naphthalene black, 6% glacial acetic acid, and 1.36% anhydrous sodium acetate). The percent of plaque formation was compared to the condition with no compounds. The EC50 values of compounds **1-3** were calculated from best fit dose response curves with variable slope.

1.6 Supporting information

1.6.1 Scheme and Figure captions

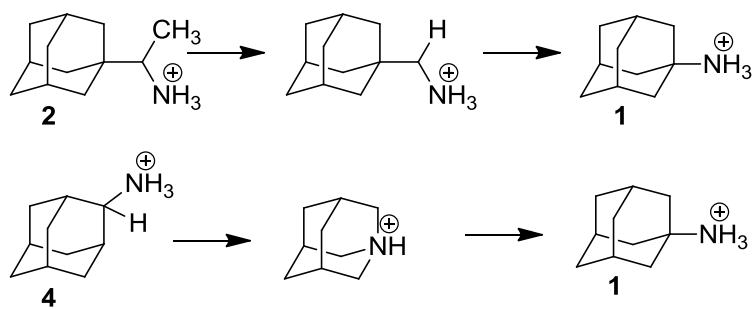
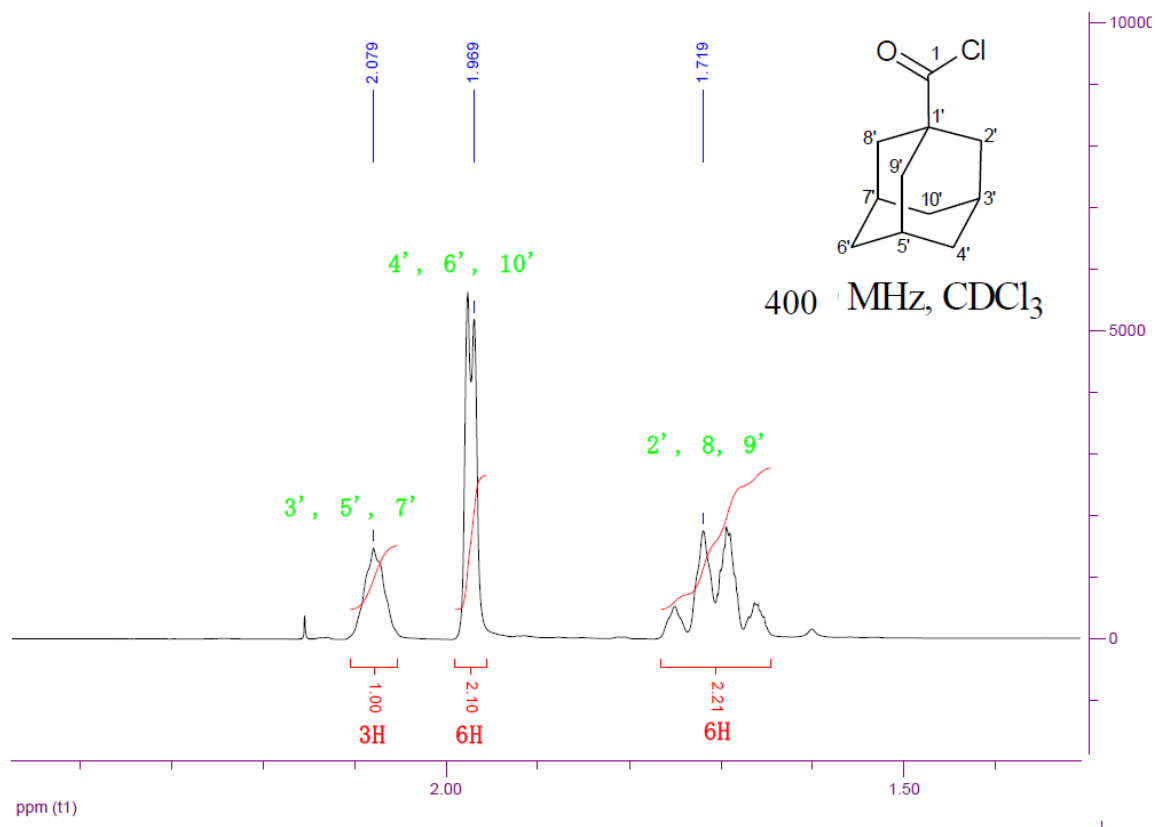


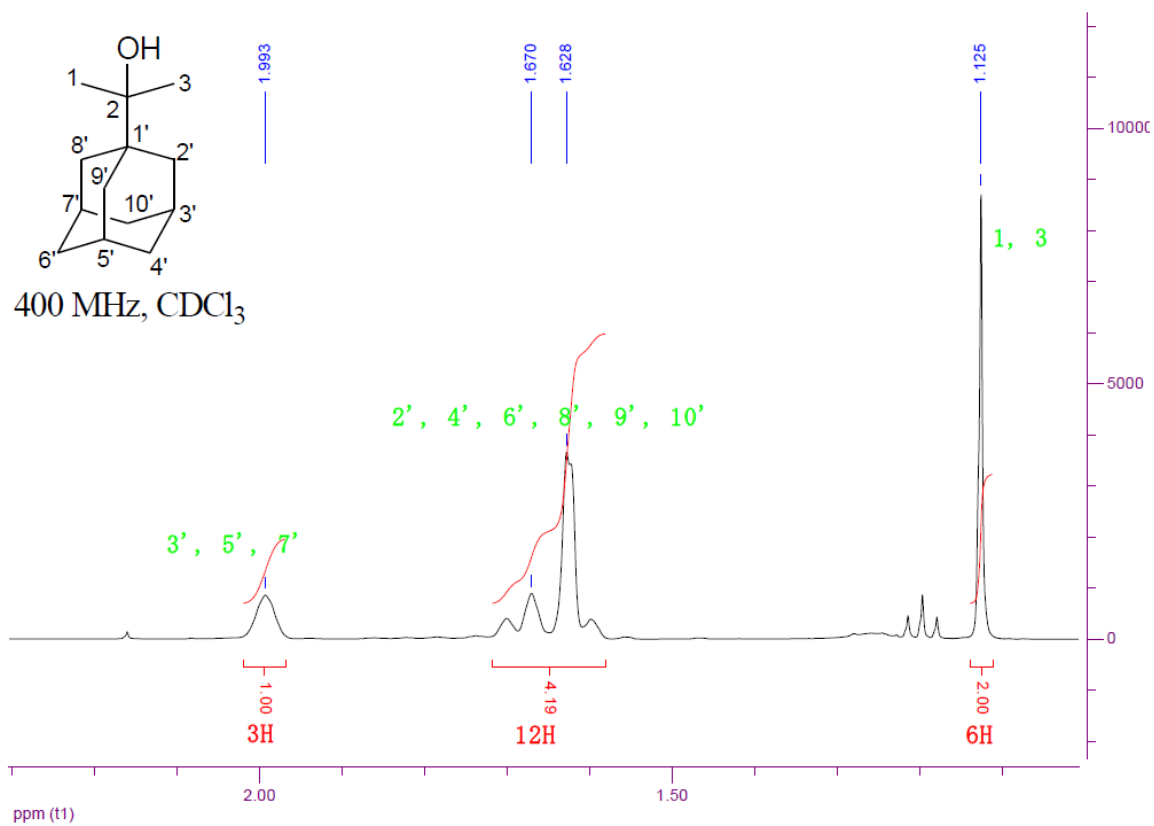
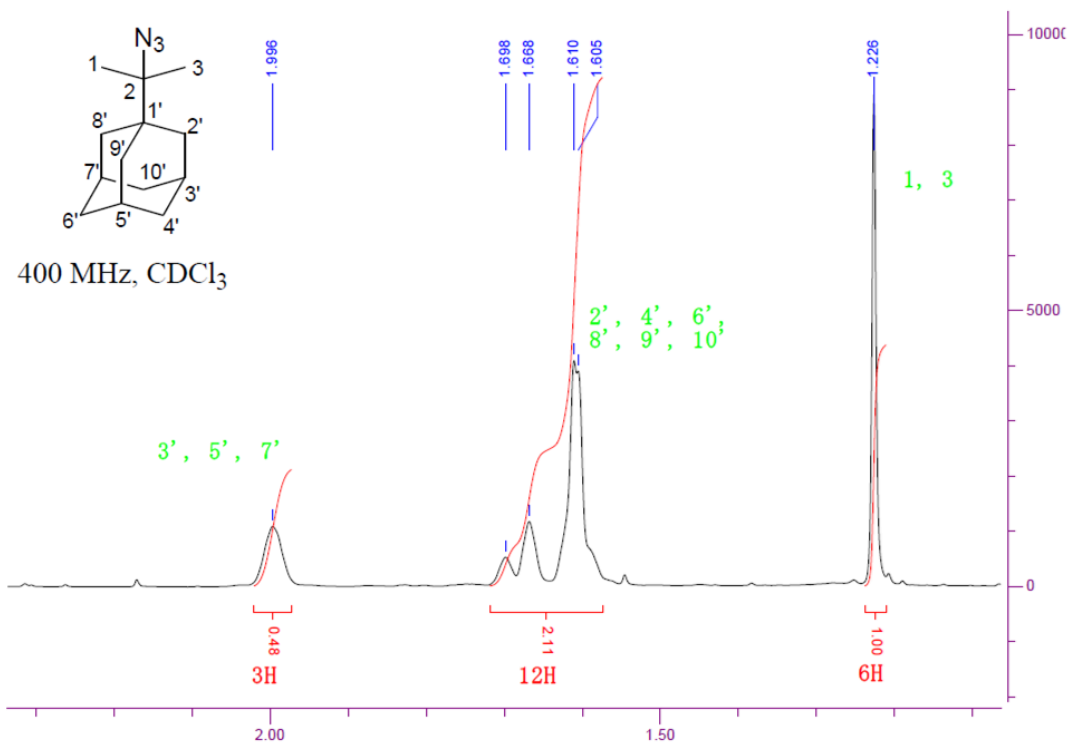
Figure 12. Two step transformations conducted in FEP calculations using the BAR approach to sufficiently sample the configurational space between the start and end states.

1.6.2 NMR Spectra of aminoadamantane compound 3 and synthetic intermediates 3a-3c.

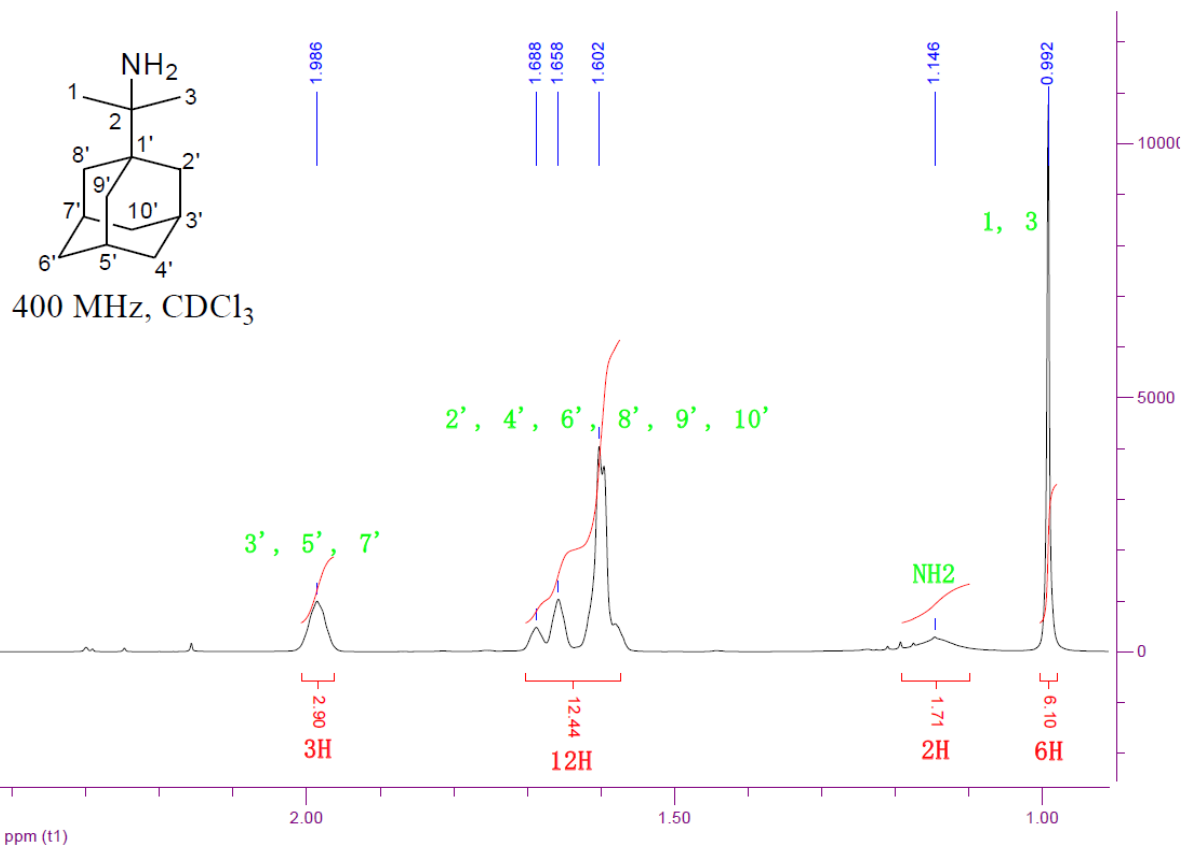
1.6.2.1 ^1H NMR spectra



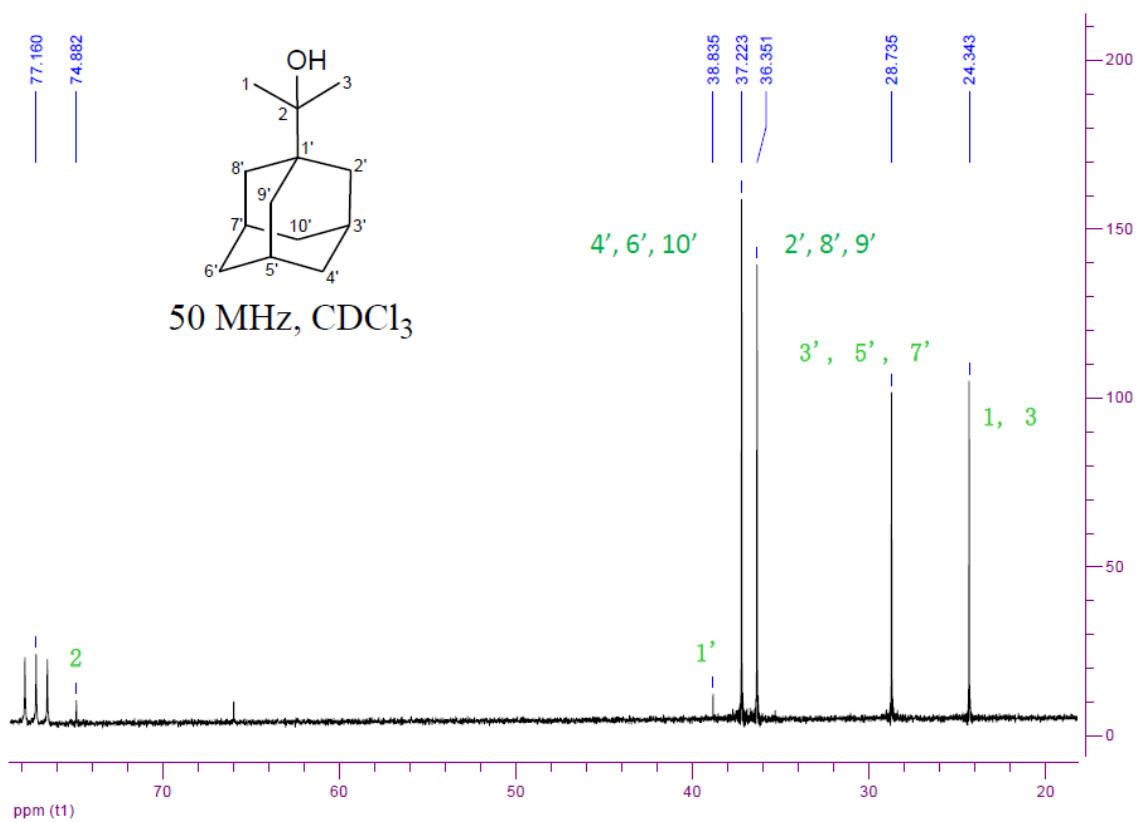
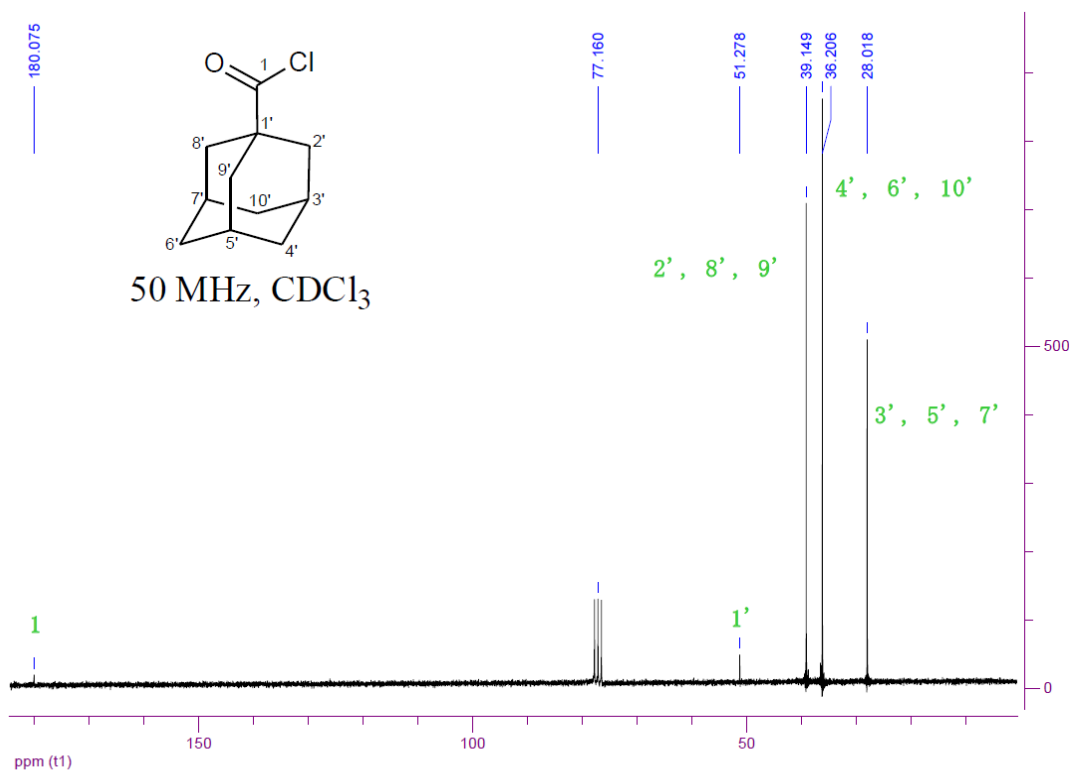
Binding Affinity of Rimantadine Enantiomers to the M2 Protein Channel



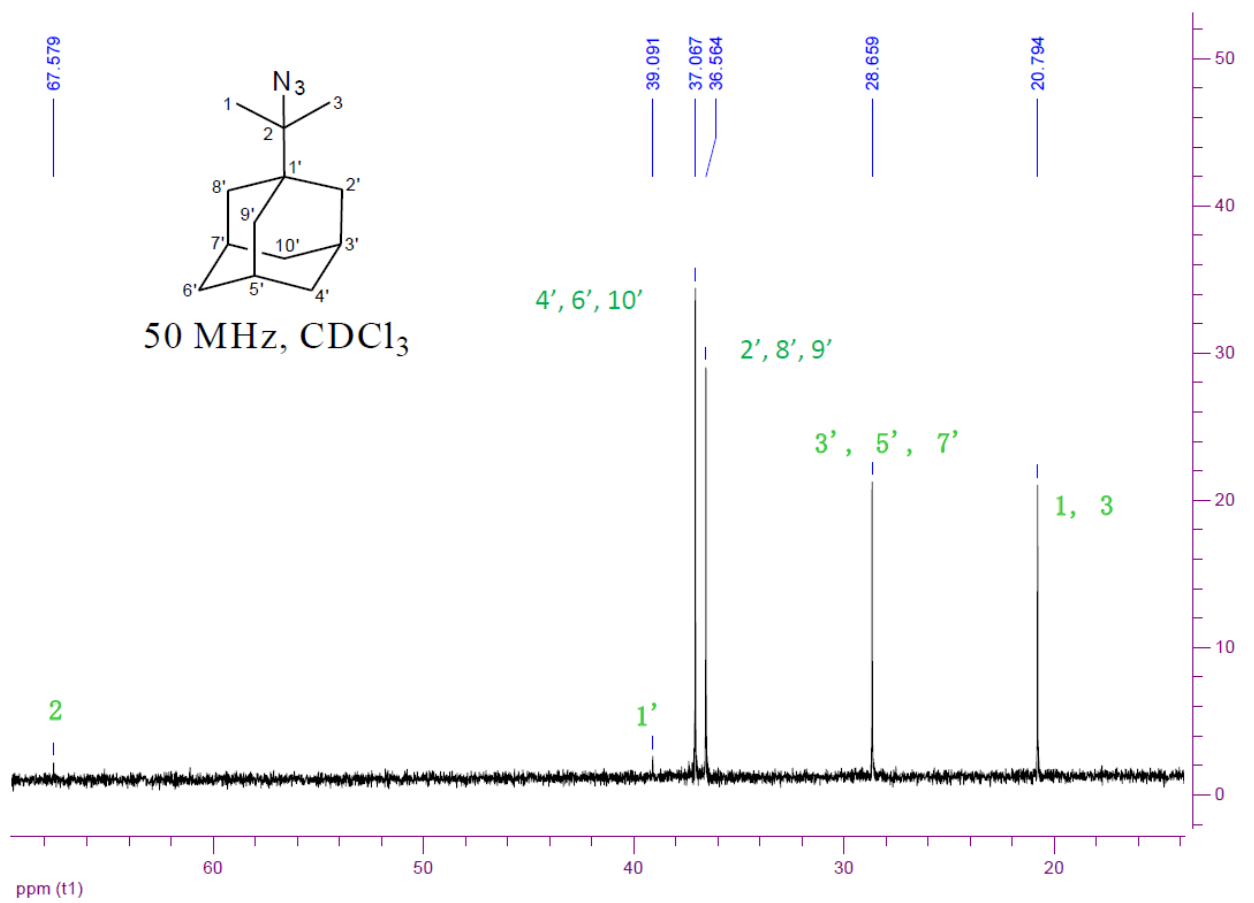
Binding Affinity of Rimantadine Enantiomers to the M2 Protein Channel



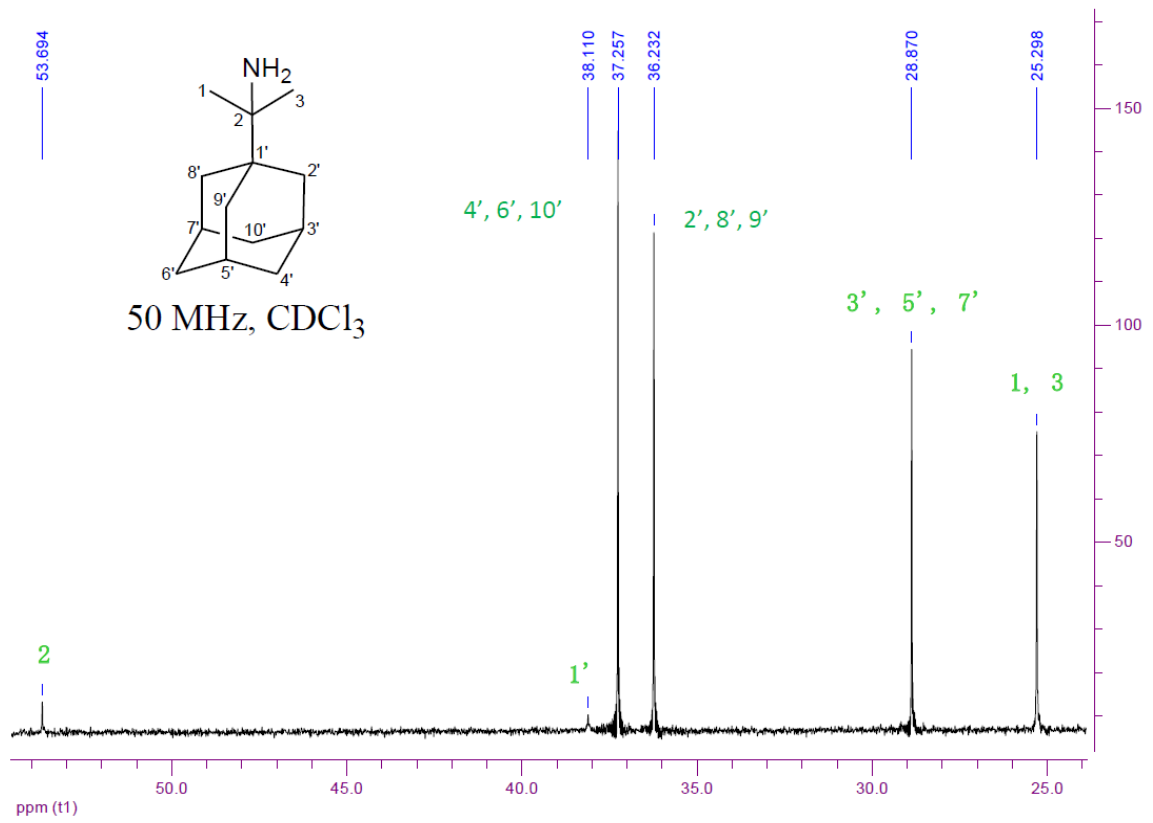
1.6.2.2 ^{13}C NMR spectra



Binding Affinity of Rimantadine Enantiomers to the M2 Protein Channel



Binding Affinity of Rimantadine Enantiomers to the M2 Protein Channel



1.7 References

- ¹Wang, C.; Takeuchi, K.; Pinto, L. H.; Lamb, R. A. Ion Channel Activity of Influenza A Virus M2 Protein: Characterization of the Amantadine Block. *J. Virol.* **1993**, *67*, 5585–5594.
- ²Chizhnikov, I. V.; Geraghty, F. M.; Ogden, D. C.; Hayhurst, A.; Antoniou, M.; Hay, A. J. Selective Proton Permeability and pH Regulation of The Influenza Virus M2 Channel Expressed In Mouse Erythroleukaemia Cells. *J. Physiol.* **1996**, *494*, 329–336.
- ³Hayden, F. G. Clinical applications of antiviral agents for chemoprophylaxis and therapy of respiratory viral infections. *Antiviral Res* **1985**, Suppl 1, 229-39.
- ⁴ Wang, C.; Lamb, R. A.; Pinto, L. H. Activation of the M2 Ion Channel of Influenza Virus: a Role for the Transmembrane Domain Histidine Residue. *Biophys. J.* **1995**, *69*, 1363–1371.
- ⁵Helenius, A. Unpacking the Incoming Influenza Virus. *Cell* **1992**, *69*, 577–578.
- ⁶Tang, Y.; Zaitseva, F.; Lamb, R. A.; Pinto, L. H. The Gate of the Influenza Virus M2 Proton Channel is Formed by a Single Tryptophan Residue. *J. Biol. Chem.* **2002**, *277*, 39880–39886.
- ⁷Hu, F.; Luo, W.; Hong, M. Mechanisms of Proton Conduction and Gating in Influenza M2 Proton Channels from Solid-State NMR. *Science* **2010**, *330*, 505–508.
- ⁸ Pinto, L. H.; Dieckmann, G. R.; Gandhi, C. S.; Papworth, C. G.; Braman, J.; Shaughnessy, M. A.; Lear, J. D.; Lamb, R. A.; DeGrado, W. F. A Functionally Defined Model for the M2 Proton Channel of Influenza A Virus Suggests a Mechanism for its Ion Selectivity. *Proc. Natl. Acad. Sci. U. S. A.* **1997**, *94*, 11301–11306.
- ⁹Ma, C.; Polishchuk, A. L.; Ohigashi, Y.; Stouffer, A. L.; Schön, A.; Magavern, E.; Jing, X.; Lear, J. D.; Freire, E.; Lamb, R. A.; DeGrado, W. F.; Pinto, L. H. Identification of the functional core of the influenza A virus A/M2 proton-selective ion channel. *Proc. Natl. Acad. Sci. USA* **2009**, *106*, 12283–12288.
- ¹⁰ Wang, J.; Qiu, J. X.; Soto, C.; DeGrado, W. F. Structural and dynamic mechanisms for the function and inhibition of the M2 proton channel from influenza A virus. *Curr. Opin. Struct. Biol.* **2011**, *21*, 68-80.
- ¹¹Hay, A. J.; Wolstenholme, A. J.; Skehel, J. J.; Smith, M. H. The Molecular Basis of the Specific Anti-Influenza Action of Amantadine. *EMBO J.* **1985**, *4*, 3021–3024.
- ¹²Balannik, V.; Carnevale, V.; Fiorin, G.; Levine, B. G.; Lamb, R. A.; Klein, M. L.; DeGrado, W. F.; Pinto, L. H. Functional Studies and Modeling of Pore-Lining Residue Mutants of the Influenza A Virus M2 Ion Channel. *Biochemistry*, **2010**, *49*, 696–708.
- ¹³Hu, J.; Asbury, T.; Achuthan, S.; Li, C.; Bertram, R.; Quine, J. R.; Fu, R.; Cross, T. A. Backbone structure of the amantadine-blocked trans-membrane domain M2 proton channel from Influenza A virus. *Biophys. J.* **2007**, *92*, 4335-43.

- ¹⁴ Stouffer, A. L.; Acharya, R.; Salom, D.; Levine, A. S.; Di Costanzo, L.; Soto, C. S.; Tereshko, V.; Nanda, V.; Stayrook, S.; DeGrado, W. F. Structural basis for the function and inhibition of an influenza virus proton channel. *Nature* **2008**, *451*, 596-9.
- ¹⁵ Cady, S. D.; Schmidt-Rohr, K.; Wang, J.; Soto, C. S.; DeGrado, W. F.; Hong, M. Structure of the amantadine binding site of influenza M2 proton channels in lipid bilayers. *Nature* **2010**, *463*, 689-92.
- ¹⁶ Pielak, R. M.; Oxenoid, K.; Chou, J. J. Structural investigation of rimantadine inhibition of the AM2-BM2 chimera channel of influenza viruses. *Structure* **2011**, *19*, 1655-1663.
- ¹⁷ Cady, S. D.; Wang, J.; Wu, Y.; DeGrado, W. F.; Hong, M. Specific binding of adamantane drugs and direction of their polar amines in the pore of the influenza M2 transmembrane domain in lipid bilayers and dodecylphosphocholine micelles determined by NMR spectroscopy. *J. Am. Chem. Soc.* **2011**, *133*, 4274-84.
- ¹⁸ Kolocouris, A.; Tzitzoglaki, C.; Johnson, F. B.; Zell, R.; Wright, A. K.; Cross, T. A.; Tietjen, I.; Fedida, D.; Busath, D. D. Aminoadamantanes with persistent in vitro efficacy against H1N1 (2009) influenza A. *J. Med. Chem.* **2014**, *57*, 4629-39.
- ¹⁹ Ioannidis, H.; Drakopoulos, A.; Tzitzoglaki, C.; Homeyer, N.; Kolarov, F.; Gkeka, P.; Freudenberger, K.; Liolios, C.; Gauglitz, G.; Cournia, Z.; Gohlke, H.; Kolocouris, A. Alchemical free energy calculations and isothermal titration calorimetry measurements of aminoadamantanes bound to the closed state of influenza A/M2TM. *J. Chem. Info. Model.* **2016**, *56*, 862-876.
- ²⁰ Andreas, L. B.; Barnes, A. B.; Corzilius, B.; Chou, J. J.; Miller, E. A.; Caporini, M.; Rosay, M.; Griffin, R. G. Dynamic nuclear polarization study of inhibitor binding to the M2(18-60) proton transporter from influenza A. *Biochemistry* **2013**, *52*, 2774-82.
- ²¹ Andreas, L. B.; Barnes, A. B.; Corzilius, B.; Chou, J. J.; Miller, E. A.; Caporini, M.; Rosay, M.; Griffin, R. G. Dynamic nuclear polarization study of inhibitor binding to the M2(18-60) proton transporter from influenza A. *Biochemistry* **2013**, *52*, 2774-82.
- ²² Yi, M.; Cross, T. A.; Zhou, H.-X. Conformational heterogeneity of the M2 proton channel and a structural model for channel activation. *Proc. Natl. Acad. Sci. U. S. A.* **2009**, *106*, 13311-13316.
- ²³ Luo, W.; Hong, M. Conformational changes of an ion channel detected through water-protein interactions using solid-state NMR spectroscopy. *J. Am. Chem. Soc.* **2010**, *132*, 2378-84.
- ²⁴ Intharathap, P.; Laohpongspaisan, C.; Rungrotmongkol, T.; Loisuangsinsin, A.; Malaisree, M.; Decha, P.; Aruksakunwong, O.; Chuenpenit, K.; Kaiyawet, N.; Sompornpisut, P.; Pianwanit, S.; Hannongbua, S. How amantadine and rimantadine inhibit proton transport in the M2 protein channel. *J. Mol. Graph. Model.* **2008**, *27*, 342-348.
- ²⁵ Khurana, E.; Devane, R. H.; Dal Peraro, M.; Klein, M. L. Computational study of drug binding to the membrane-bound tetrameric M2 peptide bundle from influenza A virus. *Biochim. Biophys. Acta* **2011**, *1808*, 530-537.

- ²⁶ Leonov, H.; Astrahan, P.; Krugliak, M.; Arkin, I. T. How Do aminoadamantanes block the influenza M2 channel, and how does resistance develop? *J. Am. Chem. Soc.* **2011**, *133*, 9903-9911.
- ²⁷ Gianti, E.; Carnevale, V.; DeGrado, W. F.; Klein, M. L.; Fiorin, G. Hydrogen-bonded water molecules in the M2 channel of the influenza A virus guide the binding preferences of ammonium-based inhibitors. *J. Phys. Chem. B* **2015**, *119*, 1173-83.
- ²⁸ Gleed, M. L.; Ioannidis, H.; Kolocouris, A.; Busath, D. D. Resistance-mutation (N31) effects on drug orientation and channel hydration in amantadine-bound influenza A M2. *J. Phys. Chem. B* **2015**, *119*, 11548-59.
- ²⁹ Wright, A. K.; Batsomboon, P.; Dai, J.; Hung, I.; Zhou, H.-X.; Dudley, G. B.; Cross, T. A. Differential binding of rimantadine enantiomers to influenza A M2 proton channel. *J. Am. Chem. Soc.* **2016**, *138*, 1506-1509.
- ³⁰ Hu, F.; Schmidt-Rohr, K.; Hong, M. NMR Detection of pH-Dependent Histidine-Water Proton Exchange Reveals the Conduction Mechanism of a Transmembrane Proton Channel. *J. Am. Chem. Soc.* **2012**, *134*, 3703-3713.
- ³¹ Hu, J.; Fu, R.; Cross, T. A. The chemical and Dynamical Influence of the Anti-Viral Drug Amantadine on the M2 Proton Channel Transmembrane Domain. *Biophys. J.* **2007**, *93*, 276-283.
- ³² Aldrich, P. E.; Hermann, E. C.; Meier, W. E.; Paulshock, M.; Prichard, W. W.; Snyder, J. A.; Watts, J. C. Antiviral agents. 2. Structure-activity relationships of compounds related to 1-adamantanamine. *J. Med. Chem.* **1971**, *14*, 535-543.
- ³³ Chaires, J. B. Calorimetry and thermodynamics in drug design. *Annu. Rev. Biophys.* **2008**, *37*, 135-151.
- ³⁴ Salom, D.; Hill, B. R.; Lear, J. D.; DeGrado, W. F. pH-Dependent tetramerization and amantadine binding of the transmembrane helix of M2 from the influenza A virus. *Biochemistry* **2000**, *39*, 14160-14170.
- ³⁵ Fokkens, J.; Klebe, G. A simple protocol to estimate differences in protein binding affinity for enantiomers without prior resolution of racemates. *Angew. Chem. Int. Ed.* **2006**, *45*, 985-989
- ³⁶ Fujii, I.; Akimoto, T.; Watadani, T.; Nunomura, S.; Takahashi, Y. Optical separation of rimantadine and in silico prediction of chiral selectivity of M2 protein. *Acta Crystallogr., Sect. A: Found. Crystallogr.* **2008**, *A64*, C380.
- ³⁷ Chipot, C.; Pohorille, A. *Free energy calculations. Theory and applications in chemistry and biology.* **2007**. Eds.; Springer Verlag: Berlin, New York.
- ³⁸ Cady, S.; Wang, T.; Hong, M. Membrane-dependent effects of a cytoplasmic helix on the structure and drug binding of the influenza virus M2 Protein. *J. Am. Chem. Soc.* **2011**, *133*, 11572-11579.

- ³⁹Gkeka, P.; Eleftheratos, S.; Kolocouris, A.; Cournia, Z. Free energy calculations reveal the origin of binding preference for aminoadamantane blockers of influenza A/M2TM pore. *J. Chem. Theory Comput.* **2013**, *9*, 1272-1281.
- ⁴⁰ Wang, J.; Ma, C.; Fiorin, G.; Carnevale, V.; Wang, T.; Hu, F.; Lamb, R. A.; Pinto, L. H.; Hong, M.; Klein, M. L.; DeGrado, W. F. Molecular dynamics simulation directed rational design of inhibitors targeting drug-resistant mutants of influenza A virus M2. *J. Am. Chem. Soc.* **2011**, *133*, 12834-12841.
- ⁴¹Balannik, V.; Wang, J.; Ohigashi, Y.; Jing, X.; Magavern, E.; Lamb, R. A.; DeGrado, W. F.; Pinto, L. H. Design and pharmacological characterization of inhibitors of amantadine-resistant mutants of the M2 ion channel of influenza A virus. *Biochemistry* **2009**, *48*, 11872.
- ⁴²Schade, D.; Kotthaus, J.; Riebling, L.; Kotthaus, J.; Müller-Fielitz, H.; Raasch, W.; Hoffmann, A.; Schmidtke, M.; Clement, B.; ZanamivirAmidoxime- and N-Hydroxyguanidine-Based Prodrug Approaches to Tackle Poor Oral Bioavailability. *J. Pharm. Sci.* **2015**, *104*, 3208-3219.
- ⁴³Choma, N.; Davis, P. P.; Edorn, R. W.; Fukuda, E. K. Quantitation of the enantiomers of rimantadine and its hydroxylated metabolites in human plasma by gas chromatography/mass spectrometry. *Biomed. Chromatogr.* **1992**, *6*, 12-15.
- ⁴⁴Manchand, P. S.; Cerutti, R. L.; Martin, J. A.; Hill, C. H.; Merrett, E. K.; Keech, E.; Belshe, R. B.; Connell, E. V.; Sim, I. S. Synthesis and antiviral activity of metabolite of rimantadine. *J. Med. Chem.* **1990**, *33*, 1992-1995.
- ⁴⁵ Kolocouris, N.; Foscolos, G. B.; Kolocouris, A.; Marakos, P.; Pouli, N.; Fytas, G.; Ikeda, S.; De Clercq, E. Synthesis and Antiviral Activity Evaluation of Some Aminoadamantane Derivatives. *J. Med. Chem.* **1994**, *37*, 2896-2902.
- ⁴⁶Hansen, R. K.; Broadhurst, R. W.; Skelton, P. C.; Arkin, I. T. Hydrogen/deuterium exchange of hydrophobic peptides in model membranes by electrospray ionization mass spectrometry. *Journal of the American Society for Mass Spectrometry* **2002**, *13*, 1376-87.
- ⁴⁷Kolocouris, A.; Zikos, C.; Broadhurst, R. W. ¹⁹F NMR detection of the complex between amantadine and the receptor portion of the influenza A M2 ion channel in DPC micelles. *Bioorg. Med. Chem. Letters* **2007**, *17*, 3947-3952.
- ⁴⁸Ladbury, J. E.; Klebe, G.; Freire, E. Adding Calorimetric Data to Decision Making in Lead Discovery: a Hot Tip. *Nat. Rev. Drug Discovery* **2010**, *9*, 23-27.
- ⁴⁹Perozzo, R.; Folkers, G.; Scapozza, L. Thermodynamics of Protein-Ligand Interactions: History, Presence, and Future Aspects. *J. Recept. Signal Transduction Res.* **2004**, *24*, 1-52.
- ⁵⁰Wang, C.; Takeuchi, K.; Pinto, L. H.; Lamb, R. A. Ion channel activity of influenza A virus M2 protein: characterization of the amantadine block. *J. Virol.* **1993**, *67*, 5585-5594;

- ⁵¹, T.; Williston, S.; Brandts, J. F.; Lin, L. N. Rapid measurement of binding constants and heats of binding using a new titration calorimeter. *Analytical biochemistry* **1989**, *179*, 131-137
- ⁵²Doyle, M. L. Characterization of binding interactions by isothermal titration calorimetry. *Current opinion in biotechnology* **1997**, *8*, 31-35.
- ⁵³*Origin 8.1G SR1*, v8.1.13.88; OriginLab Corporation, Northampton, MA, USA: **2009**.
- ⁵⁴Stouffer, A. L.; Nanda, V.; Lear, J. D.; DeGrado, W. F. Sequence Determinants of a Transmembrane Proton Channel: An Inverse Relationship between Stability and Function. *J. Mol. Biol.* **2005**, *347*, 169–179.
- ⁵⁵ Halgren, T. A. Merck molecular force field. V. Extension of MMFF94 Using Experimental Data, Additional Computational Data, and Empirical Rules. *J. Comput. Chem.* **1996**, *17*, 616-641.
- ⁵⁶ Halgren, T. A. MMFF VII. Characterization of MMFF94, MMFF94s, and Other Widely Available Force fields for Conformational Energies and for Intermolecular-Interaction Energies and Geometries. *J. Comp. Chem.* **1999**, *20*, 730-748.
- ⁵⁷ Jones, G.; Willett, P.; Glen, R. C.; Leach, A. R.; Taylor, R. Development and Validation of a Genetic Algorithm for Flexible Docking. *J. Mol. Biol.* **1997**, *267*, 727-748.
- ⁵⁸ Verdonk, M. L.; Chessari, G.; Cole, J. C.; Hartshorn, M. J.; Murray, C. W.; Nissink, J. W.; Taylor, R. D.; Taylor, R. Modeling Water Molecules in Protein-Ligand Docking Using GOLD. *J. Med. Chem.* **2005**, *48*, 6504-6515.
- ⁵⁹Korb, O.; Stützle, T.; Exner, T. E. Empirical Scoring Functions for Advanced Protein-Ligand Docking with PLANTS. *J. Chem. Inf. Model.* **2009**, *49*, 84-96.
- ⁶⁰ Mooij, W. T.; Verdonk, M. L. General and Targeted Statistical Potentials for Protein-Ligand Interactions. *Proteins: Struct., Funct., Bioinf.* **2005**, *61*, 272-287.
- ⁶¹ Pettersen, E. F.; Goddard, T. D.; Huang, C. C.; Couch, G. S.; Greenblatt, D. M.; Meng, E. C.; Ferrin, T. E. UCSF Chimera--A Visualization System for Exploratory Research and Analysis. *J. Comput. Chem.* **2004**, *25*, 1605-1612.
- ⁶¹Cristian, L.; Lear, J. D.; DeGrado, W. F. Use of Thiol-Disulfide Equilibria to Measure the Energetics of Assembly of Transmembrane Helices in Phospholipid Bilayers. *Proc. Natl. Acad. Sci. U. S. A.* **2003**, *100*, 14772-14777.
- ⁶¹Cady, S. D.; Luo, W. B.; Hu, F.; Hong, M. Structure and function of the influenza M2 proton channel. *Biochemistry* **2009**, *48*, 7356–7364.
- ⁶¹ Cady, S. D.; Hong, M. Effects of amantadine binding on the dynamics of bilayer-bound influenza A M2 transmembrane peptide studied by NMR relaxation. *J. Biomol. NMR* **2009**, *45*, 185–196.

⁶¹Hu, F.; Luo, W.; Cady, S. D.; Hong, M. Conformational plasticity of the influenza A M2 transmembrane helix in lipid bilayers under varying pH, drug binding and membrane thickness. *Biochim.Biophys.Acta*.**2011**, *1808*, 415–423.

⁶¹Saotome, K.; Duong-Ly, K.; Howard, K.P. Influenza A M2 protein conformation depends on choice of model membrane. *Biopolymers***2015**, *104*, 405-411.

⁶¹ Bennett, C.H. Efficient Estimation of Free Energy Differences from Monte Carlo Data. *J. Comp. Phys.* **1976**, *22*, 245–268.

⁶¹*Desmond Molecular Dynamics System*, version 3.0; D. E. Shaw Research: New York, NY, **2012**.

⁶¹ Bowers, K. J.; Chow, E.; Xu, H.; Dror, R. O.; Eastwood, M. P.; Gregersen, B. A.; Klepeis, J. L.; Kolossvary, I.; Moraes, M. A.; Sacerdoti, F. D.; Salmon, J. K.; Shan, Y.; Shaw, D. E. Scalable Algorithms for Molecular Dynamics Simulations on Commodity Clusters. In Proceedings of the ACM/IEEE Conference on Supercomputing (SC06), Tampa, Florida, **2006**; Tampa, Florida, 2006.

⁶¹*Maestro-Desmond Interoperability Tools*, version 3.1; Schrodinger: New York, NY, **2012**.

⁶¹ Jorgensen, W. L.; Chandrasekhar, J.; Madura, J. D.; Impey, R. W.; Klein, M. L. Comparison of Simple Potential Functions for Simulating Liquid Water. *J. Chem. Phys.* **1983**, *79*, 926-935.

⁶¹ Jorgensen, W. L.; Maxwell, D. S.; Tirado-Rives, J. Development and Testing of the OPLS All-Atom Force Field on Conformational Energetics and Properties of Organic Liquids. *J. Am. Chem. Soc.* **1996**, *118*, 11225-11236.

⁶¹ Rizzo, R. C.; Jorgensen, W. L. OPLS All-Atom Model for Amines: Resolution of the Amine Hydration Problem. *J. Am. Chem. Soc.* **1999**, *121*, 4827–4836.

⁶¹ Kaminski, G.; Friesner, R. A.; Tirado-Rives, J.; Jorgensen, W. L. Evaluation and Reparametrization of the OPLS-AA Force Field for Proteins via Comparison with Accurate Quantum Chemical Calculations on Peptides. *J. Phys. Chem. B* **2001**, *105*, 6474-6487.

⁶³Cady, S. D.; Luo, W. B.; Hu, F.; Hong, M. Structure and function of the influenza M2 proton channel. *Biochemistry***2009**, *48*, 7356–7364.

⁶⁴ Cady, S. D.; Hong, M. Effects of amantadine binding on the dynamics of bilayer-bound influenza A M2 transmembrane peptide studied by NMR relaxation. *J. Biomol. NMR***2009**, *45*, 185–196.

⁶⁵Hu, F.; Luo, W.; Cady, S. D.; Hong, M. Conformational plasticity of the influenza A M2 transmembrane helix in lipid bilayers under varying pH, drug binding and membrane thickness. *Biochim.Biophys.Acta*.**2011**, *1808*, 415–423.

- ⁶⁶Saotome, K.; Duong-Ly, K.; Howard, K.P. Influenza A M2 protein conformation depends on choice of model membrane. *Biopolymers***2015**, *104*, 405-411.
- ⁶⁷ Bennett, C.H. Efficient Estimation of Free Energy Differences from Monte Carlo Data. *J. Comp. Phys.* **1976**, *22*, 245–268.
- ⁶⁸*Desmond Molecular Dynamics System*, version 3.0; D. E. Shaw Research: New York, NY, **2012**.
- ⁶⁹ Bowers, K. J.; Chow, E.; Xu, H.; Dror, R. O.; Eastwood, M. P.; Gregersen, B. A.; Klepeis, J. L.; Kolossvary, I.; Moraes, M. A.; Sacerdoti, F. D.; Salmon, J. K.; Shan, Y.; Shaw, D. E. Scalable Algorithms for Molecular Dynamics Simulations on Commodity Clusters. In Proceedings of the ACM/IEEE Conference on Supercomputing (SC06), Tampa, Florida, **2006**; Tampa, Florida, 2006.
- ⁷⁰*Maestro-Desmond Interoperability Tools*, version 3.1; Schrodinger: New York, NY, **2012**.
- ⁷¹ Jorgensen, W. L.; Chandrasekhar, J.; Madura, J. D.; Impey, R. W.; Klein, M. L. Comparison of Simple Potential Functions for Simulating Liquid Water. *J. Chem. Phys.* **1983**, *79*, 926-935.
- ⁷² Jorgensen, W. L.; Maxwell, D. S.; Tirado-Rives, J. Development and Testing of the OPLS All-Atom Force Field on Conformational Energetics and Properties of Organic Liquids. *J. Am. Chem. Soc.* **1996**, *118*, 11225-11236.
- ⁷³ Rizzo, R. C.; Jorgensen, W. L. OPLS All-Atom Model for Amines: Resolution of the Amine Hydration Problem. *J. Am. Chem. Soc.* **1999**, *121*, 4827–4836.
- ⁷⁴ Kaminski, G.; Friesner, R. A.; Tirado-Rives, J.; Jorgensen, W. L. Evaluation and Reparametrization of the OPLS-AA Force Field for Proteins via Comparison with Accurate Quantum Chemical Calculations on Peptides. *J. Phys. Chem. B* **2001**, *105*, 6474-6487.
- ⁷⁵ Shivakumar, D.; Williams, J.; Wu, Y.; Damm, W.; Shelley, J.; Sherman, W. Prediction of Absolute Solvation Free Energies using Molecular Dynamics Free Energy Perturbation and the OPLS Force Field. *J. Chem. Theory Comput.* **2010**, *6*, 1509–1519.
- ⁷⁶ Darden, T.; York, D.; Pedersen, L. Particle Mesh Ewald: An N log(N) Method for Ewald Sums in Large Systems. *J. Chem. Phys.* **1993**, *98*, 10089–10092.
- ⁷⁷ Essmann, U.; Perera, L.; Berkowitz, M. L.; Darden, T.; Lee, H.; Pedersen, L. G. A Smooth Particle Mesh Ewald Method. *J. Chem. Phys.* **1995**, *103*, 8577–8593.
- ⁷⁸ Martyna, G. J. T., D. J.; Klein, M. L. Constant-Pressure Molecular-Dynamics Algorithms. *J. Chem. Phys.* **1994**, *101*, 4177-4189.
- ⁷⁹ Humphreys, D. D.; Friesner, R. A.; Berne, B. J. A Multiple-Time-Step Molecular-Dynamics Algorithm for Macromolecules. *J. Phys. Chem.* **1994**, *98*, 6885-6892.

⁸⁰Koynova, R.; Caffrey, M. Phases and Phase Transitions of the Phosphatidylcholines. *Biochim.Biophys.Acta***1998**, *1376*, 91-145.

⁸¹Humphrey, W.; Dalke, A.; Schulten, K. VMD: Visual Molecular Dynamics. *J. Mol. Graph.* **1996**, *14*, 33-38.

⁸²Berendsen, H. J. C.; van der Spoel, D.; van Drunen, R. GROMACS: A Message-Passing Parallel Molecular Dynamics Implementation. *Comput. Phys. Commun.* **1995**, *91*, 43–56.

⁸³Hess, B.; Kutzner, C.; van der Spoel, D.; Lindahl, E. GROMACS 4: Algorithms for Highly Efficient, Load-Balanced, and Scalable Molecular Simulation. *J. Chem. Theory Comput.* **2008**, *4*, 435-447.

⁸⁴Wang, J.; Wu, Y.; Ma, C.; Fiorin, G.; Wang, J.; Pinto, L. H.; Lamb, R. A.; Klein, M. L.; Degrado, W. F. Structure and inhibition of the drug-resistant S31N mutant of the M2 ion channel of influenza A virus. *Proc. Natl. Acad. Sci. U. S. A.* **2013**, *110*, 1315-1320.

⁸⁵Hoffmann, E.; Neumann, G.; Kawaoka, Y.; Hobom, G.; Webster, R. G. A DNA transfection system for generation of influenza A virus from eight plasmids. *Proc. Natl. Acad. Sci. U. S. A.***2000**, *97*, 6108-6113.

⁸⁶Schmidtke, M.; Schnittler, U.; Jahn, B.; Dahse, H.-M.; Stelzner, A. A rapid assay for evaluation of antiviral activity against coxsackie virus B3, influenza virus A, and herpes simplex virus type 1. *J. Virol. Meth.***2001**, *95*, 133-143.

⁸⁷Torres, E.; Duque, M. D.; Vanderlinden, E.; Ma, C.; Pinto, L. H.; Camps, P.; Froeyen, M.; Vázquez, S.; Naesens, L. *Antiviral Res.***2013**, *99*, 281.

CHAPTER 2

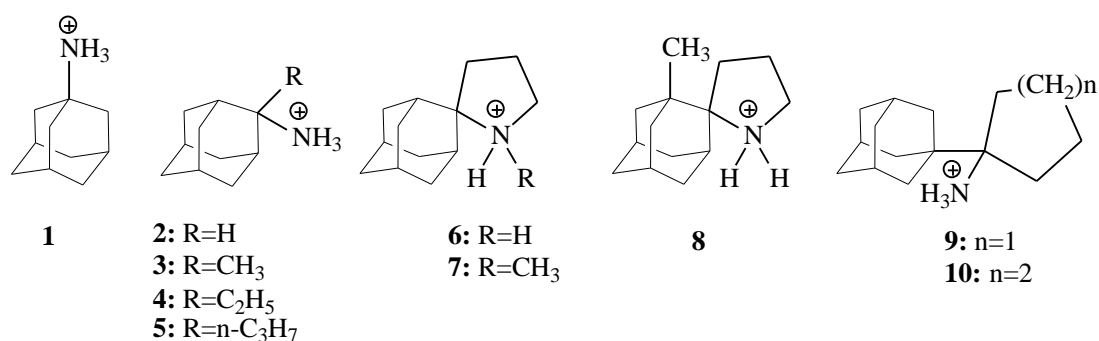
Binding and Proton Blockage by Amantadine Variants of the Influenza M2_{WT} and M2_{S31N} Explained

2.1 Abstract

While aminoadamantanes are well-established inhibitors of the influenza A M2 proton channel, the mechanisms by which they are rendered ineffective against M2_{S31N} are unclear. Solid state NMR, isothermal titration calorimetry, electrophysiology, anti-viral assays and molecular dynamics simulations suggest stronger binding interactions for aminoadamantanes to M2_{WT} compared to negligible or weak binding to M2_{S31N}. The MD simulations and ssNMR data suggest most likely that the S31N mutation produces an unfavorable contact of N31 amide side chains for adamantane ring preventing its binding in the lipophilic pocket enclosed by V27. This results in a weaker binding for derivatives with sizeable adducts or loss of binding for amantadine and derivatives with small adducts to M2TM_{S31N} in accordance to the ITC and ssNMR data. Previous experimental work and MD simulations showed that the ammonium group of amantadine has a prevalent orientation toward the C-terminus of M2TM_{WT} (Udorn), with the adamantane hydrocarbon cage shifted slightly toward N-terminus of the A30/S31 C α sites producing a region of the pore devoid of water consistent with blockage of proton transport and in agreement with ssNMR findings. In contrast our MD simulations of Amt and other aminoadamantane derivatives in M2TM_{S31N} suggested that these compounds have a variable orientation, but with a propensity to have the ammonium group toward the N-terminus of the M2TM_{S31N} pore. In this orientation water occupancy is not widely occluded in any configuration. Sizeable adducts are weakly accommodated in the region between A30 and G34 in M2TM_{S31N} pore. The reshaping of the M2pore when N31 is present, which in contrast to wild type (WT), leads: A) to the loss of the V27 pocket for the adamantyl cage and to a predominant orientation of the ligand's ammonium group toward the N-terminus and, B) to the lack of a helical kink upon ligand binding. The kink, which reduces the tilt of the C-terminal helical domain relative to the bilayer normal includes the W41 primary gate for proton conductance and may prevent the gate from opening, representing an alternative view for how these drugs prevent proton conductance.

2.2 Introduction

A proven vulnerability of influenza A infections is the blockage of the viral M2 proton channel. M2 is required for acidification of the virion interior during infection and neutralization of the trans-Golgi network during viral egress.¹ Amantadine ((*Amt*), **1**) (Scheme 1) is an established inhibitor of the influenza A/M2-mediated proton currents² and a licensed influenza A infection therapy.³ The primary binding site of **1** is located within the pore of the tetrameric M2 transmembrane (M2TM) domain that forms the transmembrane proton transit path.^{4,5} However, since 2005,⁶ the **1**-insensitive Ser-to-Asn mutation at position 31 in M2 (S31N) has become globally prevalent,⁷ abrogating the clinical usefulness of **1**⁸ and possibly other previously reported M2 inhibitors.⁹ Thus, new agents are needed to combat drug-resistant forms of influenza.



Scheme 1. Structures of aminoadamantane derivatives **1-10**.

Based on the experimental solid state NMR (ssNMR) structure of the complex M2TM-**1** 4^a,5^{a,b}, the replacement of S31 residues at the drug binding site with the more polar and bulky Asn side chains may induce the adamantyl ring to move deeper into the M2 pore, toward the C-terminus close to G34, where the pore of the helical bundle has its largest diameter, and drugs larger than **1** might be effective. We and others have searched for such larger drugs and found, for example compounds **5-7**, which are active against A/Calif/07/2009 (H1N1) virus encoding S31N but not against WSN/33 also bearing the same mutation.¹⁰ However, while a preliminary ssNMR experiment of the S31N M2TM domain complexed with compound **5** showed evidence of drug binding, electrophysiology (EP) studies showed no blockage for the full length S31N M2 protein.^{10a} These studies therefore indicate that more detailed experimental investigation and modeling are needed to explain the mechanisms by which aminoadamantanes are rendered ineffective against M2_{S31N} in order to design effective drugs.

Recent molecular dynamics (MD) simulations showed that the ammonium group of **1** has a prevalent orientation toward the C-terminus of M2TM_{WT}(Udorn), with the adamantane hydrocarbon cage shifted slightly toward N-terminus of the A30/S31 Ca^{11,12,13,14,15, 16,17, 18} producing a region of the pore devoid of water^{17,19} consistent with blockage of proton transport and in agreement with ssNMR findings.^{5c,20, 21} In contrast, MD simulations of **1** in M2TM_{S31N} from Gleed et al.^{17b} and rimantadine in M2TM_{S31N} from Alhadeff et al.¹⁶ suggested that these compounds have a variable orientation, but with a propensity to have the ammonium group toward the N-terminus^{17b, 22} of the M2TM_{S31N} pore (Figure 1). In this orientation water occupancy is not widely occluded in any configuration.¹⁷ These studies^{16,17b} presented a description of the Potential of Mean Force (PMF) curves of amantadine and rimantadine in interaction with the M2TM_{S31N} pore but the main structural/interaction changes due to S31N and leading to aminoadamantane resistance were not defined. In addition, no experimental evidence is presented to date for the binding of aminoadamantane ligands in M2TM_{S31N} pore. Nevertheless, the propensity of **1**'s amino group to orient towards the N-end was used for the successful design of **1**-polar head conjugates that were shown to be potent inhibitors of WSN/33 virus and proton conductance by M2_{S31N}²³. A ssNMR analysis of a system including one of these compounds, a phenylisoxazole derivative linked with amantadine through a methylene bridge, with M2TM in membrane bilayers was realized. The results showed that the compound's heterocyclic ring system may be trapped by the V27 side chains at N-terminus of the M2TM-pore²⁴ with the isoxazole group forming hydrogen bonds with the N31 amide side chains.

We are interested to investigate how subtle changes in amantadine structure are related with the binding affinity against M2TM variants. We previously used molecular mechanics Poisson-Boltzmann surface area (MM/PBSA) to interpret thermodynamic profiles measured using isothermal titration calorimetry (ITC) for aminoadamantanes binding to the avian M2TM_{Weybridge} (M2TM_{Weybridge} has different two amino acids that do not line into the pore, i.e., V28→I28 and L38→F38 compared to M2TM_{WT}) in order to successfully prioritize aminoadamantane derivatives.²⁵ We also applied rigorous free energy binding calculations by the Bennett acceptance ratio (BAR) approach to accurately predict relative binding affinities of aminoadamantane derivatives towards M2TM_{WT} or M2TM_{Weybridge} measured by ITC or other methods respectively.^{26,27}

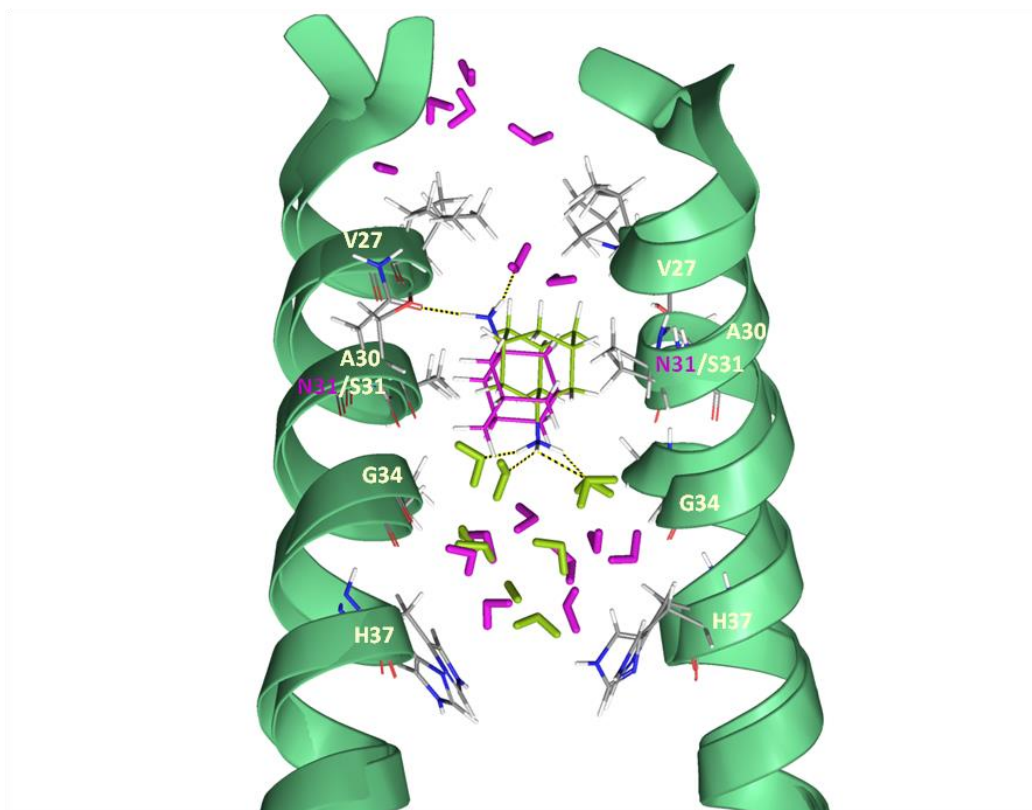


Figure 1. *Amt* (**1**) orients toward the protein C-terminus in M2TM_{WT} and toward the protein N-terminus in M2TM_{S31N}. Superposition of final snapshots, constant temperature and pressure molecular dynamics simulations at 310 K of **1** in complex with S31 or N31 M2 [PDB ID: 2KQT] in 150 mM NaCl, water, and DMPC lipid. **1** and waters are shown in yellow-green and purple in WT and S31N respectively. Two of four M2TM backbones are shown as green ribbons. In the S31 case, the ammonium group of **1** is projecting toward the C-terminus and hydrogen bonding with four water molecules. In the N31 case, the adamantane cage (purple) is lower, and the amantadine amine projects toward the N-terminus and hydrogen bonds with the one N31 side chain and a water molecule.

Here we investigate the interaction of aminoadamantane derivatives (Scheme 1) with M2TM_{WT} and M2TM_{S31N} both experimentally and by MD simulations, with the aim of determining how the S31N mutation leads to the inability of **1** and other aminoadamantanes to block S31N M2 proton transport. First, we measured binding constants of selected aminoadamantane derivatives with ITC against M2TM_{WT} and M2TM_{S31N} in dodecylphosphocholine (DPC) micelles at alkaline pH. Second, we applied a series of MD simulations (80 ns trajectories) of the M2TM_{WT} and M2TM_{S31N} complexes with **1-10** (Scheme 1) to analyze in some detail how the polar N31 amide side chains affect binding of an aminoadamantane ligand inside the M2TM pore. To this end, we suggest that repulsive forces between N31 and the adamantane ring may influence the orientation and binding interactions of the ligand, the overall stability of the complexes, and

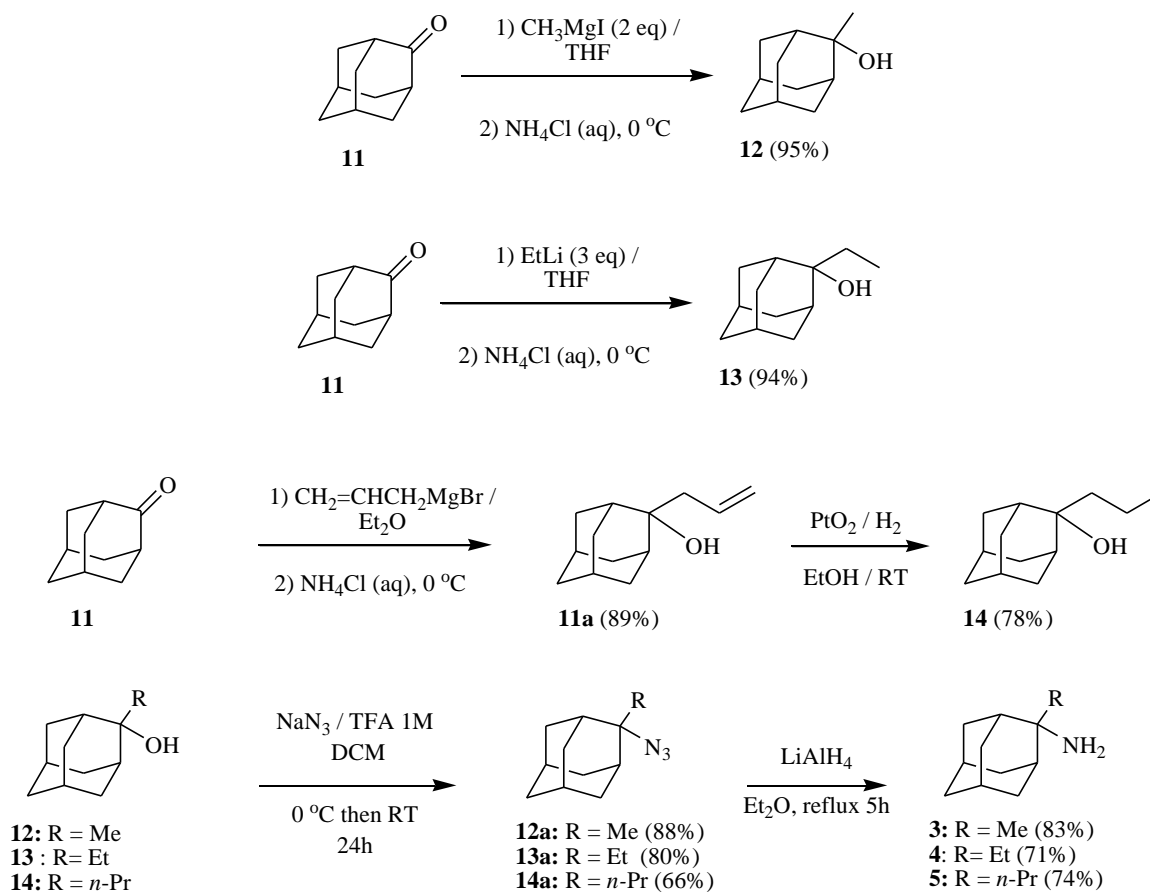
the shape of M2TM. Third, we performed Oriented Sample (OS) and Magic Angle Spinning (MAS) ssNMR experiments^{28,29,30} on representative M2TM-ligand complexes at alkaline pH using both M2TM_{WT} and M2TM_{S31N} sequences to characterize the structural influence of compounds on the channel. Fourth, we selected and tested new synthetic derivatives with slightly larger or similarly-sized adducts, like **8** and **10**, than previously synthesized compounds **5-7**, **9** for their abilities to bind M2TM_{S31N}. We realized EP experiments for selected compounds against both WT and S31N M2 proteins to test M2 channel blockage and additionally measured the antiviral potency of the compounds against the naturally amantadine-resistant H1N1 influenza strain A/WSN/1933 (WSN/33 with M2_{N31}) and its reverse genetics-generated amantadine-sensitive variant with the amino acid substitution N31S in M2 (WSN/33-M2-N31S) using cytopathic effect inhibition (CPE) assays.

2.3 Results

2.3.1 Chemistry

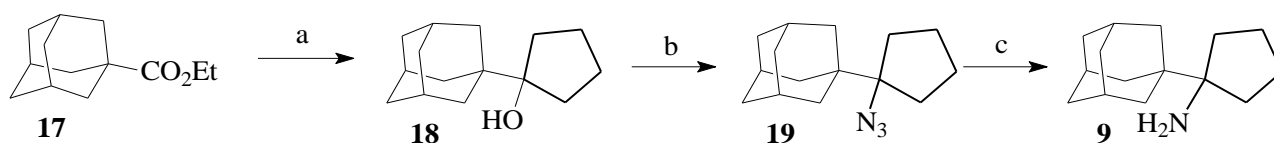
The synthesis of compounds **3-5**^{10a} and **6-7**^{9a} were previously published and resynthesized for the required measurements. The synthetic schemes of **2**, **6** and **7** are included in the SI, (Schemes S1 and S2). The multistep synthesis of 1'-methylspiro[pyrrolidine-2,2'-adamantane] **8** was accomplished by I. Stylianakis for his PhD thesis.

Compounds **2-8** belong to the class of 2-alkyl-2-aminoadamantanes bearing a substitution at adamantane C2 carbon. Tertiary alcohol **11a** was obtained by treating 2-adamantanone **11** with allyl magnesium bromide (Scheme 2). The unsaturated alcohol **11a** was converted to the *n*-propyl derivative **14** through catalytic hydrogenation over PtO₂. After a lot of experiments with tertiary alcohols in the adamantane series and in acyclic series we concluded that the conversion of tertiary alcohols to the corresponding azides through NaN₃/H₂SO₄(various concentrations)/CHCl₃ or NaN₃/TFA/CHCl₃ can result in unreacted alcohol and found that the transformation proceeds efficiently using NaN₃/TFA 1M in CH₂Cl₂. (see Chapter 4 for the details). The amine **5** was prepared by means of LiAlH₄ reduction of the azide **14a** in refluxing ether for 5 h. The amines **3, 4** were also synthesized according to Scheme 2. Tertiary alcohols **12, 13** were obtained by treating 2-adamantanone **11** with an organolithium (R = Et) or organomagnesium reagent (R = Me) (Scheme 3). While 2-methyl-2-adamantanol **12** was obtained after treating 2-adamantanone **11** with CH₃MgI, this is not an efficient method for the preparation of alcohol **13**, due to the bulky 2-adamantanone **11** and to the soft carbanion character of the Grignard reagent making the β-hydride transfer a competitive reaction to the alkyl addition and leading to a mixture of the desired tertiary alcohol with 2-adamantanol. The conversion of tertiary alcohols **12, 13** to the corresponding azides **12a, 13a** was accomplished efficiently through treatment with NaN₃/TFA 1M in dichloromethane or dichloroethane for 24 h at room temperature. The primary tert-alkyl amines **3,4** were prepared by means of LiAlH₄ reduction of the azides **12a, 13a** in refluxing ether for 5 h.



Scheme 2. Synthetic scheme for the preparation of aminoadamantanes **3-5**.

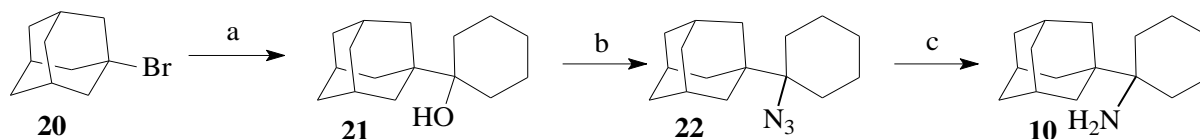
The synthesis of the 1-(1-adamantyl) cyclopentanamine **9** and of the precursor alcohol **18** was realized according to a published procedure²⁹ based on the reaction of ethyl 1-adamantanecarboxylate **17** with 1,4-bis(bromomagnesiobutane). The formation of the precursor azide **19** of the amine **9** was accomplished more efficiently using $\text{NaN}_3/\text{TFA}/\text{CH}_2\text{Cl}_2$ 1M instead of the $\text{NaN}_3/\text{trichloroacetic}/\text{CHCl}_3/\text{H}_2\text{O}$ mixture (Scheme 3).²⁹



Reagents and conditions: (a) $\text{BrMg}(\text{CH}_2)_4\text{MgBr}$, dry ether, rt 24h, $\text{NH}_4\text{Cl}_{\text{sat}}$ (70%); (b) NaN_3 , TFA, CH_2Cl_2 , 0 °C, 5h, then r.t. 24 h (88%). (c) LiAlH_4 , dry ether, reflux, 5 h, then H_2O , NaOH 10% (65%).

Scheme 3. Synthesis of 1-(1-adamantyl)cyclopentanamine **9**.²⁹

For the synthesis of 1-(1-adamantyl)cyclohexanamine **10** the alcohol **21** was prepared according to a published procedure³⁰ from 1-adamantyl lithium (1-bromoadamantane **20** + lithium wire) and cyclohexanone. Subsequent treatment of alcohols **18** or **21** with $\text{NaN}_3/\text{TFA}/\text{CH}_2\text{Cl}_2$ afforded the corresponding azides **19** or **22**. The amines **9** or **10** respectively were prepared through reduction of the azides **19** or **22** by means of $\text{LiAlH}_4/\text{ether}/\text{reflux}$, 5h (Scheme 4).



Reagents and conditions: (a) Li, dry THF, cyclohexanone, sonication, 0 °C, 5h (70%); (b) NaN_3 , TFA, CH_2Cl_2 , 0 °C, 5h, then r.t. 24 h (60%). (c) LiAlH_4 , dry ether, reflux, 5 h, then H_2O , NaOH 10% (30%).

Scheme 4. Synthesis of 1-(1-adamantyl)cyclohexanamine **10**.³⁰

2.3.2 Binding affinities of aminoadamantanes to M2TM by ITC

ITC measurements³¹ were determined for both M2TM_{WT} and M2TM_{S31N} tetramers at pH 8 corresponding to the closed state of the M2TM pore³² (Table 1). Binding data for compounds **1**, **5**, **6-8** to M2TM_{WT} measured in our previous work²⁶ were included in Table 1. Thus, as has been published recently²⁶ (see Table 1) compounds **1-8** bind M2TM_{WT}. Compound **9** and the newly synthesized analogue **10**, which has a cyclohexane ring instead of the cyclopentane in **9**, bind M2TM_{WT} with at least an order of magnitude lower dissociation constant (K_d) than those for **1-8**, possibly because their size do not enable them to fit well inside M2TM_{WT}. We note that techniques for measuring affinity against M2TM such as ITC correspond to models of molecular recognition for ligand binding to M2TM and do not necessarily reflect functional inhibition of M2 proton currents or in vitro inhibition of influenza A virus. For example, **9** inhibits M2_{WT}-dependent currents as measured by electrophysiology with an IC_{50} of $10 \pm 2 \mu\text{M}$ (Table 7) and inhibited influenza A virus replication in infected cells with an IC_{50} of $4.34 \pm 2.94 \mu\text{M}$ (Table 8) while compound **10** was inactive. Nevertheless, ITC and related techniques like Surface Plasmon Resonance (SPR) and structural techniques like ssNMR can provide useful insights for M2TM binding and trends in structure-activity relationships for the M2-aminoadamantane system. For example, compounds **1-4** did not bind efficiently to M2TM_{S31N} according to ITC and previous SPR measurements for **1**³³ while **5**, **6** with larger adducts connected to adamantane bind weakly to M2TM_{S31N} compared to M2TM_{WT} according to ITC (Table 1) and ssNMR. The K_d values of low affinity binders (e.g. **5**, **6**, **9**, **10**) against M2TM_{S31N}, and **9** against M2TM_{WT}, possess relatively large errors due to the limitations of the ITC method (Table 1). Subsequently comparison of the relative K_d values of compounds **5**, **6**, **9**, **10** do not reflect relative binding affinity strength against M2TM_{S31N}. Nevertheless, although the quantitation of the ITC results against M2TM_{S31N} is limited for this method, the measurements suggest that the K_d values of **5** and **6** against M2TM_{S31N} are much smaller compared to M2TM_{WT} suggest weaker binding to M2TM_{S31N} (Table 1). Narrower linewidths and larger chemical shifts changes for **5** bound to M2TM_{WT} compared to M2TM_{S31N} were observed in the ssNMR spectra described below suggesting a reduction in dynamics for binding to M2TM_{WT} and a more specific binding site, which in turn causes a significant reduction in hydration due to drug induced desolvation of the binding pocket.³¹

Table 1. Binding constants, and other thermodynamic parameters derived from ITC measurements for influenza A M2TM_{WT} and M2TM_{S31N}.

M2TM _{WT}				
Ligand ¹	K _d ²	ΔG ^{3,4}	ΔH ^{3,5}	TΔS ^{3,6}
1 ⁷	2.17 ± 0.52	-32.51 ± 0.59	-27.87 ± 2.09	4.64 ± 2.18
2 ⁷	1.60 ± 0.34	-33.30 ± 0.54	-29.41 ± 1.76	3.89 ± 1.84
3 ⁷	0.89 ± 0.19	-34.77 ± 0.54	-28.41 ± 1.09	6.32 ± 1.21
4 ⁷	0.62 ± 0.14	-35.65 ± 0.54	-29.87 ± 0.88	5.77 ± 1.05
5 ⁷	0.63 ± 0.17	-36.43 ± 0.69	-32.62 ± 1.29	3.90 ± 1.45
6 ⁷	0.36 ± 0.22	-38.11 ± 1.84	-21.49 ± 1.76	16.61 ± 2.57
7 ⁷	0.93 ± 0.36	-34.64 ± 0.96	-15.98 ± 1.17	18.66 ± 1.51
8 ⁷	1.30 ± 0.43	-33.81 ± 0.84	-21.25 ± 1.30	12.55 ± 1.55
9	14.61 ± 4.62	-27.77 ± 0.79	- ⁸	- ⁸
10	> 10	- ⁸	- ⁸	- ⁸
M2TM _{S31N}				
Ligand ¹	K _d ²	ΔG ^{3,4}	ΔH ^{3,5}	TΔS ^{3,6}
1-4	- ⁹	-	-	-
5	> 10	- ⁸	- ⁸	- ⁸
6	17.5 ± 8.5	-27.95 ± 1.24	- ⁸	- ⁸
9	15.8 ± 5.95	-28.22 ± 0.96	- ⁸	- ⁸
10	9.90 ± 4.99	-29.41 ± 1.29	- ⁸	- ⁸

¹ See Scheme 1.

² Binding constant K_d in μM calculated from measured K_a in M⁻¹ by K_d = 1/K_a × 10⁻⁶ and error in K_d in μM determined by K_{d, error} = (K_{a, error}/K_a²) × 10⁻⁶.

³ In kJ mol⁻¹.

⁴ Free energy of binding computed from K_d by ΔG = -RTln(K_d^{ref}/K_d) with K_d^{ref} = 1 M and T = 300 K and error in ΔG determined according to $\Delta G_{\text{error}} = \sqrt{\left(\frac{RT K_{d, \text{error}}}{K_d}\right)^2}$, with T = 300 K.

⁵ Enthalpy of binding and error in the enthalpy of binding calculated from measured binding enthalpy and measured error by ΔH = ΔH_{measured} (T / T_{measured}) with T = 300 K and the temperature at which the ITC measurements were performed T_{measured} = 293.15 K.

⁶ Entropy of binding calculated by ΔS = (-ΔG + ΔH)/T and error in ΔS computed by the equation

$$\Delta S_{\text{error}} = \sqrt{\Delta G_{\text{error}}^2 + \Delta H_{\text{error}}^2}$$

⁷ Measured in ref. 26.

⁸ Values could not be determined reliably due to the limitations of the methods in the area of very weak binding.

⁹ No detectable binding.

2.3.3 Solid state NMR of M2TM - aminoadamantanes complexes

2.3.3.1 OS ssNMR spectra

Drug binding to the channel pore of M2TM_{WT} and M2TM_{S31N} was evaluated using OS ssNMR experiments. Spectral correlation observed in these data sets, between anisotropic ¹⁵N chemical shifts and ¹H-¹⁵N dipolar coupling values for selectively ¹⁵N-labeled backbone amide sites, gives rise to resonance patterns known as PISA (polarity index slant angle) wheels.^{34,35} The shape, size and position of the PISA wheel for α -helical membrane proteins in uniformly oriented lipid bilayer preparations is determined by the helical tilt relative to the bilayer normal, and is sensitive to drug-induced structural perturbations. Previous investigations by Cross and co-workers have reported dramatic changes in anisotropic chemical shifts and dipolar coupling values for M2TM_{WT} in the presence of **1**.³⁵ PISA wheel analysis of M2TM_{WT} spectra in the *apo* state and in the presence of **1**³⁵ or **5** correlates the shifts with a substantial reduction in the tilt angle for the C-terminal region of the M2TM_{WT} helix, following ligand binding. In contrast, M2TM_{S31N} in the presence of **5** results in a uniform $5 \pm 2^\circ$ decrease in the helical tilt imparting a change to the entire helix-helix interface.^{10a}

Here, to monitor changes in the resonance frequencies and to the resulting PISA wheel in the presence of other variants of **1**, a ¹⁵N-V28,A30,I42 (VAI-M2TM) labeling scheme was used. Residues 28 and 30 are in the N-terminal domain of the M2TM helix and I42 in the C-terminal region, and hence the labels effectively sample both segments. Resonance frequencies for these sites are well resolved allowing for a PISA wheel analysis of drug binding in the channel pore that induces small structural perturbations. The signals of these three pertinent and isotopically labeled backbone amides were shifted in nearly an identical fashion when **1** or **5** bind to the M2TM_{WT} (Figure 2). As before, changes suggest only a slight perturbation to the N-terminus and a much more significant structural perturbation to the C-terminus with a change in the tilt angle from 32° to just 22° , while the N-terminal tilt changes by only a degree or two (Table 2).^{4b,35} These results imply similar drug induced structural perturbations to the TM configuration of WT M2 protein in the presence of **1** or **5**.

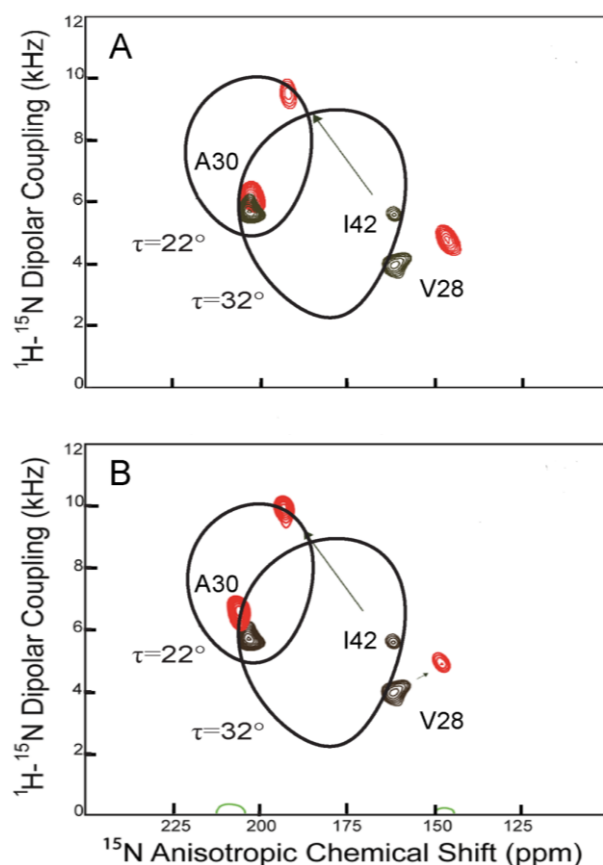


Figure 2. Superimposed PISEMA spectra of the M2TM_{WT} (residues 22-46), ¹⁵N-labeled at V28, A30, and I42, in DMPC lipid bilayers uniformly aligned on glass slides with (red) and without (black) compound **1** (A) and compound **5** (B). Assignments without drug were made based on the known structure and spectra of M2TM_{WT}.³⁵ Assignments with drug follow the rotational orientation of the helices. Change in the resonance frequencies of the ¹⁵N-labeled backbone amide sites are indicated with black arrows. All spectra were collected at 720 MHz, pH 7.5, 303K. The molar ratio of lipid/protein was 30:1. PISA wheels are drawn for helix tilts of 22° and 32° for the N- and C-terminal residues respectively when the drugs are bound.

Table 2. Mean helical tilt values relative to the bilayer normal from MD simulations of **1**, **5** in complex with M2TM_{WT} in DMPC bilayer.

Ligand ¹	MD simulations ² N-terminus/C-terminus	ssNMR Experiment ³ N-terminus/C-terminus	2QQT ^{4a,5b} N-terminus/C-terminus
1	31° ± 4.6° / 18° ± 4.9°	32 ± 2° / 22° ± 2°	30° / 19°
5	31° ± 5.1° / 19° ± 5.0°	32 ± 2° / 22° ± 2°	

¹ See Scheme 1.

² Calculated using Gromacs tools.

³ This study.

For the binding studies to M2TM_{S31N}, no observable effect was detected for binding of **1**, while **5** induces smaller changes compared to those induced by the binding of **1** or **5** to M2TM_{WT} based on the signals from the same three backbone amides (Figure 3). In addition, the linewidths are narrower when **5** is bound to M2TM_{WT} compared to M2TM_{S31N}, suggesting less dynamics in the WT complex implying a tighter complex.

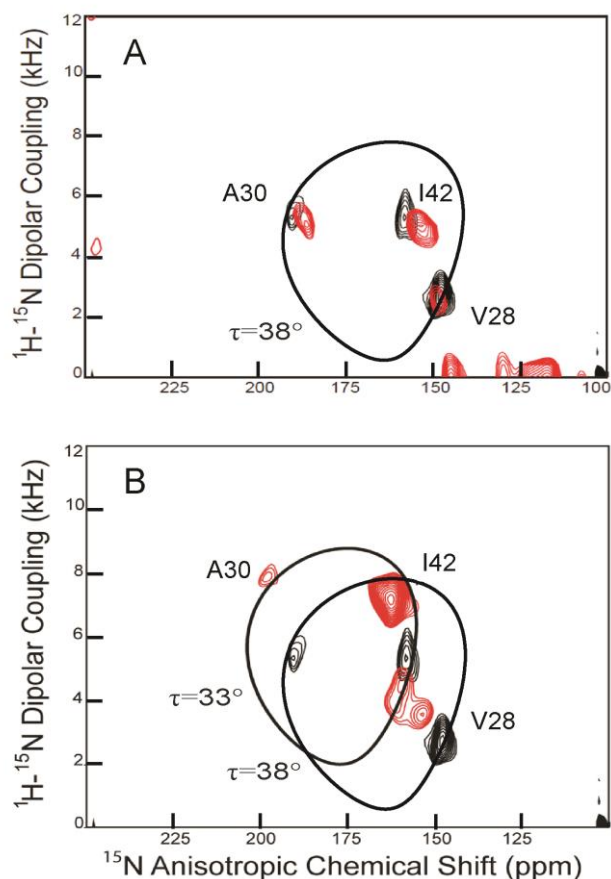


Figure 3. Superimposed PISEMA spectra of the M2TM_{S31N}, ¹⁵N-labeled at residues V28, A30, and I42, in DMPC lipid bilayers uniformly aligned on glass slides with (red) and without (black) compound **1** (A) and compound **5** (B). Assignments without drug were made based on the known structure and spectra of M2TM_{WT}.³⁵ Assignments with drug follow the rotational orientation of the helices. Theoretical PISA wheel calculated for an ideal helix $[(\phi, \varphi)] = (-60^\circ, -45^\circ)$ with a 33° tilt angle relative to the bilayer normal is superimposed on M2TM_{S31N} resonance frequencies, which are shifted after compound **5** addition. All spectra were collected at 720 MHz, pH 7.5, 303K. The molar ratio of lipid/protein was 30:1.

There is a small difference in the structure of M2TM_{S31N} versus M2TM_{WT} without drugs in lipid bilayers (black resonances in Figure 2 versus Figure 3). The M2TM_{S31N} data suggests a helical tilt of approximately 38° , somewhat greater than the helical tilt observed in the WT structure (32°) consistent with prior

characterizations.^{4,35} While the binding of **1** to M2TM_{WT} produced a 10° kink near G34 in each helix of the tetramer,^{4,35} binding of **1** produced no such structural change for the **1**-resistant M2TM_{S31N}. The shifts in the anisotropic resonance frequencies which resulted when **5** binds to M2TM_{S31N} demonstrates a significant change in helical tilt from 38° to 33° in the tetrameric complex (Table 5). Based on these resonances that sample the N- and C- regions of the TM helix, the structural change appears to be a uniform change in tilt. Consequently, the residues facing the pore remain the same, but the interactions between helices that provide the tetrameric stability may change substantially. Upon binding of **1** or **5** to M2TM_{WT} a kinked helix at G34 is produced but when adding these compounds to M2TM_{S31N} helices are not kinked at G34. Instead, when **5** bind to M2TM_{S31N}, the entire helix-helix interface changes with the ~5° reduction in tilt for each of the four helices.

The structurally similar aminoadamantanes **6-8** produced similar ssNMR results when added to M2TM_{S31N} (Figure 4) in that the change in structure always reflected a uniform change in helical tilt. **8** is a new derivative, which was synthesized to test the effect of C-methylation to binding compared to N-methylation in **6**. The measured helical tilt angles are 28° for **6**, 31° for **7**, and 33° for **8**, with the latter compound yielding results that are similar to those induced by **5** (Table 5). For **5-8**, there is no evidence for partial binding, since the unbound states are not observed in the spectra with drugs present. With **5**, V28 appears to have multiple resonances (Figure 3) clustered on an anisotropic chemical shift of 160 ppm and a dipolar interaction of 4 kHz. The structural differences would be small, i.e. no more than 1° change in the orientation of the V27-V28 peptide plane with respect to the bilayer normal. This suggests that even with **5** on the timescale of 10-100µs there is no significant evidence for asymmetry in this tetrameric structure, i.e. there is no evidence from these three labeled sites that M2TM_{S31N} bound with different compounds **1**, **5-8** forms a dimer of dimer, as has been suggested for the S31N structure.^{36,37} If such structures are present they must interconvert on a timescale faster than the difference in spectral frequencies in Hz. Furthermore, if this was occurring with significantly different structures there would be a reduction in the width and height of the PISA wheel, which was not observed. The intensity of the resonances varies, again especially for **5**, suggesting that the compound may have competing binding interactions with the pore leading to heterogeneity in the frequencies, the weakening of the A30 resonance and the small dispersion of the V28 resonances as described above. These dynamics are in sharp contrast to the intense resonance for I42 for M2TM_{S31N} bound with **5**. The uniformity of the resonance intensities that result from the interaction with heterocyclic compounds **6-8** may suggest less dynamics and more potent binders than **5** to M2TM_{S31N}.

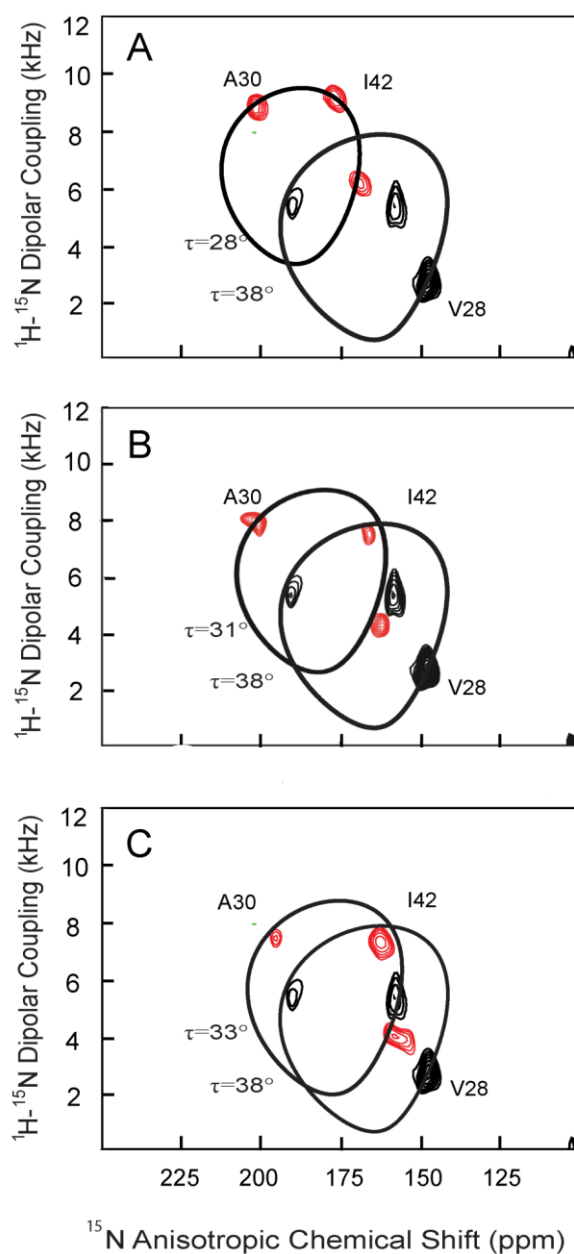


Figure 4. Superimposed PISEMA spectra of the M2TM_{S31N} (residues 22-46), ¹⁵N labeled at residues V28, A30, and I42, in DMPC bilayers uniformly aligned on glass slides with (red) and without (black) **6**, **7**, and **8** (Figures 4 A-C respectively). Assignments without drug were made based on the known structure and spectra of M2TM_{WT}.³⁵ Assignments with drug follow the rotational orientation of the helices. Theoretical PISA wheels calculated for an ideal helix $[(\phi, \varphi)] = (-60^\circ, -45^\circ)$ with varying tilt angles relative to the bilayer normal were superimposed on drug bound M2TM_{S31N} spectra (Fig. 4A-C). All spectra were collected at 720 MHz, pH 7.5, 303K. The molar ratio of lipid/protein was 30:1.

2.3.4 MAS spectra

To evaluate further the effect of **6** binding to M2TM_{S31N}, 2D N-C α correlation magic angle spinning (MAS) ssNMR experiments were performed using uniformly ¹³C, ¹⁵N-labeled V7, A30, S31 and G34 M2TM_{S31N}(¹³C, ¹⁵N-VANG labeled M2TM_{S31N}). The labeling used aims to explore the binding interactions of amantadine analogs into M2TM_{S31N} pore through measuring the effect of binding to the chemical shifts of V27, A30, G34 and N31. In the M2TM_{WT} the binding area includes the expanded area including V27, A30 and also G34, S31.^{4,5} Spectra were obtained (Figure 5) for both the *apo* protein (blue) and for **6** bound (red) to the labeled M2TM_{S31N}. Addition of the drug to the M2TM_{S31N} sample resulted in chemical shift changes for N31 and G34 of 1.2 and 2.1 ppm, respectively, V27 and A30 resonances remain unchanged, suggesting that they are not involved in binding, while the isotropic chemical shift perturbation of the N31 and G34 residues suggest the drug binding site for M2TM_{S31N} suggesting either direct hydrogen bonding with the backbone or indirect hydrogen bonding through water molecules.²¹ Significant ¹⁵N and/or ¹³C α chemical shift changes at V27, S31, G34 have been reported when rimantadine is bound to M2TM_{WT}^{20,21} with S31 experiencing a dramatic 7 ppm shift relative to the *apo* state.²¹ Despite the observed chemical shift changes at residues N31 and G34 when **6** bound to the M2TM_{S31N}, cross peak intensity was not increased as was observed for the WT full length M2 in complex with rimantadine.²¹ This suggests that the conformational heterogeneity of M2TM_{S31N} was not increased for these residues in the presence of the drug. A reduction in dynamics which is in agreement with narrower linewidths would be anticipated with a specific binding site or a significant reduction in hydration due to drug induced desolvation of the binding pocket. The narrower linewidths and increased anisotropic chemical shifts for the M2TM_{WT} and M2TM_{S31N} bound to **5** (Figures 2, 3) illustrate reduced dynamics and weaker or less specific binding of the drug to the M2TM_{S31N}.

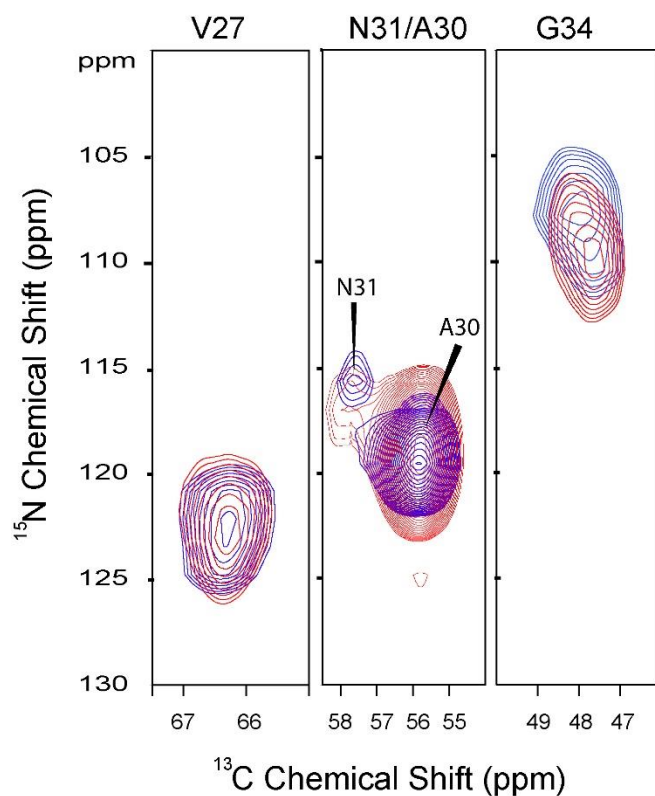


Figure 5. Superimposed 2D strip plots for $^{15}\text{N}/^{13}\text{C}$ (NCA) correlation spectra of $^{13}\text{C},^{15}\text{N}$ -V₂₇A₃₀N₃₁G₃₄ labeled M2TM_{S31N}(residues 22-46) in DMPC lipid bilayers with (red) and without (blue) compound 6. Spectra were collected at 600 MHz proton frequency, at pH 7.5, 10-kHz spinning rate and a calibrated temperature at sample of 263K.

2.3.5 MD simulations of M2TM - aminoadamantanes complexes

2.3.5.1 Starting structure of protein ligand-complex

MD simulations of the complexes between **1**, 2-alkyl-2-aminoadamantanes **2-5** and cyclic derivatives **6-10** with both M2TM_{WT} and M2TM_{S31N} provide insights for the binding interactions and possible structural changes in the binding area. All of the ligands 1 amino groups were considered to be protonated according to model calculations performed previously for ligands **1** and **6**.^{25,26} The structure of the complex M2TM_{WT}-**1** (PDB ID 2KQT4^{a,5b}) was used as a starting structure for the simulations of M2TM_{WT}-ligand complexes and of M2TM_{S31N}-ligand complexes. The PDB ID 2KQT4^{a,5b} structure was chosen since it was determined at pH 7.5 and DMPC planar bilayers and vesicles^{4a,5b}, i.e., similar conditions to those used in our simulations. Subsequently only small structural changes are to be expected in M2TM structure during MD simulations of its complexes with ligands and the equilibration phase should be short. It has been shown that the stability of the binding region for **1** in the M2TM tetramer is increased considerably when using DMPC compared to other lipids.^{38,39,40,41} In addition, 2KQT (ref. 5b) should be considered as the best structure of the amantadine bound state of M2TM since it utilized both isotropic chemical shift restraints and all of the orientation restraints of an earlier structure characterized by Cross and coworkers (see ref. 4a). The structure of the M2TM_{S31N}-ligand (**1-10**) complexes were generated from M2TM_{WT}-complexes by mutating S31 to N. (see also 3.8.2).

2.3.5.2 Complexes of ligands with M2TM_{WT}

The MD simulations of the M2TM_{WT}-ligand complexes reached equilibration in less than 40 ns with the protein system having full flexibility. The RMSDs values (Table 3) were ≤ 1.6 Å for M2TM C α -carbons with respect to the initial structure of the production period^{4a,5b} suggesting that M2TM_{WT}-ligand (**1-8**) complexes were very stable and the M2TM tetramer structure was considerably unchanged in the course of the simulation. The mean values of the N-terminal and the C-terminal helical tilt of M2TM_{WT} for the complexes with **1**, **5** from the corresponding MD trajectories were measured to be 31°, 18° and 31°, 19° respectively and are in very good agreement with the values of 32°, 22° and 32°, 22° determined by OS ssNMR (Table 2). As noted above the starting structure 2KQT4^{a,5b} having helical domain tilt angles of 31°, 19° were determined in similar conditions to those used in our MD simulations by Cross and coworkers.^{4a} Even so these findings suggest that the ligand-M2TM_{WT} complex was successfully equilibrated and the conditions were well adjusted to produce consistent results. Consistent with the experimental findings^{5b,c} and previous observations,^{25,26} the ammonium group of the aminoadamantane compounds was oriented towards the C-terminus with angles of $< 77^\circ$ between the C-N bond of the ligand and the membrane's normal (Table 3). The complexes of compounds **1-8** inside the M2TM lumen are stabilized through: a) formation of hydrogen

bonds between their ammonium group and water molecules in the region between H37 residues and the ligand and b) van der Waals interactions between adamantyl group and a lipophilic pocket formed by V27 and A30 side chains (see Figure 6). This binding area is in accordance (a) with the ^{15}N chemical shifts perturbations for V27, A30 and S31 in complexes between **1** or 3-azaspiro[5,5]undecane and M2TM_{WT} compared to the *apo* M2TM_{WT}.³⁸ and, (b) with the measured distance of 4.5 Å between G34Ca and the methyl group of rimantadine from REDOR ssNMR experiments in studies of the full length protein.²¹ In addition, for complexes of M2TM_{WT} with **1-8**, the distance between the adamantyl ring of the ligand and the center of mass of the four V27 (V27-Ad) varies between 4 and 4.9 Å, and the distance between the adamantyl ring of the ligand and the center of mass of the four A30 (A30-Ad) varies between 0.5 and 1.4 Å (Table 3). The position of the adamantyl ring inside the lumen was similar for ligands **2-8** differing from **1** only by 0.2-0.6 Å. To account for the position of the ligands towards the C-end we measured the distance between the center of mass of the four V27 and the ammonium nitrogen of the ligand (V27-N⁺) which varied between 7.1 and 7.8 Å (Table 3). According to the measures in Table 3 hydrogen bonding ability is higher for the subset of ligands **1-5, 9, 10** than for the subset **6, 8** or **7**. Thus **1-5, 9, 10** can form on average 3 hydrogen bonds with neighboring water molecules, **6, 8** can form 2 hydrogen bonds, and **7** one hydrogen bond respectively (Table 3). This is what was expected since **1-5, 9, 10** have a primary ammonium group, **6, 8** have a secondary ammonium group and **7** have a tertiary ammonium group. For ligands **3-8** which include a carbon substituent at C-2 adamantane position the molecule is rotated in order to avoid repulsive van der Waals forces of the alkyl group with the symmetric M2TM pore. The average angle between the pore axis and C-N bond vector was increased progressively according to the alkyl group size, i.e., from 13.5° for **1** to 25-35° for **2-8** (Table 3). Although all ligands **1-8** have similar binding mode as shown from the OS ssNMR spectra of complexes including **1, 5** (Figure 2), a subtle compromise between hydrogen bonding and hydrophobic interactions with key pore residues, such as V27, A30, affects the ligand tilt inside the pore and its different binding strength as shown by the ITC results (Table 1). The adamantyl ring is slightly toward the N-terminus compared to the A30/S31 C α , producing a region without water molecules. Snapshots of the simulation complexes with **5, 6** are shown in Figure 6.

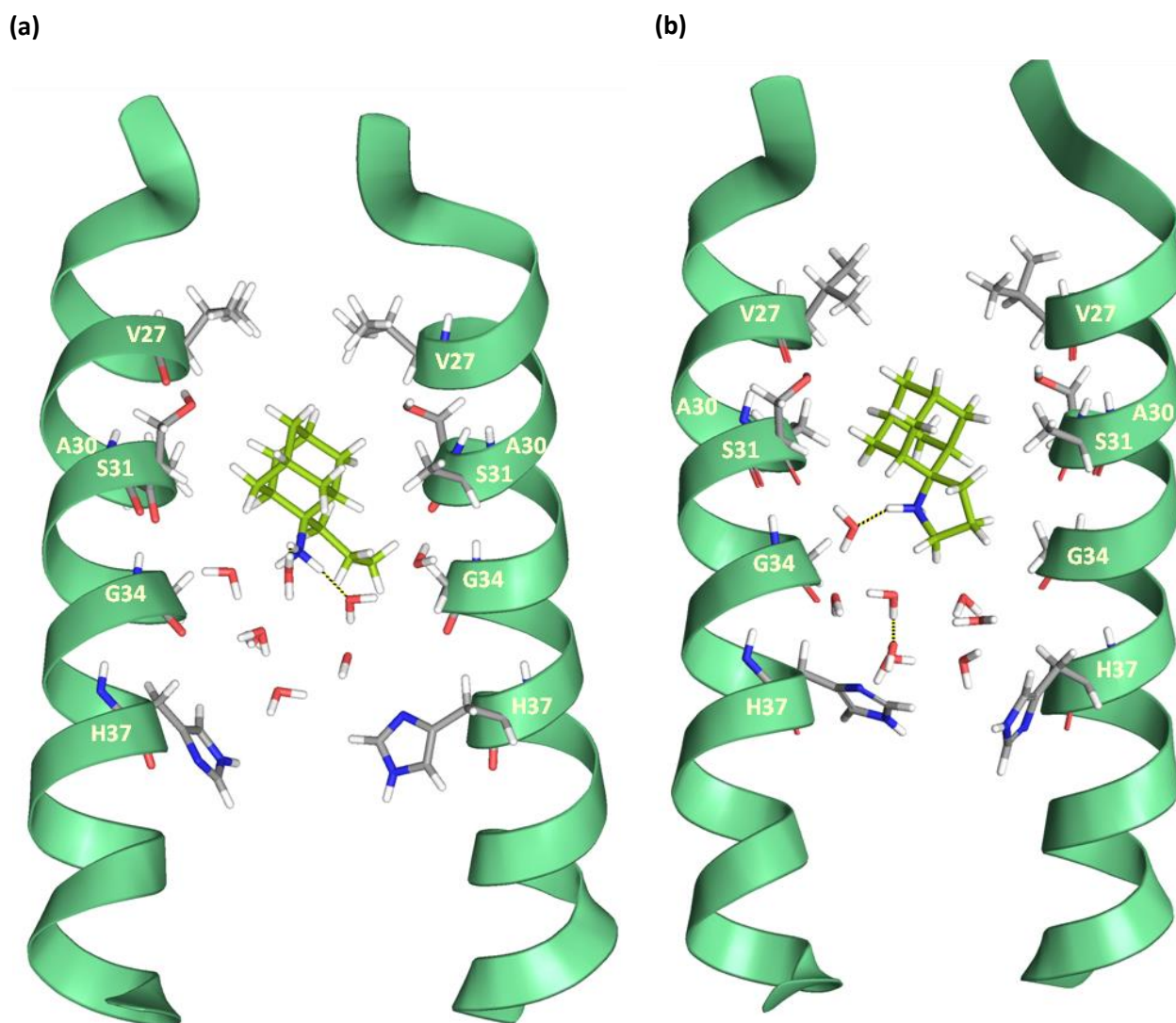


Figure 6. Snapshots from the simulation of ligands bound to M2TM_{WT}. Waters within 10 Å from ligand are shown. **(a)** **5** bound to M2TM_{WT}. Eight waters are shown between the ligand and H37 residues. Three hydrogen bonds between the secondary ammonium group of the ligand and three water molecules are shown (see Table 3). Hydrogen bonding together with van der Waals interactions of the adamantane core with V27 and A30 stabilize the ligand inside the pore with its ammonium group oriented towards the C-terminus. **(b)** **6** bound to M2TM_{WT}. Eight waters are shown between the ligand and H37 residues. Two hydrogen bonds between the secondary ammonium group of the ligand and two water molecules are shown (see also Table 3). Hydrogen bonding together with van der Waals interactions of the adamantane core with V27 and A30 stabilize the ligand inside the pore with its ammonium group oriented towards the C-terminus.

Table 3. Structural and dynamic measures from MD simulations of M2TM_{Udown}-ligand complexes in DMPC bilayer.

Ligand ¹	RMSD (C-alpha) ²	Angle C-N vector ³	V27-Ad ⁴	V27-N ⁺ ⁵	A30-Ad ⁶	G34-Ad ⁷	H-bonds ⁸	RMSF ligand ⁹
1	1.6 ± 0.3	13.5 ± 6.7	4.5 ± 0.3	7.2 ± 0.2	1.1 ± 0.2	5.5 ± 0.3	2.7 ± 0.5	0.2
2	1.4 ± 0.2	25.7 ± 9.0	3.9 ± 0.2	7.1 ± 0.2	1.4 ± 0.3	6.1 ± 0.3	2.6 ± 0.6	0.1
3	2.1 ± 0.4	33.5 ± 7.2	4.3 ± 0.3	7.3 ± 0.3	0.9 ± 0.3	5.2 ± 0.3	2.7 ± 0.5	0.3
4	1.3 ± 0.2	35.2 ± 8.8	4.0 ± 0.2	7.2 ± 0.2	1.2 ± 0.3	5.9 ± 0.3	2.6 ± 0.6	0.3
5	1.3 ± 0.2	28.2 ± 7.1	4.6 ± 0.2	7.5 ± 0.2	0.7 ± 0.2	5.2 ± 0.3	2.7 ± 0.5	0.2
6	1.4 ± 0.2	77.0 ± 14.1	4.3 ± 0.3	7.0 ± 0.5	0.9 ± 0.3	4.3 ± 0.3	2.1 ± 0.4	0.3
7-S	1.6 ± 0.3	37.2 ± 10.1	4.3 ± 0.3	7.3 ± 0.3	0.9 ± 0.3	5.3 ± 0.3	0.8 ± 0.4	0.3
7-R	1.3 ± 0.2	33.5 ± 7.0	4.3 ± 0.3	7.3 ± 0.3	0.9 ± 0.3	5.3 ± 0.3	0.8 ± 0.4	0.3
8-S	1.5 ± 0.2	30.2 ± 5.5	4.6 ± 0.3	7.6 ± 0.3	0.7 ± 0.2	5.1 ± 0.3	1.9 ± 0.3	0.3
8-R	1.1 ± 0.2	33.7 ± 6.0	4.9 ± 0.3	7.8 ± 0.3	0.5 ± 0.2	4.5 ± 0.3	2.0 ± 0.2	0.2
9	2.4 ± 0.5	73.2 ± 23.4	3.7 ± 0.6	5.5 ± 0.8	2.6 ± 0.5	7.4 ± 0.6	2.7 ± 0.5	0.2
10	2.1 ± 0.3	41.7 ± 16.2	3.5 ± 0.4	2.1 ± 0.7	4.7 ± 0.7	6.5 ± 0.5	2.5 ± 0.7	0.2

¹ See Scheme 1.

² Maximum root-mean-square deviation (RMSD) for C α atoms of M2TM relative to the initial structure (PDB entry: 2KQT) after root-mean-square fitting of C α atoms of M2TM; in Å.

³ Angle between the vector along the bond from the carbon atom of the adamantane core to the ligand nitrogen atom and the normal of the membrane; in degree.

⁴ Mean distance between the center of mass of V27 and the center of mass of the adamantane core calculated using Gromacs tools; in Å.

⁵ Mean distance between the center of mass of V27 and ammonium nitrogen of the ligand calculated using Gromacs tools; in Å.

⁶ Mean distance between the center of mass of A30 and the center of mass of the adamantane core calculated using Gromacs tools; in Å.

⁷ Mean distance between the center of mass of G34 and the center of mass of the adamantane core calculated using Gromacs tools; in Å.

⁸ Mean number of H-bonds between a ligand's ammonium group and waters.

⁹ Root-mean-square fluctuation of a ligand after fitting of the ligand to the average structure considering all ligand atoms; in Å.

The MD simulations suggest that the M2TM_{WT}-ligand complex stability is reduced when a sizeable adduct is attached to adamantane, i.e., the M2TM pore does not efficiently accommodate the large adducts in compounds **9** and **10**. This is in accordance with the weak or no binding respectively of these drugs according to the ITC results (Table 1). For example, the MD simulations showed that the stability of the complex is considerably reduced in the case of **10** where after 80 ns the ligand is shifted toward the N-terminus; the mean distances of the trajectory V27-Ad, A30-Ad and V27-N⁺ are 3.5 Å, 4.7 Å and 2.1 Å, respectively, suggesting a loosening of the M2TM-complex integrity at the N-terminus (a snapshot of the simulation complex with **10** is depicted in Figure 7).

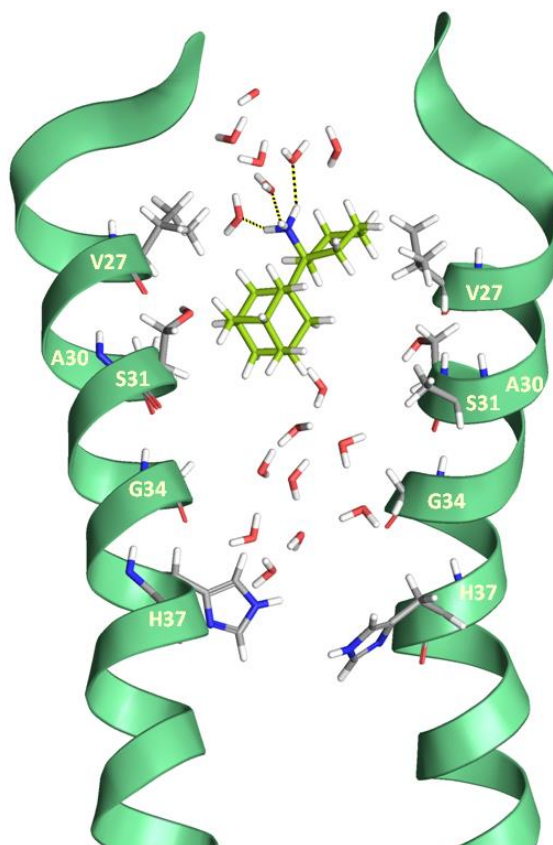


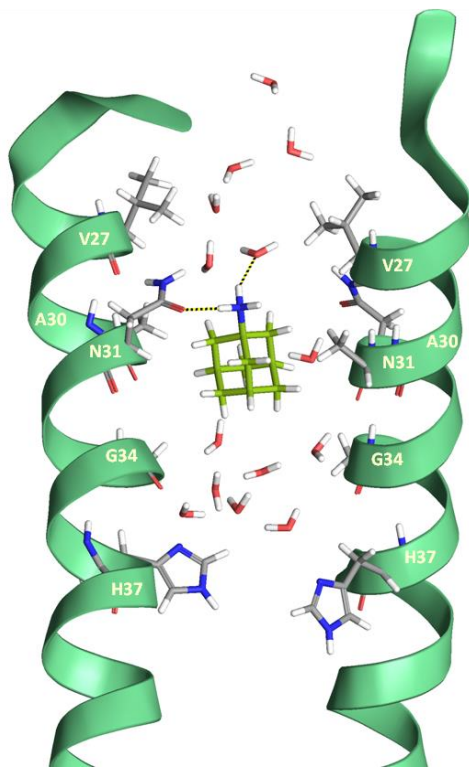
Figure 7. Snapshots from the simulation of ligand **10** bound to M2TM_{WT}. Waters within 10 Å from ligand are shown. Nine waters are shown between the ligand and His37 residues and seven waters between Asn31 and the mouth of the pore. Three hydrogen bonds between the ammonium group of the ligand and three waters are shown (see Table 3).

2.3.5.3 Complexes of ligands with M2TM_{S31N}

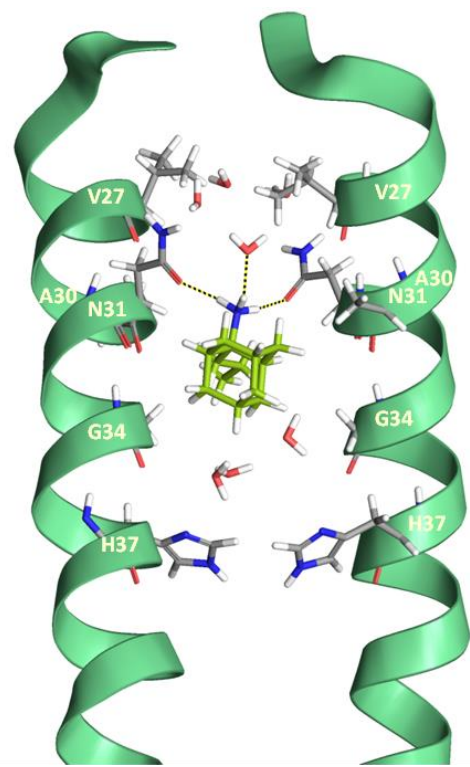
In the starting configuration of M2TM_{S31N}-aminoadamantane ligand complex the ammonium group points toward the C-terminus forming H-bonds with waters between the ligand and H37 residues as in the M2TM_{WT} pore. The MD simulations of the complexes between M2TM_{S31N} and **1-8** reach equilibration in less than 60 ns with the protein system having full flexibility. In complexes with M2TM_{S31N} the ligand is more mobile inside the pore having a propensity to orient its ammonium group toward the N-terminus, in contrast to M2TM_{WT}-ligand complexes where the ligand forms a strong complex with ammonium group oriented toward the C-terminus. Thus, after a few ns of unrestrained dynamics the ligand moves toward the C-terminus by ~2 Å, probably because the adamantyl group is repelled by the polar N31 side chains resulting in the loss of the V27 lipophilic pocket, and the molecule rotates 180° through an attraction to the polar environment around N31. This finding is consistent with the narrower linewidths and larger chemical shifts changes for M2TM_{WT} when bound with compound **5** compared to M2TM_{S31N} as observed in the ssNMR spectra suggesting a

stronger binding interaction with M2TM_{WT}. In addition waters are transferred from the region between the ligand and H37 to the area around N31 where the drug's amine can interact with the carbonyls of the N31 amide groups and waters around the amide side chains. Snapshots of the MD simulation complexes of M2TM_{S31N} with **1**, **5**, **6** and **10** are depicted in Figure 8. The MD runs showed that by progressively increasing the size of the adduct connected to the adamantyl moiety in complexes with **2-8** the ammonium group orientation turns toward the N-terminus, and the drug keeps this orientation during the entire simulation period. While this change was observed for **1** after ~ 20 ns of production, the time needed for the aminoadamantane ligand to rotate towards the N-terminus may be increased for some larger adducts. For example, in the case of **5** the ligand's ammonium group keeps its orientation toward the C-terminus during the first 40 ns and then the molecule turns towards the N-terminus until the end of the 80 ns production time. While no significant conformational change was observed for M2TM_{S31N} tetramer in its complexes with **1-8** during the production period, the RMSDs for M2TM_{S31N} C α -carbons were ≤ 2.8 Å from the initial structure^{4a,5b}, i.e., 1 to 1.5 Å higher than the RMSDs for M2TM_{WT} C α -carbons suggesting less dynamics for M2TM_{WT} complexes (Table 4). The mean values of the helical tilt angles for the complexes of **1**, **5-8** with M2TM_{S31N} from the corresponding MD trajectories were measured to be ~ 34°, 31°, 28°, 33°, 31° respectively and are close to 38°, 33°, 28°, 31° and 33° determined by OS ssNMR (Table 5). The uniformly tilted helical structure is a conversion form the initial kinked state in the 80-ns MD, where the starting structure reflects a homology model of 2KQT.^{4a,5b} Here the major finding is the lack of kinked helices in M2TM_{S31N} compared to the OS ssNMR structure when **1** binds M2TM_{WT} suggesting that the MD simulations describe well the ligand-M2TM_{S31N} structure.

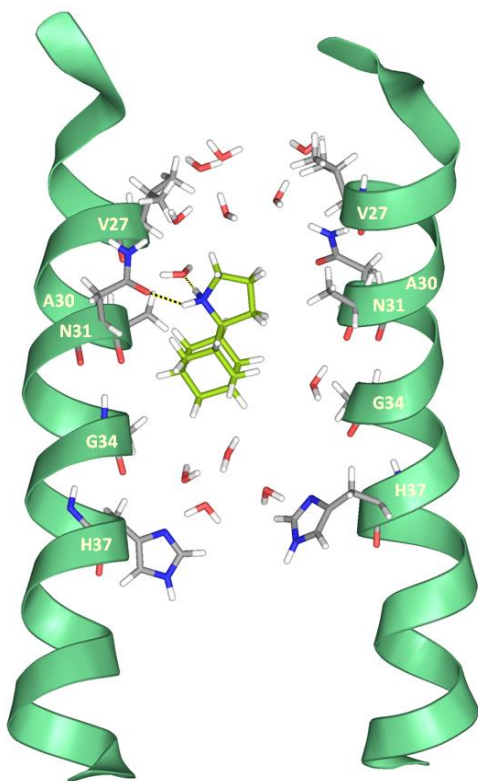
(a)



(b)



(c)



(d)

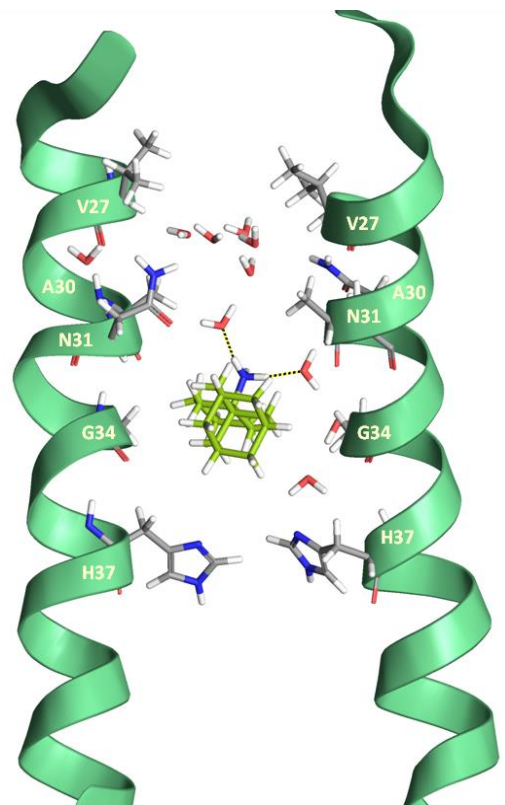


Figure 8. Snapshots from the simulation of various ligands bound to M2TM_{S31N}. Waters within 10 Å from ligand are shown. Several waters are shown covering the region between the mouth the ligand and H37 residues. Few waters may be found between the ligands and the wall of the pore, suggesting a relatively free passage through the lumen. **(a) 1** bound to M2TM_{S31N}. Seven waters are shown between the ligand and H37 residues and six waters between N31 and the mouth of the pore. In the depicted shapshot one hydrogen bond between the ammonium group of the ligand and one water, and one hydrogen bond between the ligand and the carbonyl group of N31 amide side chain are shown (see also Table 4). No efficient van der Waals interactions can be formed for the adamantane core in the region close to A30 and the ligand can't be stabilized inside the pore. **(b) 5** bound to M2TM_{S31N}. Three waters are shown between the ligand and the region close to H37 residues and three waters between N31 and the mouth of the pore. One water is shown between the ligand and the wall of the pore. One hydrogen bond between the ammonium group of the ligand, and one water and two hydrogen bonds between the ligand and the carbonyl groups of two N31 amide side chain are shown (see also Table 4). Hydrogen bonding together with weak van der Waals interactions between the adamantane core and the cleft between A30 and G34 can weakly stabilize the ligand inside the pore with its ammonium group oriented towards the N-terminus. **(c) 6** bound to M2TM_{S31N}. Four waters are shown between the ligand and H37 residues and seven waters between N31 and the mouth of the pore. Two hydrogen bonds between the ammonium group of the ligand and the carbonyl group of N31 amide side chain and one water are shown (see also Table 4). One water is shown between the ligand and the wall of the pore. Hydrogen bonding together with weak van der Waals interactions between the adamantane core and the cleft between A30 and G34 can weakly stabilize the ligand inside the pore with its ammonium group oriented towards the N-terminus. **(d) 10** bound to M2TM_{S31N}. Two waters are shown in the region between the ligand and H37 residues and six waters between N31 and the mouth of the pore. One water is shown between the ligand and the wall of the pore. Two hydrogen bonds between the ammonium group of the ligand and two waters are shown (see also Table 4). Hydrogen bonding together with weak van der Waals interactions between the adamantane core and the cleft between A30 and G34 can moderately stabilize the ligand inside the pore with its ammonium group oriented towards the N-terminus.

Table 4. Structural and dynamic measures from MD simulations of M2TM_{S31N}-ligand complexes in DMPC bilayer.

Ligand ¹	RMSD (C-alpha) ²	Angle C-N vector ³	V27-Ad ⁴	V27-N ⁵	A30-Ad ⁶	G34-Ad ⁷	H-bonds with N31-CO ⁸	H-bonds with waters ⁹
1	2.6 ± 0.4	112.7 ± 26.5	5.2 ± 0.7	3.9 ± 0.7	1.4 ± 0.9	5.1 ± 1.0	1.2 ± 0.9	1.6 ± 1.0
2	1.9 ± 0.3	146.3 ± 20.0	6.2 ± 0.5	4.2 ± 0.9	0.8 ± 0.5	3.6 ± 0.4	0.9 ± 0.8	1.8 ± 0.8
3	1.7 ± 0.3	138.1 ± 13.6	6.2 ± 0.6	3.9 ± 0.4	0.9 ± 0.4	4.5 ± 0.6	1.6 ± 0.6	1.2 ± 0.6
4	2.3 ± 0.4	145.5 ± 14.5	6.3 ± 0.7	2.4 ± 0.1	1.2 ± 0.6	3.8 ± 0.8	1.6 ± 0.7	1.0 ± 0.5
5	2.5 ± 0.9	89.7 ± 40.2 ¹⁰	6.1 ± 0.2	6.8 ± 0.7	0.2 ± 0.7	4.8 ± 1.9	0.1 ± 0.2	2.8 ± 0.4
6	2.7 ± 0.6	148.2 ± 11.9	6.6 ± 0.8	3.8 ± 0.7	1.4 ± 0.7	3.3 ± 0.7	0.6 ± 0.6	1.2 ± 0.6
7-R	2.6 ± 0.4	139.6 ± 24.3	7.5 ± 0.8	4.8 ± 0.7	2.4 ± 0.7	2.8 ± 0.8	0.1 ± 0.2	0.8 ± 0.4
7-S	2.8 ± 0.7	143.8 ± 21.6	7.1 ± 0.9	4.4 ± 0.7	1.8 ± 0.7	3.4 ± 0.7	0.5 ± 0.5	0.3 ± 0.4
8-R	2.5 ± 0.4	148.9 ± 15.4	7.4 ± 0.7	4.5 ± 0.5	2.1 ± 0.6	3.7 ± 0.6	0.8 ± 0.7	0.7 ± 0.6
8-S	2.2 ± 0.5	144.2 ± 15.0	6.8 ± 0.5	4.1 ± 0.5	1.5 ± 0.5	3.5 ± 0.7	0.5 ± 0.5	1.3 ± 0.6
9	2.4 ± 0.5	73.2 ± 23.4	4.1 ± 0.6	6.5 ± 0.7	2.7 ± 0.5	7.4 ± 0.6	0.03	2.7 ± 0.5
10	0.7 ± 0.2	156.8 ± 25.3	8.9 ± 0.1	6.8 ± 0.8	3.7 ± 0.1	2.7 ± 1.0	0.01	2.8 ± 0.6

¹See Scheme 1.

²Maximum root-mean-square deviation (RMSD) for C α atoms of M2TM relative to the initial structure (PDB entry: 2KQT) after root-mean-square fitting of C α atoms of M2TM; in Å.

³Angle between the vector along the bond from the carbon atom of the adamantane core to the ligand nitrogen atom and the normal of the membrane; in degree.

⁴Mean distance between the center of mass of the four V27 of the pore and the center of mass of the adamantane core calculated using Gromacs tools; in Å.

⁵Mean distance between the center of mass of the four V27 of the pore and ammonium nitrogen of the ligand calculated using Gromacs tools; in Å.

⁶Mean distance between the center of mass of the four A30 of the pore and the center of mass of the adamantane core calculated using Gromacs tools; in Å.

⁷Mean distance between the center of mass of the four G34 of the pore and the center of mass of the adamantane core calculated using Gromacs tools; in Å.

⁸Mean number of H-bonds between a ligand's ammonium group and N31 carbonyl group.

⁹Mean number of H-bonds between a ligand's ammonium group and waters.

¹⁰5 has values ~ 30° for the first 40 ns and ~ 150° for the last 40 ns resulting to a mean of ~ 90°.

Table 5. Mean helical tilt values relative to the bilayer normal from MD simulations of **5-8** in complex with M2TM_{S31N} in DMPC bilayer.

Ligand ¹	MD simulations ²	Experiment ^{3,4}
1	34° ± 4°	38° ± 1°
5	31° ± 6°	33° ± 1°
6	28° ± 5°	28° ± 1°
7	33° ± 4°	31° ± 1°
8	31° ± 4°	33° ± 1°

¹ See Scheme 1.

² Calculated using Gromacs tools.

³ This study.

⁴ Helical tilt is uniform.

For most of the ligands **1-8** the mean angle between the C-N bond vector and the normal of the membrane is > 140° for more than 40 ns of the simulation reflecting the propensity of ammonium group to orient towards the N-terminus (Table 4). The distance between the center of mass of the four V27 and the adamantyl ring of the ligands **1-8** (V27-Ad) was longer than in complexes with the M2TM_{WT}, which is consistent with an orientation of the ammonium group towards the N-terminus. On average, the adamantyl ring in the M2TM_{S31N} was found to be ~ 1-2 Å toward the C-terminus compared to the M2TM_{WT} complexes. Accordingly, the distance between the center of mass of the four V27 and the ligand's amine nitrogen in M2TM_{S31N} complexes was shorter by 3-3.5 Å compared to M2TM_{WT} complexes. In addition especially for the ligands with large adducts the adamantyl ring is positioned toward the C-terminus close to G34 (see distances A30-Ad and G34-Ad in Table 4) whereas in the M2TM_{WT} complexes, adamantyl ring is shifted toward the N-terminus embraced by V27 and A30. The sum of the H-bonds between the ammonium groups of the ligands and waters and between the ammonium groups and the N31 side chain amides was on average three hydrogen bonds for the primary ammonium groups (ligands **1-5**), two hydrogen bonds for secondary (ligands **6** and **8**) and one hydrogen bond for tertiary ones (ligand **7**) (Table 4). Compounds **9** and **10** form three hydrogen bonds only with water molecules in the vicinity of N31 close to the wall of the pore, possibly because the ammonium group is sterically crowded between the adamantyl and cycloalkane rings and cannot reach the side chains carbonyls of N31 (Table 4). In compound **10**, due to the large hydrocarbon framework, the adamantyl ring moves more than in any other compound toward the C-terminus, i.e., the distance between the center of mass of the four V27 to the adamantyl cage was 3.7-2.3 Å longer than **1-8** to fit inside the pore close to G34 and the distance between the center of mass of the four G34 to the adamantyl cage was 2.7 Å. A snapshot of the simulation complex with ligand **10** is depicted in Figure 7.

2.3.5.4 Additional MD simulations runs

The MD simulation for M2TM_{S31N}-**1** complex was run seven times. In five runs and starting with different N31 rotamers (as discussed above) the same flipping behaviour was observed. Noteworthy in one simulation run, after **1** turning its ammonium towards the N-terminus was shifted considerably towards the N-terminus and moves out of the pore after unfolding partially N-terminus. In another trial **1** keeps the ammonium group pointing to the C-terminus till the end of the 80 ns simulation run (a close-up view of a snapshot is depicted in Figure 9). Three repeats were also performed for **2**, **5** and **6**. In one trial **2** and **5** kept the ammonium group pointing to the C-terminus while in **6** all trials resulted to a N-ward orientation for the ammonium group. As discussed above in one of the three MD runs **1** or **5** keep the ammonium group pointing to the C-terminus till the end of the 80 ns simulation and the lipophilic framework of **5** fitted between A30 and G34 and this may explain the dynamics for V28 residue suggested from OS ssNMR results (see Figure 3); in these trajectories ligands move ~ 2.5 Å above the relevant position in M2TM_{WT} pore (see Table 6).

Table 6. Structural and dynamic measures from MD simulations of M2TM_{S31N}-ligand complexes in DMPC bilayer in which **1** and **5** keep a C-ward orientation.

Ligand ¹	RMSD (C-alpha) ²	Angle C-N vector ³	V27-Ad ⁴	V27-N ⁺⁵	A30-Ad ⁶	G34-Ad ⁷	H-bonds with Asn31-CO ⁸	H-bonds with waters ⁹
1	1.9 ± 0.3	65.5 ± 5	7.0 ± 0.4	8.2 ± 0.2	1.7 ± 0.4	3.0 ± 0.4	0.5 ± 0.8	2.4 ± 0.8
5	2.4 ± 0.3	31.2 ± 7	5.3 ± 0.5	6.9 ± 0.6	1.1 ± 0.4	5.3 ± 0.4	0	2.8 ± 0.4

¹ See Scheme 1.

² Maximum root-mean-square deviation (RMSD) for C α atoms of M2TM relative to the initial structure (PDB entry: 2KQT) after root-mean-square fitting of C α atoms of M2TM; in Å.

³ Angle between the vector along the bond from the carbon atom of the adamantane core to the ligand nitrogen atom and the normal of the membrane; in degree.

⁴ Mean distance between the center of mass of the four V27 of the pore and the center of mass of the adamantane core calculated using Gromacs tools; in Å.

⁵ Mean distance between the center of mass of the four V27 of the pore and ammonium nitrogen of the ligand calculated using Gromacs tools; in Å.

⁶ Mean distance between the center of mass of the four A30 of the pore and the center of mass of the adamantane core calculated using Gromacs tools; in Å.

⁷ Mean distance between the center of mass of the four G34 of the pore and the center of mass of the adamantane core calculated using Gromacs tools; in Å.

⁸ Mean number of H-bonds between a ligand's ammonium group and N31 carbonyl group.

⁹ Mean number of H-bonds between a ligand's ammonium group and waters.

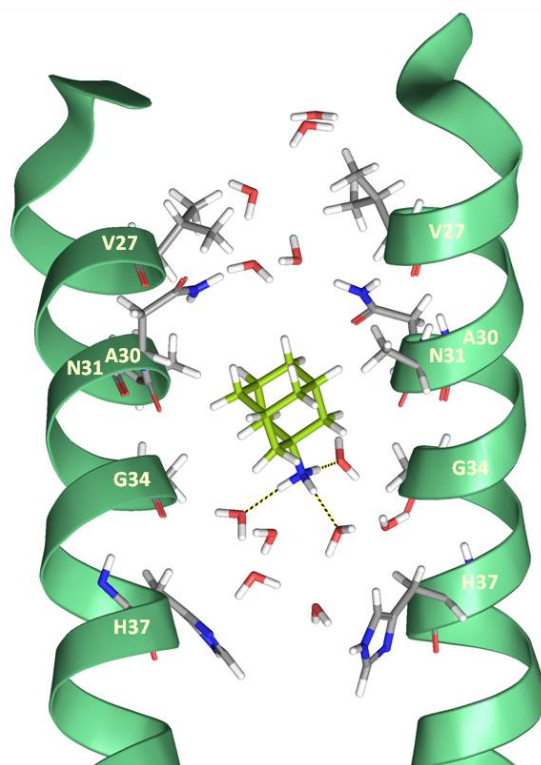


Figure 9. Snapshots from the simulation of ligand **1** bound to M2TM_{S31N}. **1** bound to M2TM_{S31N} keeping a C-ward orientation during 80 ns of the MD simulation. Waters within 10 Å from ligand are shown. Five waters are shown between the ligand and His37 residues and five waters between Asn31 and the mouth of the pore. Three hydrogen bonds between the ammonium group of the ligand and three waters are shown (see Table 6). No efficient van der Waals interactions can be formed for the adamantane core in the region close to A30 and the ligand can't be stabilized inside the pore.

2.3.6 Electrophysiology results of aminoadamantanes blockage using full-length M2

1, its isomer **2**, and three compounds with sizeable adducts (**5**, **6**, and **9**) were assessed for their ability to inhibit low pH-dependent proton currents induced by full-length M2 protein (A/California/07/2009 with M2_{N31}) in transiently-transfected, voltage clamped HEK cells (Table 7).^{10a,42} Data for compounds **1**, **2**, **5** were reported previously.^{10a} It was found that none of these compounds blocked inward proton currents better than **1**, either following a standard 3-minute exposure to compound or after prolonged exposure for 30 minutes. These EP-based results indicated that the compounds were unable to block the full-length M2 channel encoding N31. However, when this M2 protein was modified to encode the **1**-sensitive S31 sequence (through an N31S mutation), all compounds inhibited proton currents with IC₅₀s of 10 μM or less (Table 7); by increasing adduct size the blocking effect of inward proton currents is reduced.

Table 7. Block of full-length M2-dependent currents by select compounds in transfected HEK cells.¹

Compound	A/California/07/2009 (H1N1) M2: N31		A/California/09/2009 (H1N1) M2: S31	
	% Block after 3m	% Block after 30m	% Block after 3m	IC ₅₀
1 ²	14 ± 2 (100 μM; 26)	(N/A)	75 ± 9 (10 μM; 4)	2 ± 3 (3)
2 ²	13 ± 3 (100 μM; 2)	16 (100 μM; 1)	95 ± 8 (10 μM; 2)	2 ± 1 μM (2)
5 ²	0 ± 5 (100 μM; 2)	9 ± 10 (100 μM, 3)	63 ± 5 (10 μM; 2)	7 ± 2 μM (2)
6	4 ± 3 (100 μM; 2)	5 ± 4 (100 μM, 2)	66 ± 6 (10 μM; 3)	5 ± 2 μM (3)
9	4 ± 4 (100 μM; 2)	4 ± 10 (100 μM; 4)	46 ± 2 (10 μM; 2)	10 ± 2 μM (2)

¹ For each compound, percent block of pH-dependent M2 current at listed concentrations (+/- s.e.m.) and/or IC₅₀ (μM) is shown. Parenthesis show number of replicates.

² Data were also reported in Ref. 10a.

2.3.7 In vitro testing of aminoadamantanes against influenza A virus

The antiviral potency of the compounds **1-10** was measured against WSN/33 (H1N1) bearing the M2 S31N mutation⁴³ and its amantadine-sensitive variant WSN/33-M2-N31S²⁶ in MDCK cells with CPE inhibitory assay.^{44, 45} Compounds **1-9** showed sub-micromolar IC₅₀ values against WSN/33-M2-N31S but were inactive against WSN/33 (Table 8). Compound **10** was inactive against both strains. The selectivity index (CC₅₀/IC₅₀) of compounds **4-7** was comparable to **1**. The inhibition efficiency showed stringent head-ammonium group requirements for inhibition of amantadine-sensitive influenza A viruses - a result consistent with ITC and EP results.

Table 8. Antiviral activity of compounds **1-10** against influenza virus A/WSN/33 (H1N1) variants in Madin-Darby canine kidney cells.

Compound	IC ₅₀ (μM) ¹		CC ₅₀ (μM) ²
	A/WSN/33-M2-N31S	A/WSN/33-M2-N31	
1	0.27±0.16	N.A. ³	>100
2	0.42±0.46	N.A.	70.50±25.31
3	0.33±0.10	N.A.	25.63±7.65
4	0.34±0.26	N.A.	>100
5	0.34±0.10	N.A.	>100
6	0.34±0.08	N.A.	>100
7	0.90±0.29	N.A.	>100
8	6.12±2.59	N.A.	>100
9	4.34±2.94	N.A.	>100
10	N.A.	N.A.	>100
Oseltamivir	0.02±0.01	0.02±0.01	Not determined

¹ Mean and standard deviations of the 50% inhibitory concentration (IC₅₀) of at least three independent measures.

² Mean and standard deviations of the 50% cytotoxic concentration (CC₅₀) of at least three independent measures.

³ N.A., not active, maximum concentration tested: 100 μM.

2.4 Discussion

2.4.1 Unraveling the binding differences for aminoadamantanes to M2TM_{S31N} and M2TM_{WT}

Based on the MD simulations results and experimental findings, the molecular basis for weak binding and the inability of aminoadamantanes to effectively block M2_{S31N} is described. The results of the experimental data from ssNMR and ITC experiments directly correlate with the MD simulation results showing that aminoadamantane derivatives are weaker binders in the pore of M2TM_{S31N} compared to M2TM_{WT} and that **5-8** are stronger binders compared to **1-4** against M2TM_{S31N}.

The S31N mutation of M2TM results in a shift of the hydrophobic adamantyl ring toward the C-terminus thereby losing the stabilizing hydrophobic interactions of the V27 isopropyl groups with the adamantyl ring that is present in the M2TM_{WT}. The bulky N31 side chains are oriented toward the N-terminus and the V27 side chains and the ammonium group of the ligands is also turned toward the N-terminus to form significant hydrogen bonding interactions with the polar N31 side chains and surrounding waters. This ammonium group orientational preference of amantadine and rimantadine has been previously noted by Gleed et al.^{17b} and Alhadeff et al.¹⁶. The hydrogen bonding interactions with N31 is consistent with the MAS experimental data performed with compound **6** showing a chemical shift perturbation for N31 and G34 compared to the *apo* M2TM_{S31N}. Distance measurements from ssNMR experiments showed the preference for the ammonium group of the aminoadamantane drugs orienting toward the C-terminus in M2TM_{WT}^{5c} and toward the N-terminus in a complex of M2TM_{S31N} with a conjugate of **1** having a phenylisoxazole polar head.²⁴ In this class of conjugates^{23b-d} additional van der Waals interactions with the N-terminus stabilizes the ligand resulting in potential anti-influenza drugs. Here, where the aminoadamantane ligands, such as **1-8**, are hydrogen-bonded with the polar N31 environment, favorable van der Waals and hydrophobic interactions as those in M2TM_{WT} are missing. In the M2TM_{WT} the adamantyl ring is well accommodated by the V27 and A30 side chains and sizeable adducts such as ligands **5-8** additionally fill the region between A30 and G34 (Figures 1 and 8) but in M2TM_{S31N} the adamantyl ring is close to A30 and in the vicinity of G34 (see Tables 3, 4) lacking a favorable hydrophobic pocket. This is consistent with the absence of chemical shift perturbations for V27 in the NCA MAS spectrum of **6** bound to M2TM_{S31N} in comparison with the *apo* M2TM_{S31N} compared to the significant chemical shift changes at V27, S31, G34 which have been reported when rimantadine is bound to M2TM_{WT} relative to the *apo* state.^{20,21} These structural differences can be clearly observed in Figures 6 and 8. The lack of favorable van der Waals interactions results to less stable complexes and a weaker binding for aminoadamantane ligands consistent with the much smaller K_d values of **5** and **6** by ITC against M2TM_{S31N} compared to M2TM_{WT} (Table 1). In addition, linewidths are narrower for the M2TM_{WT}-complex with **5** compared to the M2TM_{S31N} complex suggesting less dynamics

consistent with stronger interactions for the aminoadamantane derivatives in complexes with M2TM_{WT}. The RMSDs for M2TM α -carbons are 1.0-1.5 Å higher for the trajectories of M2TM_{S31N} compared to M2TM_{WT} complexes further suggesting more dynamics and weaker interactions in the S31N complexes.

In **1** and analogs with small adducts the adamantyl ring has a only a limited hydrophobic contact with A30 and is close to polar N31 side chains which exert repulsive forces on adamantyl ring. It should be noted that trajectories sampled in the MD simulations of ligands in the pore were of 80 ns length, i.e., they are much shorter than the microsecond to millisecond time scales sampled by ssNMR. The MD runs of the complexes of **1-4** with M2TM_{S31N} showed qualitatively that these molecules can't bind M2TM_{S31N} because significant favorable van der Waals interactions are missing. This can be observed from snapshot for complex of **1** with M2TM_{S31N} in Figure 9. In molecules **5-8** with sizeable adducts of the adamantyl ring fill effectively the region between A30 and G34 and the interactions needed for binding are slightly improved resulting in weak binding to M2TM_{S31N} as compared to no binding for **1-4**. This can be observed from snapshots for complexes of **5, 6** with M2TM_{S31N} in Figure 9. Indeed, **1** did not bind as documented by the OS ssNMR spectra (Figure 3), but larger adducts as those present in compounds **5-8** appear to stabilize weak binding of the drug in the region between A30 and G34 (see Figure 8) and this is in accordance with the results from OS ssNMR spectra for weak binding of compounds **5-8** (Figures 3, 4) to M2TM_{S31N}. In addition, we were not able to detect any binding for **1-4** with M2TM_{S31N} using ITC while we obtained approximate binding constants for **5,6,9,10** (Table 1). NMR data were not obtained for **9** and **10** because they produced disordered lipid bilayers. Thus, the results from the combination of simulations and experiments showed that **1** (and similarly **2-4**) did not bind M2TM_{S31N} contrary to the weak binding for **1** previously suggested from short simulations^{17b} but **5-8** having sizeable adducts display weak binding.

While binding strength of aminoadamantanes against M2TM_{WT} was sensitive to modification of the adduct, the M2TM_{WT}-aminoadamantane complex stability was found to be very sensitive to the adduct size, as shown by the ITC and MD simulation results when considering **9** and **10** that produces unstable complexes. The MD simulations clearly show that **10** moves considerably toward the N-terminus of the pore losing specific binding interactions. Ligands **9** and **10** cause a dramatic reduction in affinity for M2TM_{WT} compared to **1-8** but did not affect M2TM_{S31N} affinity, which seems to be similar with that of **5** and **6**. The forces that cause the rotation of the adamantyl ring in the M2 pore appear to be inherent in the shared amine group and are not greatly perturbed by the other ligand variations as characterized by MD and OS ssNMR for adducts **1-4, 5-8** against M2TM_{S31N}. Taken together, the results from the combination of MD simulations, ITC and OS ssNMR showed no binding for **1** and similar in size analogues and only weak binding for sizeable adducts. The binding is more specific as showed by the more stringent head-ammonium group requirements in the binding pocket of M2TM_{WT} than in the M2TM_{S31N} according to the ITC but also as showed by the EP experiments and anti-viral assay results.

Thus, EP experiments indicate that the aminoadamantanes block the S31 but not the N31 full-length M2 protein. Notably, while the secondary gate formed by the V27 residues in the M2TM_{WT}¹¹ has the potential to limit water access to the pore the hydrophilic asparagine sidechains make this environment less hydrophobic and diminish the effectiveness of the V27 gate in the M2TM_{S31N} pore. In the mutant waters are observed above and below the ligand and in a few snapshots between the ligand and the wall of the pore suggesting a relatively free passage through the M2TM_{S31N} lumen despite the presence of the ligand.^{12,17,18} (snapshots from the simulation of the complexes of M2TM_{S31N} with **1**, **6**, **10** are depicted in Figure 8).

2.4.2 Changes in C-terminus structure-function of M2TM_{S31N} and M2TM_{WT} induced by V27 interactions with the adamantyl cage of amantadine variants

Furthermore it is suggested that the 10° helical kink that reduces the tilt of the C-terminal portion of the transmembrane helix in the WT is likely induced by the formation of a strong binding pocket for the aminoadamantanes. This hydrophobic pocket formed by the V27 aliphatic sidechains coupled with the aliphatic adamantyl cage of the aminoadamantanes may prevent the W41 gate from opening further defeating proton conductance. In contrast the aminoadamantanes in M2TM_{S31N} included a loss of V27 lipophilic pocket and have their amino group drawn toward the N-terminus by the asparagine sidechains resulting in the presence of multiple water molecules in this region. In addition the weak binding of the amino adamantanes results in no perturbation of the helical tilt and the W41 gate can function normally.

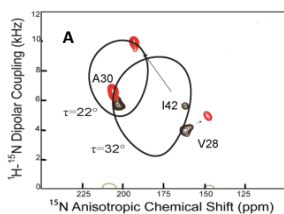
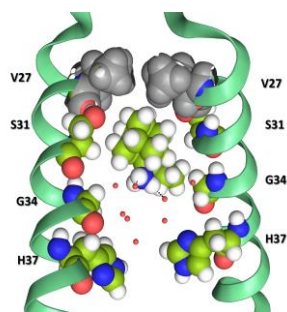
2.5 Conclusions

This work represents a study of the binding of amantadine variants against the proton channel formed by the tetrameric structure of the influenza A M2 protein. Significantly, we focus on aminoadamantane variants of **1** binding to M2TM_{S31N} compared to M2TM_{WT} aiming at investigating why these variants are ineffective in blocking proton conductance of the M2_{S31N} channel. The results of this effort are based on a combination of experimental techniques and MD simulations both performed in liquid crystalline lipid bilayer environments. Aminoadamantane derivatives are known to be blockers of the M2 WT protein. They are known to bind in the pore and are presumed to block proton access to the H37 tetrad that is known to shuttle protons through aqueous pore into the viral interior.⁴⁶ There are two gates that can inhibit conductance, the V27 tetrad, known as the secondary gate at the external entrance to the pore and the W41 tetrad near the exit of the pore into the viral interior, known as the primary gate. These aminoadamantane derivatives were weaker binders to M2TM_{S31N} compared to M2TM_{WT} as observed by a reduced influence on the protein structure and by reduced amplitude of the channel dynamics as observed by both the MD and experimental data. Moreover, these aminoadamantane derivatives were ineffective against M2_{S31N} while blocking M2_{WT} protein. We suggest that **1** and the similar sized analogs **2-4** lack of binding affinity and the larger sized analogs **5-8** showed weak binding affinity to M2TM_{S31N} because of a lack of effective hydrophobic interactions as a result of reshaping the cavity when N31 is present which included loss of V27 lipophilic pocket. In contrast V27 interactions are present with **1-8** in M2TM_{WT} pore and these ligands are effective binders to M2TM_{WT} (see Figure 10). All ligands **1-8** have a tight binding for M2TM_{WT} and the binding is more specific as showed by the more stringent head-ammonium group requirements in the binding pocket of M2TM_{WT} than in the M2TM_{S31N} according to the ITC, EP and CPE results. The weak binding of **5-8** to M2TM_{S31N} was significant enough to induce observable changes in the helix tilt angles characterized by the experimental data and by the MD simulations.

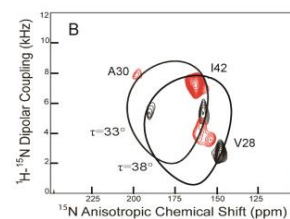
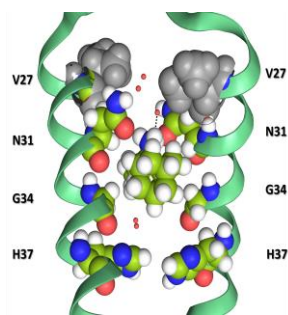
It is interesting to note that the blockage of M2TM_{WT} by both **1** and **5** involved a 10° kink in the TM helix and a very significant change in the helix orientation in the C-terminal half of the TM. This is likely due to the V27 side chains - adamantane hydrophobic interactions that are not possible in M2TM_{S31N}. While aminoadamantane ligand binding causes a kink in the C-terminal half of M2TM_{WT} and a blockage for proton conductance by the M2 channel, aminoadamantane ligand interactions with M2TM_{S31N} did not result in a helix kink in the TM helix and proton conductance was not blocked (see Figure 10). While the helix kink has been associated with blockage and potential disabling the opening of W41 gate in M2TM_{WT} previously⁴⁷ here, the explanation for the helix kink in the M2TM_{WT} and its absence in M2TM_{S31N} has been suggested to be induced by the V27 interactions with the adamantyl cage in the M2TM_{WT} and the absence of such significant interactions in the M2TM_{S31N}.

Figure 10. Summary of the most important binding consequences by amantadine variants to the influenza M2TM_{WT} and M2TM_{S31N}.

A Tight M2TM_{WT}-5 complex; strong C-terminus direction, V27 lipophilic pocket, 10° kink in C-terminus half



B Weak M2TM_{S31N}-5 complex; propensity for N-terminus direction, loss of V27 lipophilic pocket, uniform helical tilt



2.6 Experimental Work

2.6.1 Ligands synthesis

Melting points were determined using a Buchi capillary apparatus and are uncorrected. IR spectra were recorded on a Perkin-Elmer 833 spectrometer. ^1H and ^{13}C NMR spectra were recorded on a Bruker DRX 400 and AC 200 spectrometer at 400 and 50 MHz, respectively, using CDCl_3 as solvent and TMS as internal standard. Carbon multiplicities were established by DEPT experiments. 2D NMR experiments (HMQC and COSY) were used for the elucidation of the structures of intermediates and final products. Microanalyses were carried out by the Service Central de Microanalyse (CNRS) France or by a relevant service in Demokritos, National Center for Scientific Research, Athens, Greece. The results obtained had a maximum deviation of $\pm 0.4\%$ from the theoretical value. Thus, the purity of the tested compounds was $\geq 95\%$ as determined by elemental analysis. **1** was purchased from Merck ($> 99\%$ purity). Details for the synthesis of compounds **2**, **6** and **7** can be found in ref. 10a and 9a, respectively. The synthetic scheme of **2** and **6,7** is also included in the SI (Schemes S1, S2). All compounds purity was $\geq 95\%$ as determined by elemental analysis.

2-Methyl-tricyclo[3.3.1.1^{3,7}]decan-2-amine 3. Tertiary alcohol **12** was obtained after treating a solution of adamantanone **11** (500 mg, 3.33 mmol) in dry THF (30% solution w/v) with 2-molar excess CH_3MgI (obtained from 20% solution w/v solution of CH_3I (940 mg, 6.67 mmol) in dry ether and 1.3 equivalents of Mg (210 mg, 8.67 mmol)) under argon atmosphere and stirring the mixture overnight. After treating the mixture with saturated ammonium chloride the organic phase was separated and the aqueous phase was extracted twice with an equal volume of diethyl ether. The combined organic phase was washed with water and brine, dried (Na_2SO_4) and evaporated to afford the corresponding tertiary alcohol **12**; yield 525 mg, (95%); IR (Nujol) $\nu(\text{OH})$ 2923 cm^{-1} ; ^1H NMR (CDCl_3 , 400 MHz): δ (ppm) ^{13}C NMR (CDCl_3 , 50 MHz) δ 27.16-27.5 (5,7adamantane-C), 27.4 (CH_3), 33.1 (8,10adamantane -C), 35.2 (4,9adamantane-C), 38.4 (1,3adamantane -C), 39.3 (6adamantane -C), 74.0 (2adamantane-C).

To a stirred mixture of sodium azide (187 mg, 2.88 mmol) and dry dichloromethane (5 mL), trifluoroacetic acid (0.8 mL, 9.6 mmol) was added at 0 °C. The resulting mixture was stirred for 10 min at 0 °C and a solution of the tertiary alcohol **12** (160 mg, 0.96 mmol) in 5 mL of dichloromethane was added dropwise. The mixture was stirred at 0-5 °C for 4 h and 24 h at ambient temperature. The mixture was made alkaline by adding NH_3 12% (30 mL) and the organic phase was separated. The aqueous phase was extracted with dichloromethane and the combined organic phases were washed with water, brine and dried (Na_2SO_4). Solvent was evaporated in vacuo to afford azide **12a**; yield 0.161g (88%); IR (Nujol) $\nu(\text{N}_3)$ 2913 cm^{-1} ;

To a stirred suspension of LiAlH_4 (127 mg, 3.35 mmol) in dry ether (10 mL) was added dropwise at 0 °C a solution of the azide **12a** (160 mg, 0.84 mmol) in dry ether (5 mL). The mixture was refluxed for 5 h and then was treated with water, NaOH 10 % and water. The insoluble inorganic material was filtered-off, washed with ether and the filtrate was extracted with HCl 6%. The aqueous phase was made alkaline with solid sodium carbonate and was extracted with dichloromethane or ether. The organic phase was washed with brine, dried (Na_2SO_4) and evaporated in vacuo to afford the amine **3**; yield 117 mg, (83 %); ^1H NMR (CDCl_3 , 400 MHz): δ (ppm) 1.17 (br s, 3H, CH_3), 1.46-1.48 (d, $J \sim 9\text{ Hz}$, 2H, 4eq, 9eqadamantane-H), 1.54 (d, $J \sim 12\text{ Hz}$, 2H, 8eq, 10eqadamantane-H), 1.63 (br m, 3H, 1, 3, 6adamantane-H), 1.76 (br s, 2H, 5, 7adamantane-H), 1.93 (d, $J \sim 12\text{ Hz}$, 2H, 8ax, 10axadamantane-H), 2.01 (d, $J \sim 12\text{ Hz}$, 2H, 4ax, 9axadamantane-H); ^{13}C NMR (CDCl_3 , 50 MHz) δ (ppm) 27.3 (7adamantane-C), 27.7 (5adamantane-C), 27.9 (CH_3), 33.2 (4,9adamantane-C), 34.7 (8,10adamantane-C), 38.9(6adamantane-C), 39.6 (1,3adamantane-C), 52.9 (2adamantane-C). Hydrochloride: mp > 250 °C (EtOH-Et₂O); Anal. ($\text{C}_{11}\text{H}_{20}\text{NCl}$) C, H, N.

2-Ethyl-tricyclo[3.3.1.1^{3,7}]decan-2-amine 4. Tertiary alcohol **13** was obtained after treating a solution of adamantanone **11** (500 mg, 3.33 mmol) in dry THF (30% solution w/v) with n-ethylolithium (0.5 M in benzene), (20 mL, 10,0 mmol) at 0 °C and stirring the mixture overnight; yield 560 mg (94%); ^1H NMR (CDCl_3 , 400 MHz): δ (ppm) 0.86 (t, $J \sim 7\text{ Hz}$, CH_2CH_3), 1.40-1.70 (m, 10 H, 1, 3, 4eq, 9eq, 6, 8eq, 10eqadamantane-H, CH_2CH_3), 1.75-1.83 (m, 2H, 5, 7adamantane-H), 1.94 (d, $J \sim 12\text{ Hz}$, 2H, 8ax, 10axadamantane-H), 2.07 (d, $J \sim 12\text{ Hz}$, 2H, 4ax, 9axadamantane-H); ^{13}C NMR (CDCl_3 , 50 MHz) δ 6.4 (CH_2CH_3), 27.4, 27.5 (5, 7adamantane-C), 30.6 (CH_2CH_3), 33.0 (8, 10adamantane-C), 34.6 (4, 9adamantane-C), 36.6 (1, 3adamantane-C), 38.5 (6adamantane-C), 74.9 (2adamantane-C).

The tertiary azide **13a** was prepared by treatment of the tertiary alcohol **13** (0.180g, 1.0mmol) with CH_2Cl_2 (5 mL) / NaN_3 (195 mg, 3.00 mmol) / TFA (0.8 mL, 10,0 mmol) according to the same procedure followed for the azide **12a**; yield 0.160 g (80%); IR (Nujol) $\nu(\text{N}_3)$ 2100 cm^{-1} .

The oily amine **4** was prepared through LiAlH_4 (0.120 g, 0.78 mmol) reduction of azide **13a** (160 mg, 3.12 mmol) in refluxing ether (10 mL) for 5h according to the same procedure followed for amine **3**; yield 100 mg (71%); ^1H NMR (CDCl_3 , 400 MHz): δ (ppm) 0.85 (t, $J \sim 7\text{ Hz}$, 3H, CH_2CH_3), 1.55 (br s, 2H, 1, 3adamantane-H), 1.58-1.68 (m, 7H, 4eq, 9eq-H, 8eq, 6adamantane-H, CH_2CH_3), 1.78 (br s, 1H, 5adamantane-H), 1.81 (br s, 1H, 7adamantane-H), 1.93 (d, $J \sim 12\text{ Hz}$, 2H, 8ax, 10axadamantane-H), 2.06 (d, $J \sim 12\text{ Hz}$, 2H, 4ax, 9axadamantane-H); ^{13}C NMR (CDCl_3 , 50 MHz) δ (ppm) 6.5 (CH_2CH_3), 27.2, 27.6 (5, 7adamantane-C), 30.7 (CH_2CH_3), 33.0 (4, 9adamantane-C), 33.8 (8, 10adamantane-C), 36.6 (1, 3adamantane-C), 38.5 (6adamantane-C), 74.9 (2adamantane-C). Hydrochloride: mp > 250 °C (EtOH-Et₂O); Anal. ($\text{C}_{12}\text{H}_{22}\text{NCl}$) C, H, N.

2-*n*-Propyl-tricyclo[3.3.1.1^{3,7}]decan-2-amine 5. Tertiary alcohol **11a** was obtained after treating adamantanone **11** (1000 mg, 6.67 mmol) in dry diethyl ether (30% solution w/v) with $\text{CH}_2\text{CH}=\text{CH}_2\text{MgBr}$ with 2-molar excess (obtained from 20% solution w/v solution of $\text{CH}_2\text{CH}=\text{CH}_2\text{Br}$ (1.6 g, 13.34 mmol) in dry ether and 1.05 equivalents of Mg (340 mg, 14.01 mmol)) under argon atmosphere and stirring the mixture overnight. After treating the mixture with saturated ammonium chloride following usual workup the corresponding tertiary alcohol **11a**; yield 1.1 g, (89%); δ (ppm) 1.52 (d, $J \sim 12$ Hz, 2H, 4eq, 9eqadamantane-H), 1.53-1.90 (m, 10H, 1, 3, 5, 6, 7, 8eq, 10eq, 8ax, 10ax adamantane-H), 2.15 (d, $J \sim 12$ Hz, 1H, 4ax, 9ax-H), 2.40 (d, $J \sim 6$ Hz, 2H, $\text{CH}_2\text{CH}=\text{CH}_2$), 5.05-5.15 (m, 2H, $\text{CH}_2\text{CH}=\text{CH}_2$), 5.75-6.0 (m, 1H, $\text{CH}_2\text{CH}=\text{CH}_2$); the unsaturated alcohol **11a** was hydrogenated under PtO_2 (catalyst was used in 1/20 percentage to the weight of the unsaturated compound) to afford the *n*-propyl analogue **14**; yield quant.: ^1H NMR (CDCl_3 , 400 MHz): δ (ppm) 0.92 (t, $J \sim 7$ Hz, 3H, $\text{CH}_2\text{CH}_2\text{CH}_3$), 1.30-1.40 (m, 2H, $\text{CH}_2\text{CH}_2\text{CH}_3$), 1.52 (d, $J \sim 12$ Hz, 2H, 4eq, 9eqadamantane-H), 1.58-1.61 (m, 2H, $\text{CH}_2\text{CH}_2\text{CH}_3$), 1.68 (d, $J \sim 12$ Hz, 2H, 8eq, 10eqadamantane-H), 1.67 (~ br s, 2H, 6adamantane-H), 1.68 (~ br s, 2H, 1, 3adamantane-H), 1.79 (m, 2H, 5, 7adamantane-H), 1.83 (d, $J \sim 12$ Hz, 2H, 8ax, 10axadamantane-H), 2.16 (d, $J \sim 12$ Hz, 2H, 4ax, 9axadamantane-H); ^{13}C NMR (CDCl_3 , 50 MHz) δ (ppm) 14.9 ($\text{CH}_2\text{CH}_2\text{CH}_3$), 15.4 ($\text{CH}_2\text{CH}_2\text{CH}_3$), 27.4, 27.6 (5, 7adamantane-C), 33.1 ($\text{CH}_2\text{CH}_2\text{CH}_3$), 34.7 (4, 9adamantane-C), 37.1 (8, 10adamantane-C), 38.5 (1, 3adamantane-C), 40.9 (6adamantane-C), 75.2 (2adamantane-C).

The tertiary azide **14a** was prepared by treatment of the tertiary alcohol **14** (640 mg, 3.27 mmol) with CH_2Cl_2 (20 mL) / NaN_3 (640 mg, 9.83 mmol) / TFA (2.6 mL, 32.7 mmol) according to the same procedure followed for the azide **12a**; yield 470 mg (66%); IR (Nujol) $\nu(\text{N}_3)$ 2100 cm^{-1} ; ^1H NMR (CDCl_3 , 400 MHz): δ (ppm) 0.96 (t, $J \sim 7$ Hz, 3H, $\text{CH}_2\text{CH}_2\text{CH}_3$), 1.42 (m, 2H, $\text{CH}_2\text{CH}_2\text{CH}_3$), 1.59 (d, $J \sim 12$ Hz, 2H, 8eq, 10eqadamantane-H), 1.68 – 2.03 (m, 12H, $\text{CH}_2\text{CH}_2\text{CH}_3$, 1, 3, 4eq, 5, 7, 8ax, 9eq, 10ax adamantane-H), 2.10 (d, $J \sim 12$ Hz, 1H, 4ax, 9axadamantane-H); ^{13}C NMR (CDCl_3 , 50 MHz) δ (ppm) 14.7 ($\text{CH}_2\text{CH}_2\text{CH}_3$), 16.4 ($\text{CH}_2\text{CH}_2\text{CH}_3$), 27.2, 27.4 (5, 7adamantane-C), 33.8 ($\text{CH}_2\text{CH}_2\text{CH}_3$), 34.4 (4, 9adamantane-C), 37.9 (8, 10adamantane-C), 38.5 (1, 3adamantane-C), 40.0 (6adamantane-C), 69.7 (2adamantane-C).

The oily amine **5** was prepared through LiAlH_4 (390 mg, 10.3 mmol) reduction of azide **14a** (490 mg, 2.57 mmol) in refluxing ether (10 mL) for 5h according to the same procedure followed for amine **3**; yield 350 mg (74%); ^1H NMR (CDCl_3 , 400 MHz): δ (ppm) 0.92 (t, $J \sim 7$ Hz, 3H, $\text{CH}_2\text{CH}_2\text{CH}_3$), 1.29-1.40 (m, 2H, $\text{CH}_2\text{CH}_2\text{CH}_3$), 1.52 (d, $J \sim 12$ Hz, 2H, 4eq, 9eqadamantane-H), 1.58-1.61 (m, 2H, $\text{CH}_2\text{CH}_2\text{CH}_3$), 1.67 (d, $J \sim 12$ Hz, 2H, 8eq, 10eqadamantane-H), 1.66 (~ br s, 2H, 6adamantane-H), 1.68 (~ br s, 2H, 1, 3adamantane-H), 1.78 (br s, 2H, 5, 7adamantane-H), 1.83 (d, $J \sim 12$ Hz, 2H, 8ax, 10axadamantane-H), 2.16 (d, $J \sim 12$ Hz, 1H, 4ax, 9axadamantane-H); Hydrochloride: mp > 250 °C (EtOH-Et₂O); Anal. ($\text{C}_{13}\text{H}_{24}\text{NCl}$) C, H.

1-(1-Adamantyl)cyclopentanamine 9. The corresponding cyclopentanol **18** used as a starting material was prepared from ethyl 1-adamantanecarboxylate **17** and 1,4-bis(bromomagnesiobutane) in dry ether with a

70% yield according to a published procedure⁴⁸, ¹H NMR (CDCl₃, 400 MHz): δ 1.30-1.40 (m, 2H, cyclopentane-H), 1.50-1.80 (m, 18H, adamantane-H, cyclopentane-H), 1.98 (br s, 3H, 3',5',7'-H), 2.16 (s, 1H, OH); ¹³C NMR (CDCl₃, 50 MHz) δ 24.2 (3,4-cyclopentane-C), 28.6 (3',5',7'-C), 33.8 (2,5-cyclopentane-C), 37.1 (4',6',10'-C), 37.3 (2',8',9'-C), 39.5 (1'-C), 87.6 (1-cyclopentane-C).

To a stirred mixture of NaN₃ (0.270 g, 4.08mmol) and dry dichloromethane (40 mL) at 0 °C, TFA (13.6mmol) was added. To the stirred mixture a solution of tertiary alcohol **18** (0.300 g, 1.36 mmol) in dry dichloromethane (20 mL) was added and stirring was maintained at 0 °C for 4 h. The mixture was stirred at ambient temperature for 24 h and then was treated with NH₃ 12% (30 mL) at 0 °C. The organic phase was separated and the aqueous phase was extracted twice with an equal volume of dichloromethane. The combined organic phase was washed with water and brine, dried (Na₂SO₄) and evaporated to afford oily azide**19**; yield 0.290 g (88%); IR (Nujol) ν (N₃) 2097 cm⁻¹; ¹H NMR (CDCl₃, 400 MHz): δ 1.50-1.80 (m, 20H, adamantane-H, cyclopentane-H), 1.99 (br s, 3H, 3',5',7'-H); ¹³C NMR (CDCl₃, 50 MHz) δ 24.2 (3,4-cyclohexane-C), 28.6 (3',5',7'-C), 30.7 (2,5-cyclohexane-C), 37.1 (4',6',10'-C), 36.7 (2',8',9'-C), 41.8 (1'-C), 81.2 (1-cyclopentane-C).

To a stirred suspension of LiAlH₄ (161 mg, 4.24 mmol) in dry ether (20 mL) was added, drop-wise at 0 °C, a solution of the azide**19** (260 mg, 1.06 mmol) in dry ether (10 mL). The reaction mixture was refluxed for 5 h (TLC monitoring) and then hydrolyzed with water and NaOH (15%) under ice cooling. The inorganic precipitate was filtered off and washed with ether, and the filtrate was extracted with HCl (6%). The aqueous layer was made alkaline with solid Na₂CO₃ and the mixture was extracted with ether. The combined ether extracts were washed with water and brine and dried (Na₂SO₄). After evaporation of the solvent the oily amine **9** was obtained; yield: 151 mg (65%); ¹H NMR (CDCl₃, 400 MHz): δ 1.08-1.18 (m, 4H, 3,4-cyclopentane-H), 1.50-1.80 (m, 18H, adamantane-H, cyclopentane-H, NH₂), 1.98 (br s, 3H, 3',5',7'-H); ¹³C NMR (CDCl₃, 50 MHz) δ 24.9 (3,4-cyclopentane-C), 28.8 (3',5',7'-C), 34.4 (2,5-cyclopentane -C), 37.0 (4',6',10'-C), 37.4 (2',8',9'-C), 39.0 (1'-C), 66.8 (1-cyclopentane-C). Fumarate: mp 255 °C (EtOH-Et₂O); Anal. (C₁₉H₂₉NO₄) C, H, N.

1-(1-Adamantyl)cyclohexanamine (10): Tertiary alcohol **21** was obtained from 1-adamantyl lithium (formed by 1-bromoadamantane **20** and lithium wire under sonication) and cyclohexanone in dry THF according to a published procedure with 70% yield.⁴⁹

To a stirred mixture of NaN₃ (0.170 g, 2.61mmol) and dry dichloromethane (20 mL) at 0 °C, TFA (8.70mmol) was added. To the stirred mixture a solution of tertiary alcohol **21** (0.204 g, 0.87 mmol) in dry dichloromethane (10 mL) was added and stirring was maintained at 0 °C for 4 h. The mixture was stirred at ambient temperature for 24 h and then was treated with NH₃ 12% (30 mL) at 0 °C. The organic phase was separated and the aqueous phase was extracted twice with an equal volume of dichloromethane. The combined organic phase was washed with water and brine, dried (Na₂SO₄) and evaporated to afford oily

azide **22**; yield 0.140 g (60%); IR (Nujol) $\nu(\text{N}_3)$ 2101 cm^{-1} ; ^{13}C NMR (CDCl_3 , 50 MHz) δ 21.9 (4-cyclohexane-C), 25.6 (3,5-cyclohexane-C), 28.8 (3',5',7'-C), 30.8 (2,6-cyclohexane-C), 35.7 (4',6',10'-C), 37.2 (2',8',9'-C), 42.0 (1'-C), 70.1 (1-cyclohexane-C).

To a stirred suspension of LiAlH_4 (65 mg, 1.70 mmol) in dry ether (7 mL) was added, drop-wise at 0 °C, a solution of the azide **22** (110 mg, 0.425 mmol) in dry ether (5 mL). The reaction mixture was refluxed for 5 h (TLC monitoring) and then hydrolyzed with water and NaOH (15%) under ice cooling. The inorganic precipitate was filtered off and washed with ether, and the filtrate was extracted with HCl (6%). The aqueous layer was made alkaline with solid Na_2CO_3 and the mixture was extracted with ether. The combined ether extracts were washed with water and brine and dried (Na_2SO_4). After evaporation of the solvent the oily amine **10** was obtained; yield: 50 mg (30%); ^1H NMR (CDCl_3 , 400 MHz): δ 1.35-1.42 (m, 6H, 3,4,5-cyclohexane-H), 1.48-1.55 (m, 3H, 2',8',9'-H), 1.56-1.70 (m, 12H, 2,6-cyclohexane-H, 4',6',10'-H, NH_2), 1.98 (br s, 3H, 3',5',7'-H); ^{13}C NMR (CDCl_3 , 50 MHz) δ 22.1 (4-cyclohexane-C), 26.4 (3,5-cyclohexane-C), 29.0 (3',5',7'-C), 30.5 (2,6-cyclohexane-C), 35.7 (4',6',10'-C), 37.5 (2',8',9'-C), 38.7 (1'-C), 54.5 (1-cyclohexane-C). Fumarate: mp 264 °C (EtOH-Et₂O); Anal. ($\text{C}_{20}\text{H}_{31}\text{NO}_4$) C, H, N.

2.6.2 M2TM peptide synthesis

M2TM_{WT} peptides corresponding to residues 22-46 of the Udorn (A/Udorn/307/72) sequence of M2 (C-terminally amidatedSSDPLVVAASIIGILHLILWILDRL) and of the new S31N mutant peptide (C-terminally amidatedSSDPLVVAANIIGILHLILWILDRL) were synthesized by standard Fmoc (9-fluorenylmethoxycarbonyl) solid phase peptide synthesis using an aminomethyl polystyrene resin loaded with the amide linker and purified by reverse phase HPLC before used for the ITC experiments. Details for peptide synthesis and purification, can be found in Chapter 1, i.e., in 1.3.2. Additional quantities of these peptides needed were purchased from CenticBiotec, Heildeberg, Germany. For ssNMR experiments M2TM_{WT} and M2TM_{S31N} (22-46) peptides with ¹⁵N labeled at V28, A30 and I42 and M2TM_{S31N} (22-46) peptides with ¹³C, ¹⁵N labeled at structurally important residues V27, A30^{a,5b} and N31, G34 (¹³C, ¹⁵N-VANG) were synthesized using Fmoc chemistry. Fmoc-[¹⁵N]-Val, Fmoc-[¹⁵N]-Ala, Fmoc-[¹⁵N]-Ile and Fmoc-[¹³C, ¹⁵N]-Val, Fmoc-[¹³C, ¹⁵N]-Ala, Fmoc-[¹³C, ¹⁵N]-Ser and Fmoc-[¹³C, ¹⁵N]-Gly were purchased from Cambridge Isotope Laboratory (Andover, MA). Solid-phase syntheses of M2TM peptides (0.25 mmol) were performed on an Applied Biosystems 430A peptide synthesizer as previously described.^{50,51} The peptide was cleaved from the resin by the treatment with ice cold 95 % TFA, 2.5 % H₂O, 1.25 % ethanedithiol, 1.25 % thioanisole and precipitated from TFA using ice cold ether. Following centrifugation, the supernatant was discarded and the pellet was washed with cold ether again. The precipitated peptide was dried under vacuum. A purification procedure previously described⁵² and modified⁵¹ was used. Peptide purity and identity was confirmed using ESI mass spectrometry (positive ion mode).

Figure 10 illustrates the analytical spectrum obtained by RP-HPLC, while Figure 11 shows the mass spectrum obtained after purification and lyophilization of the fractions containing the pure peptide. The retention time was R_f = 26.85 min and the purity was ~ 98 %.

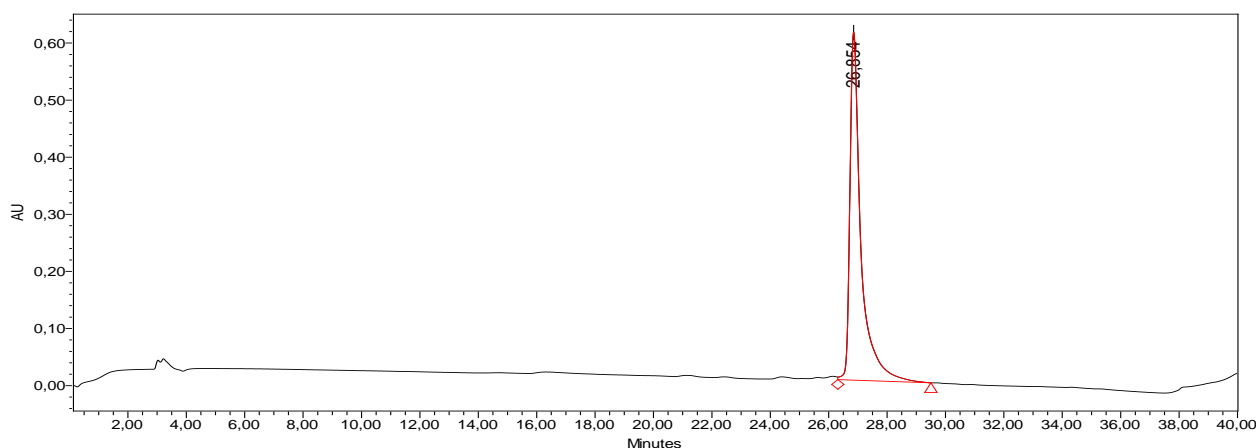


Figure 10. Analytical RP-HPLC chromatograph of M2TM_{S31N} peptide sequence after purification. The retention time is noted.

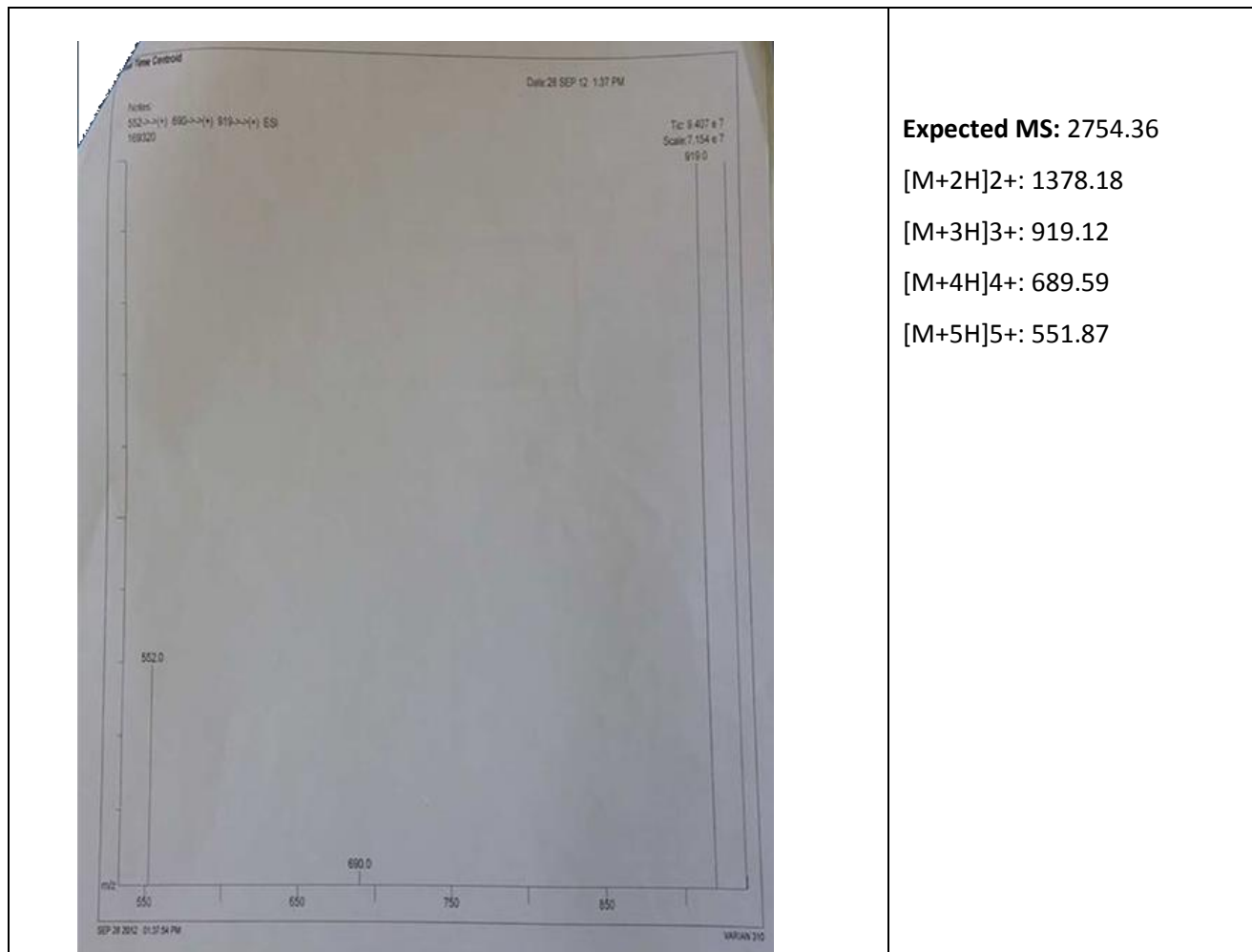


Figure 11. MS Analysis of the new S31N mutant peptide, C-terminally amidated SSDPLVVAANIIGILHLILWILDRL.

2.6.3 ITC measurements of aminoadamantane ligands binding to M2TM

Binding affinities of the aminoadamantane derivatives **1-5**, **6**, **9**, **10** for M2TM_{S31N} were measured by ITC experiments^{53,54} in DPC micelles at pH 8. Compounds **7**, **8** were not measured. M2TM fragments form stable tetramers at this pH, in contrast to low pH (< 6.5) conditions.⁵⁵ Furthermore, experimental data indicate that **1** binds with higher affinity at alkaline pH to M2TM, where the pore of the M2 channel is in the closed state, than at low pH, where the open state of M2TM is prevalent.^{55a,2^a}

Synthetic M2TM_{S31N} (residues 22-46) was reconstituted in DPC micelles at pH 8 at a 1:40 monomer/DPC ratio - which guarantees the quantitative formation of M2TM tetramers⁵⁵ - by dissolving and sonicating 334 nmol of M2TM with the 40-fold amount of DPC in the aforementioned buffer system (for M2TM_{WT} a 1:26 ratio was applied for the measurements of ligands **9**, **10** compared to 1:57 applied previously²⁶). Solutions of the ligands in the buffer were titrated into the calorimetric cell at 20 °C. The released heat of binding was derived by subtracting the heat of dilution from the heat of reaction.^{56,57} The measured heat per amount of substance against the molar ratio of titrant to peptide tetramer was plotted and the affinity constants were calculated by non-linear regression of the measured heat per injection using Origin 8.0⁵⁸ and are included in Table 1. Compounds **1-8** have been measured against M2TM_{WT} in a previous work (Table 7).²⁶ For the calculation, the concentration of the peptide was kept variable because the M2TM tetramer formation is not complete. Details for isothermal titration calorimetry measurements can be found in Chapter 1, i.e., 1.3.3.

2.6.4 Solid state NMR

2.6.4.1 Sample preparation for solid state NMR

$^{15}\text{N-V}_{28}\text{A}_{30}\text{I}_{42}$ M2TM_{WT} or M2TM_{S31N} was co-dissolved in trifluoroethanol (TFE) with DMPC in a 1:30 molar ratio. (The molar ratio of 1 protein tetramer to 120 DMPC lipids was used. The molecular weight of the M2TM_{WT} peptide is MW = 2729 g/mole and the lipid is MW = 678 g/mole). The solvent was removed under a stream of nitrogen gas to yield a lipid film, and then dried to remove residual organic solvent under vacuum for 12 hours. Thoroughly dried lipid film was hydrated with 10 mM HEPES buffer at pH 7.5 to form multilamellar vesicles containing M2TM in tetrameric state. This suspension was bath sonicated, dialyzed against 2L HEPES 10 mM pH 7.5 buffer for 1 day and centrifuged at 196,000xg to harvest unilamellar proteoliposomes. The pellet was re-suspended in a 1 mL aliquot of the decanted supernatant containing the ligand, resulting in a 1:6 molar ratio of the M2TM tetramer to drug. Typically a preparation for solid state NMR would include 5 mg of protein and 37 mg of DMPC. For samples that included drug the molar ratio of drug to tetramer was 6:1. For **1** with a molecular weight of $M_w = 187.5$ g/mole that would mean the addition 0.52 mg for a 5 mg protein sample (There is sufficient evidence in the literature to demonstrate that M2 structure is not perturbed by drug concentration. The most obvious example in this manuscript, is the absence of structural changes in the S31N spectra in the presence of **1**) Following overnight incubation at 37°C, the pellet was deposited on 5.7x10mm glass strips (Matsunami Trading, Osaka, Japan). The bulk of the water from the sample was removed during a two day period in a 98 % relative humidity environment at 298 K. Rehydration of the slides, before stacking and sealing into a rectangular sample cell, increased the sample weight by 40-50 %. Compounds **1**, **5** were used for ssNMR experiments against M2TM_{WT}; compounds **1**, **5-8** were used for ssNMR experiments against M2TM_{S31N}; compounds **9** and **10** produce disordered lipid bilayers according to the ^{31}P spectra (not shown).

2.6.4.2 Solid state NMR experiments of M2TM-aminoadamantanes complexes

2.6.4.2.1 OS ssNMR spectra

PISEMA²⁸ and SAMPI4^{29,30} spectra were acquired at 720 MHz utilizing a low-E $^1\text{H}/^{15}\text{N}$ double resonance probe.⁵⁹ Acquisition took place at 303 K, above the gel to liquid crystalline phase transition temperature of DMPC lipids. Experimental parameters included a 90° pulse of 5 μs and cross-polarization contact time of 0.8-1 ms, a 4 s recycle delay and a SPINAL decoupling sequence.⁵⁹ 32 t_1 increments were obtained for the spectrum of $^{15}\text{N-V}_{28}\text{A}_{30}\text{I}_{42}$ M2TM_{WT} with compounds **1**, **5** and nine t_1 for the sample of $^{15}\text{N-V}_{28}\text{A}_{30}\text{I}_{42}$ M2TM_{WT} without drug. 16-28 t_1 increments were obtained for the spectrum of $^{15}\text{N-V}_{28}\text{A}_{30}\text{I}_{42}$ M2TM_{S31N} with compounds **1**, **5-8** and nine t_1 increments for the sample of $^{15}\text{N-V}_{28}\text{A}_{30}\text{I}_{42}$ M2TM_{S31N} without drug. Spectral

processing was done with NMRPIPE⁶⁰ and plotting with SPARKY. ¹⁵N chemical shifts were referenced to a concentrated solution of N₂H₈SO₄, defined as 26.8 ppm relative to liquid ammonia.

2.6.4.2.2 NCA MAS spectra

¹⁵N-¹³C α correlation experiments were performed on a BrukerAvance 600 MHz NMR Spectrometer with an NHMFL 3.2 mm low-E-field triple resonance probe.^{61,62} The ¹³C chemical shifts were referenced using the published chemical shifts of adamantane relative to DSS⁶³ and ¹⁵N chemical shifts were calculated with IUPAC relative frequency ratios between the DSS (¹³C) and liquid ammonia (¹⁵N).^{64,65} Spectra were acquired at magic angle spinning (MAS) frequency of 10-12 kHz and a calibrated sample temperature of -10 °C. 30 points were collected in the ¹⁵N dimension for an acquisition time of 5-6.25 ms, while in the direct dimension the acquisition time was 10.2 ms. 92 kHz of proton decoupling was used in all experiments. To get one bond ¹⁵N-¹³C correlation a mixing time of 5 ms was used. Spectra were processed with Topspin.

2.6.5 MD simulations of M2TM-aminoadamantane complexes

2.6.5.1 Docking calculations

The M2TM_{Udorn}-**1** complex structure (PDB ID 2KQT^{13,15}) served as a model structure for the docking calculations of M2TM_{Udorn} complexes with ligands **1-10** (Scheme 1). Details for Docking calculations can be found in Chapter 1, i.e., 1.3.4.1.

2.6.5.2 MD simulations

Models of M2TM_{S31N}-aminoadamantane complexes were generated from M2TM_{WT}-aminoadamantane complexes by mutating amino acids S31 to N31 with Maestro⁶⁶ and preparing the structure as described above i.e. N- and C-termini of the M2TM peptides were capped by acetyl- and methylamino groups, respectively. For N31, the side chain rotamers may have χ_1 angles -160° or -80° corresponding to N31 side chains placed at the interface between helices or inside the lumen respectively. Structures of M2TM_{S31N}(18-60) in DPC micelles solved by solution NMR spectroscopy show residue 31 in the helix-helix interface⁶⁷ while MAS ssNMR studies in 1,2-diphytanoyl-sn-glycero-3-phosphocholine (DPhPC) bilayers showed the side chain of the N31 residue oriented toward the pore in two helices and toward an adjacent helix in the other two, with neighboring N31 side chains close enough to form polar contacts.³⁶ A just-released X-ray structure shows that N31 residues are oriented into the channel pore forming a hydrogen-bonding network⁶⁸ and it was suggested that this may prevent drug from entering the channel. Preliminary OS ssNMR results in liquid crystalline lipid bilayers confirm that all four of the M2_{S31N} N31 residues are oriented toward the pore. Simulations of M2TM_{S31N}-ligands were run a) with N31 side chains placed at the interface between helices⁶⁷ (χ_1 angle is -80°) to avoid a biased starting conformer in which N31 repel adamantane and b) with N31

pointing toward the pore in two helices (χ_1 angle is $\sim -160^\circ$) and toward an adjacent helix in the other two³⁶ (χ_1 angle is $\sim -80^\circ$). For comparison reasons few MD simulations with **1**, **5**, **6** were also performed with the starting structure of M2TM_{S31N} having N31 residues pointing into the center of the channel pore (χ_1 angle is -160°).⁶⁸ It should be mentioned that when the starting structure has all four N31 side chains placed at the interface between helices after a few ns of simulation the side chains of at least two N31 residues change orientation pointing inside the pore lumen. This was also observed with the *apo* protein M2TM_{S31N} after a few ns. Configurations with different N31 rotamers produced MD trajectories with similar behavior for aminoadamantane ligands. MD simulations were run in triplicate or more for **1**, **2**, **5**, **6** to test reproducibility of the behavior of the system.

The M2TM_{WT} complexes or M2TM_{S31N} complexes were embedded in a DMPC lipid bilayer extending 10 Å beyond the solutes. Complex and ligand systems were solvated using the TIP3P⁶⁹ water model. Na⁺ and Cl⁻ ions were placed in the water phase to neutralize the systems and to reach the experimental salt concentration of 0.150 M NaCl. Membrane creation and system solvation were conducted with the “System Builder” utility of Desmond.^{70,71} The M2TM_{WT}-**1** complex structure in the hydrated DMPC bilayer with ions included 18617 atoms.

The OPLS 2005 force field^{72, 73, 74} was used to model all protein and ligand interactions, and the TIP3P model⁶⁹ was used for water. The particle mesh Ewald method (PME)^{75,76} was employed to calculate long-range electrostatic interactions with a grid spacing of 0.8 Å. Van der Waals and short range electrostatic interactions were smoothly truncated at 9.0 Å. The Nosé-Hoover thermostat⁷⁷ was utilized to maintain a constant temperature in all simulations, and the Martyna-Tobias-Klein method⁷⁷ was used to control the pressure. Periodic boundary conditions were applied (50×50×80)Å³. The equations of motion were integrated using the multistep RESPA integrator⁷⁸ with an inner time step of 2 fs for bonded interactions and non-bonded interactions within a cutoff of 9 Å. An outer time step of 6.0 fs was used for non-bonded interactions beyond the cut-off.

Each system was equilibrated in MD simulations with a modification of the default protocol provided in Desmond, which consists of a series of restrained minimizations and MD simulations designed to relax the system, while not deviating substantially from the initial coordinates. First, two rounds of steepest descent minimization were performed with a maximum of 2000 steps with harmonic restraints of 50 kcal mol⁻¹ Å⁻² applied on all solute atoms, followed by 10000 steps of minimization without restraints. The first simulation was run for 200 ps at a temperature of 10 K in the NVT (constant number of particles, volume, and temperature) ensemble with solute heavy atoms restrained with a force constant of 50 kcal mol⁻¹ Å⁻². The temperature was then raised during a 200 ps MD simulation to 310 K in the NVT ensemble with the force constant retained. The temperature of 310 K was used in our MD simulations in order to ensure that the membrane state is above the melting temperature state of 297 K for DMPC lipids.⁷⁹

The heating was followed by equilibration runs. First, two stages of NPT equilibration (constant number of particles, pressure, and temperature) were performed, one with the heavy atoms of the system restrained for 1 ns and one for solvent and lipids for 10 ns, with a force constant of 10 kcal/mol/Å² for the harmonic constraints, respectively. A NPT simulation followed with the C_α atoms restrained for 1 ns with a force constant of 2 kcal/mol/Å². The above-mentioned equilibration was followed by a 80 ns NPT simulation without restraints. Within this time, the total energy and the RMSD reached a plateau, and the systems were considered equilibrated.

2.6.6 Electrophysiology experiments of M2 blockage by aminoadamantanes

Electrophysiology was performed as previously described.^{10a} pcDNA3 vectors encoding the full-length A/California/07/2009 (H1N1) M2 protein containing either an N31 or an S31 mutation was co-transfected with a pcDNA3 vector encoding eGFP into TSA-201 (HEK parental) cells using standard transfection protocols (Lipofectamine 2000, Life Technologies). This construct was previously annotated as A/England/195/2009 (H1N1)^{10a} but is identical in amino acid sequence to A/California/07/2009 (H1N1). Macroscopic ionic currents were recorded in the whole-cell configuration from GFP-positive cells 24–48 h after transfection. Cells were perfused continuously at 3–5 mL min⁻¹ with external (bath) solution containing (in mM) 150 NMG, 10 HEPES, 10 D-glucose, 2 CaCl₂, and 1 MgCl₂ buffered at pH 7.4 with HCl. For low pH (pH = 5.5) solution, HEPES was replaced by MES. Patch electrodes were pulled from thin-walled borosilicate glass (World Precision Instruments, Fl) and fire-polished before filling with standard pipet solution containing (in mM) 140 NMG, 10 EGTA, 10 MES, and 1 MgCl₂ buffered at pH 6.0 with HCl. Voltage-clamp experiments were performed with an Axopatch 200B amplifier (Molecular Devices, CA) connected to a Digidata 1322A 16-bit digitizer. Data were acquired with the pCLAMP8.0 software (Molecular Devices, CA) sampled at 10 kHz and low-pass-filtered at 5 kHz. Cells were held at –40 mV. The voltage protocol consisted of a 100 ms pulse to –80 mV followed by a 300 ms ramp to +40 mV and a 200 ms step to 0 mV before stepping back to –40 mV, which was repeated every 4 s. All drugs were prepared as DMSO stocks (50 or 100 mM) and diluted with external solution to desired concentrations. To measure block of M2 currents by compounds, cells were recurrently treated with pH 7.4 and pH 5.5 solutions until stable, pH-dependent inward currents were reproducibly observed, followed by treatment with compound at pH 5.5 for 2–30 min. At the end of each experiment, cells were treated with a 100 μM solution of **1**.

2.6.7 Anti-viral assays

2.6.7.1 Cells and viruses

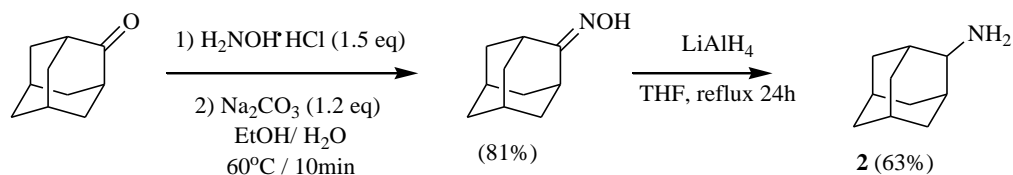
Information for cells and viruses can be found in Chapter 1. i.e., see section 1.3.6.

2.6.7.2 CPE inhibition assay of influenza A viruses by aminoadamantanes

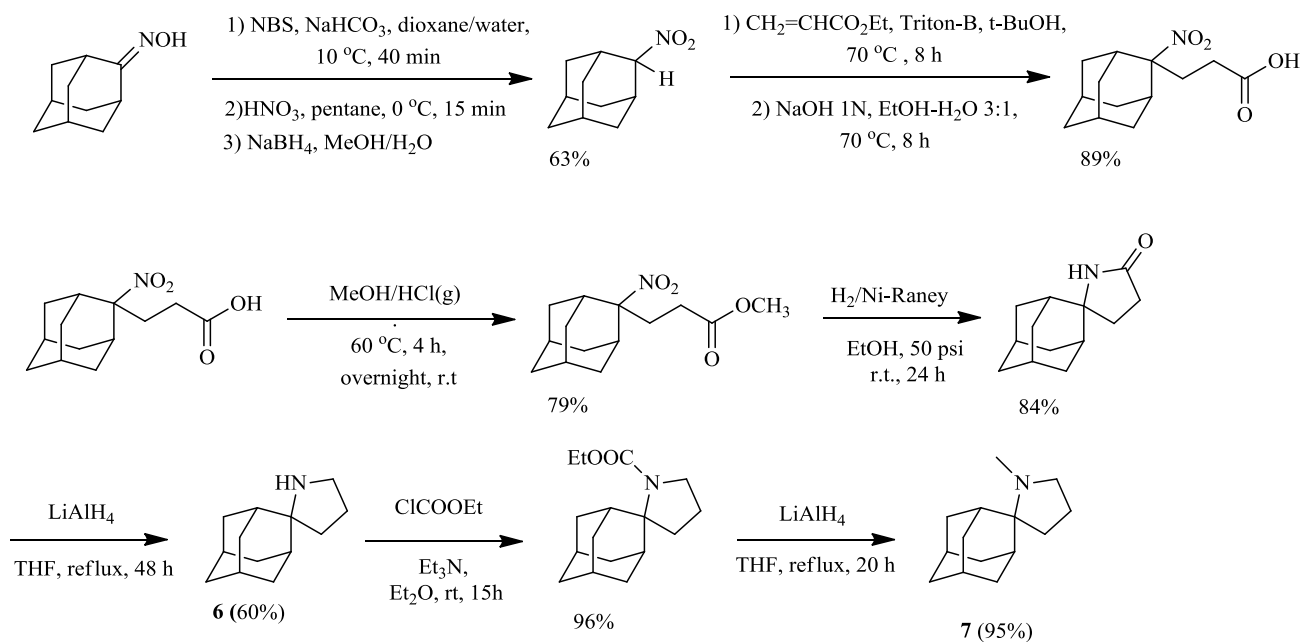
Information for CPE inhibition studies can be found in Chapter 1, 1.3.7. Cytotoxicity and CPE inhibition studies were performed on two-day-old confluent monolayers of MDCK cells grown in 96-well plates as published.⁴⁵ Cytotoxicity was analyzed 72 h after compound addition (two-fold or half-log dilutions; at least two parallels per concentration; maximum concentration 100 μ M).

2.8 Supporting information

2.8.1 Synthetic Schemes for the preparation of compounds 2, 6, 7

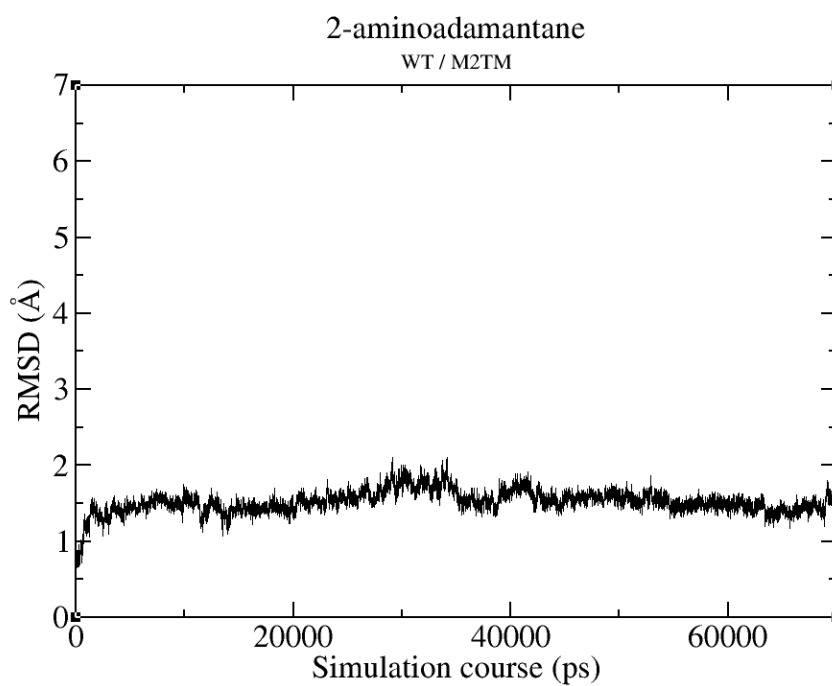
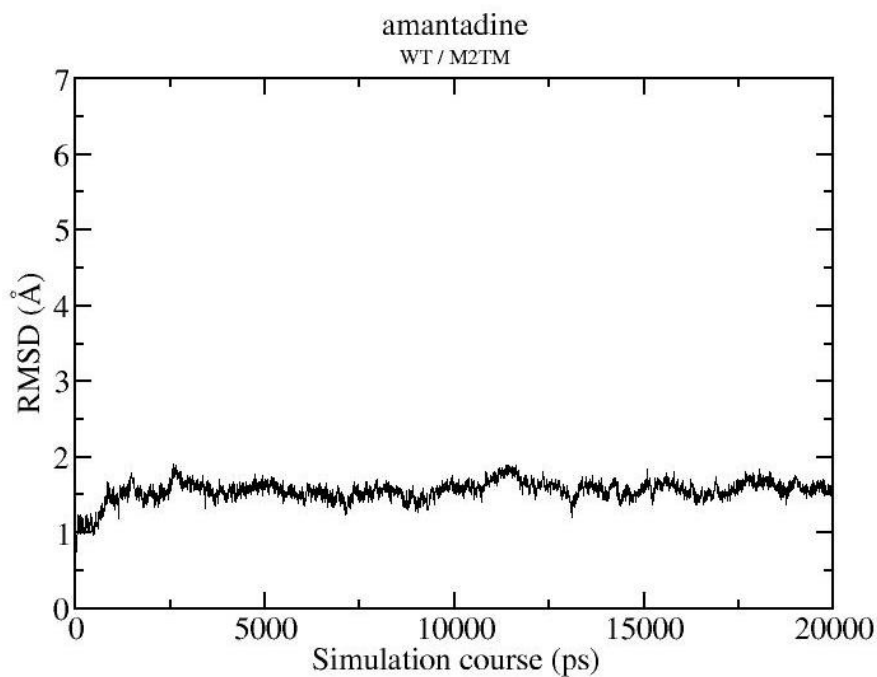


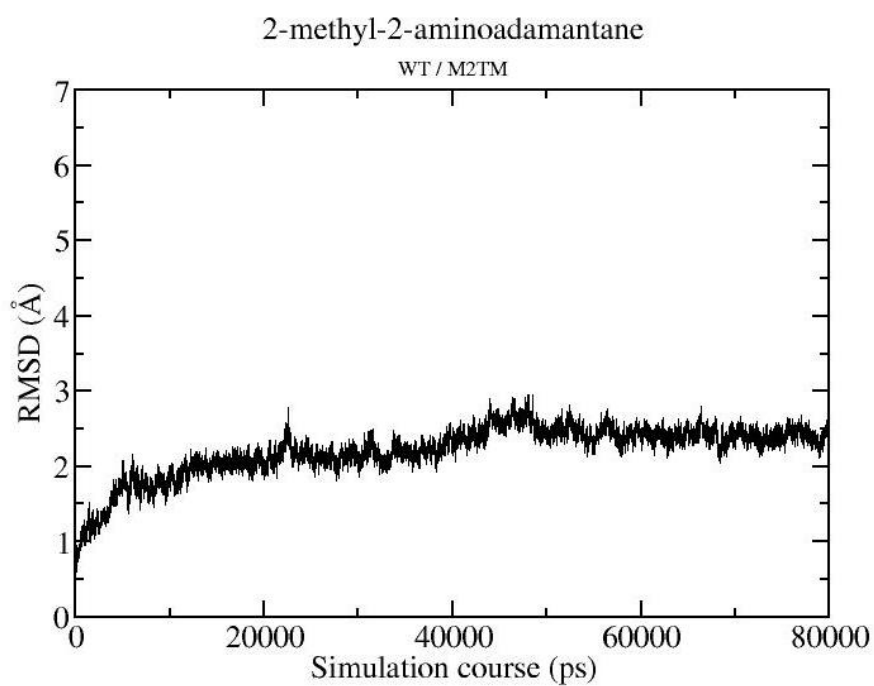
Scheme S1

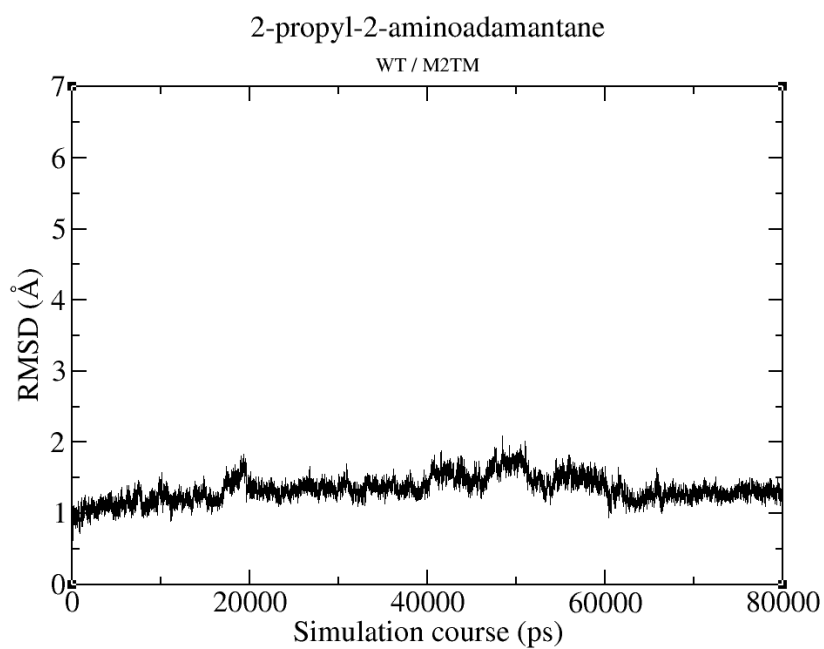
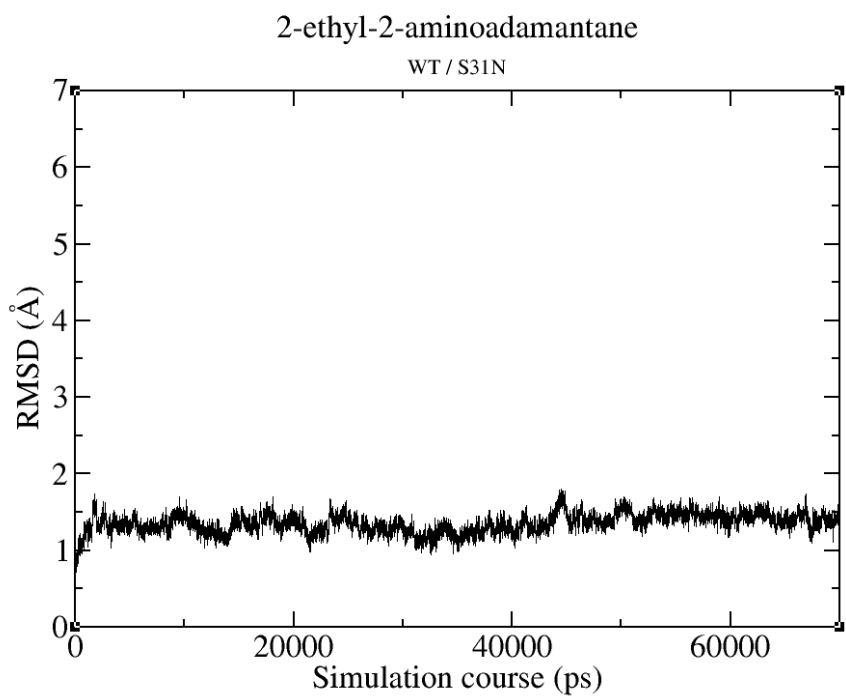


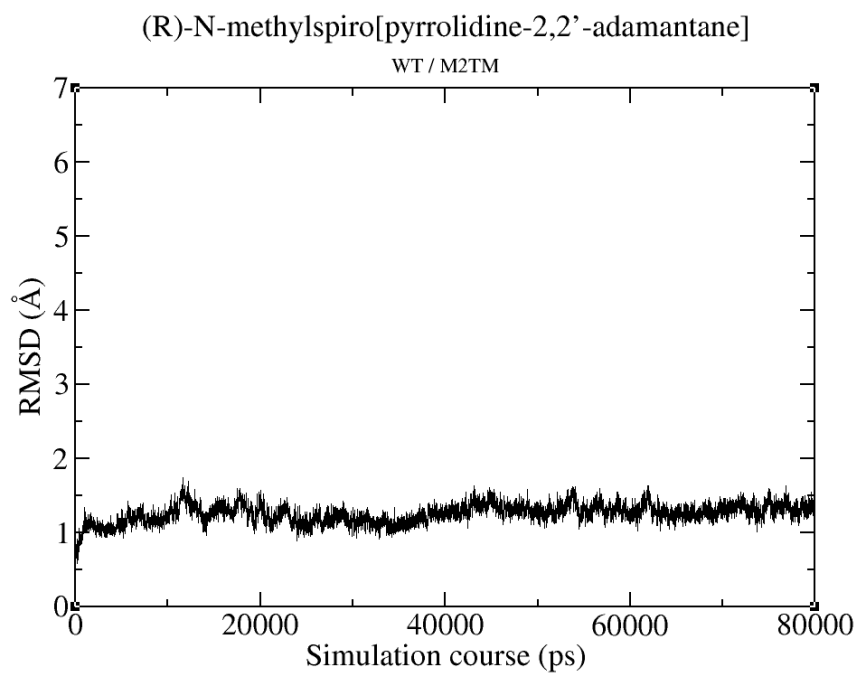
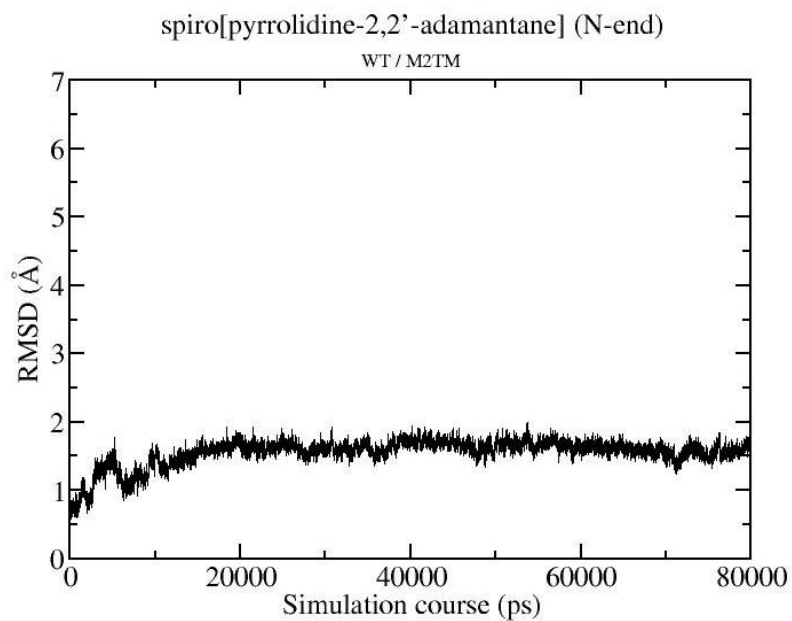
Scheme S2

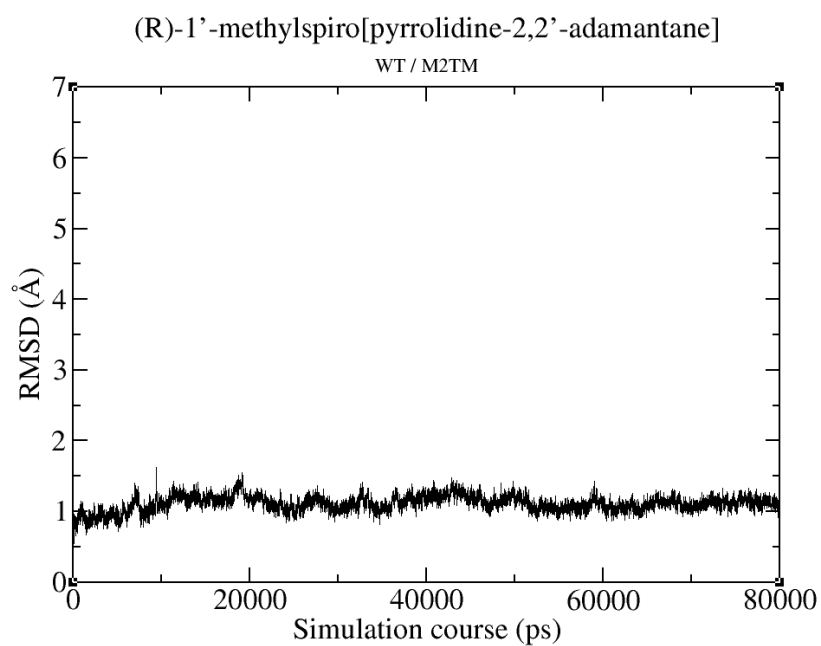
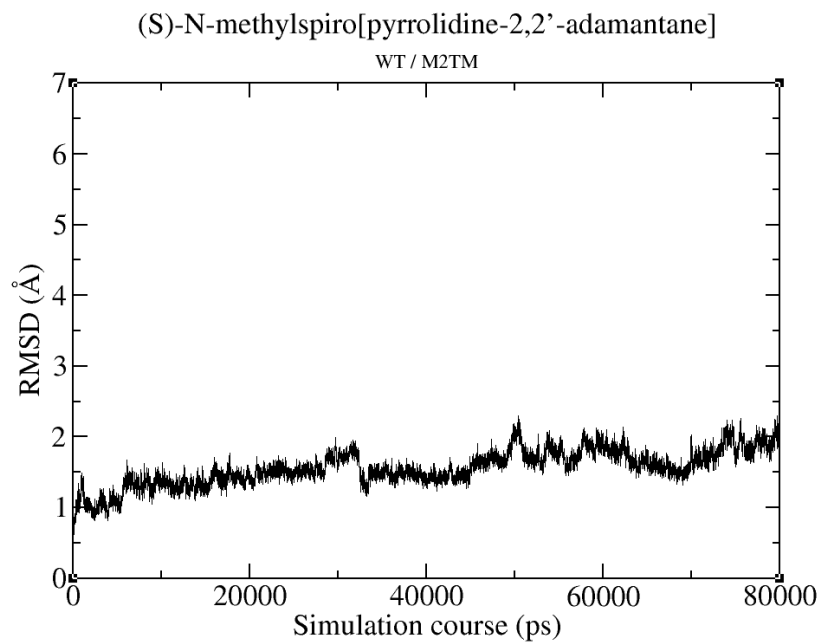
2.8.1.1 Few representative RMSD plots from the MD simulations of M2TM_{WT}-ligand and M2TM_{S31N} ligand complexes in DMPC bilayer (M2TM C α -carbons with respect to the initial structure of the production period)

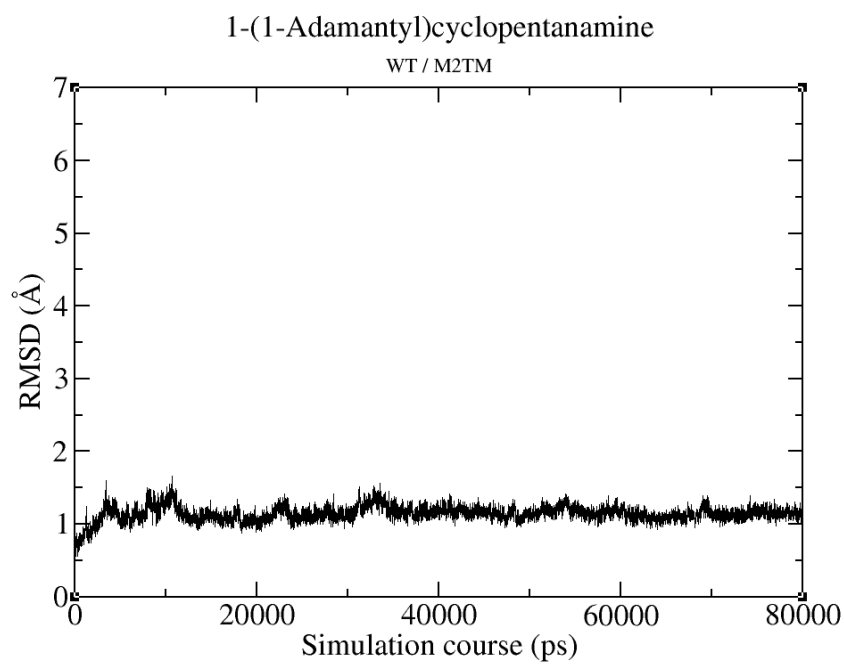
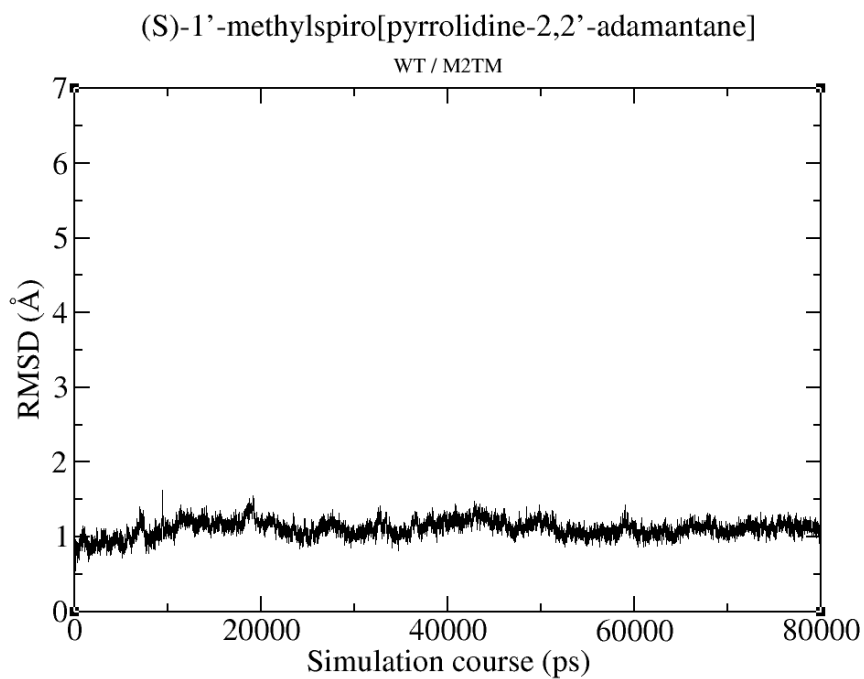


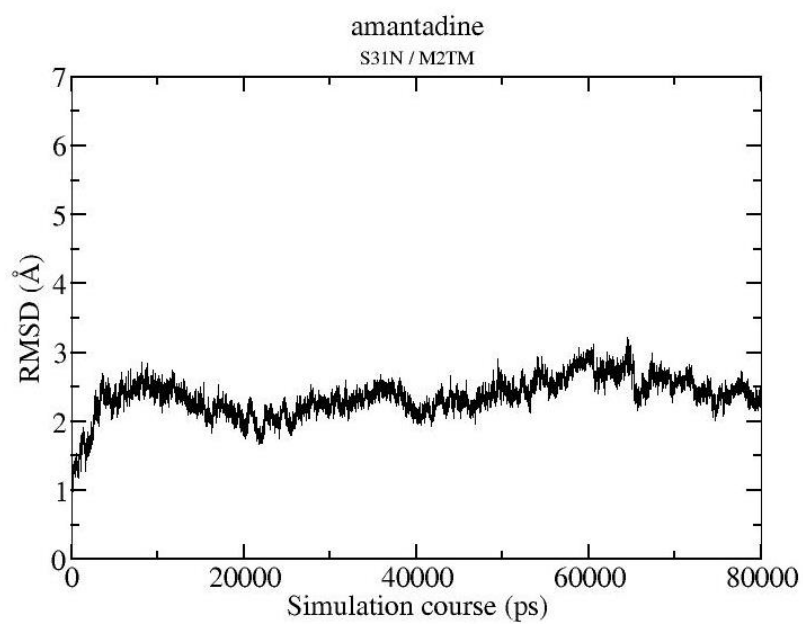
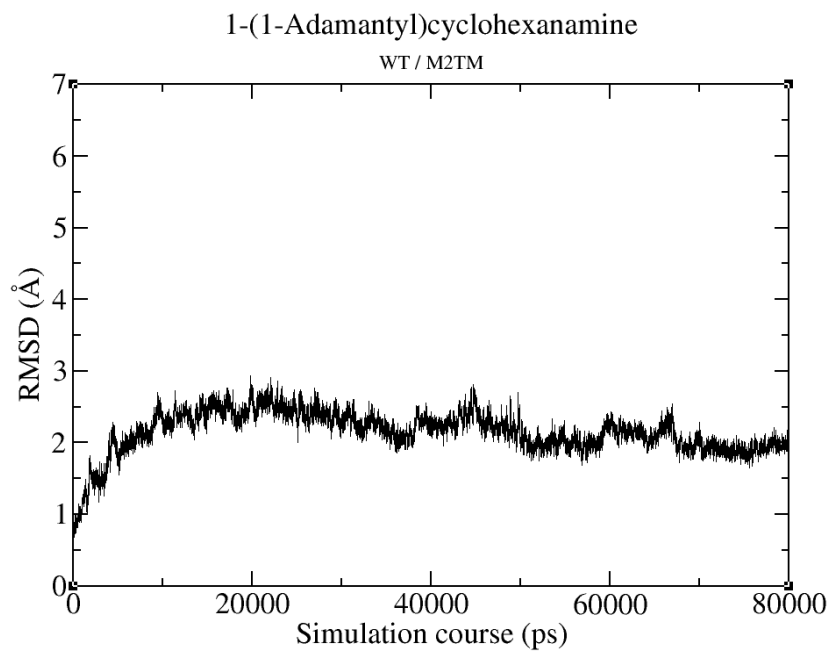


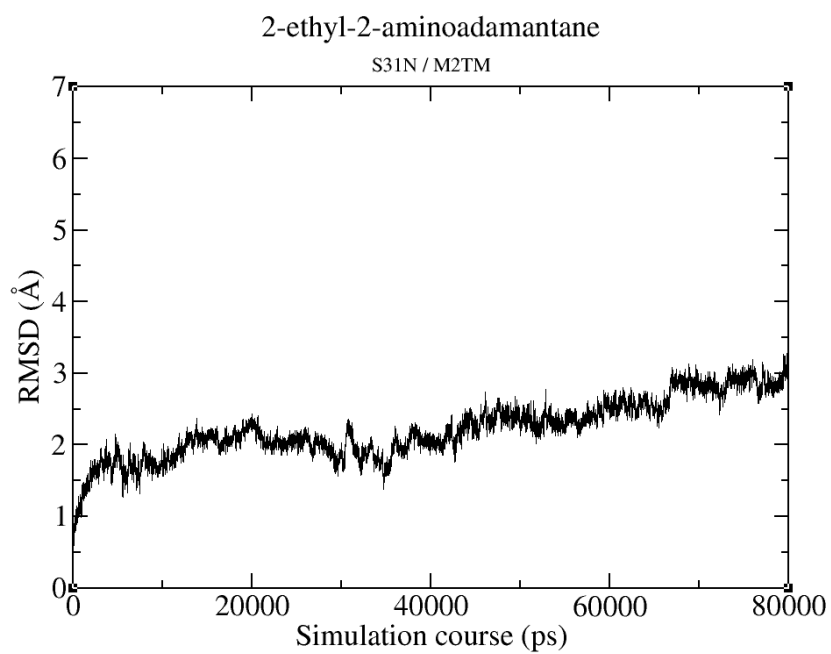
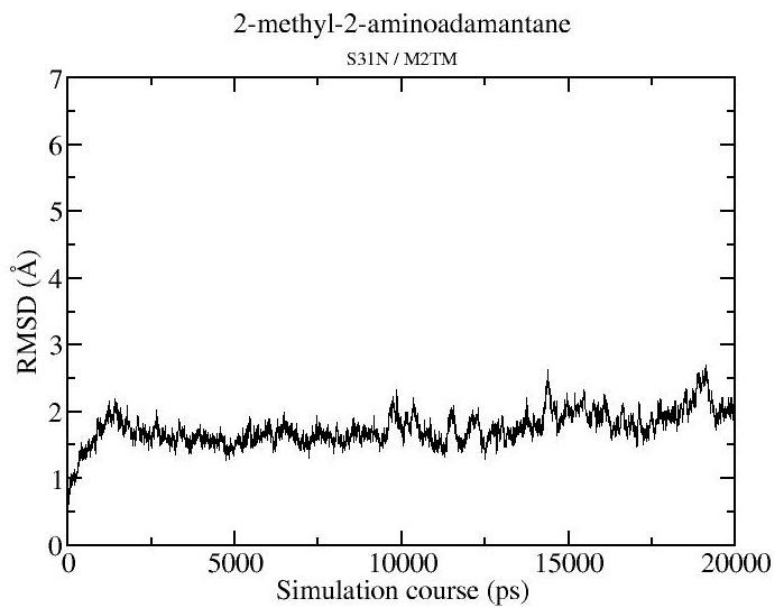


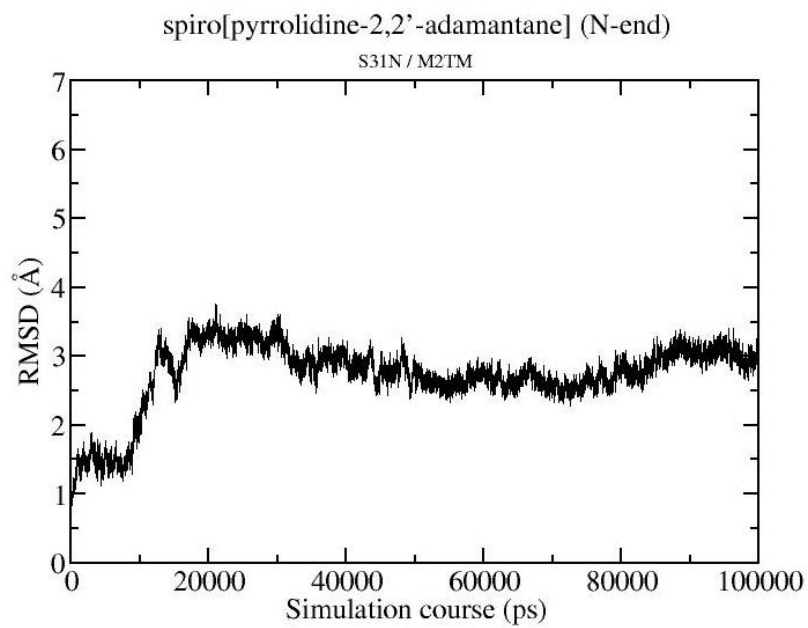
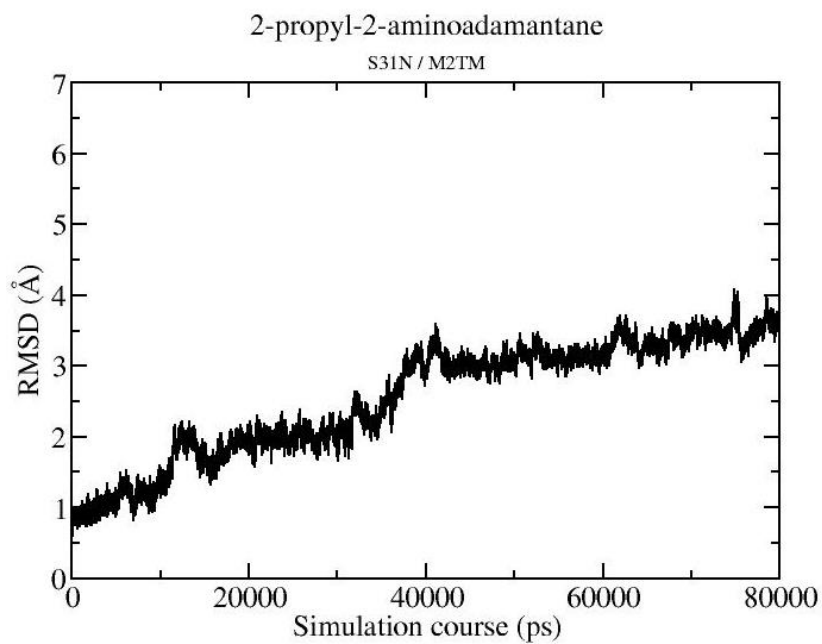


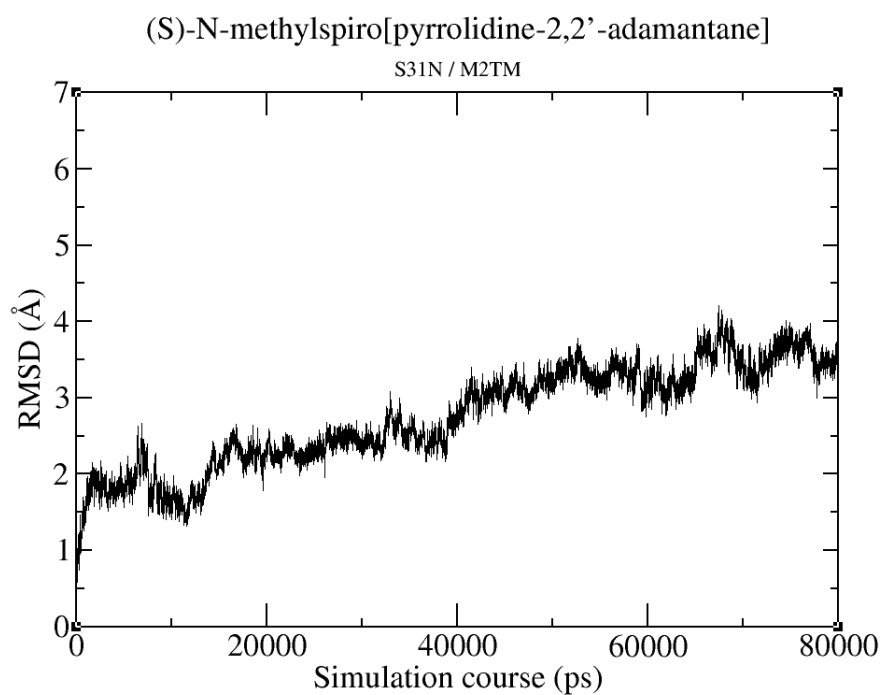
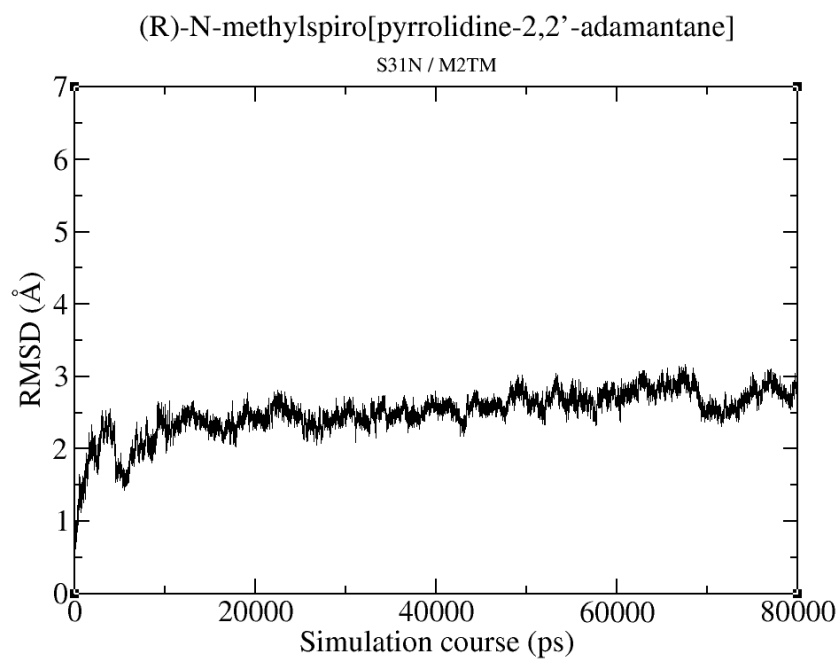


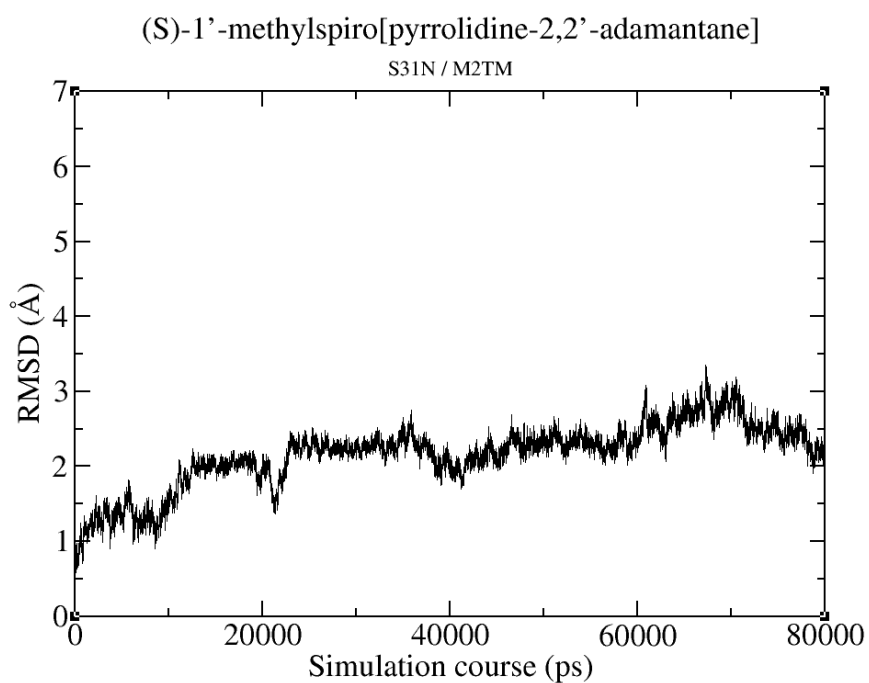
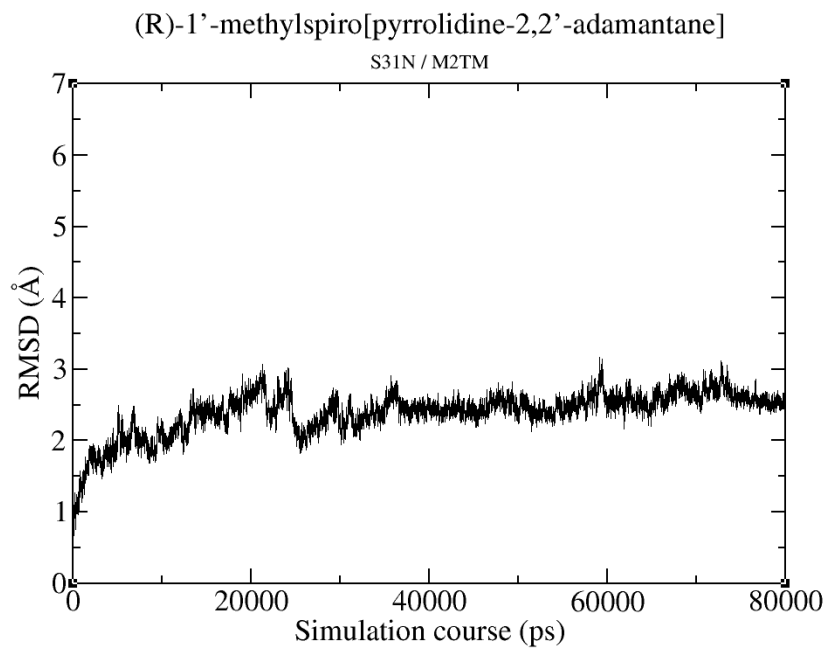


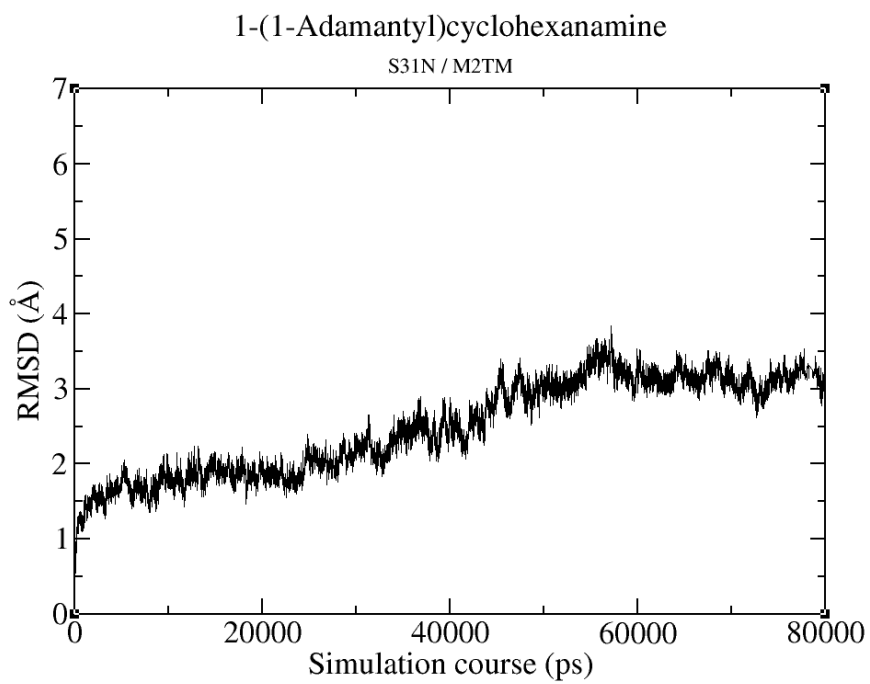
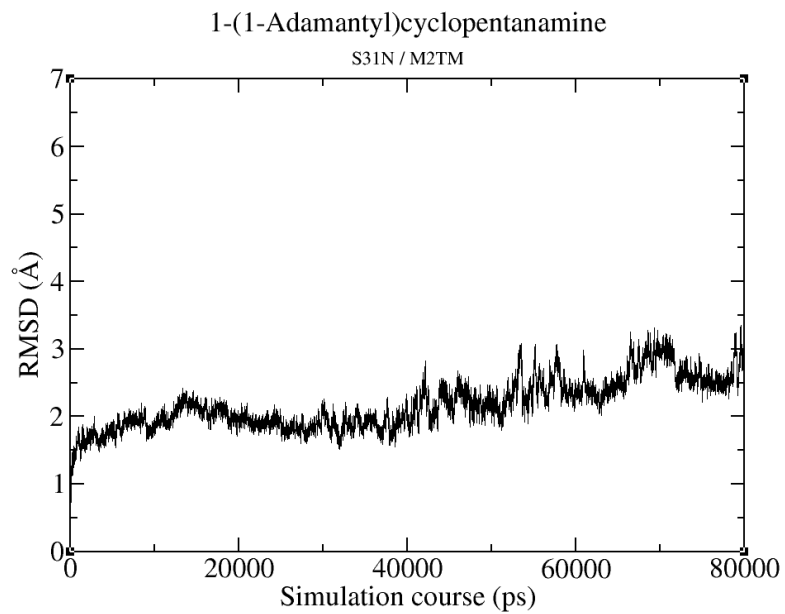






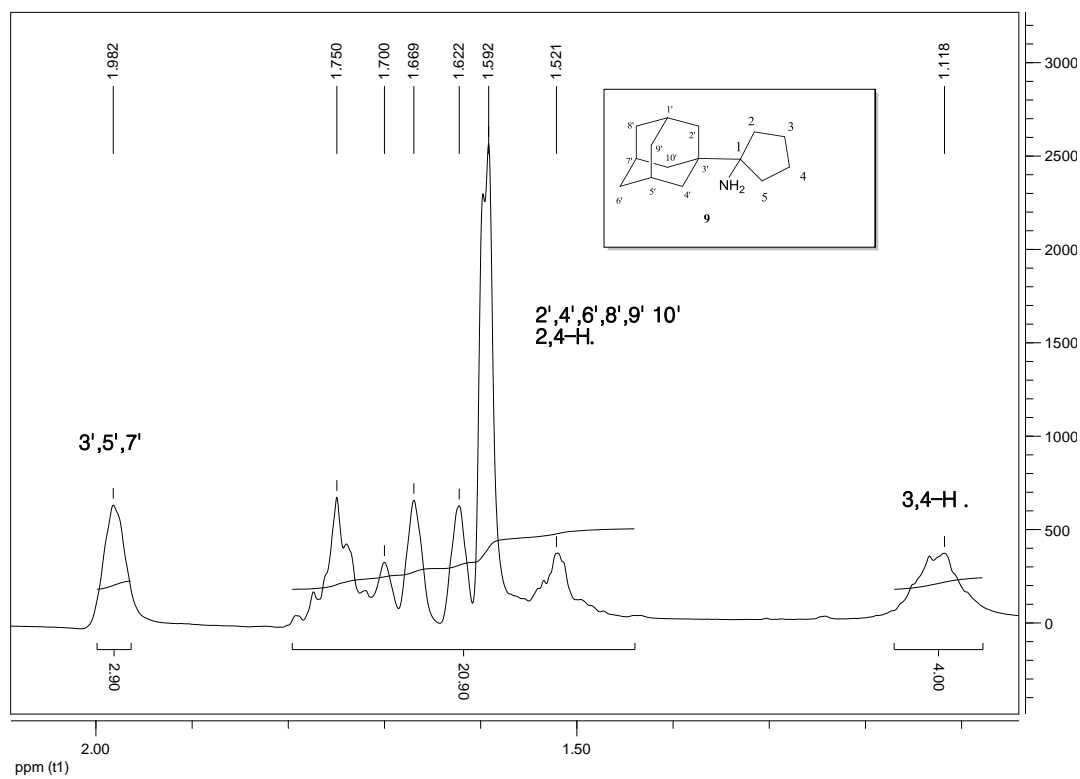


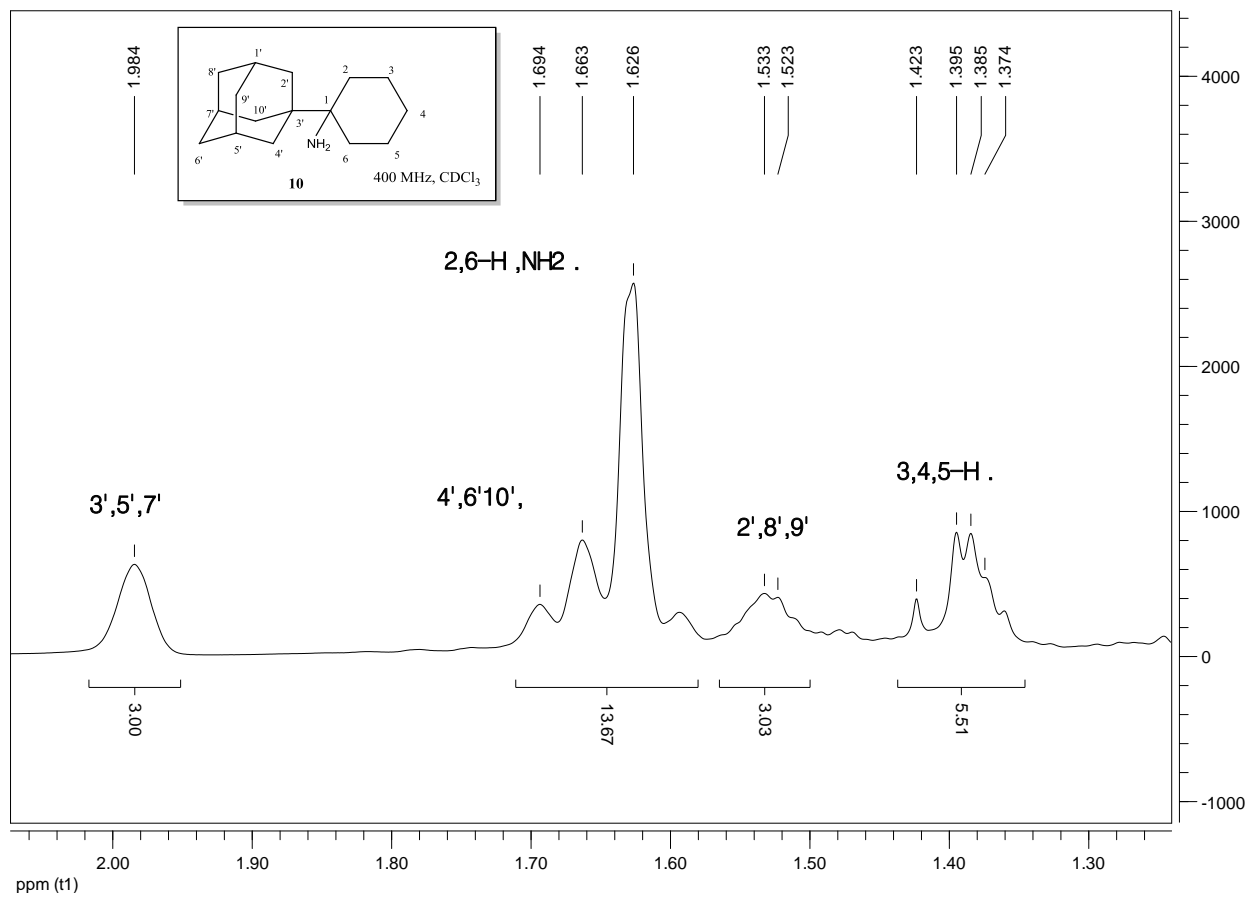




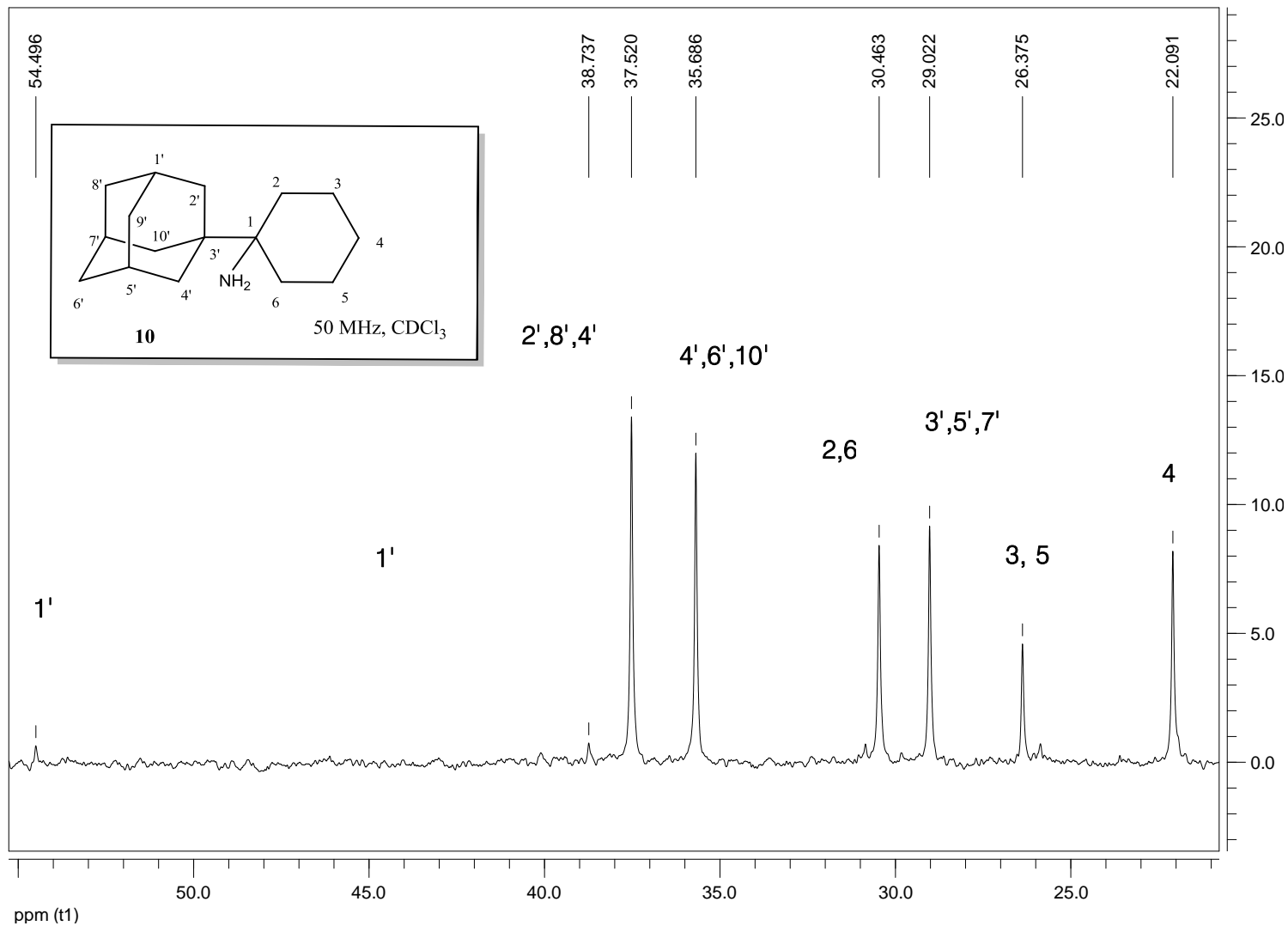
2.8.1.2 Nuclear Magnetic Resonance (NMR) Spectra of aminoadamantane compounds 8, 9 and 10 and intermediate derivatives 3a, 3b and 3c.

2.8.1.2.1 ^1H NMR spectra





2.8.1.2.2 ¹³C NMR spectra



2.9 References

¹Helenius, A. Unpacking the incoming influenza virus. *Cell*, **1992**, *69*, 577-578.

²(a) Wang, C.; Takeuchi, K.; Pinto, L. H.; Lamb, R. A. Ion channel activity of influenza A virus M2 protein: characterization of the amantadine block. *J. Virol.* **1993**, *67*, 5585-5594; (b) Chizhnikov, I. V.; Geraghty, F. M.; Ogden, D. C.; Hayhurst, A.; Antoniou, M.; Hay, A. J. Selective proton permeability and pH regulation of the influenza virus M2 channel expressed in mouse erythroleukaemia cells. *J. Physiol.* **1996**, *494*, 329-336.

³Hayden, F. G. Clinical applications of antiviral agents for chemoprophylaxis and therapy of respiratory viral infections. *Antiviral Res.* **1985**, 229-239.

⁴(a) Hu, J.; Asbury, T.; Achuthan, S.; Li, C.; Bertram, R.; Quine, J. R.; Fu, R.; Cross, T. A. Backbone structure of the amantadine-blocked trans-membrane domain M2 proton channel from influenza A virus. *Biophys. J.* **2007**, *92*, 4335-4343; (b) Hu, J.; Fu, R.; Cross, T. A. The chemical and dynamical influence of the anti-viral drug amantadine on the M2 proton channel transmembrane domain. *Biophys. J.* **2007**, *93*, 276-283.

⁵(a) Stouffer, A. L.; Acharya, R.; Salom, D.; Levine, A. S.; Di Costanzo, L.; Soto, C. S.; Tereshko, V.; Nanda, V.; Stayrook, S.; DeGrado, W. F. Structural basis for the function and inhibition of an influenza virus proton channel. *Nature* **2008**, *451*, 596-599; (b) Cady, S. D.; Schmidt-Rohr, K.; Wang, J.; Soto, C. S.; DeGrado, W. F.; Hong, M. Structure of the amantadine binding site of influenza M2 proton channels in lipid bilayers. *Nature* **2010**, *463*, 689-692; (c) Cady, S. D.; Wang, J.; Wu, Y.; DeGrado, W. F.; Hong, M. Specific binding of adamantane drugs and direction of their polar amines in the pore of the influenza M2 transmembrane domain in lipid bilayers and dodecylphosphocholine micelles determined by NMR spectroscopy. *J. Am. Chem. Soc.* **2011**, *133*, 4274-4284; (d) Jing, X.; Ma, C.; Ohigashi, Y.; Oliveira, F. A.; Jardetzky, T. S.; Pinto, L. H.; Lamb, R. A., Functional studies indicate amantadine binds to the pore of the influenza A virus M2 proton-selective ion channel. *Proc. Natl. Acad. Sci. U. S. A.* **2008**, *105*, 10967-10972. (e) Pielak, R. M.; Oxenoid, K.; Chou, J. J. Structural investigation of rimantadine inhibition of the AM2-BM2 chimera channel of influenza viruses. *Structure* **2011**, *19*, 1655-1663.

⁶Bright, R. A.; Medina, M. J.; Xu, X.; Perez-Oroz, G.; Wallis, T. R.; Davis, X. M.; Povinelli, L.; Cox, N. J.; Klimov, A. I. Incidence of adamantane resistance among influenza A (H3N2) viruses isolated worldwide from 1994 to 2005: a cause for concern. *Lancet* **2005**, *366*, 1175-1181.

⁷(a) Bright, R. A.; Shay, D. K.; Shu, B.; Cox, N. J.; Klimov, A. I. Adamantane resistance among influenza A viruses isolated early during the 2005-2006 influenza season in the United States. *J. Am. Med. Assoc.* **2006**, *295*, 891-894; (b) Lan, Y.; Zhang, Y.; Dong, L.; Wang, D.; Huang, W.; Xin, L.; Yang, L.; Zhao, X.; Li, Z.; Wang, W.; Li, X.; Xu, C.; Guo, J.; Wang, M.; Peng, Y.; Gao, Y.; Guo, Y.; Wen, L.; Jiang, T.; Shu, Y. A comprehensive surveillance of adamantane resistance among human influenza A virus isolated from mainland China between 1956 and 2009. *Antivir. Ther.* **2010**, *15*, 853-859.

⁸High levels of adamantane resistance among influenza A (H3N2) viruses and interim guidelines for use of antiviral agents--United States, 2005-06 influenza season. *MMWR Morb. Mortal Wkly Rep.* **2006**, *55*, 44-46.

⁹See for example: (a) Kolocouris, N.; Foscolos, G. B.; Kolocouris, A.; Marakos, P.; Pouli, N.; Fytas, G.; Ikeda, S.; De Clercq, E. Synthesis and antiviral activity evaluation of some aminoadamantane derivatives. *J. Med. Chem.* **1994**, *37*, 2896-2902. (b) Kolocouris, N.; Kolocouris, A.; Foscolos, G. B.; Fytas, G.; Neyts, J.; Padalko, E.; Balzarini, J.; Snoeck, R.; Andrei, G.; De Clercq, E. Synthesis and antiviral activity evaluation of some new aminoadamantane derivatives. 2. *J. Med. Chem.* **1996**, *39*, 3307-3318. (c) Kolocouris, A.; Spearpoint, P.; Martin, S. R.; Hay, A. J.; Lopez-Querol, M.; Sureda, F. X.; Padalko, E.; Neyts, J.; De Clercq, E. Comparisons of the influenza virus A M2 channel binding affinities, anti-influenza virus potencies and NMDA antagonistic activities of 2-alkyl-2-aminoadamantanes and analogues. *Bioorg. Med. Chem. Lett.* **2008**, *18*, 6156-6160.

¹⁰(a) Kolocouris, A.; Tzitzoglaki, C.; Johnson, F. B.; Zell, R.; Wright, A. K.; Cross, T. A.; Tietjen, I.; Fedida, D.; Busath, D. D. Aminoadamantanes with persistent in vitro efficacy against H1N1 (2009) influenza A. *J. Med. Chem.* **2014**, *57*, 4629-4639. (b) Torres, E.; Fernández, R.; Miquet, S. P.; Font-Bardia, M.; Vanderlinden, E.; Naesens, L.; Vázquez, S. Synthesis and anti-influenza A virus activity of 2,2-dialkylamantadines and related compounds. *ACS Med. Chem. Lett.* **2012**, *3*, 1065-1069. (c) Torres, E.; Duque, M. D.; Vanderlinden, E.; Ma, C.; Pinto, L. H.; Camps, P.; Froeyen, M.; Vazquez, S.; Naesens, L. Role of the viral hemagglutinin in the anti-influenza virus activity of newly synthesized polycyclic amine compounds. *Antiviral Res.* **2013**, *99*, 281-291.

¹¹Yi, M.; Cross, T. A.; Zhou, H.-X. A secondary gate as a mechanism for inhibition of the M2 proton channel by amantadine. *J. Phys. Chem. B.* **2008**, *112*, 7977-7979.

¹²Laohpongspaisan, C.; Rungrotmongkol, T.; Intharathep, P.; Malaisree, M.; Decha, P.; Aruksakunwong, O.; Sompornpisut, P.; Hannongbua, S. Why amantadine loses its function in influenza M2 mutants: MD Simulations. *J. Chem. Inf. Model.* **2009**, *49*, 847-852.

¹³Khurana, E.; Devane, R. H.; Dal Peraro, M.; Klein, M. L. Computational study of drug binding to the membrane-bound tetrameric M2 peptide bundle from influenza A virus. *Biochim. Biophys. Acta* **2011**, *1808*, 530-537.

¹⁴Wang, J.; Ma, C.; Fiorin, G.; Carnevale, V.; Wang, T.; Hu, F.; Lamb, R. A.; Pinto, L. H.; Hong, M.; Klein, M. L.; DeGrado, W. F. Molecular dynamics simulation directed rational design of inhibitors targeting drug-resistant mutants of influenza A virus M2. *J. Am. Chem. Soc.* **2011**, *133*, 12834-12841.

¹⁵Gu, R.-X.; Liu, L. A.; Wang, Y.-H.; Xu, Q.; Wei, D.-Q. Structural comparison of the wild-type and drug-resistant mutants of the influenza A M2 proton channel by molecular dynamics simulations. *J. Phys. Chem. B* **2013**, *117*, 6042-6051.

¹⁶Alhadeff, R.; Assa, D.; Astrahan, P.; Krugliak, M.; Arkin, I. T. Computational and experimental analysis of drug binding to the influenza M2 channel. *Biochim. Biophys. Acta* **2014**, *1838*, 1068-1073.

¹⁷(a) Gleed, M. L.; Busath, D. D. Why bound amantadine fails to inhibit proton conductance according to simulations of the drug-resistant influenza A M2 (S31N). *J. Phys. Chem. B* **2015**, *119*, 1225-12231. (b) Gleed, M. L.; Ioannidis, H.; Kolocouris, A.; Busath, D. D. Resistance-mutation (N31) effects on drug orientation and channel hydration in amantadine-bound influenza A M2. *J. Phys. Chem. B.* **2015**, *119*, 11548-11559.

- ¹⁸Llabres, S.; Juarez-Jimenez, J.; Masetti, M.; Leiva, R.; Vazquez, S.; Gazzarrini, S.; Moroni, A.; Cavalli, A.; Luque, F. J. Mechanism of the pseudoirreversible binding of amantadine to the M2 proton channel. *J. Am. Chem. Soc.*, **2016**, *138*, 15345–15358.
- ¹⁹Gianti, E.; Carnevale, V.; DeGrado, W. F.; Klein, M. L.; Fiorin, G., Hydrogen-Bonded Water Molecules in the M2 Channel of the Influenza A Virus Guide the Binding Preferences of Ammonium-Based Inhibitors. *J. Phys. Chem. B* **2015**, *119*, 1173-83.
- ²⁰(a) Andreas, L.B.; Barnes, A.B.; Corzilus, B.; Chou, J.J.; Miller, E.A.; Caporini, M.; Rosay, M.; Griffin, R.G. *Biochemistry* **2013**, *52*, 2774-82. (b) Andreas, L. B.; Eddy, M. T.; Pielak, R. M.; Chou, J.; Griffin, R. G. Magic angle spinning NMR investigation of influenza A M2(18-60): support for an allosteric mechanism of inhibition. *J. Am. Chem. Soc.* **2010**, *132*, 10958-10960.
- ²¹Wright, A. K.; Batsomboon, P.; Dai, J.; Hung, I.; Zhou, H.-X.; Dudley, G. B.; Cross, T. A. Differential Binding of Rimantadine Enantiomers to Influenza A M2 Proton Channel. *J. Am. Chem. Soc.* **2016**, *138*, 1506-1509.
- ²²Rey-Carrizo, M.; Barniol-Xicota, M.; Ma, C.; Frigolé-Vivas, M.; Torres, E.; Naesens, L.; Llabrés, S.; Juárez-Jiménez, J.; Luque, F. J.; DeGrado, W. F.; Lamb, R. A.; Pinto, L. H.; Vázquez, S. Easily Accessible Polycyclic Amines that Inhibit the Wild-Type and Amantadine-Resistant Mutants of the M2 Channel of Influenza A Virus. *J. Med. Chem.* **2014**, *57*, 5738–5747.
- ²³(a) Zhao, X.; Jie, Y.; Rosenberg, M. R.; Wan, J.; Zeng, S.; Cui, W.; Xiao, Y.; Li, Z.; Tu, Z.; Casarotto, M. G.; Hu, W. Design and synthesis of pinanamine derivatives as anti-influenza A M2 ion channel inhibitors. *Antiviral Res.* **2012**, *96*, 91-99; (b) Wang, J.; Wu, Y.; Ma, C.; Fiorin, G.; Pinto, L. H.; Lamb, R. A.; Klein, M. L.; DeGrado, W. F. Structure and inhibition of the drug-resistant S31N mutant of the M2 ion channel of influenza A virus. *Proc. Natl. Acad. Sci. U. S. A.* **2013**, *110*, 1315-1320. (c) Wang, J.; Ma, C.; Jo, H.; Canturk, B.; Fiorin, G.; Pinto, L. H.; Lamb, R. A.; Klein, M. L.; DeGrado, W. F. Discovery of novel dual inhibitors of wild-type and the most prevalent drug-resistant mutant, S31N, of M2 proton channel from influenza A virus. *J. Med. Chem.* **2013**, *56*, 2804-2812. (d) Wu, Y.; Canturk, B.; Jo, H.; Ma, C.; Gianti, E.; Klein, M. L.; Pinto, L. H.; Lamb, R. A.; Fiorin, G.; Wang, J.; DeGrado, W. F. Flipping in the pore: discovery of dual inhibitors that bind in different orientations to the wild-type versus the amantadine-resistant S31N mutant of the influenza A virus M2 proton channel. *J. Am. Chem. Soc.* **2014**, *136*, 17987–17995.
- ²⁴Williams, J. K.; Tietze, D.; Wang, J.; Wu, Y.; DeGrado, W. F.; Hong, M. Drug-induced conformational and dynamical changes of the S31N mutant of the influenza M2 proton channel investigated by solid-state NMR. *J. Am. Chem. Soc.* **2013**, *135*, 9885-97.
- ²⁵Homeyer, N.; Ioannidis, H.; Kolarov, F.; Gauglitz, G.; Zikos, C.; Kolocouris, A.; Gohlke, H. Interpreting Thermodynamic Profiles of Aminoadamantane Compounds Inhibiting the M2 Proton Channel of Influenza A by Free Energy Calculations. *J. Chem. Inf. Model.* **2016**, *56*, 110–126.

- ²⁶Ioannidis, H.; Drakopoulos, A.; Tzitzoglaki, C.; Homeyer, N.; Kolarov, F.; Gkeka, P.; Freudenberger, K.; Liolios, C.; Gauglitz, G.; Cournia, Z.; Gohlke, H.; Kolocouris, A. Alchemical Free Energy Calculations and Isothermal Titration Calorimetry Measurements of Aminoadamantanes Bound to the Closed State of Influenza A/M2TM. *J. Chem. Inf. Model.* **2016**, *56*, 862–876.
- ²⁷Gkeka, P.; Eleftheratos, S.; Kolocouris, A.; Cournia, Z. Free Energy Calculations Reveal the Origin of Binding Preference for Aminoadamantane Blockers of Influenza A/M2TM Pore. *J. Chem. Theory Comput.* **2013**, *9*, 1272-1281.
- ²⁸(a) Wu, C. H.; Ramamoorthy, A.; Opella, S. J. High-Resolution Heteronuclear Dipolar Solid-State NMR Spectroscopy. *J. Magn. Reson.* **1994**, *109*, 270-272. (b) Ahuja, S.; Jahr, N.; Im, S.-C.; Vivekanandan, S.; Popovych, N.; Le Clair, S. V.; Huang, R.; Soong, R.; Xu, J.; Yamamoto, K.; Nanga, R.P.; Bridges, A.; Waskell, L.; Ramamoorthy, A. *J. Biol. Chem.* **2013**, *288*, 22080-22095. (c) De Simone, A.; Mote, K. R.; Veglia, G. Structural Dynamics and Conformational Equilibria of SERCA Regulatory Proteins in Membranes by Solid-State NMR Restrained Simulations. *Biophys. J.* **2014**, *106*, 2566-2576.
- ²⁹Nevezorov, A.A.; Opella, S.J. Selective averaging for high-resolution solid-state NMR spectroscopy of aligned samples. *J. Magn. Reson.* **2007**, *185*, 59-70.
- ³⁰De Simone, A.; Mote, K. R.; Veglia, G. Structural dynamics and conformational equilibria of SERCA regulatory proteins in membranes by solid-state NMR restrained simulations. *Biophys. J.* **2014**, *106*, 2566-2576.
- ³¹Rühmann, E. H.; Rupp, M.; Betz, M.; Heine, A.; Klebe, G. Boosting affinity by correct ligand preorganization for the S2 pocket of thrombin: a study by isothermal titration calorimetry, molecular dynamics, and high-resolution crystal structures. *ChemMedChem* **2016**, *11*, 309-319.
- ³²Ma, C.; Polishchuk, A. L.; Ohigashia, Y.; Stouffer, A. L.; Schon, A.; Magavern, E.; Jing, X.; Lear, J. D.; Freirec, E.; Lamb, R. A.; DeGrado, W. F.; Pinto, L. H. Identification of the functional core of the influenza A virus A/M2 proton-selective ion channel. *Proc. Natl. Acad. Sci. U. S. A.* **2009**, *106*, 12283-12288.
- ³³Rosenberg, M. R.; Casarottol, M. G. Coexistence of two adamantane binding sites in the influenza A M2 ion channel. *Proc. Natl. Acad. Sci. U. S. A.* **2010**, *107*, 13866-13871.
- ³⁴Marassi, F.M.; Opella, S.J. A solid-state NMR index of helical membrane protein structure and topology. *J. Magn. Reson.* **2000**, *144*, 150-155.
- ³⁵Wang, J.; Denny, J.; Tian, C.; Kim, S.; Mo, Y.; Kovacs, F.; Song, Z.; Nishimura, K.; Gan, Z.; Fu, R.; Quine, J. R.; Cross, T. A. Imaging membrane protein helical wheels. *J. Magn. Reson.* **2000**, *144*, 162-167.
- ³⁶Andreas, L. B.; Eddy, M. T.; Chou, J. J.; Griffin, R. G. Magic-angle-spinning NMR of the drug resistant S31N M2 proton transporter from influenza A. *J. Am. Chem. Soc.* **2012**, *134*, 7215–7218.

- ³⁷Andreas, L. B.; Reese, M.; Eddy, M. T.; Gelev, V.; Ni, Q.-Z.; Miller, E. A.; Emsley, L.; Pintacuda, G.; Chou, J. J.; Griffin, R. G. Structure and mechanism of the influenza A M2₁₈₋₆₀ dimer of dimers. *J. Am. Chem. Soc.* **2015**, *137*, 14877–14886.
- ³⁸(a) Cady, S. D.; Luo, W. B.; Hu, F.; Hong, M. Structure and function of the influenza M2 proton channel. *Biochemistry* **2009**, *48*, 7356–7364. (b) Cady, S. D.; Hong, M. Effects of amantadine binding on the dynamics of bilayer-bound influenza A M2 transmembrane peptide studied by NMR relaxation. *J. Biomol. NMR* **2009**, *45*, 185–196. (c) Hu, F.; Luo, W.; Cady, S. D.; Hong, M. Conformational plasticity of the influenza A M2 transmembrane helix in lipid bilayers under varying pH, drug binding and membrane thickness. *Biochim. Biophys. Acta.* **2011**, *1808*, 415–423.
- ³⁹Cristian, L.; Lear, J. D.; DeGrado, W. F. Use of thiol-disulfide equilibria to measure the energetics of assembly of transmembrane helices in phospholipid bilayers. *Proc. Natl. Acad. Sci. U. S. A.* **2003**, *100*, 14772-14777.
- ⁴⁰Cady, S.; Wang, T.; Hong, M. Membrane-dependent effects of a cytoplasmic helix on the structure and drug binding of the influenza virus M2 protein. *J. Am. Chem. Soc.* **2011**, *133*, 11572–11579.
- ⁴¹Saotome, K.; Duong-Ly, K.; Howard, K.P. Influenza A M2 protein conformation depends on choice of model membrane. *Biopolymers* **2015**, *104*, 405-411.
- ⁴²(a) Chizhnikov, I. V.; Geraghty, F. M.; Ogden, D. C.; Hayhurst, A.; Antoniou, M.; Hay, A. J. Selective proton permeability and pH regulation of the influenza virus M2 channel expressed in mouse erythroleukaemia cells. *J. Physiol.* **1996**, *494*, 329–336. (b) Balannik, V.; Carnevale, V.; Fiorin, G.; Levine, B. G.; Lamb, R. A.; Klein, M. L.; DeGrado, W. F.; L Pinto, L. H. Functional studies and modeling of pore-lining residue mutants of the influenza A virus M2 ion channel. *Biochemistry* **2010**, *49*, 696–708. (c) Duque, M. D.; Ma, C.; Torres, E.; Wang, J.; Naesens, L.; Juarez-Jimenez, J.; Camps, P.; Luque, F. J.; DeGrado, W. F.; Lamb, R. A.; Pinto, L. H.; Vazquez, S. Exploring the size limit of templates for inhibitors of the M2 ion channel of influenza A virus. *J. Med. Chem.* **2011**, *54*, 2646-2457.
- ⁴³Schade, D.; Kotthaus, J.; Riebling, L.; Kotthaus, J.; Müller-Fielitz, H.; Raasch, W.; Hoffmann, A.; Schmidtke, M.; Clement, B.; ZanamivirAmidoxime- and N-Hydroxyguanidine-Based Prodrug Approaches to Tackle Poor Oral Bioavailability. *J. Pharm. Sci.* **2015**, *104*, 3208-3219.
- ⁴⁴Torres, E.; Duque, M. D.; Vanderlinden, E.; Ma, C.; Pinto, L. H.; Camps, P.; Froeyen, M.; Vázquez, S.; Naesens, L. Role of the viral hemagglutinin in the anti-influenza virus activity of newly synthesized polycyclic amine compounds. *Antiviral Res.* **2013**, *99*, 281.
- ⁴⁵Schmidtke, M.; Schnittler, U.; Jahn, B.; Dahse, H.-M.; Stelzner, A. A rapid assay for evaluation of antiviral activity against coxsackie virus B3, influenza virus A, and herpes simplex virus type 1. *J. Virol. Methods* **2001**, *95*, 133-143.

- ⁴⁶ Miao, Y.; Fu, R.; Zhou, H. X.; Cross, T. A. Dynamic short hydrogen bonds in histidine tetrad of full-length M2 proton channel reveal tetrameric structural heterogeneity and functional mechanism. *Structure* **2015**, *23*, 2300-2308.
- ⁴⁷ Yi, M.; Cross, T. A.; Zhou, H. X. Conformational heterogeneity of the M2 proton channel and a structural model for channel activation. *Proc. Natl. Acad. Sci. U. S. A.* **2009**, *106*, 13311-13316.
- ⁴⁸ Fytas, G.; Kolocouris, N.; Foscolos, G. B.; Vamvakides, A., Synthesis and pharmacological study of some adamantylcyclopentanamines. *Eur. J. Med. Chem.* **1991**, *26*, 563-566.
- ⁴⁹ (a) Stamatiou, G.; Foscolos, G. B.; Fytas, G.; Kolocouris, A.; Kolocouris, N.; Pannecouque, C.; Witvrouw, M.; Padalko, E.; Neyts, J.; De Clercq, E. Heterocyclic rimantadine analogues with antiviral activity. *Bioorg. Med. Chem.* **2003**, *11*, 5485-92. (b) Kraus, G. A.; Siclovan, T. M., Bridgehead intermediates in organic synthesis. A reproducible synthesis of adamantane-containing compounds. *J. Org. Chem.* **1994**, *59*, 922-923.
- ⁵⁰ Kovacs, F. A.; Cross, T. A. Transmembrane four-helix bundle of influenza A M2 protein channel: structural implications from helix tilt and orientation. *Biophys. J.* **1997**, *73*, 2511-2517.
- ⁵¹ Kolocouris, A.; Zikos, C.; Broadhurst, R. W. ¹⁹F NMR detection of the complex between amantadine and the receptor portion of the influenza A M2 ion channel in DPC micelles. *Bioorg. Med. Chem. Letters* **2007**, *17*, 3947-3952.
- ⁵² Hansen, R. K.; Broadhurst, R. W.; Skelton, P. C.; Arkin, I. T. Hydrogen/deuterium exchange of hydrophobic peptides in model membranes by electrospray ionization mass spectrometry. *J. Am. Soc. Mass Spectr.* **2002**, *13*, 1376-87.
- ⁵³ Ladbury, J. E.; Klebe, G.; Freire, E. Adding calorimetric data to decision making in lead discovery: a hot tip. *Nat. Rev. Drug Discov.* **2010**, *9*, 23-27.
- ⁵⁴ Perozzo, R.; Folkers, G.; Scapozza, L. Thermodynamics of protein-ligand interactions: history, presence, and future aspects. *J. Recept. Signal Transduct. Res.* **2004**, *24*, 1-52.
- ⁵⁵ (a) Salom, D.; Hill, B. R.; Lear, J. D.; DeGrado, W. F. pH-dependent tetramerization and amantadine binding of the transmembrane helix of M2 from the influenza A virus. *Biochemistry* **2000**, *39*, 14160-14170. (b) Stouffer, A. L.; Ma, C.; Cristian, L.; Ohigashi, Y.; Lamb, R. A.; Lear, J. D.; Pinto, L. H.; DeGrado, W. F. The interplay of functional tuning, drug resistance, and thermodynamic stability in the evolution of the M2 proton channel from the influenza A virus. *Structure* **2008**, *16*, 1067-1076. (c) Stouffer, A. L.; Nanda, V.; Lear, J. D.; DeGrado, W. F. Sequence determinants of a transmembrane proton channel: an inverse relationship between stability and function. *J. Mol. Biol.* **2005**, *347*, 169-179.
- ⁵⁶ Wiseman, T., Willison, S., Brandts, J.F., Lin, L.-N. Rapid measurement of binding constants and heats of binding using a new titration calorimeter *Anal. Biochem.* **1989**, *179* 131-137.

- ⁵⁷ Doyle, M. L. Characterization of binding interactions by isothermal titration calorimetry. *Curr. Opin. Biotech.* **1997**, *8*, 31-35.
- ⁵⁸ *Origin 8.1G SR1*, v8.1.13.88; OriginLab Corporation, Northampton, MA, USA: **2009**.
- ⁵⁹ Fung, B. M.; Khitrin, A. K.; Ermolaev, K. An improved broadband decoupling sequence for liquid crystals and solids. *J. Magn. Reson.* **2000**, *142*, 97-101.
- ⁶⁰ Delaglio, F.; Grzesiek, S.; Vuister, G. W.; Zhu, G.; Pfeifer, J.; Bax, A. NMRPipe: a multidimensional spectral processing system based on UNIX pipes. *J. Biomol. NMR* **1995**, *6*, 277-293.
- ⁶¹ Gorkov, P. L.; Chekmenev, E. Y.; Li, C.; Cotten, M.; Buffy, J. J.; Traaseth, N. J.; Veglia, G.; Brey, W. W. Using low-E resonators to reduce RF heating in biological samples for static solid-state NMR up to 900 MHz. *J. Magn. Reson.* **2007**, *185*, 77-93.
- ⁶² McNeill, S. A., P. L. Gorkov, K. Shetty, W. W. Brey, and J. R. Long. A low-E magic angle spinning probe for biological solid state NMR at 750 MHz. *J. Magn. Reson.* **2009**, *197*, 135-144.
- ⁶³ Morcombe, C. R., Zilm, K. W. Chemical shift referencing in MAS solid state NMR. *J. Magn. Reson.* **2003**, *162*, 479-486.
- ⁶⁴ Markley, J. L., Bax, A.; Arata, Y.; Hilbers, C. W.; Kaptein, R.; Sykes, B. D.; Wright, P. E.; Wüthrich, K. Recommendations for the presentation of NMR structures of proteins and nucleic acids. *J. Mol. Biol.* **1998**, *280*, 933-952.
- ⁶⁵ Harris, R. K.; Becker, E. D.; Cabral de Menezes, S. M.; Goodfellow, R.; Granger, P. NMR nomenclature: nuclear spin properties and conventions for chemical shifts. IUPAC recommendations 2001. *Solid State Nucl. Magn. Reson.* **2002**, *22*, 458-483.
- ⁶⁶ *Maestro*, version 8.5; Schrodinger, Inc.: New York, NY, **2008**.
- ⁶⁷ Pielak, R. M.; Schnell, J. R.; Chou, J. J. Mechanism of drug inhibition and drug resistance of influenza A M2 channel. *Proc. Natl. Acad. Sci. U. S. A.* **2009**, *106*, 7379-7384.
- ⁶⁸ Thomaston, J. L.; DeGrado, W. F. Crystal structure of the drug-resistant S31N influenza M2 proton channel. *Protein Sci.* **2016**, *25*, 1551-1554.
- ⁶⁹ Jorgensen, W. L.; Chandrasekhar, J.; Madura, J. D.; Impey, R. W.; Klein, M. L. Comparison of simple potential functions for simulating liquid water. *J. Chem. Phys.* **1983**, *79*, 926-935.
- ⁷⁰ (a) *Desmond Molecular Dynamics System*, version 3.0; D. E. Shaw Research: New York, NY, **2011**. (b) *Desmond Molecular Dynamics System*, version 3.1; D. E. Shaw Research: New York, NY, **2012**. (c) Bowers, K. J.; Chow, E.; Xu, H.; Dror, R. O.; Eastwood, M. P.; Gregersen, B. A.; Klepeis, J. L.; Kolossvary, I.; Moraes, M. A.;

Sacerdoti, F. D.; Salmon, J. K.; Shan, Y.; Shaw, D. E. Scalable algorithms for molecular dynamics simulations on commodity clusters. In *Proceedings of the ACM/IEEE Conference on Supercomputing(SC06)*, Tampa, Florida, **2006**.

⁷¹*Maestro-Desmond Interoperability Tools*, version 3.1; Schrodinger: New York, NY, **2012**.

⁷²(a) Jorgensen, W. L.; Maxwell, D. S.; Tirado-Rives, J. Development and testing of the OPLS all-atom force field on conformational energetics and properties of organic liquids. *J. Am. Chem. Soc.* **1996**, *118*, 11225-11236. (b) Rizzo, R. C.; Jorgensen, W. L. OPLS all-atom model for amines: resolution of the amine hydration problem. *J. Am. Chem. Soc.* **1999**, *121*, 4827-4836.

⁷³Kaminski, G.; Friesner, R. A.; Tirado-Rives, J.; Jorgensen, W. L. Evaluation and reparametrization of the OPLS-AA force field for proteins via comparison with accurate quantum chemical calculations on peptides. *J. Phys. Chem. B* **2001**, *105*, 6474-6487.

⁷⁴Shivakumar, D.; Williams, J.; Wu, Y.; Damm, W.; Shelley, J.; Sherman, W. Prediction of absolute solvation free energies using molecular dynamics free energy perturbation and the OPLS force field. *J. Chem. Theory Comput.* **2010**, *6*, 1509-1519.

⁷⁵Darden, T.; York, D.; Pedersen, L. Particle mesh Ewald: an N log(N) method for Ewald sums in large systems *J. Chem. Phys.* **1993**, *98*, 10089-10092.

⁷⁶Essmann, U.; Perera, L.; Berkowitz, M. L.; Darden, T.; Lee, H.; Pedersen, L. G. A Smooth particle mesh Ewald method. *J. Chem. Phys.* **1995**, *103*, 8577-8593.

⁷⁷Martyna, G. J. T., D. J.; Klein, M. L. Constant-pressure molecular-dynamics algorithms. *J. Chem. Phys.* **1994**, *101*, 4177-4189.

⁷⁸Humphreys, D. D.; Friesner, R. A.; Berne, B. J. A multiple-time-step molecular-dynamics algorithm for macromolecules. *J. Phys. Chem.* **1994**, *98*, 6885-6892.

⁷⁹Koynova, R.; Caffrey, M. Phases and phase transitions of the phosphatidylcholines. *Biochim. Biophys. Acta* **1998**, *1376*, 91-145.

CHAPTER 3

Unraveling the Binding, Proton Blockage and Inhibition of the influenza M2 WT and S31N by Rimantadine variants

3.1 Abstract

Recently, the binding kinetics of a ligand-target interaction, such as the residence time of a small molecule on its protein target, are seen as increasingly important for drug efficacy. Here we investigate these concepts to explain binding and proton blockage of rimantadine variants bearing progressively larger alkyl group size to influenza A virus M2 WT (wild type) and M2 S31N protein proton channel. We showed that resistance of M2 S31N to rimantadine analogues compared to M2 WT resulted from their higher k_{off} rates compared to the k_{on} rates according to electrophysiology (EP) measurements. This is due to the fact that, in M2 S31N, the loss of the V27 pocket for the adamantyl cage resulted in low residence time inside the M2 pore. Both rimantadine enantiomers have similar channel blockage and binding k_{on} and k_{off} against M2 WT. To compare the potency between the rimantadine variants against M2 we applied approaches using different mimicry of M2, i.e., isothermal titration calorimetry (ITC) and molecular dynamics (MD) simulations, EP and antiviral assays, which all prioritize the same rimantadine analogue as an agent against M2 WT bearing influenza A viruses. It was also shown that a small change in an amino acid at site 28 (V28I) of M2 WT, which does not line the pore, seriously affects M2 WT blockage efficiency.

3.2 Introduction

The details of the complex formed between a drug molecule and its protein target is of key importance for *in vivo* drug efficacy. Most efforts in early drug discovery focus on optimization of drug-receptor interactions, such as target affinity and selectivity, while minimizing potential adverse ADMET effects. However, novel approaches are necessary in early drug discovery for optimal drug design and improved therapy. Recently, the kinetics of a ligand-target interaction, such as the residence time of a small molecule on its protein target, is seen as increasingly important for *in vivo* efficacy and safety.¹

1 and **2** are effective prophylactics and therapeutics against IAVs, provided they contain the WT M2TM such as A/Udorn/72 H3N2 (Udorn) and A/Hong Kong/68 H3N2 (HK), but not those containing M2 S31N such as A/WSN/33 H1N1 (WSN) (Figure 1). Recent comparison of oriented sample (OS) ssNMR spectra revealed that the binding mode of many aminoadamantane ligands to M2TM WT is similar to **1**.² On the assumption that M2TM is a minimal model for M2 binding,¹¹ these high resolution structures have been used for the design of new aminoadamantane ligands against M2 by employing MD simulations.^{3,4,5} We have measured binding affinities of aminoadamantane derivatives using ITC^{6,7} and other methods⁸ and used them as probes for accessing free energy methods to predict relative binding affinities.^{6,7,9}

ssNMR, ITC, EP, antiviral assays and MD simulations suggest stronger binding interactions for aminoadamantanes to M2 WT compared to negligible or weak binding to M2 S31N.² We showed that this is due to reshaping of the M2 pore when N31 is present, which in contrast to M2 WT, leads: a) to the loss of the V27 pocket for the adamantyl cage and to a predominant orientation of the ligand's ammonium group toward the N-terminus and, b) to the lack of a helical kink upon ligand binding.² We published recently that rimantadine enantiomers showed no significant difference in terms of their M2 WT channel blockage (%-blocking at 2 or 5 min), in binding to the corresponding M2TM WT (using ITC), or in antiviral potency against M2 WT influenza viruses within the limits of detection.¹⁰ This is consistent with the findings reported many decades ago that the biological activity of **2-R** and **2-S** *in vivo* against IAV is the same.¹¹

Rimantadine **2** is ranked among the best binders to M2TM WT 2'3'6'7'8'9'^{12,13,14,10} and most potent anti-IAV agents among the aminoadamantane derivatives. 2'3'4'5'6'7'8'¹⁰ Thus, the synthesis of symmetrical analogues of **2** with the addition of two methyl (**3**), ethyl (**4**) and n-propyl (**5**) groups on the carbon bridge was accomplished [see compounds **3-5** with structure AdCR₂NH₂ (R=Me, Et, Pr) in Scheme 1] aiming at filling progressively from **3** to **5** the extra space between the ligand and the walls in M2 WT or M2 S31N with a few alkyl groups. Binding affinities of **1**, **2**, **2-R**, **2-S**, and **3-5** were measured by ITC and interpreted using MD simulations against the

M2TM WT and its S31N variant in their closed form at pH 8. Furthermore, we measured the antiviral activity of the rimantadine analogues against IAV strains and the blocking effect of the compounds against full length M2 using EP. Antiviral potency to the aminoadamantanes is exhibited by IAV containing M2 WT and not by IAV with M2 S31N. More specifically, the antiviral potency of the compounds was measured against Udorn and HK influenza viruses in MDCK cells. The amino acid sequences of M2 WT in Udorn and HK are identical, not just in the TM region but in the full length protein. The antiviral potency of the compounds was additionally measured against amantadine-resistant WSN, and the amantadine-sensitive WSN M2 N31S (generated by reverse genetics from WSN) in MDCK cells. Then, the blocking effect of **1**, **2**, **2-R**, **2-S**, and **3-5** against full length Udorn M2 protein (amantadine sensitive) and Udorn M2 S31N (amantadine resistant) was determined using EP with a two-electrode voltage clamp (TEVC) assay, and the kinetics of binding (i.e. the k_{on} and k_{off} rate constants) were compared.

In this context we seek also to investigate further the block of rimantadine enantiomers against Udorn M2 WT protein in EP, considering the differences in resonances seen in ssNMR studies³² of **2-R** or **2-S** bound to the full-length Udorn M2 protein. EP was also performed using full length Udorn M2 V28I to examine whether small changes in WSN in the side chains of amino acids that do not line the pore (Figure 1) affect aminoadamantane blocking properties. In summary, we compared the potency between the rimantadine ligands against M2 using four different M2 mimicry methods, i.e. ITC, MD simulations, EP and antiviral assays (Figure 2).

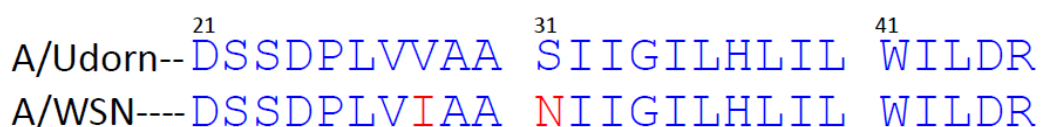


Figure 1. Transmembrane domain sequence for A/Udorn/72 (and A/Hong Kong/68) compared to A/WSN/33, which differ at positions 28 and 31.

Effect of Subtle Changes of Aminoadamantanes Structure and Influenza M2TM Structure in the Binding Kinetics, Affinity and Potency

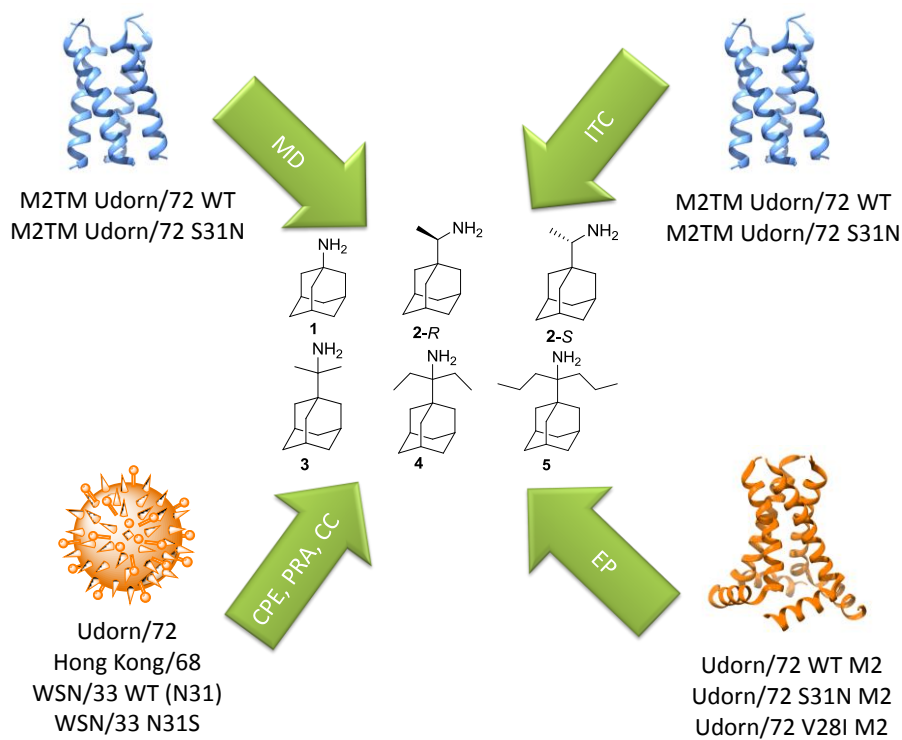
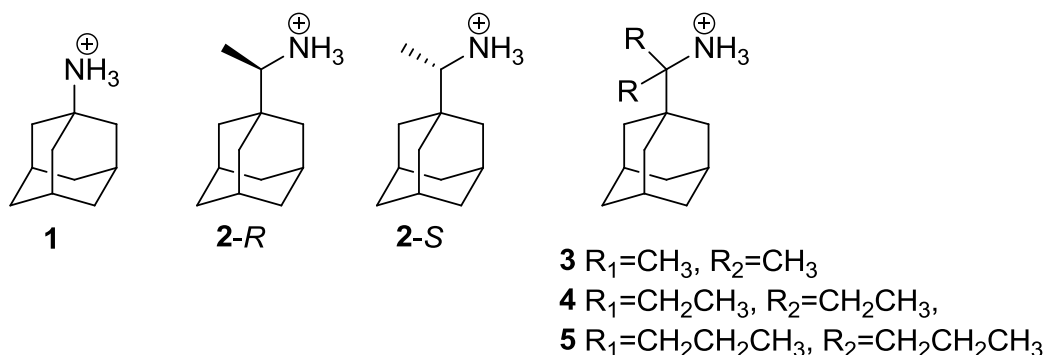


Figure 2. Comparison of the potency between the rimantadine ligands against M2 using different mimicry of M2 i.e. ITC and MD simulations, EP and antiviral assays.

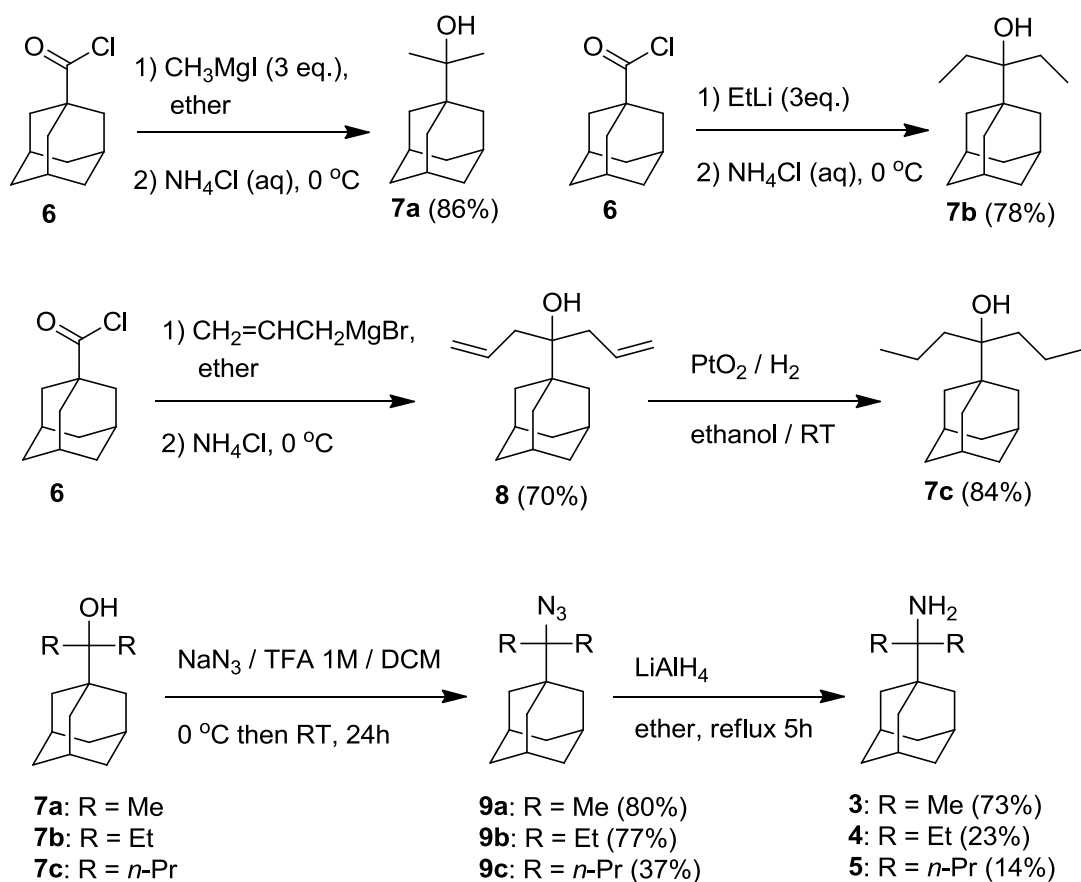
3.3 Results and Discussion

3.3.1 Compound synthesis

For the synthesis of primary *tert*-alkyl amines **3-5** the raw *tert*-alkyl alcohols **7a-c** were prepared according to Scheme 2 from the reaction between 1-adamantane carbonyl chloride **6** and an organometallic reagent. *Tert*-alkyl alcohol **7a** was prepared in high yield from the reaction between 1-adamantane carbonyl chloride **6** and methylmagnesium iodide. *Tert*-alkyl alcohol **7b** was prepared in high yield from the reaction between 1-adamantane carbonyl chloride **6** and ethyl lithium. The reaction of allylmagnesium bromide with 1-adamantane carbonyl chloride **6** afforded diallyl alcohol **8** which was subsequently hydrogenated under PtO₂ as the catalyst to afford *tert*-alkyl alcohol **7c**. Treatment of *tert*-alkyl alcohols **7a,b** with NaN₃/TFA in dichloromethane afforded azides **9a,b** in high yields. Azides **9a, b** were subjected to reduction through LiAlH₄ to form *tert*-alkyl amine **3** in a good yield and **4** in a moderate yield. The same procedure when applied for the synthesis of amine **5** afforded azide **9c** with 37% yield but the yield for the reduction step was 14% due to the formation of unsaturated products and extensive decomposition.



Scheme 1. Structures of studied aminoadamantane derivatives **1-5**



Scheme 2. Synthetic scheme for the preparation of corresponding *tert*-alkyl amines **3-5**.

3.3.2 ITC measurements

Table 1 includes thermodynamic parameters of binding against M2TM WT and M2TM S31N. Binding affinities were determined by ITC^{15,16,17} for M2TM-ligand systems in dodecylphosphocholine (DPC) micelles at pH 8, where M2TM fragments form stable tetramers.^{18,19} ITC measurements yield the enthalpy of binding (ΔH) as well as the dissociation constant (K_d). From K_d , the binding free energy (ΔG) is calculated (Table 1). The estimation of the binding entropy is based on the difference between ΔG and ΔH . The thermodynamic parameters for rimantadine's enantiomers **2-R** and **2-S** were taken from our previous paper¹⁰ and included in Table 1 for comparison with achiral **1** and rimantadine analogues **3-5**. **1** has a K_d of 2.17 μM . As depicted in Table 1, enantiomers **2-R** and **2-S** have the same K_d values against M2TM WT ($K_d = 0.34$ and $0.32 \mu\text{M}$ respectively). Compound **3**, having two methyl groups instead of one methyl group in **2**, has the smallest $K_d = 0.13 \mu\text{M}$, i.e., the highest binding affinity of all studied aminoadamantane compounds, suggesting that polar and lipophilic characteristics are well balanced in its structure. The diethyl derivative **4** and dipropyl derivative **5** exhibit lower binding affinities against M2TM WT ($K_d = 4.59 \mu\text{M}$ and $K_d = 3.43 \mu\text{M}$, respectively). A balance between enthalpy and entropy determines the free energy of binding as shown in Table 1. For each compound, enthalpy goes down and entropy goes up on binding. The entropy presumably changes on binding because the ordered clathrate water surrounding the ligand is dispersed as the ligand enters the water-poor channel cavity. This is more prominent for **3** and **4**, as expected due to their larger hydrophobic surfaces. Presumably, it would have gone up even more for **5**, but this clathrate effect was probably countered by a reduced ligand entropy in the channel due to restricted rotation inside the receptor binding area. Compounds **1-3** did not bind efficiently to M2TM S31N according to ITC and previous SPR measurements for **1**²⁰ while **5**, with a larger adduct connected to adamantane, binds weakly to M2TM S31N compared to M2TM WT according to ITC.

Table 1. Binding constant, free energy, enthalpy, and entropy of binding derived from ITC measurements for M2TM WT (upper table) and the M2TM S31N (lower table)

Ligand ¹	K_d ²	ΔG ^{3,4}	ΔH ^{3,5}	$-T\Delta S$ ^{3,6}
1	2.17 ± 0.52	-7.77 ± 0.14	-6.66 ± 0.50	-1.11 ± 0.52
2	0.51 ± 0.26	-8.64 ± 0.30	-7.60 ± 0.28	-1.04 ± 0.41
2-R ⁷	0.32 ± 0.16	-8.97 ± 0.26	-7.54 ± 0.34	-1.42 ± 0.43
2-S ⁷	0.34 ± 0.12	-8.88 ± 0.21	-7.73 ± 0.28	-1.15 ± 0.35
3	0.13 ± 0.12	-9.30 ± 0.43	-4.19 ± 0.28	-5.12 ± 0.51
4	4.59 ± 2.21	-7.33 ± 0.28	-3.29 ± 0.62	-4.03 ± 0.68
5	3.43 ± 1.05	-7.50 ± 0.18	-6.23 ± 0.45	-1.27 ± 0.48

Ligand ¹	K_d ²	ΔG ^{3,4}	ΔH ^{3,5}	$-T\Delta S$ ^{3,6}
1-3	₋₈	₋₈	₋₈	₋₈
5	> 10	₋₉	₋₉	₋₉

¹ See Scheme 1.

² Binding constant K_d in μM calculated from measured K_a in M^{-1} by $K_d = 1/K_a \times 10^{-6}$ and error in K_d in μM determined by $K_{d, \text{error}} = (K_{a, \text{error}}/K_a^2) \times 10^{-6}$.

³ In kcal mol^{-1} .

⁴ Free energy of binding computed from K_d by $\Delta G = -RT \ln(K_d^{\text{ref}}/K_d)$ with $K_d^{\text{ref}} = 1 \text{ M}$ and $T = 300 \text{ K}$ and error in ΔG determined according to

$$\Delta G_{\text{error}} = \sqrt{\left(\frac{RT K_{d, \text{error}}}{K_d}\right)^2} \text{ with } T = 300 \text{ K.}$$

⁵ Enthalpy of binding and error in the enthalpy of binding calculated from measured binding enthalpy and measured error by $\Delta H = \Delta H_{\text{measured}} (T / T_{\text{measured}})$ with $T = 300 \text{ K}$ and the temperature at which the ITC measurements were performed $T_{\text{measured}} = 293.15 \text{ K}$.

⁶ Entropy of binding calculated by $\Delta S = (-\Delta G + \Delta H)/T$ and error in ΔS computed by the equation

$$\Delta S_{\text{error}} = \sqrt{\Delta G_{\text{error}}^2 + \Delta H_{\text{error}}^2}$$

⁷ The purity of each enantiomer used was 90% for **2-R** and 95% for **2-S**; the enantiomeric excess (*ee*) of both **2-R** and **2-S** is 99% (Mosher's method); the purity of compound **3** used was > 99%. Values for **2-R** and **2-S** are close to the $K_d = 0.51 \mu\text{M}$ of the racemic **2** considering the errors of the measurements and that the commercially available enantiomers have a lower chemical purity compared to racemic **2**.

⁸ No detectable binding.

⁹ Values could not be determined reliably due to the limitations of the methods in the area of very weak binding.

3.3.3 In vitro testing against Influenza A Virus

The cytopathic effect (CPE) inhibition assay was used^{21,22} to compare the antiviral potency of **1-5** against HK, Udorn, WSN, and WSN M2 N31S in MDCK cells (Table 2). There was no potency against WSN with the compound concentrations used. All compounds showed low micromolar activity against Udorn, HK and WSN M2 N31S with **3** being the most potent agent exhibiting submicromolar potency. Inhibition of replication of Udorn was further confirmed with plaque-reduction assay (results not shown). It is of note that **5** only reduced the plaque size but not the number of plaques. The cytotoxicity data (Table 2) showed that **1-4** are non-toxic with CC₅₀ values > 100 μM, but **5** is mildly toxic with a CC₅₀ ~ 57 μM.

Table 2. Cytotoxicity (CC₅₀) and antiviral activity (EC₅₀) of compounds **1–5** against IAVs HK, Udorn, WSN, and WSN M2 N31S in Madin-Darby canine kidney cells.

Compound	EC ₅₀ (μM) ¹				CC ₅₀ (μM) ¹
	HK	Udorn	WSN		
	M2 (V28; S31)	M2 (V28; S31)	M2 (I28, N31S)	M2 (I28, N31)	
1	ND ³	0.78 ± 0.44	0.48 ± 0.05	>100	>100
2	0.05 ± 0.04	0.09 ± 0.03	0.04 ± 0.02	>100	>100
2-R	ND ³	0.05 ± 0.01	0.04 ± 0.01	>100	>100
2-S	ND ³	0.06 ± 0.02	0.02 ± 0.01	>100	>100
3	0.012 ± 0.003	0.01 ± 0.001	0.03 ± 0.02	>100	>100
4	0.46 ± 0.25	0.41 ± 0.23	1.01 ± 0.13	>100	>100
5	0.45 ± 0.34	1.07 ± 0.31 ²	1.06 ± 0.23	>100	57.3 ± 11.3
Oseltamivir	0.002 ± 0.001	0.001	0.02 ± 0.01	0.03 ± 0.01	>100

¹ Mean and standard deviations of the 50% inhibitory concentration (EC₅₀) and the 50% cytotoxic concentration (CC₅₀) of at least three independent assays; ² Inhibition of plaque size without reduction of plaque number; ³ ND: Not determined.

3.3.4 Electrophysiology measurements

The inhibitors were tested with TEVC using *X. laevis* frog oocytes microinjected with RNA expressing the M2 protein as in previous reports.^{10,29} The blocking effect of the aminoadamantane derivatives against M2 was investigated with EP experiments using Udorn M2 and Udorn M2 S31N. Because WSN has the V28I substitution in M2, Udorn M2 V28I was generated and studied in parallel. The potency of the inhibitors was expressed as the inhibition percentage of the M2 current observed after 2, 5, and/or 10 min of incubation with 100 μ M compound (Tables 3-5). After 5 min, **3** and **4** block Udorn M2 and Udorn M2 V28I as well as **1** (about 90% and 80% respectively). Generally after 2 and 5 min the percentage of current inhibition was progressively increased for **3** and **4**. It is noteworthy that **5** against Udorn M2 exhibited 27% blocking at 2 min, 38% at 5 min and 61% at 10 min (Table 3). The IC₅₀ values were calculated from a nonlinear regression fit of the inhibition percentage at both 100 μ M and 30 μ M for these compounds. The IC₅₀ values of **3** and **4** for Udorn M2 and Udorn M2 V28I were reduced from 2- to 5-minute time points (Table 3). The IC₅₀ values of **3** and **4** for Udorn M2 at 5-minute time point was 4.0 μ M and 13.2 μ M, respectively. For Udorn M2 V28I, **3** has IC₅₀ (5 min) = 17.9 μ M and **4** has IC₅₀ (5 min) = 53.8 μ M (Tables 3 and 4). As discussed previously,³ these measurements at 2, 5 or 10 min are made prior to the establishment of equilibrium due to very slow on- and off-rates for entry (see the k_{on} and k_{off} rate values in Tables 3 and 5), especially of the bulky ligands like **5**, together with the difficulty of maintaining cells at low pH for extended periods. Hence the %-blocking/IC₅₀ values determined by the TEVC procedure can be significantly lower/higher than expected for the equilibrium block state or K_d (from ITC). Thus, the very slow binding of **5** (Table 3) should not be viewed as inconsistent with the high antiviral potency (submicromolar EC₅₀) against WT (V28; S31) viruses (Table 2), the latter representing much longer exposure times than EP experiments.

Compounds **1-3** have similar blocking efficiency for Udorn M2, with **3** being slightly more active; and, **4** was ~ 3-fold less potent than **3** according to the IC₅₀ (Table 3). For Udorn M2 V28I the percentage of current inhibition is lower for **3** and **4** and the IC₅₀ values are ~ 5-fold higher (Table 4). Thus, the comparative experiments regarding the blocking effect of the compounds in EP against M2 WT (present in Udorn and HK viruses) and M2 V28I (present in WSN M2 N31S virus) showed that **1-4** inhibit Udorn M2 more than Udorn M2 V28I. The inhibition of **3** and **4** on both Udorn M2 and Udorn M2 V28I are irreversible in our experimental time frame, as was also observed for **1** with both proteins (data not shown).

Compounds **1, 2, 3** and **5** were tested as aminoadamantane representatives for their blocking effect against Udorn M2 S31N (Table 5). Although **1** and **3** showed some block after 2 minutes, it proved to saturate at a modest level after 5 minutes. Compounds **2** and **5** were very weak blockers with high dissociation rate

constants and equilibrium constants. When rate constants are compared in Tables 3 and 5, it is seen that aminoadamantane analogues can have comparable k_{on} values in the two constructs, but their residence time inside Udorn M2 WT is much higher than in S31N, judging by the much lower k_{off} values. Thus it is the high dissociation rate constants, not low association rate constants, that render aminoadamantanes useless against S31N viruses like WSN. We previously studied Udorn M2 S31N using a broad set of methods, i.e., ssNMR, ITC, EP, antiviral assays and MD simulations, 2 where we concluded that the weaker binding is due to reshaping of the M2 pore when N31 is present, leading to the loss of the V27 pocket for the adamantyl cage.²

In a very recent paper²³ the authors showed that when K_d (TEVC) = k_{off}/k_{on} was smaller than a threshold, an *in vitro* antiviral activity was exhibited. For example for amantadine (**1**) a $k_{off}/k_{on} = 10^{-6}$ M (1 μ M) was measured against M2 WT, which correlates with good *in vitro* antiviral potency. When $k_{off}/k_{on} \sim 100$ μ M or higher, antiviral potency was not observed even for quick binders. For example 4-(2-adamantyl)piperidine (compound **3** in ref. 23) although a quick blocker against Udorn M2 and the amantadine resistant Udorn M2 V27A was ineffective against the corresponding influenza A strains. 4-(1-Adamantyl)piperidine (compound **2** in ref. 23) had high blocking efficiency of 90% at 2 min against Udorn M2 V27A; similarly for N-amidyl-4-(1-adamantyl)piperidine (compound **7** in ref. 23) against Udorn M2. Both 4-(1-adamantyl)piperidine and N-amidyl-4-(1-adamantyl)piperidine inhibited the corresponding influenza A strains effectively. The authors also showed that 2-(1-adamantyl)piperidine (compound **8** in ref. 23) was a slow binder against Udorn M2 (48% at 2 min, but 90% at 6 min) but still has good antiviral efficacy, possibly because although k_{on} is low, k_{off} is really low. This is the case with compound **5** against Udorn M2 WT in the present study (see Table 3): It has a reduced onset of block compared to **1**, **2**, and **3**, but also has a low dissociation rate constant, so it still has μ M efficacy against infections of cell cultures by viral strains with M2 WT.

In the S31N variants, TEVC (Table 5) shows very high exit rate constants, especially for **2** (0.9 s^{-1}) and **5**, (0.14 s^{-1}), consistent with the unmeasurably high K_d in ITC (Table 1, lower) and EC_{50} in CPE (Table 2, WSN). Interestingly, in these two cases, **2** and **5** have low %-block of inward currents at 2, 5 and 10 min in Udorn M2 S31N (Table 5), and somewhat similar k_{on} rates to **1** and **3**, albeit lower compared to M2 WT, Table 3), demonstrating that mutations can have complex, ligand-dependent effects on entry and exit rates.

We previously showed¹⁰ that **2-R** and **2-S** showed similar channel blockage against Udorn M2 WT when tested in EP at 100 μ M at the 2- or 5-minute time point, and this result is consistent with that from ITC measurements (see Table 1) and antiviral assays (see Table 2). The EP measurements showed a $k_{off} = 0.0013$ s^{-1} for **2-R** and a $k_{off} = 0.0016$ s^{-1} for **2-S** (Table 3), i.e. the two enantiomers had very similar binding kinetics. Thus, **2-R** has a bit longer residence time inside the receptor than **2-S**, as reflected by its slightly lower k_{off} and K_d values

(2.4 vs 3.2 μM). In ref.32, the first ssNMR study of the full length M2 in complex with rimantadine enantiomers was published. **2-R** was argued to have a higher affinity than **2-S** based on differences in peak intensities and position restrained MD simulations. The results published in ref. 32 are in qualitative agreement with those reported here, but not quantitative agreement, as here we see no statistically significant (ITC and EC_{50}) or meaningful (EP) difference. Perhaps this is a consequence of the different methodologies applied, i.e., EP vs ssNMR spectroscopy. Chemical shifts differences and peak intensities do not provide an accurate quantitative estimate of binding affinity values. The EP results, antiviral assays and ITC results showed clearly that the two enantiomers form complexes with M2 protein of essentially equal stability.

Table 3. Block¹ of inward currents in oocytes² transfected with full-length Udorn M2 by selected compounds.

Compound	Udorn M2							
	% Block after 2 min	% Block after 5 min	% Block after 10 min	IC_{50} after 2 min (μM)	IC_{50} after 5 min (μM)	k_{on} ($\text{M}^{-1}\text{s}^{-1}$)	k_{off} (s^{-1})	K_{d} ⁴
1	90 \pm 2%	95 \pm 1%	ND ³	12.5	4.7	327	0.003	9 μM
2	96 \pm 1%	96 \pm 1%	ND ³	10.8	ND ³	416	0.003	7 μM
2-R	95 \pm 1%	96 \pm 1%	ND ³	ND ³	ND ³	412	0.0013	3.2 μM
2-S	93 \pm 1%	95 \pm 1%	ND ³	ND ³	ND ³	407	0.0016	3.9 μM
3	90 \pm 2%	96 \pm 1%	ND ³	9.3	4.0	230	0.003	13 μM
4	78 \pm 2%	91 \pm 1%	ND ³	24.3	13.2	ND ³	ND ³	ND ³
5	27 \pm 1.2%	38 \pm 1.6%	61 \pm 2.3%	ND ³	ND ³	34	0.003	88 μM

¹ For each compound, percent block of pH-dependent M2 current at listed concentrations (+/- s.e.m.) and IC_{50} (μM) is shown. ² Three replicates were used for measurements at 100 μM . ³ ND: Not determined. ⁴ $K_{\text{d}} = k_{\text{off}}/k_{\text{on}}$.

Table 4. Block¹ of full-length Udorn M2 V28I-dependent current² by selected compounds.

Compound	Udorn M2 V28I			
	% Block after 2 min	% Block after 5 min	IC ₅₀ after 2 min (μ M)	IC ₅₀ after 5 min (μ M)
1	66.5 \pm 1.4%	88.8 \pm 1.4%	ND ³	ND ³
2	84 \pm 1%	93 \pm 0%	ND ³	ND ³
2-R	71 \pm 1%	90 \pm 1%	ND ³	ND ³
2-S	78 \pm 1%	92 \pm 0%	ND ³	ND ³
3	56 \pm 3%	80 \pm 2%	52.0	17.9
4	43 \pm 2%	72 \pm 2%	124.5	53.8
5	ND ³	ND ³	ND ³	ND ³

¹ For each compound, percent block of pH-dependent M2 current at listed concentrations (+/- s.e.m.) and IC₅₀ (μ M) is shown. ² Three or four (for compound 2-S) or two (for 1) replicates were used for measurements at 100 μ M. ³ ND: Not determined

Table 5. Block¹ of full-length Udorn M2 S31N-dependent current² by selected compounds.

Compound	Udorn M2 S31N					
	% Block after 2 min	% Block after 5 min	% Block after 10 min	k_{on}	k_{off}	K_d ⁵
1	35 \pm 2%	36 \pm 1%	36.3 \pm 1%	143 M ⁻¹ s ⁻¹	0.03 s ⁻¹	210 μ M
2 ³	1.0 \pm 0.2%	1.5 \pm 0.4%	ND ⁴	22 M ⁻¹ s ⁻¹	0.9 s ⁻¹	>10 mM
3	21 \pm 2%	30 \pm 3%	33 \pm 1%	18 M ⁻¹ s ⁻¹	0.008 s ⁻¹	444 μ M
5	7.0 \pm 0.4%	7.6 \pm 0.2%	8.0 \pm 0.4%	79 M ⁻¹ s ⁻¹	0.14 s ⁻¹	1.8 mM

¹ For each compound, percent block of pH-dependent M2 current at listed concentrations (+/- s.e.m.) and IC₅₀ (μ M) is shown. ² Three replicates were used for measurements at 100 μ M. ³ Racemic. ⁴ ND: Not determined. ⁵ $K_d = k_{off}/k_{on}$.

3.3.5 MD simulations

M2TM WT complexes were simulated in the closed conformation found at high pH and assigning a neutral form for all H37. M2TM-ligand complexes were simulated in DMPC bilayers which represents a better membrane mimetic system for retaining proper M2TM structure compared to other glycerophospholipids.^{24,25} We used an experimental structure (PDB ID 2KQT^{26,27}) determined at pH 7.5, in the presence of **1**, and in DMPC bilayers. This M2TM structure is already adapted to the high pH condition, and only a short equilibration phase was required. MD simulations of the complexes between aminoadamantane variants **1**, **2**, **2-R**, **2-S**, **3-5** with M2TM provide insights for the binding interactions and possible structural changes in the binding area. The simulated M2TM-ligand complexes were stable, and in all cases the M2TM tetramer showed no large conformational changes in the course of the simulations, as demonstrated by RMSDs ≤ 1.8 Å for M2TM C α -carbons with respect to the initial structure^{26,27} (Table 6, 7). No significant differences in measures were detected between trajectories with production times of 4 ns and 80 ns (Table 6, 7).

The axial position of the ligands inside the pore differed only lightly, that is, 0-0.3 Å towards the C-end, relative to **1** (Table 7). The center of mass between the four V27 residues and the adamantane cage of the ligand varies between 4.1 Å and 4.5 Å on average (Table 7). For rimantadine enantiomers **2-R**, **2-S** and rimantadine analogues **3-5**, the average angle between the pore axis (membrane normal, from the N- to the C-terminus of the channel) and the C-N bond vector ranges between 51° and 61° (Table 7), i.e. the ammonium group of all aminoadamantane compounds oriented towards the C-terminus, consistent with previous experimental findings^{27,28} and observations.^{6,7,9,10} The ligand ammonium groups form hydrogen bonds with water molecules between the ligand and the H37 residues. The adamantane is embraced by V27 and A30 side chains, which define the binding site of the ligands. The 6 compounds, **1**, **2**, **2-R**, **2-S**, and **3-5**, all include a primary ammonium group and form, on average, 3 hydrogen bonds with neighbouring water molecules (Table 7). The CHCH₃ group that includes the chiral carbon in **2-R** and **2-S** is positioned in the cleft between G34 and A30. A30 has different van der Waals interactions between the two enantiomers, being a chiral amino acid. However, the distance between the ligand CH₃ and the A30 CH₃ is similar for the two enantiomers (3.9 ± 0.3 and 3.5 ± 0.3 Å respectively); also the distance between V27-Ad (4.2 ± 0.3 and 4.1 ± 0.3 Å respectively see Table 7). Thus, hydrogen bonding interactions for **2-R** and **2-S** and geometric measures which reflect van der Waals contacts were found to be similar for the two enantiomers, suggesting equal binding interactions. In diethyl and di-n-propyl derivatives (**4** and **5**), the alkyl groups seem to better fill the space between the ligand and the pore walls; but, in these cases, restricted motion and the resulting entropy cost of binding may be significant and decrease

the binding affinities compared to **3** (Table 1-4). Configurations from the simulations of ligands **2-R**, **2-S**, **3** and **5** are depicted in Figure 3. In all cases, in the region located above the adamantane core (i.e. towards the N-terminus) no water molecules were found^{15,16}, which is consistent with the proton blocking effect of the aminoadamantane derivatives.^{2,2,23,29} No Cl⁻ ion entered the pore as it is indicated by the average Cl-N distance (Table 7).

Table 6. Structural and dynamic measures from MD trajectories of A/Udorn/72 M2TM-ligand complexes in DMPC bilayer (4 ns).

Ligand ¹	RMSD (C α) ²	Angle C-N vector ³	V27-Ad ⁴	H-bonds ⁵	Cl-N distance ⁶
1 ²	1.5 \pm 0.1	11.2 \pm 5.9	4.2 \pm 0.3	2.7 \pm 0.5	32.3 \pm 6.6
2-R	1.5 \pm 0.2	44.7 \pm 7.6	3.9 \pm 0.273	2.6 \pm 0.6	33.3 \pm 5.8
2-S	1.1 \pm 0.2	55.7 \pm 6.1	4.2 \pm 0.259	2.8 \pm 0.4	35.9 \pm 5.9
3	1.4 \pm 0.2	51.5 \pm 4.9	4.4 \pm 0.3	2.9 \pm 0.3	33.7 \pm 6.3
4	1.0 \pm 0.1	47.5 \pm 6.9	4.5 \pm 0.3	2.9 \pm 0.3	35.7 \pm 7.5
5	1.5 \pm 0.2	49.4 \pm 4.3	4.4 \pm 0.2	2.9 \pm 0.3	30.0 \pm 6.0

Table 7. Structural and dynamic measures from MD trajectories of A/Udorn/72 M2TM-ligand complexes in DMPC bilayer (80 ns).

Ligand ¹	RMSD (C α) ²	Angle C-N vector ³	V27-Ad ⁴	H-bonds ⁵	Cl-N distance ⁶
1 ²	1.2 \pm 0.2	9.8 \pm 5.4	4.2 \pm 0.3	2.7 \pm 0.5	23.5 \pm 9.3
2-R	1.8 \pm 0.5	52.0 \pm 6.7	4.2 \pm 0.3	2.6 \pm 0.5	34.2 \pm 6.5
2-S	1.2 \pm 0.2	50.9 \pm 5.3	4.1 \pm 0.3	2.9 \pm 0.3	33.7 \pm 7.4
3	1.2 \pm 0.2	53.8 \pm 8.3	4.1 \pm 0.2	2.9 \pm 0.3	32.7 \pm 6.1
4	1.6 \pm 0.5	54.3 \pm 6.9	4.4 \pm 0.3	2.9 \pm 0.3	33.9 \pm 7.7
5	1.0 \pm 0.2	61.5 \pm 7.1	4.5 \pm 0.4	2.9 \pm 0.3	32.4 \pm 7.4

¹See Scheme 1; measures for **1** were added for comparison reasons.

²Maximum root-mean-square deviation (RMSD) for C α atoms of M2TM relative to the initial structure (PDB entry: 2KQT) after root-mean-square fitting of C α atoms of M2TM; in Å.

³Angle between the vector along the bond from the carbon atom of the adamantane core to the ligand nitrogen atom and the normal to the membrane; in degrees.

⁴Mean distance between center of mass of V27 and centers of mass of adamantane calculated using Gromacs tools; in Å.

⁵Mean number of H-bonds between ligand's ammonium group and waters.

⁶Mean distance in Å between the ligand N and the nearest Cl⁻.

The MD simulations of the complex of **3** or **5** with M2TM S31N (Table 8) showed that the ligand can't bind tightly to M2TM S31N because significant favourable van der Waals interactions are missing (Figure 4). The S31N mutation of M2TM results in a shift of the hydrophobic adamantyl ring towards the C-terminus, due to the repulsive forces of amide side chains to adamantyl ring and attraction to water molecules. As a consequence the stabilizing hydrophobic interactions of the V27 isopropyl groups with the adamantyl ring that are present in the M2TM WT are lost in M2TM S31N. The bulky N31 side chains are oriented toward the N-terminus; and, the V27 side chains and the ammonium group of the ligands are also turned toward the N-terminus allowing significant hydrogen bonding interactions between the polar N31 side chains and the nearby water molecules.^{2,30} The hydrogen bonding interactions with N31 are consistent with the magic angle spinning (MAS) experimental data performed by us using a spiropyrrolidine adamantane derivative and the same M2TM S31N channel. With the adamantane compound present, there was a chemical shift perturbation for N31 and G34 compared to the *apo* M2TM S31N. In the M2TM WT, the adamantyl ring is well accommodated by the V27 and A30 side chains and sizeable adducts such as ligands **4** and **5** additionally fill the region between A30 and G34 (Figure 3); but, in M2TM S31N, the adamantyl ring is between A30 and G34 (Figure 4), due to the lack of a favorable hydrophobic pocket. We have also found an absence of chemical shift perturbations for V27 in M2TM S31N in the presence of bulky ligand, in comparison with the *apo* M2TM S31N, contrasting with the significant chemical shift changes at V27, S31, and G34 relative to the *apo* state reported when rimantadine is bound to M2TM WT.^{31,32}

The MD runs of the complexes of **1-3** with M2TM S31N showed qualitatively that these molecules can't bind M2TM S31N because significant favorable van der Waals interactions are missing. This can be observed from the snapshot of the complex of **3** with M2TM S31N in Figure 4a. Compound **5** has sizeable adducts in addition to the adamantyl ring that effectively fill the region between A30 and G34 and the interactions needed for binding are slightly improved resulting in weak binding to M2TM S31N according to ITC compared to no binding for **1-3**. This can be observed from the snapshot for the complex of **5** with M2TM S31N in Figure 4b. Indeed, **1** does not bind as documented by the oriented sample (OS) ssNMR spectra, but larger adducts like those present in compound **5** appear to stabilize weak binding of the drug in the region between A30 and G34. The last point is in agreement with the results from MAS and OS ssNMR spectra. Taken together, the results from the combination of MD simulations, ITC and EP showed no binding of **1** and similar in size analogues to M2 S31N and M2TM S31N, and only possible weak binding for sizeable adducts.

Table 8. Structural and dynamic measures from MD trajectories of M2TM S31N-ligand complexes in DMPC bilayer (80 ns).

Ligand ¹	RMSD (C α) ²	Angle C-N vector ³	V27-Ad ⁴	H-bonds with waters ⁵	H-bonds with N31-CO ⁶	Cl-N distance ⁷
1	2.6 \pm 0.4	112.3 \pm 27	5.2 \pm 0.7	1.4 \pm 0.7	1.2 \pm 0.9	34.3 \pm 7.9
3	1.8 \pm 0.3	122.3 \pm 8.7	6.9 \pm 0.1	1.9 \pm 0.7	1.0 \pm 0.7	34.3 \pm 7.9
5	1.8 \pm 0.3	115.1 \pm 5.2	6.3 \pm 0.4	1.7 \pm 0.8	1.1 \pm 0.8	33.4 \pm 7.1

¹ See Scheme 1; values taken from ref. 27 of the draft; measures for **1** were added for comparison reasons.

² Maximum root-mean-square deviation (RMSD) for Ca atoms of M2TM relative to the initial structure (PDB entry: 2KQT) after root-mean-square fitting of Ca atoms of M2TM; in Å.

³ Angle between the vector along the bond from the carbon atom of the adamantane core to the ligand nitrogen atom and the normal of the membrane; in degree.

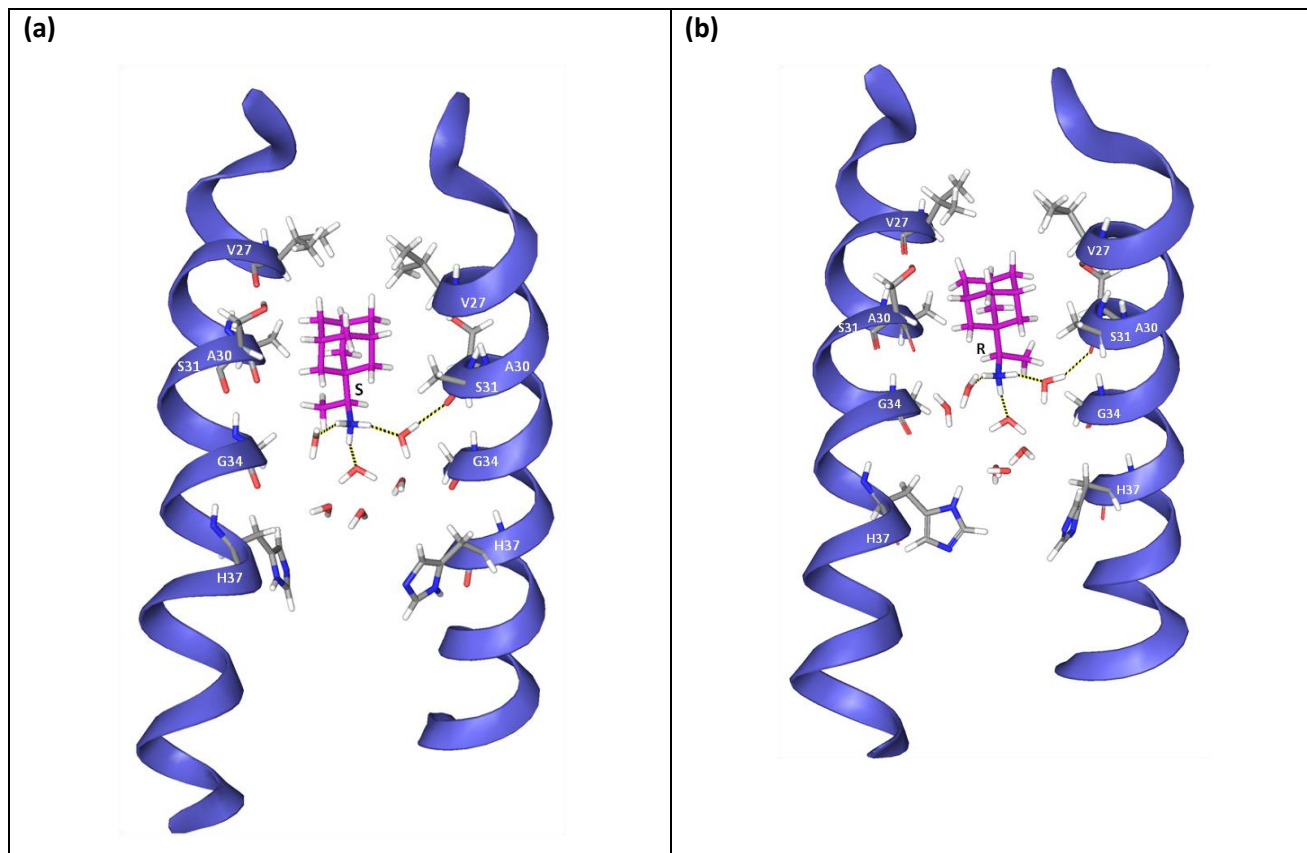
⁴ Mean distance between center of mass of V27 and centers of mass of adamantane calculated using Gromacs tools; in Å.

⁵ Mean number of H-bonds between ligand's ammonium group and waters.

⁶ Mean number of H-bonds between a ligand's ammonium group and N31 carbonyl group.

⁷ Mean distance in Å between the ligand N and the nearest Cl⁻.

Effect of Subtle Changes of Aminoadamantanes Structure and Influenza M2TM Structure in the Binding Kinetics, Affinity and Potency



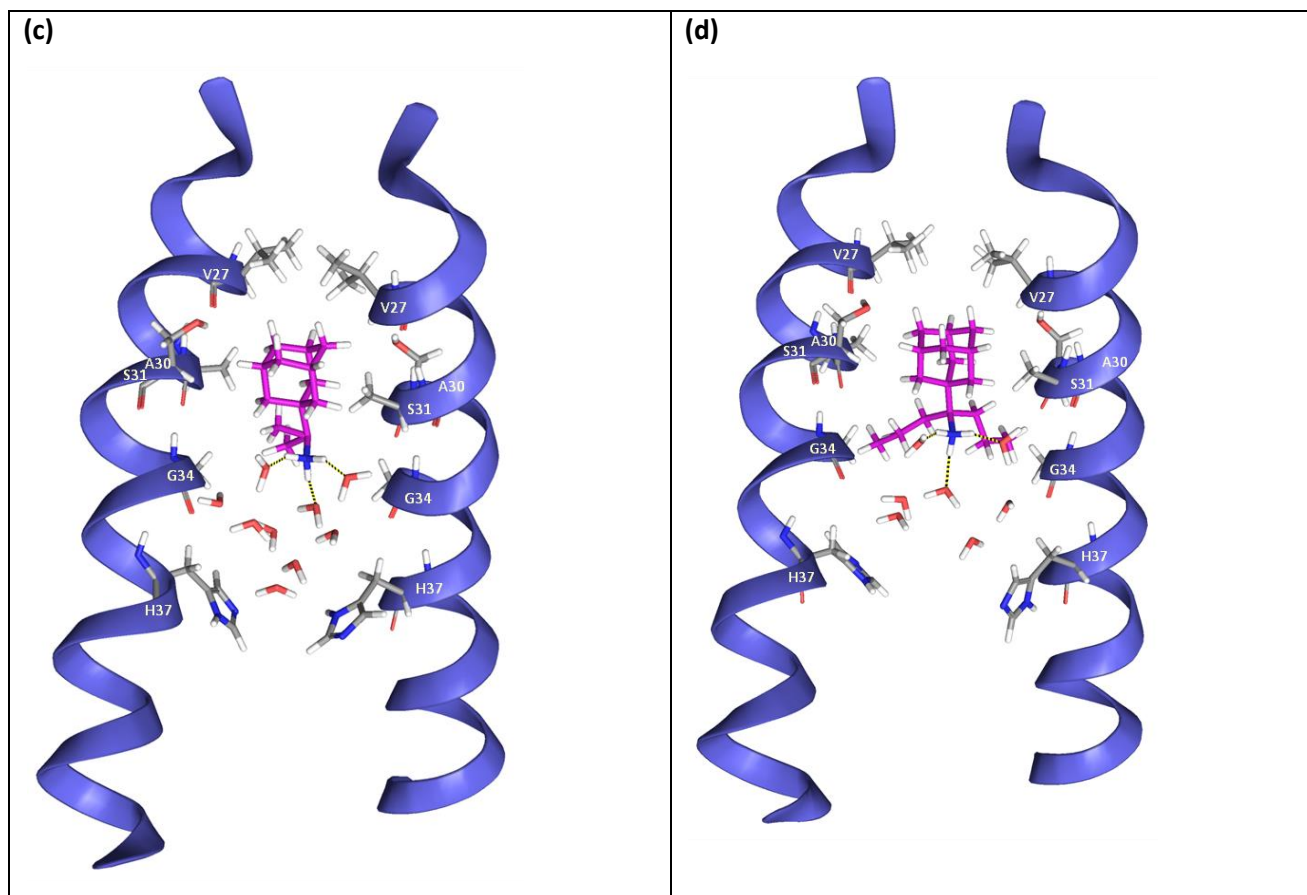
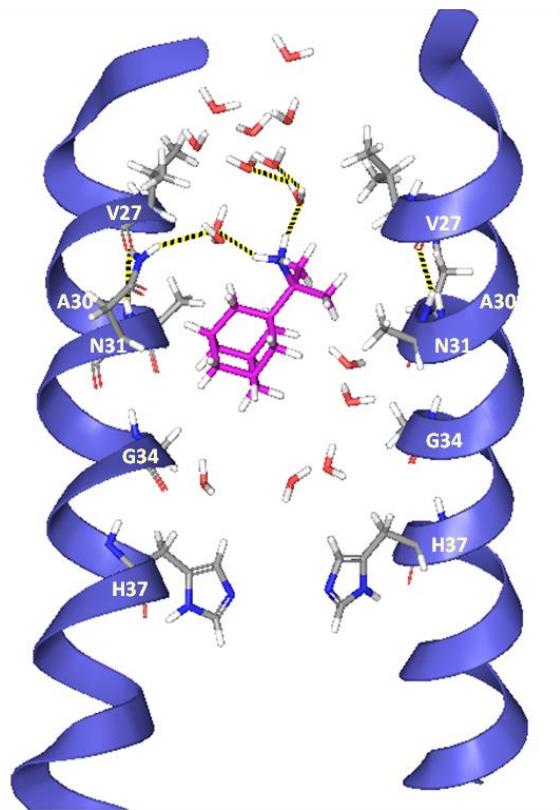


Figure 3. Representative snapshots from the simulation of ligands **2-R** (a), **2-S** (b), **3** (c), and **5** (d) bound to M2TM WT. Six and seven water molecules are shown between the ligand and H37 residues for **2-S** and **2-R** respectively, nine for **3** and seven for **5**. Three hydrogen bonds between the ammonium group of the ligand and three water molecules are shown. Hydrogen bonding with water molecules and van der Waals interactions of the adamantane core with V27 and A30 side chains stabilize the ligand inside the pore with its ammonium group oriented towards the C-terminus of the channel. The CHCH₃ group that includes the chiral carbon in **2-R** and **2-S** is positioned in the cleft between G34 and A30. A30 has different van der Waals interactions between the two enantiomers, being a chiral amino acid. However, the distance between the ligand CH₃ and the A30 CH₃ is similar for the two enantiomers (3.9 ± 0.3 and 3.5 ± 0.3 Å respectively); also the distance between V27-Ad (4.2 ± 0.3 and 4.1 ± 0.3 Å respectively see Table 7).

(a)



(b)

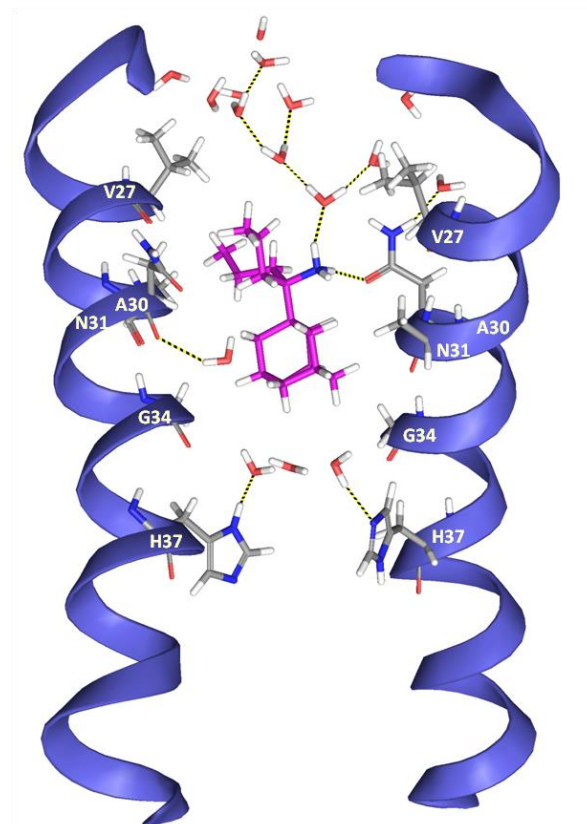


Figure 4. Representative snapshots from the simulations of ligand **3** (a) and **5** (b) bound to M2TM S31N. Five and three water molecules are shown between ligand **3** and **5**, respectively and the H37 residues and ten and twelve water molecules, respectively between N31 and the mouth of the pore. In these representative snapshots for the S31N variant, the ammonium group of the ligand is oriented towards the N-terminus, where it forms hydrogen bonds with water molecules or the carbonyl group of the N31 amide side chain. In this orientation, loss of the V27 pocket for the adamantyl cage would be expected to lead to weak binding of aminoadamantane ligands.

3.3.6 Compound prioritization against M2 WT

The IC₅₀ values after 2 or 5 minutes for **1-5** (Table 3) prioritize the same derivative for blocking M2 WT, i.e. **3**, in agreement to the results from the K_d values from ITC experiments based on M2TM WT binding (Table 1), as well as with IC₅₀ values from TEVC experiments based on full length Udorn M2 WT protein inhibition (Table 3). While it seems that the correlation between CPE assay for M2 WT viruses (Table 2) and percent block in TEVC results experiments at 2 min for **5** is poor, it should be considered that **5** is a slow blocker having an 27% blockage at 2 min, 38% at 5 min and 61% at 10 min at a concentration of 100 μ M. In studies focusing on the development of aminoadamantane ligands against IAV, derivatives are often initially tested in TEVC assays at 100 μ M concentration at 2 min and only the most potent compounds are then tested using whole cell assays.^{23,5} If the same procedure had been applied here, **5** would not have been tested, even though it proved to be a low μ M inhibitor according to K_d values from ITC experiments with M2TM WT (Table 1) and CPE assay (Table 2) results. Similarly **4** would not be tested based on percent block at 2 minutes in TEVC with Udorn M2 V28I (Table 4). The results suggested that TEVC results, when used for compound filtering, need careful interpretation for compounds having low association rate constant for binding to the full length M2 which also depends on the M2 pore. The reduction of M2 blocking efficiency by increasing drug's size has been also observed for other lipophilic amines.²

3.4 Conclusions

The role of the kinetic behaviour of an aminoadamantane derivative when binding to the influenza A M2 protein pore, reflected by association (k_{on}) and dissociation (k_{off}) rate constants, was studied in this work. We investigated the binding kinetics of selected rimantadine analogues with M2 WT and M2 S31N and how they influenced the outcome of potency. Overall, this work aimed at comparing and explaining binding, proton transport blockage, and antiviral potency of aminoadamantane derivatives against M2 WT and M2 S31N. Binding was assessed for M2TM with ITC and illuminated with MD simulations. The kinetics of block and unblock of proton transport were measured for full length IAV M2 using TEVC EP. Antiviral potency was measured as the prevention of infection in cell cultures using CPE assays. The two rimantadine enantiomers have similar binding free energies, channel blockage and k_{on} and k_{off} rate constants, and similar antiviral potencies. We conclude that they form equally stable complexes and have the same residence time inside M2 WT.

The inhibitory potency for M2 WT, as determined by ITC, EP, and anti-viral assays with Udorn, HK and WSN M2 N31S strains of IAV in MDCK cells, prioritize **3** which is almost equal in structure with rimantadine (**2**) without having a chiral center. Compound **3** has also a promising selectivity index based on the *in vitro* cytotoxicity data. TEVC percent block for 100 μ M at 2 minutes also prioritizes **3** in accordance with the ITC, but perhaps “underrated” the potential of **5**, being only 27%, growing to 38% at 5 minutes and 61% at 10 minutes. Slow block could be associated with tight block, and this phenomenon should not be overlooked in short-lasting experiments. In this regard, ITC measurements are seen to be an important additional tool for clarifying the binding energies of novel derivatives to M2TM given its capacity for sufficient relaxations of equilibrium between titration injections. Nevertheless, it is clear from the ITC, CPE (all strains with M2 WT), that **5** (and **4** where tested) are \sim 10-fold less active than **3**.

It was also shown that a small change in an amino acid at site 28 (V28I) of M2, which does not line the pore, seriously affects M2 blockage kinetics. The IC_{50} s of blocking compounds measured for Udorn M2 and its V28I mutant showed that both **3** and **4** inhibit M2 WT more rapidly than the V28I mutant.

The compounds did not bind to Udorn M2TM S31N according to ITC and did not exhibit antiviral potency against WSN virus, which contains both the S31N and the V28I mutations. We showed that a valuable parameter to explain the resistance of M2 S31N viruses to rimantadine analogues compared to M2 WT is a higher k_{off} rate (i.e. a smaller residence time inside M2 S31N). According to MD simulations and previous ssNMR results this is due to the fact that, in M2 S31N, the loss of the V27 pocket for the adamantyl cage resulted in low residence time inside M2TM and a lack of antiviral potency; but, for **5**, the sizeable adducts resulted in a weak binding

which is albeit not sufficient for antiviral potency. It is the high dissociation rate constants that render aminoadamantanes useless against S31N viruses like WSN leading to K_d (TEVC) in the mM range compared to the μM range for M2 WT binding. Thus, we provided a kinetic perspective to explain rimantadine variant binding, proton transport blockage and antiviral potency against influenza M2 WT and M2 S31N.

3.5 Experimental Part

3.5.1 Synthesis of the ligands

1 was purchased from Merck and **2** from Alfa chemicals (> 99 % purity). Enantiomers of **2** were purchased from Enamine; **2-S** has 95% chemical purity and **2-R** has 90% chemical purity and the enantiomeric excess of each enantiomer sample is 99%. The procedure leading to the synthesis of **3** was described in 1.3.1 (chapter 1).

3-(Tricyclo[3.3.1.1^{3,7}]dec-1-yl)-pentan-3-ol (AdEt₂C-OH) 7b. A solution of 1-adamantanecarbonyl chloride **6** (700 mg, 3.53 mmol) in 25 mL of dry diethyl ether was added dropwise under Ar atmosphere and stirring, to a solution of 5 mL ethyl lithium (0.5 M in benzene/cyclohexane, 12.5 mmol). The mixture was stirred for 26 h under Ar atmosphere at room temperature. The reaction mixture was hydrolyzed with an equal volume of saturated ammonium chloride solution under ice-cooling. The organic layer was separated and the aqueous phase was extracted with diethyl ether two times. The combined organic phase was washed two times with a solution of sodium hydroxide 3% w/v, water and brine, and dried over anhydrous sodium sulfate. After evaporation of the solvent under vacuum, a light yellow coloured solid residue of the alcohol **7b** was obtained. Yield 357mg (45.5%); IR (Nujol): $\nu(\text{OH})$ 3502 cm^{-1} (br s); ¹H-NMR (400MHz, CDCl₃) δ (ppm) 0.93 (t, $J \sim 7$ Hz, 6H, 2xCH₃), 1.56 (q, $J \sim 7$ Hz, 4H, 2xCH₃CH₂), 1.61-1.70 (m, 12H, 2,4,6,8,9,10-H, adamantane H), 2.05 (br s, 3H, 3,5,7-H, adamantane H); ¹³C-NMR (200MHz, CDCl₃) δ : 9.47 (CH₃), 25.93 (CH₃CH₂), 28.90 (3,5,7-C, adamantane C), 36.71 (2,8,9-C, adamantane C), 37.40 (4,6,10-C, adamantane C), 38.51 (1-C, adamantane C), 40.48 (C-OH).

3-(Tricyclo[3.3.1.1^{3,7}]dec-1-yl)-pentan-3-amine (AdEt₂C-NH₂) 4. The oily 3-(1-adamantyl)-3-azido-pentane **8b** was prepared by treatment of the tertiary alcohol **7b** with CH₂Cl₂/NaN₃/TFA according to the same procedure followed for 2-(1-adamantyl)-2-azido-propane **9a**. The reaction afforded an oily mixture of azide **9b** along with 3-(1-adamantyl)-pent-2-ene as an elimination by-product. The yield of the azide preparation was 65 % based on the integration of ¹³C NMR peaks. The crude oily mixture was used without further purification for the LiAlH₄ reduction step.

3-(1-Adamantyl)-3-pentanamine**4** was prepared through LiAlH₄ reduction of azide **9b** in refluxing ether for 5h according to the same procedure followed for 2-(1-adamantyl)-propan-2-amine **3**. Amine **4** was afforded as a light yellow colored oil. Yield: 10.9%; MS: 222.4; ¹H-NMR (400 MHz, CDCl₃) δ (ppm) 0.88 (t, $J \sim 7$ Hz, 6H, 2xCH₃),

1.08 (br s, 2H, NH₂), 1.33-1.52 (m, 2H, 2xCH₃CH₂), 1.60-1.69 (m, 12H, 2,4,6,8,9,10-H, adamantane H), 1.97 (br s, 3H, 3,5,7-H, adamantane H); ¹³C-NMR (200MHz, CDCl₃) δ (ppm) 9.90 (CH₃), 26.73 (CH₃CH₂), 29.04 (3,5,7-C, adamantane C), 36.75 (2,8,9-C, adamantane C), 37.45 (4,6,10-C, adamantane C), 38.60 (1-C, adamantane C), 39.86 (C-NH₂). Anal. Fumarate (C₁₉H₃₁NO₄) (EtOH-Ether).

4-(Tricyclo[3.3.1.1^{3,7}]dec-1-yl)-hept-1,6-dien-4-ol (AdAllyl₂C-OH) 8. Allylmagnesium bromide was prepared from magnesium turnings (1.33 g, 55.4 mmol) and allyl bromide (6.1 g, 50.4 mmol) in 60 mL of dry diethyl ether. A solution of 1-adamantanecarbonyl chloride **6** (2 g, 10.1 mmol) in 60 mL of dry diethyl ether was added dropwise to the first solution, under Ar atmosphere and stirring. The reaction mixture was heated at gentle reflux for 4h under stirring and Ar atmosphere and an additional 24 h at room temperature under stirring and Ar atmosphere. The mixture was hydrolyzed with an equal volume of saturated solution of ammonium chloride under ice-cooling. The organic layer was separated and the aqueous phase was extracted with diethyl ether two times. The combined organic phase was washed with water and brine, dried (Na₂SO₄) and evaporated under vacuum to yield a yellow colored oil residue of 4-(adamant-1-yl)-hept-1,6-dien-4-ol **8**. Yield: 1.74 g (70%); IR (Film) δ: ν(OH) 3568 cm⁻¹ (s), ν(=C-H) 3074 cm⁻¹ (s), 3008 cm⁻¹ (m), ν(C=C) 1636 cm⁻¹ (s); ¹H-NMR (400MHz, CDCl₃) δ (ppm) 1.70 (m, 12H, 2,4,6,8,9,10-H, adamantane H), 1.99 (br s, 3H, 3,5,7-H, adamantane H), 2.28-2.40 (m, *J*~7 Hz, 4H, 3,5-CH₂), 5.09 (t, *J*~7 Hz, 4H, 2xCH₂=), 5.88-5.98 (m, *J*~7 Hz, 2H, 2xCH=); ¹³C-NMR (200MHz, CDCl₃) δ (ppm) 28.81 (3,5,7-C, adamantane C), 36.57 (2,8,9-C, adamantane C), 37.29 (4,6,10-C, adamantane C), 39.29 (CH₂), 40.34 (1-C, adamantane C), 76.08 (C-OH), 118.11 (=CH₂), 135.82 (CH=).

4-(Tricyclo[3.3.1.1^{3,7}]dec-1-yl)-heptan-4-ol (AdPr₂C-OH) 7c. The 4-(adamant-1-yl)-hept-1,6-dien-4-ol **8** (840 mg, 3.42 mmol) was dissolved in 80 mL of absolute ethanol and the solution was hydrogenated over Adams catalyst (80 mg) for 20 h. Vacuum filtration of the catalyst and solvent evaporation under vacuum yields a white solid residue of 4-(1-adamant-1-yl)-heptan-4-ol **7c**. Yield: 720 mg (84%); IR (Nujol): ν(OH) 3469 cm⁻¹ (s), ¹H-NMR (400MHz, CDCl₃) δ (ppm) 0.90 (t, *J*~7 Hz, 6H, 1, 2xCH₃), 1.29-1.39 (m, *J*~7 Hz, 4H, 2,6-CH₂), 1.41-1.50 (m, *J*~7 Hz, 4H, 3,5-CH₂), 1.65 (m, 12H, 2,4,6,8,9,10-H, adamantane H), 1.98 (br s, 3H, 3,5,7-H, adamantane H), 2.17 (s, 1H, -OH); ¹³C-NMR (200MHz, CDCl₃) δ (ppm) 15.29 (CH₃), 18.19 (CH₂), 28.89 (3,5,7-C, adamantane C), 36.59 (2,8,9-C, adamantane C), 36.88 (CH₂), 37.39 (4,6,10-C, adamantane C), 40.28 (1-C, adamantane C), 41.39 (C-OH).

4-(Tricyclo[3.3.1.1^{3,7}]dec-1-yl)-heptan-4-amine (AdPr₂C-NH₂) 5. The oily 3-(adamant-1-yl)-heptan-4-azide **9c** was prepared by treatment of the tertiary alcohol **7c** with CH₂Cl₂/NaN₃/TFA as previously described. The reaction

afforded a yellow colored oily mixture consisting of the desired 3-(adamant-1-yl)-4-azido-heptane **9c** (54 %) and of 4-(adamant-1-yl)-hept-3-ene (46%) as an elimination byproduct. Yield of the azide: 37%. The crude oily mixture was used without further purification for the LiAlH₄ reduction step. 4-(Adamant-1-yl)-heptan-4-amine **5** was prepared through LiAlH₄ reduction of azide **9c** in refluxing ether for 5h according to the same procedure described previously. Amine **5** was afforded as a light yellow coloured oil. Yield (based on azide): 14%; MS: 250.1; ¹H-NMR (400MHz, CDCl₃) δ (ppm) 0.89 (t, *J*~7 Hz, 6H, 2xCH₃), 1.19 (br s, 2H, NH₂), 1.25-1.41 (m, *J*~7 Hz, 8H, 4xCH₂), 1.61 (m, 12H, 2,4,6,8,9,10-H, adamantane H), 1.98 (br s, 3H, 3,5,7-H, adamantane H); ¹³C-NMR (200MHz, CDCl₃) δ (ppm) 15.45 (CH₃), 18.59 (CH₂), 29.07 (3,5,7-C, adamantane C), 36.65 (2,8,9-C, adamantane C), 37.45 (CH₂), 37.97 (4,6,10-C, adamantane C), 39.53 (1-C, adamantane C), 56.94 (C-N). Anal. Fumarate (C₂₁H₃₅NO₄) (EtOH-Ether).

3.5.2 Peptide synthesis and ITC measurements

Binding affinities of aminoadamantane derivatives **1**, **2**, **2-R**, **2-S** and **3-5** (Scheme 1) for Udorn M2TM were determined by ITC experiments for M2TM-ligand systems in dodecylphosphocholine (DPC) micelles at pH 8. M2TM peptides corresponding to residues 22-46 of Udorn/72 wild type sequence of M2 (C-terminally amidated M2TM_{Udorn/72}: SSDPLVVAASIIIGILHLILWILDRL) were synthesized by standard Fmoc solid phase peptide synthesis using an aminomethyl polystyrene resin loaded with the amide linker and purified by reverse phase HPLC. The final peptide purity was 98%. Details for a) peptide synthesis and purification, and b) isothermal titration calorimetry measurements can be found in Chapter 1, i.e., in 1.3.2 and 1.1.3.2 respectively.

3.5.3 Two-electrode voltage clamp assay

The inhibitors were tested in a TEVC assay using *Xenopus laevis* frog oocytes microinjected with RNA expressing either the WT or the S31N mutant of the M2 protein as previously reported.²⁹ Oocytes from *Xenopus laevis* (Ecocyte, Austin, TX) were maintained in ND-96⁺⁺ solution (96 mM NaCl, 2 mM KCl, 1.8 mM CaCl₂, 1mM MgCl₂, 2.5 mM sodium pyruvate, 5 mM HEPES-NaOH, pH 7.4) at 17 °C until injection of ~ 40 ng of Udorn or Udorn S31N mRNA. After injection, the oocytes were maintained in ND96⁺⁺ pH 7.4 until electrophysiological recording. 72 hrs after mRNA injection, whole-cell currents were recorded with a TEVC apparatus at V_m = -20 mV. Oocyte currents were recorded in standard Barth's solution (0.3 mM NaNO₃, 0.71 mM CaCl₂, 0.82 mM MgSO₄, 1.0 mM KCl, 2.4 mM NaHCO₃, 88 mM NaCl, 15.0 mM HEPES, pH 7.5. Inward proton current was induced by perfusion

with Barth's pH 5.3. A concentration of 100 μM compound in Barth's was used to perfuse the oocytes transfected with either M2 WT or mutant M2. The potency of the inhibitors was expressed as percentage inhibition of M2 current observed after 2, 5, or 10 min of incubation with either 100 or 30 μM of compounds. The IC_{50} values were calculated from a nonlinear regression fit of the inhibition percentage using a simple sigmoid function at 100 μM and 30 μM for these compounds.

3.5.4 Cells and viruses

Information for cells and viruses can be found in Chapter 1, 1.3.6. Amantadine-sensitive IAVs Udorn and HK (identical amino acid composition in M2 with V28 and S31), naturally amantadine-resistant WSN M2 WT (with I28 and N31 in M2 WSN M2 N31) and its mutated amantadine-sensitive variant WSN M2 N31S³³ were used in this study.

3.5.5 Evaluation of cytotoxicity and CPE inhibition activity

Information for CPE inhibition studies can be found in Chapter 1, 1.3.7. Cytotoxicity and CPE inhibition studies were performed on two-day-old confluent monolayers of MDCK cells grown in 96-well plates as published.³³ Cytotoxicity was analyzed 72 h after compound addition (six half-log dilutions; at least two parallels per concentration; maximum concentration 100 μM). The neuraminidase inhibitor oseltamivir carboxylate (GS4071; GlaxoSmithKline) that inhibits all studied IAVs similarly was used as positive control.

3.5.6 Evaluation of inhibition activity using Plaque Reduction Assay

Cytotoxicity and CPE inhibition studies were performed on two-day-old confluent monolayers of MDCK cells grown in 96-well plates as published.³³ Cytotoxicity was analyzed 72 h after compound addition (six half-log dilutions; at least two parallels per concentration; maximum concentration 100 μM). In the CPE inhibition assay, 50 μL of at least six serial half-log dilutions of compound in test medium and a constant multiplicity of infection of test virus (0.03 for WSN and for WSN M2 N31S; 0.003 for HK; and 0.002 for Udorn in a volume of 50 μL of the test medium were added to cells. Then, plates were incubated at 37 °C with 5% CO_2 for 48 h. The neuraminidase

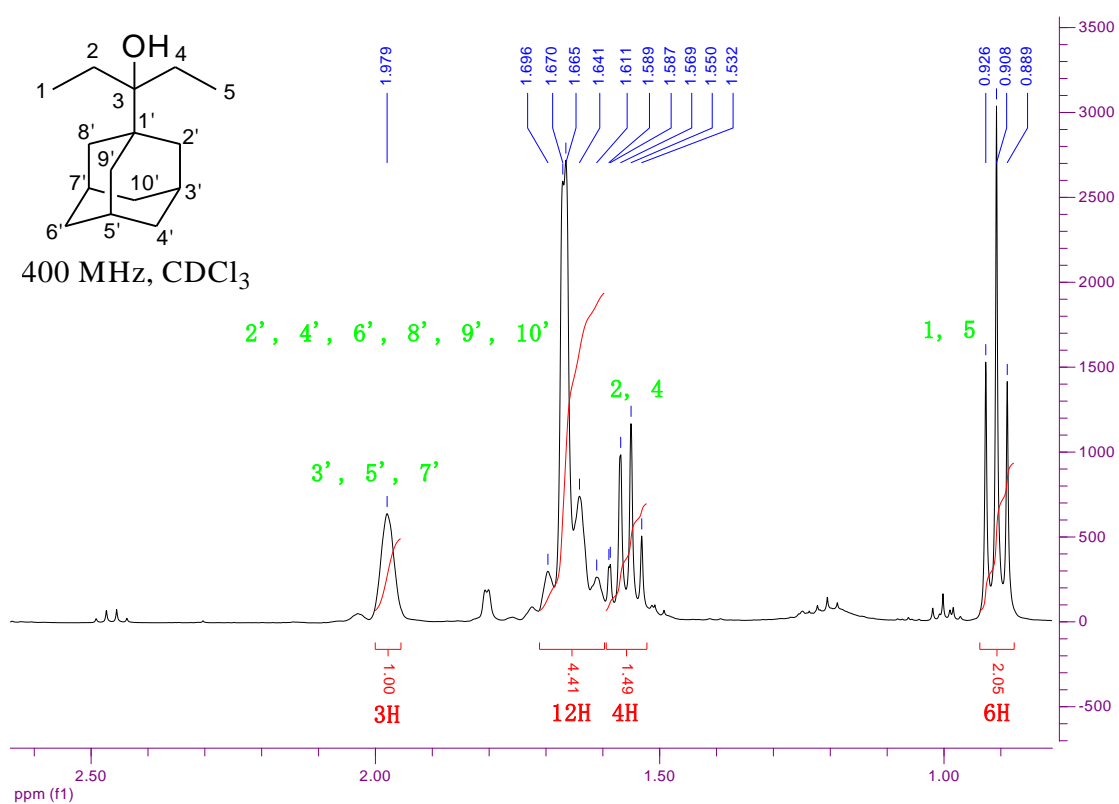
inhibitor oseltamivir carboxylate (GS4071; GlaxoSmithKline) that inhibits all studied IAVs similarly was used as positive control. Crystal violet staining and optical density determination were performed as described before.^{34,33} After log transformation of compound concentrations, linear regression was used to determine the 50% cytotoxic (CC_{50}) and 50% inhibitory concentration (EC_{50}). At least three independent assays were conducted to calculate the mean CC_{50} and EC_{50} and their standard deviations

3.6 Supporting Information

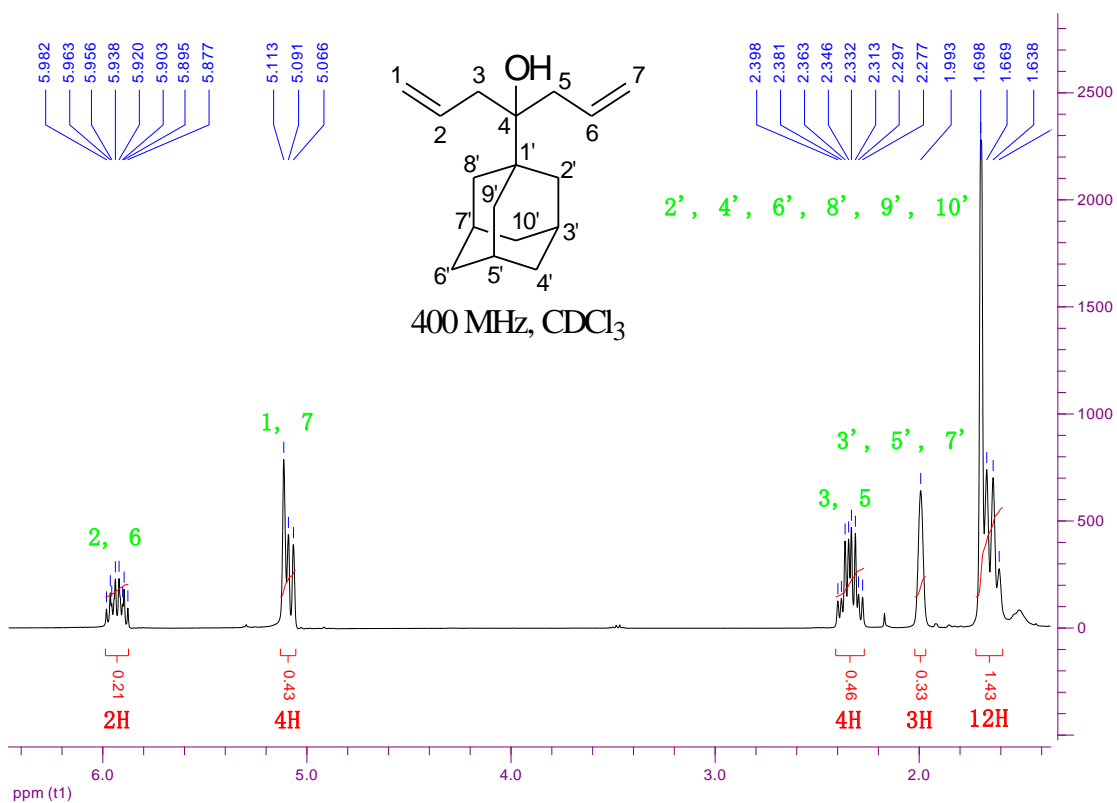
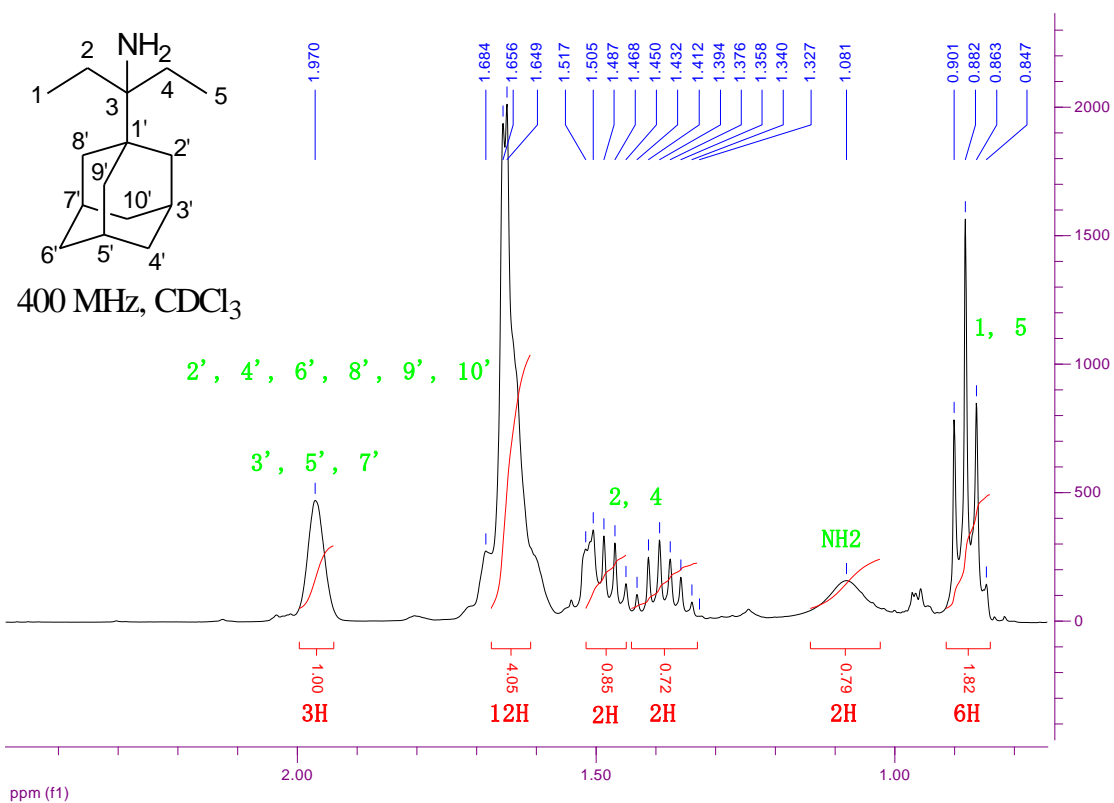
3.6.1 Nuclear Magnetic Resonance (NMR) Spectra of aminoadamantane compounds 4 and 5 and the intermediate derivatives 7b, 7c and 8.

Spectra of aminoadamantane compound 3 and the intermediate derivatives **6**, **7a**, **9a** can be found in Chapter 1, 1.4.2.

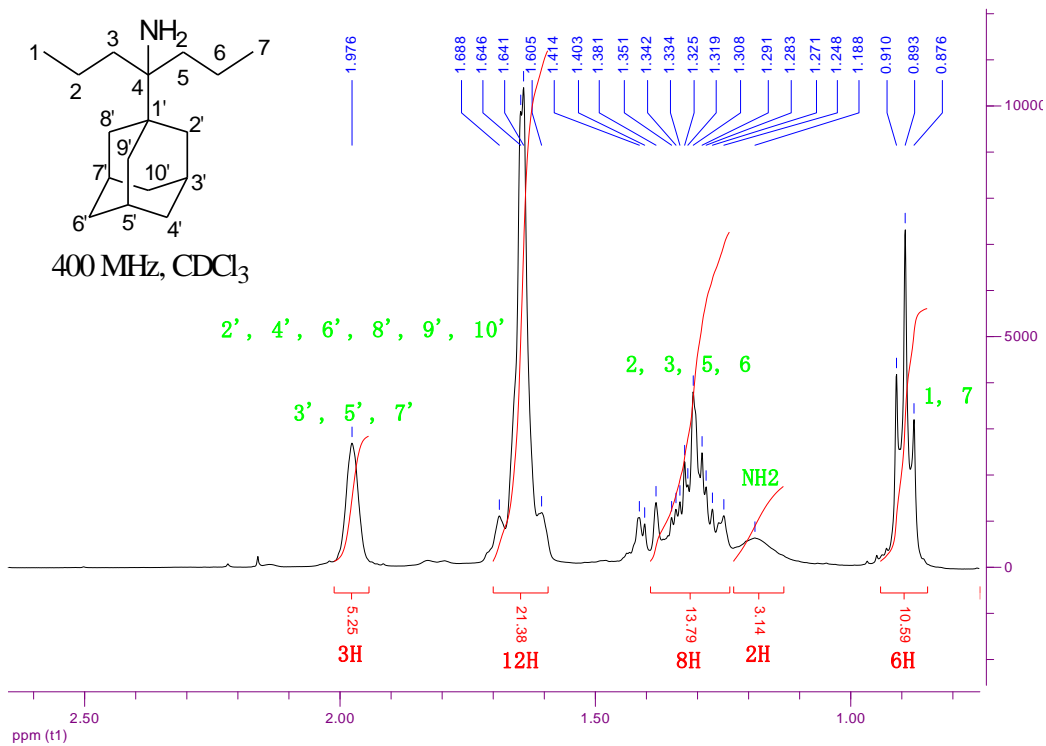
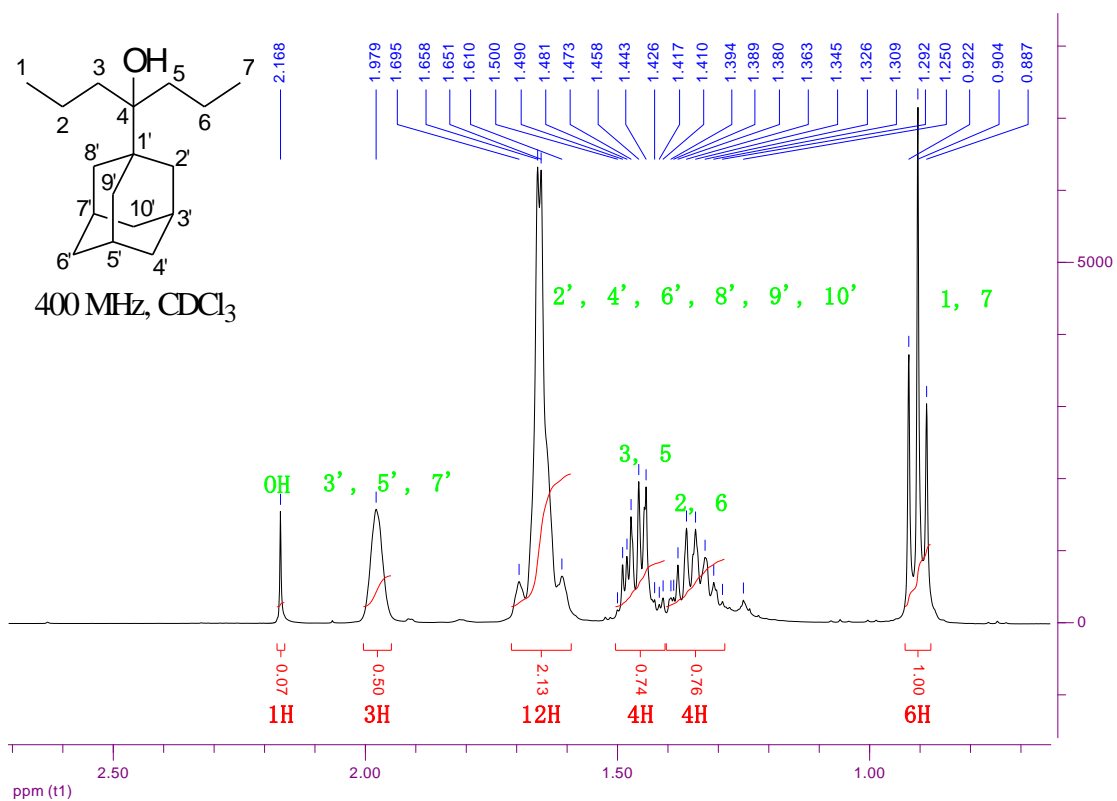
3.6.1.1 ^1H NMR spectra



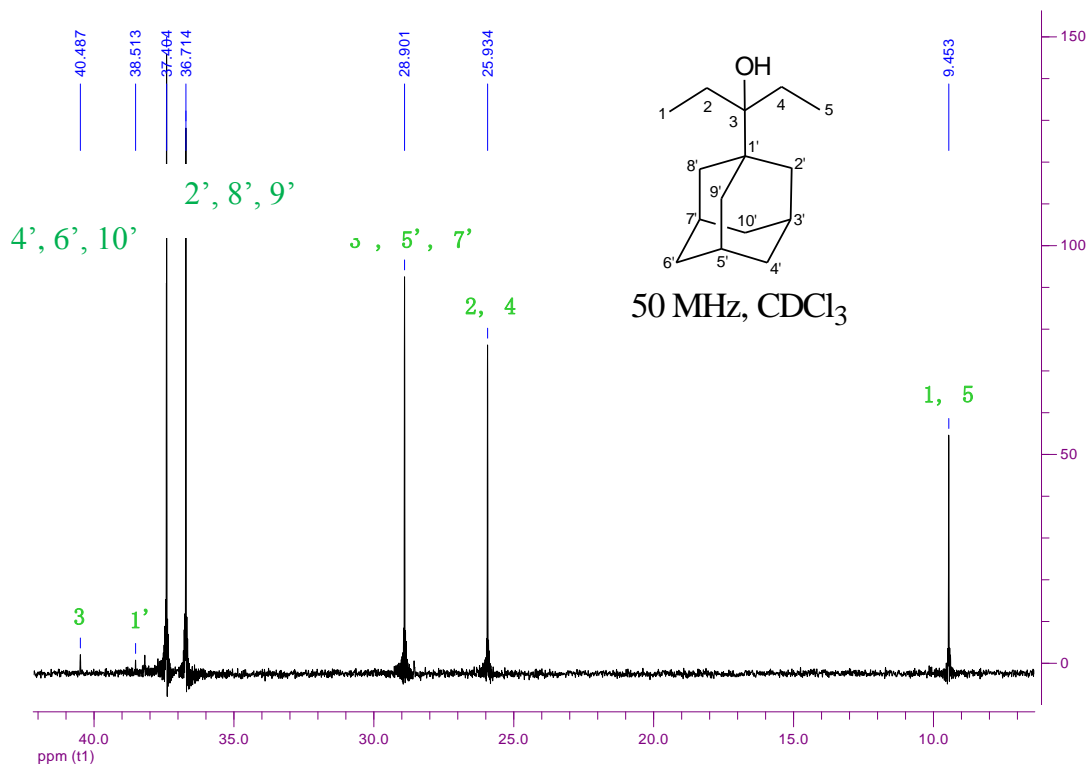
Effect of Subtle Changes of Aminoadamantanes Structure and Influenza M2TM Structure in the Binding Kinetics, Affinity and Potency



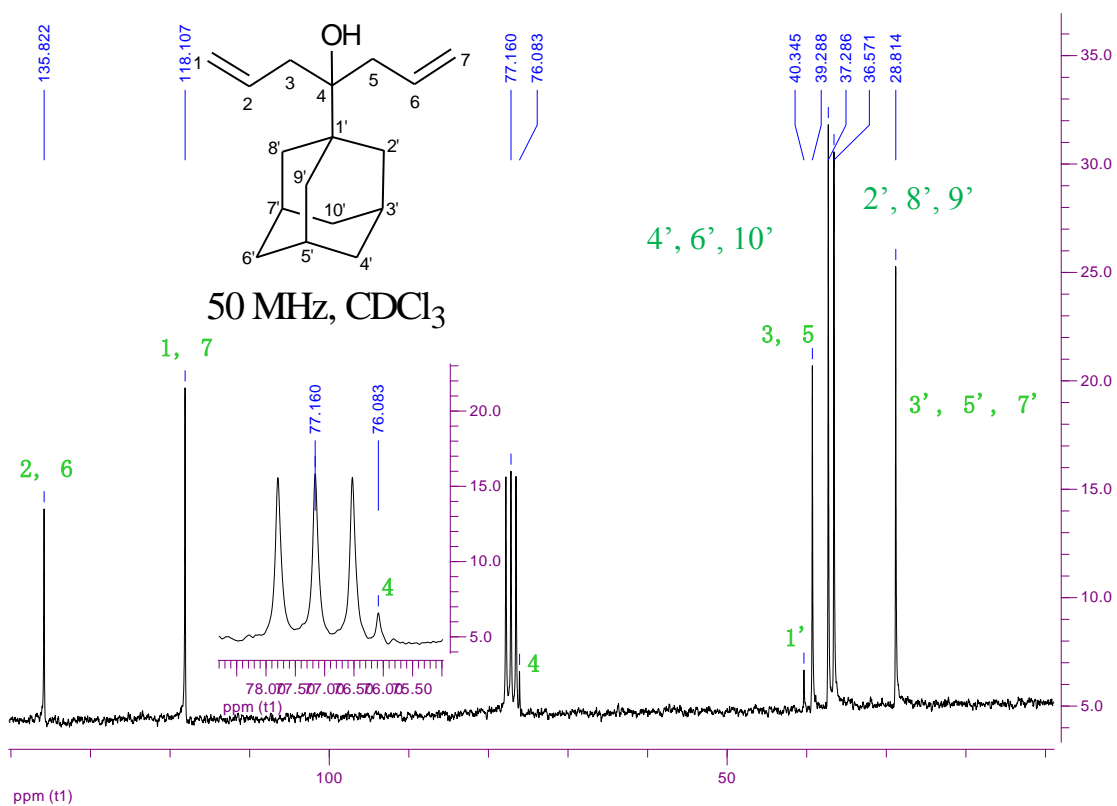
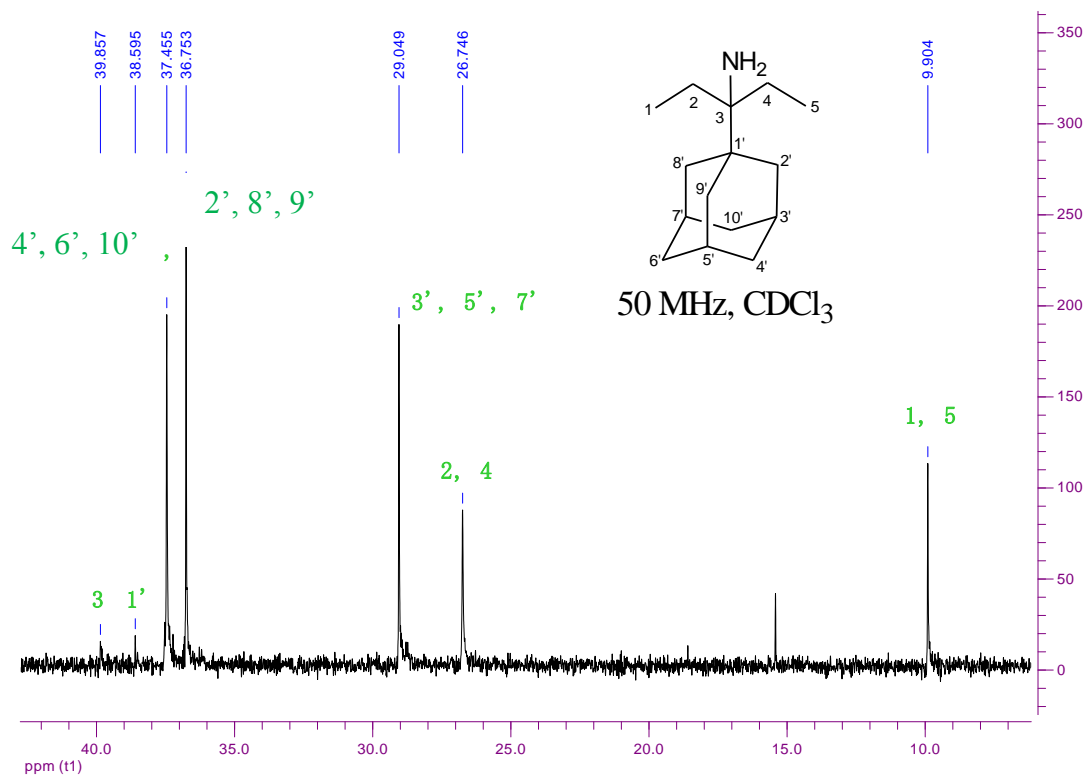
Effect of Subtle Changes of Aminoadamantanes Structure and Influenza M2TM Structure in the Binding Kinetics, Affinity and Potency



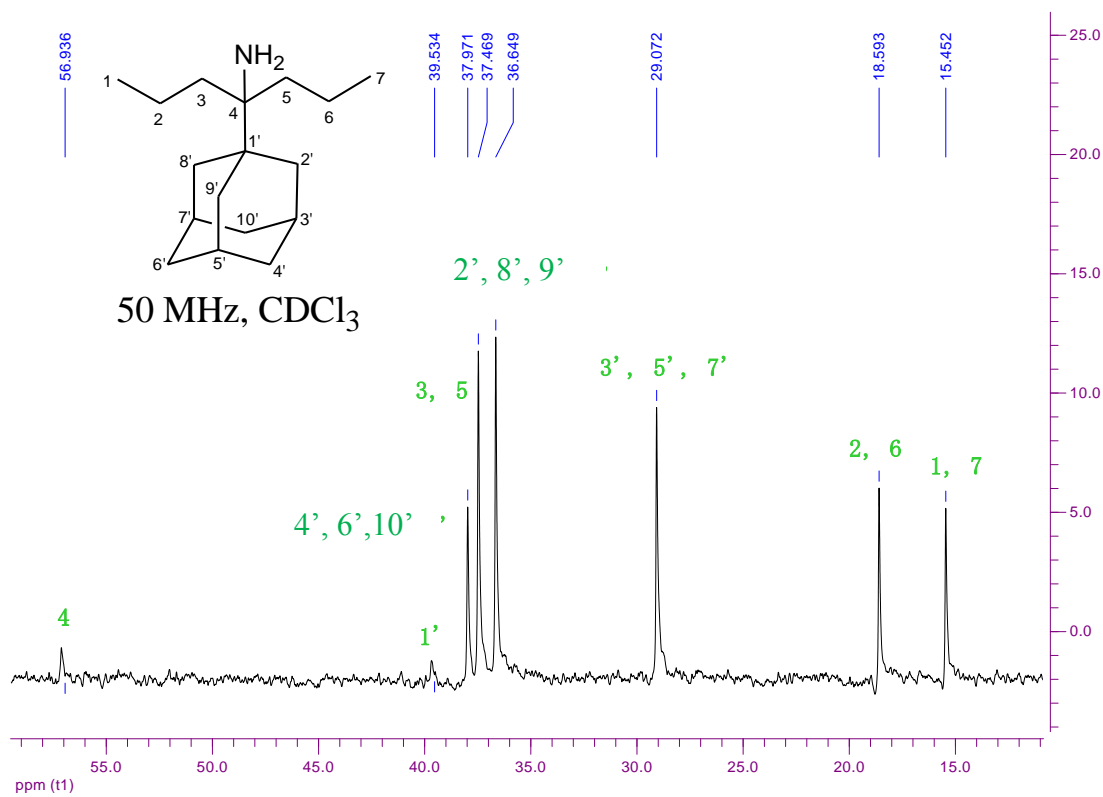
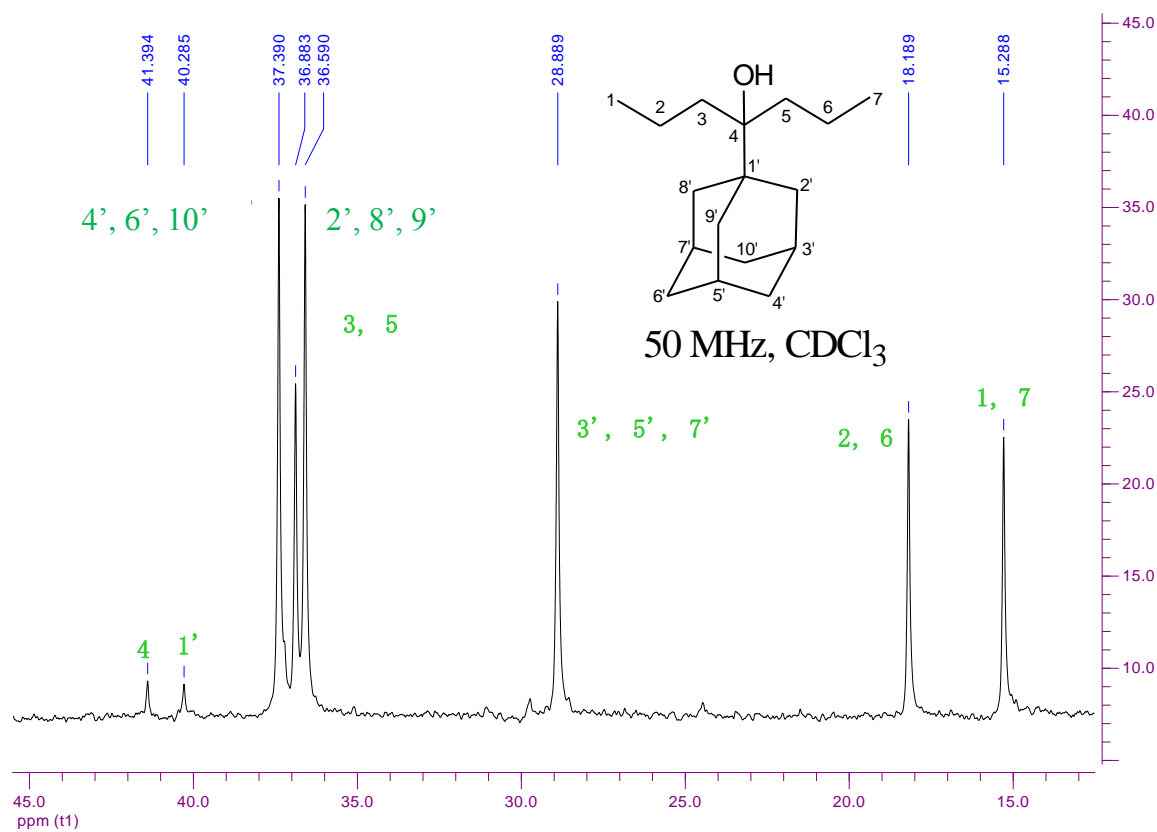
3.6.1.2 ^{13}C NMR spectra



Effect of Subtle Changes of Aminoadamantanes Structure and Influenza M2TM Structure in the Binding Kinetics, Affinity and Potency



Effect of Subtle Changes of Aminoadamantanes Structure and Influenza M2TM Structure in the Binding Kinetics, Affinity and Potency



3.7 References

- ¹ (a) Ferruz, N.; De Fabritiis, G. Binding Kinetics in Drug Discovery. *Molecular Informatics* **2016**, *35*, 216-226. (b) Hothersall, D. J.; Brown, A. J.; Dale, I.; Rawlins, P. Can residence time offer a useful strategy to target agonist drugs for sustained GPCR responses? *Drug Discovery Today* **2016**, *21*, 90-96. (c) Guo, D.; Heitman, L. H.; Ijzerman, A. P. Kinetic Aspects of the Interaction between Ligand and G Protein-Coupled Receptor: The Case of the Adenosine Receptors. *Chemical Reviews* **2017**, *117*, 38-66. (d) 13th EFMC Short Course on Medicinal Chemistry: A matter of time; a kinetic perspective on drug-target interactions (Netherlands, April 23-26, 2017).
- ² Tzitzoglaki, C.; Wright, A. K.; Freudenberger, K. M.; Hoffmann, A.; Tietjen, I.; Stylianakis, I.; Kolarov, F.; Fedida, D.; Schmidtke, M.; Gauglitz, G.; Cross, T. A. Kolocouris, A. Binding and Proton Blockage by Amantadine Variants of the Influenza M2_{WT} and M2_{S31N} Explained. *J. Med. Chem.* **2017**, *60*, 1716–1733.
- ³ Wang, J.; Ma, C.; Fiorin, G.; Carnevale, V.; Wang, T.; Hu, F.; Lamb, R. A.; Pinto, L. H.; Hong, M.; Klein, M. L.; DeGrado, W. F. Molecular dynamics simulation directed rational design of inhibitors targeting drug-resistant mutants of influenza A virus M2. *J. Am. Chem. Soc.* **2011**, *133*, 12834-12841.
- ⁴ Wang, J.; Wu, Y.; Ma, C.; Fiorin, G.; Wang, J.; Pinto, L. H.; Lamb, R. A.; Klein, M. L.; Degrado, W. F. Structure and inhibition of the drug-resistant S31N mutant of the M2 ion channel of influenza A virus. *Proc. Natl. Acad. Sci. U. S. A.* **2013**, *110*, 1315-1320.
- ⁵ Wu, Y.; Canturk, B.; Jo, H.; Ma, C.; Gianti, E.; Klein, M. L.; Pinto, L. H.; Lamb, R. A.; Fiorin, G.; Wang, J.; Degrado, W. F. Flipping in the Pore: Discovery of Dual Inhibitors That Bind in Different Orientations to the Wild-Type versus the Amantadine-Resistant S31N Mutant of the Influenza a Virus M2 Proton Channel. *J. Am. Chem. Soc.* **2014**, *136*, 17987–17995.
- ⁶ Homeyer, N.; Ioannidis, H.; Kolarov, F.; Gauglitz, G.; Zikos, C.; Kolocouris, A.; Gohlke, H. Interpreting Thermodynamic Profiles of Aminoadamantane Compounds Inhibiting the M2 Proton Channel of Influenza A by Free Energy Calculations. *J. Chem. Inf. Model.* **2016**, *56*, 110–126.
- ⁷ Ioannidis, H.; Drakopoulos, A.; Tzitzoglaki, C.; Homeyer, N.; Kolarov, F.; Gkeka, P.; Freudenberger, K.; Liolios, C.; Gauglitz, G.; Cournia, Z.; Gohlke, H.; Kolocouris, A. Alchemical Free Energy Calculations and Isothermal Titration Calorimetry Measurements of Aminoadamantanes Bound to the Closed State of Influenza A/M2TM. *J. Chem. Info. Model.* **2016**, *56*, 862–876.

- ⁸ Eleftheratos, S.; Spearpoint, P.; Ortore, G.; Kolocouris, A.; Martinelli, A.; Martin, S.; Hay, A. Interaction of Aminoadamantane Derivatives with the Influenza A Virus M2 Channel-Docking Using a Pore Blocking Model. *Bioorg. Med. Chem. Lett.* **2010**, *20*, 4182-4187.
- ⁹ Gkeka, P.; Eleftheratos, S.; Kolocouris, A.; Cournia, Z. Free energy calculations reveal the origin of binding preference for aminoadamantane blockers of influenza A/M2TM pore. *J. Chem. Theory Comput.* **2013**, *9*, 1272-1281.
- ¹⁰ Drakopoulos, A.; Tzitzoglaki, C.; Ma, C.; Freudenberger, K.; Hoffmann, A.; Hu, Y.; Gauglitz, G.; Schmidtke, M.; Wang, J.; Kolocouris, A. Affinity of Rimantadine Enantiomers against Influenza A/M2 Protein Revisited. *ACS Med. Chem. Lett.* **2017**, *8*, 145–150.
- ¹¹ Aldrich, P. E.; Hermann, E. C.; Meier, W. E.; Paulshock, M.; Prichard, W. W.; Snyder, J. A.; Watts, J. C. Antiviral agents. 2. Structure-activity relationships of compounds related to 1-adamantanamine. *J. Med. Chem.* **1971**, *14*, 535-543.
- ¹² Bright, R. A.; Medina, M. J.; Xu, X.; Perez-Orozco, G.; Wallis, T. R.; Davis, X. M.; Povinelli, L.; Cox, N. J.; Klimov, A. I. Incidence of adamantane resistance among influenza A (H3N2) viruses isolated worldwide from 1994 to 2005: a cause for concern. *Lancet* **2005**, *366*, 1175-1181.
- ¹³ (a) Bright, R. A.; Shay, D. K.; Shu, B.; Cox, N. J.; Klimov, A. I. Adamantane resistance among influenza A viruses isolated early during the 2005-2006 influenza season in the United States. *J. Am. Med. Assoc.* **2006**, *295*, 891-894; (b) Lan, Y.; Zhang, Y.; Dong, L.; Wang, D.; Huang, W.; Xin, L.; Yang, L.; Zhao, X.; Li, Z.; Wang, W.; Li, X.; Xu, C.; Guo, J.; Wang, M.; Peng, Y.; Gao, Y.; Guo, Y.; Wen, L.; Jiang, T.; Shu, Y. A comprehensive surveillance of adamantane resistance among human influenza A virus isolated from mainland China between 1956 and 2009. *Antivir. Ther.* **2010**, *15*, 853-859.
- ¹⁴ High levels of adamantane resistance among influenza A (H3N2) viruses and interim guidelines for use of antiviral agents--United States, 2005-06 influenza season. *MMWR Morb. Mortal Wkly Rep.* **2006**, *55*, 44-46.
- ¹⁵ Chaires, J. B. Calorimetry and thermodynamics in drug design. *Annu. Rev. Biophys.* **2008**, *37*, 135-151.

- ¹⁶ Ladbury, J. E.; Klebe, G.; Freire, E. Adding calorimetric data to decision making in lead discovery: a hot tip. *Nat. Rev. Drug Discov.* **2010**, *9*, 23-27.
- ¹⁷ Perozzo, R.; Folkers, G.; Scapozza, L. Thermodynamics of protein-ligand interactions: history, presence, and future aspects. *J. Recept. Signal Transduct. Res.* **2004**, *24*, 1-52.
- ¹⁸ Salom, D.; Hill, B. R.; Lear, J. D.; DeGrado, W. F. pH-dependent tetramerization and amantadine binding of the transmembrane helix of M2 from the influenza A virus. *Biochemistry* **2000**, *39*, 14160–14170.
- ¹⁹ Stouffer, A. L.; Ma, C.; Cristian, L.; Ohigashi, Y.; Lamb, R. A.; Lear, J. D.; Pinto, L. H.; DeGrado, W. F. The Interplay of Functional Tuning, Drug Resistance, and Thermodynamic Stability in the Evolution of the M2 Proton Channel from the Influenza A Virus. *Structure* **2008**, *16*, 1067-1076.
- ²⁰ Rosenberg, M. R.; Casarottol, M. G. Coexistence of two adamantane binding sites in the influenza A M2 ion channel. *Proc. Natl. Acad. Sci. U. S. A.* **2010**, *107*, 13866-13871.
- ²¹ Schmidtke, M.; Schnittler, U.; Jahn, B.; Dahse, H.-M.; Stelzner, A. A rapid assay for evaluation of antiviral activity against coxsackie virus B3, influenza virus A, and herpes simplex virus type 1. *Journal of Virological Methods* **2001**, *95*, 133-143.
- ²² Dong, J.; Chen, S.; Li, R.; Cui, W.; Jiang, H.; Ling, Y.; Yang, Z.; Hu, W. Imidazole-based pinanamine derivatives: Discovery of dual inhibitors of the wild-type and drug-resistant mutant of the influenza A virus. *Eur. J. Med. Chem.* **2016**, *108*, 605-615.
- ²³ Barniol-Xicotá, M.; Gazzarrini, S.; Torres, E.; Hu, Y.; Wang, J.; Naesens, L.; Moroni, A.; Vazquez, S. Slow but Steady Wins the Race: Dissimilarities among New Dual Inhibitors of the Wild-Type and the V27A Mutant M2 Channels of Influenza A Virus. *J. Med. Chem.* **2017**, *60*, 3727-3738.
- ²⁴ Cristian, L.; Lear, J. D.; DeGrado, W. F. Use of Thiol-Disulfide Equilibria to Measure the Energetics of Assembly of Transmembrane Helices in Phospholipid Bilayers. *Proc. Natl. Acad. Sci. U. S. A.* **2003**, *100*, 14772-14777.
- ²⁵ Cady, S.; Wang, T.; Hong, M. Membrane-Dependent Effects of a Cytoplasmic Helix on the Structure and Drug Binding of the Influenza Virus M2 Protein. *J. Am. Chem. Soc.* **2011**, *133*, 11572–11579.

- ²⁶ Hu, J.; Asbury, T.; Achuthan, S.; Li, C.; Bertram, R.; Quine, J. R.; Fu, R.; Cross, T. A. Backbone structure of the amantadine-blocked trans-membrane domain M2 proton channel from Influenza A virus. *Biophys. J.* **2007**, *92*, 4335-43.
- ²⁷ Cady, S. D.; Schmidt-Rohr, K.; Wang, J.; Soto, C. S.; Degrado, W. F.; Hong, M., Structure of the amantadine binding site of influenza M2 proton channels in lipid bilayers. *Nature* **2010**, *463*, 689-92.
- ²⁸ Ma, C.; Polishchuk, A. L.; Ohigashi, Y.; Stouffer, A. L.; Schön, A.; Magavern, E.; Jing, X.; Lear, J. D.; Freire, E.; Lamb, R. A.; DeGrado, W. F.; Pinto, L. H. Identification of the functional core of the influenza A virus A/M2 proton-selective ion channel. *Proc. Natl. Acad. Sci. USA* **2009**, *106*, 12283-12288.
- ²⁹ Balannik, V.; Wang, J.; Ohigashi, Y.; Jing, X.; Magavern, E.; Lamb, R. A.; DeGrado, W. F.; Pinto, L. H. *Biochemistry* **2009**, *48*, 11872.
- ³⁰ (a) Gleed, M. L.; Ioannidis, H.; Kolocouris, A.; Busath, D. D. Resistance-Mutation (N31) Effects on Drug Orientation and Channel Hydration in Amantadine-Bound Influenza A M2. *J. Phys. Chem. B* **2015**, *119*, 11548-59. (b) Alhadeff, R.; Assa, D.; Astrahan, P. Krugliak, M.; Arkin, I. T. Computational and experimental analysis of drug binding to the influenza M2 channel. *Biochim. Biophys. Acta* **2014**, *1838*, 1068–1073.
- ³¹ Andreas, L. B.; Eddy, M. T.; Pielak, R. M.; Chou, J.; Griffin, R. G. Magic angle spinning NMR investigation of influenza A M2(18-60): support for an allosteric mechanism of inhibition. *J. Am. Chem. Soc.* **2010**, *132*, 10958-10960.
- ³² Wright, A. K.; Batsomboon, P.; Dai, J.; Hung, I.; Zhou, H.-X.; Dudley, G. B.; Cross, T. A. Differential binding of rimantadine enantiomers to influenza A M2 proton channel. *J. Am. Chem. Soc.* **2016**, *138*, 1506-1509.
- ³³ Schade, D.; Kotthaus, J.; Riebling, L.; Kotthaus, J.; Müller-Fielitz, H.; Raasch, W.; Hoffmann, A.; Schmidtke, M.; Clement, B.; Zanamivir Amidoxime- and N-Hydroxyguanidine-Based Prodrug Approaches to Tackle Poor Oral Bioavailability. *J. Pharm. Sci.* **2015**, *104*, 3208-3219.
- ³⁴ Torres, E.; Fernández, R.; Miquet, S.; Font-Bardia, M.; Vanderlinden, E.; Naesens, L.; Vázquez, S. Synthesis and anti-influenza A virus activity of 2,2-dialkylamantadines and related compounds. *ACS Med. Chem. Lett.* **2012**, *3*, 1065–1069. (f) Kolocouris, A.; Tzitzoglaki, C.; Johnson, F. B.; Zell, R.; Wright, A. K.; Cross, T. A.; Tietjen, I.; Fedida, D.; Busath, D. D. Aminoadamantanes with Persistent in Vitro Efficacy against H1N1 (2009) Influenza A. *J. Med. Chem.* **2014**, *57*, 4629-39.

CHAPTER 4

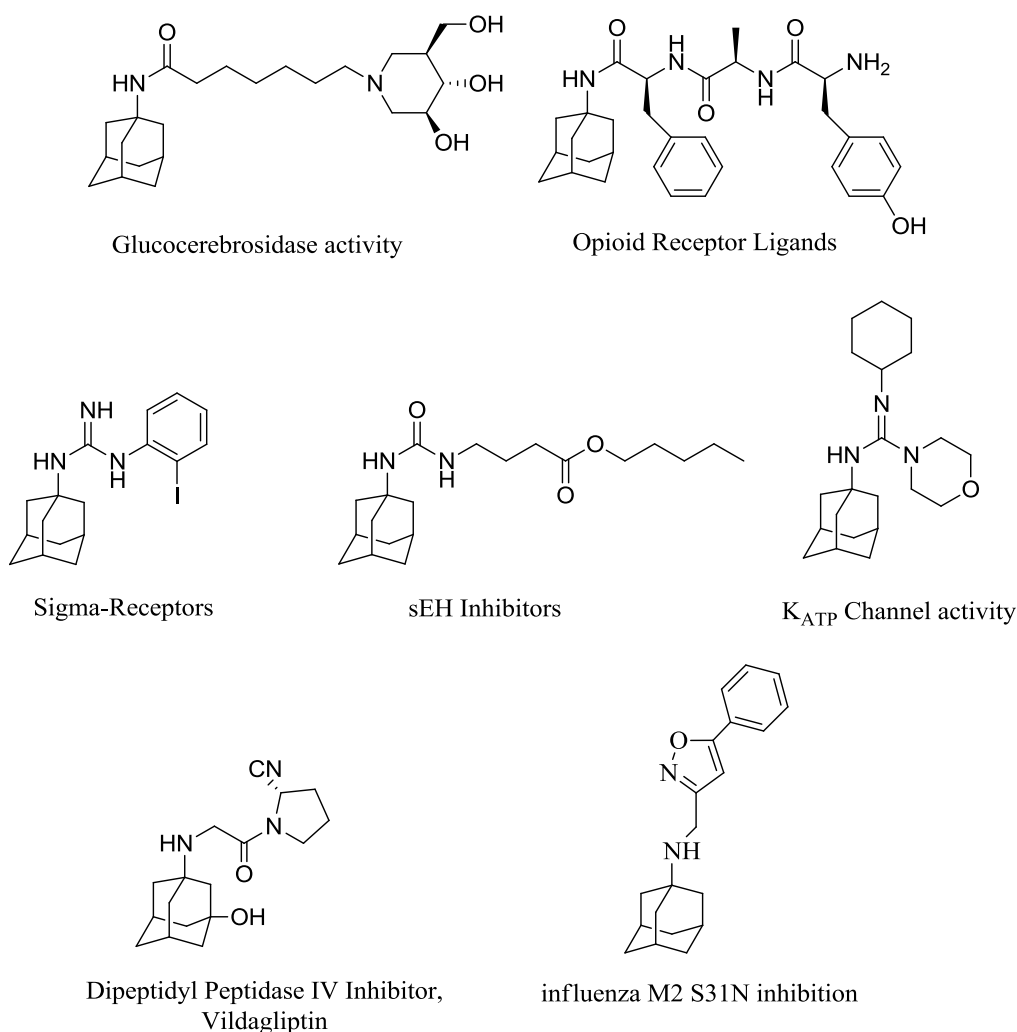
Approaches to primary *tert*-alkyl amines as medicinal chemistry building blocks

4.1 Abstract

Amantadine is a lipophilic symmetrical hydrocarbon cage amine and represents a building block which can be favorably modified and linked with known pharmacophoric groups resulting in enhanced biological activity. Five procedures were tested for the synthesis of primary *tert*-alkyl primary amines in aliphatic series including also adamantane adducts. The synthesized amines are analogues of amantadine or other cage-like amines. The first procedure included the formation and reduction of *tert*-alkyl azides (procedure A), where yield depends from the selection of solvent for azide formation and the reagent and conditions for its reduction. Dichloromethane or 1,2-dichloroethane and LiAlH₄ were found to be optimal choices. The yields of the amine products were diminished when the *tert*-alkyl substrate includes longer alkyl groups than Pr₃. This procedure was the most general covering a broader range of substrates including also bulky adamantane adducts. Standard Ritter reaction (procedure B) was not affordable. A modified Ritter scheme (procedure C), which proceeds through a *tert*-alkyl chloroacetamide produced *tert*-alkyl amines with good yields also for long alkyl groups. The procedure failed when the substrate included an adamantane adduct. Procedure D included the addition of organometallic reagents to *N-tert*-butyl sulfinyl ketimines and has also limitations. The synthesis of primary *tert*-alkyl amines from nitriles using organometallic reagents and Ti(*i*-PrO)₄ was a useful one-flask transformation (procedure E). Triggered by the effects of the adamantane adduct in reactivity and conformational strain the rotation of the 1-adamantyl group was investigated using dynamic NMR (DNMR) in the synthesized Ad-C(Et₂)OH and Ad-C(Et₂)Cl which were related synthetic intermediates in the present study. Their NMR spectra resulted in decoalescence for carbons 2', 8', 9'-C and 4', 6', 10'-C signals at temperatures as low as -100 °C. The free energy for bond rotation was calculated to be $\Delta G^\ddagger = 8.7 \pm 0.2 \text{ kcal mol}^{-1}$ for Ad-C(Et₂)OH and $10.0 \pm 0.4 \text{ kcal mol}^{-1}$ for Ad-C(Et₂)Cl compared to $9.3 \text{ kcal mol}^{-1}$ for Ad-C(Me₂)Cl or $10.6 \text{ kcal mol}^{-1}$ for Ad-CMe(*t*-Bu)Cl.

4.2 Introduction

Remarkably simple aminoadamantane structures hit targets like viroporins to combat Influenza virus A and the NMDA receptor for symptomatic relief in Parkinson Disease and Alzheimer Disease.¹ Adamantane is a lipophilic symmetrical hydrocarbon cage and when is included itself or favorably modified as a substituent in drug molecules can result in enhanced biological activity. Amantadine or simple amantadine analogues represent building blocks which can be favorably modified and linked with known pharmacophoric groups resulting in enhanced biological activity.



Scheme 1. Few examples of molecules bearing 1-adamantyl linked with a pharmacophoric group.

Examples¹ are molecules with glucocerebrosidase activity potentially useful for atherosclerosis,^{2a} K⁺ channel activity and hypoglycemic properties,^{2b} affinity for opioid receptor,^{2c} affinity for σ -receptor^{2d} which is involved in psychotic disorders, depression, neuroprotection, affinity for soluble epoxide hydrolase^{2e} which seems valuable for various diseases, dipeptidyl peptidase IV inhibitory potency^{2f} for the treatment of type 2 diabetes mellitus, influenza A amantadine resistance etc^{2g} etc (Scheme 1).

Our efforts for more than 25 years include research on synthetic aminoadamantanes, that is, synthesis and biological evaluation of new derivatives mainly against influenza virus A, dynamic NMR spectroscopy and other physical organic chemistry studies, and biophysical studies of aminoadamantanes interaction with the transmembrane domain of M2 protein (M2TM) or the full M2 protein, i.e., solution NMR and solid state NMR (ssNMR) studies for mapping the binding site, measurements of binding constants using Isothermal Titration Calorimetry (ITC) and other assays used as experimental probes for binding free energy calculations, electrophysiology for studying kinetics of binding, biomolecular simulations.³ It was only after 2008 that high resolution structures from X-ray and ssNMR experiments showed that the primary binding site of amantadine is the lumen of the four-helix bundle of tetrameric M2 (M2TM: amino acids 22-46) that forms the proton transport path.⁴⁻¹³

We are interested in the preparation of primary *tert*-alkyl amines in aliphatic series including common alkyl chain or adamantane substituents which may be used as lipophilic amine building blocks for the development of drug molecules acting in WT and mutant M2 protein of influenza A viruses which are resistant to amantadine^{2g, 3h-n, 13-18} or other biological targets (Scheme 1). For example it was reported that 1,1,3,3-tetramethylbutylamine (*tert*-octylamine, nPeMe₂CNH₂)¹⁵ and 2-(1-adamantyl)-2-propanamine (AdCMe₂NH₂)^{3m,n} block M2 channel with an efficiency comparable to amantadine (Figure 1).

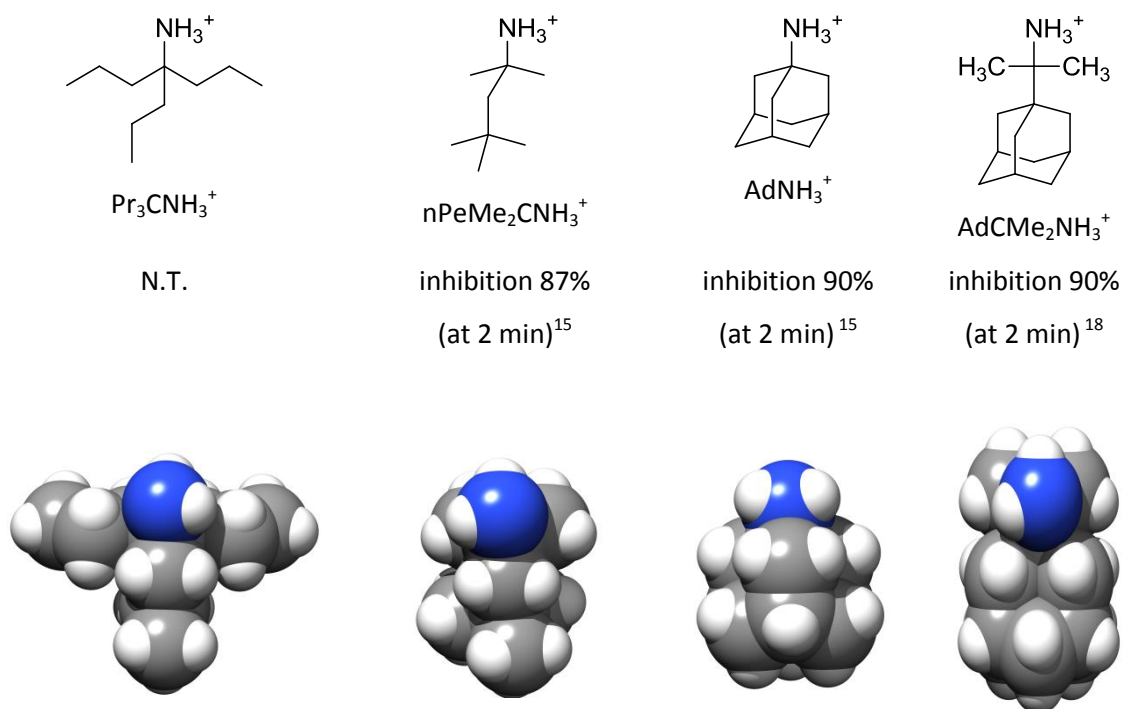


Figure 1. Up: $\text{Pr}_3\text{CNH}_3^+$ and $\text{nPeMe}_2\text{CNH}_3^+$ are open cage analogues of amantadine and $\text{nPeMe}_2\text{CNH}_3^+$, AdNH_3^+ and $\text{Ad-CMe}_2\text{-NH}_3^+$ are potent influenza A WT M2 pore blockers. Down: van der Waals spheres representation of Pr_3CNH_2 , $\text{nPeMe}_2\text{CNH}_2$, AdNH_2 and $\text{Ad-CMe}_2\text{-NH}_2$.

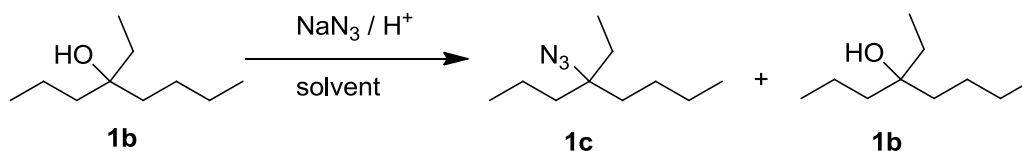
The preparation of primary *tert*-alkyl amines is considered to be a difficult problem.¹⁹ When one of the substituent of the α,α,α -trisubstituted primary amine is a *tert*-alkyl group like adamantyl steric crowding is expected to increase the difficulty of conformational motions and the reactivity. When the starting material is a *tert*-alkyl alcohol a general and widely used route is the Ritter reaction²⁰ providing the primary *tert*-alkyl amine in two steps. However, this procedure has some considerable disadvantages such as the drastic conditions and moderate overall yields. While several procedures are widely applied to convert primary and secondary alcohols to the corresponding azides -based on $\text{S}_{\text{N}}2$ mechanism- only limited examples of robust procedures have been published on the conversion of *tert*-alkyl alcohols²¹ and some of the latter procedures used elaborate reactants.^{21d-g} In addition, while several reagents have been developed for the reduction of primary and secondary azides to the corresponding amines, this is not the case when a *tert*-alkyl azide is the substrate and its reduction is considered to be inconvenient¹⁹. In this work we present results obtained during our synthetic efforts to prepare primary *tert*-alkyl amines with various alkyl groups including adamantyl group.

4.3 Results and Discussion

4.3.1 Synthetic studies

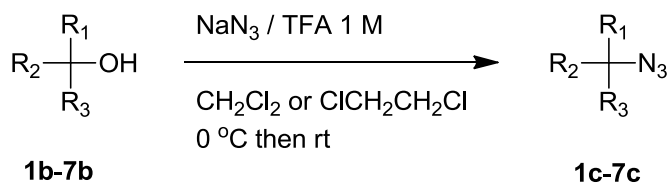
4.3.3.1 From *tert*-alkyl alcohols through *tert*-alkyl azides reduction (Procedure A)

The conversion of tertiary adamantanol to the corresponding azides (*tert*-alkyl alcohol → *tert*-alkyl azide → primary *tert*-alkyl amine, procedure A) was routinely realized in our lab using a mixture of $\text{CHCl}_3/\text{H}_2\text{SO}_4$ 57 % and sodium azide in good yields.^{21a,b,22,23} When these reaction conditions were applied to *tert*-alkyl alcohols, like *n*-BuEt(*n*-Pr)C-OH (**1b**) - obtained from 3-heptanone (**1a**) + *n*-PrMgBr - a mixture of the azide BuEtPrC-N₃ (**1c**) and the precursor alcohol **1a** was obtained in 60:40 ratio based on the integration of ¹³C NMR signals (Table 1, entry 1). The reaction proceed via the formation of a carbonium ions which is trapped by the azide anion. It seems that the 2-alkyl-2-adamantyl carbonium intermediates from tertiary 2-alkyl-2-adamantanol are more stable and formed more efficiently compared to those formed by *tert*-alkyl alcohols.²⁴ A more efficient formation of the azide was not achieved after increasing the sulfuric acid concentration to 70 % (Table 1, entry 2); instead a ketone product was also formed along with the azide. This ketone may be obtained through a Schmidt rearrangement²⁵ mechanism where an imine is formed which can be hydrolyzed to a ketone as has been reported for the *tert*-butyl substrate.^{25b} The *tert*-alkyl alcohol **1b** was treated with CHCl_3/TFA 0.5M/ NaN_3 mixture, and the reaction product was a mixture of the azide **1c** and the precursor alcohol **1b** in a 70:30 ratio according to the ¹³C NMR spectrum. An increase in TFA concentration to 1 M was tested but the same mixture was afforded (Table 1, entries 3, 4). Increase of the TFA concentration to 5M caused a decomposition of the substrate. Changing the solvent from CHCl_3 to CH_2Cl_2 or $\text{ClCH}_2\text{CH}_2\text{Cl}$ (i.e., from CHCl_3/TFA 1 M/ NaN_3 to CH_2Cl_2 or $\text{ClCH}_2\text{CH}_2\text{Cl}/\text{TFA}$ 1 M/ NaN_3) resulted to the azide as the only product (Table 1, entry 5). The reactions conditions were then tested against *tert*-alkyl alcohols **1b-7b** (Table 2, entries 1-7). Alcohols **1b-4b**, **6b** were obtained from the reaction between ketone **1a-3a** and the suitable Grignard reagent (Table 2, entries 1-4,6). However, the reaction applied for the preparation of *i*BuPr₂C-OH (**5b**) (Table 2, entry 5) including 3-heptanone (**1a**) and freshly prepared isobutyl magnesium bromide yielded a mixture of the *tert*-alkyl alcohol **5b** and 3-heptanol in a ratio of 70:30 according to the ¹³C NMR spectrum; 3-heptanol was formed through a β -hydride transfer of the Grignard reagent.²⁶ The desired *i*-BuPr₂C-OH (**5b**) was obtained from the addition of isobutyl lithium to 4-heptanone (**2a**) and similarly *i*-BuBu₂C-OH (**7b**) (Table 2, entry 7) was afforded through addition of isobutyl lithium to 5-nonanone (**3a**). Starting from alcohols **1b-7b** and using the conditions shown in Table 2, i.e., CH_2Cl_2 or $\text{ClCH}_2\text{CH}_2\text{Cl}/\text{TFA}$ 1 M/ NaN_3 , the azides **1c-7c** respectively were afforded with yields 71-87% (Table 2).

Table 1. Optimization of the reaction conditions for the conversion of a *tert*-alkyl alcohol to the corresponding *tert*-alkyl azide using NaN₃ in an acidic environment.

Entry	Solvent/acid	Product (percentage) ^a
1	CHCl ₃ /H ₂ SO ₄ 57 %	1c (~ 60%) + 1b (~ 40%)
2	CHCl ₃ /H ₂ SO ₄ 70 %	1c (~ 45%) + ketone product (~ 55%)
3	CHCl ₃ /TFA 0.5 M	1c (~ 70%) + 1b (~ 30%)
4	CHCl ₃ /TFA 1 M	1c (~ 70%) + 1b (~ 30%)
5	CH ₂ Cl ₂ or ClCH ₂ CH ₂ Cl /TFA 1 M	1c

^aApproximate percentages were measured from integration of ¹³C NMR signals.

Table 2. Conversion of *tert*-alkyl alcohols to *tert*-alkyl azides using a NaN₃/TFA in CH₂Cl₂ or ClCH₂CH₂Cl (Procedure A).

Entry	Ketone + organometallic reagent	Isolated Yield	Alcohol R ₁ ,R ₂ ,R ₃	Azide R ₁ ,R ₂ ,R ₃	Isolated Yield ^a
1	3-heptanone 1a + PrMgBr	80%	Bu,Et,Pr, 1b	Bu,Et,Pr, 1c ^b	87%
2	4-heptanone 2a + PrMgBr	78%	Pr,Pr,Pr, 2b	Pr,Pr,Pr,, 2c ^b	78%
3	5-nonanone 3a + BuMgBr	80%	Bu,Bu,Bu, 3b	Bu,Bu,Bu, 3c ^b	82%
4	4-heptanone 2a + BuMgBr	71%	Bu,Pr,Pr, 4b	Bu,Pr,Pr, 4c ^b	71%
5	4-heptanone 2a + iBuLi	80%	iBu,Pr,Pr, 5b	iBu,Pr,Pr, 5c ^b	86%
6	5-nonanone 3a + PrMgBr	70%	Bu,Bu,Pr, 6b	Bu,Bu,Pr, 6c ^b	75%
7	2,6-dimethyl-heptan-4-one 4a + BuLi	80%	iBu,iBu,Bu, 7b	iBu,iBu,Bu, 7c ^c	76%

^aCompletion of reaction was checked by ¹³C NMR peaks integration; ^bCH₂Cl₂ used; ^cClCH₂CH₂Cl used

Thus, according to the reactions conditions included by Table 2 changing the solvent from CHCl₃ to CH₂Cl₂ or ClCH₂CH₂Cl increased considerably *tert*-alkyl azide yield. The *tert*-alkyl azide formation proceeds through an ion pair intermediate (*tert*-alkyl carbocation/TFA anion) - generated by the *tert*-alkyl alcohol treatment with TFA - which is more favored in dichloromethane compared to chloroform. The higher dielectric constant of CH₂Cl₂ ($\epsilon = 8.93$) or ClCH₂CH₂Cl ($\epsilon = 10.4$) compared to CHCl₃ ($\epsilon = 4.81$) may stabilize the carbonium ion and thus facilitate its formation (nucleophilic solvation).²⁷ Protic solvents have also high dielectric constants but *tert*-alkyl azides are formed in low yields in protic solvents due to competitive solvolysis reactions.²⁸ The stability of various carbonium ions in different solvents can be compared by calculating the difference in the free energy for the isodesmic reaction between 1-adamantyl cation (1-Ad⁺) and the related hydrocarbon,²⁹ i.e, for the reaction R₃CH + 1-Ad⁺ → R₃C⁺ + Ad-H. We investigated the comparative efficiency for the formation of Pr₃C⁺ and of Bu₃C⁺ in CHCl₃, CH₂Cl₂ and ClCH₂CH₂Cl using this isodesmic reaction (R=Pr,Bu). Calculations were performed using the standard B3LYP/6-31G(d,p) level³⁰ and the Polarizable Continuum Model of Tomasi (PCM)³¹ as the implicit solvent model (see Supporting Information). The results in Table 3 suggested the easier formation of Pr₃C⁺ and of Bu₃C⁺ in CH₂Cl₂ and ClCH₂CH₂Cl than in CHCl₃.

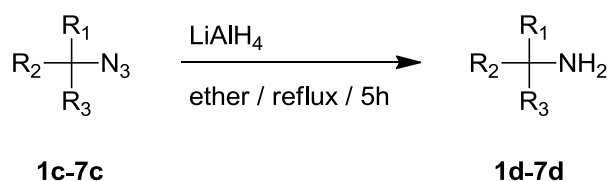
Table 3. Difference in free energy (kcal mol⁻¹) calculated for the isodesmic reaction R₃CH + 1-Ad⁺ → R₃C⁺ + Ad-H (R=Pr, Bu), in CHCl₃, CH₂Cl₂, ClCH₂CH₂Cl at B3LYP/6-31+G(d,p) level using PCM as continuous solvent model.

Solvent	ΔG (kcal mol ⁻¹)	
	Pr ₃ C ⁺	Bu ₃ C ⁺
CHCl ₃	+ 3.2	+ 2.1
CH ₂ Cl ₂	+ 2.8	+ 1.7
ClCH ₂ CH ₂ Cl	+ 2.7	+ 1.6

It was tested if primary *tert*-alkyl amines **1d-7d** could be formed conventionally from primary *tert*-alkyl azides **1c-7c** through a LiAlH₄ reduction^{21g,32,33} or a catalytic hydrogenation, for example using Pd/C.³³ In general, these methods are considered to be high yielding^{21g,33,34d} without never being explored systematically regarding the structure of the *tert*-alkyl substrate; for example in one case it was found that the reduction took a different route yielding a triazene.³⁵ As previously mentioned the reduction of *tert*-alkyl azides for the preparation of *tert*-alkyl amines was reported to be an inconvenient transformation without further explanations and citations.¹⁹ The reduction of the *tert*-alkyl azides **1c-7c** using LiAlH₄ in refluxing ether

for 5 h yielded the primary *tert*-alkyl amines **1d-7d** in good (Table 4, entries 1,2,5) to moderate yields (entries 3,4,6,7); 4 equivalents of LiAlH₄ were used in a slurry having a concentration of 1 g LiAlH₄/80 mL dry ether. Amines were isolated through standard hydrolysis conditions and filtration of the reaction mixture. The ethereal solution was extracted with hydrochloride solution 6%, the acidic solution was made alkaline with solid sodium carbonate and the mixture was extracted with ether to afford amines **1d-7d** having a purity > 95% (according to the relative integration of amine signals with impurities signals detected in ¹³C NMR spectra). The amines were further purified through formation of crystalline fumaric acid salts and recrystallization of the ammonium salts using ethanol/ether. A suspicious competitive reaction of the reduction is the formation of an imine which can be formed through an intramolecular Schmidt rearrangement via a nitrene intermediate.³⁶ When refluxing THF was used lower yields were obtained. The yield was not improved when the refluxing conditions were changed to ambient temperature for avoiding possible azide decomposition at refluxing ether conditions. It is noteworthy that a critical reduction in yield was noted upon the transition from Pr₃ to Bu₃ substrate (Table 4, see entries 2 and 3).

Table 4. Reaction of *tert*-alkyl azides with LiAlH₄ in refluxing dry ether (Procedure A).



Entry	Azide R ₁ ,R ₂ ,R ₃	Amine product R ₁ ,R ₂ ,R ₃	Isolated Yield ^a
1	Bu,Et,Pr, 1c	Bu,Et,Pr, 1d	65 %
2	Pr,Pr,Pr, 2c	Pr,Pr,Pr, 2d	60 %
3	Bu,Bu,Bu, 3c	Bu,Bu,Bu, 3d	20 %
4	iBu,Pr,Pr, 4c	iBu,Pr,Pr, 4d	14 %
5	Bu,Pr,Pr, 5c	Bu,Pr,Pr, 5d	58 %
6	Bu,Bu,Pr, 6c	Bu,Bu,Pr, 6d	35 %
7	iBu,iBu,Bu, 7c	iBu,iBu,Bu, 7d	20 %

^aCompletion of reaction was observed by NMR

To investigate further the effect of the structure of the *tert*-alkyl group to the reduction yield of the azido group, we synthesized the alcohols **5b**, **6b** and the corresponding azides **5c**, **6c** including the

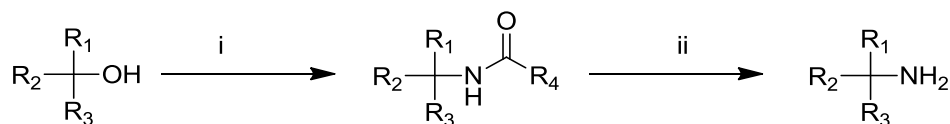
combination of BuPr₂ and Bu₂Pr substitution on the tertiary carbon (see Table 4, entries 5, 6). As depicted in Table 4, the yield for the BuPr₂ substrate (amine **5d**, 58%; Table 4, entry 5) was similar to that obtained with Pr₃ substrate (amine **2d**, 60%; Table 4, entry 2) and reduced progressively from Bu₂Pr (amine **6d**, 35%; Table 4, entry 6) to Bu₃ or *i*-Bu₂Bu substrate (amines **3d**, **7d**, 20%, Table 4, entries 3,7). Also, changing the tri-alkyl group from Pr₃ to *i*-BuPr₂ reduced significantly the yield (amine **4d**, 14%, Table 4, entry 4).

We tested few other reagents for reduction of the *tert*-alkyl azido group. Some representative trials are described below showing that no improvement was achieved in yield compared to LiAlH₄ reduction. The catalytic hydrogenation with Pd/C (10%)³² for 18 h was tested using different solvents (AcOEt, MeOH, MeOH/NH₃(g), MeOH/CHCl₃)³⁴ or different pressure conditions (50 psi or 1 Atm). For example, for the BuEtPrC-N₃ (**1c**) the higher yield achieved with catalytic hydrogenation was 57% for amine **1d** and Bu₃C-N₃ (**3c**) provided Bu₃C-NH₂ (**3d**) with 11% yield. The yields were poor when reduction of EtPrBuC-N₃ (**1c**) was attempted with FeCl₃/NaI³⁷ (10%) or Me₃SiCl/NaI³⁸ (4%) or by applying Staudinger reaction conditions and then hydrolysis of the phosphazene in THF/H₂O under reflux⁴⁰ (13%) or NaBH₄/CuSO₄·5H₂O³⁹ (23%). When Pr₃C-N₃ (**2c**) was used in combination with (EtO)₃P/benzene/TosOH/EtOH^{21d,40} or SnCl₂/PhSH/Et₃N⁴¹ the yields of the obtained amine **2d** were 35% and 33% respectively; when Bu₃C-N₃ (**3c**) was used as substrate the same reagents afforded Bu₃C-NH₂ (**3d**) with yields 18% and 8%.

The conclusion drawn from the trials described above, is that the weak spot of procedure A, which is responsible for the serious decrease of the overall yield, is the reduction step of the *tert*-alkyl azide to the corresponding primary *tert*-alkyl amine; especially when the alkyl chain length is increasing. We investigated other possibly more affordable procedures especially for the synthesis of crowded amines like **3d** (Bu₃) which was produced in low yield with procedure A.

4.3.3.2 From *tert*-alkyl alcohols using Ritter reaction (Procedure B)

The Ritter reaction²⁰ using standard^{20,42} (KCN, c. H₂SO₄, heat; Table 5, entries 1, 2) or slightly modified conditions (urea, c. H₂SO₄, heat; Table 5, entry 3)⁴³ was tested. The results showed that standard Ritter reaction conditions proved at best equally affordable compared to procedure A for the preparation of the BuEtPrC-NH₂ (**1d**), and significantly worst for the preparation of Bu₃C-NH₂ (**3d**).

Table 5. Standard Ritter reaction conditions for the formation of primary *tert*-alkyl amines from *tert*-alkyl alcohols (Procedure B).

Entry	Alcohol R ₁ ,R ₂ ,R ₃	step	Intermediate R ₁ ,R ₂ ,R ₃ ,R ₄	step	Amine product R ₁ ,R ₂ ,R ₃	Overall yield
		i		ii		
1	Bu,Et,Pr, 1b	c. H ₂ SO ₄ , AcOH, KCN / 70°C, 2h ^{20,42}	Bu,Et,Pr,H	NaOH 40%, HOCH ₂ CH ₂ OH / 180 °C, 24 h	Bu,Et,Pr, 1d	47%
2	Bu,Bu,Bu, 3b	c. H ₂ SO ₄ , AcOH, KCN / 70°C, 2h ^{20,42}	Bu,Bu,Bu,H	NaOH 40%, HOCH ₂ CH ₂ OH / 180 °C, 24 h	Bu,Bu,Bu, 3d	4%
3	Bu,Bu,Bu, 3b	Urea, H ₂ SO ₄ 86% / 70°C, 0.5h and overnight rt ⁴³	Bu,Bu,Bu,NH ₂	KOH 40%, HOCH ₂ CH ₂ OH / 180 °C, 24 h	Bu,Bu,Bu, 3d	5%

We then tested a modified Ritter reaction scheme, proposed as a general scheme for the synthesis of primary *tert*-alkyl amines (Procedure C).⁴⁴ This methodology includes the formation of *N-tert*-alkyl chloroacetamides after reaction of *tert*-alkyl alcohols with chloroacetonitrile (ClCH₂CN) and the smooth cleavage of the chloroacetyl group in the intermediate chloroacetamide with thiourea (Table 6).

Using this procedure, Pr₃C-NH₂ (**2d**) and Bu₃C-NH₂ (**3d**) were successfully obtained from the corresponding *tert*-alkyl alcohols **2b** and **3b** through intermediate chloroacetamides **8** and **9**; in the latter case the yield of the chloroacetyl group cleavage step was lower. Increasing alkyl group size reduced the efficiency of Ritter-like procedures for the synthesis of primary *tert*-alkyl amines, possibly due to a retro-Ritter reaction. Especially when standard reaction conditions were applied, the yield was reduced dramatically (Scheme 3).⁴⁵ After work-up of the reaction mixture in the second step, described in Tables 5 and 6, and isolation of amines **2d** or **3d** through extraction with diluted hydrochloric acid, the organic layer contained an unsaturated product, possibly formed through a retro-Ritter reaction. However, the modified Ritter reaction scheme (procedure C) includes as a second step a more efficient chloroacetyl group cleavage,

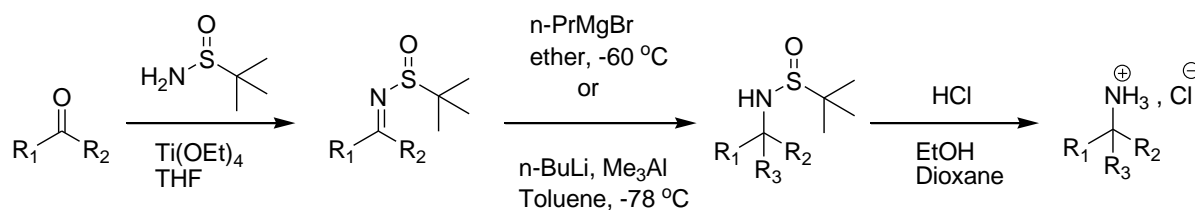
providing the primary *tert*-alkyl amine in yields 80% and 60% for Pr₃C and Bu₃C substrate respectively. The second step of procedure A i.e., the azide reduction had moderate to low yields (60% and 20%) for the same substrates. However, in the first step the *tert*-alkyl azides **2c**, **3c** are formed in higher yields compared to the *tert*-alkyl chloroacetamides **8** and **9**. Starting from the same commercially available ketone, both procedures include three steps, procedure C the sequence ketone → *tert*-alkyl alcohol → *tert*-alkyl chloroacetamide → *tert*-alkyl amine, and procedure A the sequence ketone → *tert*-alkyl alcohol → *tert*-alkyl azide → *tert*-alkyl amine. The overall three steps yields for amines **2d** (Pr₃C), **3d** (Bu₃C) were for procedure C 30%, 25% while for procedure A were 37% and 13% respectively.

Table 6. Modified Ritter reaction through chloroacetamides which are hydrolyzed with thiourea for the preparation of primary *tert*-alkyl amines (Procedure C).

Entry	Alcohol R ₁ ,R ₂ ,R ₃	Chloroacetamide R ₁ ,R ₂ ,R ₃	Isolated Yield	Amine R ₁ ,R ₂ ,R ₃	Isolated Yield
1	Pr,Pr,Pr, 2b	Pr,Pr,Pr, 8	48%	Pr,Pr,Pr, 2d	80%
2	Bu,Bu,Bu, 3b	Bu,Bu,Bu, 9	51%	Bu,Bu,Bu, 3d	61%

4.3.3.3 From the addition of organometallic reagents to *N*-*tert*-butylsulfinyl imines (Procedure D)

The procedure including the addition of organomagnesium or organolithium reagents to *N*-*tert*-butylsulfinyl imines⁴⁶ **10** and **12** was tested and proved to be successful for the synthesis of the *tert*-alkyl amines **2d** and **3d** (Procedure D, Scheme 5). However, it included more elaborate conditions and more expensive reagents like *tert*-butanesulfinamide compared to the previous procedures. For the preparation of Bu₃C-NH₂ (**3d**) the addition of BuLi/AlMe₃ to imine **13** was applied, which proved to be more efficient compared to BuMgBr or BuLi.⁴⁶ Procedure D afforded Pr₃C-NH₂ (**2d**) and Bu₃C-NH₂ (**3d**) with 28% and 19% yield starting from ketones **2a** and **3a** respectively. It is recalled that, using the same ketone as starting material, procedure A afforded **2d** and **3d** in 37% and 13% yield respectively, while procedure C in 30% and 25% respectively. Again, procedure C proved to be optimal for the test case of the crowded amine **3d**.

Table 7. Synthesis of primary *tert*-alkyl amines by the addition of organometallic reagents to *N*-*tert*-butylsulfinyl imines (Procedure D).

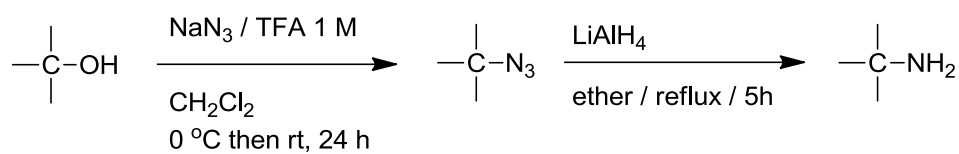
Entry	Ketone R ₁ ,R ₂	<i>N</i> - <i>t</i> Bu-sulfinylimine R ₁ ,R ₂	Isolated Yield	<i>t</i> Bu-sulfinamide ^a R ₁ ,R ₂ ,R ₃	Amine R ₁ ,R ₂ ,R ₃	Isolated ^b Yield
1	Pr,Pr, 2a	Pr,Pr, 10	70%	Pr,Pr,Pr, 11	Pr,Pr,Pr, 2d	40%
2	Bu,Bu, 3a	Bu,Bu, 12	77%	Bu,Bu,Bu, 13	Bu,Bu,Bu, 3d	25%

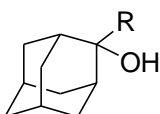
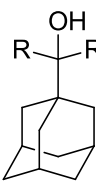
^ayield not determined; ^bfrom imine

The efficiency of procedures A, C, D depends from the reactant substrate. For example starting from 5-nonanone **3a** the synthesis of Bu₃C-NH₂ **3d** was accomplished in three steps with a yield of 13%, 25%, 19%, respectively. Starting from 4-heptanone **2a** the synthesis of Pr₃C-NH₂ **2d** was accomplished in three steps with a yield of 37%, 30%, 22% respectively. The gradual reduction in yield for procedure A from Pr₃C to Bu₃C is notable.

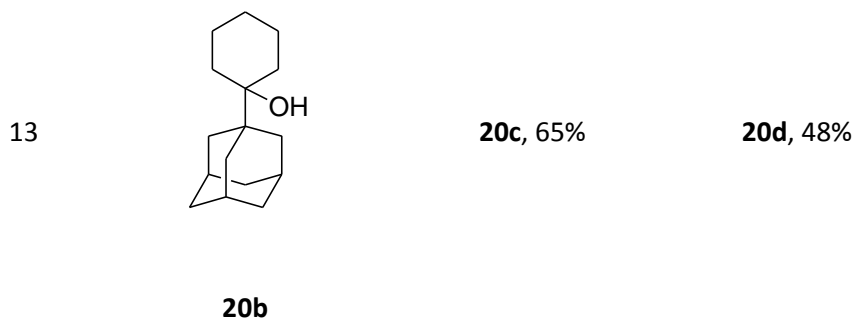
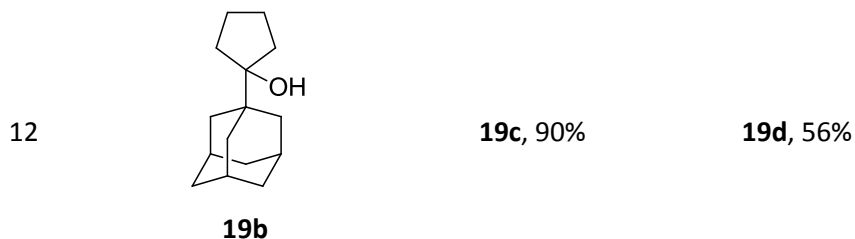
4.3.3.4 Examples for the preparation of primary *tert*-alkyl amines in adamantane series (Procedures A-D)

The synthesis of the antiviral bulky aminoadamantanes **8d-20d**^{3m,n,23} was considered through procedure A (Table 8, entries 1-13). Although the yields included in Table 8 are not optimized, the procedure seems general and efficient for all the substrates applied except entry 10 in which treatment of the diallyl azide with LiAlH₄ did not afford the diallylamine. While in all cases refluxing ether seems to be an optimal choice for LiAlH₄ reduction of *tert*-alkyl azides we noticed that these conditions did not work well in one of the last reactions tested before submission of this manuscript (Table 8, entry 7). I.e., it was observed that between Bn and pMeOBn substrates (Table 8, entries 6 and 7) while refluxing ether was enough to complete reduction for Bn substrate, for pMeOBn the reduction yield was only 18% and most of azide **14c** was isolated unreacted. Refluxing THF was applied for effective reduction of the azide **14c**.

Table 8. Conversion of some tertiary alcohols in adamantane series to *tert*-alkyl amines using procedureA.^{3m,n,23}

Entry	Alcohol	Azide, yield	Amine, yield
			
1	8b : R = Me	8c , 88%	8d , 77%
2	9b : R = Et	9c , 80%	9d , 71%
3	10b : R = <i>n</i> -Pr	10c , 66%	10d , 74%
4	11b : R = <i>n</i> -Bu	11c , 76%	11d , 23%
5	12b : R = Ph	12c , 95%	12d , 55%
6	13b : R = Bn	13c , 50%	13d , 45%
7	14b : R = <i>p</i> MeOBn	14c , 53%	14d , 18%, 48% ^a
			
8	15b : R = Me	15c , 80%	15d , 73%
9	16b : R = Et	16c , 77%	16d , 23%

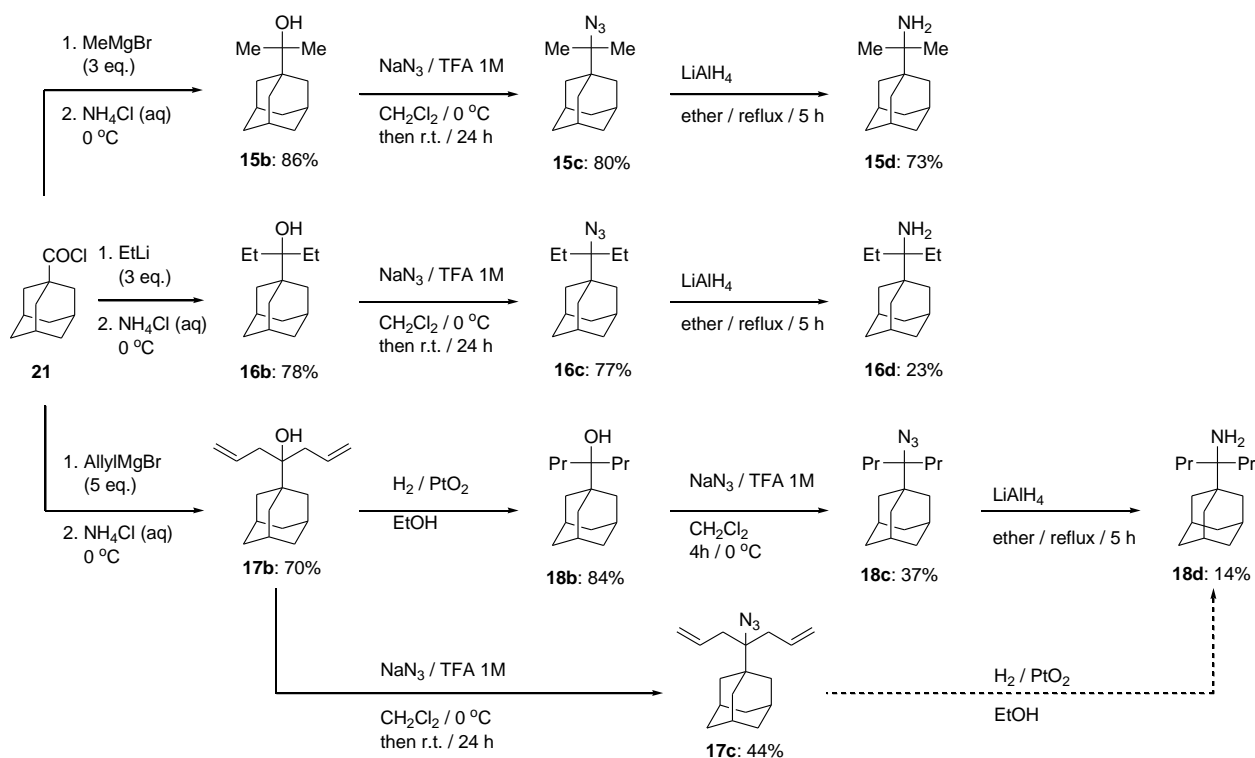
10	17b : R = allyl	17c , 44%	17d ^b
11	18b : R = <i>n</i> -Pr	18c , 37%	18d , 14%



^aTHF, reflux; ^bcomplex mixture

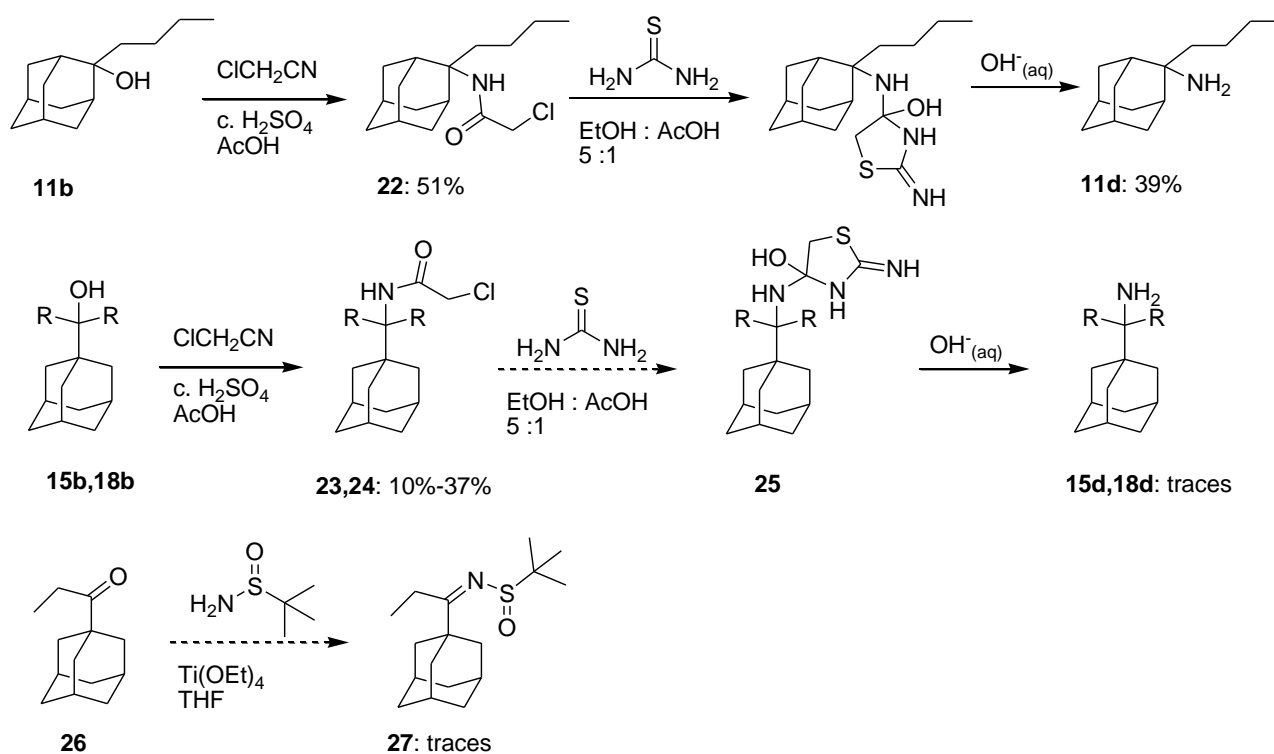
In scheme 2 the synthesis of aminoadamantanes **15d**, **16d**, **18d** is representatively showed ^{3m,n} from the starting *tert*-alkyl alcohols **15b**, **16b**, **18b**. Compound **15b** can be prepared conveniently from the reaction between 1-adamantane carbonyl chloride **16** or the corresponding ethyl ester and CH₃MgI. However, the reaction between **21** and CH₃CH₂MgBr afforded a mixture of the *tert*-alkyl alcohol Ad(Et)₂C-OH **16d** and the *sec*-alkyl alcohol AdEtCH-OH. This alcohol was formed via a β-hydride addition from the organometallic reagent to the carbonyl group, instead of an alkyl addition, due to the crowded electrophilic carbonyl in **16**. Thus, **16d** was prepared in high yield from the reaction between 1-adamantane carbonyl chloride **21** and EtLi. Application of procedure A afforded AdMe₂C-NH₂ **15d** in high overall yield, including a high yield both for formation of the azide **15c** (80%) and for the azide reduction through LiAlH₄ (73%). The same procedure when applied for the synthesis of amine **16d** afforded azide **16c** with 77% yield, but the yield for the reduction step was 23%, due to the formation of unsaturated products and extensive decomposition. Compounds **15d**, **16d**, **18d** yields were improved compared to previous results.³ⁿ The reaction of allylmagnesium bromide with **21** afforded diallyl alcohol **17b** which was subsequently

hydrogenated under PtO₂ as the catalyst to afford alcohol **18b**. A trial to afford cyclopentenol precursor of cyclopentanol **19b** through cyclization of diallyl alcohol using first generation Grubbs catalyst was unsuccessful as noted in ref. 47. Diallyl azide **17c** was prepared with 44% from diallyl alcohol **17b** but the catalytic hydrogenation led to a complex mixture of products; reduction through LiAlH₄ of diallyl azide **17c** did not afford diallylamine but led to decomposition.



Scheme 2. Synthetic scheme applied for the conversion of **15b**, **16b** and **18b** to the corresponding *tert*-alkyl amines **15d**, **16d** and **18d** (procedure A).

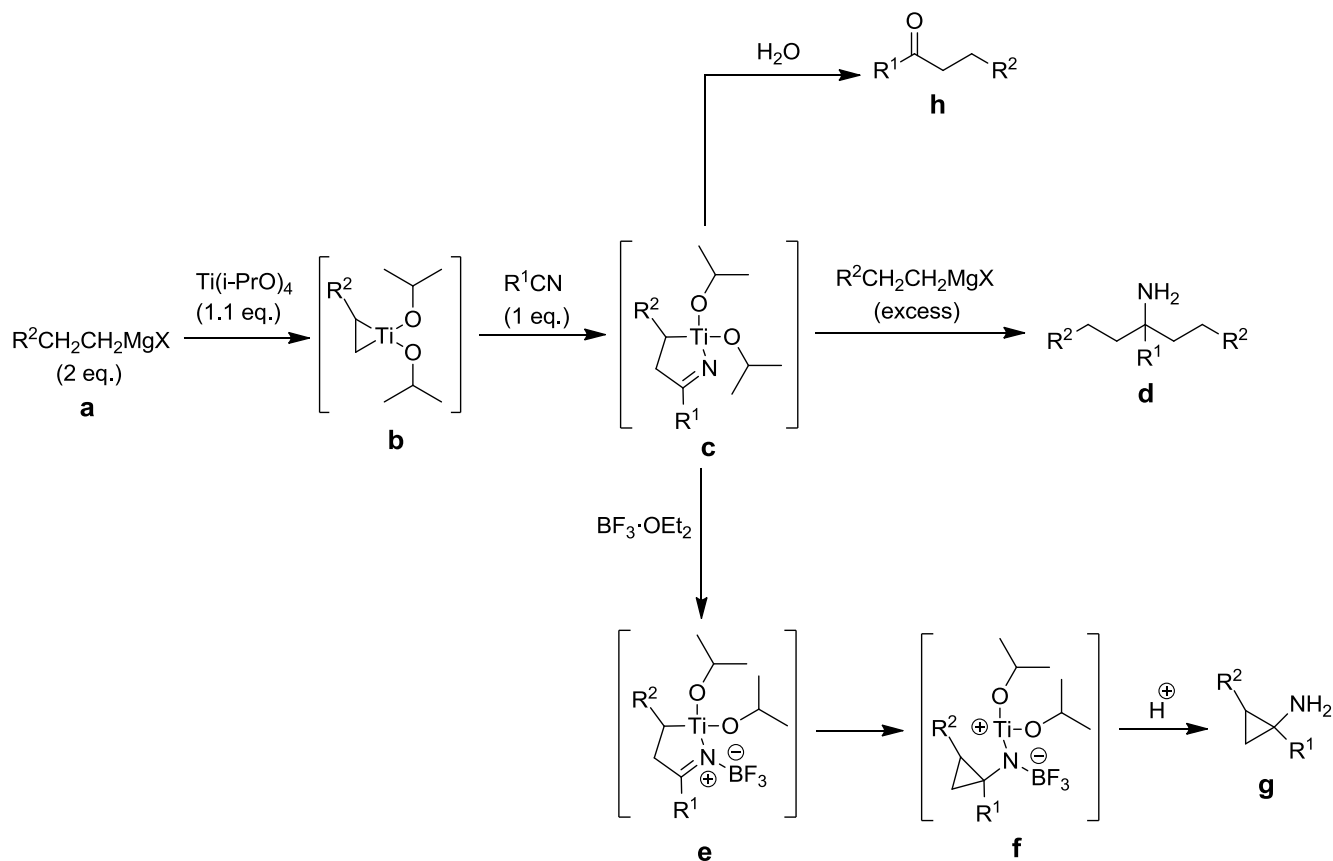
Procedure C, while provided amine **11d** through chloroacetamide **22** successfully, was not productive when applied for the synthesis of **15d** or **18d**. The relevant trials afforded chloroacetamides **23**, **24** with low to moderate yield, due to the formation of an alkene by-product, and the cleavage of the chloroacetyl group with thiourea gave the *tert*-alkyl amines **15d**, **18d** respectively only in traces (Scheme 3). Procedure D was also not productive since the reaction of 1-adamantyl ethyl ketone **26** with *tert*-butanesulfinamide did not afford the corresponding *N-tert*-butylsulfinyl imine **27**. The formation of intermediates **25** or **27** is suffering from steric hindrance (Scheme 3) as suggested by the molecular mechanics calculation (the structures of the derivatives were generated and minimized in Maestro⁴⁸ using the MMFF94 force field⁴⁹ implemented with Macromodel 9.6⁴⁸).



Scheme 3. Results from the application of procedures C and D for the synthesis of amines **10d**, **15d** and **18d**.

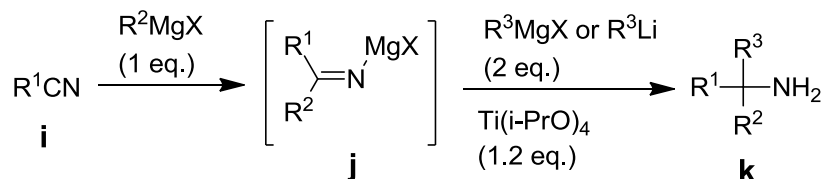
4.3.3.5 From the addition of organometallic reagents to nitriles (Procedure E)

The one flask synthesis of primary *tert*-alkyl amines by the addition of organometallic reagents to nitriles in the presence of Lewis acid catalysts was investigated^{50-56,58} after a recent report which applied $\text{Ti}(\text{O}i\text{-Pr})_4$ in combination with ethylmagnesium bromide to afford **16d** in 52% yield.⁵⁷ As will be discussed below this result was not reproduced in our hands. In the original Kulinkovich-Szymoniak protocol for the synthesis of cyclopropanamines (Scheme 4),^{50,52} $\text{Ti}(\text{O}i\text{-Pr})_4$ is already present in ethereal solution of two equivalents of the Grignard reagent, before nitrile is added. These reaction conditions allow first the formation of the suggested three-membered titanocene ring **b**, formed by the reaction of the Grignard reagent with $\text{Ti}(\text{O}i\text{-Pr})_4$, which reacts then with nitrile to form a five-membered titanocene complex **c** including an electrophilic imine bond. The fate of this latter reactive intermediate is depending upon treatment of the reaction mixture with the next reagent. A cyclopropanamine **g** can be formed by the addition of $\text{BF}_3 \cdot \text{Et}_2\text{O}$ through a rearrangement transformation (**e**→**f**→**g**) or a primary *tert*-alkyl amine **d** upon addition of an organometallic reagent to the imino bond.⁵⁰ In order this reaction scheme to proceed the starting Grignard reagent should have a β -hydrogen to allow the formation of the three-membered titanocene (Scheme 4).



Scheme 4. Kulinkovich-Szymoniak reaction protocol.

In the Kulinkovich-de Meijere reaction conditions^{19,53} for the synthesis of primary *tert*-alkyl amines the reaction scheme has been simplified (Scheme 5). The Grignard reagent reacts first with the nitrile **i** to form an imino derivative **j** and then $\text{Ti}(\text{O}i\text{-Pr})_4$ is added to activate the imino functionality for the addition of a second equivalent of an organometallic reagent. The equivalent of the organometallic reagent needed for nucleophilic addition to the imino bond can be provided from an initial excess of the Grignard reagent in the reaction flask or can be added separately. In the latter case the organometallic reagent can be a Grignard or an organolithium reagent including the same or different alkyl group as regards the first step. These reaction conditions were considered to be optimized for the synthesis of primary *tert*-alkyl amines **k**. Both procedures can combine the introduction of different alkyl groups using Grignard or the combination of Grignard and organolithium reagents.^{19,53}



Scheme 5. Kulinkovich-de Meijere reaction protocol.

The synthesis of few *tert*-alkyl amines was firstly tested through a procedure which included the addition of an excess of organometallic reagent (3-4 equivalents) to nitriles mediated by $\text{Ti}(\text{OiPr})_4$ in one flask according to the Kulinkovich-de Meijere reaction conditions (Table 9, procedure E).¹⁹ Starting from commercially available butanenitrile **14** and pentanenitrile **15** the preparation of $\text{PrBu}_2\text{C-NH}_2$ (**6d**) and $\text{Bu}_3\text{C-NH}_2$ (**3d**) was accomplished in 25% and 20% yield respectively (Table 9, entries 1, 2) but the reaction took place in one flask with non-expensive reagents. Thus, regarding the preparation of the amine **3d**, this procedure has a higher yield (20%) compared to procedure A (three steps from ketone, yield 13%), but has slightly lower or similar yields compared to procedure C (three steps from ketone, yield 25%) and procedure D (three steps from ketone, yield 19%).

There was no particular limitation to the structure of the Grignard reagent but this reaction was originally tested for nitriles up to secondary or benzonitrile in the relevant papers.^{19,53} We then applied the Kulinkovich-de Meijere reaction to pivalonitrile (**28**). Treatment of nitrile **28** with propylmagnesium bromide (3 eq)/ $\text{Ti}(\text{Oi-Pr})_4$ afforded the $t\text{-BuPr}_2\text{C-NH}_2$ (**29**) in 20% yield (Table 9, entry 3). Following common workup of the reaction mixture, the yield was determined for the reactions depicted in Table 9 after fumarate salt formation and recrystallization of the amine product.

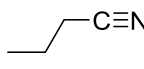
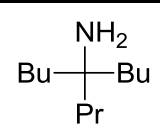
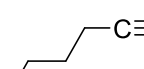
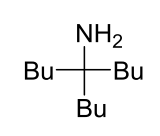
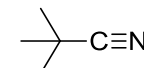
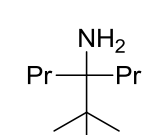
4.3.3.6 Examples for the preparation of primary *tert*-alkyl amines in adamantane series (Procedure E)

The Kulinkovich-de Meijere protocol was applied using 1-adamantanecarbonitrile (**30**) and the simple Grignard reagents RMgBr ($\text{R}=\text{Me}, \text{Et}$) for the synthesis of primary *tert*-alkyl adamantanamines having the structure AdCR_2NH_2 ($\text{R}=\text{Me}, \text{Et}$ groups) by the addition of organometallic reagents to 1-adamantanecarbonitrile (**30**) using $\text{Ti}(\text{O-}i\text{Pr})$ (Table 9, entries 4-10). As mentioned above the reaction of **30** with ethylmagnesium bromide/ $\text{Ti}(\text{OiPr})_4$ using a Kulinkovich-Szymoniak protocol was reported to produce **16d** in 52% yield.⁵⁷ The addition of ethylmagnesium bromide to 1-adamantanecarbonitrile (**30**) using $\text{Ti}(\text{O-}i\text{Pr})$ and Kulinkovich-de Meijere protocol afforded a mixture of AdEtCH-NH_2 (**32**) in 3% yield and $\text{AdEt}_2\text{C-NH}_2$ **16d** in a 4% yield (ratio 60:40 according to ^{13}C NMR spectrum) (Table 9, entry 5). We thought that a β -hydride addition from the second equivalent of the organometallic reagent to an imino group may explain the formation of the *sec*-alkyl amine **32** with the desired *tert*-alkyl amine **16d**. However, it was striking that

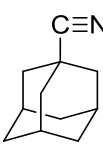
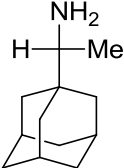
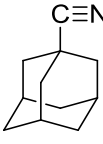
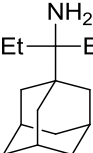
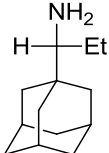
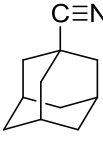
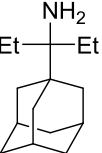
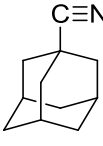
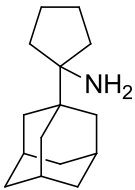
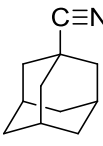
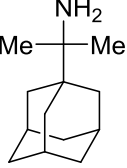
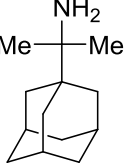
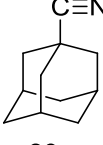
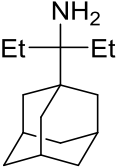
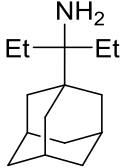
the application of MeMgBr afforded the secondary amine, that is, the rimantadine AdMeCH-NH₂ (**31**) in 15% yield (measured after fumarate salt formation) (Table 9, entry 4); unreacted AdMeC=NH imine was identified in the filtrate after filtration of the solid fumarate salt of amine **31**. The reaction of adamantanacarbonitrile **30** with 1,4-bis(bromomagnesiobutane) afforded cyclopentanamine²³ **19d** in 10% yield (Table 9, entry 7). The overall yield using procedure A for the transformation of alcohol to amine **19d** starting from the commercially available 1-adamantanacarboxylic acid using treatment of 1-adamantanacarboxylic ethylester with 1,4-bis(bromomagnesiobutane)²³ was ~ 32%.

Table 9. One flask synthesis of primary *tert*-alkyl amines by the addition of organometallic reagents to nitriles mediated by Ti(OiPr)₄ (Procedure E).

$$\text{RCN} \xrightarrow{\text{organometallic reagent, Ti(OiPr)}_4} \text{product}$$

Entry	nitrile	reagents, conditions	Product: yield, protocol	
			Kulinkovich-De Meijere	Kulinkovich- Szymoniak
1	 14	nBuMgBr (3 eq) Ti(OiPr) ₄ ether / 24h / reflux	 6d : 25%	N/A
2	 15	nBuMgBr (3 eq) Ti(OiPr) ₄ ether / 24h / reflux	 3d : 20%	N/A
3	 28	nPrMgBr (3 eq) Ti(OiPr) ₄ ether / 24h / reflux	 29 : 20%	N/A

Tert-alkyl amines analogues of amantadine

4	 30	MeMgBr (3 eq) Ti(OiPr) ₄ ether / 24h / reflux	 31: 15%	N/A	
5	 30	EtMgBr (3 eq) Ti(OiPr) ₄ ether / 24h / reflux	 16d: 4%	+  32: 3%	N/A
6	 30	EtLi (3 eq) Ti(OiPr) ₄ ether / 24h / reflux	 16d: 2%		N/A
7	 30	BrMg(CH ₂) ₄ MgBr (2 eq) Ti(OiPr) ₄ ether / 24h / reflux	 19d: 10%		N/A
8	 30	1. MeMgBr (1 eq), Ti(OiPr) ₄ ether / 1h / rt 2. MeLi (2 eq) ether / 24h / reflux	 15d: 10%	 15d: 11%	
9	 30	1. EtMgBr (1 eq), Ti(OiPr) ₄ ether / 1h / rt 2. EtLi (2 eq) ether / 24h / reflux	 16d: 10%	 16d: 10%	

10	<p>30</p>	<p>1. MeMgBr (2 eq), Ti(OiPr)₄ ether / 1h / rt 2. MeMgBr (1 eq), ether / 1h / rt</p>	N/A	<p>15d: 10%</p>
11	<p>30</p>	<p>1. MeMgBr (1 eq), Ti(OiPr)₄ ether / 1h / rt 2. MeMgBr (2 eq), ether / 1h / rt</p>	<p>15d: 8 %</p>	

The application of an organolithium reagent as the organometallic reagent of the second step was also tested using the Kulinkovich-de Meijere protocol (Scheme 5). The Grignard reagent was added to the nitrile (Scheme 5, from **i** to **j**) followed by Ti(O-*i*Pr)₄ and then an organolithium reagent was added (see Scheme 5, from **j** to **k**). As mentioned before, this scheme was used as an equivalent set of reaction conditions.^{19,53} The desired *tert*-alkyl amine **16d** was obtained in 10% yield (Table 9, entry 9). In the fumarate salt, a small amount of the secondary amine **32** was again detected (10% contamination). When Kulinkovich-Szymoniak⁵⁰ reaction conditions were used i.e., when nitrile and Ti(O-*i*Pr)₄ were placed in the reaction flask following by treatment with EtMgBr and then EtLi or with two equivalents of EtMgBr, according to ref. 52, pure amine **16d** was isolated as crystalline fumarate, in 10% yield (Table 9, entry 9). Application of the Kulinkovich-de Meijere protocol or the Kulinkovich-Szymoniak protocol for the treatment of 1-adamantanecarbonitrile **30** with Ti(O-*i*Pr)₄, MeMgBr and MeLi afforded *tert*-alkyl amine **15d** in 10 or 11% yield respectively (Table 9, entry 8). Application of the Kulinkovich-de Meijere protocol for the treatment of 1-adamantanecarbonitrile **30** with Ti(O-*i*Pr)₄, MeMgBr and MeMgBr afforded *tert*-alkyl amine **15d** in 8% yield (Table 9, entry 11). Application of Kulinkovich-Szymoniak reaction conditions for the treatment of 1-adamantanecarbonitrile **30** with Ti(O-*i*Pr)₄ and 2 equivalents MeMgBr amines **15d** in 10% yield respectively (Table 9, entry 10). The reaction of **30** with three equivalents of EtLi afforded **16d** in 2% yield (Table 9, entry 6); organolithium

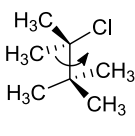
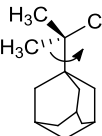
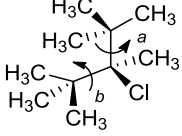
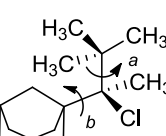
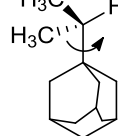
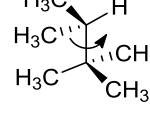
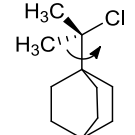
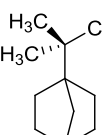
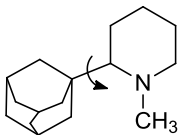
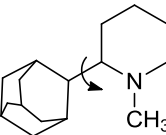
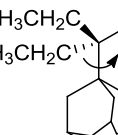
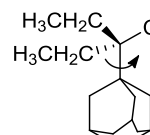
reagent may be consumed by the reaction with $\text{Ti}(\text{O}-i\text{Pr})_4$.⁵⁹ Trials using allylmagnesium bromide afforded a complex mixture of products either using Kulinkovich-de Meijere or Kulinkovich-Szymoniak.

4.3.2 Dynamic NMR spectroscopy

From previous studies using DNMR⁶⁰ it has been shown that single bond rotational barriers were found lower than expected when bulky but rigid groups, like 1-adamantyl, were attached to one end of an ethane bond compared to smaller but flexible *tert*-butyl group (see Table 10). For example, the 1-adamantyl rotation barrier for **35** was about 1 kcal mol^{-1} lower than the barrier of the corresponding *tert*-butyl analogue **34**.⁶¹ This results because of the more negative entropy of activation for the *tert*-butyl compound **34**. The effect is due to the flexibility in attaining a stable rotational ground state in *tert*-butyl compound **34**. In contrast in 1-adamantyl analogue **35** similar constraints are present in both the ground state and transition state (see also Table 10, rotation barriers b in **36** and **37**). On the other hand, when the same groups are acting only as substituents on an ethane bond rather than forming one end of it, the bulkier adamantyl group in **37** hinders rotation more than the smaller *tert*-butyl group in **36** (see Table 10, rotation barriers a in **36** and **37**). It was presented above that pivalonitrile **28** reacted more efficiently with Grignard reagents in presence of $\text{Ti}(\text{iPrO})_4$ compared to 1-adamantanecarbonitrile **30** since reaction transition states are more hindered for 1-adamantyl substitution compared to *tert*-butyl (Table 9). We studied also 2-(1-adamantyl)-1-methylpiperidine **42** and 2-(2-adamantyl)-1-methylpiperidine **43** and show that the rotational barrier is much higher in the latter case due to rotational flexibility of 1-adamantyl compared to 2-adamantyl group in the transition state.^{3e} The relative size of each substituent group as regards its effect in rotational barrier investigated depends on the context and the substitution pattern.

The rotation of the *tert*-butyl group has been studied,⁶¹⁻⁶⁴ and recently also the rotation of the adamantyl group or other cage like compounds has received attention.^{65-67,3e} The compounds depicted in Table 10 and other compounds^{3e,61-64} have been studied so far. We were intrigued to further investigate the behavior of the 1-adamantyl group in rotation barriers via DNMR, following up our previous studies in the field (see for example ref. 3d,e). We investigated the tertiary alcohol AdCET_2OH **16b** and its chloride AdCET_2Cl **44** prepared from reaction of **16b** with $\text{HCl}(\text{g})$ in anhydrous CH_2Cl_2 (-50°C , 15 min).⁶⁵ We studied compounds **16b** and **44** since it is interesting to compare the energy barrier by rotation around Ad-C bond with compounds **35**, **37** (rotation barrier b, see Table 10) previously studied.⁶¹

Table 10. Energy barriers (kcal mol⁻¹) for rotation around specified C-C bond as determined from previous DNMR spectroscopy studies for compounds **34-43**^{61,3e} and for compounds **16b** and **44** in the present study.

Compound						
	34	35	36	37	38	39
ΔG^\ddagger	10.4	9.3	11.4, ^a 11.4 ^b	12.2, ^a 10.6 ^b	6.1	6.9
Compound						
	40	41	42	43	16b	44
ΔG^\ddagger	9.8	8.2	7.6	n.d. ^c	8.7	10.0

^a bond rotation a; ^b bond rotation b; ^c n.d., not determined since was too high to be detectable.

By lowering the temperature of an NMR sample of alcohol **16b** in CDCl₂, the dynamic behavior was identified by following the lineshape of the signals of carbons 2', 8', 9'-C and 4', 6', 10'-C. At 181 K (-92 °C) a broadening of these signals was observed and the splitting of each signals to two peaks with a ratio of 2:1 was observed at 166 K (-107 °C).^{3e} One adamantyl carbon of the set of carbons 2', 8', 9'-C (designated as α in the upper part of Figure 3) has a gauche orientation relative to two ethyl group carbons while the other two adamantyl carbons of the set of carbons 2', 8', 9'-C (designated as β in the upper part of Figure 3) have one ethyl group carbon to a gauche position and the hydroxyl group also to a gauche position, thus explaining the observed 2:1 ratio. The signals of carbons 4', 6', 10'-C were also affected but the dynamic effect was smaller since these carbons are more distant from the hindered bond rotation. Decalescence occurs at 178 K (-95 °C) for carbons 2', 8', 9'-C signal and at 173 K (-100 °C) for carbons 4', 6', 10'-C signal (Figure 3). The peaks separation for carbons 2', 8', 9'-C was 1.7 ppm and 0.3 ppm for carbons 4', 6', 10'-C. From lineshape analysis the free energy for bond rotation was calculated to be $\Delta G^\ddagger = 8.7 \pm 0.2$ kcal mol⁻¹.⁶⁸

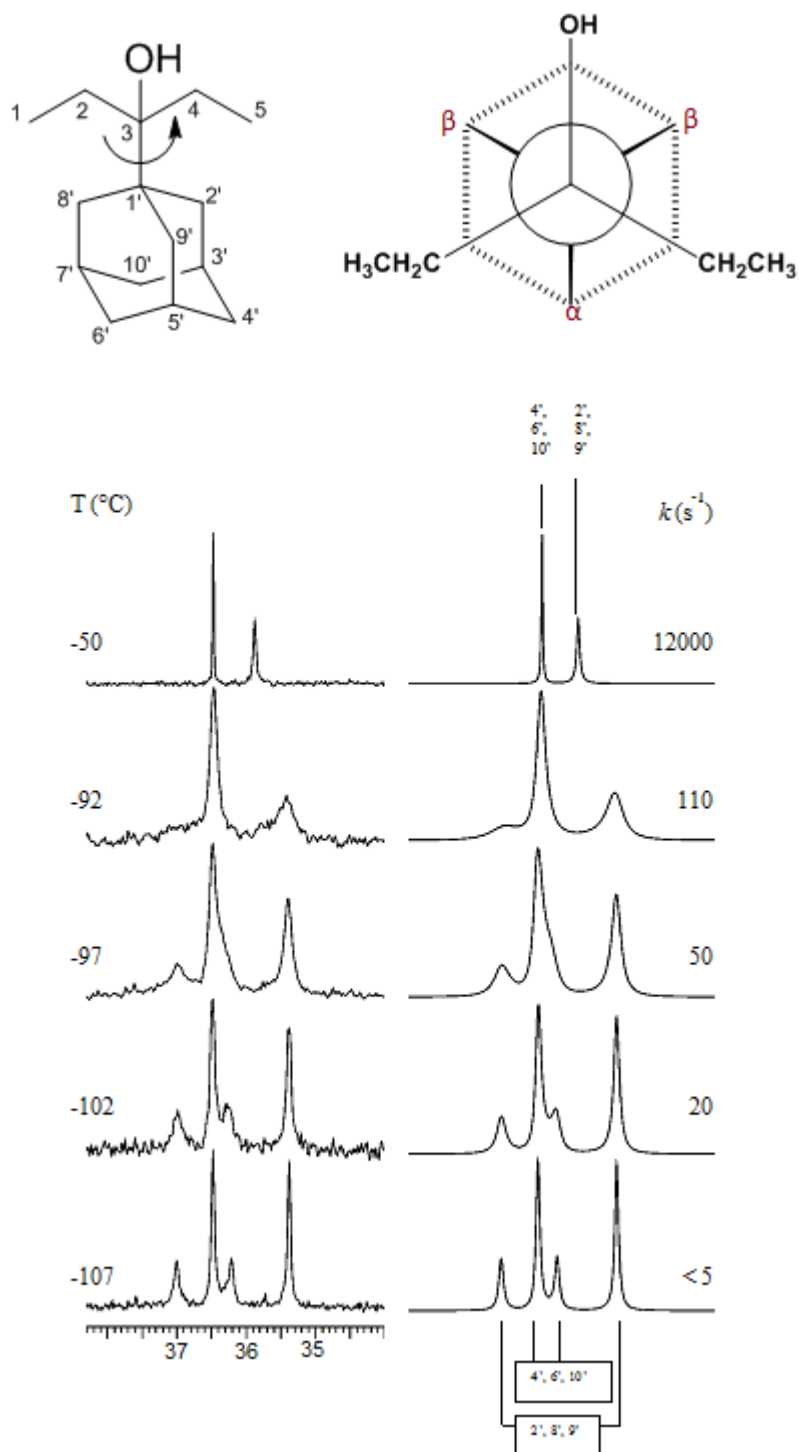


Figure 3. VT spectra for compound **16b** (^1H NMR 600 MHz in CDCl_2). On the left is shown the evolution of the CH_2 signals on lowering the temperature. On the right are reported the line-shape simulations with the corresponding rate constants. The bond rotation studied is shown in the upper scheme of the figure.

In the case of the chloride **44** the lineshape analysis is hampered by the presence of some alkene due to the elimination in the presence of HCl. However, the coalescence temperature of the signals is reached at

higher temperature, between -50 and -60 °C, with a separation of 185 Hz between signals at -130 °C (Figure 3).

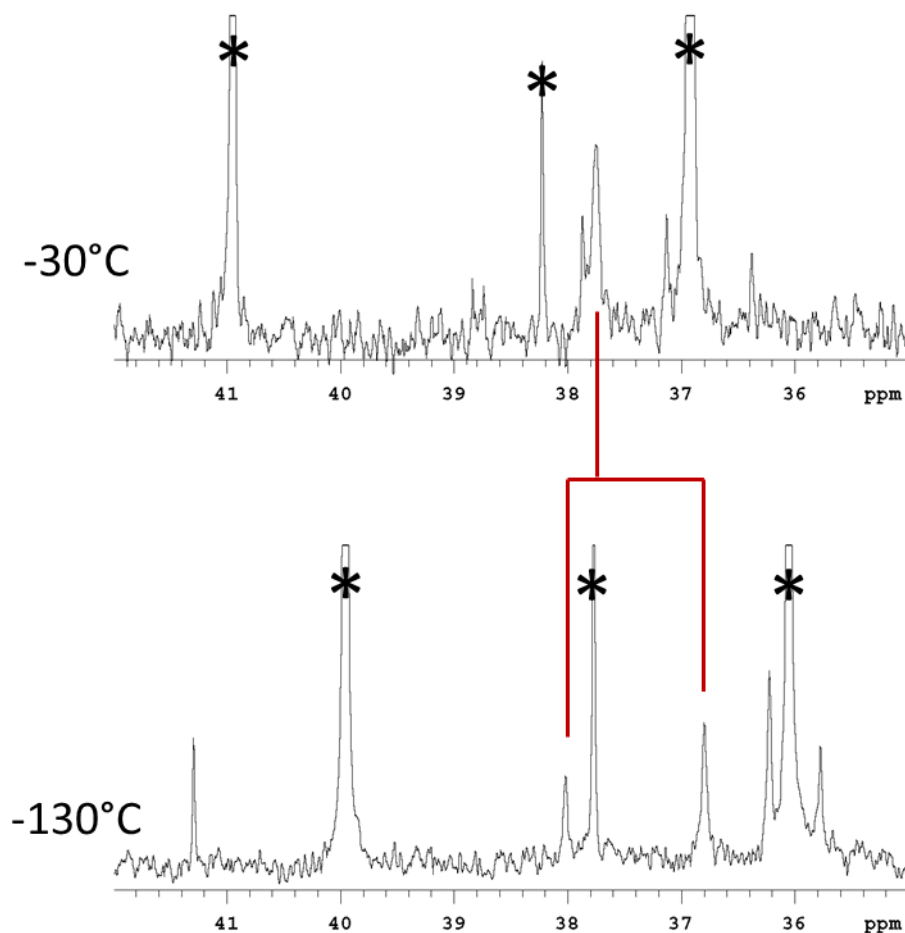


Figure 3. Low temperature ^{13}C -NMR spectra of compound **44** in CDCl_2 . The asterisks indicate the signals of the alkene due to elimination of chloride **44**.

According to the dynamic NMR theory for a biased equilibrium,^{69,70} at the temperature of maximum broadening the major form converts to the minor with a rate constant approximated using equation (1):

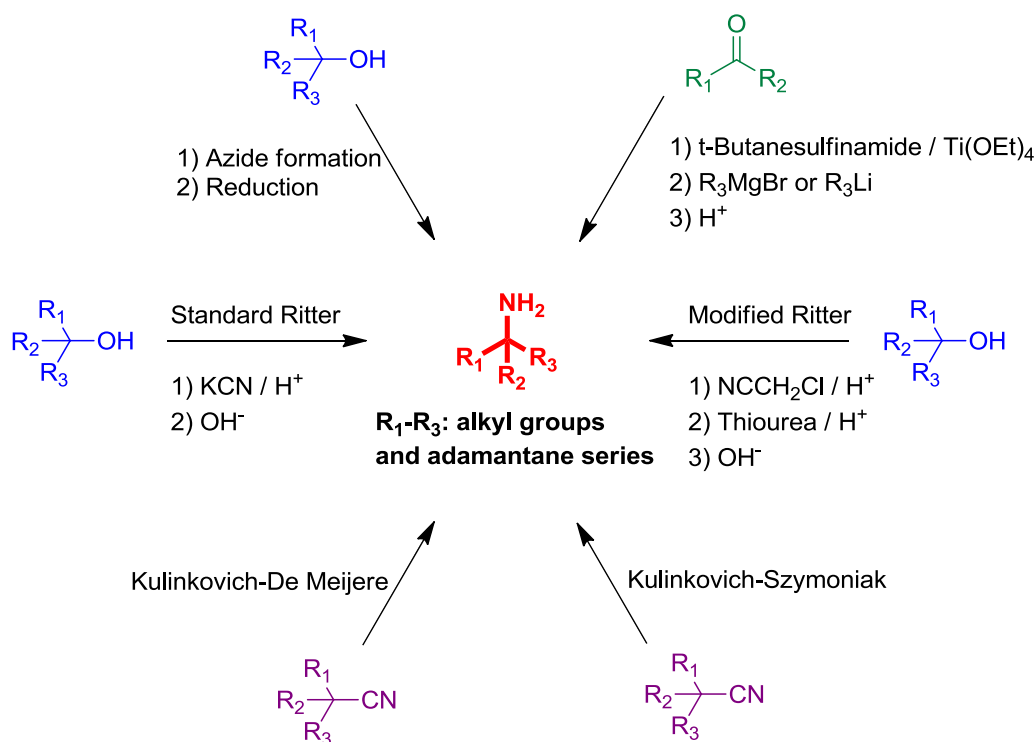
$$k_c = 2\pi \cdot \rho \cdot \delta\nu \quad (1)$$

where p = population of the minor signal and $\delta\nu$ = carbons signals separation at frozen rotation temperature. For the set of carbons 4', 6', 10'-C, $p = 0.33$ and $\delta\nu = 185$ Hz resulting to $k_c = 383$ s⁻¹ and $\Delta G^\ddagger = 10.0 \pm 0.4$ kcal mol⁻¹.

The bond rotation barriers of alcohol **16b** and chloride **44** showed that replacement of hydroxyl group with a bulkier chlorine raises the energetic requirements for bond rotation. Similarly comparison of the bond rotation barrier between chlorides **35** and **40** (see Table 10) clearly show that by increasing the size of the alkyl groups the bond rotation barrier is raised.

4.4 Conclusion

Five procedures were tested for the synthesis of *tert*-alkyl amines included aliphatic alkyl chains or alkyl chains and an adamantyl group. These compounds represent analogues of amantadine or other cage-like amines and may provide useful building blocks for drug molecules targeting various biological targets.¹⁻³



Scheme 6. Procedure tested of the preparation of primary *tert*-alkyl amines.

The first procedure included the formation and reduction of *tert*-alkyl azides (procedure A), where yield depends from the selection of solvent for azide formation and the reagent and conditions for azide reduction. Dichloromethane or 1,2-dichloroethane and LiAlH₄ were found to be optimal choices between those tested. Procedure B and procedure C correspond to the the standard and the modified Ritter reaction. The modified scheme which proceeds through a *tert*-alkyl chloroacetamide. Procedure D included the addition of organometallic reagents to *N-tert*-butyl sulfinyl ketimines. Procedure E applied the one flask reaction of nitriles with organometallic reagent in the presence of Ti(iPrO)₄. For bulky amines including adamantane adducts like **11d**, **15d-20d** procedures C and D were not affordable and the reduced reactivity of the relevant substrate was due to the bulky adamantane moiety. This suggests that procedure A is valuable for a broader range of substrates. The applicability of Ti(iPrO)₄ mediated reactions between nitriles

and Grignard/organolithium reagents was further investigated using few additional nitriles and 1-adamantanecarbonitrile. The results from previous and ongoing antiviral testing showed that few *tert*-alkyl amines bearing an hydrocarbon framework of branched alkyl chains or alkyl chains and adamantane may provide useful analogues of amantadine or aminoadamantane derivatives for antiviral projects. To study also how adamantane ring effected conformational restrictions, and as a continuation also to previous efforts for the investigation of the rotation around 1-adamantyl group,^{3e,61-65} DNMR experiments in Ad-C(Et₂)OH **16d** and its Ad-C(Et₂)Cl **44** were performed. The NMR signals resulted in decoalescence for carbons 2', 8', 9'-C and 4', 6', 10'-C signals at temperatures as low as -100 °C and the free energy for bond rotation was $\Delta G^\ddagger = 8.7 \pm 0.2$ kcal mol⁻¹ for Ad-C(Et₂)OH and 10.0 ± 0.4 kcal mol⁻¹ for Ad-C(Et₂)Cl, compared to 9.3 kcal mol⁻¹ for Ad-C(Me₂)Cl **35** or 10.6 kcal mol⁻¹ for Ad-CMe(t-Bu)Cl **37**.

4.5 Experimental Section

4.5.1 Chemistry

IR spectra were recorded on a Perkin-Elmer 833 spectrometer. ^1H and ^{13}C NMR spectra were recorded on a Bruker DRX 400 and AC 200 spectrometer at 400 and 50 MHz, respectively, using CDCl_3 as solvent and TMS as internal standard. Carbon multiplicities were established by DEPT experiments. The 2D NMR techniques (HMQC and COSY) were used for the elucidation of the structures of intermediates and final products. Microanalyses were carried out by the Microanalyses lab of the National Center for Scientific Research, Demokritos, Athens, and the results obtained had a maximum deviation of $\pm 0.4\%$ from the theoretical value. Preparation of compounds **15d-18d** in Scheme 2^{3m,n} was described in chapter 3. Preparation of compounds **8d-110d** in Table 8^{3h} was described in chapter 3. Preparation of compounds **19d, 20d** in Table 8³ⁱ was described in chapter 2.

4.5.1.1 Procedure A

4-Ethyl-octan-4-amine (BuEtPr-CNH₂) 1d. 4-Ethyl-octan-4-ol **1b** was obtained after treating a solution of 3-heptanone **1a** (1g, 8.77 mmol) in dry ether (30% solution w/v) with 1.2-molar excess of $\text{CH}_3\text{CH}_2\text{CH}_2\text{MgBr}$ (obtained from an 20% solution w/v solution of 1-bromopropane (2.1 g, 17.54 mmol) in dry ether and 1.3 equivalents of Mg (548 mg, 22.8 mmol)) under argon atmosphere and stirring the mixture overnight. After treating the mixture with saturated ammonium chloride following usual workup the corresponding tertiary alcohol **1b** was obtained. Yield 1.1 g, (80%); IR (Nujol) $\nu(\text{N}_3)$ 3392 cm^{-1} ; ^1H NMR (CDCl_3 , 400 MHz): δ (ppm) 0.85 (t, $J \sim 7$ Hz, 3H, $(\text{CH}_2)_3\text{CH}_3$), 0.91 (t, $J \sim 7$ Hz, 6H, $(\text{CH}_2)_2\text{CH}_3$, CH_2CH_3), 1.22-1.48 (m, 13H, $(\text{CH}_2)_3\text{CH}_3$, $(\text{CH}_2)_2\text{CH}_3$, CH_2CH_3 , OH); ^{13}C NMR (CDCl_3 , 50 MHz) δ (ppm) 7.9 ($(\text{CH}_2)_3\text{CH}_3$), 14.3 ($(\text{CH}_2)_2\text{CH}_3$), 14.9 (CH_2CH_3), 16.9 ($(\text{CH}_2)_2\text{CH}_2\text{CH}_3$), 23.5 ($\text{CH}_2\text{CH}_2\text{CH}_3$), 25.8 ($\text{CH}_2\text{CH}_2\text{CH}_2\text{CH}_3$), 31.7 (CH_2CH_3), 38.6 ($\text{CH}_2(\text{CH}_2)_2\text{CH}_3$), 41.4 ($\text{CH}_2\text{CH}_2\text{CH}_3$), 74.3 (COH).

To a stirred mixture of sodium azide (488 mg, 7.50 mmol) and dry dichloromethane (15 mL), trifluoroacetic acid (2 mL, 25 mmol) was added at 0 °C. The resulting mixture was stirred for 10 min at 0 °C and a solution of the 4-ethyl-4-octanol **1b** (400 mg, 2.50 mmol) in 10 mL of dichloromethane was added dropwise. The mixture was stirred at 0-5 °C for 4 h and 24 h at ambient temperature. The mixture was made alkaline by adding NH_3 12 % (40 mL) and the organic phase was separated. The aqueous phase was extracted with dichloromethane and the combined organic phases were washed with water, brine and dried (Na_2SO_4). Solvent was evaporated in vacuo to afford 4-azido-4-ethyl-octane, **1c**. Yield 398 mg, (87%); IR (Nujol) $\nu(\text{N}_3)$ 2093 cm^{-1} ; ^{13}C NMR (CDCl_3 , 50 MHz) δ (ppm) 8.1 ($(\text{CH}_2)_3\text{CH}_3$), 14.2 ($(\text{CH}_2)_2\text{CH}_3$), 14.6 (CH_2CH_3),

17.0((CH₂)₂CH₂CH₃), 23.2 (CH₂CH₂CH₃), 25.8 (CH₂CH₂CH₂CH₃), 29.3 (CH₂CH₃), 35.8 (CH₂(CH₂)₂CH₃), 38.5 (CH₂CH₂CH₃), 67.3 (CN₃).

To a stirred suspension of LiAlH₄ (223 mg, 5.87 mmol) in dry ether (20 mL) was added dropwise at 0 °C a solution of the alkyl azide **1c** (269 mg, 1.47 mmol) in dry ether (15 mL). The mixture was refluxed for 5 h and then was treated with water, NaOH 10 % and water. The insoluble inorganic material was filtered-off, washed with ether and the filtrate was extracted with HCl 6%. The aqueous phase was made alkaline with solid sodium carbonate and was extracted with dichloromethane or ether. The organic phase was washed with brine, dried (Na₂SO₄) and evaporated in vacuo to afford the amine **1d**. Yield 150 mg, (65%); ¹H NMR (CDCl₃, 400 MHz): δ (ppm) 0.81 (t, *J* ~ 7 Hz, 3H, ((CH₂)₃CH₃), 0.89 (t, *J* ~ 7 Hz, 6H, (CH₂)₂CH₃, CH₂CH₃), 1.21-1.39 (m, 14H, (CH₂)₃CH₃, (CH₂)₂CH₃, CH₂CH₃, NH₂); ¹³C NMR (CDCl₃, 50 MHz) δ (ppm) 7.9 ((CH₂)₃CH₃), 14.3((CH₂)₂CH₃), 15.0(CH₂CH₃), 16.8((CH₂)₂CH₂CH₃), 23.6 (CH₂CH₂CH₃), 25.9 (CH₂CH₂CH₂CH₃), 32.6 (CH₂CH₃), 39.6 (CH₂(CH₂)₂CH₃), 42.4 (CH₂CH₂CH₃), 53.6 (CNH₂). MS (ES+) : C₁₀H₂₄N⁺ (M+H⁺) 158.190 Found: 158.178. Anal. Calcd. for C₁₄H₂₇NO₄ : C, 61.51; H, 9.96; N, 5.12. Found: C, 61.54; H, 10.16; N, 5.01.

4-Propylheptan-4-amine (Pr₃C-NH₂) 2d. Tertiary alcohol **2b** was obtained after treating a solution of 4-heptanone **2a** (1g, 8.77 mmol) in dry diethyl ether (30% solution w/v) with 1.2-molar excess CH₃CH₂CH₂MgBr (obtained from an 20% solution w/v solution of 1-bromopropane (2.1 g, 17.54 mmol) in dry ether and 1.3 equivalents of Mg (548 mg, 22.8 mmol)) under argon atmosphere and stirring the mixture overnight. After treating the mixture with saturated ammonium chloride following usual workup 4-propylheptan-4-ol **2b** was obtained. Yield 1.1 g, (78%); IR (Nujol) ν(N₃) 3392 cm⁻¹; ¹H NMR (CDCl₃, 400 MHz): δ (ppm) 0.91 (t, *J* ~ 7 Hz, 9H, 3x CH₂CH₂CH₃), 1.15-1.41 (m, 12H, 3xCH₂CH₂CH₃, 3xCH₂CH₂CH₃), 2.10 (br s, OH); ¹³C NMR (CDCl₃, 50 MHz) δ 14.9 (CH₃), 17.0 (CH₂CH₂CH₃), 42.0 (CH₂CH₂CH₃), 74.7 (COH).

The 4-azido-4-propylheptane **2c** was prepared by treatment of the tertiary alcohol **2b** (400 mg, 2.50 mmol) with CH₂Cl₂ (15 mL) / NaN₃ (488 mg, 7.50 mmol) / TFA (2 mL, 25 mmol) according to the same procedure followed for 4-azido-4-ethyloctane **1c**. Yield 356 mg, (78%); IR (Nujol) ν(N₃) 2101 cm⁻¹; ¹³C NMR (CDCl₃, 50 MHz) δ (ppm) 14.4 (3xCH₂CH₂CH₃), 16.9 (3xCH₂CH₂CH₃), 38.9 (3xCH₂CH₂CH₃), 66.8 (CN₃).

The oily amine **2d** was prepared through LiAlH₄ (288 mg, 7.60 mmol) reduction of azide **2c** (350 mg, 1.90 mmol) in refluxing ether (20 mL) for 5h according to the same procedure followed for 4-ethyloctan-4-amine **1d**. 950 mg, Yield 50%; ¹H NMR (CDCl₃, 400 MHz): δ (ppm) 0.81 (t, *J* ~ 7 Hz, 9H), 1.27 (m, 12H), 2.11(s, NH₂); ¹³C NMR (CDCl₃, 50 MHz) δ (ppm) 14.9 (CH₃), 16.8(CH₂CH₂CH₃), 42.9(CH₂CH₂CH₃), 53.4 (CNH₂). MS (ES+): C₁₀H₂₄N⁺ (M+H⁺) 158.190 Found: 158.178. Anal. Calcd. for C₁₄H₂₇NO₄ : C, 61.51; H, 9.96; N, 5.12. Found: C, 61.66; H, 10.06; N, 5.13.

4-Propyl-octan-4-amine (BuPr₂C-NH₂) 5d. 4-Propyl-octan-4-ol **5b** was obtained after treating a solution of 4-heptanone **2a** (1g, 8.77 mmol) in dry diethyl ether (30% solution w/v) with 1.2-molar excess CH₃CH₂CH₂CH₂MgBr (obtained from an 20% solution w/v solution of 1-bromobutane (2,4 g, 17.54 mmol) in dry ether and 1.3 equivalents of Mg (548 mg, 22.8 mmol)) under argon atmosphere and stirring the mixture overnight. After treating the mixture with saturated ammonium chloride following usual workup the corresponding tertiary alcohol **5b** was obtained. Yield 990 mg, (71 %); IR (Nujol) $\nu(\text{N}_3)$ 3392 cm⁻¹; ¹H NMR (CDCl₃, 400 MHz): δ (ppm) 0.85-0.91 (m, 9H, CH₃), 1.21-1.31 (m, 9H, 2xCH₃CH₂CH₂, CH₃CH₂CH₂CH₂, OH), 1.34-1.42 (m, 6H, 2x CH₃CH₂CH₂, CH₃CH₂CH₂CH₂); ¹³C NMR (CDCl₃, 50 MHz) δ (ppm) 14.2 ((CH₂)₃CH₃), 14.8 (2x(CH₂)₂CH₃), 16.8 ((CH₂)₂CH₂CH₃), 23.5 (2xCH₂CH₂CH₃), 25.8 (CH₂CH₂CH₂CH₃), 39.1 (2xCH₂CH₂CH₃), 41.8 (CH₃CH₂CH₂COH), 74.5 (COH).

The 4-azido-4-propyloctane **5c** was prepared by treatment of the tertiary alcohol **5b** (900 mg, 5.23 mmol) with CH₂Cl₂ (20 mL) / NaN₃ (1 g, 15.7 mmol) / TFA (4.1 mL, 52 mmol) according to the same procedure followed for 4-azido-4-ethyloctane **1c**. Yield 730 mg, (71%); IR (Nujol) $\nu(\text{N}_3)$ 2095 cm⁻¹; ¹³C NMR (CDCl₃, 50 MHz) δ (ppm) 14.2 ((CH₂)₃CH₃), 14.6 (2x(CH₂)₂CH₃), 17.0 ((CH₂)₂CH₂CH₃), 23.2 (2xCH₂CH₂CH₃), 25.9 (CH₂CH₂CH₂CH₃), 36.4 (2xCH₂CH₂CH₃), 39.0 (CH₃CH₂CH₂CN₃), 66.9 (CN₃).

The oily amine **5d** was prepared through LiAlH₄ (540 mg, 14.2 mmol) reduction of azide **5c** (700 mg, 3.55 mmol) in refluxing ether (25 mL) for 5h according to the same procedure followed for 4-ethyloctan-4-amine **1d**. Yield 365 mg, (60%); ¹H NMR (CDCl₃, 400 MHz): δ (ppm) 0.85-0.89 (m, 9H, CH₃), 1.16-1.27 (m, 14H, 2xCH₃CH₂CH₂, CH₃CH₂CH₂CH₂); ¹³C NMR (CDCl₃, 50 MHz) δ (ppm) 14.0 ((CH₂)₃CH₃), 14.8 (2x(CH₂)₂CH₃), 16.7 ((CH₂)₂CH₂CH₃), 23.4 (2xCH₂CH₂CH₃), 25.7 (CH₂CH₂CH₂CH₃), 39.9 (2xCH₂CH₂CH₃), 42.8 (CH₃CH₂CH₂CNH₂), 53.2 (CNH₂). Anal. Calcd. for C₁₅H₂₉NO₄: C, 62.69; H, 10.17; N, 4.87. Found: C, 62.66; H, 10.53; N, 4.89.

5-Butyl-nonan-5-amine (Bu₃C-NH₂) 3d. 5-Butyl-nonan-5-ol, **3b** was obtained after treating a solution of 5-nonanone **3a** (1 g, 7.04 mmol) in dry diethyl ether (30% solution w/v) with 1.2-molar excess CH₃CH₂CH₂CH₂MgBr (obtained from an 20% solution w/v solution of 1-bromobutane (1.9 g, 14.08 mmol) in dry ether and 1.3 equivalents of Mg (440 mg, 18.3 mmol)) under argon atmosphere and stirring the mixture overnight. After treating the mixture with saturated ammonium chloride following usual workup the corresponding tertiary alcohol **3b** was obtained. Yield 1.1g, (80%); IR (Nujol) $\nu(\text{N}_3)$ 3392 cm⁻¹; ¹H NMR (CDCl₃, 400 MHz): δ (ppm) 0.88 (t, *J* ~ 7 Hz, 9H, 3xCH₃CH₂CH₂CH₂), 1.18-1.31 (m, 13H, 3xCH₃CH₂CH₂CH₂, 3xCH₃CH₂CH₂CH₂, OH), 1.34-1.42 (m, 6H, 3x CH₃CH₂CH₂CH₂); ¹³C NMR (CDCl₃, 50 MHz) δ (ppm) 14.2 (3xCH₃), 23.4 (3xCH₃CH₂CH₂CH₂), 25.8 (3xCH₃CH₂CH₂CH₂), 39.1 (3xCH₃CH₂CH₂CH₂), 74.4 (COH).

The 5-azido-5-butylnonane **3c** was prepared by treatment of the tertiary alcohol **3b** (500 mg, 2.50 mmol) with CH₂Cl₂ (20 mL) / NaN₃ (489 mg, 7.50 mmol) / TFA (2 mL, 25 mmol) according to the same procedure followed for 4-azido-4-ethyloctane **1c**. Yield 460 mg, (82%); IR (Nujol) $\nu(\text{N}_3)$ 2095 cm⁻¹; ¹³C NMR

(CDCl₃, 50 MHz) δ (ppm) 14.2 (3xCH₃), 23.2 (3xCH₃CH₂CH₂CH₂), 25.9 (3xCH₃CH₂CH₂CH₂), 36.4 (3xCH₃CH₂CH₂CH₂), 66.9 (CN₃).

The oily amine **3d** was prepared through LiAlH₄ (270 mg, 7.11 mmol) reduction of azide **3c** (400 mg, 1.78 mmol) in refluxing ether (20 mL) for 5h according to the same procedure followed for 4-ethyloctan-4-amine **1d**. Yield 20%; ¹H NMR (CDCl₃, 400 MHz): δ (ppm) 0.89 (t, *J* ~ 7 Hz, 9H, 3xCH₃CH₂CH₂CH₂), 1.15-1.30 (m, 12H, 3xCH₃CH₂CH₂CH₂); ¹³C NMR (CDCl₃, 50 MHz) δ (ppm) 14.3 (3xCH₃), 23.6(3xCH₃CH₂CH₂CH₂), 25.9 (3xCH₃CH₂CH₂CH₂), 40.1 (3xCH₃CH₂CH₂CH₂), 53.2 (CNH₂). MS (ES+) : C₁₃H₃₀N⁺ (M+H⁺) 200.240 Found: 200.045. Anal. Calcd. for C₁₇H₃₃NO₄ : C, 64.73; H, 10.54; N, 4.44. Found: C, 64.54; H, 10.42; N, 4.63.

5-Propyl-nonan-5-amine (Bu₂PrC-NH₂) 6d. 5-Propyl-nonan-5-ol **6b** was obtained after treating a solution of 5-nonanone **3a** (1 g, 7.04 mmol) in dry diethyl ether (30% solution w/v) with 1.2-molar excess CH₃CH₂CH₂MgBr (obtained from 20% solution w/v solution of 1-bromopropane (1.9 g, 14.08 mmol) in dry ether and 1.3 equivalents of Mg (440 mg, 18.3 mmol)) under argon atmosphere and stirring the mixture overnight. After treating the mixture with saturated ammonium chloride following usual workup the corresponding tertiary alcohol **6b** was obtained. Yield 915 mg, (70%); IR (Nujol) ν (N₃) 3392 cm⁻¹; ¹³C NMR (CDCl₃, 50 MHz) δ (ppm) 14.2 (2x CH₃(CH₂)₃), 14.8 (CH₃(CH₂)₂), 16.8 (2xCH₃CH₂(CH₂)₂), 23.5 (2xCH₃CH₂CH₂CH₂), 25.8 (CH₂CH₂CH₃), 39.2 (2xCH₃(CH₂)₂CH₂), 41.8 (CH₂CH₂CH₃), 74.5 (COH).

The 5-azido-5-propylnonane **6c** was prepared by treatment of the tertiary alcohol **6b** (500 mg, 2.69 mmol) with CH₂Cl₂ (20 mL) / NaN₃ (524 mg, 8.06 mmol) / TFA (2.2 mL, 27 mmol) according to the same procedure followed for 4-azido-4-ethyloctane **1c**. Yield 425 mg, (75%); IR (Nujol) ν (N₃) 2094 cm⁻¹; ¹³C NMR (CDCl₃, 50 MHz) δ (ppm) 14.1 (2x CH₃(CH₂)₃), 14.6 (CH₃(CH₂)₂), 17.0 (2xCH₃CH₂(CH₂)₂), 23.2 (2xCH₃CH₂CH₂CH₂), 25.8 (CH₂CH₂CH₃), 36.4 (2xCH₃(CH₂)₂CH₂), 39.1 (CH₂CH₂CH₃), 66.9 (CN₃).

The oily amine **6d** was prepared through LiAlH₄ (289 mg, 7.60 mmol) reduction of azide **6c** (400 mg, 1.90 mmol) in refluxing ether (20 mL) for 5h according to the same procedure followed for 4-ethyloctan-4-amine **1c**. Yield 35%; ¹H NMR (CDCl₃, 400 MHz): δ 0.86-0.89 (m, 9H, CH₃), 1.15-1.28 (m, 16H, CH₂); ¹³C NMR (CDCl₃, 50 MHz) δ (ppm) 14.4 2x CH₃(CH₂)₃, 15.1 (CH₃(CH₂)₂), 16.9 (2xCH₃CH₂(CH₂)₂), 23.7 (2xCH₃CH₂CH₂CH₂), 25.9 (CH₂CH₂CH₃), 40.4 (2xCH₃(CH₂)₂CH₂), 42.9 (CH₂CH₂CH₃), 53.4 (CNH₂). Anal. Calcd. for C₁₆H₃₁NO₄: C, 63.75; H, 10.37; N, 4.65. Found: C, 6.84; H, 10.16; N, 5.01.

2-Methyl-4-propyl-heptan-4-amine (i-BuPr₂C-NH₂) 4d. 2-methyl-4-propyl-heptan-4-ol **4b** was obtained after adding to i-butyllithium (14 mL, 21.9 mmol) reagent (1.6 M in hexanes) a solution of 4-heptanone **2a** (1g, 8.77 mmol) in dry ether (30% solution w/v) at 0 °C under argon atmosphere and stirring the mixture overnight, with lithium reagent being in a 2.5 molar excess. After treating the mixture with saturated ammonium chloride following usual workup the corresponding tertiary alcohol **4b** was obtained. Yield 1.2 g,

(80%); IR (Nujol) $\nu(\text{N}_3)$ 3422 cm^{-1} ; ^1H NMR (CDCl_3 , 400 MHz): δ (ppm) 0.86-0.89 (m, 6H, $2\times(\text{CH}_2)_2\text{CH}_3$) 0.92 (d, $J \sim 4$ Hz, 6H, $\text{CH}_2\text{CH}(\text{CH}_3)_2$), 1.23-1.25 (m, 4H, $2\times\text{CH}_2\text{CH}_2\text{CH}_3$), 1.31 (d, $J \sim 6$ Hz, 2H, $\text{CH}_2\text{CH}(\text{CH}_3)_2$), 1.37-1.41 (m, 4H, $2\times\text{CH}_2\text{CH}_2\text{CH}_3$), 1.73 (sep, $J \sim 6$ Hz, 1H, $\text{CH}_2\text{CH}(\text{CH}_3)_2$); ^{13}C NMR (CDCl_3 , 50 MHz) δ (ppm) 14.78 ($2\times\text{CH}_2\text{CH}_2\text{CH}_3$), 17.01 ($2\times\text{CH}_2\text{CH}_2\text{CH}_3$), 23.8 ($\text{CH}_2\text{CH}(\text{CH}_3)_2$), 24.9 ($\text{CH}_2\text{CH}(\text{CH}_3)_2$), 42.23 ($2\times\text{CH}_2\text{CH}_2\text{CH}_3$), 48.13 ($\text{CH}_2\text{CH}(\text{CH}_3)_2$), 75.22 (COH).

The 4-azido-2-methyl-4-propylheptane **4c** was prepared by treatment of the tertiary alcohol **4b** (500 mg, 2.90 mmol) with CH_2Cl_2 (25 mL) / NaN_3 (570 mg, 8.72 mmol) / TFA (2.3 mL, 29 mmol) according to the same procedure followed for 4-azido-4-ethyloctane **1c**. Yield 490 mg, (86%); IR (Nujol) $\nu(\text{N}_3)$ 2101 cm^{-1} ; ^{13}C NMR (CDCl_3 , 50 MHz) δ (ppm) 14.6 ($2\times\text{CH}_2\text{CH}_2\text{CH}_3$), 17.1 ($2\times\text{CH}_2\text{CH}_2\text{CH}_3$), 23.9 ($\text{CH}_2\text{CH}(\text{CH}_3)_2$), 24.4 ($\text{CH}_2\text{CH}(\text{CH}_3)_2$), 39.1 ($2\times\text{CH}_2\text{CH}_2\text{CH}_3$), 45.1 ($\text{CH}_2\text{CH}(\text{CH}_3)_2$), 67.0 (CN_3).

The oily amine **4d** was prepared through LiAlH_4 (309 mg, 8.12 mmol) reduction of azide **4c** (400 mg, 2.03 mmol) in refluxing ether (20 mL) for 5h according to the same procedure followed for 4-ethyloctan-4-amine **1d**. Yield 49 mg, (14%); ^1H NMR (CDCl_3 , 400 MHz): δ (ppm) 0.84-0.88 m, 6H, $2\times(\text{CH}_2)_2\text{CH}_3$ 0.89 (d, $J \sim 4$ Hz, 6H, $\text{CH}_2\text{CH}(\text{CH}_3)_2$), 1.92-1.27 (m, 11H, $2\times\text{CH}_2\text{CH}_2\text{CH}_3$, $\text{CH}_2\text{CH}(\text{CH}_3)_2$); ^{13}C NMR (CDCl_3 , 50 MHz) δ (ppm) 14.86 ($2\times\text{CH}_2\text{CH}_2\text{CH}_3$), 16.93 ($2\times\text{CH}_2\text{CH}_2\text{CH}_3$), 23.8 ($\text{CH}_2\text{CH}(\text{CH}_3)_2$), 25.4 ($\text{CH}_2\text{CH}(\text{CH}_3)_2$), 43.36 ($2\times\text{CH}_2\text{CH}_2\text{CH}_3$), 49.15 ($\text{CH}_2\text{CH}(\text{CH}_3)_2$), 54.17 (CNH_2). MS (ES+) : $\text{C}_{11}\text{H}_{26}\text{N}^+$ ($\text{M}+\text{H}^+$) 172.210 Found: 172.090. Anal. Calcd. for $\text{C}_{15}\text{H}_{29}\text{NO}_4$: C, 62.69; H, 10.17; N, 4.87. Found: C, 62.34; H, 10.16; N, 4.61.

2-Methyl-4-isobutyl-octan-4-amine (i-Bu₂BuC-NH₂) 7d. 2-Methyl-4-isobutyl-octan-4-ol **7b** was obtained after adding a solution of 2,6-dimethyl-heptan-4-one **4a** (1 g, 7.04 mmol) in dry diethyl ether (30% solution w/v) to n-butyllithium (1.6 M in hexanes), (13.5 mL, 21.1 mmol) at 0 °C under argon atmosphere and stirring the mixture overnight, with lithium reagent being in a 3.0 molar excess; After treating the mixture with saturated ammonium chloride following usual workup the corresponding tertiary alcohol **7b** was obtained. Yield 1.1 g, (80%); IR (Nujol) $\nu(\text{N}_3)$ 3460 cm^{-1} ; ^1H NMR (CDCl_3 , 400 MHz): δ (ppm) 0.88 (t, $J \sim 7$ Hz, 3H, $(\text{CH}_2)_2\text{CH}_3$) 0.92-0.95 (m, 12H, $2\times\text{CH}_2\text{CH}(\text{CH}_3)_2$), 1.19-1.35 (m, 10H, $\text{CH}_2\text{CH}_2\text{CH}_2\text{CH}_3$, $2\times\text{CH}_2\text{CH}(\text{CH}_3)_2$), 1.74 (sep, 2H, $J \sim 6$ Hz, $2\times\text{CH}_2\text{CH}(\text{CH}_3)_2$); ^{13}C NMR (CDCl_3 , 50 MHz) δ (ppm) 14.2 ($\text{CH}_3(\text{CH}_2)_3$), 23.5 ($\text{CH}_3\text{CH}_2(\text{CH}_2)_2$), 23.9 ($2\times\text{CH}_2\text{CH}(\text{CH}_3)_2$), 25.0 ($2\times\text{CH}_2\text{CH}(\text{CH}_3)_2$), 26.4 ($\text{CH}_2\text{CH}_2\text{CH}_2\text{CH}_3$), 39.9 ($\text{CH}_2(\text{CH}_2)_2\text{CH}_3$), 48.7 ($2\times\text{CH}_2\text{CH}(\text{CH}_3)_2$), 75.9 (COH).

The 4-azido-2-methyl-4-isobutyloctane **7c** was prepared by treatment of the tertiary alcohol **7b** (500 mg, 2.69 mmol) with CH_2Cl_2 (25 mL) / NaN_3 (525 mg, 8.07 mmol) / TFA (2.2 mL, 26.9 mmol) according to the same procedure followed for 4-azido-4-ethyloctane **1c**. Yield 430 mg, (76%); IR (Nujol) $\nu(\text{N}_3)$ 2099 cm^{-1} ; ^{13}C NMR (CDCl_3 , 50 MHz) δ (ppm) 14.2 ($\text{CH}_3(\text{CH}_2)_3$), 24.0 ($\text{CH}_3\text{CH}_2(\text{CH}_2)_3$), 24.2 ($2\times\text{CH}_2\text{CH}(\text{CH}_3)_2$), 24.6 ($2\times\text{CH}_2\text{CH}(\text{CH}_3)_2$), 26.3 ($\text{CH}_2\text{CH}_2\text{CH}_2\text{CH}_3$), 36.4 ($\text{CH}_2(\text{CH}_2)_2\text{CH}_3$), 45.5 ($2\times\text{CH}_2\text{CH}(\text{CH}_3)_2$), 67.1 (CN_3).

The oily amine **7d** was prepared through LiAlH_4 (288 mg, 7.58 mmol) reduction of azide **7c** (400 mg, 1.90 mmol) in refluxing ether (20 mL) for 5h according to the same procedure followed for 4-ethyloctan-4-amine **1d**. Yield 70 mg, (20%); ^1H NMR (CDCl_3 , 400 MHz): δ (ppm) 0.89 (t, $J \sim 7$ Hz, 3H, $\text{CH}_3(\text{CH}_2)_3$) 0.92-0.94 (m, 12H, 2x $\text{CH}_2\text{CH}(\text{CH}_3)_2$), 1.19-1.37 (m, 10H, $\text{CH}_2\text{CH}_2\text{CH}_2\text{CH}_3$, 2x $\text{CH}_2\text{CH}(\text{CH}_3)_2$), 1.63-1.76 (m, 2H, 2x $\text{CH}_2\text{CH}(\text{CH}_3)_2$); ^{13}C NMR (CDCl_3 , 50 MHz) δ (ppm) 14.3 ($\text{CH}_3(\text{CH}_2)_3$), 23.5 ($\text{CH}_3\text{CH}_2(\text{CH}_2)_2$), 23.8 (2x $\text{CH}_2\text{CH}(\text{CH}_3)_2$), 25.5 (2x $\text{CH}_2\text{CH}(\text{CH}_3)_2$), 26.3 ($\text{CH}_2\text{CH}_2\text{CH}_2\text{CH}_3$), 40.9 ($\text{CH}_2(\text{CH}_2)_2\text{CH}_3$), 49.7 (2x $\text{CH}_2\text{CH}(\text{CH}_3)_2$), 55.1 (CNH_2). Anal. Calcd. for $\text{C}_{17}\text{H}_{33}\text{NO}_4$: C, 64.73; H, 10.54; N, 4.44. Found: C, 64.34; H, 10.08; N, 4.81.

2-*n*-Butyl-(tricyclo[3.3.1.1^{3,7}]decan)-2-amine 11d. The 2-*n*-Butyl-tricyclo[3.3.1.1^{3,7}]decan-2-azide **11c** was prepared by treatment of the tertiary alcohol **11b** (300 mg, 1.44 mmol) with CH_2Cl_2 (20 mL) / NaN_3 (281 mg, 4.32 mmol) / TFA (1.2 mL, 14.4 mmol) according to the same procedure followed for 4-azido-4-ethyloctane **1c**. Yield 255 mg, (76%); IR (Nujol) $\nu(\text{N}_3)$ 2088 cm^{-1} ; ^1H NMR (CDCl_3 , 400 MHz): δ (ppm) 0.96 (t, $J \sim 7$ Hz, 3H, $\text{CH}_3\text{CH}_2\text{CH}_2\text{CH}$), 1.32-1.42 (m, 4H, $\text{CH}_3\text{CH}_2\text{CH}_2\text{CH}_2$), 1.62 (d, $J \sim 12$ Hz, 2H, 4eq,9eq-adamantane-H), 1.70-1.93 (m, 12H, adamantane-H, $\text{CH}_3\text{CH}_2\text{CH}_2\text{CH}_2$), 2.14 (d, $J \sim 12$ Hz, 2H, 4ax,9ax-adamantane-H); ^{13}C NMR (CDCl_3 , 50 MHz) δ (ppm) 14.2 ($\text{CH}_3\text{CH}_2\text{CH}_2\text{CH}_2$), 23.3 ($\text{CH}_2\text{CH}_2\text{CH}_2\text{CH}_3$), 24.9 ($\text{CH}_3\text{CH}_2\text{CH}_2\text{CH}_3$), 27.2, 27.4 (5,7-adamantane C), 33.8 (4,9-adamantane C), 33.7 (8,10-adamantane C), 34.4 (1,3-adamantane C), 35.2 ($\text{CH}_3\text{CH}_2\text{CH}_2\text{CH}_2$), 38.5 (6-adamantane C), 69.7 (2-adamantane C). The oily amine **11d** was prepared through LiAlH_4 (130 mg, 3.43 mmol) reduction of azide **11c** (200 mg, 0.860 mmol) in refluxing ether (15 mL) for 5h according to the same procedure followed for 4-ethyloctan-4-amine **1d**. Yield 41 mg, (23%); ^1H NMR (CDCl_3 , 400 MHz): δ (ppm) 0.88 (t, $J \sim 7$ Hz, 3H, $\text{CH}_3\text{CH}_2\text{CH}_2\text{CH}$), 1.18-1.32 (m, 4H, $\text{CH}_3\text{CH}_2\text{CH}_2\text{CH}_2$), 1.45-1.65 (m, 10H, adamantane-H, $\text{CH}_3\text{CH}_2\text{CH}_2\text{CH}_2$), 1.77 (br s, 2H, 5,7-adamantane-H), 1.93 (d, $J \sim 12$ Hz, 2H, 8ax,10ax-adamantane-H), 2.03 (d, $J \sim 12$ Hz, 2H, 4ax,9ax-adamantane-H), 2.13 (~ br s, 2H, NH_2); ^{13}C NMR (CDCl_3 , 50 MHz) δ (ppm) 14.3 ($\text{CH}_3\text{CH}_2\text{CH}_2\text{CH}_2$), 23.7 ($\text{CH}_2\text{CH}_2\text{CH}_2\text{CH}_3$), 24.6 ($\text{CH}_3\text{CH}_2\text{CH}_2\text{CH}_3$), 27.5, 27.8 (5,7 adamantane-C), 34.1 (4,9 adamantane-C), 33.2 (8,10 adamantane-C), 37.5 (1,3 adamantane-C), 38.6 (6 adamantane-C), 39.1 ($\text{CH}_3\text{CH}_2\text{CH}_2\text{CH}_2$), 54.5 (2 adamantane-C). Fumarate: mp 220 °C (EtOH-Et₂O); Anal. . Calcd. for ($\text{C}_{18}\text{H}_{29}\text{NO}_4$): C, 66.84; H, 9.04; N, 4.33. Found: C, 66.34; H, 9.22; N, 4.84.

2-Phenyl-(tricyclo[3.3.1.1^{3,7}]decan)-2-amine 12d. The 2-Phenyl-tricyclo[3.3.1.1^{3,7}]decan-2-azide **12c** was prepared by treatment of the tertiary alcohol **12b** (300 mg, 1.32 mmol) with CH_2Cl_2 (20 mL) / NaN_3 (265 mg, 3.95 mmol) / TFA (1.1 mL, 13.2 mmol) according to the same procedure followed for 4-azido-4-ethyloctane **1c**. Yield 290 mg, (95%); IR (Nujol) $\nu(\text{N}_3)$ 2098 cm^{-1} ; ^{13}C NMR (CDCl_3 , 50 MHz) δ (ppm) 26.8, 27.4 (5,7-adamantane-C), 33.1 (4,9-adamantane-C), 33.4 (8,10-adamantane-C), 34.1 (1,3-adamantane-C), 37.7 (6-adamantane-C), 70.3 (2-adamantane-C), 125.6, 127.3, 127.8, 128.9, 140.3 (phenyl).

The oily amine **12d** was prepared through LiAlH₄ (897 mg, 3.95 mmol) reduction of azide **12c** in refluxing ether (15 mL) for 5h according to the same procedure followed for 4-ethyloctan-4-amine **1d**. Yield 123 mg, (55%); ¹H NMR (CDCl₃, 400 MHz): δ (ppm) 1.53 (br s, 2H, 6-adamantane-H), 1.61-1.80 (m, 6H, adamantane-H), 1.90 (br s, 2H, 5,7-adamantane-H), 2.33 (d, *J* ~ 12 Hz, 1H, 4ax, 9ax-adamantane-H), 2.45 (br s, 2H, 1,3-adamantane-H), 7.18-7.25 (m, 5H, phenyl-H); ¹³C NMR (CDCl₃, 50 MHz) δ (ppm) 27.2, 27.6 (5,7 adamantane-C), 32.9 (4,9 adamantane-C), 34.6 (8,10 adamantane-C), 35.8 (1,3 adamantane-C), 38.2 (6 adamantane-C), 57.8 (2 adamantane-C), 125.2, 126.2, 128.8, 148.7 (Ph). Hydrochloride: mp > 265 °C (EtOH-Et₂O); Anal. (C₁₆H₂₂NCl): C, 72.84; H, 8.41; N, 5.31. Found: C, 72.12; H, 8.32; N, 5.02.

2-Benzyl-(tricyclo[3.3.1.1^{3,7}]decan)-2-amine 13d. The 2-Benzyl-tricyclo[3.3.1.1^{3,7}]decan-2-azide **13c** was prepared by treatment of the tertiary alcohol **13b** (500 mg, 2.07 mmol) with CH₂Cl₂ (25 mL) / NaN₃ (540 mg, 8.28 mmol) / TFA (1.7 mL, 20.7 mmol) according to the same procedure followed for 4-azido-4-ethyloctane **1c**. Yield 280 mg, (50%); IR (Nujol) ν(N₃) 2096 cm⁻¹; ¹³C NMR (CDCl₃, 50 MHz) δ (ppm) 27.1, 27.4 (5,7-adamantane C), 33.7 (4,9-adamantane C), 33.8 (8,10-adamantane C), 34.1 (1,3-adamantane C), 38.4 (6-adamantane C), 41.4 (CH₂Ph), 69.8 (2-adamantane C), 126.7, 128.2, 130.3, 136.6 (Ph).

The oily amine **13d** was prepared through LiAlH₄ reduction of azide **13c** in refluxing ether for 5h according to the same procedure followed for 4-ethyloctan-4-amine **1d**. Yield 45%; ¹H NMR (CDCl₃, 400 MHz): δ (ppm) 1.61 (d, *J* ~ 12 Hz, 2H, 4eq, 9eq-adamantane-H), 1.61 (br s, 1H, 6-adamantane-H), 1.73 (br s, 1H, 5,7-adamantane-H), 1.78 (d, *J* ~ 12 Hz, 2H, 8eq, 10eq-adamantane-H), 1.87 (br s, 1H, 3-adamantane-H), 1.97 (br s, 1H, 1-adamantane-H), 2.09 (d, *J* ~ 12 Hz, 1H, 8ax, 10ax-adamantane-H), 2.29 (d, *J* ~ 12 Hz, 1H, 4ax, 9ax-adamantane-H), 2.97 (s, 2H, CH₂Ph), 7.10-7.32 (m, 5H, phenyl-H); ¹³C NMR (CDCl₃, 50 MHz) δ (ppm) 27.6, 27.8 (5,7-adamantane C), 33.2 (4,9- adamantane C), 34.3 (8,10- adamantane C), 37.3 (1,3- adamantane C), 39.2 (6- adamantane C), 44.2 (CH₂Ph), 55.1 (2-adamantane C), 126.3, 128.1, 130.7, 138.4 (Ph). Fumarate: mp 205 °C (EtOH-Et₂O); Anal. (C₂₁H₂₇NO₄) : C, 70.56; H, 8.41; N, 5.31. Found: C, 70.99; H, 8.53; N, 5.02.

2-(p-Methoxy)benzyl-(tricyclo[3.3.1.1^{3,7}]decan)-2-amine 14d. 2-(p-Methoxy)benzyl-2-adamantanol **14b** was obtained after adding dropwise a solution of 2-adamantanone (500 mg, 3.33 mmol) in dry THF (6 mL) to a solution of pMeOBnMgCl (0.25 M in THF, 27 mL, 6.66 mmol) at room temperature and under argon atmosphere. The resulting mixture was stirred overnight and then heated at 45 °C for 2 hours. After treating the mixture with saturated ammonium chloride following usual workup the corresponding tertiary alcohol **14b** was obtained. Yield 725 mg, (80%); ¹H NMR (CDCl₃, 400 MHz) δ (ppm) 1.48 (d, *J* = 12 Hz, 2H, 4eq, 9eq adamantane-H), 1.53 (br s, 1H, OH), 1.66 (br s, 1H, 6 adamantane-H), 1.71 (br s, 1H, 5,7 adamantane-H), 1.77 (br s, 1H, 3 adamantane-H), 1.80 (d, *J* = 12 Hz, 2H, 8eq, 10eq adamantane-H), 1.91 (br s, 1H, 1 adamantane-H), 2.08 (d, *J* = 12 Hz, 1H, 8ax, 10ax adamantane-H), 2.22 (d, *J* = 12 Hz, 1H, 4ax, 9ax adamantane-H), 2.93 (s,

2H, CH₂Ar), 3.79 (s, 3H, OCH₃), 6.85 (d, *J* = 6 Hz, 2H, phenyl-H), 7.15 (d, *J* = 6 Hz, 2H, phenyl-H); ¹³C NMR (CDCl₃, 50 MHz) δ (ppm) 27.4, 27.5 (5,7 adamantane-C), 33.1 (4,9 adamantane-C), 34.7 (8,10 adamantane-C), 36.9 (1,3 adamantane-C), 38.5 (6 adamantane-C), 43.9 (CH₂Ar), 74.7 (2 adamantane-C), 126.5, 128.3, 130.7, 137.4 (Ar).

The corresponding azide **14c** was prepared from alcohol **14b** (720 mg, 2.64 mmol) according to the same procedure followed for 4-azido-4-ethyloctane **1c** using CH₂Cl₂ (30 mL) / NaN₃ (515.5 mg, 7.93 mmol) / TFA (3.01 mg, 26.4 mmol). Yield 730mg, (93 %).

The oily amine **14d** was prepared through LiAlH₄ (358 mg, 9.43 mmol) reduction of azide **14c** (700 mg, 2.36mmol) in refluxing THF (20 mL) for 5h. Yield 307 mg, (48%); ¹H NMR (CDCl₃, 400 MHz) δ (ppm) 1.62 (d, *J* = 12 Hz, 2H, 4eq, 9eq adamantane-H), 1.73 (d, *J* = 12 Hz, 2H, 8eq, 10eq adamantane-H), 1.77 (br s, 1H, 5,7 adamantane-H), 1.84 (br s, 1H, 6 adamantane-H), 1.93 (br s, 1H, 3 adamantane-H), 1.97 (br s, 1H, 1 adamantane-H), 2.09 (d, *J* = 12 Hz, 1H, 8ax, 10ax adamantane-H), 2.24 (d, *J* = 12 Hz, 1H, 4ax, 9ax adamantane-H), 2.93 (s, 2H, CH₂Ar), 3.80 (s, 3H, OCH₃), 6.84 (d, *J* = 6 Hz, 2H, phenyl-H), 7.15 (d, *J* = 6 Hz, 2H, phenyl-H). Fumarate: mp 205 °C (EtOH–Et₂O). Anal. Calcd for C₂₁H₃₆NO₅ C, 65.94; H, 9.49; N, 3.66. Found: C, 65.05; H, 9.58; N, 3.72.

4-(Tricyclo[3.3.1.1^{3,7}]dec-1-yl)-hept-1,6-dien-4-azide (AdAllyl₂C-N₃) 17c. The 4-(1-Adamantyl)-hept-1,6-dien-4-azide **17c** was prepared by treatment of the tertiary alcohol **17b** (500 mg, 2.03 mmol) with CH₂Cl₂ (20 mL) / NaN₃ (396 mg, 6.09 mmol) / TFA (1.6 mL, 20.3 mmol) according to the same procedure followed for 4-azido-4-ethyloctane **1c**. Yield 265 mg, (44%); ¹H-NMR (400MHz, CDCl₃) δ (ppm) 1.64-1.75 (m, 12H, 2,4,6,8,9,10-H, adamantane-H), 1.82 (br s, 3H, 3,5,7-H, adamantane-H), 1.99-2.20 (m, 4H, 3,5-CH₂), 5.09 (t, *J*~7 Hz, 4H, 2xCH₂=), 5.90-5.98 (m, 2H, 2xCH=); ¹³C-NMR (200MHz, CDCl₃) δ (ppm) 28.78 (3,5,7-C, adamantane-C), 36.57 (2,8,9-C, adamantane-C), 37.01 (4,6,10-C, adamantane-C), 39.28 (CH₂), 41.09 (1-C, adamantane-C), 55.14 (C-N₃), 118.06 (=CH₂), 135.61 (CH=).

1-(Tricyclo[3.3.1.1^{3,7}]dec-1-yl)cyclopentanamine 19d. The synthetic details and characterization were included in Chapter 2.

1-(Tricyclo[3.3.1.1^{3,7}]dec-1-yl)cyclohexanamine 20d. The synthetic details and characterization were included in Chapter 2.

2-(Tricyclo[3.3.1.1^{3,7}]dec-1-yl)-propan-2-amine (AdMe₂C-NH₂) 15d. The synthetic details and characterization were included in Chapter 1.

3-(Tricyclo[3.3.1.1^{3,7}]dec-1-yl)-pentan-3-amine (AdEt₂C-NH₂) 16d. The synthetic details and characterization were included in Chapter 3.

4-(Tricyclo[3.3.1.1^{3,7}]dec-1-yl)-hept-1,6-dien-4-ol (AdAllyl₂C-OH) 17b. The synthetic details and characterization were included in Chapter 3.

4-(Tricyclo[3.3.1.1^{3,7}]dec-1-yl)-heptan-4-amine (AdPr₂C-NH₂) 18d. The synthetic details and characterization were included in Chapter 3.

4.5.1.2 Procedure B

4-Ethyl octan-4-amine (BuEtPr-CNH₂) 1d. A solution of conc. H₂SO₄ (6 mL) and AcOH (6 mL) was added dropwise to a mixture of alcohol **1b** (500 mg, 3.16 mmol), AcOH (6 mL) and KCN (258 mg, 3.96 mmol) at 70 °C and heating was maintained for 2 h. The resulting mixture was treated with water (10 mL) and NaOH 10% (10 mL) and stirred for 15 min. The mixture was extracted with ether (2x15 mL), the combined organic phases were washed with water and the solvent was evaporated in vacuo to afford the amine **1d** acetamide. A mixture of the amine **1d** acetamide (430 mg, 2.32 mmol) and KOH (1.04 g, 18.6 mmol) in di(ethylene glycol) (2 mL) was heated for 24h in a sealed tube at 180 °C. After cooling, the tube was opened and the mixture poured into water (50 mL). The mixture was extracted with dichloromethane (3x20 mL) and washed with HCl 6%. The aqueous phase was made alkaline with solid sodium carbonate and was extracted with dichloromethane. The organic phase was washed with brine, dried (Na₂SO₄) and evaporated in vacuo to afford the 4-ethyl octan-4-amine **1d**; Yield 47%. Amine **3d** was prepared according to the same procedure; Characterization of compound **1d** is included in compounds synthesized by Procedure A.

5-Butyl nonan-5-amine (Bu₃C-NH₂) 3d. The amine **3d** acetamide was prepared as above for the preparation of tert-alkyl amine **1d** through treatment of alcohol **3b** (500 mg, 2.50 mmol), with conc.H₂SO₄ (6 mL) / AcOH (6 mL) / KCN (203 mg, 3.13 mmol). The amine **3d** was prepared through treatment of **3d** acetamide (400 mg, 1.76 mmol) with KOH (780 mg, 18.6 mmol) in di(ethylene glycol) (2 mL) and following the same workup. Yield 20 mg (4%). Characterization of compound **3d** is included in compounds synthesized by Procedure A.

4.5.1.3 Procedure C

4-propylheptan-4-amine (Pr₃C-NH₂) 2d. To a mixture of the alcohol **2b** (300 mg, 1.90 mmol) and ClCH₂CN (287 mg, 3.80 mmol), AcOH (0.3 mL, 5.25 mmol) was added and the mixture was cooled to 0-3 °C. H₂SO₄ (0.3 mL, 5.70 mmol) was added dropwise keeping the temperature below 10 °C. The reaction mixture was allowed to reach rt, stirred for 24 h and poured into ice water (10 mL). Chloroacetamide **8** was extracted with ether (3 × 10 mL). The combined extracts were washed with NaHCO₃ 10% and brine, and dried (NaSO₄). Solvent was evaporated in vacuo to afford compound **8** which was used without further purification for the next step. Yield 200 mg (45%); IR (Nujol) $\nu(\text{C=O})$ 1668 cm⁻¹; ¹H NMR (CDCl₃, 400 MHz) δ (ppm) 0.96 (t, *J* ~ 7 Hz, 9H, 3xCH₂CH₂CH₃), 1.33-1.47 (m, 12H, 3xCH₂CH₂CH₃, 3xCH₂CH₂CH₃), 4.27 (s, COCH₂Cl).

A solution of the amide **8** (180 mg, 0.772 mmol) and thiourea (70.6 mg, 0.927 mmol) in EtOH (6 mL)/AcOH (1.2 mL) was refluxed for 10 h. Then water (15 mL) was added to the reaction mixture and the resulting precipitate was filtered off. The filtrate was made alkaline with NaOH 20%, washed with ether (3 × 30 mL) and extracted with HCl 6%. The aqueous phase was made alkaline with solid sodium carbonate and was extracted with dichloromethane or ether. The organic phase was washed with brine, dried (Na₂SO₄) and evaporated in vacuo to afford the amine **2d**. Yield 100 mg (80 %); Characterization of compound **2d** is included in compounds synthesized by Procedure A.

5-Butylnonan-5-amine (Bu₃C-NH₂) 3d. Chloroacetamide **9** was prepared through treatment of tributylsubstituted methanol **3b** (300 mg, 1.50 mmol) with NCCH₂Cl (282 mg, 3.00 mmol), H₂SO₄ (0.3 mL, 5.70 mmol) / AcOH (0.3 mL, 5.25 mmol) according to the same procedure followed for the chloroacetamide **8**. Yield 252 mg, (61%); IR (Nujol) $\nu(\text{C=O})$ 1689 cm⁻¹; ¹H NMR (CDCl₃, 400 MHz) δ (ppm) 0.97 (t, *J* ~ 7 Hz, 9H, 3xCH₃CH₂CH₂CH₂), 1.29-1.35 (m, 12H, 3xCH₃CH₂CH₂CH₂, 3x CH₃CH₂CH₂CH₂), 1.38-1.47 (m, 6H, 3x CH₃CH₂CH₂CH₂), 4.27 (s, COCH₂Cl). The amine **3d** was prepared as above for the preparation of tert-alkyl amine **2d** through treatment of **9** (200 mg, 0.725 mmol) with thiourea (66 mg, 0.871 mmol) in EtOH (6 mL)/AcOH (1.2 mL) and following the same workup. Yield 19 mg (13%). Characterization of compound **3d** is included in compounds synthesized by Procedure A.

2-*n*-Butyl-(tricyclo[3.3.1.1^{3,7}]decan)-2-amine 11d. Chloroacetamide **22** was prepared through treatment of tributylsubstituted methanol **3b** (300 mg, 1.44 mmol) with NCCH₂Cl (271 mg, 2.88 mmol), H₂SO₄ (0.3 mL, 5.70 mmol) / AcOH (0.3 mL, 5.25 mmol) according to the same procedure followed for the chloroacetamide **8**. Yield 209 mg, (51%); IR (Nujol) $\nu(\text{C=O})$ 1690 cm⁻¹; ¹H NMR (CDCl₃, 400 MHz) δ (ppm) 0.96 (t, *J* ~ 7 Hz, 3H, CH₃CH₂CH₂CH), 1.35-1.45 (m, 4H, CH₃CH₂CH₂CH₂), 1.63 (d, *J* ~ 12 Hz, 2H, 4eq,9eq-adamantane-H), 1.76-2.02 (m, 12H, adamantane-H, CH₃CH₂CH₂CH₂), 2.05 (d, *J* ~ 12 Hz, 2H, 4ax,9ax-adamantane-H), 4.32 (s, COCH₂Cl).

The amine **11d** was prepared as above for the preparation of tert-alkyl amine **2d** through treatment of **22** (200 mg, 0.704 mmol) with thiourea (67 mg, 0.880 mmol) in EtOH (6 mL)/AcOH (1.2 mL) and following the same workup. Yield 57 mg (39%). Characterization of compound **11d** is included in compounds synthesized by Procedure A.

2-(Tricyclo[3.3.1.1^{3,7}]dec-1-yl)-propan-2-amine 15d. Chloroacetamide **23** was prepared through treatment of tributylsubstituted methanol **15b** (300 mg, 1.55 mmol) with NCCH₂Cl (290 mg, 3.09 mmol), H₂SO₄ (0.3 mL, 5.70 mmol) / AcOH (0.3 mL, 5.25 mmol) according to the same procedure followed for the chloroacetamide **8**. Yield 42 mg, (10%); IR (Nujol) $\nu(\text{C=O})$ 1673 cm⁻¹; ¹H NMR (CDCl₃, 400 MHz) δ (ppm) 0.80 (s, 6H, 2xCH₃), 1.58-1.70 (m, 12H, 2,4,6,8,9,10-H, adamantane H), 2.01 (br s, 3H, 3,5,7-H, adamantane H), 4.30 (s, COCH₂Cl). The amine **15d** was prepared as above for the preparation of tert-alkyl amine **2d** through treatment of **23** (40 mg, 0.150 mmol) with thiourea (9 mg, 0.118 mmol) in EtOH (3 mL) / AcOH (0.6 mL) and following the same workup. Yield traces. Characterization of compound **15d** is included in Chapter 1.

4-(Tricyclo[3.3.1.1^{3,7}]dec-1-yl)-heptan-4-amine 18d. Chloroacetamide **24** was prepared through treatment of tributylsubstituted methanol **18d** (300 mg, 1.20 mmol) with NCCH₂Cl (226 mg, 2.40 mmol), H₂SO₄ (0.3 mL, 5.70 mmol) / AcOH (0.3 mL, 5.25 mmol) according to the same procedure followed for the chloroacetamide **8**. Yield 144 mg, (37%); IR (Nujol) $\nu(\text{C=O})$ 1690 cm⁻¹; ¹H NMR (CDCl₃, 400 MHz) δ (ppm) 0.92 (t, *J*~7 Hz, 6H, 2xCH₃), 1.35-1.43 (m, 8H, 2x CH₂CH₂CH₃), 1.63-1.70 (m, 12H, 2,4,6,8,9,10-H, adamantane H), 2.01 (br s, 3H, 3,5,7-H, adamantane H), 4.28 (s, COCH₂Cl). The amine **18d** was prepared as above for the preparation of tert-alkyl amine **2d** through treatment of **24** (140 mg, 0.430 mmol) with thiourea (26 mg, 0.344 mmol) in EtOH (3 mL) / AcOH (0.6 mL) and following the same workup. Yield traces. Characterization of compound **18d** is included in Chapter 3.

4.5.1.4 Procedure D

4-Propylheptan-4-amine (Pr₃C-NH₂) 2d. To a stirred mixture of 4-heptanone **2a** (224 mg, 1.97 mmol) and Ti(EtO)₄ (900 mg, 3.93 mmol) in dry THF (4 mL), *tert*-butanesulfinamide (250 mg, 2.06 mmol) was added and the resulting reaction mixture was refluxed overnight. The mixture was cooled at 0 °C and the solvent was evaporated in vacuo. The residue was purified by flash chromatography on silica gel (40-63 μm) using 40:60 Et₂O/hexane as an eluent to afford the sulfinyl ketimine **10**. Yield 48%; ¹H NMR (CDCl₃, 400 MHz) δ (ppm) 0.88-0.98 (m, 6H, (CH₂)₂CH₃), 1.20 (s, 9H, C(CH₃)₃), 1.56-1.60 (sex, *J*~7, 4H CH₂CH₂CH₃), 2.32-2.38 (m, 2H, CH₂CH₂CH₃), 2.54-2.71 (m, 2H, CH₂CH₂CH₃).

Propylmagnesium bromide (2.07 mmol) (obtained from 20% solution w/v 1-bromopropane in dry ether and 1.3 equivalents of Mg) was cooled at -78 °C and treated dropwise with a solution of the *tert*-butyl sulfinyl ketimine **10** (205 mg, 0.942 mmol) in dry ether (2 mL). The resulting mixture was stirred for 1 h at -78 °C and then allowed to reach slowly ambient temperature and stirred for additional 15 h. The mixture was then cooled at 0 °C, treated with sat. aq. Na₂SO₄ (5 mL) and stirred for 10 min. After suction filtration, the mixture was extracted with ethyl acetate (2 x 15 mL) and the organic phase was washed with brine, dried (Na₂SO₄) and evaporated in vacuo to afford crude *tert*-butyl sulfinamide **11** which was used without further purification for the next step.

A solution of sulfinamide **11** (121 mg, 0.463 mmol) in dioxane (1 mL) was cooled at 0 °C and treated dropwise with HCl 2.5 M in ethanol (4.0 mL, 2.31 mmol). The resulting solution was allowed to reach ambient temperature and stirred for 40 min. The solution was concentrated under vacuum to a volume of 1 mL and 2 mL of ether was added to afford amine **2d** hydrochloride as a precipitate. Yield 13 mg (18%); Characterization of compound **2d** is included in compounds synthesized by Procedure A.

5-Butylnonan-5-amine (Bu₃C-NH₂) 3d. *Tert*-butyl sulfinyl aldimine **12** was prepared according to the same procedure followed for *tert*-butyl sulfinyl ketimine **10**. Yield 77%; ¹H NMR (CDCl₃, 400 MHz) δ (ppm) 0.89 (t, J ~ 7, 6H, (CH₂)₃CH₃), 1.19 (s, 9H, C(CH₃)₃), 1.33 (sex, J ~ 7, 4H, (CH₂)₂CH₂CH₃), 1.54 (q, J ~ 7, 4H, CH₂CH₂CH₂CH₃), 2.38 (t, J ~ 7, 2H, CH₂(CH₂)₂CH₃), 2.58-2.73 (m, 2H, CH₂(CH₂)₂CH₃); ¹³C NMR (CDCl₃, 50 MHz): δ (ppm) 13.9 (2x(CH₂)₃CH₃), 22.3 (C(CH₃)₃), 23.0 (2x(CH₂)₂CH₂CH₃), 27.8 (CH₂CH₂CH₂CH₃), 29.6 (CH₂CH₂CH₂CH₃), 36.4 (2xCH₂CH₂CH₂CH₃), 56.2 (C(CH₃)₃), 189.1 (C=N).

A 0.7 M solution of sulfinyl ketimine **12** (387 mg, 1.58 mmol) in dry toluene (2 mL) was cooled at -78 °C and treated dropwise with a 2M solution of AlMe₃ in toluene (0.8 mL, 1.1 molar excess). The mixture was stirred for 5 min and a solution of 1.6M n-butyl lithium in hexanes (2 mL, 0.4 M in toluene, 2.2 molar excess) was added dropwise at -78 °C. The resulting mixture was stirred for additional 4 h at -78 °C and then allow to reach 0 °C. The mixture was treated with sat. aq. Na₂SO₄ (5 mL) and stirred for 10 min. After suction filtration, the mixture was extracted with ethyl acetate (2 x 15 mL) and the organic phase was washed with brine, dried (Na₂SO₄) and evaporated in vacuo to afford crude *tert*-butyl sulfinamide **13** which was used without further purification for the next step.

A solution of sulfinamide **13** (227 mg, 0.750 mmol) in dioxane (1 mL) was cooled at 0 °C and treated dropwise with HCl 2.5 M in ethanol (6.5 mL, 3.75 mmol). The resulting solution was allowed to reach ambient temperature and stirred for 40 min. The solution was concentrated under vacuum to a volume of 1 mL and 2 mL of ether was added to afford amine **3d** hydrochloride as a precipitate. Yield 45 mg (25 %); Characterization of compound **3d** is included in compounds synthesized by Procedure A.

4.5.1.5 Procedure E

5-Propyl-nonan-5-amine (Bu₂PrC-NH₂) 6d. Kulinkovich-de Meijere reaction protocol: A solution of butanenitrile **14** (1.0 g, 14.5 mmol) in 40 mL anhydrous ether was added dropwise to a 3.2 molar excess of BuMgBr (3M in dry ether, obtained from 1-bromobutane (5.9 g, 46.4 mmol) with 1.2 equivalents of Mg (1.4 g, 55.7 mmol)). After stirring the mixture for 30 min, 1 equiv of Ti(Oi-Pr)₄ (4.1 g, 14.5 mmol) was added successively at rt and the reaction mixture was gently refluxed for 24 h. After treating the mixture with NaOH 10%, following usual workup the corresponding amine **6d** was obtained. Yield 670 mg (25%), (Table 9, entry 1); Characterization of compound **6d** is included in compounds synthesized by Procedure A.

5-Butyl-nonan-5-amine (Bu₃C-NH₂) 3d. Kulinkovich-de Meijere reaction protocol: A solution of pentanenitrile **15** (1.0 g, 12.0 mmol) in 40 mL anhydrous ether was added dropwise to a 3.2 molar excess of BuMgBr (3M in dry ether, obtained from 1-bromobutane (4.9 g, 36.0 mmol) and 1.2 equivalents of Mg (1.0 g, 43.2 mmol)). After stirring the mixture for 30 min, 1 equiv of Ti(Oi-Pr)₄ (3.4 g, 12.0 mmol) was added successively at rt and the reaction mixture was gently refluxed for 24 h. After treating the mixture with NaOH 10% following usual workup the corresponding amine **3c** was obtained. Yield 510 mg (20%), (Table 9, entry 2); Characterization of compound **3d** is included in compounds synthesized by Procedure A.

4-(Tert-butyl)-heptane-4-amine (tBuMe₂C-NH₂) 29. Kulinkovich-de Meijere reaction protocol: *Tert*-alkyl amine **29** was prepared through the reaction of pivalonitrile **28** (500 mg, 6.02 mmol) in 30 mL of anhydrous diethyl ether with a 3M PrMgBr in dry ether (obtained from PrBr (2.20 g, 18.07 mmol) and 1.2 equivalents of Mg (520 mg, 21.7 mmol)) and Ti(Oi-Pr)₄ (2.0 g, 7.22 mmol) according to the same procedure described above for the amines **3d** and **6d** (Procedure E). Fumaric salt formation and recrystallization afforded 340 mg of fumaric salt of amine **29**. Yield 20%, (Table 9, entry 3); ¹H NMR (CDCl₃, 400 MHz) δ (ppm) 0.84-0.90 (m, 15H, (CH₂)₂CH₃, (CH₂)₂CH₃, C(CH₃)₃), 1.28-1.40 (m, 8H, (CH₂)₂CH₃); ¹³C NMR (CDCl₃, 50 MHz) δ (ppm) 15.37 (2x(CH₂)₂CH₃), 18.62 (2xCH₂CH₂CH₃), 26.3 (C(CH₃)₃), 38.9 (2xCH₂CH₂CH₃), 42.2 (C(CH₃)₃), 57.5(CNH₂).

3-(Tricyclo[3.3.1.1^{3,7}]dec-1-yl)-propan-2-amine (AdMe₂CNH₂) 15d. Kulinkovich-de Meijere reaction protocol: A solution of 3M MeMgBr (1 mL, 3.11 mmol) in diethyl ether was added dropwise to 1-adamantanenitrile **30** (500 mg, 3.11 mmol) in ether (30 mL). After stirring the mixture for 30 min, 1.2 equiv of Ti(Oi-Pr)₄ (975 mg, 3.43 mmol) was added successively at rt. The mixture was allowed to stir at room temperature under argon atmosphere for 1 h. Then, 4 mL of methylithium solution (1.6 M in diethyl ether, 6.22 mmol) was added dropwise and the reaction mixture was gently refluxed for 24 h. After treating the mixture with NaOH 10%

following usual workup the corresponding amine **15d** was obtained. Yield 60 mg (10%), (Table 9, entry 8); Characterization of compound **15d** is included in compounds synthesized by Procedure A.

3-(Tricyclo[3.3.1.1^{3,7}]dec-1-yl)-propan-2-amine (AdMe₂CNH₂) 15d. Kulinkovich-de Meijere reaction protocol: A solution of 3M MeMgBr (1 mL, 3.11 mmol) in diethyl ether was added dropwise to 1-adamantanenitrile **30** (500 mg, 3.11 mmol) in ether (30 mL). After stirring the mixture for 30 min, 1.2 equiv of Ti(Oi-Pr)₄ (975 mg, 3.43 mmol) was added successively at rt. The mixture was allowed to stir at room temperature under argon atmosphere for 1 h. Then, 2.1 mL of MeMgBr solution (3 M in diethyl ether, 6.22 mmol) was added dropwise and the reaction mixture was gently refluxed for 24 h. After treating the mixture with NaOH 10% following usual workup the corresponding amine **15d** was obtained. Yield 60 mg (10%), (Table 9, entry 11); Characterization of compound **15d** is included in compounds synthesized by Procedure A.

3-(Tricyclo[3.3.1.1^{3,7}]dec-1-yl)-propan-2-amine (AdMe₂CNH₂) 15d. Kulinkovich-Szymoniak reaction protocol: Tetraisopropoxy titanium (975 mg, 3.43 mmol) was added in a solution of 1-adamantanenitrile **30** (500 mg, 3.11 mmol) in 30 mL of anhydrous diethyl ether, under stirring and argon atmosphere. After 20 min, 1 mL of MeMgBr solution in diethyl ether (3 M, 6.22 mmol) was added dropwise and the mixture was allowed to stir at room temperature under argon atmosphere for 1 h. Then, 4 mL of methylithium solution (1.6 M in diethyl ether, 6.22 mmol) was added dropwise and the reaction mixture was gently refluxed for 24 h. After treating the mixture with NaOH 10% following usual workup the corresponding amine **15d** was obtained. Yield 66 mg (11%), (Table 9, entry 8); Characterization of compound **15d** is included in compounds synthesized by Procedure A.

3-(Tricyclo[3.3.1.1^{3,7}]dec-1-yl)-propan-2-amine (AdMe₂CNH₂) 15d. Kulinkovich-Szymoniak reaction protocol: A solution of 3M MeMgBr (2.1 mL, 6.22 mmol) in diethyl ether was added dropwise to 1-adamantanenitrile **30** (500 mg, 3.11 mmol) in ether (30 mL). After stirring the mixture for 30 min, 1.2 equiv of Ti(Oi-Pr)₄ (975 mg, 3.43 mmol) was added successively at rt. The mixture was allowed to stir at room temperature under argon atmosphere for 1 h. Then, 1 mL of MeMgBr solution (3 M in diethyl ether, 3.11 mmol) was added dropwise and the reaction mixture was gently refluxed for 24 h. After treating the mixture with NaOH 10% following usual workup the corresponding amine **15d** was obtained. Yield 60 mg (10%), (Table 9, entry 10); Characterization of compound **15d** is included in compounds synthesized by Procedure A.

3-(Tricyclo[3.3.1.1^{3,7}]dec-1-yl)-pentan-3-amine (AdEt₂CNH₂) 16d. Kulinkovich-de Meijere reaction protocol: Amine **16d** was prepared through the reaction of 1-adamantanenitrile **30** (500 mg, 3.11 mmol) in 30 mL of anhydrous diethyl ether with EtMgBr 3M in dry ether (obtained from EtBr (1.02 g, 9.33 mmol) and 1.2

equivalents of Mg (672 mg, 28.0 mmol)) and Ti(Oi-Pr)₄ (970 mg, 3.42 mmol) according to the same procedure described above for the amines **3d** and **6d** (Procedure E) to afford 120 mg of mixture. For purification of the crude product 2 mL of an ethanolic solution of fumaric acid (66 mg, 0.569 mmol) was added to a solution of the crude amine in 2 mL ethanol. The mixture was evaporated under vacuum, to yield a white colored crystal residue which was treated with diethyl ether and filtered under vacuum to afford a non-separable mixture of AdEtCH-NH₂ (**32**) in 3% yield and AdEt₂C-NH₂ **16d** in a 4% yield (ratio 60:40 according to ¹³C NMR spectrum), (Table 9, entry 5). Characterization of compound **16d** is included in compounds synthesized by Procedure A.

3-(Tricyclo[3.3.1.1^{3,7}]dec-1-yl)-pentan-3-amine (AdEt₂CNH₂) 16d. Kulinkovich-de Meijere reaction protocol: Amine **16d** was prepared through the reaction of 1-adamantanenitrile **30** (500 mg, 3.11 mmol) in 30 mL of anhydrous diethyl ether with 19 mL of ethyllithium solution (0.5 M in cyclohexane/benzene, 9.33 mmol) and Ti(Oi-Pr)₄ (970 mg, 3.42 mmol) according to the same procedure described above for the amines **3d** and **6d** (Procedure E). Yield 14 mg (2%), (Table 9, entry 6). Characterization of compound **16d** is included in compounds synthesized by Procedure A.

3-(Tricyclo[3.3.1.1^{3,7}]dec-1-yl)-pentan-3-amine (AdEt₂CNH₂) 16d. Kulinkovich-de Meijere reaction protocol: Amine **16d** was prepared through the reaction of 1-adamantanenitrile **30** (500 mg, 3.11 mmol) in 30 mL of anhydrous diethyl ether with EtMgBr 3M in dry ether (obtained from EtBr (340 mg, 3.11 mmol) and 1.2 equivalents of Mg (90 mg, 3.73 mmol)) and Ti(Oi-Pr)₄ (970 mg, 3.42 mmol) according to the same procedure described above for the amines **3d** and **6d** (Procedure E). The mixture was allowed to stir at room temperature under argon atmosphere for 1 h. Then, 12 mL of ethyllithium solution (0.5 M in cyclohexane/benzene, 6.22 mmol) was added dropwise and the reaction mixture was gently refluxed for 24 h. After treating the mixture with NaOH 10% following usual workup the corresponding amine **16d** was obtained. Yield 70 mg (10%), (Table 9, entry 9); Characterization of compound **16d** is included in compounds synthesized by Procedure A.

3-(Tricyclo[3.3.1.1^{3,7}]dec-1-yl)-pentan-3-amine (AdEt₂CNH₂) 16d. Kulinkovich-Szymoniak reaction protocol: Tetraisopropoxy titanium (975 mg, 3.43 mmol) was added in a solution of 1-adamantanenitrile **30** (500 mg, 3.11 mmol) in 30 mL of anhydrous diethyl ether, under stirring and argon atmosphere. After 20 min, 3.1 mL of ethyl magnesium bromide solution in diethyl ether (1 M, 3.11 mmol) was added dropwise and the mixture was allowed to stir at room temperature under argon atmosphere for 1 h. Then, 12 mL of ethyllithium solution (0.5 M in cyclohexane/benzene, 6.22 mmol) was added dropwise and the reaction mixture was gently refluxed for 24 h. After treating the mixture with NaOH 10% following usual workup to yield 300 mg of

a yellow oily product, which was purified by recrystallization; 2 mL of an ethanolic solution of fumaric acid (166 mg, 1.43 mmol) was added to a solution of the crude amine in 2 mL ethanol. The mixture was evaporated under vacuum, to yield a white colored crystal residue which was treated with diethyl ether and filtered under vacuum to afford 60 mg (yield 10%) of the fumarate salt of amine **16d**; Yield 65 mg (10%), (Table 9, entry 9); Characterization of compound **16d** is included in compounds synthesized by Procedure A.

1-(Tricyclo[3.3.1.1^{3,7}]dec-1-yl)cyclopentanamine 19d. Kulinkovich-de Meijere reaction protocol: A solution of 1-adamantanenitrile **30** (300 mg, 1.86 mmol) in ether (5 mL) was added dropwise to a 2 molar excess of $\text{BrMg}(\text{CH}_2)_2\text{MgBr}$ (3M in dry ether, obtained from dibromobutane with 2.2 equivalents of Mg). After stirring the mixture for 30 min, 1 equiv of $\text{Ti}(\text{O}i\text{-Pr})_4$ (529 mg, 1.86 mmol) was added successively at rt and the reaction mixture was allowed to stir at room temperature under argon atmosphere for 24 h. After a dropwise addition of an equal volume of a sodium hydroxide 10% w/v solution under ice cooling, the mixture was stirred for 30 min and filtered under vacuum. The filtrate was extracted with diethyl ether (2x10mL). The combined ethereal phases were extracted with 30 mL (2x15 mL) of hydrochloric acid 6% w/v. The aqueous phase was separated and made alkaline through addition of an excess solid sodium carbonate under ice-cooling. The aqueous phase was extracted two times with 15 mL of dichloromethane. The combined organic extracts were washed 2 times with an equal volume of water and brine, dried (Na_2SO_4) and evaporated under vacuum to yield 173 mg of a yellow oily product, which was purified by recrystallization; 2 mL of an ethanolic solution of fumaric acid (94 mg, 0.829 mmol) was added to a solution of the crude amine in 2 mL ethanol. The mixture was evaporated under vacuum, to yield a white colored crystal residue which was treated with diethyl ether and filtered under vacuum to afford 60 mg (yield 10%) of the fumarate salt of 3-(1-adamantyl)-pentan-3-amine **19d**; Characterization of compound **19d** is included in compounds synthesized by Procedure A.

4.5.2 Computational chemistry details

All structures included by the isodesmic reaction $R_3CH + 1-Ad^+ \rightarrow R_3C^+ + AdH$ were fully optimized at the B3LYP/6-31+G**³⁰ level using PCM³¹ as continuous solvent model; calculations were performed using the GAUSSIAN 03 package (detailed results of the thermochemistry calculations, that is, SCF energies, SCF + ZPVE energies, enthalpies, free energies and cartesian coordinates for the optimized structures of the species included in the isodesmic reaction can be found in the Supporting Information). Frequency calculations were also performed at the B3LYP/6-31+G** to locate minima; no imaginary frequencies were found.

4.5.3 Dynamic NMR Spectroscopy

The low temperature NMR spectra were obtained by using a flow of dry nitrogen which entered into an inox steel heat exchanger immersed in liquid nitrogen and connected to the NMR probe head by a vacuum-insulated transfer line. The 600 MHz ¹H spectra were acquired using a 5 mm direct probe with a 9000 Hz spectral width, 2.0 μ s (20° tip angle) pulse width, 3 s acquisition time and 1 s delay time. A shifted sine bell weighting function equal to the acquisition time (i.e., 3 s) was applied before the Fourier transformation. Temperature calibrations were performed before the experiments, using a digital thermometer and a Cu/Ni thermocouple placed in an NMR tube filled with isopentane. The uncertainty in the temperature measurements can be estimated from the calibration curve as ± 1 °C. Line shape simulations were performed using a PC version of the QCPE DNMR6 program.⁶⁸ Electronic superimposition of the original and the simulated spectra enabled the determination of the most reliable rate constants at a few different temperatures. These constants provided the free energies of activation (ΔG^\ddagger) by means of the Eyring equation. Within the experimental uncertainty, the latter values were found essentially invariant in the examined temperature range, thus implying an almost negligible activation entropy ΔS^\ddagger .⁷⁰

4.6 References and Notes

¹ Wanka, L.; Iqbal, K.; Schreiner, P. R. *Chem. Rev.* **2013**, *113*, 3516.

² (a) Yu, Z.; Sawkar, A. R.; Whalen, L. J.; Wong, C.-H.; Kelly, J. W. *J. Med. Chem.* **2007**, *50*, 94; (b) Meisheri, K. D.; Humphrey, S. J.; Khan, S. A.; Cipkus-Dubray, L. A.; Smith, M. P.; Jones, A. W. *J. Pharmacol. Exp. Ther.* **1993**, *266*, 655; (c) Horvat, S.; Varga-Defterdarovic, L.; Horvat, J.; Jukic, R.; Kantoci, D.; Chung, N. N.; Schiller, P. W.; Biesert, L.; Pfutzner, A.; Suhartono, H.; Rubsamen-Waigmann, H. *J. Pept. Sci.* **1995**, *1*, 303; (d) Scherz, M. W.; Fialeix, M.; Fischer, J. B.; Reddy, N. L.; Server, A. C.; Sonders, M. S.; Tester, B. C.; Weber, E.; Wong, S. T.; Keana, J. F. W. *J. Med. Chem.* **1990**, *33*, 2421; (e) Kim, I.-H.; Morisseau, C.; Watanabe, T.; Hammock, B. D. *J. Med. Chem.* **2004**, *47*, 2110.; (f) Villhauer, E. B.; Brinkman, J. A.; Naderi, G. B.; Burkey, B. F.; Dunning, B. E.; Prasad, K.; Mangold, B. L.; Russell, M. E.; Hughes, T. E. *J. Med. Chem.* **2003**, *46*, 2774; (g) Wang, J.; Wu, Y.; Ma, C.; Fiorin, G.; Wang, J.; Pinto, L. H.; Lamb, R. A.; Klein, M. L.; Degrado, W. F. *Proc. Natl. Acad. Sci. U. S. A.* **2013**, *110*, 1315.

³ Some references that cover various research disciplines in our group are given. Dynamic NMR spectroscopy, physical organic chemistry, computational chemistry: (a) Lopez, S. C.; Faza, O. N.; De Proft, F.; Kolocouris, A. *J. Comp. Chem.* **2016**, *37*, 2647; (b) Kolocouris, A.; Zervos, N.; De Proft, F.; Koch, A. *J. Org. Chem.* **2011**, *76*, 4432; (c) Kolocouris, A.; Mikros, E.; Kolocouris, N. *J. Chem Soc., Perkin Trans. 2* **1998**, 1701; (d) Kolocouris, A. *Tetrahedron* **2009**, *65*, 9428-9435; (e) Kolocouris, A., Outeiriño, J. G.; Anderson, J. E.; Fytas, G.; Foscolos, G. B.; Kolocouris, N. *J. Org. Chem.* **2001**, *66*, 4989. Medicinal Chemistry (synthetic antivirals): (f) Kolocouris, N.; Foscolos, G. B.; Kolocouris, A.; Marakos, P.; Pouli, N.; Fytas, G.; Ikeda, S.; De Clercq, E. *J. Med. Chem.* **1994**, *37*, 2896. (g) Kolocouris, N.; Kolocouris, A.; Foscolos, G. B.; Fytas, G.; Neyts, J.; Padalko, E.; Balzarini, J.; Snoeck, R.; Andrei, G.; De Clercq, E. *J. Med. Chem.* **1996**, *39*, 3307. (h) Kolocouris, A.; Tzitzoglaki, C.; Johnson, F. B.; Zell, R.; Wright, A. K.; Cross, T. A.; Tietjen, I.; Fedida, D.; Busath, D. D. *J. Med. Chem.* **2014**, *57*, 4629. Drug-receptor interactions (solution NMR): (i) Kolocouris, A.; Zikos, C.; Broadhurst, R. W. *Bioorg. Med. Chem. Lett.* **2007**, *17*, 3947. Drug-receptor interactions (Computational medicinal chemistry, ITC): (g) Gueka, P.; Eleftheratos, S.; Kolocouris, A.; Cournia, Z. *J. Chem. Theory Comput.* **2013**, *9*, 1272; (k) Ioannidis, H.; Drakopoulos, A.; Tzitzoglaki, C.; Homeyer, N.; Kolarov, F.; Gkeka, P.; Freudenberger, K.; Liolios, C.; Gauglitz, G.; Cournia, Z.; Gohlke, H.; Kolocouris, A. *J. Chem. Inf. Model.* **2016**, *56*, 862. Drug-receptor interactions (Computational medicinal chemistry, ssNMR, ITC, electrophysiology) (l) Tzitzoglaki, C.; Wright, A.; Freudenberger, K.; Kolarov, F.; Tejen, I.; Fedida, D.; Gauglitz, G.; Cross, T.; Kolocouris, A. *J. Med. Chem.* **2017**, *60*, 1716. (m) Drakopoulos, A.; Tzitzoglaki, C.; Ma, C.; Freudenberger, K.; Hoffmann, A.; Hu, Y.; Gauglitz, G.; Schmidtke, M.; Wang, J.; Kolocouris, A. *ACS Med. Chem. Lett.* **2017**, *8*, 145. (n) Drakopoulos, A.; Tzitzoglaki, C.; Hoffmann, A.; Ma, C.; Freudenberger, K.; Hutterer, J.; Konstantinidi, A.; Kolocouris, D.; McGuire, K.; Hutterer, J.; Busath, D.; Gauglitz, G.; Schmidtke, M.; Wang, J.; Kolocouris, A. *ACS Med. Chem. Lett.* **2018**, <http://dx.doi.org/10.1021/acsmchemlett.7b00458>.

⁴ Wang, C.; Takeuchi, K.; Pinto, L. H.; Lamb, R. A. *J. Virol.* **1993**, *67*, 5585.

⁵ Chizhnikov, I. V.; Geraghty, F. M.; Ogden, D. C.; Hayhurst, A.; Antoniou, M.; Hay, A. J. *J. Physiol.* **1996**, *494*, 329.

⁶ Hayden, F. G. *Antiviral Res* **1985**, *Suppl 1*, 229.

- ⁷ Wang, J.; Qiu, J. X.; Soto, C.; DeGrado, W. F. *Curr. Opin. Struct. Biol.* **2011**, *21*, 68.
- ⁸ Hu, J.; Asbury, T.; Achuthan, S.; Li, C.; Bertram, R.; Quine, J. R.; Fu, R.; Cross, T. A. *Biophys. J.* **2007**, *92*, 4335.
- ⁹ Stouffer, A. L.; Acharya, R.; Salom, D.; Levine, A. S.; Di Costanzo, L.; Soto, C. S.; Tereshko, V.; Nanda, V.; Stayrook, S.; DeGrado, W. F. *Nature* **2008**, *451*, 596.
- ¹⁰ Cady, S. D.; Schmidt-Rohr, K.; Wang, J.; Soto, C. S.; DeGrado, W. F.; Hong, M. *Nature* **2010**, *463*, 689.
- ¹¹ Pielak, R. M.; Oxenoid, K.; Chou, J. J. *Structure* **2011**, *19*, 1655.
- ¹² Cady, S. D.; Wang, J.; Wu, Y.; DeGrado, W. F.; Hong, M. *J. Am. Chem. Soc.* **2011**, *133*, 4274.
- ¹³ Wang, J.; Ma, C.; Wang, J.; Jo, H.; Canturk, B.; Fiorin, G.; Pinto, L. H.; Lamb, R. A.; Klein, M. L.; DeGrado, W. F. *J. Med. Chem.* **2013**, *56*, 2804–2812.
- ¹⁴ Hu, W.; Zeng, S.; Li, C.; Jie, Y.; Li, Z.; Chen, L. *J. Med. Chem.* **2010**, *53*, 3831.
- ¹⁵ Wang, J.; Ma, C.; Balannik, V.; Pinto, L. H.; Lamb, R. A.; DeGrado, W. *ACS Med. Chem. Lett.* **2011**, *2*, 307.
- ¹⁶ Torres, E.; Fernández, R.; Miquet, S.; Font-Bardia, M.; Vanderlinden, E.; Naesens, L.; Vázquez, S. *ACS Med. Chem. Lett.* **2012**, *3*, 1065.
- ¹⁷ Wang, J.; Ma, C.; Fiorin, G.; Carnevale, V.; Wang, T.; Hu, F.; Lamb, R. A.; Pinto, L. H.; Hong, M.; Klein, M. L.; DeGrado, W. F. *J. Am. Chem. Soc.* **2011**, *133*, 12834.
- ¹⁸ Wang, J.; Ma, C.; Wang, J.; Jo, H.; Canturk, B.; Fiorin, G.; Pinto, L. H.; Lamb, R. A.; Klein, M. L.; DeGrado, W. F. *J. Med. Chem.* **2013**, *56*, 2804–2812.
- ¹⁹ Tomashenko, O.; Sokolov, V.; Tomashevskii, A.; Potekhin, A.; de Meijere, A. *Russian J. Org. Chem.* **2007**, *43*, 1421.
- ²⁰ Ritter, J. J.; Kalish, J. J. *J. Am. Chem. Soc.* **1948**, *70*, 4045, 4048.
- ²¹ (a) Sasaki, T.; Egushi, S.; Toi, N. *J. Org. Chem.* **1979**, *44*, 3711. (b) Kalir, A.; Balderman, D.; *Organic Syntheses* **1990**, Coll. Vol. 7, 433. (c) Setti, E. L.; Mascaretti, O. A. *J. Org. Chem.* **1986**, *51*, 3217; (d) Koziara, A.; Zwierzak, A. *Tetrahedron Lett.* **1987**, *28*, 6513. (e) Iranpoor, N.; Firouzabadi, H.; Akhlaghinia, B.; Nowrouzi, N. *Tetrahedron Lett.* **2004**, *45*, 3291. (f) Akhlaghinia, B.; Samiei, S. *J. Braz. Chem. Soc.* **2007**, *18*, 1311. (g) Kuroda, K.; Hayashi, Y.; Mukaiyama, T. *Tetrahedron* **2007**, *63*, 6358. For literature related to the preparation of azides from primary and secondary substrates see references in 21e,f.
- ²² Kolocouris, A.; Spearpoint, P.; Martin, S. R.; Hay, A. J.; Lopez-Querol, M.; Sureda, F. X.; Padalko, E.; Neyts, J. De Clercq, E. *Bioorg. Med. Chem. Lett.* **2008**, *18*, 6156.

- ²³ Fytas, G.; Kolocouris, N.; Foscolos, G. B.; Vamvakides, A *Eur. J. Med. Chem.* **1991**, *26*, 563.
- ²⁴ See for example: Abboud, M. J.-L.; Castano, O.; Della, E. W. Herreros, M.; Muller, P.; Notario, R.; Rossier, J.-C. *J. Am. Chem. Soc.* **1997**, *119*, 2262.
- ²⁵ See for example: (a) Smith, P. A. S. In *Molecular Rearrangements*; de Mayo, P., Ed.; Wiley: New York, 1963; Vol. 1, Chapter 8. (b) Bottaro, J. C.; Penwell, P. E.; Schmitt, R. J. *Synthetic Communications* **1997**, *27*, 1465. (c) Akimoto, R.; Tokugawa, T.; Yamamoto, Y.; Yamataka, H. *J. Org. Chem.* **2012**, *77*, 4073.
- ²⁶ Whitmore, F. C.; George, R. S. *J. Am. Chem. Soc.* **1942**, *64*, 1239.
- ²⁷ Richard, J. P.; Toteva, M. M.; Amyes, T. L. *Organic Letters* **2001**, *3*, 2225. It should be also noted that when ether ($\epsilon = 4.33$) was used as a solvent the starting alcohol was afforded.
- ²⁸ Toteva, M. M.; Richard, J. P. *J. Am. Chem. Soc.* **1996**, *118*, 11434.
- ²⁹ Abboud, J.-L. M.; Castano, O.; Della, E. W.; Herreros, M.; Muller, P.; Notario, R.; Rossier, J.-C. *J. Am. Chem. Soc.* **1997**, *119*, 2262.
- ³⁰ 6-31+G(d,p): Francl, M. M.; Pietro, W. J.; Hehre, W. J.; Binkley, J. S.; Gordon, M. S.; Defrees, D. J.; Pople, J. A. *J. Chem. Phys.* **1982**, *77*, 3654; MP2: Pople, J. A.; Binkley, J. S.; Seeger, R. *International Journal of Quantum Chemistry* **1976**, *10* (S10), 1; B3LYP: (a) Becke, A. D. *J. Chem. Phys.* **1993**, *98*, 5648. (b) Lee, C. T.; Yang, W. T.; Parr, R. G. *Phys. Rev. B* **1988**, *37*, 785.
- ³¹ Tomasi, J.; Menucci, B.; Cammi, R. *Chem. Rev.* **2005**, *105*, 2999.
- ³² Amantini, D.; Fringuelli, F.; Pizzo, F.; Vaccaro, L. *Organic Preparations and Procedures Int.* **2002**, *34*, 109.
- ³³ He, X.-S.; Raymon, L. P.; Mattson, M. V.; Eldefrawi, M. E.; de Costa, B. R. *J. Med. Chem.* **1993**, *36*, 1188.
- ³⁴ (a) Jung, M. E.; Shaw, T. J. *J. Am. Chem. Soc.* **1980**, *102*, 6304. (b) Goksu, S.; Secen, H. *Tetrahedron*, **2005**, *61*, 6801. (c) Radchenko, D. S.; Pavlenko, S. O.; Grygorenko, O. O.; Volochnyuk, D. M.; Shishkina, S. V.; Shishkin, O. V.; Komarov, I. V. *J. Org. Chem.* **2010**, *75*, 5941. (d) Bartra, M.; Romea, P.; Urpi, F.; Vilarrasa, J. *Tetrahedron Lett.* **1990**, *46*, 587.
- ³⁵ Gaoni, Y. *J. Org. Chem.* **1994**, *59*, 6853.
- ³⁶ See for example: (a) Lang, S.; Murphy, J. A. *Chem. Soc. Rev.* **2006**, *35*, 146-156. (b) Chen, C.-C.; McQuaid, M. J. *J. Am. Chem. Soc.* **1996**, *118*, 11434. (c) Brase, S.; Gil, C.; Knepper, K.; Zimmermann, V. *Angew. Chem. Int. Ed.* **2005**, *44*, 5188.
- ³⁷ Kamal, A.; Ramana, K. V.; Ankati, H. B.; Ramana, A. V. *Tetrahedron Lett.* **2002**, *43*, 6861.
- ³⁸ Kamal, A.; Rao, N. V.; Laxman, E. *Tetrahedron Lett.* **1997**, *38*, 6945.
- ³⁹ (a) Waser, J.; Gaspar, B.; Nambu, H. *J. Am. Chem. Soc.* **2006**, *128*, 11693. (b) Rao, H. S. P.; Siva, P. *Synth. Communications* **1994**, *24*, 549.

⁴⁰ (a) Vaultier, M.; Knouzi, N.; Carrie, R. *Tetrahedron Lett.* **1983**, *24*, 763. (b) Butcher, J. W.; Liverton, N. J.; Selnick, H. G.; Elliot, J. M.; Smith, G. R. *Tetrahedron Lett.* **1996**, *37*, 6685.

⁴¹ (a) Bartra, M.; Urpi, F.; Vilarrasa, J. *Tetrahedron Lett.* **1987**, *28*, 5941. (b) Bosch, I.; Costa, A. M.; Martin, M.; Urpi, F.; Vilarrasa, J. *Organic Lett.* **2000**, *2*, 397.

⁴² (a) Aldrich, P. E.; Hermann, E. C.; Meier, W. E.; Paulshock, M.; Prichard, W. W.; Snyder, J. A.; Watis, J. C. *J. Med. Chem.* **1971**, *14*, 535. (b) Martinez, A. G.; Vilar, E. T.; Fraile, A. G.; Cerero, S. de la Moya.; Herrero, M. E. R.; Ruiz, P. M.; Subramanian, L. R.; Gancedo, A. G. *J. Med. Chem.* **1995**, *38*, 4474. (c) Pigerol, C.; Vernieres, J.-C.; Broll, M.; Eymard, P.; Werbenec, J.-P. *Eur. J. Med. Chem.* **1977**, *12*, 351.

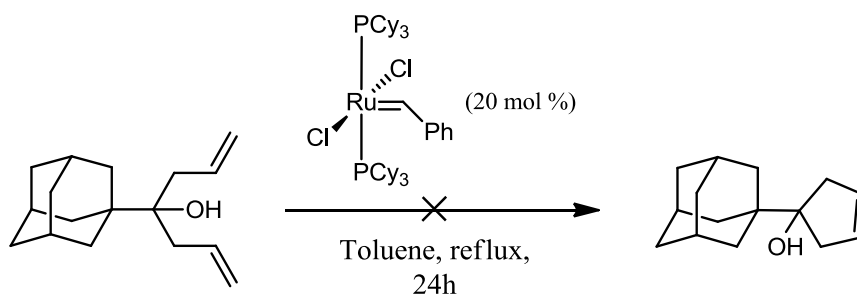
⁴³ (a) Smith, L. I.; Emerson, O. H. *Organic Syntheses*, **1955**, Coll. Vol. 3, 149. (b) Furman, F. M. US Patent 3,673,249, June 27, 1972.

⁴⁴ Jirgensons, A.; Kauss, V.; Kalvinsh, I.; Gold, M. R. *Synthesis* **2000**, 1709.

⁴⁵ See for example: Bishop, R.; Burgess, G. *Tetrahedron Lett.* **1987**, *28*, 1585.

⁴⁶ (a) Cogan, D. A.; Ellman, J. A. *J. Am. Chem. Soc.* **1999**, *121*, 268; McMahon, J. P.; Ellman, J. A. *Org. Letters* **2004**, *6*, 1645. (b) Liu, G.; Cogan, D. A.; Owens, T. D.; Tang, T. P.; Ellman, J. A. *J. Org. Chem.* **1999**, *64*, 1278.

⁴⁷ The reaction of the unsuccessful trial is described below. We did not attempt the cyclization using newer generation catalysts.



⁴⁸ (a) *Maestro*, version 8.5; Schrodinger, Inc.: New York, NY, **2008**. (b) *Maestro-Desmond Interoperability Tools*, version 3.1; Schrodinger: New York, NY, **2012**.

⁴⁹ (a) Halgren, T. A. *J. Comput. Chem.* **1996**, *17*, 616-641. (b) Halgren, T. A. MMFF VII. *J. Comp. Chem.* **1999**, *20*, 730.

⁵⁰ (a) Bertus, P.; Szymoniak, J. *Chem. Commun.* **2001**, 1792. (b) Bertus, P.; Szymoniak, J. Ti(II)- *J. Org. Chem.* **2002**, *67*, 3965. (c) Laroche, C.; Bertus, P.; Szymoniak, J. *Chem. Commun.* **2005**, 3030.

⁵¹ Wolan, A.; Six, Y. *Tetrahedron* **2010**, *66*, 15.

⁵² Bertus, P.; Szymoniak, J. *J. Org. Chem.* **2002**, *67*, 3965.

⁵³ (a) Tomashenko, O.; Sokolov, V.; Tomashevskiy, A.; de Meijere, A. *Synlett* **2007**, 652. (b) Henze, H. R.; Allen, B. B.; Leslie, W. B. *J. Am. Chem. Soc.* **1943**, *65*, 87

- ⁵⁴ Wang, R.; Gregg, B. T.; Zhang, W.; Golden, K. C.; Quinn, J. F.; Cui, P.; Tymoshenko, D. O. *Tetrahedron Lett.* **2009**, *50*, 7070.
- ⁵⁵ Tomashenko, O.; Rudenko, A.; Sokolov, V.; Tomashevskiy, A.; de Meijere, A. *Eur. J. Org. Chem.* **2010**, 1574.
- ⁵⁶ Ciganek, E. *J. Org. Chem.* **1992**, *57*, 4521.
- ⁵⁷ Fan, Z.; Shu, S.; Ni, J.; Yao, Q.; Zhang, A. *ACS Catal.* **2016**, *6*, 769.
- ⁵⁸ Wolan, A.; Six, Y. *Tetrahedron* **2010**, *66*, 3097.
- ⁵⁹ Eisch, J. J.; Gitua, J. N. *Eur. J. Inorg. Chem.* **2002**, *2002*, 3091.
- ⁶⁰ Sternhell, S. in *Dynamic Nuclear Magnetic Resonance Spectroscopy*; Jackman, L. M.; Cotton, F. A., Eds.; Academic Press: New York, 1975; Chapter 6, II.
- ⁶¹ Anderson, J. E.; Pearson, H.; Rawson, D. I. *J. Am. Chem. Soc.* **1985**, *107*, 1446.
- ⁶² Bushweller, C. H.; Anderson, W. G. *Tetrahedron Lett.* **1972**, *13*, 1811.
- ⁶³ Anderson, J. E.; Pearson, H. *Tetrahedron Lett.* **1972**, *13*, 2779.
- ⁶⁴ Anderson J. E., *Conformational Analysis of Acyclic and Alicyclic Saturated Hydrocarbons in The Chemistry of Alkanes and Cycloalkanes*, Patai, S; Rappoport, Z. Eds.; Wiley, Chichester, 1992, Chapter 3.II.D.
- ⁶⁵ Anderson, J. E.; de Meijere, A.; Kozhushkov, S. I.; Lunazzi, L.; Mazzanti, A. *J. Org. Chem.* **2003**, *68*, 8494.
- ⁶⁶ Casarini, D.; Coluccini, C.; Lunazzi, L.; Mazzanti, A.; Rompietti, R. *J. Org. Chem.* **2004**, *69*, 5746.
- ⁶⁷ Kozhushkov, S. I.; Yufit, D. S.; Boese, R.; Blaser, D.; Schreiner, P. R.; de Meijere, A. *Eur. J. Org. Chem.* **2005**, 1409.
- ⁶⁸ Brown, J.H.; Bushweller, C.H. *QCPE Bulletin*, **1983**, *3*, 103–103. A copy of the program is available on request from the authors (A.M.).
- ⁶⁹ (a) Anet, F. A. L.; Basus, V. J. *J. Magn. Reson.* **1978**, *32*, 339. (b) Okazawa, N.; Sorensen, T. S. *Can. J. Chem.* **1978**, *56*, 2737.
- ⁷⁰ This is usual in the majority of conformational processes investigated by DNMR. For a review see: Casarini, D.; Lunazzi, L.; Mazzanti, A. *Eur. J. Org. Chem.* **2010**, 2035.

4.7 Supporting Information

Detailed results of the thermochemistry calculations (SCF energies, SCF + ZPVE energies, enthalpies, free energies and cartesian coordinates for the optimized structures of the species included in the isodesmic reaction in Table 3).

Table S1. Calculated results for the species included in the isodesmic reaction $R_3CH + 1-Ad^+ \rightarrow R_3C^+ + Ad$ (R=Et, Pr, Bu) in 1,2-dichloroethane (DCE), dichloromethane (DCM) and chloroform (CFM) using PCM model as the continuous solvent model.

4-n-propyl-heptane	Solvent	SCF Energy	SCF Energy + zpve	Enthalpy	Entropy	Free Energy
	DCE	-247473.95	-247284.5753	-247275.3773	34.67177642	-247310.0491
	DCM	-247473.95	-247284.5602	-247275.3616	34.67114891	-247310.0327
	CFM	-247473.91	-247284.4522	-247275.2554	34.66738385	-247309.9228

5-n-butyl-nonane	Solvent	SCF Energy	SCF Energy + zpve	Enthalpy	Entropy	Free Energy
	DCE	-321490.21	-321247.5404	-321235.7357	41.78585039	-321277.5216
	DCM	-321490.20	-321247.5209	-321235.7162	41.78522288	-321277.5014
	CFM	-321490.1455	-321247.3847	-321235.5812	41.78459537	-321277.3658

adamantane	Solvent	SCF Energy	SCF Energy + zpve	Enthalpy	Entropy	Free Energy
	DCE	-245202.58	-245049.7712	-245044.8766	22.68697455	-245067.5636
	DCM	-245202.58	-245049.7613	-245044.8668	22.68634704	-245067.5531
	CFM	-245202.56	-245049.6924	-245044.7991	22.68446451	-245067.4835

Adamantane1-cation	Solvent	SCF Energy	SCF Energy + zpve	Enthalpy	Entropy	Free Energy
	DCE	-244683.99	-244539.1033	-244534.0073	24.45592352	-244558.4632
	DCM	-244683.28	-244538.5125	-244533.3957	24.49545661	-244557.8912
	CFM	-244678.65	-244533.9013	-244528.7808	24.50235922	-244553.2832

Tri n-propyl cation	Solvent	SCF Energy	SCF Energy + zpve	Enthalpy	Entropy	Free Energy
	DCE	-246955.13	-246772.81	-246763.64	34.5764	-246798.22
	DCM	-246954.50	-246772.16	-246763.00	34.5350	-246797.53
	CFM	-246949.79	-246767.33	-246758.21	34.3549	-246792.57

Tri n-butyl cation	Solvent	SCF Energy	SCF Energy + zpve	Enthalpy	Entropy	Free Energy
	DCE	-320972.37	-320737.95	-320726.25	40.6293	-320766.87
	DCM	-320971.70	-320737.26	-320725.57	40.5992	-320766.17
	CFM	-320966.76	-320732.23	-320720.57	40.4913	-320761.06

Example of a Gaussian program format used to run a representative calculation for 3-ethylpentane in chloroform

```
$RunGaus
%mem=12000Mb
%nproc=8
%chk=3_ethyl_pentane_chloroform.chk
# opt b3lyp/6-31+g(d,p) scrf=(iefpcm,solvent=chloroform)
```

3_ethyl_pentane_chloroform

0 1

--Link1--

```
%mem=12000Mb
%nproc=8
%chk=3_ethyl_pentane_chloroform.chk
#freq b3lyp/6-31+g(d,p) scrf=(iefpcm,solvent=chloroform)
guess=read geom=check
```

3_ethyl_pentane_chloroform

0 1

--Link1--

```
$RunGaus
%mem=12000Mb
%nproc=8
%chk=3_ethyl_pentane_chloroform.chk
#b3lyp/6-31+g(d,p) scrf=(iefpcm,solvent=chloroform)
POP=NBOREAD
guess=read geom=check
```

3_ethyl_pentane_chloroform

0 1

\$NBO BNDIDX \$END

--Link1--

%mem=12000Mb

%nproc=8

%chk=3_ethyl_pentane_chloroform.chk

#b3lyp/6-31+g(d,p) scrf=(iefpcm,solvent=chloroform)

Output=wfn

guess=read geom=check

3_ethyl_pentane_chloroform

0 1

3_ethyl_pentane_chloroform.wfn

Cartesian coordinates level of species optimized at the B3LYP/6-31+G ; species are included by the isodesmic reaction $R_3CH + 1-Ad^+ \rightarrow R_3C^+ + Ad$ (R=Et, Pr, Bu) in 1,2-dichloroethane (DCE), dichloromethane (DCM) and chloroform (CFM) using PCM model as the continuous solvent model.**

1-adamantane cation-DCE

1 1

C	0.637672	1.29647	1.122213
C	0.640062	1.300002	-0.50405
H	1.668962	1.351515	1.472194
C	1.460316	0.094449	-0.98463
C	-0.81502	1.213551	-0.98665
H	1.106148	2.247125	-0.78958
C	0.806831	-1.20667	-0.49758
H	1.496925	0.093732	-2.07997
H	2.494833	0.1639	-0.63254

Tert-alkyl amines analogues of amantadine

C	0.802274	-1.19501	1.128337
C	-0.64678	-1.31671	-0.97936
H	1.394651	-2.08502	-0.77824
C	0.000573	0.00385	1.343753
H	0.333768	-2.11394	1.482169
H	1.831025	-1.11161	1.48001
C	-1.43812	-0.0913	1.1264
H	0.052386	2.147348	1.472013
H	-1.99958	0.775992	1.475517
H	-1.88151	-1.02183	1.482143
H	-1.1041	-2.2457	-0.62292
H	-0.66443	-1.35458	-2.07452
H	-0.83599	1.242432	-2.08203
C	-1.44771	-0.09795	-0.49951
H	-1.39198	2.075523	-0.63579
H	-2.50169	-0.16895	-0.78196

1-adamantane cation-DCM

1 1

C	-1.12221	-0.89533	1.132329
C	-1.14184	-0.89876	-0.49333
H	-2.07354	-0.5024	1.492225
C	-1.3677	0.541524	-0.97395
C	0.204641	-1.4482	-0.98569
H	-1.97252	-1.55358	-0.77084
C	-0.2134	1.435558	-0.4989
H	-1.41185	0.555776	-2.06888
H	-2.32837	0.923959	-0.61315
C	-0.20138	1.425976	1.127203
C	1.142164	0.907672	-0.99077
H	-0.36798	2.480879	-0.78037
C	0.009522	-0.00043	1.343565
H	0.619046	2.054986	1.474497
H	-1.16387	1.793375	1.484818

Tert-alkyl amines analogues of amantadine

C	1.347796	-0.53201	1.117589
H	-0.95438	-1.91481	1.480935
H	1.486731	-1.55506	1.468374
H	2.150805	0.120328	1.461762
H	1.957726	1.54985	-0.64199
H	1.165471	0.932057	-2.08624
H	0.203018	-1.48483	-2.08107
C	1.344043	-0.53607	-0.50934
H	0.356147	-2.47403	-0.63384
H	2.323723	-0.9262	-0.79853

1-adamantane cation-CMF

1 1

C	-0.21545	1.42355	1.127981
C	-0.21924	1.434797	-0.49832
H	0.599615	2.056968	1.479989
C	1.141827	0.916075	-0.98389
C	-1.36542	0.534387	-0.98084
H	-0.37873	2.479501	-0.77962
C	1.350668	-0.52705	-0.50273
H	1.169824	0.941164	-2.07919
H	1.951978	1.563419	-0.63196
C	1.344693	-0.52604	1.12343
C	0.219347	-1.44573	-0.98604
H	2.334111	-0.91105	-0.78788
C	0.001695	-0.0025	1.344061
H	1.488648	-1.54864	1.47413
H	2.141829	0.129817	1.475042
C	-1.12442	-0.90273	1.126226
H	-1.18093	1.786481	1.482014
H	-2.0804	-0.51476	1.479415
H	-0.95565	-1.92201	1.475391
H	0.375666	-2.47126	-0.63551
H	0.22385	-1.48181	-2.08147

Tert-alkyl amines analogues of amantadine

H	-1.4032	0.550409	-2.07601
C	-1.13324	-0.90538	-0.5007
H	-2.33087	0.910566	-0.62602
H	-1.95845	-1.565	-0.78338

Adamantane DCE

0 1

C	0	1.781806	0
C	0.893024	0.893024	0.893024
H	-0.62427	2.435782	0.624265
C	0	0	1.781806
C	1.781806	0	0
H	1.526924	1.526924	1.526924
C	-0.89302	-0.89302	0.893024
H	0.624265	-0.62427	2.435782
H	-0.62427	0.624265	2.435782
C	-1.78181	0	0
C	0	-1.78181	0
H	-1.52692	-1.52692	1.526924
C	-0.89302	0.893024	-0.89302
H	-2.43578	-0.62427	-0.62427
H	-2.43578	0.624265	0.624265
C	0	0	-1.78181
H	-1.52692	1.526924	-1.52692
H	0.624265	2.435782	-0.62427
H	0.624265	0.624265	-2.43578
H	-0.62427	-0.62427	-2.43578
H	-0.62427	-2.43578	-0.62427
H	0.624265	-2.43578	0.624265
H	2.435782	-0.62427	0.624265
C	0.893024	-0.89302	-0.89302
H	2.435782	0.624265	-0.62427
H	1.526924	-1.52692	-1.52692

Adamantane DCM

0 1

C	0	1.781804	0
C	0.893024	0.893024	0.893024
H	-0.62425	2.435799	0.624254
C	0	0	1.781804
C	1.781804	0	0
H	1.526924	1.526924	1.526924
C	-0.89302	-0.89302	0.893024
H	0.624254	-0.62425	2.435799
H	-0.62425	0.624254	2.435799
C	-1.7818	0	0
C	0	-1.7818	0
H	-1.52692	-1.52692	1.526924
C	-0.89302	0.893024	-0.89302
H	-2.4358	-0.62425	-0.62425
H	-2.4358	0.624254	0.624254
C	0	0	-1.7818
H	-1.52692	1.526924	-1.52692
H	0.624254	2.435799	-0.62425
H	0.624254	0.624254	-2.4358
H	-0.62425	-0.62425	-2.4358
H	-0.62425	-2.4358	-0.62425
H	0.624254	-2.4358	0.624254
H	2.435799	-0.62425	0.624254
C	0.893024	-0.89302	-0.89302
H	2.435799	0.624254	-0.62425
H	1.526924	-1.52692	-1.52692

Adamantane CFM

0 1

C	0	1.78179	0
C	0.893024	0.893024	0.893024
H	-0.62418	2.435913	0.624181

Tert-alkyl amines analogues of amantadine

C	0	0	1.78179
C	1.78179	0	0
H	1.526918	1.526918	1.526918
C	-0.89302	-0.89302	0.893024
H	0.624181	-0.62418	2.435913
H	-0.62418	0.624181	2.435913
C	-1.78179	0	0
C	0	-1.78179	0
H	-1.52692	-1.52692	1.526918
C	-0.89302	0.893024	-0.89302
H	-2.43591	-0.62418	-0.62418
H	-2.43591	0.624181	0.624181
C	0	0	-1.78179
H	-1.52692	1.526918	-1.52692
H	0.624181	2.435913	-0.62418
H	0.624181	0.624181	-2.43591
H	-0.62418	-0.62418	-2.43591
H	-0.62418	-2.43591	-0.62418
H	0.624181	-2.43591	0.624181
H	2.435913	-0.62418	0.624181
C	0.893024	-0.89302	-0.89302
H	2.435913	0.624181	-0.62418
H	1.526918	-1.52692	-1.52692

Tripropylcation DCE

1 1

C	-0.0693	-0.03906	0.149056
C	0.970347	-1.06126	-0.07011
C	-1.3848	-0.21802	-0.47302
C	0.155197	1.093323	1.054553
H	-1.94945	0.71666	-0.4921
H	-1.29256	-0.63523	-1.47996
C	-2.21087	-1.25355	0.398949
C	2.453433	-0.6249	-0.12076

Tert-alkyl amines analogues of amantadine

H	0.844603	-1.70128	0.829715
H	0.714794	-1.6944	-0.92477
C	0.692358	2.363763	0.264038
H	-0.78405	1.385923	1.534447
H	0.903237	0.847318	1.811205
C	-3.62027	-1.4132	-0.17426
H	-1.68589	-2.21257	0.401067
H	-2.25819	-0.89471	1.431363
C	3.380186	-1.84041	-0.22282
H	2.598449	0.023013	-0.99142
H	2.709622	-0.04033	0.767717
H	4.422494	-1.51483	-0.28751
H	3.282583	-2.49022	0.653478
H	3.158902	-2.43651	-1.11448
H	-4.17681	-2.13616	0.43064
H	-4.16735	-0.4656	-0.15914
H	-3.59268	-1.78097	-1.20452
H	0.975027	3.057225	1.06131
H	1.609988	2.098404	-0.2657
C	-0.30768	3.029717	-0.67828
H	0.123576	3.963941	-1.05187
H	-0.54612	2.412285	-1.5491
H	-1.24181	3.279638	-0.16439

Tripropylation DCM

1 1

C	-0.06975	-0.03864	0.148671
C	0.969354	-1.06134	-0.07131
C	-1.38555	-0.21654	-0.47298
C	0.15558	1.093295	1.054474
H	-1.94979	0.718391	-0.49125
H	-1.29434	-0.63344	-1.48017
C	-2.21156	-1.25212	0.399241
C	2.452932	-0.6264	-0.12061

Tert-alkyl amines analogues of amantadine

H	0.842746	-1.7026	0.82754
H	0.713686	-1.69327	-0.92683
C	0.694545	2.363093	0.263896
H	-0.78346	1.387096	1.534066
H	0.903152	0.846565	1.81138
C	-3.62078	-1.41252	-0.17422
H	-1.68626	-2.21098	0.402007
H	-2.25926	-0.89273	1.43147
C	3.378563	-1.8428	-0.2222
H	2.599391	0.021714	-0.99088
H	2.708919	-0.04228	0.768242
H	4.421156	-1.51823	-0.28688
H	3.280283	-2.49223	0.654295
H	3.156906	-2.439	-1.11368
H	-4.17734	-2.13488	0.431357
H	-4.16807	-0.46503	-0.16022
H	-3.59297	-1.78144	-1.20405
H	0.978558	3.055976	1.061196
H	1.61161	2.096373	-0.26612
C	-0.30489	3.030639	-0.6779
H	0.127808	3.963944	-1.05203
H	-0.54516	2.413517	-1.54845
H	-1.2382	3.282489	-0.16345

Tripropylation CFM

1 1

C	-0.07181	-0.03839	0.147385
C	0.966929	-1.06219	-0.0725
C	-1.38657	-0.21403	-0.47641
C	0.152909	1.091627	1.055409
H	-1.95002	0.721402	-0.49589
H	-1.29675	-0.63285	-1.48298

Tert-alkyl amines analogues of amantadine

C	-2.21365	-1.24812	0.398302
C	2.451762	-0.62992	-0.11733
H	0.838155	-1.70662	0.823779
H	0.712375	-1.69179	-0.93025
C	0.699861	2.36036	0.266647
H	-0.78702	1.389381	1.530858
H	0.896937	0.843159	1.815432
C	-3.62423	-1.40622	-0.17281
H	-1.68976	-2.20792	0.400592
H	-2.25899	-0.88824	1.430605
C	3.375084	-1.8477	-0.22261
H	2.601453	0.022199	-0.98409
H	2.706854	-0.05017	0.774738
H	4.418291	-1.52501	-0.28388
H	3.274513	-2.50089	0.650791
H	3.154588	-2.43971	-1.11709
H	-4.18056	-2.12749	0.434075
H	-4.17047	-0.4582	-0.15791
H	-3.59941	-1.7758	-1.20238
H	0.982287	3.052107	1.065547
H	1.61901	2.090603	-0.2582
C	-0.29305	3.031209	-0.67957
H	0.143743	3.963888	-1.0502
H	-0.53032	2.416542	-1.55274
H	-1.22832	3.285657	-0.16993

Tri-n-butyl cation DCE

1 1

C	-0.09311	-0.14241	0.306147
C	-1.3479	0.545709	-0.03391
C	1.179101	0.60228	0.281538
C	-0.11374	-1.55344	0.717467
H	1.80236	0.071487	-0.46105

Tert-alkyl amines analogues of amantadine

C	1.187619	2.109506	0.016014
H	1.698166	0.363604	1.22485
C	-2.68879	-0.18293	0.072041
H	-1.35591	1.488846	0.537721
H	-1.17945	0.91529	-1.0651
C	1.169867	-2.39379	0.74933
H	-0.52583	-1.44748	1.746385
H	-0.92523	-2.07364	0.194247
H	0.972697	-3.25245	1.400025
C	1.598907	-2.91135	-0.63478
H	1.990569	-1.84216	1.220573
C	2.854723	-3.78641	-0.56318
H	0.77242	-3.48753	-1.06977
H	1.779929	-2.07238	-1.31923
H	3.133618	-4.15303	-1.5561
H	3.70609	-3.22576	-0.16089
H	2.691838	-4.65698	0.08226
C	2.616113	2.674771	0.02273
H	0.718915	2.326192	-0.95135
H	0.59324	2.624107	0.781328
C	2.651629	4.18506	-0.2316
H	3.088814	2.453149	0.988598
H	3.213131	2.159134	-0.7409
H	3.679981	4.559785	-0.22071
H	2.21541	4.432837	-1.20611
H	2.089001	4.729401	0.53552
C	-3.86051	0.733864	-0.30999
H	-2.69405	-1.0615	-0.58438
H	-2.83182	-0.54782	1.096572
C	-5.21562	0.026318	-0.21201
H	-3.85845	1.61714	0.342171
H	-3.71024	1.10302	-1.33296
H	-6.03104	0.701861	-0.4891
H	-5.25856	-0.84181	-0.87973

Tert-alkyl amines analogues of amantadine

H	-5.40539	-0.32638	0.808302
---	----------	----------	----------

Tri-n-butyl cation DCM

1 1

C	-0.09308	-0.14224	0.305606
C	-1.34781	0.546166	-0.03419
C	1.179299	0.60215	0.280587
C	-0.11406	-1.55319	0.717185
H	1.801728	0.071525	-0.46292
C	1.18824	2.109568	0.016104
H	1.699443	0.362523	1.223064
C	-2.68873	-0.18246	0.071158
H	-1.35561	1.488693	0.538632
H	-1.17957	0.917493	-1.06478
C	1.169338	-2.39393	0.749502
H	-0.52664	-1.447	1.745932
H	-0.9256	-2.07328	0.193832
H	0.972079	-3.25203	1.400878
C	1.597817	-2.91259	-0.63436
H	1.990381	-1.84226	1.220126
C	2.853697	-3.78751	-0.56267
H	0.771201	-3.48921	-1.06853
H	1.778442	-2.07415	-1.31963
H	3.132137	-4.15483	-1.55543
H	3.705242	-3.22661	-0.16116
H	2.691144	-4.65765	0.083409
C	2.61694	2.674394	0.022487
H	0.719059	2.327282	-0.9508
H	0.594386	2.623804	0.782101
C	2.652854	4.184784	-0.23107
H	3.089977	2.452128	0.988046
H	3.213496	2.158941	-0.74163
H	3.681351	4.559026	-0.22055
H	2.21626	4.433313	-1.20521

Tert-alkyl amines analogues of amantadine

H	2.090964	4.728996	0.53666
C	-3.86054	0.734769	-0.30954
H	-2.69415	-1.06028	-0.58633
H	-2.83159	-0.54869	1.095253
C	-5.21565	0.027299	-0.21137
H	-3.85803	1.617603	0.343223
H	-3.71069	1.104641	-1.3323
H	-6.03107	0.703107	-0.48771
H	-5.25906	-0.84039	-0.87961
H	-5.40508	-0.32596	0.808796

Tri-n-butyl cation CFM

1 1

C	-0.09335	-0.14103	0.304274
C	-1.34767	0.548901	-0.03484
C	1.180418	0.600972	0.276896
C	-0.11653	-1.55173	0.717546
H	1.79966	0.068978	-0.46881
C	1.193701	2.108778	0.014216
H	1.704491	0.358094	1.216546
C	-2.68987	-0.17752	0.071423
H	-1.35316	1.491494	0.538482
H	-1.18139	0.923055	-1.06487
C	1.165299	-2.39512	0.750155
H	-0.53002	-1.4446	1.746043
H	-0.92972	-2.07063	0.195095
H	0.967546	-3.25156	1.403418
C	1.590911	-2.91735	-0.63339
H	1.988379	-1.84462	1.218754
C	2.843665	-3.79661	-0.56147
H	0.762051	-3.49181	-1.06614
H	1.773928	-2.08049	-1.3204
H	3.12083	-4.16453	-1.55413
H	3.697283	-3.23926	-0.15967

Tert-alkyl amines analogues of amantadine

H	2.677903	-4.66642	0.083937
C	2.624106	2.669922	0.021894
H	0.725559	2.32945	-0.95258
H	0.600633	2.623946	0.780355
C	2.664444	4.180584	-0.22871
H	3.096502	2.444316	0.987015
H	3.219361	2.154306	-0.74316
H	3.69402	4.551147	-0.21694
H	2.229657	4.432712	-1.20263
H	2.104473	4.725434	0.539818
C	-3.86056	0.741884	-0.30795
H	-2.69744	-1.05514	-0.58653
H	-2.83245	-0.54451	1.095389
C	-5.21659	0.036282	-0.21104
H	-3.85676	1.623994	0.345819
H	-3.70957	1.112907	-1.33011
H	-6.03032	0.713417	-0.48819
H	-5.26112	-0.83108	-0.87946
H	-5.40819	-0.31645	0.808833

4-n-propyl-heptane-DCE

0 1

C	0.20492	-0.00465	0.592223
H	0.429043	0.357282	1.608794
C	-0.83658	-1.13703	0.76458
C	-0.32918	1.20453	-0.20839
C	1.531168	-0.53994	0.00544
C	-1.35989	-1.79164	-0.52378
H	-0.38733	-1.91784	1.395202
H	-1.69393	-0.7536	1.333888
H	-0.52459	0.899855	-1.24682
C	-1.5872	1.872659	0.365631
H	0.461258	1.964074	-0.26519

Tert-alkyl amines analogues of amantadine

C	-2.37362	-2.90827	-0.24262
H	-1.83001	-1.03391	-1.16372
H	-0.52261	-2.20405	-1.10109
H	-2.73639	-3.36332	-1.17106
H	-1.92711	-3.70375	0.366396
H	-3.24397	-2.52375	0.302808
C	-1.98194	3.145324	-0.39434
H	-2.42967	1.170204	0.346946
H	-1.41568	2.117592	1.42345
H	-2.88427	3.600962	0.028568
H	-1.18093	3.893511	-0.35716
H	-2.18282	2.928009	-1.45052
H	1.398942	-0.76544	-1.06253
C	2.743022	0.389562	0.174136
H	1.765042	-1.49828	0.491733
C	4.04523	-0.22707	-0.35143
H	2.565026	1.340836	-0.34247
H	2.860263	0.63552	1.239093
H	4.893168	0.453469	-0.21542
H	4.280368	-1.16192	0.171737
H	3.97055	-0.45633	-1.42134

4-n-propyl-heptane-DCM

0 1

C	0.204926	-0.00466	0.592252
H	0.429039	0.357254	1.608832
C	-0.83659	-1.13703	0.764587
C	-0.32913	1.204541	-0.20835
C	1.531173	-0.53996	0.005477
C	-1.35991	-1.79161	-0.52378
H	-0.38738	-1.91785	1.39521
H	-1.69392	-0.7536	1.333926

Tert-alkyl amines analogues of amantadine

H	-0.52443	0.899921	-1.24682
C	-1.58722	1.872627	0.36559
H	0.461288	1.964102	-0.26506
C	-2.37366	-2.90823	-0.24265
H	-1.83001	-1.03386	-1.16373
H	-0.52265	-2.20401	-1.1011
H	-2.73644	-3.36325	-1.17109
H	-1.92719	-3.70373	0.366351
H	-3.24401	-2.52373	0.30279
C	-1.9819	3.145337	-0.39433
H	-2.42969	1.170167	0.346794
H	-1.41581	2.117483	1.423446
H	-2.88428	3.600931	0.028507
H	-1.18093	3.893548	-0.35702
H	-2.18266	2.928123	-1.45055
H	1.398932	-0.76554	-1.06247
C	2.743024	0.389558	0.174083
H	1.765067	-1.49828	0.491804
C	4.045236	-0.22711	-0.35142
H	2.565021	1.340783	-0.34261
H	2.860265	0.63564	1.239011
H	4.893168	0.453444	-0.21548
H	4.280401	-1.16191	0.171816
H	3.970579	-0.45648	-1.4213

4-n-propyl-heptane-CFM

0 1

C	-2.37392	-2.90797	-0.24283
C	-1.36004	-1.79145	-0.52377
C	-0.83668	-1.13699	0.764626
C	0.204968	-0.00472	0.592417
C	1.531204	-0.54008	0.005689
C	2.743038	0.38955	0.173747
C	4.045283	-0.22733	-0.35135

Tert-alkyl amines analogues of amantadine

C	-0.32889	1.204614	-0.2081
C	-1.58734	1.872426	0.365332
C	-1.9817	3.145409	-0.39425
H	0.42902	0.357085	1.609056
H	-0.38768	-1.91789	1.395288
H	-1.69388	-0.7536	1.334159
H	-0.52346	0.900341	-1.24681
H	0.461454	1.964284	-0.2643
H	-1.82996	-1.03363	-1.16381
H	-0.52283	-2.20388	-1.10114
H	-2.73672	-3.36289	-1.17127
H	-1.92769	-3.70361	0.366122
H	-3.24431	-2.52363	0.302639
H	-2.42978	1.169925	0.345851
H	-1.4167	2.116787	1.423422
H	-2.8844	3.600721	0.02813
H	-1.18095	3.893792	-0.35613
H	-2.18168	2.928849	-1.45073
H	1.398871	-0.76613	-1.06214
H	1.765226	-1.49828	0.492192
H	2.564999	1.340465	-0.3435
H	2.86026	0.636422	1.238498
H	4.893177	0.453317	-0.21584
H	4.280639	-1.16179	0.172349
H	3.970799	-0.45742	-1.42107

5_nButyl_nonane-DCE

0 1

C	3.802276	-1.46243	-0.511
C	2.601864	-0.94539	0.29456
H	3.839145	-0.94075	-1.47764
H	3.650417	-2.52571	-0.74338
C	5.14153	-1.2853	0.214143
H	5.14715	-1.82229	1.170404

Tert-alkyl amines analogues of amantadine

H	5.975517	-1.6655	-0.38622
H	5.338981	-0.22775	0.427173
H	2.556571	-1.47905	1.255747
H	2.771388	0.111732	0.538855
C	1.265202	-1.11093	-0.44223
C	0.001499	-0.75181	0.371425
H	1.288016	-0.51828	-1.36793
H	1.172878	-2.15897	-0.76137
C	-1.26177	-1.11364	-0.44172
H	0.002415	-1.39933	1.263288
C	0.000051	0.704254	0.897929
C	-2.59867	-0.94921	0.294836
H	-1.2854	-0.522	-1.36805
H	-1.16794	-2.16189	-0.75974
C	-3.79837	-1.46835	-0.51048
H	-2.55284	-1.48208	1.256434
H	-2.76956	0.107883	0.538302
C	-5.13794	-1.29223	0.214293
H	-3.83569	-0.94746	-1.47754
H	-3.64519	-2.53162	-0.74201
H	-5.97133	-1.67424	-0.38574
H	-5.14295	-1.82816	1.171154
H	-5.33686	-0.23471	0.426112
H	-0.87202	0.840047	1.550949
H	0.873828	0.842856	1.548052
C	-0.00355	1.815089	-0.16329
C	-0.00312	3.223946	0.44761
H	0.872945	1.713911	-0.818
H	-0.88332	1.712442	-0.81333
C	-0.00825	4.341372	-0.60204
H	-0.87933	3.334022	1.101834
H	0.877421	3.336202	1.095598
H	-0.00755	5.331626	-0.13295
H	0.874187	4.279387	-1.25045

Tert-alkyl amines analogues of amantadine

H	-0.89542	4.277482	-1.24378
---	----------	----------	----------

5_nButyl_nonane_DCM

0 1

C	3.802265	-1.4625	-0.51097
C	2.601854	-0.94537	0.294536
H	3.839147	-0.94092	-1.47767
H	3.650385	-2.52578	-0.74328
C	5.141517	-1.28534	0.214164
H	5.147146	-1.82225	1.170465
H	5.975502	-1.66558	-0.38616
H	5.339009	-0.22778	0.427139
H	2.55655	-1.47893	1.255778
H	2.771402	0.111763	0.538778
C	1.265191	-1.11093	-0.44224
C	0.00149	-0.7518	0.371409
H	1.287983	-0.51834	-1.36798
H	1.172874	-2.15897	-0.76138
C	-1.26178	-1.11363	-0.44174
H	0.002401	-1.3993	1.263283
C	0.00005	0.704259	0.897921
C	-2.59868	-0.94917	0.294811
H	-1.28538	-0.52205	-1.3681
H	-1.16796	-2.16188	-0.75976
C	-3.79838	-1.46838	-0.51046
H	-2.55285	-1.48194	1.256461
H	-2.76958	0.107937	0.538228
C	-5.13794	-1.29223	0.214314
H	-3.83572	-0.94759	-1.47757
H	-3.64519	-2.53166	-0.74192
H	-5.97134	-1.67428	-0.38568
H	-5.14297	-1.82808	1.171213
H	-5.3369	-0.2347	0.426079
H	-0.87201	0.840052	1.550955

Tert-alkyl amines analogues of amantadine

H	0.873803	0.842845	1.548076
C	-0.00352	1.815102	-0.16329
C	-0.0031	3.223964	0.447602
H	0.872959	1.713919	-0.81801
H	-0.88327	1.712458	-0.81337
C	-0.0082	4.341389	-0.60204
H	-0.87931	3.334051	1.10183
H	0.877408	3.336217	1.095632
H	-0.0075	5.331642	-0.13296
H	0.874239	4.279422	-1.25045
H	-0.89534	4.277528	-1.24381

5_nButyl_nonane-CFM

0 1

C	3.802203	-1.46286	-0.5108
C	2.601797	-0.94526	0.294412
H	3.839124	-0.94193	-1.47784
H	3.650211	-2.5262	-0.74275
C	5.141448	-1.28553	0.214247
H	5.147193	-1.82197	1.170784
H	5.975416	-1.66606	-0.38587
H	5.339195	-0.22797	0.426885
H	2.556453	-1.47821	1.255986
H	2.771472	0.111936	0.538351
C	1.265112	-1.11099	-0.44227
C	0.001432	-0.75176	0.37135
H	1.287762	-0.51877	-1.36824
H	1.172849	-2.15903	-0.76141
C	-1.26184	-1.11359	-0.44179
H	0.00231	-1.39918	1.263298
C	0.000048	0.704271	0.897902
C	-2.59875	-0.94891	0.294679
H	-1.28527	-0.52235	-1.36836
H	-1.16813	-2.16182	-0.75984

Tert-alkyl amines analogues of amantadine

C	-3.79847	-1.46851	-0.51031
H	-2.5529	-1.48112	1.256643
H	-2.76972	0.108258	0.537829
C	-5.13802	-1.29214	0.214388
H	-3.83583	-0.94833	-1.47774
H	-3.64523	-2.53184	-0.74145
H	-5.97142	-1.67443	-0.3854
H	-5.14318	-1.82754	1.171514
H	-5.33719	-0.23461	0.425838
H	-0.87192	0.840074	1.55103
H	0.873643	0.842758	1.548265
C	-0.00339	1.815151	-0.16327
C	-0.00298	3.224053	0.447544
H	0.873041	1.713927	-0.81807
H	-0.88296	1.712529	-0.8136
C	-0.00788	4.341459	-0.60208
H	-0.87913	3.334223	1.101807
H	0.877333	3.3363	1.095839
H	-0.0072	5.331709	-0.13306
H	0.874567	4.279599	-1.25046
H	-0.89485	4.277786	-1.24407

CHAPTER 5

Discovery of resistance-breaking inhibitors targeting the M2 proton channel of influenza A viruses

5.1 Abstract

Influenza virus infections lead to numerous deaths and millions of hospitalizations each year. One challenge facing anti-influenza drug development is the heterogeneity of the circulating influenza viruses, which comprise several strains with variable susceptibility to antiviral drugs. For example, the wild-type (WT) influenza A viruses, such as the seasonal H1N1, tend to be sensitive to antiviral drugs, amantadine and rimantadine, while the S31N mutant viruses, such as the pandemic 2009 H1N1 (H1N1pdm09) and seasonal H3N2, as well as L26F, V27A, A30T, G34E are resistant to this class of drugs. We report here lead compounds that represent resistance-breaking inhibitors with good antiviral potencies against WT, S31N, L26F and at the same time moderate potencies against V27A, A30T, G34E. Electrophysiology and molecular dynamics (MD) simulations of drug-M2 interactions supported the potency of the compounds against WT and S31N M2. Namely, the dual inhibitor binds in the WT M2 channel with an aromatic group facing down toward the C-terminus, while the same drug binds in the S31N M2 channel with its aromatic group facing up toward the N-terminus.

5.2 Introduction

Amantadine **1** and rimantadine **2** (Scheme 1) are blockers of proton transport by viral ion channels,^{1,2} and approved as prophylactics and therapeutics against influenza A viruses (IAV).³ The primary binding site of **1** and **2** is the transmembrane domain lumen (TM, amino acids 22-46) in the four-helix bundle of tetrameric M2, that forms the proton transport path.^{1,4} According to high resolution structures from X-ray and solid state NMR (ssNMR) experiments the M2TM protein channel is blocked by **1** and **2** via a pore-binding mechanism.^{5,6,7,8,9,10,11} The adamantyl cage in these molecules is tightly contacted on all sides by V27 and A30 side chains, producing a steric occlusion of proton transport^{6,7,8,9} and thereby preventing the continuation of the viral life cycle. The ssNMR results also demonstrated that the ammonium group of the drug is pointing towards the four H37 residues at the C-end (Figure 1).⁹ This orientation can be stabilized only through hydrogen bonds with water molecules in the channel lumen between the imidazoles of H37 and the ligand and possibly with A30 carbonyls in the vicinity according to experimental and MD simulations data.^{9,12,13,14,15,16,17,18} Provided that M2TM is a minimal model for M2 binding¹⁰, these high resolution structures can be used for the prediction of new ligands binding more effectively to the M2TM pore for example through MD simulations or more precisely by free energy calculations^{19,20,21}

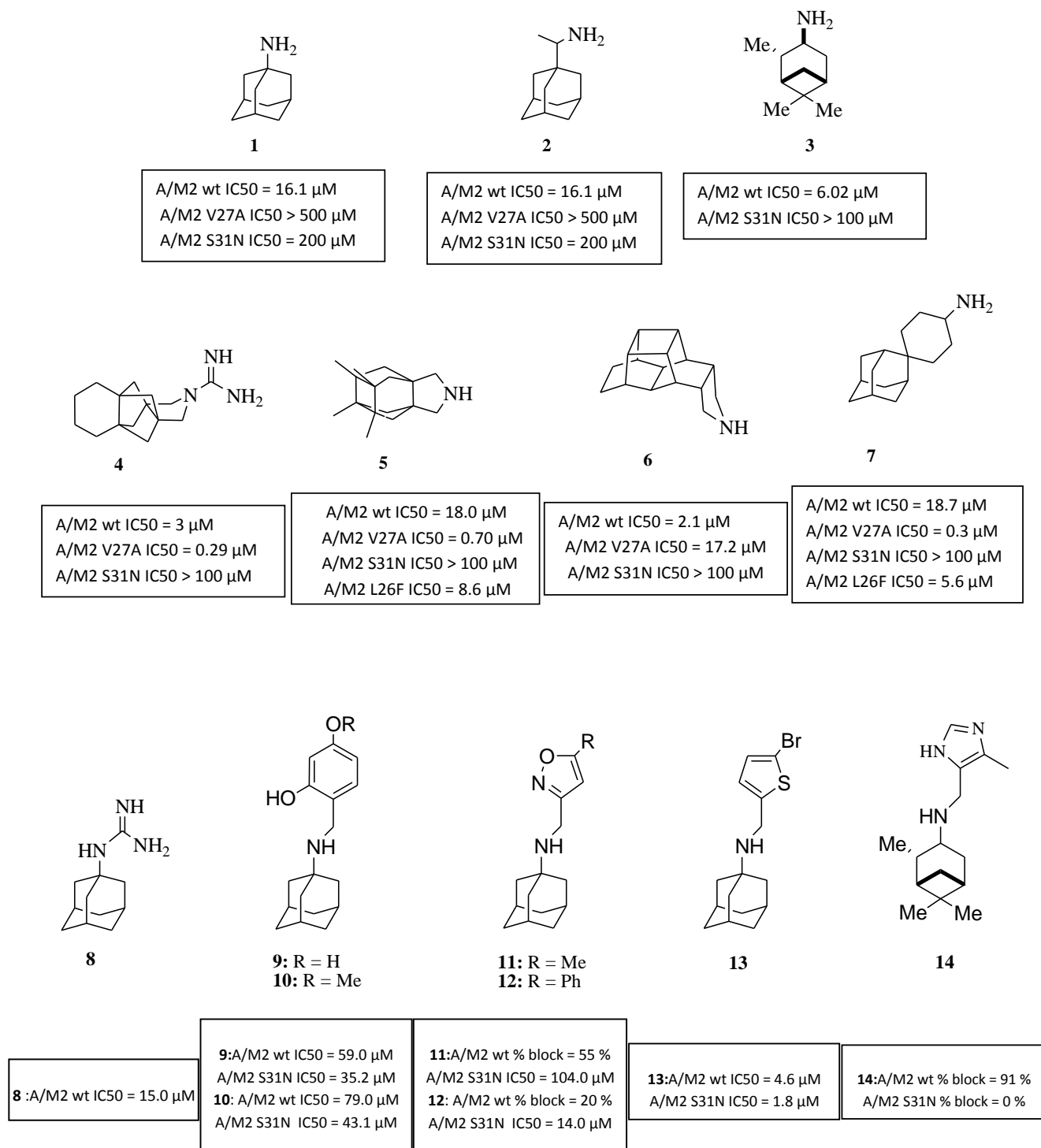
Resistance to M2 WT proton channel drugs is associated with mutations in the transmembrane domain of the M2 protein. The homotetrameric structure of the M2 channel places constraints on the types of drug-resistant mutations that can be accommodated.²² Amino acid substitution L26F, V27A, A30T, G34E and S31N were shown to confer cross-resistance to **1** and **2** demonstrating their impact for inhibitor binding in IAV.^{23,24,25,26,27} The vast majority, 95%, of resistant viruses bear the S31N substitution in M2, 1% have V27A, and L26F, A30T, and G34E are rare.^{28,29} The substitution V27A most often emerged under drug selection pressure.^{24,25} The other mutations confer amantadine resistance but this is not a result of the amantadine drug selection pressure.²⁴ The M2 S31N mutant is a natural mutation and one of the most conserved viral proteins among currently circulating influenza A viruses that happens to maintain nearly identical channel function as the M2 WT but is resistant to amantadine. The presence of L26F, V27A, and particularly S31N in IAV circulating worldwide pushed the search for novel ion channel blockers with stronger, preferably resistance-overcoming activity.

Few polycyclic amines^{30,31} from Vazquez group were dual M2 WT as well as V27A inhibitors, see for example compounds **4-6** in Scheme 1. A 7,8,9,10-tetramethyl-3-azapentacyclotridecane³⁰ was found to be active against WT, V27A, and L26F mutant viruses, see compound **5** in Scheme 1. Between the aminoadamantane analogues synthesized by DeGrado group,^{32,33} a spiroadamantanamine analogue,³⁴ see

compound **7** in Scheme 1, was reported as active against active against M2 WT, V27A, and L26F and 4-(1- and 2-adamantyl)piperidines was a dual V27A and WT inhibitor. Numerous other aminoadamantanes have been synthesized^{35,36,37,38,39} but have not been tested for their ability to block M2 proton transport. Recently it was observed that few of these inhibit S31N viruses through a mechanism that was not M2 proton blockage.^{38, 39}

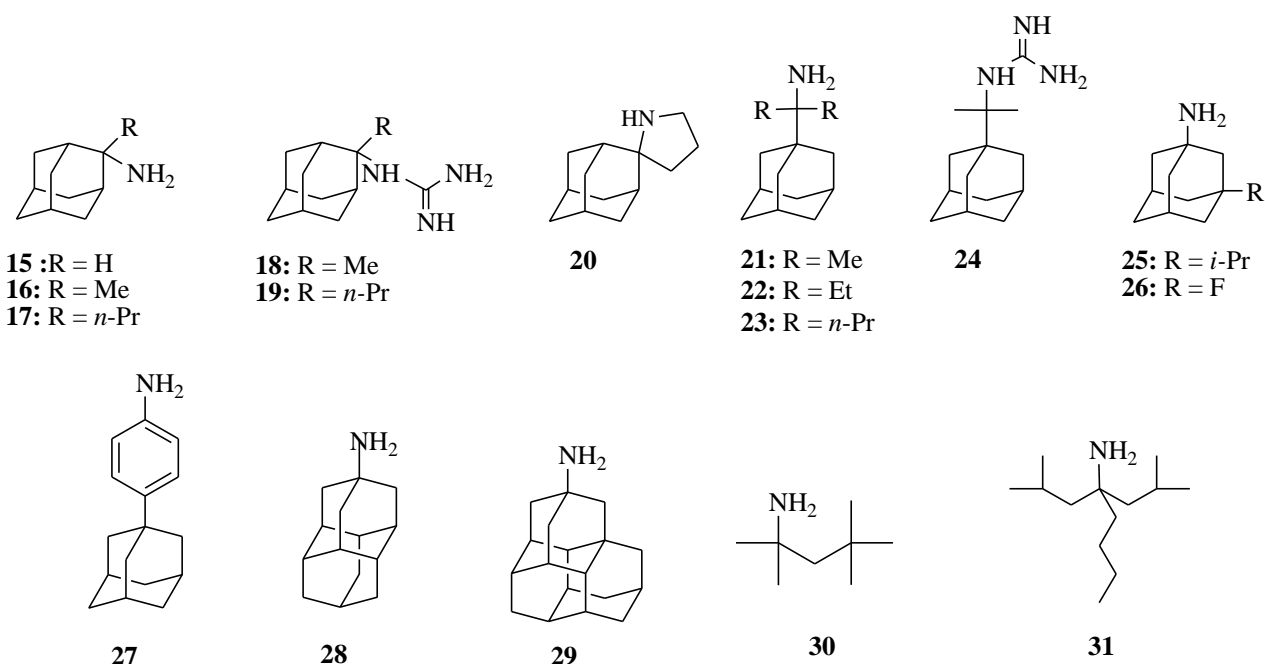
Hu after testing that pinanamine is more active than amantadine against a M2 WT strain⁴⁰ found that the attachment of the 4-imidazole or p-hydroxyphenyl to the lipophilic amine pinanamine through a methylene bridge, see for example compound **14** in Scheme 1, led to dual activity against M2 WT and S31N viruses.^{41,42}

Aminoadamantane-polar head conjugates inhibiting multiple-influenza A viruses resistant to amantadine



Scheme 1. Representative aminoadamantanes or analogues and their polar head conjugates potency against M2 WT and amantantadine resistant M2 V27A, M2 L26F and M2 S31N viruses.

Extensive SAR investigations of molecules including an aryl derivative linked with amantadine analogue through a methylene bridge, see for example compounds **9-13** in Scheme 1, using electrophysiological testing, and antiviral assaying combined with MD simulations and solution NMR structural investigations of complexes with M2TM S31N were performed from DeGrado and Wang.^{43,44,45,46,47,48} A ssNMR analysis of a system including compound **12** in complex with M2TM S31N in membrane bilayers showed that the compound's heterocyclic ring system may be trapped by the V27 side chains at N-terminus of the M2TM-pore with the isoxazole group forming hydrogen bonds with the N31 amide side chains.⁴⁹ Recent findings from MD simulations and OS (Oriented Sample) ssNMR spectra, ITC and electrophysiology revealed that different aminoadamantane ligands, for example compounds **17**, **20** in Scheme 2, bind similarly to M2 WT. However the M2 N31 M2 mutation abolishes the lipophilic pocket enclosed by V27 side chains causing a propensity for amantadine variants to change orientation pointing ammonium group N-ward in the M2TM S31N pore compared to the tight C-ward orientation in the M2TM WT pore, see Chapters 2 and 3.^{14,50,51}

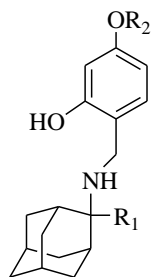


Scheme 2. Aminoadamantanes tested and used as templates for connecting with polar heads through a methylene bridge.

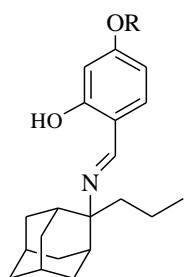
DeGrado and Wang suggested using solution NMR studies and MD simulations that dual inhibitors having an aminoadamantane-polar head conjugate structure, see for example compound **13** in Scheme 1, inhibiting both M2 WT and S31N. They showed that these compounds bind with different orientations to the

M2 WT relative to S31N proton channel. They oriented with their polar head C-ward inside the WT M2TM pore and N-ward inside the S31N M2TM pore i.e., there is a flipping in the pore.⁴⁵

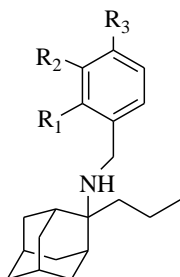
In this campaign was investigated the potency of aminoadamantane analogues or other lipophilic amines and of their conjugates with polar head groups against the amantadine resistant strains L26F, V27A, A30T, G34E and S31N. Several modifications of amantadine template was tested: (a) the substitution at 3-position of adamantane with a propyl or fluorine group, see compounds **25**, **26**); (b) the 2-alkyl-2-aminoadamantane skeleton in compounds **15-17**, **20**; the addition of a CR₂ methylene bridge or a phenyl group between adamantane and amino group resulting in rimantadine derivatives **21-23** or compound **27**; (c) the guanidine group in derivatives **18**, **19**, **24** since this group was reported to boost in some cases the antiviral potency; (d) the expansion of adamantane to the diadamantoids in compounds **28**, **29**; (e) the *tert*-alkyl as open adamantane analogues in compounds **30**, **31**. The addition of a substituted isoxazolyl or thiophenyl or hydroxylphenyl group attached with lipophilic amine through a methylene bridge as applied by Wang and DeGrado in previous reported series^{43,44,45,46,47,48} resulted in the polar head conjugates **32-62** (Scheme 3). These efforts resulted in several potent lead compounds with a high selectivity index against amantadine resistant influenza A viruses.



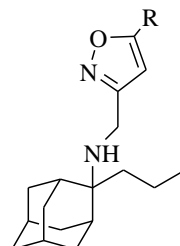
32: R₁ = H, R₂ = Me
33: R₁ = H, R₂ = H
34: R₁ = Me, R₂ = Me



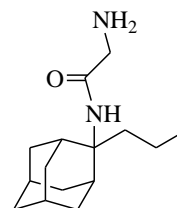
35: R = Me
36: R = H



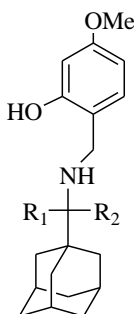
37: R₁ = OH, R₂ = H, R₃ = H
38: R₁ = H, R₂ = OH, R₃ = H
39: R₁ = H, R₂ = H, R₃ = OH
40: R₁ = OH, R₂ = H, R₃ = OMe
41: R₁ = OH, R₂ = H, R₃ = OH



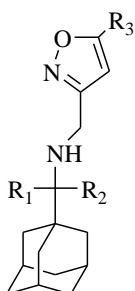
42: R = Me
43: R = Ph



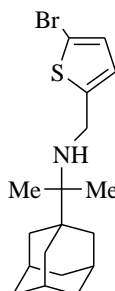
44



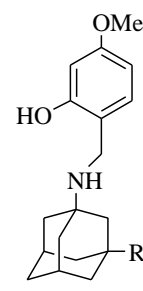
45: R₁ = Me, R₂ = H
46: R₁ = Me, R₂ = Me
47: R₁ = Et, R₂ = Et
48: R₁ = Pr, R₂ = Pr



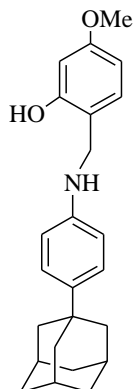
49: R₁ = Me, R₂ = H, R₃ = Me
50: R₁ = Me, R₂ = H, R₃ = Ph
51: R₁ = Me, R₂ = Me, R₃ = Ph
52: R₁ = Et, R₂ = Et, R₃ = Ph
53: R₁ = Pr, R₂ = Pr, R₃ = Ph



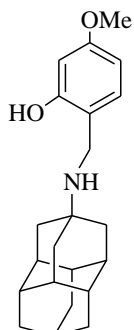
54



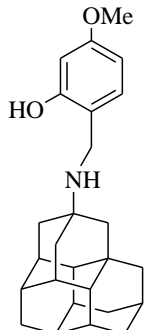
55: R = *i*Pr
56: R = F



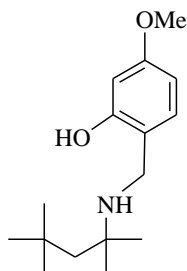
57



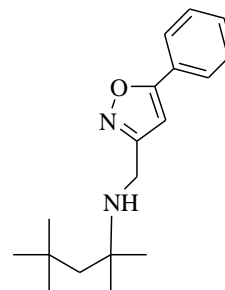
58



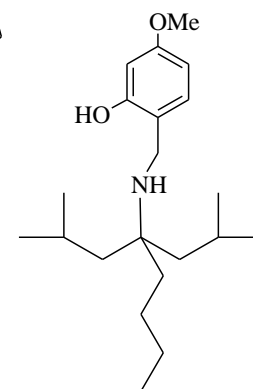
59



60



61



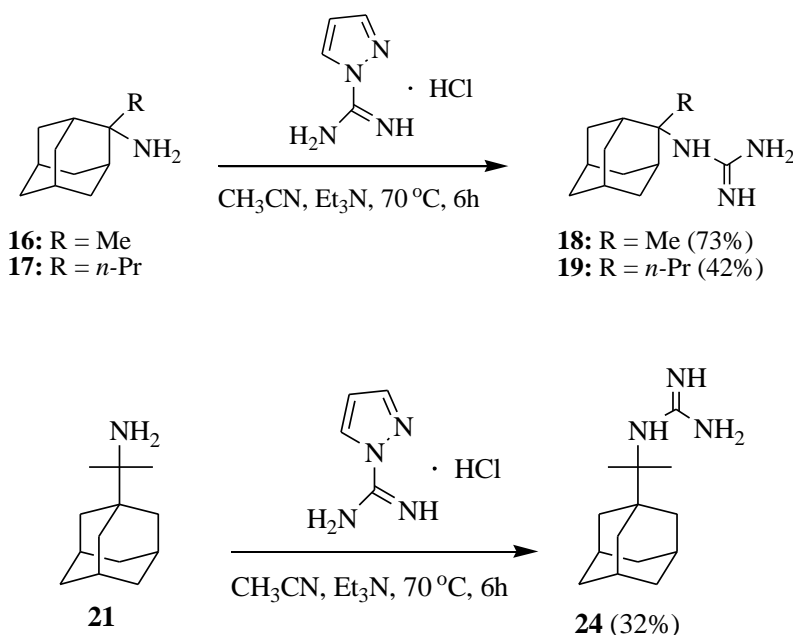
62

Scheme 3. Chemical structures of synthesized aminoadamantane-polar heads conjugates.

5.3 Results and Discussion

5.3.1 Synthesis of aminoadamantane derivatives and other lipophilic amine analogues 15-31

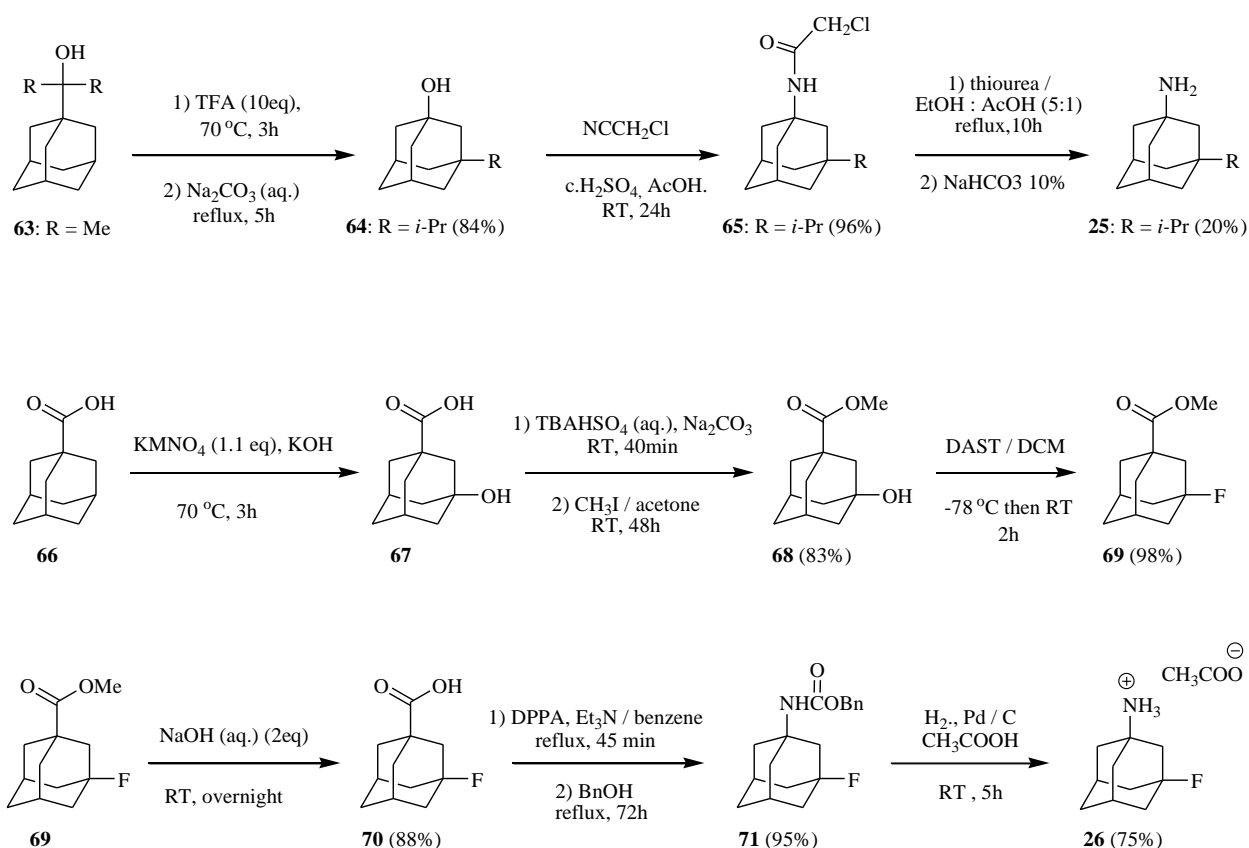
The synthesis of aminoadamantanes **15-17**³⁸ **20**⁵² and **21-23**⁵³ and diamantoids analogs **28** and **29**⁵⁴ was realized as previously described. Guanidine derivatives **18**, **19** and **24** were prepared through the reaction of the corresponding amines **16**, **17** and **21** with 1H-pyrazole-1-carboxamide.³⁹ (Scheme 4). The yield was good to moderate depending the steric crowding around starting compound nucleophilic amine group.



Scheme 4. Synthetic scheme of compounds **18**, **19** and **24**, analogues of 2-alkyl-2-aminoadamantane derivatives **16** and **17** and of *tert*-alkyl amine **21** respectively.

For the synthesis of 3-isopropyl-1-aminoadamantane **25**, *tert*-alkyl alcohol **63** was used as starting material prepared from the reaction of 1-adamantanecarbonyl chloride with methyl magnesium iodide. The alkyl metathesis of alcohol **63** afforded 3-isopropyl-1-adamantanol **64** after treatment with TFA in high yield.⁵⁵ A modified Ritter included formation of chloroacetamide **65** in excellent yield which afforded amine **25** in 20% yield after treatment with thiourea in a mixture of ethanol and acetic acid.⁵⁶ The synthesis of amines **16**, **17** and **21-23** has been previously described in Chapters 2 and 3. The synthesis of 3-fluoroamantadine **2** was accomplished with a sequence of high yield reactions based on the fluorination of methyl 3-hydroxyadamantyl

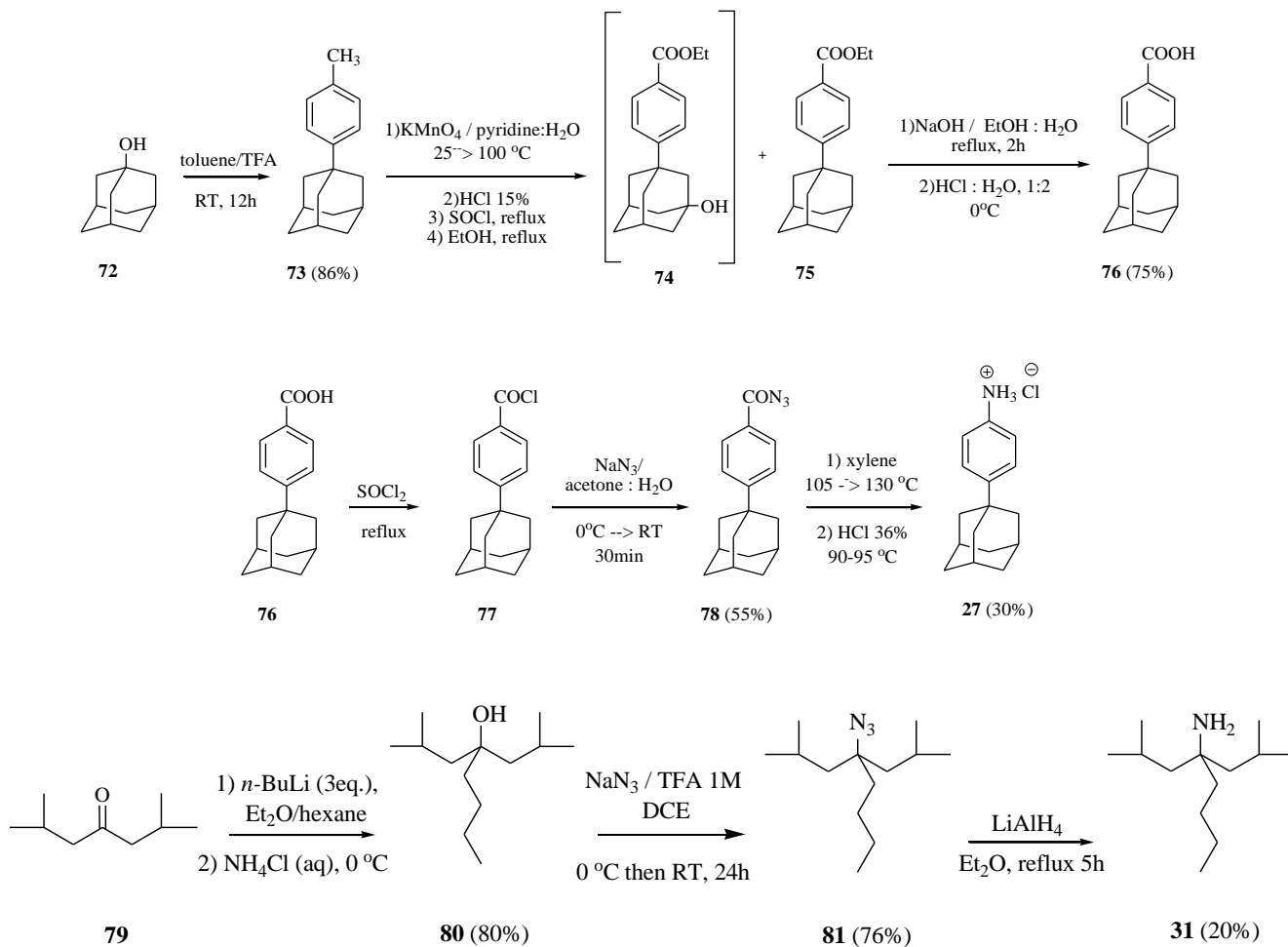
carboxylate ester using diethylaminosulfur trifluoride (DAST.)⁵⁷ Thus potassium permanganate-mediated bridgehead hydroxylation followed by DAST fluorination was utilized to sequentially insert bridgehead fluorine atoms. 3-Fluoroadamantyl Carboxylic acid was treated with diphenylphosphoryl azide⁵⁸, triethylamine and benzyl alcohol 70 °C to afford benzyl carbamate **71**. Hydrogenolysis (10 % Pd/C, HOAc) cleanly yielded amine **26** as its acetate salt.



Scheme 5. Synthesis of 1-alkyl-3-aminoadamantane derivatives **25**, 1-fluoro-3-aminoadamantane **26**.

For the synthesis of 4-(1-adamantyl)aniline **27**, the reaction between 1-adamantanol **72** and toluene in the presence of TFA afforded 4-(1-adamantyl)toluene **73**. Compound **73** was oxidized with potassium permanganate to yield a mixture of two carboxylic acids which were converted to the corresponding esters **75** and the hydroxyderivative **74** in 48% and a 20% yield respectively from the hydrocarbon **73**. Ester **74** was converted to carboxylic acid **76**, acid chloride **77** and acyl azide **78** which produced the desired amine **27** after Curtius rearrangement in xylene at 105-130 °C. For the synthesis of 4-isobutyl-2-methyloctan-4-amine **31** the reaction including di-isobutylketone **79** and freshly prepared butyl magnesium bromide yielded a mixture of the *tert*-alkyl alcohol **80** and 2,6-heptan-4-ol; heptanol was formed through a β -hydride transfer of the Grignard reagent.⁵⁹ The desired *i*-Bu₂BuCOH (**80**) was obtained from the addition of *n*-butyl lithium to ketone

79. Starting from alcohols **1b-7b** and using $\text{CH}_2\text{Cl}_2/\text{TFA}$ 1 M/ NaN_3 , the azide **81** was afforded in 76% yield. The reduction of the *tert*-alkyl azides **81** using LiAlH_4 in refluxing ether for 5 h yielded the primary *tert*-alkyl amine **31** in 20% yield.



Scheme 6. Synthesis of 4-(1-adamantyl)aniline **27** and 4-isobutyl-2-methyloctan-4-amine **31**.

5.3.2 Binding of lipophilic amines to M2TM WT

In order to test if aminoadamantanes may provide useful templates for attaching a CH₂-polar head fragment we estimate their ability to fit between M2TM WT pore walls by measuring their K_d values using Isothermal Titration Calorimetry (ITC).

Table 1. Binding constants, and other thermodynamic parameters derived from ITC measurements for influenza A M2TM WT.

M2TM WT				
Ligand ¹	K _d ²	ΔG ^{3,4}	ΔH ³	TΔS ^{3,5}
1	2.17 ± 0.52	-31.78 ± 0.59	-27.73 ± 2.05	4.56 ± 2.13
2	0.51 ± 0.26	-35.54 ± 0.29	-31.16 ± 0.27	4.26 ± 0.40
15	1.60 ± 0.34	-32.52 ± 0.51	-29.41 ± 1.76	3.89 ± 1.83
16	0.89 ± 0.19	-33.96 ± 0.53	-27.78 ± 1.08	6.18 ± 1.20
17	0.71 ± 0.15	-34.52 ± 0.50	-35.17 ± 1.13	0.65 ± 1.23
21	0.13 ± 0.12	-38.02 ± 1.77	-17.12 ± 1.11	20.91 ± 2.09
22	4.59 ± 2.21	-29.95 ± 1.17	-13.48 ± 2.58	16.47 ± 2.83
23	3.43 ± 1.05	-30.67 ± 0.75	-25.47 ± 1.87	5.20 ± 2.01
25	⁸	⁸	⁸	⁸
26	6.33 ± 1.53	-29.18 ± 0.59	-14.71 ± 1.25	-14.46 ± 1.38
28	13.56	-27.32	-25.21	2.55
29	⁸	⁸	⁸	⁸

¹ See Scheme 2.

² Binding constant K_d in μM calculated from measured K_a in M⁻¹ by K_d = 1/K_a × 10⁻⁶ and error in K_d in μM determined by K_{d, error} = (K_{a, error}/K_a²) × 10⁻⁶.

³ In kJ mol⁻¹.

⁴ Free energy of binding computed from K_d by ΔG = -RT ln(K_d^{ref}/K_d) with K_d^{ref} = 1 M and T = 293.15 K and error in ΔG determined according to

$$\Delta G_{\text{error}} = \sqrt{\left(\frac{RT K_{d, \text{error}}}{K_d}\right)^2}$$

with T = 293.15 K.

⁵ Entropy of binding calculated by ΔS = (-ΔG + ΔH)/T and error in ΔS computed by the equation

$$\Delta S_{\text{error}} = \sqrt{\Delta G_{\text{error}}^2 + \Delta H_{\text{error}}^2}$$

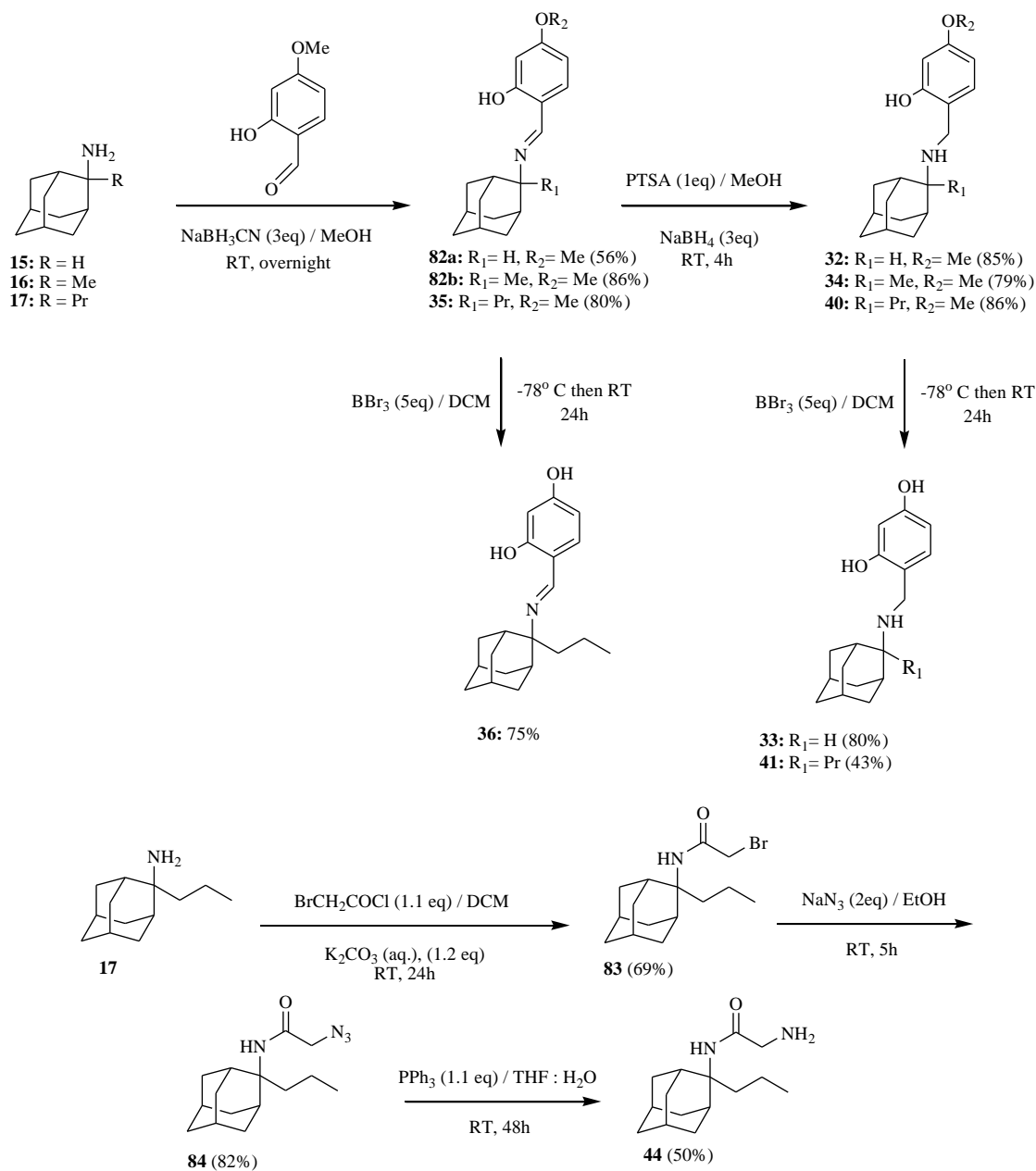
⁸ No detectable binding.

Table 1 includes thermodynamic parameters of binding against M2TM WT. Binding affinities were measured for the M2TM-ligand systems in dodecylphosphocholine (DPC) micelles at pH 8, where M2TM fragments form stable tetramers (see Chapters 1-3).⁶⁰ As described in Chapters 1-3 compounds **1,2,15-17, 21-**

23, 26 bind M2TM. The 4-aminodiamantane **28** and the aminotriamantane **29** can also fit between M2TM pore walls. No detectable binding was observed for **25** and **29**.

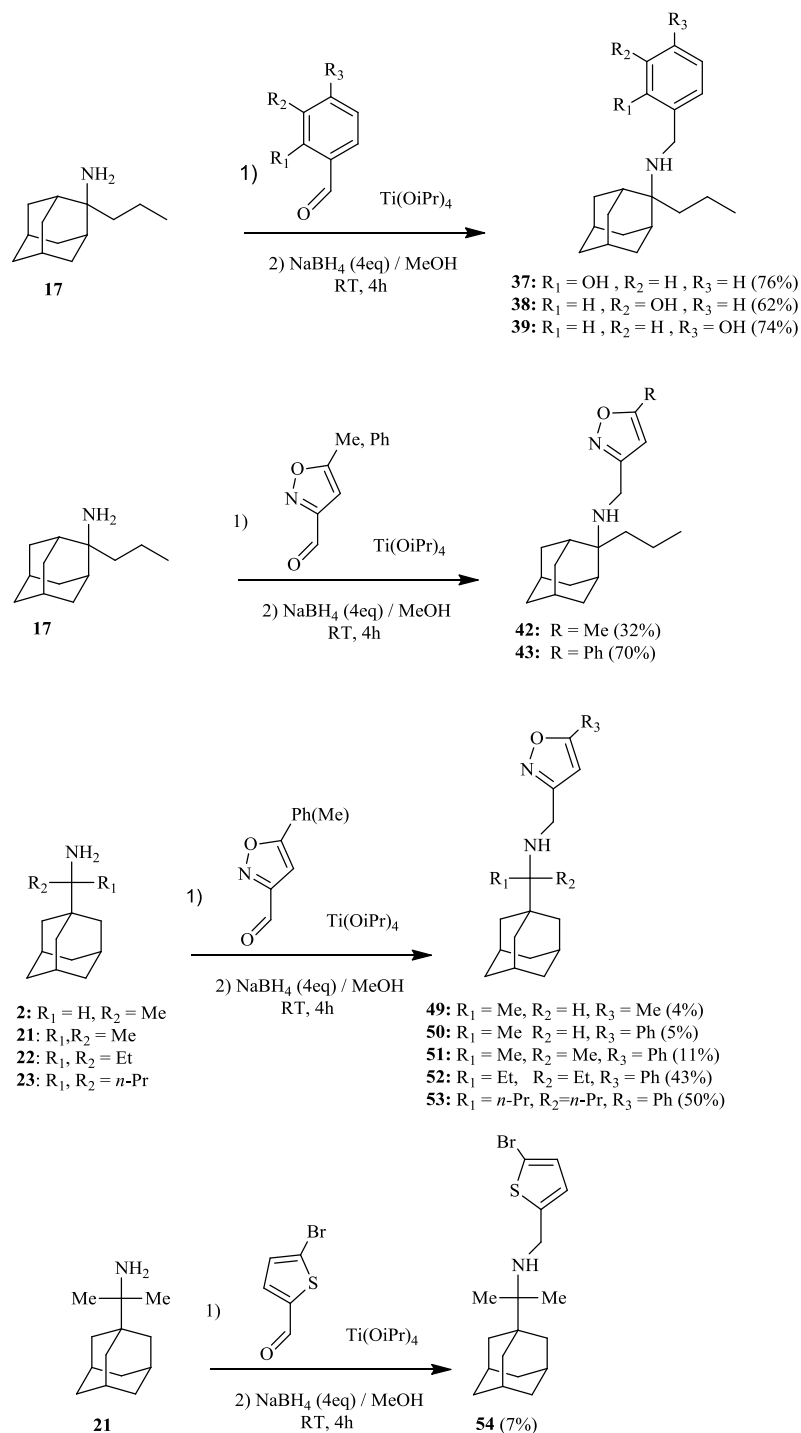
5.3.3 Synthesis of aminoadamantanes-polar head conjugates 32-62

Few polar head groups found to be efficient in previous works^{43,44,45} were installed on the N-terminal of lipophilic amines **15-31** through reductive amination. The reaction of the primary amine with 2-hydroxy-4-methoxy-benzaldehyde using NaCNBH₃ in methanol for 15 min, as described earlier,⁴⁴ afforded the corresponding imine. Elongation of the reduction for few hours led to cleavage of the adduct affording the starting amine from the reaction mixture. These imines can be formed by refluxing the starting amine with the suitable aldehydes in benzene using a Dean-Stark adaptor for the separation of water. They were also formed by treating amine with aldehyde in methanol but was found that the yield was increased when was present possibly increasing carbonyl reactivity acting as a Lewis acid. We found that after imine isolation the reduction proceeded to the formation of the amine after treatment of the imine with PTSA and NaBH₄ in methanol. Thus, using this protocol the N-(2-hydroxy-4-methoxy-benzyl)methyl derivatives **32, 34, 45-48, 55-62** were obtained. Demethylation of the methoxy group from the 2-hydroxy-4-methoxy-benzyl moiety of compounds **32, 35, 40** through treatment with excess BBr₃ in dichloromethane at -78 °C afforded derivatives **33, 36, 41**. In compound **44** the aminoacetyl group was installed to the amino group of **17**. Starting from **17** the N-azidoacetyl derivative **84** was prepared through the N-bromoacetyl derivative in compound **83**. Reduction of the azido group under Staudinger reaction conditions⁶¹ afforded compound **44**.

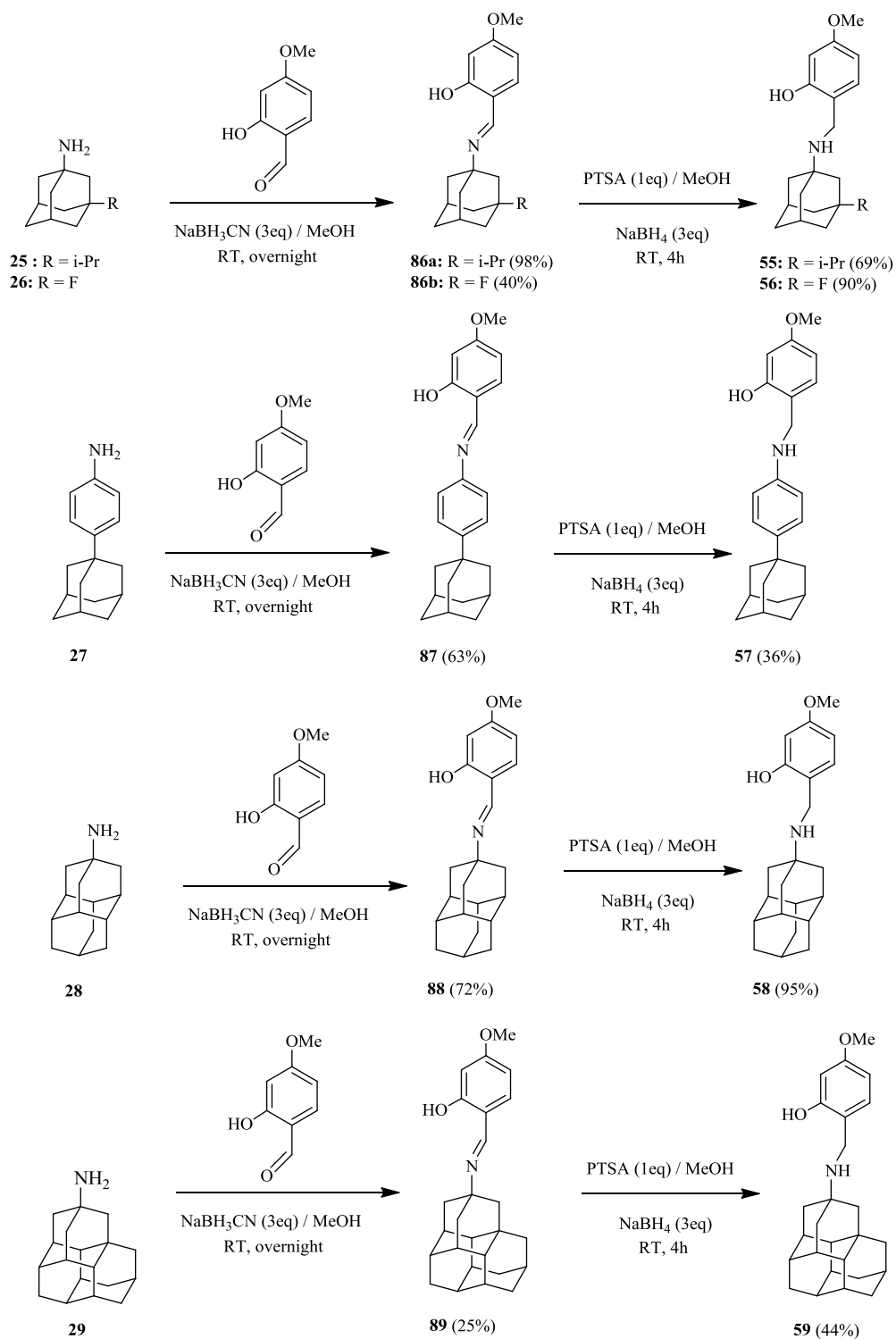


Scheme 7. Reductive amination reaction scheme using NaCNBH₃ in methanol applied for the synthesis of compounds **32**, **24**, **40** through imines **82a**, **82b**, **35** starting from amines **15-17**. Demethylation of **35**, **32**, **40** led to **36**, **33**, **41**. Synthesis of the aminoacetamide derivative **44** starting from amine **17**.

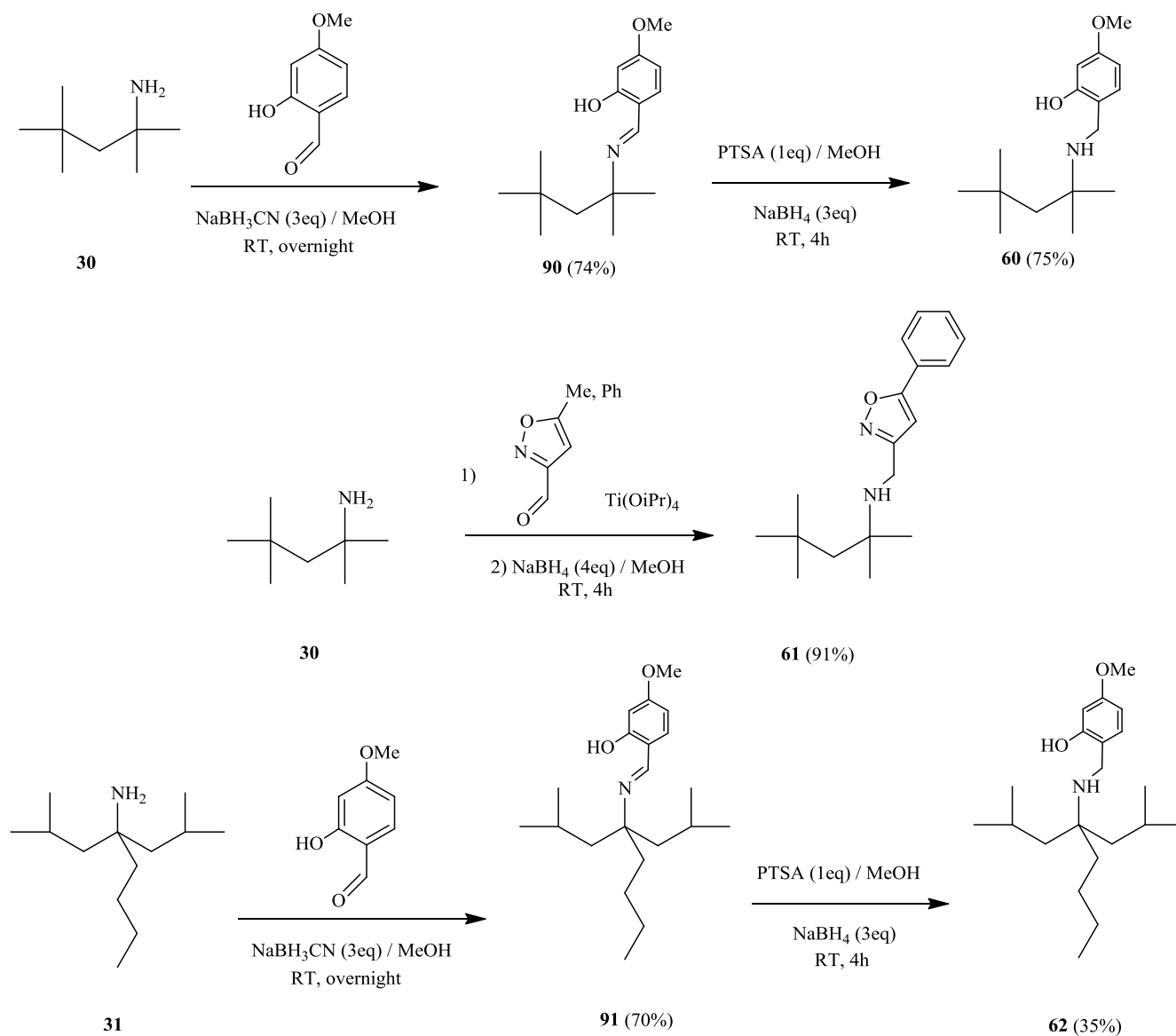
Reductive amination of aminoadamantanes **17** with NaBH₄ in methanol and Ti(OiPr)₄⁴³ as the Lewis acid afforded N-(hydroxyphenyl)methyl derivatives **37-39** or the isoxazolylmethyl derivatives **42**, **43**. Similarly rimantadine analogues **2**, **21-23** were converted to the isoxazolylmethyl derivatives **49-53** respectively and from **2** derivative **54** was formed.



Scheme 8. Reductive amination reaction scheme using NaBH_4 in methanol and Ti(OiPr)_4 applied for the synthesis of compounds **37-39**, **42**, **43** and **49-54** starting from amines **17**, **2**, **21-23**.



Scheme 9. Reductive amination reaction scheme using NaCNBH_3 in methanol applied for the synthesis of compounds **55-59** through imines **86-89**.



Scheme 10. Reductive amination scheme using NaCNBH_3 in methanol through imines **90**, **91** or NaBH_4 in methanol and $\text{Ti}(\text{O}i\text{Pr})_4$ applied for the synthesis of compounds **60**, **62** or **61** respectively.

5.3.4 In vitro testing against Influenza Virus A

The cytopathic effect (CPE) inhibition assay was used^{30,62} to compare the antiviral activity of the compounds in Table 2 against WSN/33 variants without (WSN/33-M2-N31S, generated by reverse genetics from the amantadine-resistant WSN/33-M2-WT consisting N31) or with drug resistance-conferring mutations in M2 (WSN/33-M2-WT, WSN/33-M2-L26F/N31S, WSN/33-M2-V27A/N31S, WSN/33-M2-A30T/N31S, WSN/33-M2-G34E/N31S) in MDCK cells. All aminoadamantyl compounds **1, 2, 8, 23, 15-30** showed low micromolar activity against WSN/33-M2-S31. Compounds **21, 24** and the diamantanoid analogue **28** were the most potent compounds exhibiting equal potency to rimantadine (**2**) against WSN/33-M2-N31S. Guanidine derivatives **18, 19, 24** exhibited comparable potency to the parent amines **16, 17, 21**. When a polar head was installed in the amino group of aminoadamantane analogues the micromolar potency was maintained for many compounds and rimantadine derivatives **45-48** and **51-54** and **57, 58** exhibited similar potency to **1**. The activity testing against WSN virus confirmed the published potency of compounds **10, 12**.^{43,44} From the new lipophilic amine-polar head conjugates, compounds **33, 34, 45, 46, 49, 52, 53, 57, 58, 62** exhibited potency. In particular **46, 57** and **58** were the most interesting exhibiting potency comparable to **10**. Compared to **10** in **46, 57, 58** the amantadine **1** scaffold was replaced with 2-(1-adamantyl)-propan-2-amine **21**, 4-(1-adamantyl)-1-benzenamine **27** and 4-aminodiamantane **28** respectively.

Table 2. In Vitro Efficacy (IC₅₀, μM) of aminoadamantane derivatives tested against initial cell infection.

Compound ID	CC ₅₀ [μM]	IC ₅₀ ± SD (μM) ^a					
		A/WSN/33 (M2 N31S)	A/WSN/33 WT (M2 N31)	A/WSN/33 (M2 L26F/N31S)	A/WSN/33 (M2 V27A/N31S)	A/WSN/33 (M2 A30T/N31S)	A/WSN/33 (M2 G34E/N31S)
1	>100	0.25 ± 0.06	n.a	55.78 ± 6.80	n.a	n.a	n.a
2	>100	0.04 ± 0.01	n.a	3.10 ± 0.40	n.a.	n.a.	n.a.
8	>100	0.29 ± 0.10	n.a	39.22 ± 23.09	n.a	n.a	n.a
10	49.86±12.28	1.13 ± 0.03	8.70± 4.38	n.a.	n.a.	n.a.	n.a.
12	67.80±0.62	n.a.	1.18 ± 0.17	n.a.	n.a.	n.a.	n.a.
15	70.50 ±25.31	0.50 ±0.38	n.a.	20.97 ± 5.00	n.a	n.a	n.a
16	25.63±7.65	0.33 ±0.10	n.a	16.10 ± 8.72	n.a	n.a	n.a
17	12.24	0.34 ± 0.10	n.a	1.99 ± 0.74	n.a	n.a	n.a
18	38.51 ± 0.13	0.69 ± 0.26	n.a	23.13 ± 6.34	n.a	n.a	n.a
19	>100	0.29± 0.14	n.a	1.79 ±1.05	n.a	n.a	n.a
20	>100	0.34 ± 0.08	n.a	8.75 ± 4.72	n.a	n.a	n.a
21	>100	0.03 ± 0.02	n.a	0.79 ± 0.37	n.a	n.a	n.a
22	>100	1.01 ± 0.13	n.a	5.95 ± 3.35	n.a	n.a	n.a
23	71.28±11.46	1.06 ± 0.23	n.a	0.55 ± 0.23	n.a	n.a	n.a
24	>100	0.04± 0.01	n.a	1.01 ± 0.50	n.a	n.a	n.a
25	>100	14.12 ± 3.72	n.a.	69.45 ± 28.73	n.a.	n.a	n.a.
26	>100	16.19 ± 5.36	58.80±20.99	n.a	n.a	n.a	n.a
27	>100	2.51 ± 1.24	56.80±17.09	45.30 ± 10.76	n.a.	40.64± 18.78	n.a
28	>100	0.07 ±0.02	n.a	0.74 ±0.26	15.46 ± 6.97	n.a	n.a
29	17.66 ± 0.09	0.72 ±0.33	n.a.	n.a.	n.a.	n.a.	n.a.
30	>100	5.63 ±2.01	n.a	n.a	n.a	n.a	n.a
31	>100	n.a	n.a	n.a	n.a	n.a	n.a
32	68.10 ± 3.65	12.47 ± 6.70	n.a	n.a	n.a	n.a	n.a
33	>100	1.08 ± 0.33	36.98 ± 8.52	48.86 ± 13.71	n.a	n.a	37.75± 12.57
34	>100	4.88 ± 2.76	37.73±13.38	30.25 ± 24.51	63.51 ± 30.59	50.15 ± 12.80	49.18 ± 9.05
35	69.40 ± 12.02	1.72 ± 0.78	n.a	23.03 ± 10.29	n.a	n.a	n.a
36	>100	7.50 ± 1.64	n.a	28.73 ± 7.58	n.a	n.a	n.a
37	>100	n.a	n.a	n.a	n.a	N.T	N.T
38	>100	n.a	n.a	n.a	n.a	n.a	n.a
39	30.22 ± 3.05	1.17 ± 0.08	n.a	3.67 ± 1.73	n.a	n.a	n.a
40	>100	1.06 ± 0.59	n.a	4.20 ± 0.60	n.a	n.a	17.89 ± 6.56
41	>100	0.66 ± 0.37	n.a	9.29 ± 2.74	n.a	56.58 ± 24.98	n.a
42	>100	n.a	n.a	n.a	n.a	N.T	N.T
43	35.36 ± 3.23	n.a	n.a	n.a	n.a	N.T	N.T
44	>100	5.98 ± 0.49	n.a	30.82 ± 12.17	n.a	n.a	n.a
45	>100	0.27 ± 0.08	41.74 ± 1.76	17.55 ± 9.26	78.16 ± 15.42	34.90 ± 1.32	50.65 ± 2.08
46	>100	0.13 ± 0.02	19.86 ± 6.92	1.80 ± 0.29	n.a	43.98 ± 8.50	19.22 ± 9.36
47	>100	0.19 ± 0.08	n.a	1.44 ± 0.44	n.a	n.a	n.a
48	27.34 ± 3.37	0.37 ± 0.10	n.a	0.60 ± 0.23	n.a	n.a	n.a
49	>100	1.00 ± 0.65	86.37 ± 8.47	91.30 ± 7.25	n.a	n.a	n.a
50	21.70 ± 8.61	1.14 ± 0.46	n.a.	n.a.	n.a.	n.a.	n.a.

51	67.60 ± 1.45	0.19 ± 0.09	n.a	n.a	n.a	n.a	n.a
52	>100	0.89 ± 0.64	56.97±31.59	14.27 ± 3.04	n.a	n.a	n.a
53	>100	0.69 ± 0.13	70.15 ± 7.86	1.52 ± 0.49	n.a	n.a	n.a
54	85.99 ± 3.60	0.29 ± 0.17	n.a	9.06 ± 2.53	n.a	n.a	n.a
55	57.24 ± 6.07	13.21 ± 5.97	n.a	n.a	n.a	19.10 ± 7.17	23.44 ± 4.14
56	>100	63.43 ±17.64	n.a	n.a	n.a	n.a	n.a
57	>100	0.66 ± 0.21	17.43 ± 11.94	21.57 ± 10.65	55.02 ± 21.57	22.53 ± 13.06	47.99 ± 14.34
58	>100	0.29 ± 0.11	21.24 ± 8.92	17.31 ± 12.09	47.47 ± 15.20	38.40 ± 6.22	55.79 ± 11.58
59	27.14 ± 9.43	8.10 ± 2.72	n.a	n.a	n.a	n.a	n.a
60	>100	26.35 ±10.42	n.a	40.33 ± 17.18	n.a	38.02 ± 3.68	37.01 ± 7.23
61	>100	n.a	n.a	n.a	n.a	n.a	n.a
62	65.30 ± 5.80	58.94 ± 10.98	60.36 ± 2.76	n.a	n.a	n.a	n.a
Oseltamivir		0.03±0.02	0.01± 0.00	0.04± 0.02	0.03±0.01	0.01 ±0.00	0.04±0.03

^a measured in triplicate

Testing against WSN/33-M2-V27A/N31S revealed that only 4-aminodiamantane **28** showed significant potency while conjugates **34** and **45** very weak potency. The addition of a sizeable substituent in amantadine **1** in proximity to 1-amino group seems to favor potency against WSN/33-M2-L26F/N31S and compounds **2**, **17**, **19-24**, **28** exhibited low micromolar potency compared to **1** and **15** for example which exhibited weak or moderate potency. In other cases where lipophilic skeleton size was increased like in compounds **27**, **29** potency was abolished. The addition of the guanidino group in compounds **18**, **19**, **24** retained potency. The addition of a CH₂-polar head in **17**, **21**, **23** resulted in inhibitors **39-41**, **46-48**, **52-54** covering a potency from submicromolar to micromolar range and in **27** resulted in micromolar inhibitors **57**, **58**. Testing against WSN/33-M2-A30T/N31S revealed that compound **27** was the only aminoadamantane showing some potency; the polar head conjugates **34**, **41**, **45**, **46**, **57**, **60** exhibited moderate potency while **55**, **57** inhibited viruses with a micromolar potency. None of the aminoadamantanes was proved to be active against WSN/33-M2-G34E/N31S; compounds **33**, **34**, **45**, **57**, **58**, **60** exhibited moderate potency while **40**, **46**, **55** inhibited viruses with a micromolar potency.

Table 3. In vitro efficacy (IC_{50} , μM) of Scheme 1 compounds against influenza virus A(H1N1)pdm09 viruses. ^a

Compound	IC_{50}	
	Jena/8178	Calif/07
46	24.23 \pm 7.63	13.99 \pm 3.76
32	74.33 \pm 0.00	54.59 \pm 0.00
33	40.96 \pm 8.41	62.64 \pm 26.04
62	n.a	73.58 \pm 6.85
52	58.77 \pm 21.70	53.83 \pm 38.83
45	18.19 \pm 6.79	13.23 \pm 2.95
49	13.23 \pm 3.98	8.16 \pm 5.39
27	37.82 \pm 1.54	19.88 \pm 7.35
57	12.96 \pm 5.22	15.71 \pm 5.06
58	18.43 \pm 7.25	21.88 \pm 5.88
Oseltamivir	0.14 \pm 0.13	0.29 \pm 0.27
Amantadine	-	-

^a measured in triplicate

Between the various adamantyl scaffolds used for installation of a polar head compounds **21**, **25**, **27** and **28** were the most successful. (a) Compound **21** as part of compounds **46** which exhibited potency against WSN/33, WSN/33-M2-N31S, WSN/33-M2-L26F/N31S, WSN/33-M2-G34E/N31S; (b) compound **27** led to derivative **57** which exhibited potency against WSN/33, WSN/33-M2-N31S, WSN/33-M2-L26F/N31S, WSN/33-M2-A30T/N31S; (c) compound **28** led to derivative **58** which was potent especially against WSN/33, WSN/33-M2-N31S, WSN/33-M2-L26F/N31S. Additionally aminoadamantane **25** was the lipophilic amine part of compound **55** which exhibited potency against WSN/33-M2-A30T/N31S and WSN/33-M2-G34E/N31S. The cytotoxicity data showed that compounds **46**, **57**, **58** are non-toxic with CC_{50} values $> 100 \mu M$. In order to confirm the potency of the most interesting compounds against epidemic viruses testing was performed against Calif/07 and a German domestic strain Jena/8178 using few representative compounds (Table 3). As can be observed compounds **45**, **46**, **49**, **57** and **58** exhibited potency against these epidemic strains. Noteworthy is that aminoadamantane **27** exhibited some potency against Calif/07 but not against Jena/8178 strain. We have also previously noted that aminoadamantane derivatives can inhibit S31N viruses through a mechanism other than M2 pore blocking. ⁶³

5.3.5 TEVC experiments

Verification of the M2 as the protein target for inhibition of influenza A viruses was performed by measuring the blocking effect of the compounds against full length M2 using EP. The blocking effect against full length M2 protein was determined with a two-electrode voltage clamp (TEVC) assay at 10 min following 3 min washout. Compounds **46**, **57** and **58** exhibiting high antiviral potencies against WSN/33-M2-N31S were tested. Testing confirmed that the drugs are acting by efficiently blocking M2 WT.

Table 4. Block of full-length Udorn M2 WT current by selected compounds

Ligand	Udorn M2 WT	
	% Block after 10 min wash-in ¹	% Block after 3 min wash-out
46	80.0 ± 1.7%	2.0 ± 0.8%
57 ³	81.0 ± 2.1%	0%
58	81.0 ± 1.6%	0%

¹ For each compound, percent block of pH-dependent M2 current at listed concentrations (+/- s.e.m.). ² Three replicates were used for measurements at 100 µM.

5.3.6 MD simulations

We used MD simulations of M2TM in a phospholipid bilayer to investigate the dual inhibitory behavior adopted by compounds **40**, **46**, and **57-59** against M2 WT and S31N proton channels. A structure of M2TM S31N - **12** complex used as a template was generated using: (a) the coordinates of ligand **12** from the PDB ID 2LY0⁴³ (22-65), obtained using NMR spectroscopy in micelles solution at alkaline pH,⁴³ and (b) the structure of M2TM S31N obtained from M2TM WT (22-46), determined at pH 7.5 (PDB ID 2KQT^{6,8}) and in DMPC bilayers, in the presence of **1**, after mutation of Ser31 to Asn (see experimental methods). The molecules were firstly docked inside the M2TM S31N (22-46) pore. The program GOLD5.2,^{64,65,66} and the GoldScore⁶⁵ as the scoring function were applied. The highest-scored docking solutions adopt an orientation of the polar head towards the N-end. The orientations of the compounds towards the C-end were obtained as lower in score docking solutions. M2TM-ligand complexes were simulated in DMPC bilayers which represents a better membrane mimetic system for retaining proper M2TM structure compared to other glycerophospholipids.^{67, 68} We used an experimental structure of M2TM which is already adapted to the high pH condition and DMPC bilayers.

MD simulations of M2TM WT in complex with ligands **1**, **28**, **29**, **40**, **46**, **57**, **58** were performed. Trajectories of 80 ns were obtained. In the M2TM WT the ammonium's position of the ligands aligned itself with the backbone carbonyl of G34, in most cases slightly above the experimental binding position for amantadine.^{5,6,7,9} The M2TM backbone showed a kink at G34 in contrast to the low pH apo protein structure.^{5,16} The average angle between the pore axis, which is equal to the membrane normal, from the N- to the C-terminus of the channel, and the C-N bond vector ranges between 11° and 47° (Table 5A), i.e. the ammonium group of all aminoadamantyl compounds oriented towards the C-terminus, consistent with previous experimental findings^{5,6,7,9} and observations.^{13,14,15,19,20,21} The center of mass between the four V27 residues and the adamantyl Cage of the ligands **1**, **28**, **40**, **46**, **57**, **58** varies between 4.2 Å and 5.8 Å on average (Table 5A). However in triadamantane analogue **29** the ammonium's position shifts by about 1.3 Å toward C-end where pore is broader and can accommodate the larger size of lipophilic moiety close to G34. Diadamantane and triadamantane analogues of amantadine, **28** and **29** fit inside the M2TM pore according to the ITC results (see Table 1 and Figure 1). Two layers of waters are observed, one close to Ala30 and the other deeper close to Gly34 being enabling the protons transport through the channel. These two layers were observed also in the recent crystal structure of aminoadamantane drugs-M2TM complexes.⁶⁹ The top most layer of waters close to Ala30 is completely displaced in the structure of triadamantane analogue **29**. The inhibitor ammonium group is within H-bonding distance of the layer of waters immediately above the gating His37 residues. This is consistent with the X-ray structure⁶⁹ of the complex between a spiroadamantanamine⁷⁰ and M2TM complex

and with the shift of ammonium's position of triadamantane analogue **29** by about 1.3 Å toward C-end which causes the displacement of waters layer close to Ala30.

The primary ammonium groups in **28** and **29** group form, on average, three hydrogen bonds with neighbouring water molecules (Table 5A) and the lipophilic cage is embraced by V27 and A30 side chains, which define the binding site of these ligands. For conjugate molecules **40, 46, 57, 58** the ammonium group gradually converges to stable positions along the pore and the ligand is spanning the M2TM pore from V27 to H37. The ligand ammonium group form hydrogen bonds with two water molecules between the ligand and the H37 residues. The 4-MeO-2-OH phenyl group adopted an anti conformation around the N-CH₂ bond which is aligned with M2TM pore axis forming a hydrogen bond with G34 carbonyls. The simulated M2TM-ligands **1, 28, 29, 40, 46, 58** were stable, and in all cases the M2TM tetramer showed no large conformational changes in the course of the simulations, as demonstrated by RMSDs ≤ 1.8 Å for M2TM C α -carbons with respect to the initial structure (PDB ID 2KQT)^{5,6,7} (see Figure S1). The movement of **57** accompanied by a more distinct conformational change of the M2TM backbone, in the direction toward the low pH structure.^{16 6} After 80 ns, the root-mean-square deviation (RMSD) of the backbone atoms from the starting structure^{5,6,7} was 3 Å. The region located above the adamantyl core, i.e. towards the N-terminus, no water molecules were found,^{13 14 50} which is consistent with the proton blocking effect of the aminoadamantane derivatives.^{1,71,30,32,} No Cl⁻ ion entered the pore as it is indicated by the average Cl-N distance (Table 5A).

MD simulations were also performed for the complexes of few ligands exhibited potency in complex with S31N M2TM mutant. They were stabilized inside the pore in a similar orientation compared to the S31N M2TM-M2WJ332 structure PDB ID 2LYO.⁴³ In the simulated M2TM S31N - complexes including ligands **1, 28, 29, 40, 46, 57, 58** the M2TM tetramer showed RMSDs ≤ 2.6 Å for M2TM C α -carbons with respect to the initial PDB ID 2KQT^{5,6,7}, see Figure S2 and Table 5B.

The lipophilic amine is spanning the region between G34 and A30, the 4-MeO-2-OH moiety facing toward V27, and the ammonium is forming hydrogen bonds with the side chain of N31 and waters distributed in the N-end. The V27 side chains are packed tightly around the 4-MeO-2-OH group only partially exposed to the outer solvent and the C γ atoms from opposite monomers are separated by 7.2 Å (Figure 2). During the simulation, the N-terminal residues slightly expand to accommodate the thermal fluctuations of the ligand **58** i.e., the separation between opposing C γ s increases to 9.2 Å. The ligand is more flexible and the RMSF values are higher than those in M2TM WT complexes. Water molecules that are initially positioned around **58** leave the region between V27 and G34, with the exception of two water molecules coordinating the ammonium group, also seen in the previous S31N-M2WJ332 simulations.⁴³ MD simulations with ligand **58** having its polar head towards the N-end were tested. They resulted to higher RMSD values of 3.0-3.5 Å suggesting this orientation is not preferred inside M2TM S31N pore walls compared the orientation towards the C-end.

Table 5A. Structural and dynamic measures from MD trajectories of M2TM_{Udorn/72}-ligand complexes in DMPC bilayer (80 ns).

Ligand ¹	RMSD (C-alpha) ²	Angle C-N vector ³	V27-N	V27-Ad ⁴	H-bonds ⁵	Cl-N distance ⁶	RMSF ligand ⁷
1	1.5 ± 0.1	11.2 ± 5.9	7.2 ± 0.2	4.2 ± 0.3	2.7 ± 0.5	32.3 ± 6.6	0.4
28	1.8 ± 0.4	12.2 ± 2.0	8.6 ± 0.3	4.9 ± 0.3	2.8 ± 0.4	34.0 ± 6.6	0.4
29	1.5 ± 0.2	15.8 ± 7.8	9.9 ± 0.4	5.8 ± 0.4	2.8 ± 0.3	29.3 ± 8.9	0.1
40	1.7 ± 0.4	46.6 ± 6.7	7.4 ± 0.2	4.8 ± 0.2	2.9 ± 0.3	33.9 ± 5.9	0.5
46	1.8 ± 0.3	36.1 ± 7.0	8.3 ± 0.3	4.9 ± 0.3	3.0 ± 0.6	35.5 ± 6.4	0.6
57	3.0 ± 0.4	12.1 ± 5.7	11.7 ± 0.4	4.3 ± 0.4	2.9 ± 0.9	33.9 ± 7.7	0.8
58	1.7 ± 0.3	13.0 ± 6.7	8.0 ± 0.2	4.2 ± 0.2	2.6 ± 0.9	32.0 ± 7.5	0.9

Table 5B. Structural and dynamic measures from MD trajectories of M2TM_{S31N}-ligand complexes in DMPC bilayer (80 ns).

Ligand ¹	RMSD (C-alpha) ²	Angle C-N vector ³	V27-N	V27-Ad ⁴	H-bonds (lig-Asn31)	H-bonds ⁵	Cl-N distance ⁶	RMSF ligand ⁷
40	2.3 ± 0.6	37.8 ± 11.3	5.9 ± 0.4	7.3 ± 0.5	0.8 ± 0.6	1.5 ± 0.6	37.0 ± 7.9	0.6
46	2.3 ± 0.3	45.7 ± 12.2	3.0 ± 0.7	6.8 ± 0.8	0.6 ± 0.5	2.0 ± 1.1	32.1 ± 7.9	1.4
57	2.6 ± 0.4	11.1 ± 4.5	4.0 ± 0.2	11.2 ± 0.2	3.7 ± 0.7	0.5 ± 0.6	32.4 ± 8.2	1.4
58	1.7 ± 0.3	11.0 ± 6.9	3.0 ± 0.9	6.5 ± 0.4	1.8 ± 0.9	2.3 ± 0.8	31.1 ± 7.2	0.8
59	2.3 ± 0.5	30.8 ± 5.6	2.7 ± 0.3	6.1 ± 0.4	1.1 ± 0.3	2.0 ± 0.8	33.3 ± 7.5	0.4

¹ See Scheme 1; values taken from ref. 53; measures for **1** were added for comparison reasons.

² Maximum root-mean-square deviation (RMSD) for Ca atoms of M2TM relative to the initial structure (PDB entry: 2KQT) after root-mean-square fitting of Ca atoms of M2TM; in Å.

³ Angle between the vector along the bond from the carbon atom of the adamantyl core to the ligand nitrogen atom and the normal of the membrane; in degree.

⁴ Mean distance between center of mass of V27 and centers of mass of adamantyl calculated using Gromacs tools; in Å.

⁵ Mean number of H-bonds between ligand's ammonium group and waters.

⁶ Distance from the closest chlorine atom.

⁷ Maximum root-mean-square fluctuation of the ligand.

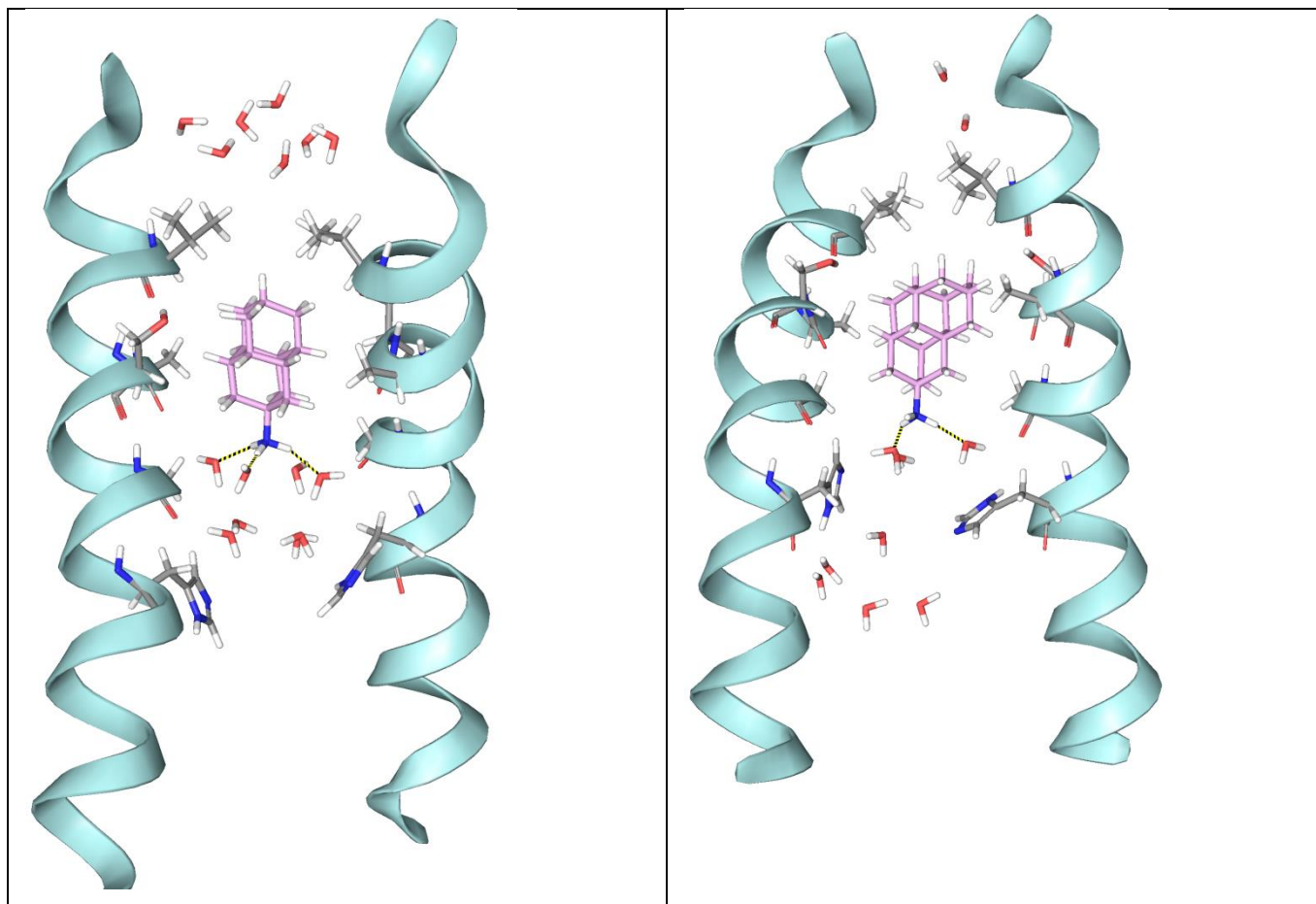


Figure 1. (a) Representative replica from the simulation of compound **28** bound to M2TM_{WT} in hydrated DMPC after 100 ns of production. Waters within 5 Å from ligand define two layers of waters between the ligand's ammonium group and His37. Three hydrogen bonds between the ammonium group of the ligand and three water molecules of an upper layer close at are shown. (b) Snapshot from the simulation of **29** bound to M2TM_{WT} in hydrated DMPC. Waters within 5 Å from ligand define one layer of waters between the ligand's ammonium group and His37. Three hydrogen bonds between the ammonium group of the ligand and three water molecules are shown. For both ligands water network that connect carbonyl groups in the protein together with van der Waals interactions of the adamantyl Core with V27 and A30 stabilize the ligand inside the pore with its ammonium group oriented towards the C-terminus.

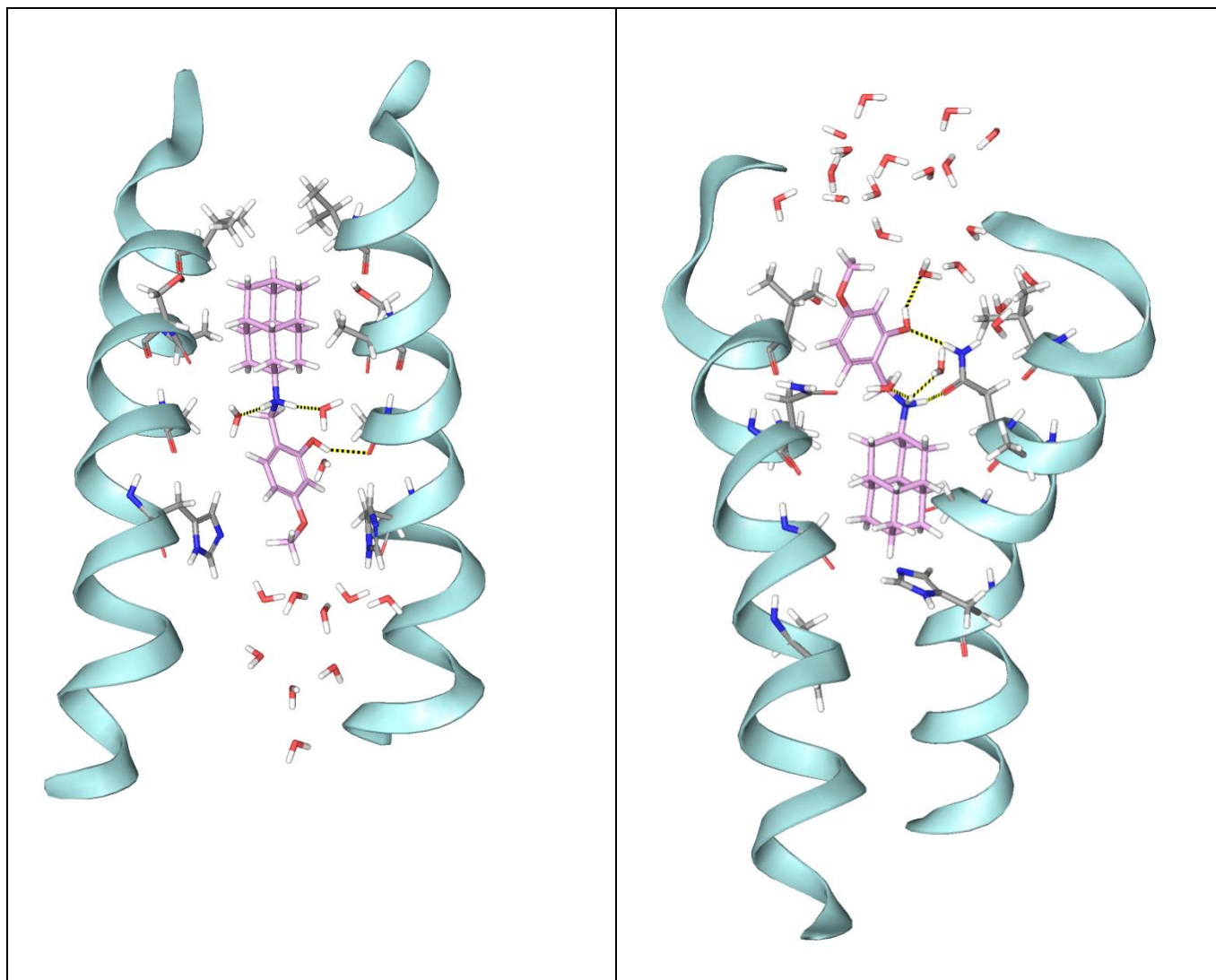


Figure 2. (a) Representative replica from the MD simulation of ligand **58** bound to M2TM WT with its ammonium group oriented towards the C-terminus of the channel. Two hydrogen bonds between the ammonium group of the ligand and two water molecules and between 4-MeO-2-OH phenyl group of the ligand and two water molecules are shown. (b) Representative replica from the MD simulation of ligand **58** bound to M2TM S31N with its ammonium group oriented towards the N-terminus of the channel. The ammonium group of the ligand forms two hydrogen bonds one with and one water molecule and one with N31 side chain carbonyl group. The 4-MeO-2-OH phenyl group of the ligand forms one hydrogen bond with one water molecule and another one with N31 side chain NH₂ group. Van der Waals interactions between the ligand and the M2TM pore walls between V27 and H37 stabilize the ligand inside the pore.

5.4 Conclusions

The heterogeneity of influenza viruses poses a great challenge in the development of anti-influenza drugs. For effective neutralization of influenza viruses, influenza vaccines normally contain two strains of influenza A viruses, /California/7/2009 (H1N1)-like virus and A/Texas/50/2012 (H3N2) virus, plus at least one strain of influenza B virus, typically B/Massachusetts/ 2/2012.⁷² Although influenza vaccines remain the cornerstone in prophylaxis of influenza infection, they are much less active than small molecule antivirals in treating influenza-infected patients.⁷³ Moreover, due to antigenic shift and antigenic drift of influenza viruses, influenza vaccines have to be reformulated each year; plus, there is generally a six-month delay in vaccine production. The limitations of influenza vaccines together with the heterogeneous makeup of influenza viruses call for broadspectrum small molecule antivirals. Our design was based on the hypothesis that dual inhibitors bind to WT and M2-S31N channels with opposite orientations: the heterocyclic headgroup faces down toward the C-termini and toward N-terminus in WT and S31N channel, respectively. Using this approach we developed a class of broad-spectrum inhibitors. Compounds like **46**, **57**, **58** have fair antiviral potencies against WT, S31N, L26F and at the same time moderate potencies against V27A, A30T, G34E. MD simulations results confirmed that the inhibitors bind to the WT and S31N channels in opposite orientations, although we cannot rule out the possibility of other minor conformational states of the drug in the S31N. The multiple starin inhibitors reported herein provide promising lead compounds for further medicinal chemistry optimization with the ultimate goal of developing broadspectrum anti-influenza drugs.

5.5 Experimental Part

5.5.1 Synthesis of aminoadamantane fragments and derivatives

3-Isopropyl-1-aminoadamantane (25). In 2-(1-adamantyl)-2-propanol **63** (430 mg, 2.22 mmol) was added dropwise trifluoroacetic acid (16.39 g, 143.77 mmol). The resulting mixture was stirred for 4 h at 65 °C and was quenched with saturated aq. Na₂CO₃ (68 mL). The mixture was refluxed for 3.5 h and then overnight at room temperature. The aqueous phase was extracted with Et₂O (2x80mL) and the combined organic phases were washed with water, brine and dried (Na₂SO₄). Solvent was evaporated *in vacuo* to afford the 3-isopropyl-1-adamantanol **64**: yield 240 mg, (56%); ¹H-NMR (400 MHz, CDCl₃) δ (ppm) 0.80-0.82 (d, *J* = 7 Hz, 6H, CH(CH₃)₂), 1.28 (m, 1H, CH(CH₃)₂), 1.38 (br s, 4H, 4, 10-adamantyl H), 1.42 (br s, 2H, 6-adamantyl H), 1.52 (br s, 3H, OH, 5,7-adamantyl H), 1.59-1.68 (m, 4H, 8,9-adamantyl H), 2.18 (br s, 2H, 2-adamantyl H); ¹³C-NMR (50 MHz, CDCl₃) δ 16.67 (CH(CH₃)₂), 30.89 (5,7-adamantyl C), 35.97 (6-adamantyl C), 37.18 (CH(CH₃)₂), 38.00 (4,10-adamantyl C), 38.63 (3-adamantyl C), 45.18 (8,9-adamantyl C), 47.21 (2-adamantyl C), 69.46 (1-adamantyl C). In a mixture of alcohol **64** (75 mg, 0.387 mmol) and chloroacetonitrile (59 mg, 0.774 mmol) was added 0.06 mL of CH₃COOH and the mixture was cooled down. Then H₂SO₄ was added dropwise (114 mg, 1.161 mmol) and the temperature is below 10 °C. The reaction mixture was then stirred for 24 h at room temperature. Then it was quenched with 10 mL of ice water and the insoluble inorganic material was filtered-off. The aqueous phase was extracted with Et₂O (3x10mL) and the combined organic phases were washed with 10 % aq NaHCO₃ (2x20mL), water, brine and dried (Na₂SO₄). Solvent was evaporated *in vacuo* to afford the acetamide **65**; yield 50 mg (48 %); IR (Nujol) ν(C=O) 1673 cm⁻¹ (s); ¹H-NMR (400 MHz, CDCl₃) δ (ppm) 0.80-0.82 (d, *J* = 7 Hz, 6H, CH(CH₃)₂), 1.28 (m, 1H, CH(CH₃)₂), 1.44 (br s, 4H, 4,10-adamantyl H), 1.52 (br s, 2H, 6-adamantyl H), 1.71 (br s, 2H, 5,7-adamantyl H), 1.87-1.99 (m, 4H, 8,9-adamantyl H), 2.15 (br s, 2H, 2-adamantyl H), 3.92 (CH₂Cl), 6.24 (NH); ¹³C-NMR (50 MHz, CDCl₃) δ 16.56 (CH(CH₃)₂), 29.69 (5,7-adamantyl C), 36.09 (6-adamantyl C), 37.31 (CH(CH₃)₂), 38.06 (4,10-adamantyl C), 41.07 (CH₂Cl), 45.24 (3-adamantyl C), 43.05 (8,9-adamantyl C), 43.30 (2-adamantyl C), 53.55 (1-adamantyl C), 164.74 (C=O). To a solution of the acetamide **65** (50 mg, 0.185 mmol) in 6 mL EtOH / CH₃COOH (5:1), thiourea (17 mg, 0.222 mmol) was added and the mixture stirred for 14h under reflux and then 15 mL H₂O was added. The insoluble inorganic material was filtered-off, washed with ether and the filtrate was extracted with HCl 6%. The aqueous phase was made alkaline with solid sodium carbonate and was extracted with dichloromethane or ether. The organic phase was washed with brine, dried (Na₂SO₄) and evaporated *in vacuo* to afford the amine **25**: yield 15 mg (12%); MS: 194.1916; ¹H-NMR (400 MHz, CDCl₃) δ (ppm) 0.77-0.73 (d, *J* = 7 Hz, 6H, CH(CH₃)₂), 1.18-1.20 (m, 1H, CH(CH₃)₂), 1.23 (br s, 4H, 4,10 adamantane-H), 1.32 (br s, 2H, 6-

adamantyl H), 1.46 (br s, 2H, 5,7- adamantyl H), 1.60 (m, 4H, 8,9-adamantyl H), 2.05 (br s., 2H, 2-adamantyl H); ^{13}C -NMR (50 MHz, CDCl_3) δ 16.62 ($\text{CH}(\underline{\text{C}}\text{H}_3)_2$), 30.03 (5,7-adamantyl C), 36.05 (6-adamantyl C), 37.20 (3-adamantyl C), 37.30 ($\underline{\text{C}}\text{H}(\text{CH}_3)_2$), 38.02 (4,10-adamantyl C), 45.12 (8,9-adamantyl C), 47.24 (2- adamantyl C), 49.36 (1-adamantyl C).

3-Fluoro-1-aminoadamantane (26). The synthetic protocol used for preparation of F-Am **26** was adapted from that described by Jasys and coworkers.⁵⁷ The reaction between 1-adamantanecarboxylic acid **66** and KMnO_4 afforded 3-hydroxyadamantanecarboxylic acid **67** which was transformed through its tetrabutylammonium salt to the corresponding methyl ester **68**. Under a N_2 atmosphere to 24 mL of dichloromethane was added DAST (26.17 mL, 200 mmol), which was cooled to -78°C . To this solution was added dropwise a dichloromethane solution (10 mL) of methyl 3-hydroxyadamantane-1-carboxylate **68** (42.0 g, 200 mmol). The suspension was allowed to warm at ambient temperature and stirred for 1 h. The resulting solution was quenched with water (500 mL). The organic layer was separated, washed with brine, dried (Na_2SO_4), filtered and concentrated *in vacuo* to afford crude **69** which slowly crystallized; yield 41.6 g (98 %); ^1H NMR (CDCl_3 , 400 MHz) δ (ppm) 1.70-1.80 (m, 6H), 2.20-2.35 (m, 3H), 2.50-2.60 (m, 6H), 7.00-7.70 (m, 5H, C_6H_5). Under an argon atmosphere was added to crude ester **69** (41.6 g, 196 mmol), 100 mL methanol, 75 mL of THF, 50 mL of water followed by NaOH pellets (16.0 g, 400 mmol). The solution was stirred overnight. The organic solvents were removed under reduced pressure, water (200 mL) was added and the solution was acidified to a pH of 1.0 with 6N HCl. The resulting solid precipitate was filtered, washed with water and air dried to afford 3-fluoroadamantane-1-carboxylic acid **70**; yield 34.1 g (88 %). Under an argon atmosphere was added 3-fluoroadamantane-1-carboxylic acid **70** (7.65 g, 38.6 mmol) to 150 mL of benzene. To this solution was added Et_3N (5.37 mL, 38.38 mmol) followed by DPPA (Diphenylphosphoryl azide) (8.31 mL, 38.8 mmol). The reaction mixture was heated to reflux for 45 min, then cooled at ambient temperature at which point benzyl alcohol (8.0 mL, 77.4 mmol) was added. The resulting reaction mixture was refluxed for 72 h. The crude reaction mixture was allowed to cool, concentrated *in vacuo* and was chromatographed on silica gel using 4:1 hexane:EtOAc to afford 3-fluoroadamantan-1ylamine benzyl carbamate **71**; yield 11.1 g (95 %); ^1H -NMR (400 MHz, CDCl_3) δ (ppm) 1.53 (m, 2H, 6-H), 1.75-1.95 (m, 10H, 2, 8, 9, 4, 10-H), 2.33 (br s, 2H, 5, 7-H), 4.76 (br s, 1H, NH), 5.03 (br s, 2H, $\underline{\text{C}}\text{H}_2\text{C}_6\text{H}_5$), 7.33 (m, 5H, C_6H_5). The benzyl carbamate **71** was dissolved in 100 mL of HOAc, 2 g of 10 % Pd/C was added and the mixture was hydrogenated (50 psi) for a period of 5 h. The crude reaction mixture was filtered, the catalyst was washed with HOAc and the filtrate was concentrated *in vacuo* to afford crude product **26** as its acetate salt; yield 7.4 g, (75 %); *Acetate*: ^1H -NMR (phosphate buffer, pH 7, 10 % D_2O , 500 MHz) δ (ppm) 1.60-1.69 (m, 2H, 6-H), 1.87 (s, 4H, 4, 10-H), 1.89-1.98 (m, 7H, 8,9-H, CH_3COO^-), 2.09 (br d, 2H, 2-H), 2.48 (br s, 2H, 5,7-H); LC-MS (m/z) 170.3 ($\text{FC}_{10}\text{H}_{14}\text{NH}_3^+$). *Base*: mp 210°C (EtOH-ether); ^1H -NMR (CDCl_3 , 400 MHz) δ (ppm) 1.41

(br s, 2H, 6-H), 1.49 (br s, 2H, NH₂), 1.51 (br s, 4H, 4,10-H), 1.74 (d, 2H, *J* = 6 Hz, 2-H), 1.79 (m, 4H, 8,9-H), 2.31 (br s, 2H, 5,7-H); ¹³C-NMR (CDCl₃, 50 MHz) δ (ppm) 31.33, 31.55 (5,7-C), 34.67 (6-C), 41.44, 41.77 (4,10-C), 44.74 (8,9-C), 51.14, 51.47 (2-C, 3-C), 93.29 (d, *J*_{C-F} = 183.8 Hz, 1-C).

4-(1-Adamantyl)aniline (27). The synthetic protocol used for preparation of 4-(1-adamantyl)aniline **27** was adapted from the literature.⁷⁴ The reaction between 1-adamantanol **72** with toluene/TFA afforded 1-(*p*-tolyl)adamantane **73** which was transformed through reaction with (a) KMnO₄ in pyridine/H₂O; (b) HCl 15%; (c) SOCl₂, reflux; (d) EtOH, reflux to the mixture of esters **74** and **75**. The crude product was purified by flash column chromatography (*n*-hexane/Et₂O, 9:1) resulting in ethyl 4-(1-adamantyl)benzoate **75** as the less polar extract; 230 mg; IR (Nujol) ν(C=O) 1715 cm⁻¹; ¹H NMR (400 MHz, CDCl₃) δ (ppm) 1.36-1.40 (t, 3H, *J* = 7Hz, CH₃), 1.75-1.80 (m, 6H, 4,6,10-adamantyl H), 1.92 (br.s, 6H, 2,8,9-adamantyl H), 2.11 (br s, 3H, 3,5,7-adamantyl H), 4.34-4.39 (q, 2H, *J* = 7Hz, CH₂O) 7.43 (d, *J* = 8 Hz, 2H, 3,5-H C₆H₅), 7.98-8.00 (m, 3H, C₆H₅). An aqueous conc. solution of NaOH (130 mg) was added to a mixture of ester **75** (230 mg, 0.809 mmol) in ethanol (10 ml), which was then refluxed under vigorous stirring for 2 h. Ethanol was removed in vacuo and water was added into the residue. The mixture was acidified by the dropwise addition of a HCl 10% solution, under stirring and cooling. The acidified mixture was allowed to stand overnight in the refrigerator and the precipitate formed was collected by filtration, washed with water and dried over P₂O₅ to give the carboxylic acid **76** as a white solid; yield 160 mg (75 %); ¹H NMR (400 MHz, DMSO-d₆) δ (ppm) 1.73 (br.s, 6H, 4,6,10-adamantyl H), 1.87 (br.s, 6H, 2,8,9-adamantyl H), 2.06 (br.s, 3H, 3,5,7-adamantyl H), 7.47 (d, *J* = 8 Hz, 2H, 3,5-H C₆H₅), 7.87-7.89 (m, 3H, C₆H₅), 12.78 (s, 1H, CO₂H). Benzoic acid **76** (160 mg, 0.625 mmol) was treated with thionyl chloride (4 ml) at 60-65 °C for 25 min. Thionyl chloride was removed under reduced pressure and the last traces were removed azeotropically with the aid of benzene. The residue was dissolved in anhydrous acetone (10 ml) and a solution of sodium azide (93 mg, 1.88 mmol) in water (5 ml) was added dropwise into the above acetone solution with stirring at 0 °C. The reaction mixture was stirred at 0 °C for 15 min and then at room temperature for 30 min. Acetone was evaporated *in vacuo* and water was added into the residue. The mixture was extracted with benzene, the combined benzene extracts were washed with water, dried over Na₂SO₄ and evaporated under reduced pressure below 40 °C. Carbonylazide **78** was obtained as a solid; yield 90 mg (55 %); mp 114-116 °C; IR (Nujol), ν(N=N) 2134.9 cm⁻¹, ν(C=O) 1694.7 cm⁻¹. A solution of carbonylazide **78** (90 mg, 0.320 mmol) in dry xylene (3 ml) was heated gradually until the appearance of gas evolution (~105 °C). Heating was continued carefully until the temperature reach at 128-130 °C. The mixture was stirred at this temperature until nitrogen evolution ceased (30-40 min). The mixture was then allowed to cool at 95-90 °C and concentrated hydrochloric acid (4-5 ml) was added rapidly dropwise into the mixture. Vigorous gas evolution was observed and stirring at this temperature was continued until the evolution of carbon dioxide ceased. The mixture was allowed to cool

at room temperature and the solvents were removed under high vacuum. The residue was treated with dry ether and the solid so formed was separated by filtration and washed with dry ether; yield 25 mg (30 %) of hydrochloride of **27**. mp>250 °C (EtOH-Et₂O); ¹H NMR (400 MHz, MeOD) δ (ppm) 1.81 (br s, 6H, 4,6,10-adamantyl H), 1.94 (br s, 6H, 2,8,9-adamantyl H), 2.09 (br s, 3H, 3,5,7-adamantyl H), 7.31 (d, *J* = 8 Hz, 2H, 3,5-H C₆H₅), 7.53-7.55 (m, 3H, C₆H₅), 8.06 (br s, 3H, NH₃⁺).

4-Amino-4-isobutyl-2-methyloctane (30). Tertiary alcohol **80** was obtained after adding a solution of 2,6-dimethyl-heptan-4-one **79** (1 g, 7.04 mmol) in anhydrous diethyl ether (30% solution w/v) in a solution of *n*-butyllithium (1.6 M in hexanes, 13 mL, 21.1 mmol) at 0 °C under argon atmosphere and stirring the mixture overnight. After treating the mixture with saturated ammonium chloride following usual workup the corresponding tertiary alcohol **80** was obtained; yield 1.1 g (80 %). To a stirred mixture of sodium azide (488 mg, 7.50 mmol) and dry dichloromethane (15 mL), trifluoroacetic acid (2.9 g, 25 mmol) was added at 0 °C. The resulting mixture was stirred for 10 min at 0 °C and a solution of the tertiary alcohol **80** (500 mg, 2.50 mmol) in 10 mL of dichloromethane was added dropwise. The mixture was stirred at 0-5 °C for 4 h and 24 h at ambient temperature. The mixture was made alkaline by adding NH₃ 12 % (40 mL) and the organic phase was separated. The aqueous phase was extracted with dichloromethane and the combined organic phases were washed with water, brine and dried (Na₂SO₄). Solvent was evaporated *in vacuo* to afford 4-azido-4-isobutyl-2-methyloctane **81**; yield 340 mg (76 %); IR (Nujol) ν(N₃) 2099 cm⁻¹; ¹³C NMR (CDCl₃, 50 MHz) δ (ppm) 14.2(n-Bu, CH₃), 24.0(n-Bu, CH₂CH₃), 24.2(2xCH), 24.6 (i-Bu, 2xCH₃), 26.3 (n-Bu, CH₂CH₂CH₃), 36.4 (n-Bu, CH₂CN₃), 45.5 (i-Bu, 2xCH₂), 67.1 (CN₃). To a stirred suspension of LiAlH₄ (230 mg, 6.04 mmol) in dry ether (20 mL) was added dropwise at 0 °C a solution of the alkyl azide **81** (340 mg, 1.51 mmol) in dry ether (15 mL). The mixture was gently refluxed for 5 h and then was treated with water, NaOH 10 % and water. The insoluble inorganic material was filtered-off, washed with ether and the filtrate was extracted with HCl 6%. The aqueous phase was made alkaline with solid sodium carbonate and was extracted with dichloromethane or ether. The organic phase was washed with brine, dried (Na₂SO₄) and evaporated *in vacuo* to afford the amine **31**; yield 60 mg (20 %); ¹H NMR (CDCl₃, 400 MHz) δ 0.89 (t, *J* = 7 Hz, 3H, n-Bu, CH₃), 0.94 (dd, *J* = 2 Hz, 6 Hz, 12H, i-Bu, 2x(CH₃)₂), 1.19-1.37 (m, 10H, 5xCH₂), 1.63-1.76 (m, 2H, 2xCH); ¹³C NMR (CDCl₃, 50 MHz) δ 14.3 (n-Bu, CH₃), 23.5 (n-Bu, CH₂CH₃), 23.8 (2xCH), 25.5 (i-Bu, 2xCH₃), 26.3 (n-Bu, CH₂CH₂CH₃), 40.9 (n-Bu, CH₂CNH₂), 49.7 (i-Bu, 2xCH₂), 55.1 (CNH₂).

1-Adamantylguanidine (8). A Mixture of the hydrochloride of amantadine **1** (0.300 g, 1.60 mmol), hydrochloride of 1H-pyrazolo-1-carboxamide (0.282 g, 1.92 mmol), Et₃N (0.400 mL, 2.88 mmol) and CH₃CN (8 mL) was stirred at 70 °C for 6 h and stirring was maintained at 4 °C for 24 h. After evaporation of the solvent the solid hydrochloride of guanidine **8** was isolated, dissolved in water and the solution was made

alkaline with NaOH 3% w/v. The aqueous phase was extracted three times with an equal volume of dichloromethane. The combined organic phase was washed with water, dried (Na₂SO₄) and evaporated to afford free guanidine **8** (yield 0.240 g, 42%). Compound **8** was dissolved in anhydrous diethyl ether (10 mL) and the solution was acidified with a saturated solution of HCl/MeOH. Solvent evaporation under vacuum yields a white solid residue of the corresponding guanidine hydrochloride (ethanol/ether); ¹H-NMR (CDCl₃, 400MHz) δ(ppm) 1.55-1.64 (m, 12H, 2,4,6,8,9,10-H), 2.02 (s, 3H, 3,5,7-H), 6.31 (s, 2H, 3-H(-NH₂)), 7.57 (s, 1H, 2-H, NH=).

2-(1-Adamantyl)propylguanidine (24). The corresponding hydrochloride of guanidine **24** was prepared according to the same procedure followed for guanidine **8** using the hydrochloride of amine **21** (0.426 g, 1.86 mmol), hydrochloride 1H-pyrazolo-1-carboxamide (0.327 g, 0.23 mmol), Et₃N (0.465 mL, 3.35 mmol) and CH₃CN (10 mL); yield of free guanidine **24** 0.140 g (32%). Hydrochloride (ethanol/ether); ¹H-NMR (CDCl₃, 400 MHz) δ (ppm) 0.98 (s, 6H, 2xCH₃), 1.59-1.67 (m, 12H, 2,4,6,8,9,10-H), 1.97 (br, s, 3H, 3,5,7-H), 6.29 (s, 2H, 3-H(NH₂)), 7.56 (s, 1H, 2-H(NH=)).

2-Methyl-2-adamantylguanidine (18). The corresponding hydrochloride of guanidine **18** was prepared according to the same procedure followed for guanidine **8** using the hydrochloride of amine **16** (0.550 g, 2.74 mmol), hydrochloride 1H-pyrazolo-1-carboxamide (0.483 g, 3.29 mmol), Et₃N (0.685 mL, 4.93 mmol) in CH₃CN (14 mL); yield of free guanidine **33** 0.420 g (73%). Hydrochloride (ethanol/ether); ¹H-NMR (CDCl₃, 400 MHz) δ (ppm) 1.18 (s, 3H, CH₃), 1.48 (br,s, 2H, 8eq,10eq-H), 1.54-1.57 (d, J = 12Hz, 2H, 4eq,9eq-H), 1.63 (br s, 4H, 1,3,5,7-H), 1.76 (br s, 2H, 6-H), 1.92-1.95 (d, J = 12Hz, 2H, 8ax,10ax-H), 2.01-2.04 (d, J = 12Hz, 2H, 4ax,9ax-H), 2.76 (s, 1H, 1-H(NH-)), 6.28 (s, 2H, 3-H(NH₂)), 7.55 (s, 1H, 2-H(NH=)). ¹³C-NMR (DMSO, 600 MHz) δ (ppm) 22.9 (CH₃), 25.9 (3-C), 26.3 (1-C), 31 (5,7-C), 32.7 (4,9-C), 34.5 (8,10-C), 37.8 (6-C), 58.1 (2-C).

2-Propyl-2-adamantylguanidine (19). The corresponding hydrochloride of guanidine **19** was prepared according to the same procedure followed for guanidine **8** using the hydrochloride of amine **17** (0.550 g, 2.40 mmol), hydrochloride 1H-pyrazolo-1-carboxamide (0.422 g, 2.88 mmol), Et₃N (0.600 mL, 4.32 mmol) in CH₃CN (12.2 mL); yield of free guanidine **33** 0.240 g (42%). Hydrochloride (ethanol/ether); ¹H-NMR (CDCl₃, 400MHz) δ (ppm) 0.90-0.94 (t, J = 7 Hz, 3H, CH₂CH₂CH₃), 1.26-1.36 (m, 2H, CH₂CH₂CH₃), 1.52-1.56 (m, 4H, 8eq,10eq-H,CH₂CH₂CH₃), 1.59-1.61 (d, J = 12 Hz, 2H, 4eq,9eq-H), 1.64-1.66 (m, 2H, 6-H), 1.80 (s, 2H, 5,7-H), 1.94-1.97 (d, J = 12 Hz, 2H, 8ax,10ax-H), 2.05-2.08 (d, J = 12Hz, 2H, 4ax,9ax-H), 6.34 (s, 2H, 3-H(-NH₂)), 7.60 (s, 1H, 2-H(NH=)).

5.5.2 Synthesis of aminoadamantane polar head conjugates

5.5.2.1 General Procedures of Reductive Amination

Procedure A

Aminoadamantane (1.2 equiv) and aldehyde (1.0 equiv) were mixed in MeOH and then treated with NaCNBH₃ (3.0 equiv). The mixture was stirred at rt under argon overnight. The reaction mixture was quenched with H₂O, and the product was extracted with EtOAc. The combined organic layer was dried over Na₂SO₄, and concentrated under reduced pressure. The crude product was separated by flash column chromatography with Et₂O /hexane 4:1 to give the target imine. The imine (1eq) was dissolved in MeOH and to the solution was added p-toluenesulfonic acid monohydrate (1eq), sodium borohydride (4eq) and the mixture was stirred at rt for 4h. The reaction mixture was quenched with saturated aqueous solution of NaHCO₃ (10 ml) and extracted with CH₂Cl₂. The combined organic extract was dried over anhydrous Na₂SO₄, filtered and concentrated. The mixture was then purified by silica gel flash column chromatography (CH₃OH/CH₂Cl₂ 1:2) to give the final product.

Procedure B

The chloride (1 equiv), and aminoadamantane (1.5 equiv) were dissolved in isopropanol. CsI (0.1 equiv) and triethyl amine (2 equiv) were then added. The reaction mixture was heated to reflux overnight. The solvent was removed under reduced pressure, and the resulting residue was extracted with ethyl acetate and water. The organic layer was separated, dried over Na₂SO₄, filtered, and concentrated under reduced pressure. The mixture was then purified by silica gel flash column chromatography (1:2 CH₃OH/CH₂Cl₂) to give the final product.

Procedure C

Aminoadamantane (1.0 equiv) and aldehyde (1.0 equiv) were mixed and 2 mL of titanium (IV) isopropoxide (15 equiv) was added. The resulting slurry was heated to 100 °C and stirred overnight. Then the solution was cooled down to 0 °C in ice-bath. MeOH added and NaBH₄ (4.0 equiv) were added portion-wise over 10 min. The solution was warmed to rt and stirred overnight. The solvent was removed under reduced pressure, and the resulting residue was extracted with EtOAc and H₂O. The organic layer was separated, dried over Na₂SO₄, filtered, and concentrated under reduced pressure. The crude mixture was purified by silica gel flash column chromatography (CH₃OH/CH₂Cl₂ 1:2) to give the desired compound.

5.5.2.2 Aminoadamantane polar head conjugates

Compound 32 (Procedure A). Reaction of 2-aminoadamantane (**15**) (88 mg, 0.583 mmol) and 2-hydroxy-4-methoxybenzaldehyde (74 mg, 0.486 mmol) in MeOH (2 mL) followed by addition of NaCNBH₃ (110 mg, 1.75 mmol) to afford imine **82a**; yield 88 mg (56 %); ¹H NMR (CDCl₃, 400 MHz) δ (ppm) 1.61 (d, J = 8 Hz, 2H, 4eq, 9eq-adamantyl H), 1.78 (br s, 4H, 1,3,8eq,10eq-adamantyl H), 1.89-1.95 (m, 8H, 5,6,7,8ax,10ax,4ax,9ax-adamantyl H), 3.50 (s, 2H, 2-adamantyl H) 3.80 (s, 3H, OCH₃), 6.30 (dd, J = 8, 2.4 Hz, 1H, phenyl H), 6.36 (d, J = 2 Hz, 1H, phenyl H), 7.05 (d, J = 8 Hz, 1H, phenyl H), 8.14 (s, 1H, CH=N).

Reaction of imine **82a** (88 mg, 0.327 mmol) with PTSA (56 mg, 0.327 mmol) and NaBH₄ (50 mg, 1.31 mmol) in MeOH (2 mL) afforded amine **32**; yield 80 mg (85 %); ¹H NMR (CDCl₃, 400 MHz) δ (ppm) 1.57 (d, J = 8 Hz, 2H, 4eq,9eq-adamantyl H), 1.74 (br s, 4H, 1,3,8eq,10eq-adamantyl H), 1.86 (br s, 4H, 5,7,6-adamantyl H), 1.95 (m, 4H, 8ax,10ax,4ax,9ax-adamantyl H), 2.82 (s, 2H, 2 adamantyl H) 3.76 (s, 3H, OCH₃), 3.92 (s, 2H, CH₂N), 5.29 (br s, OH), 6.31 (dd, J = 8, 2.4 Hz, 1H, phenyl H), 6.43 (d, J = 2 Hz, 1H, phenyl H), 6.89 (d, J = 8 Hz, 1H, phenyl H); ¹³C NMR (CDCl₃, 50 MHz) δ (ppm) 27.5 (5-adamantyl C), 27.7 (7-adamantyl C), 31.6 (4,9-adamantyl C), 31.7 (8,10 adamantane-C), 37.6 (1,3-adamantane-C), 37.8 (6-adamantyl C), 49.6 (CH₂N), 55.4 (OCH₃) 61.2 (2-adamantyl C), 102.1 (3-phenyl CH), 104.5 (5-phenyl CH), 115.6 (1-phenyl C), 128.7 (6-phenyl CH), 159.7 (2-phenyl COH), 160.5 (4-phenyl COCH₃); HRMS (m/z): [M + H⁺] calcd for C₁₈H₂₅NO₂ 287.1885, experimental 287.1890.

Compound 33. To a solution of amine **32** (35 mg, 0.129 mmol) in CH₂Cl₂ (3 mL) at -78 °C was added BBr₃ (1.0 M in CH₂Cl₂, 0.8 mL, 0.775 mmol). The mixture was warmed at 0 °C and stirred overnight at rt. Then the mixture was quenched with MeOH (3 mL) at -78 °C and warmed at rt. After evaporation of MeOH the mixture was diluted with AcOEt (15 mL) and washed with NaHCO₃ (satd) (2 x 5 mL) and the water phase was extracted with AcOEt (2 x 10 mL). The combined organic layers were dried over Na₂SO₄, filtered, and concentrated under reduced pressure to give amine **33**; yield 28 mg (80 %); ¹H NMR (CDCl₃, 400 MHz) δ (ppm) 1.56-1.61 (m, 2H, 4eq,9eq-adamantyl H), 1.72 (br s, 4H, 1,3,8eq, 10eq-adamantyl H), 1.85-1.95 (m, 8H, 5,7,6-H, 8ax,10ax,4ax,9ax-adamantyl H), 2.82 (s, 1H, 2-adamantyl H) 3.90 (s, 2H, CH₂N), 5.73 (br s, 2H, 2xOH), 6.24 (dd, J = 8, 2.4 Hz, 1H, phenyl H), 6.35 (d, J = 2 Hz, 1H, phenyl H), 6.79 (d, J = 8 Hz, 1H, phenyl H); ¹³C NMR (CDCl₃, 50 MHz) δ (ppm) 27.5 (5- adamantyl C), 27.7 (7-adamantyl C), 31.5 (4,9,8,10-adamantyl C), 37.5 (1,3-adamantyl C), 37.8 (6-C), 49.6 (CH₂N), 61.3 (2-adamantyl C), 103.9 (3-phenyl CH), 106.2 (5-phenyl CH), 115.6 (1-C, phenyl C), 129.1 (6-phenyl CH), 156.9 (2-phenyl COH,), 159.6 (4-phenyl COH,); HRMS (m/z): [M + H⁺] calcd for C₁₇H₂₃NO₂ 274.1729, experimental 274.1730.

Compound 34 (Procedure A). Reaction of 2-methyl-2-aminoadamantane **16** (50 mg, 0.280 mmol) and 2-hydroxy-4-methoxybenzaldehyde (35 mg, 0.232 mmol) in MeOH (2 mL) followed by addition of NaCNBH₃ (53 mg, 0.840 mmol) to afford imine **82b**; yield 70 mg (86 %); ¹H NMR (CDCl₃, 400 MHz) δ (ppm) 1.44 (s, 3H, CH₃), 1.60 (br s, 2H, 4eq, 9eq-adamantyl H), 1.67-1.72 (m, 6H, 1,3,8eq,10eq,5,7-adamantyl H), 1.80-2.18 (m, 6H, 8ax,10ax,4ax,9ax,6-adamantyl H), 3.75 (br s OH), 3.78 (s, 3H, OCH₃), 6.23 (dd, *J* = 8, 2.4 Hz, 1H, phenyl H), 6.27 (d, *J* = 2 Hz, 1H, phenyl H), 6.96 (d, *J* = 8 Hz, 1H, phenyl H), 7.99 (s, 1H, CH=N); ¹³C NMR (CDCl₃, 50 MHz) δ (ppm) 23.8 (CH₃), 26.9 (5-adamantyl C), 27.4 (7-adamantyl C), 33.0 (4,9-adamantyl C), 33.9 (8,10-adamantyl C), 37.6 (1, 3-adamantyl C), 38.6 (6-adamantyl C), 55.3 (OCH₃) 61.7 (2-adamantyl C), 102.4 (3-phenyl CH), 106.5 (5-phenyl CH), 111.2 (1-phenyl C), 133.5 (6-phenyl CH), 158.9 (CH=N), 165.9 (2-phenyl COH), 174.7 (4-phenyl COCH₃).

Reaction of imine **82b** (70 mg, 0.247mmol) with PTSA (43 mg, 0.247 mmol) and NaBH₄ (38 mg, 0.988 mmol) in MeOH (2 mL) afforded amine **34**; yield 55 mg (79 %); ¹H NMR (CDCl₃, 400 MHz) δ (ppm) 1.34 (s, 3H, CH₃), 1.60 (br s, 2H, 4eq, 9eq-H), 1.68-1.75 (m, 6H, 1,3,8eq,10eq,5,7-adamantyl H), 1.88 (br s, 2H, 6-adamantyl H), 1.95-2.01 (m, 4H, 8ax,10ax,4ax,9ax-adamantyl H), 3.74 (br s, OH), 3.76 (s, 3H, OCH₃), 3.84 (s, 2H, CH₂N), 6.31 (dd, *J* = 8, 2.4 Hz, 1H, phenyl H), 6.41 (d, *J* = 2 Hz, 1H, phenyl H), 6.88 (d, *J* = 8 Hz, 1H, phenyl H); ¹³C NMR (CDCl₃, 50 MHz) δ (ppm) 22.8 (CH₃), 27.0 (5-adamantyl C), 27.9 (7-adamantyl C), 32.8 (4,9- adamantyl C), 34.2 (8,10-adamantyl C), 35.8 (1,3-adamantyl C), 38.9 (6-adamantyl C), 43.6 (CH₂N), 55.4 (OCH₃) 56.8 (2-adamantyl C), 102.2 (3-phenyl CH), 104.9 (5-phenyl CH), 115.8 (1-phenyl C), 128.8 (6-phenyl CH), 160.3 (2-phenyl C-OH), 161.0 (4-phenyl COCH₃); HRMS (*m/z*): [M + H⁺] calcd for C₁₉H₂₇NO₂ 301.2042, experimental 301.2045.

Compound 40 (Procedure A). Reaction of 2-propyl-2-aminoadamantane **17** (350 mg, 1.81 mmol) and 2-hydroxy-4-methoxybenzaldehyde (230 mg, 1.51 mmol) in MeOH (2 mL) followed by addition of NaCNBH₃ (342 mg, 5.43 mmol) to afford imine **35**; yield 470 mg (80 %); ¹H NMR (CDCl₃, 400 MHz) δ (ppm) 0.87 (t, *J* = 7 Hz, 3H, CH₂CH₂CH₃), 1.22-1.3 (m, 2H, CH₂CH₂CH₃), 1.58 (d, *J* = 12 Hz, 2H, 4eq,9eq-adamantyl H), 1.71 (m, 2H, CH₂CH₂CH₃), 1.72-1.8 (4H, 1,3,8eq,10eq-adamantyl H), 1.96 (br s, 2H, 6-adamantyl H), 1.97-2.06 (m, 6H, 5,7,8ax,10ax,4ax,9ax-adamantyl H), 3.78 (s, 3H, OCH₃), 5.29 (br s, OH), 6.17 (dd, *J* = 8, 2.4 Hz, 1H, phenyl H), 6.24 (d, *J* = 2 Hz, 1H, phenyl H), 6.99 (d, *J* = 8 Hz, 1H, phenyl H), 7.83 (s, 1H, CH=N); ¹³C NMR (CDCl₃, 50 MHz) δ (ppm) 14.6 (CH₂CH₂CH₃), 15.3 (CH₂CH₂CH₃), 27.2 (5-adamantyl C), 27.5 (7-adamantyl C), 32.9 (4,9-adamantyl C), 33.5 (8,10-adamantyl C), 34.9 (1,3-adamantyl C), 38.5 (CH₂CH₂CH₃), 39.9 (6-adamantyl C), 55.4 (OCH₃), 63.8 (2-adamantyl C), 102.5 (2-phenyl CH), 106.4 (5-phenyl CH), 115.8 (1-phenyl C), 133.6 (6-phenyl CH), 159.2 (CH=N), 166.1 (2-phenyl COH), 175.4 (4-phenyl COCH₃); HRMS (*m/z*): [M + H⁺] calcd for C₂₁H₂₉NO₂ 327.2198, experimental 327.2195.

Reaction of imine **35** (70 mg, 0.213 mmol,) PTSA (40 mg, 0.213 mmol) /NaBH₄(32 mg, 0.852 mmol) in MeOH (2 mL) afforded amine **40**; yield 60 mg (86 %). ¹H NMR (CDCl₃, 400 MHz) δ (ppm) 0.97 (t, *J* = 7 Hz, 3H, CH₂CH₂CH₃), 1.19-1.29 (m, 2H, CH₂CH₂CH₃), 1.59 (d, *J* = 12 Hz, 2H, 4eq,9eq-adamantyl H), 1.63 (br s, 2H, 8eq,10eq-adamantyl H), 1.65-1.67 (m, 4H, 1,3-adamantyl H, CH₂CH₂CH₃), 1.77 (br s, 2H, 5,7-adamantyl H H), 1.88 (br s, 2H, 6-adamantyl H), 1.96 (d, *J* = 12 Hz, 2H, 8ax,10ax-adamantyl H), 2.08 (d, *J* = 12 Hz, 2H, 4ax,9ax-adamantyl H), 3.71 (s, 2H, CH₂N), 3.76 (s, 3H, OCH₃), 3.78 (br s, OH), 6.39 (dd, *J* = 8, 2.4 Hz, 1H, phenyl H), 6.42 (d, *J* = 2 Hz, 1H, phenyl H), 6.89 (d, *J* = 8 Hz, 1H, phenyl H); ¹³C NMR (CDCl₃, 50 MHz) δ (ppm) 14.6 (CH₂CH₂CH₃), 15.3 (CH₂CH₂CH₃), 27.2 (5-adamantyl C), 27.5 (7-adamantyl C), 32.9 (4,9-adamantyl C), 33.5 (8,10-adamantyl C), 34.9 (1,3-adamantyl C), 38.5 (CH₂CH₂CH₃), 39.9 (6-adamantyl C), 55.4 (OCH₃), 63.8 (2-adamantyl C), 102.0 (3-phenyl CH), 104.8 (5-phenyl CH), 111.2 (1-phenyl C), 128.9 (6-phenyl CH), 160.5 (2-phenyl COH, phenyl), 175.3 (4-phenyl COCH₃); HRMS (*m/z*): [M + H⁺] calcd for C₂₁H₃₁NO₂ 329.2355, experimental 329.2361.

Compound 36. Compound **36** was prepared following the same procedure applied for the preparation of compound **33** by treating imine **35** (250 mg, 0.768 mmol), with BBr₃ (1.0 M in CH₂Cl₂, 4.8 mL, 4.7 mmol) in CH₂Cl₂ (10 mL) at -78 °C; yield 180 mg (75 %). ¹H NMR (CDCl₃, 400 MHz) δ (ppm) 0.86 (t, *J* = 7 Hz, 3H, CH₂CH₂CH₃), 1.30-1.33 (m, 2H, CH₂CH₂CH₃), 1.60 (d, *J* = 12 Hz, 2H, 4eq,9eq-adamantyl H), 1.69 (br s, 2H, 1,3-adamantyl H), 1.75-1.95 (m, 8H, 5,6,7,8eq,10eq-adamantyl H, CH₂CH₂CH₃), 1.99-2.04 (m, 4H 4ax,9ax,8ax,10ax-adamantyl H), 5.31 (s, 2H, 2xOH), 6.16 (dd, , *J* = 8, 2.4 Hz, 1H, phenyl H), 6.36 (d, *J* = 2 Hz, 1H, phenyl H), 6.94 (d, *J* = 8 Hz, 1H, phenyl H), 7.74 (s, 1H, CH=N); HRMS (*m/z*): [M + H⁺] calcd for C₂₀H₂₇NO₂ 313.2042, experimental 313.2053.

Compound 37 (Procedure C). To a mixture of 2-propyl-2-aminoadamantane (**17**) (105 mg, 0.543 mmol) and 2-hydroxybenzaldehyde (66 mg, 0.543 mmol) in Ti(iPrO)₄ (2 mL, 8.15 mmol) was added NaBH₄ (83 mg, 2.17 mmol) and MeOH (2 mL) to afford amine **37**; yield 130 mg (76 %); ¹H NMR (CDCl₃, 400 MHz) δ (ppm) 0.98 (t, *J* = 7 Hz, 3H, CH₂CH₂CH₃), 1.19-1.29 (m, 2H, CH₂CH₂CH₃), 1.59 (d, *J* = 12 Hz, 2H, 4eq,9eq-adamantyl H), 1.68-1.72 (m, 6H, 1,3,8eq,10eq- adamantyl H, CH₂CH₂CH₃), 1.76 (1H, NH), 1.79 (br s, 2H, 5,7-adamantyl H), 1.90 (br s, 2H, 6-adamantyl H), 1.98 (d, *J* = 12 Hz, 2H, 8ax,10ax-adamantyl H), 2.10 (d, *J* = 12 Hz, 2H, 4ax,9ax- adamantyl H), 3.78 (s, 2H, CH₂N), 3.96 (br s, OH), 6.78 (t, *J* = 8 Hz, 1H, phenyl H), 6.84 (d, *J* = 8 Hz, 1H, phenyl H), 7.02 (d, *J* = 7 Hz, 1H, phenyl H), 7.19 (t, *J* = 8 Hz 1H, phenyl H); HRMS (*m/z*): [M + H⁺] calcd for C₂₀H₂₉NO 299.2249, experimental 299.2251.

Compound 38 (Procedure C). To the mixture of 2-propyl-2-aminoadamantane **17** (100 mg, 0.517 mmol) and 3-hydroxybenzaldehyde (63 mg, 0.517 mmol) in Ti(iPrO)₄ (2 mL, 7.76 mmol) was added NaBH₄ (80 mg, 2.07

mmol) and MeOH (2 mL) to afford amine **38**; yield 100 mg (62 %); ^1H NMR (CDCl_3 , 400 MHz) δ (ppm) 0.96 (t, $J = 7$ Hz, 3H, $\text{CH}_2\text{CH}_2\text{CH}_3$), 1.15-1.35 (m, 2H, $\text{CH}_2\text{CH}_2\text{CH}_3$), 1.48 (d, $J = 12$ Hz, 2H, 4eq, 9eq-adamantyl H), 1.65-1.70 (m, 6H, 1,3,8eq,10eq-adamantyl H, $\text{CH}_2\text{CH}_2\text{CH}_3$), 1.78-1.85 (m, 4H, 5,7,6- adamantyl H), 1.95 (d, $J = 12$ Hz, 2H, 8ax,10ax-adamantyl H), 2.14 (d, $J = 12$ Hz, 2H, 4ax,9ax-adamantyl H), 3.50 (s, 2H, CH_2N), 4.06 (br s, OH), 6.62 (d, $J = 8$ Hz, 1H, phenyl H), 6.83-6.85 (m, 2H, phenyl H), 7.08 (d, $J = 8$ Hz, 1H, phenyl H); ^{13}C NMR (CDCl_3 , 50 MHz) δ (ppm) 15.1 ($\text{CH}_2\text{CH}_2\text{CH}_3$), 15.2 ($\text{CH}_2\text{CH}_2\text{CH}_3$), 27.8 (5-adamantyl C), 28.0 (7-adamantyl C), 32.8 (4,9- adamantyl C), 33.8 (8,10-adamantyl C), 34.0 (1,3-adamantyl C), 34.4 ($\text{CH}_2\text{CH}_2\text{CH}_3$), 39.2 (6-adamantyl C), 44.6 (CH_2N), 57.9 (2-adamantyl C), 114.3 (6-phenyl CH), 115.9 (5-phenyl CH), 120.5 (4-phenyl CH), 129.6 (2-phenyl), 143.1 (1-phenyl C) 156.1 (3-phenyl CH); HRMS (m/z): $[\text{M} + \text{H}^+]$ calcd for $\text{C}_{20}\text{H}_{29}\text{NO}$ 299.2249, experimental 299.2254.

Compound 39 (Procedure C). To the mixture of 2-propyl-2-aminoadamantane **17** (100 mg, 0.517 mmol) and 4-hydroxybenzaldehyde (63mg, 0.517 mmol) in $\text{Ti}(\text{iPrO})_4$ (2 mL, 7.76 mmol) was added NaBH_4 (80 mg, 2.07 mmol) and MeOH (2 mL) to afford amine **39**; yield 120 mg (74 %); ^1H NMR (CDCl_3 , 400 MHz) δ (ppm) 0.97 (t, $J = 7$ Hz, 3H, $\text{CH}_2\text{CH}_2\text{CH}_3$), 1.28-1.38 (m, 2H, $\text{CH}_2\text{CH}_2\text{CH}_3$), 1.52 (d, $J = 12$ Hz, 2H, 4eq, 9eq-adamantyl H), 1.64-1.71 (m, 7H, 1,3,8eq,10eq-adamantyl H, $\text{CH}_2\text{CH}_2\text{CH}_3$, NH), 1.80 (br s, 2H, 5,7-adamantyl H), 1.84 (br s, 2H, 6-H), 1.96 (d, $J = 12$ Hz, 2H, 8ax,10ax-adamantyl H), 2.15 (d, $J = 12$ Hz, 2H, 4ax,9ax-adamantyl H), 3.46 (s, 2H, CH_2N), 4.06 (br s, OH), 6.61 (d, $J = 8$ Hz, 2H, phenyl H), 7.16 (d, $J = 8$ Hz, 2H, phenyl H); ^{13}C NMR (CDCl_3 , 50 MHz) δ (ppm) 15.1 ($\text{CH}_2\text{CH}_2\text{CH}_3$), 15.3 ($\text{CH}_2\text{CH}_2\text{CH}_3$), 27.8 (5-adamantyl C), 28.0 (7-adamantyl C), 32.8 (4,9-adamantyl C), 33.8 (8,10-adamantyl C), 33.9 (1,3-adamantyl C), 34.4 ($\text{CH}_2\text{CH}_2\text{CH}_3$), 39.3 (6-adamantyl C), 44.2 (CH_2N), 57.9 (2-adamantyl C), 115.9 (3,5-phenyl CH), 129.8 (2,6-phenyl CH), 132.9 (1-phenyl C), 155.2 (4-phenyl C); HRMS (m/z): $[\text{M} + \text{H}^+]$ calcd for $\text{C}_{20}\text{H}_{29}\text{NO}$ 299.2249, experimental 299.2246.

Compound 41. Compound **41** was prepared following the same procedure applied for the preparation of compound **33** by adding BBr_3 (1.0 M in CH_2Cl_2 , 0.5 mL, 6.0 mmol) to **40** (25 mg, 0.076 mmol) in CH_2Cl_2 (3 mL) at -78 °C; yield 10 mg (43 %). ^1H NMR (CDCl_3 , 400 MHz) δ (ppm) 0.97 (t, $J = 7$ Hz, 3H, $\text{CH}_2\text{CH}_2\text{CH}_3$), 1.21-1.31 (m, 2H, $\text{CH}_2\text{CH}_2\text{CH}_3$), 1.61 (d, $J = 12$ Hz, 2H, 4eq,9eq-adamantyl H), 1.67 (m, 2H, $\text{CH}_2\text{CH}_2\text{CH}_3$), 1.71-1.73 (4H, 1,3,8eq,10eq-adamantyl H), 1.74 (1H, NH), 1.77 (br s, 2H, 5,7-adamantyl H), 1.82 (br s, 2H, 6-adamantyl H), 1.98 (d, $J = 12$ Hz, 2H, 8ax,10ax-adamantyl H), 2.09 (d, $J = 12$ Hz, 2H, 4ax,9ax-adamantyl H), 3.71 (s, 2H, CH_2N), 3.76 (br s, OH), 6.33 (dd, $J = 8, 2.4$ Hz, 1H, phenyl H), 6.43 (d, $J = 2$ Hz, 1H, phenyl H), 6.88 (d, $J = 8$ Hz, 1H, phenyl H); HRMS (m/z): $[\text{M} + \text{H}^+]$ calcd for $\text{C}_{20}\text{H}_{29}\text{NO}_2$ 315.2198, experimental 315.2196.

Compound 42 (Procedure B). To the mixture of 2-propyl-2-aminoadamantane **17** (110 mg, 0.569 mmol) and 3-chloromethyl-5-methylisoxazole (50 mg, 0.379 mmol) in isopropanol (2 mL) was added CsI (15 mg, 0.0569

mmol) and Et₃N (115 mg, 1.14 mmol) to afford amine **42**; yield 35 mg (32%); ¹H NMR (CDCl₃, 400 MHz) δ (ppm) 0.93 (t, *J* = 7 Hz, 3H, CH₂CH₂CH₃), 1.20-1.26 (m, 2H, CH₂CH₂CH₃), 1.46 (d, *J* = 12 Hz, 2H, 4eq,9eq-adamantyl H), 1.61 (d, *J* = 12 Hz, 2H, 8eq,10eq-adamantyl H), 1.65-1.72 (m, 6H, CH₂CH₂CH₃, 6,1,3-adamantyl H), 1.80 (br s, 2H, 5,7-adamantyl H), 1.93 (d, *J* = 12 Hz, 2H, 8ax,10ax-adamantyl H), 2.20 (d, *J* = 12 Hz, 2H, 4ax,9ax-adamantyl H), 2.4 (s, 3H, CH₃), 3.6 (s, 2H, CH₂N), 6.0 (s, 1H, isoxazolyl CH=); ¹³C NMR (CDCl₃, 50 MHz) δ (ppm) 12.3 (CH₂CH₂CH₃), 14.9 (CH₃), 15.0 (CH₂CH₂CH₃), 27.8 (5,7-adamantyl C), 32.6 (4,9-adamantyl C), 33.5 (8,10-adamantyl C), 34.0 (1,3-adamantyl C), 36.0 (CH₂CH₂CH₃) 39.0 (6-adamantyl C), 57.9 (2-adamantyl C), 101.5 (isoxazolyl CH=), 165 (isoxazolyl C=N), 170 (isoxazolyl CO); HRMS (*m/z*): [M + H⁺] calcd for C₁₈H₂₈N₂O 288.2202, experimental 288.2212.

Compound 43 (Procedure C). To the mixture of 2-propyl-2-aminoadamantane **17** (150 mg, 0.777mmol) and 5-phenylisoxazole-3-carboxaldehyde (63mg, 0.517 mmol) in Ti(iPrO)₄ (3 mL, 11.7 mmol) was added NaBH₄ (118 mg, 3.11 mmol) and MeOH (3 mL) to afford amine **43**; yield 190 mg (70 %). ¹H NMR (CDCl₃, 400 MHz) δ (ppm) 0.94 (t, *J* = 7 Hz, 3H, CH₂CH₂CH₃), 1.20-1.3 (m, 2H, CH₂CH₂CH₃), 1.50 (d, *J* = 12 Hz, 2H, 4eq, 9eq-adamantyl H), 1.63 (m, 2H, CH₂CH₂CH₃), 1.63-1.69 (4H, 1,3,8eq, 10eq-adamantyl H), 1.70 (br s, 2H, 6-adamantyl H), 1.82 (br s, 2H, 5,7-adamantyl H), 1.93 (d, *J* = 12 Hz, 2H, 8ax,10ax-adamantyl H), 2.2 (d, *J* = 12 Hz, 2H, 4ax,9ax-adamantyl H), 3.7 (s, 2H, CH₂N), 6.60 (s, 1H, isoxazolyl CH), 7.4-7.5 (m, 3H, phenyl CH), 7.7 (d, *J* = 12 Hz, 2H, phenyl CH); ¹³C NMR (CDCl₃, 50 MHz) δ (ppm) 14.9 (CH₂CH₂CH₃), 15.2 (CH₂CH₂CH₃), 27.9 (5, 7-C), 32.8 (4,9-adamantyl C), 33.7 (8,10-adamantyl C), 34.2 (1,3-adamantyl C), 34.3 (CH₂CH₂CH₃) 36.3 (6-adamantyl C), 39.2 (CH₂N), 57.2 (2-adamantyl C), 99.4 (isoxazolyl CH=) 125.9 (phenyl CH) 127.8 (phenyl C), 129.0 (phenyl CH), 130.1 (phenyl CH), 165.1 (isoxazolyl C=N), 169.9 (isoxazolyl CO); HRMS (*m/z*): [M + H⁺] calcd for C₂₃H₃₀N₂O 350.2358, experimental 350.2362.

Compound 44. To a vigorously stirred mixture of 2-propyl-2-aminoadamantane **17** (100 mg, 0.517 mmol) in dichloromethane (8 mL) and K₂CO₃ (82 mg, 0.595 mmol) in 5mL H₂O (5 mL), was added, dropwise, a solution of bromoacetyl chloride (90 mg, 0.569mmol) in dichloromethane (5 mL). The reaction mixture was stirred at rt for 24 h. The resulting mixture was extracted with dichloromethane and the organic phase was washed with NaHCO₃ 10% (1x15 ml), HCl 3% (1x15mL), water and brine and evaporated under vacuum to afford the bromacetamide **83**; yield 110 mg (69 %) ; ¹³C NMR (CDCl₃, 50 MHz) δ (ppm) 14.7 (CH₂CH₂CH₃), 16.1 (CH₂CH₂CH₃), 27.2 (5,7-adamantyl C), 30.2 (CH₂CH₂CH₃), 33.0 (4,9-adamantyl C), 33.2 (1,3-adamantyl C), 33.3 (8,10-adamantyl C), 34.7 (6-adamantyl C), 38.6 (CH₂Br), 61.5 (2-adamantyl C), 163.6 (C=O). A mixture of the bromacetamide **83** (105 mg, 0.334 mmol) and NaN₃ (43 mg, 0.668 mmol) in ethanol (3 mL) was stirred for 5 h at rt. After evaporation of ethanol, water (10 mL) was added and the aqueous phase was extracted twice with

an equal volume of diethyl ether. The combined organic phase was washed with water and brine, dried (Na_2SO_4) and evaporated to afford the oily azide **84**; yield 75 mg (82 %); ^{13}C NMR (CDCl_3 , 50 MHz) δ (ppm) 14.6 ($\text{CH}_2\text{CH}_2\text{CH}_3$), 16.0 ($\text{CH}_2\text{CH}_2\text{CH}_3$), 27.2 (5,7-adamantyl C), 32.9 (4,9-adamantyl C), 33.2 (1,3-adamantyl C), 33.3 (8,10-adamantyl C), 34.9 ($\text{CH}_2\text{CH}_2\text{CH}_3$), 38.6 (6-adamantyl C), 53.3 (CH_2N_3), 61.3 (2-adamantyl C), 165.2 (C=O). A mixture of the azide **84** (75 mg, 0.271 mmol) and PPh_3 (78 mg, 0.298 mmol) in THF (3 mL) and water (5 mL) was stirred for 72 h at rt. The solvent was evaporated under vacuum and the residue was dissolved in Et_2O . The organic solution was washed with water and extracted with HCl 4% (2x10mL). The aqueous layer was made alkaline with solid Na_2CO_3 and the oily product formed was extracted with ether. The combined ether extracts were washed with water and brine and dried (Na_2SO_4). After evaporation of the solvent, amino acetamide **44** was afforded: yield 34 mg (50 %). ^1H NMR (CDCl_3 , 400 MHz) δ (ppm) 0.89 (t, $J = 7$ Hz, 3H, $\text{CH}_2\text{CH}_2\text{CH}_3$), 1.23-1.24 (m, 4H, $2 \times \text{CH}_2\text{CH}_2\text{CH}_3$), 1.58-1.61 (m, 2H, 4eq,9eq-adamantyl H), 1.65 (d, $J = 12$ Hz, 2H, 1,3-adamantyl H), 1.80 (br s, 2H, 8eq,10eq-adamantyl H), 1.95-2.01 (m, 6H, 5,7,6,8ax,10ax-adamantyl H), 2.25 (d, $J = 12$ Hz, 2H, 4ax,9ax-H), 3.28 (s, 2H, COCH_2N); ^{13}C NMR (CDCl_3 , 50 MHz) δ (ppm) 14.7 ($\text{CH}_2\text{CH}_2\text{CH}_3$), 16.1 ($\text{CH}_2\text{CH}_2\text{CH}_3$), 27.4 (5,7-adamantyl C), 33.0 (4,9-adamantyl C), 33.2 (8,10-adamantyl C), 35.1 ($\text{CH}_2\text{CH}_2\text{CH}_3$), 37.1 (1,3-adamantyl C), 38.7 (6-adamantyl C), 45.4 (CH_2N), 59.8 (2-adamantyl C), 171.2 (C=O); HRMS (m/z): $[\text{M} + \text{H}^+]$ calcd for $\text{C}_{15}\text{H}_{26}\text{N}_2\text{O}$ 250.2045, experimental 250.2052.

Compound 45 (Procedure A). Reaction of rimantadine **2** (300 mg, 1.68 mmol) and 2-hydroxy-4-methoxybenzaldehyde (212 mg, 1.40 mmol) in MeOH (5 mL) followed by addition of NaCNBH_3 (317 mg, 5.04 mmol) to afford imine **85a**; yield 25 mg (5 %). ^1H NMR (CDCl_3 , 400 MHz) δ (ppm) 1.25 (d, $J = 13$ Hz, 3H, CHCH_3), 1.51-1.68 (m, 12H, 2,4,6,8,9,10-adamantyl H), 2.02 (br s, 3H, 3,5,7-adamantyl H), 2.17 (q, $J = 6$ Hz, $\text{CH}(\text{CH}_3)\text{N}$), 3.77 (s, 3H, OCH_3), 4.77 (br s, OH), 6.43 (dd, $J = 8$, 2.4 Hz, 1H, phenyl H), 6.88 (d, $J = 2$ Hz, 1H, phenyl H), 7.02 (d, $J = 8$ Hz, 1H, phenyl H), 7.76 (s, 1H, $\text{CH}=\text{N}$).

Reaction of imine **85a** (25 mg, 0.0799 mmol) with PTSA (14 mg, 0.0799 mmol) / NaBH_4 (12 mg, 0.320 mmol) / MeOH (2 mL) afforded amine **45**; yield 6 mg (24 %); ^1H NMR (CDCl_3 , 400 MHz) δ (ppm) 1.05 (d, $J = 7$ Hz, 3H, CHCH_3), 1.52-1.67 (m, 12H, 2,4,6,8,9,10-adamantyl H), 1.99 (br s, 3H, 3,5,7-adamantyl H), 2.27 (q, $J = 6$ Hz, $\text{CH}(\text{CH}_3)\text{N}$), 3.41 (s, 1H, NCH_2), 3.76 (m, 4H, OCH_3 , NCH_2), 4.1 (br s, OH), 6.33 (dd, $J = 8$, 2.4 Hz, 1H, phenyl), 6.40 (d, $J = 2$ Hz, 1H, phenyl), 6.89 (d, $J = 8$ Hz, 1H, phenyl); ^{13}C NMR (CDCl_3 , 50 MHz) δ (ppm) 12.7 (CHCH_3), 28.7 (3,5,7-adamantyl C), 37.0 (1-adamantyl C), 37.3 (4,6,10-adamantyl C), 38.7 (2,8,9-adamantyl C), 50.9 (NCH_2), 55.4 (OCH_3), 62.1 ($\text{CH}(\text{CH}_3)\text{N}$), 116.1 (1-phenyl CH), 102.9 (3-phenyl CH), 104.8 (5-phenyl CH), 128.8 (6-phenyl CH), 151.3 (2-phenyl CH), 160.8 (4-phenyl CH); HRMS (m/z): $[\text{M} + \text{H}^+]$ calcd for $\text{C}_{20}\text{H}_{29}\text{NO}_2$ 315.2198, experimental 315.2196.

Compound 46 (Procedure A). Reaction 2-(1-adamantyl)-2-propanamine **21** (55 mg, 0.285 mmol) and 2-hydroxy-4-methoxybenzaldehyde (36 mg, 0.238 mmol) in MeOH (2 mL) followed by addition of NaCNBH₃ (54 mg, 0.855 mmol) to afford imine **85b**; yield 37 mg (67 %); ¹H NMR (CDCl₃, 400 MHz) δ (ppm) 1.25 (s, 6H, 2xCH₃), 1.62-1.64 (m, 12H, 2,4,6,8,9,10-adamantyl H), 1.99 (br s, 3H, 3,5,7-adamantyl H), 3.77 (s, 3H, OCH₃), 6.17 (dd, *J* = 8, 2.4 Hz, 1H, phenyl), 6.25 (d, *J* = 2 Hz, 1H, phenyl), 6.98 (d, *J* = 8 Hz, 1H, phenyl), 7.86 (s, 1H, CH=N).

Treatment of imine **85b** (37 mg, 0.113 mmol) with PTSA (20 mg, 0.113 mmol) and NaBH₄ (17 mg, 0.452 mmol) in MeOH (2 mL) afforded amine **46**; yield 50 mg (81 %); ¹H NMR (CDCl₃, 400 MHz) δ (ppm) 1.06 (s, 6H, 2xCH₃), 1.58-1.73 (m, 12H, 2,4,6,8,9,10-adamantyl H), 2.01 (br s, 3H, 3,5,7-adamantyl H), 3.76 (s, 3H, OCH₃), 3.86 (s, 2H, CH₂N), 6.30 (dd, *J* = 8, 2.4 Hz, 1H, phenyl), 6.41 (d, *J* = 2 Hz, 1H, phenyl), 6.86 (d, *J* = 8 Hz, 1H, phenyl); ¹³C NMR (CDCl₃, 50 MHz) δ (ppm) 19.7 (2xCH₃), 28.8 (3,5,7-adamantyl C), 36.1 (4,6,10-adamantyl C), 37.2 (2,8,9-adamantyl C), 38.8 (1-adamantyl C), 45.2 (CH₂N), 55.4 (OCH₃), 57.8 (CNH), 102.5 (2-phenyl CH), 104.8 (5-phenyl CH), 115.9 (1-phenyl C), 128.6 (6-phenyl CH), 130.8 (2-phenyl C=O), 159.8 (4-phenyl C=O); HRMS (*m/z*): [M + H⁺] calcd for C₂₁H₃₁NO₂ 329.2355, experimental 329.2364.

Compound 47 (Procedure A). Reaction of 3-(1-adamantyl)-3-pentanamine **22** (70 mg, 0.317 mmol) and 2-hydroxy-4-methoxybenzaldehyde (40 mg, 0.264 mmol) in MeOH (2 mL) followed by addition of NaCNBH₃ (60 mg, 0.951 mmol) to afford imine **85c**; yield 20 mg (18 %); ¹H NMR (CDCl₃, 400 MHz) δ (ppm) 0.96 (t, *J* = 7, 6H, 2xCH₃), 1.63-1.67 (m, 12H, 2,4,6,8,9,10-adamantyl H), 1.82-1.87 (m, 4H, 2xCH₂CH₂), 1.99 (br s, 3H, 3,5,7-adamantyl H), 3.77 (s, 3H, OCH₃), 6.16 (dd, *J* = 8, 2.4 Hz, 1H, CH, phenyl), 6.27 (d, *J* = 2 Hz, 1H, CH, phenyl), 6.98 (d, *J* = 8 Hz, 1H, CH, phenyl), 7.71 (s, 1H, CH=N).

Reaction of imine **85c** (20 mg, 0.056 mmol) with PTSA (10 mg, 0.056 mmol) and NaBH₄ (9 mg, 0.224 mmol) in MeOH (1 mL) afforded amine **47**; yield 15 mg (75 %); ¹H NMR (CDCl₃, 400 MHz) δ (ppm) 0.89 (t, *J* = 7, 6H, 2xCH₃), 1.64-1.67 (m, 12H, 2,4,6,8,9,10-adamantyl H), 1.76-1.80 (m, 4H, 2xCH₂CH₂), 2.0 (br s, 3H, 3,5,7-adamantyl H), 3.76 (s, 3H, OCH₃), 3.96 (s, 2H, CH₂N), 6.32 (dd, *J* = 8, 2.4 Hz, 1H, phenyl), 6.42 (d, *J* = 2 Hz, 1H, phenyl), 6.86 (d, *J* = 8 Hz, 1H, phenyl); HRMS (*m/z*): [M + H⁺] calcd for C₂₃H₃₅NO₂ 357.2668, experimental 357.2674.

Compound 48 (Procedure A). Reaction of 4-(1-adamantyl)-4-heptanamine **23** (45 mg, 0.181 mmol) and 2-hydroxy-4-methoxybenzaldehyde (23 mg, 0.151 mmol) in MeOH (2 mL) followed by addition of NaCNBH₃ (34 mg, 0.543 mmol) to afford imine **85d**; yield 15 mg (22 %); ¹H NMR (CDCl₃, 400 MHz) δ (ppm) 0.95 (t, 6H, *J* = 7 Hz, 2xCH₂CH₂CH₃), 1.31-1.40 (m, 4H, 2xCH₂CH₂CH₃), 1.56-1.67 (m, 12H, 2,4,6,8,9,10-adamantyl H), 1.69-1.74 (m, 4H, 2xCH₂CH₂CH₃), 1.99 (br s, 3H, 3,5,7-adamantyl H), 3.78 (s, 3H, OCH₃), 6.15 (dd, *J* = 8, 2.4 Hz, 1H, phenyl), 6.23 (d, *J* = 2 Hz, 1H, phenyl), 6.98 (d, *J* = 8 Hz, 1H, phenyl), 7.70 (s, 1H, CH=N).

Reaction of imine **85d** (15 mg, 0.039 mmol) with PTSA (7 mg, 0.039 mmol) and NaBH₄ (6 mg, 0.156 mmol) in MeOH (2 mL) afforded amine **48**; yield 10 mg (68 %); ¹H NMR (CDCl₃, 400 MHz) δ (ppm) 0.92 (t, 6H, *J* = 7 Hz, 2xCH₂CH₂CH₃), 1.44-1.50 (m, 4H, 2xCH₂CH₂CH₃), 1.52-1.56 (m, 4H, 2xCH₂CH₂CH₃), 1.57-1.68 (m, 12H, 2,4,6,8,9,10-adamantyl H), 2.0 (br s, 3H, 3,5,7-adamantyl H), 3.76 (s, 3H, OCH₃), 3.95 (s, 2H, CH₂N), 6.34 (d, *J* = 4 Hz, 1H, phenyl), 6.42 (d, *J* = 4 Hz 1H, phenyl), 6.86 (d, *J* = 8 Hz, 1H, phenyl); HRMS (*m/z*): [M + H⁺] calcd for C₂₅H₃₉NO₂ 385.2981, experimental 385.2976.

Compound 49 (Procedure B). To the mixture of rimantadine **2** (100 mg, 0.558 mmol) and 3-chloromethyl-5-methylisoxazole (49 mg, 0.372 mmol) in isopropanol (2 mL) was added CsI (15 mg, 0.0558 mmol) and Et₃N (112 mg, 1.12 mmol) to afford amine **49**; yield 6 mg (4%); ¹H NMR (CDCl₃, 400 MHz) δ (ppm) 0.95 (d, *J* = 6 Hz, 3H, CHCH₃), 1.41-1.64 (m, 12H, 2,4,6,8,9,10-adamantyl H), 1.95 (br s, 3H, 3,5,7-adamantyl H), 2.07 (q, *J* = 6 Hz, 1H, CH(CH₃)N), 2.40 (s, 3H, isoxazolyl CH₃), 3.69 (d, *J* = 14 Hz, 1H, CH₂N), 3.87 (d, *J* = 14 Hz, 1H, CH₂N), 5.9 (s, 1H, isoxazolyl CH=); ¹³C NMR (CDCl₃, 50 MHz) δ (ppm) 13.2 (CH-CH₃), 13.3 (isoxazolyl CH₃) 28.7 (3,5,7-adamantyl C), 37.4 (1-C), 37.5 (4,6,10-adamantyl C), 38.7 (2,8,9-adamantyl C), 43.7 (NHCH₂), 61.6 (CH(CH₃)N), 101.3 (isoxazolyl CH=), 163.8 (isoxazolyl C=N), 169.3 (isoxazolyl CO); HRMS (*m/z*): [M + H⁺] calcd for C₁₇H₂₆N₂O 274.2045, experimental 274.2053.

Compound 50 (Procedure C). To the mixture of rimantadine **2** (150 mg, 0.694 mmol) and 5-phenylisoxazole-3-carboxaldehyde (120 mg, 0.694 mmol) in Ti(iPrO)₄ (3 mL, 10.4 mmol) was added NaBH₄ (105 mg, 2.78 mmol) and MeOH (3 mL) to afford amine **50**; yield 12 mg (5%); ¹H NMR (CDCl₃, 400 MHz) δ (ppm) 0.96 (d, *J* = 6 Hz, 3H, CHCH₃), 1.42-1.64 (m, 12H, 2,4,6,8,9,10-adamantyl H), 1.94 (br s, 3H, 3,5,7-adamantyl H), 2.13 (q, *J* = 6 Hz, 1H, CH(CH₃)N), 3.72 (d, *J* = 14 Hz, 1H, CH₂N), 3.74 (d, *J* = 14 Hz, 1H, CH₂N), 3.93 (d, *J* = 14 Hz, 1H, CH₂N), 6.52 (s, 1H, isoxazolyl CH=), 7.39-7.42 (m, 3H, phenyl), 7.74 (d, *J* = 8 Hz, 2H, phenyl); ¹³C NMR (CDCl₃, 50 MHz) δ (ppm) 13.2 (CHCH₃), 28.6 (3,5,7-adamantyl C), 36.2 (1-adamantyl C), 37.3 (4,6,10-adamantyl C), 38.6 (2,8,9-adamantyl C), 43.7 (NCH₂), 61.5 (CH(CH₃)N), 99.1 (isoxazolyl CH=), 125.8 (CH, C₆H₅) 127.6 (C, C₆H₅), 129.0 (CH, C₆H₅), 130.0 (CH, C₆H₅), 164.3 (isoxazolyl C=N), 169.5 (isoxazolyl CO); HRMS (*m/z*): [M + H⁺] calcd for C₂₂H₂₈N₂O 336.2202, experimental 336.2215.

Compound 51 (Procedure C). To the mixture of 2-(1-adamantyl)-2-propanamine (70 mg, 0.363 mmol) and 5-phenylisoxazole-3-carboxaldehyde (63 mg, 0.363 mmol) in Ti(iPrO)₄ (1.5 mL, 5.45 mmol) was added NaBH₄ (55 mg, 1.45 mmol) and MeOH (2 mL) to afford amine **51**; yield 15 mg (11 %); ¹H NMR (CDCl₃, 400 MHz) δ (ppm) 1.03 (s, 6H, 2xCH₃), 1.61-1.670 (m, 12H, 2,4,6,8,9,10-adamantyl H), 2.0 (br s, 3H, 3,5,7-adamantyl H), 3.86 (s, 2H, CH₂N), 6.56 (s, 1H, isoxazolyl CH=C), 7.43-7.45 (m, 3H, phenyl), 7.75-7.77 (m, 2H, phenyl); ¹³C NMR (CDCl₃, 50

MHz) δ (ppm) 20.4 (2xCH₃), 28.9 (3,5,7-adamantyl C), 36.2 (4,6,10-adamantyl C), 37.4 (2,8,9-adamantyl C), 39.0 (1-adamantyl C), 57.2 (CH₂NH), 98.2 (CHNH), 99.4 (isoxazolyl CH=), 125.9 (CH, 2C, phenyl) 126.0 (C, phenyl), 129.0 (CH, 2C, phenyl), 130.1 (CH, phenyl), 165.8 (isoxazolyl C=N), 169.3 (isoxazolyl CO); HRMS (m/z): [M + H⁺] calcd for C₂₃H₃₀N₂O 350.2358, experimental 350.2374.

Compound 52 (Procedure C). To the mixture of 3-(1-adamantyl)-3-pentanamine **22** (40 mg, 0.181 mmol) and 5-phenylisoxazole-3-carboxaldehyde (31 mg, 0.181 mmol) in Ti(iPrO)₄ (1 mL, 2.72 mmol) was added NaBH₄ (28 mg, 0.724 mmol) and MeOH (2 mL) to afford amine **52**; yield 30 mg (43 %); ¹H NMR (CDCl₃, 400 MHz) δ (ppm) 0.95 (t, J = 8 Hz, 6H, 2xCH₃), 1.51-1.63 (m, 4H, 2xCH₂CH₃), 1.64-1.76 (m, 12H, 2,4,6,8,9,10-adamantyl H), 1.99 (br s, 3H, 3,5,7-adamantyl H), 3.98 (s, 2H, CH₂NH), 6.59 (s, 1H, isoxazolyl CH=C), 7.41-7.46 (m, 3H, phenyl), 7.74-7.77 (m, 2H, phenyl); ¹³C NMR (CDCl₃, 50 MHz) δ (ppm) 10.1 (2xCH₃), 25.0 (2xCH₂), 28.7 (3,5,7-adamantyl C), 36.7 (4,6,10-adamantyl C), 36.8 (2,8,9-adamantyl C), 38.0 (CH₂NH), 62.1 (CNH), 118.1 (isoxazolyl CH=), 120.1 (CH, phenyl) 128.8 (CH, phenyl), 129.2 (CH, phenyl), 150.8 (isoxazolyl C=N), 169.0 (isoxazolyl CO); HRMS (m/z): [M + H⁺] calcd for C₂₅H₃₄N₂O 378.2671, experimental 378.2695.

Compound 52 (Procedure C). To the mixture of 4-(1-adamantyl)-4-heptananamine **23** (20 mg, 0.080 mmol) and 5-phenylisoxazole-3-carboxaldehyde (14 mg, 0.080 mmol) in Ti(iPrO)₄ (0.3 mL, 1.20 mmol) was added NaBH₄ (12 mg, 0.320 mmol) and MeOH (2 mL) to afford amine **53**; yield 20 mg (50%). ¹H NMR (CDCl₃, 400 MHz) δ (ppm) 0.94 (m, 6H, 2xCH₃), 1.34-1.56 (m, 8H, 2xCH₂CH₂CH₃), 1.62-1.75 (m, 12H, 2,4,6,8,9,10-adamantyl H), 1.98 (br s, 3H, 3,5,7-adamantyl H), 3.97 (s, 2H, CH₂NH), 6.59 (s, 1H, isoxazolyl CH=C), 7.43-7.46 (m, 3H, phenyl), 7.74-7.78 (m, 2H, phenyl); ¹³C NMR (CDCl₃, 50 MHz) δ (ppm) 14.3 (2xCH₃), 18.7 (2xCH₂CH₂CH₃), 29.3 (3,5,7-adamantyl C), 35.9 (2xCH₂CH₂CH₃), 36.0 (4,6,10-adamantyl C), 36.9 (2,8,9-adamantyl C), 55.9 (CH₂NH), 69.1 (CNH), 97.9 (isoxazolyl CH=), 125.9 (CH, C₆H₅), 129.0 (CH, C₆H₅), 130.4 (CH, C₆H₅), 150.0 (isoxazolyl C=N), 169.4 (isoxazolyl CO); HRMS (m/z): [M + H⁺] calcd for C₂₇H₃₈N₂O 406.2984, experimental 406.2965.

Compound 54 (Procedure C). To the mixture of 2-(1-adamantyl)-2-propananamine **21** (60 mg, 0.314 mmol) and 5-bromo-2-thiophenecarboxaldehyde (49 mg, 0.314 mmol) in Ti(iPrO)₄ (1.5 mL, 4.71 mmol) was added NaBH₄ (48 mg, 1.26 mmol) and MeOH (2 mL) to afford amine **54**; yield 7 mg (7%); ¹H NMR (CDCl₃, 400 MHz) δ (ppm) 1.03 (s, 6H, 2xCH₃), 1.65-1.67 (m, 12H, 2,4,6,8,9,10-adamantyl H), 2.00 (br s, 3H, 3,5,7-adamantyl H), 3.92 (br s, 2H, CH₂NH), 6.88 (d, J = 4 Hz, thiophenyl CH=C), 7.27 (d, J = 4 Hz, thiophenyl CH=CBr); ¹³C NMR (CDCl₃, 50 MHz) δ (ppm) 20.5 (2xCH₃), 28.9 (3,5,7-adamantyl C), 36.2 (4,6,10-adamantyl C), 37.4 (2,8,9-adamantyl C), 39.0 (1-adamantyl C), 42.6 (CH₂NH), (CNH, ??), 129.4 (thiopenyl CH=C), 130.7 (thiopenyl CH=CBr); HRMS (m/z): [M + H⁺] calcd for C₁₈H₂₆BrNS 367.0969, experimental 367.0972.

Compound 55 (Procedure A). Reaction of 1-isopropyl-3-aminoadamantane **25** (60 mg, 0.311 mmol) with 2-hydroxy-4-methoxybenzaldehyde (40 mg, 0.259 mmol) in MeOH (2 mL) followed by addition of NaCNBH₃ (58 mg, 0.933 mmol) to afford imine **86a**; yield 100 mg (98 %) ¹H NMR (CDCl₃, 400 MHz) δ (ppm) 0.80-0.82 (d, *J* = 7 Hz, 6H, CH(CH₃)₂), 1.27 (hept, *J* = 7 Hz, 1H, CH(CH₃)₂), 1.46-1.49 (m, 4H, 4,10-adamantyl H), 1.57 (br s, 2H, 6-adamantyl H), 1.61 (br s, 2H, 5,7-adamantyl H), 1.77-1.79 (m, 4H, 8, 9-adamantyl H), 2.23 (br s, 2H, 2-adamantyl H), 3.77 (s, 3H, OCH₃), 4.75 (br s, OH), 6.19 (dd, *J* = 8, 2.4 Hz, 1H, phenyl), 6.25 (d, *J* = 2 Hz, 1H, phenyl), 7.01 (d, *J* = 8 Hz, 1H, phenyl), 7.99 (s, 1H, CH=N); ¹³C NMR (CDCl₃, 50 MHz) δ (ppm) 16.5 (CH(CH₃)₂), 29.6 (5,7-adamantyl C), 35.9 (6-adamantyl C), 36.8 (3-adamantyl C), 37.3 (CH(CH₃)₂), 37.9 (4,9-adamantyl C), 42.5 (8,10-adamantyl C), 45.1 (2-adamantyl C), 55.2 (OCH₃), 56.4 (1-adamantyl C), 101.5 (2-phenyl CH), 106.5 (5-phenyl CH), 111.1 (1-C, C₆H₅), 133.2 (6-phenyl CH), 156.8 (CH=N), 164.9 (2-COH, phenyl), 172.5 (4-COCH₃, phenyl).

Reaction of imine **86a** (100 mg, 0.306 mmol,) with PTSA (53 mg, 0.306 mmol) and NaBH₄ (47 mg, 1.22 mmol) in MeOH (2 mL) afforded amine **55**; yield 70 mg (69 %). ¹H NMR (CDCl₃, 400 MHz) δ (ppm) 0.79 (d, *J* = 4 Hz, 6H, CH(CH₃)₂), 1.21-1.26 (hept, *J* = 7 Hz, 1H, CH(CH₃)₂), 1.38-1.46 (m, 4H, 4,10-adamantyl H), 1.54-1.68 (m, 6H, 6,8,9-H), 2.15 (br s, 2H, 5,7-adamantyl H), 3.74 (s, 3H, OCH₃), 3.91 (br s, 2H, CH₂NH), 6.33 (dd, *J* = 8, 2.4 Hz, 1H, phenyl), 6.38 (d, *J* = 2 Hz, 1H, phenyl), 6.82 (d, 1H, *J* = 8 Hz, phenyl); ¹³C NMR (CDCl₃, 50 MHz) δ (ppm) 16.6 (CH(CH₃)₂), 29.7 (5,7-adamantyl C), 36.3 (6-adamantyl C), 36.8 (3-adamantyl C), 37.3 (CH(CH₃)₂), 38.3 (4,9-adamantyl C), 41.9 (8,10-adamantyl C), 43.7 (CH₂-NH), 44.4 (2-adamantyl C), 52.2 (1-adamantyl C), 55.3 (CH₃-O), 102.2 (2-CH, phenyl), 104.8 (5-CH, phenyl), 116.1 (1-C, phenyl), 128.4 (6-CH, phenyl), 159.7 (2-COH, phenyl), 160.3 (4-COCH₃, phenyl); HRMS (*m/z*): [M + H⁺] calcd for C₂₁H₃₁NO₂ 329.2355, experimental 329.2362.

Compound 56 (Procedure A). Reaction of 1-fluoro-3-aminoadamantane **26** (30 mg, 0.178 mmol) with 2-hydroxy-4-methoxybenzaldehyde (23 mg, 0.148 mmol) in MeOH (1 mL) followed by addition of NaCNBH₃ (34 mg, 0.534 mmol) to afford imine **86b**; yield 20 mg (40 %); ¹H NMR (CDCl₃, 400 MHz) δ (ppm) 1.61 (br s, 2H, 6-adamantyl H), 1.78 (br s, 4H, 4,10-adamantyl H), 1.91-1.96 (m, 4H, 8,9-adamantyl H), 1.98 (d, *J* = 6 Hz, 2H, 2-adamantyl H), 2.44 (br s, 3H, 5,7-adamantyl H), 3.80 (s, 3H, OCH₃), 6.33 (dd, *J* = 8, 2.4 Hz, 1H, phenyl), 6.38 (d, *J* = 2 Hz, 1H, phenyl), 7.06 (d, *J* = 8 Hz, 1H, phenyl), 8.16 (s, 1H, CH=N); ¹³C NMR (CDCl₃, 50 MHz) δ (ppm) 31.0, 31.2 (5,7-adamantyl C), 34.6 (6-adamantyl C), 41.6 (4,10-adamantyl C), 41.9 (8,9-adamantyl C), 47.8 (2-adamantyl C), 51.5 (3-adamantyl C), 55.5 (OCH₃), 93.0 (d, *J* = 100 Hz, CF), 101.5 (2-phenyl), 106.5 (5-phenyl CH), 112.3 (1-phenyl C), 130.0 (6-CH, C₆H₅), 158.7 (CH=N), 164.0 (2-COH, phenyl), 167.1 (4-COCH₃, phenyl).

Reaction of imine **86b** (20 mg, 0.066 mmol,) with PTSA (11 mg, 0.066 mmol) and NaBH₄ (10 mg, 0.264 mmol) in MeOH (1 mL) afforded amine **56**; yield 18 mg (90 %); ¹H NMR (CDCl₃, 400 MHz) δ (ppm) 1.55 (br s, 2H,

6-adamantyl H), 1.64-1.70 (m, 4H, 4,10-adamantyl H), 1.87-1.90 (m, 6H, 2,8,9-adamantyl H), 2.44 (br s, 3H, 5,7-adamantyl H), 3.80 (s, 3H, OCH₃), 3.92 (br s, 2H, CH₂NH), 6.30 (dd, *J* = 4 Hz, 1H, phenyl), 6.36 (d, *J* = 4 Hz, 1H, phenyl), 6.84 (d, *J* = 16 Hz 1H, phenyl); ¹³C NMR (CDCl₃, 50 MHz) δ (ppm) 31.0, 31.2 (5,7-adamantyl C), 34.9 (6-adamantyl C), 40.9 (4,10-adamantyl C), 41.7, 42.0 (8,9-adamantyl C), 44.2 (CH₂NH), 47.1 (2-adamantyl C), 51.5 (1-adamantyl C), 55.3 (3-adamantyl C), 55.4 (OCH₃), 93.0 (d, *J* = 100 Hz, CF), 102.2 (2-phenyl CH), 102.3 (5-phenyl CH), 115.7 (1-phenyl C), 128.6 (6-phenyl CH), 159.4 (2-COH, phenyl), 160.5 (4-COCH₃, phenyl); HRMS (*m/z*): [M + H⁺] calcd for C₁₈H₂₄FNO₂ 305.1791, experimental 305.1783.

Compound 57 (Procedure A). Reaction of 4-(1-adamantyl)aniline **27** (25 mg, 0.110 mmol) with 2-hydroxy-4-methoxybenzaldehyde (15 mg, 0.092 mmol) in MeOH (1 mL) followed by addition of NaCNBH₃ (21 mg, 0.330 mmol) to afford imine **87**; yield 25 mg (63 %); ¹H NMR (CDCl₃, 400 MHz) δ (ppm) 1.84 (br s, 6H, 4,6,10-adamantyl H), 1.98 (br s, 6H, 2,8,9-adamantyl H), 2.17 (br s, 3H, 3,5,7-adamantyl H), 3.89 (s, 3H, OCH₃), 6.53-6.55 (m, 2H, aromatic H), 7.30-7.50 (m, 3H, aromatic H), 8.58 (s, 1H, CH=N); ¹³C NMR (CDCl₃, 50 MHz) δ (ppm) 29.05 (3,5,7-adamantyl C), 36.22 (1-adamantyl C), 36.87 (4,10-adamantyl C), 43.3 (8,9-adamantyl C), 55.6 (OCH₃), 101.3 (2-phenyl CH), 105.7 (5-phenyl CH), 116.2 (1-phenyl C), 120.7 (3,5-C, Ph-N=), 125.9 (2,6-C, Ph-N=), 133.5 (6-phenyl CH), 145.8 (1-C, Ph-N=), 150.0 (4-C, Ph-N=), 160.7 (CH=N), 163.4 (2-COH, phenyl), 164.5 (4-COCH₃, phenyl).

Reaction of imine **87** (25 mg, 0.70 mmol,) with PTSA (120 mg, 0.70 mmol) and NaBH₄ (106 mg, 2.8 mmol) in MeOH (1 mL) afforded amine **57**; yield 10 mg (36 %); ¹H NMR (CDCl₃, 400 MHz) δ (ppm) 1.79 (br s, 6H, 4,6,10-adamantyl H), 1.91 (br s, 6H, 2,8,9-adamantyl H), 2.11 (br s, 3H, 3,5,7-adamantyl H), 3.81 (s, 3H, OCH₃), 4.37 (br s, 2H, CH₂N), 6.43-6.50 (m, 2H, aromatic H), 6.84-6.88 (m, 2H, aromatic H), 7.03-7.07 (d, *J* = 8 Hz, 1H, aromatic H), 7.24-7.30 (m, 2H, aromatic H); ¹³C NMR (CDCl₃, 50 MHz) δ (ppm) 29.03 (3,5,7-adamantyl C), 35.8 (1-adamantyl C), 37.2 (4,10-adamantyl C), 43.7 (8,9-adamantyl C), 48.9 (CH₂N), 55.4 (OCH₃), 101.3 (2-phenyl CH), 105.8 (5-phenyl CH), 115.2 (1-phenyl C), 116.3 (3,5-C, Ph-NH), 126.4 (2,6-C, Ph-NH), 130.0 (6-phenyl CH), 143.4 (1-C, Ph-NH), 145.2 (4-C, Ph-NH), 158.2 (2-COH, phenyl), 160.9 (4-COCH₃, phenyl); HRMS (*m/z*): [M + H⁺] calcd for C₂₄H₂₉NO₂ 363.2198, experimental 363.2201.

Compound 58 (Procedure A). Reaction of 4-aminodiamantane **28** (100 mg, 0.493 mmol) with 2-hydroxy-4-methoxybenzaldehyde (63 mg, 0.411 mmol) in MeOH (2 mL) followed by addition of NaCNBH₃ (93 mg, 1.48 mmol) to afford imine **88**; yield 100 mg (72%); ¹H NMR (CDCl₃, 400 MHz) δ (ppm) 1.75-1.76 (m, 9H, diadamantyl H), 1.82-1.83 (m, 7H, diadamantyl H), 1.97 (br s, 3H, 3,5,7-diadamantyl H), 3.77 (s, 3H, OCH₃), 6.21 (dd, *J* = 8, 2.4 Hz, 1H, phenyl), 6.27 (d, *J* = 2 Hz, 1H, phenyl), 6.99 (d, *J* = 8 Hz, 1H, phenyl), 8.01 (s, 1H, CH=N).

Reaction of imine **88** (100 mg, 0.297 mmol,) with PTSA (51 mg, 0.297 mmol) and NaBH₄(45 mg, 1.19 mmol) in MeOH (2 mL) afforded amine **58**; yield 95 mg (95 %); ¹H NMR (CDCl₃, 400 MHz) δ (ppm) ¹H NMR (CDCl₃, 400 MHz) δ (ppm) 1.67-1.70 (m, 9H, diadamantyl H), 1.71-1.74 (m, 7H, diadamantyl H), 1.91 (br s, 3H, 3,5,7-diadamantyl H), 3.75 (s, 3H, OCH₃), 3.91 (s, 2H, CH₂N), 6.30 (dd, *J* = 8, 2.4 Hz, 1H, phenyl), 6.38 (d, *J* = 2 Hz, 1H, phenyl), 6.83 (d, *J* = 8 Hz, 1H, phenyl); HRMS (*m/z*): [M + H⁺] calcd for C₂₂H₂₉NO₂ 339.2198, experimental 339.2189.

Compound 59 (Procedure A). Reaction of 9-aminotriadamantane **29** (40 mg, 0.157 mmol) with 2-hydroxy-4-methoxybenzaldehyde (20 mg, 0.131 mmol) in MeOH (1 mL) followed by addition of NaCNBH₃ (30 mg, 0.471 mmol) afforded imine **89**; yield 15 mg (25 %); ¹H NMR (CDCl₃, 400 MHz) δ (ppm) 1.25-1.37 (m, 5H, triadamantyl-H), 1.44 (br s, 2H, triadamantyl-H), 1.68-1.77 (m, 13H, triadamantyl-H), 1.87 (br s, 3H, triadamantyl-H), 3.78 (s, 3H, OCH₃), 6.21 (d, *J* = 4 Hz, 1H, phenyl), 6.24 (d, *J* = 4 Hz 1H, phenyl), 7.0 (d, *J* = 8 Hz 1H, phenyl), 9.7 (s, 1H, CH=N).

Reaction of imine **89** (15 mg, 0.039 mmol,) with PTSA (7 mg, 0.039 mmol) and NaBH₄(6 mg, 0.156 mmol) in MeOH (1 mL) gives amine **59**; yield 7 mg (44 %). ¹H NMR (CDCl₃, 400 MHz) δ (ppm) 1.28-1.31 (m, 5H, triadamantyl-H), 1.32 (br s, 2H, triadamantyl-H), 1.64-1.72 (m, 15H, triadamantyl-H), 1.86 (br s, 3H, triadamantyl-H), 3.77 (s, 3H, OCH₃), 3.91 (s, 2H, CH₂N), 6.33 (dd, *J* = 8, 2.4 Hz, 1H, phenyl), 6.39 (d, *J* = 2 Hz 1H, phenyl), 6.84 (d, *J* = 8 Hz 1H, phenyl); HRMS (*m/z*): [M + H⁺] calcd for C₂₆H₃₃NO₂ 391.2511, experimental 391.2523.

Compound 60 (Procedure A). Reaction of *tert*-octylamine **30** (300 mg, 2.33 mmol) with 2-hydroxy-4-methoxybenzaldehyde (440 mg, 6.99 mmol) in MeOH (5 mL) followed by addition of NaCNBH₃ (440 mg, 6.69 mmol) afforded imine **90**; yield 450 mg (74%); ¹H NMR (CDCl₃, 400 MHz) δ (ppm) 0.85 (br s, 9H, C(CH₃)₃) 1.28 (br s, 6H, CH₂C(CH₃)₂), 1.57 (br s, 2H, CH₂), 3.65 (s, 3H, OCH₃), 6.13 (dd, *J* = 8, 2.4 Hz, 1H, phenyl), 6.19 (d, *J* = 2 Hz 1H, phenyl), 6.93 (d, *J* = 8 Hz 1H, phenyl), 7.92 (s, 1H, CH=N); ¹³C NMR (CDCl₃, 50 MHz) δ (ppm) 30.2 (C(CH₃)₃), 31.4 (C(CH₃)₂), 31.7 (C(CH₃)₃), 54.9 (OCH₃), 55.7 (CH₂), 58.8 (C(CH₃)₂), 101.7 (2-phenyl CH), 105.9 (5-phenyl CH), 111.4 (1-phenyl C), 133.0 (6-phenyl CH), 158.0 (CH=N), 164.5 (2-COH, phenyl), 170.8 (4-COCH₃, phenyl).

Reaction of imine **90** (450 mg, 1.70 mmol,) with PTSA (292 mg, 1.70 mmol) and NaBH₄(260 mg, 6.80 mmol) in MeOH (5 mL) afforded amine **60**; yield 330 mg (70%); ¹H NMR (CDCl₃, 400 MHz) δ (ppm) 1.04 (br s, 9H, C(CH₃)₃) 1.25 (br s, 6H, CH₂(CH₃)₂), 1.52 (br s, 2H, CH₂), 3.74 (s, 3H, OCH₃), 3.86 (s, 2H, CH₂N), 6.30 (dd, *J* = 8, 2.4 Hz, 1H, phenyl), 6.35 (d, *J* = 2 Hz, 1H, phenyl), 6.84 (d, *J* = 8 Hz 1H, phenyl); HRMS (*m/z*): [M + H⁺] calcd for C₁₆H₂₇NO₂ 265.2042, experimental 265.2055.

Compound 61 (Procedure A). Reaction of *tert*-octylamine **30** (150 mg, 1.16 mmol) with 5-phenylisoxazole-3-carboxaldehyde (200 mg, 1.16 mmol) in MeOH (3 mL) followed by addition of NaCNBH₃ (219 mg, 3.48 mmol) afforded amine **61**; yield 300 mg (91%); ¹H NMR (CDCl₃, 400 MHz) δ (ppm) 1.05 (br s, 9H, C(CH₃)₃) 1.15 (br s, 6H, C(CH₃)₂), 1.25 (br s, 2H, CH₂), 3.81 (s, 2H, CH₂N), 6.62 (s, 1H, CH=N), 7.30-7.50 (m, 3H, phenyl), 7.48 (d, *J* = 6 Hz, 2H, phenyl); ¹³C NMR (CDCl₃, 50 MHz) δ (ppm) 29.0 (C(CH₃)₃), 31.8 (C(CH₃)₂), 31.9 (C(CH₃)₃), 38.3 (NHCH₂), 52.9 ((CH₃)₂CCH₂C(CH₃)₃), 54.7 (C(CH₃)₂), 99.2 (isoxazolyl CH=), 125.8 (CH, C₆H₅) 127.3 (C, C₆H₅), 128.9 (CH, C₆H₅), 130.0 (CH, C₆H₅), 164.7 (isoxazolyl C=N), 168.9 (isoxazolyl CO); HRMS (*m/z*): [M + H⁺] calcd for C₁₈H₂₆N₂O 286.2045, experimental 286.2052.

Compound 62 (Procedure A). Reaction of 4-isobutyl-2-methyloctan-4-amine **31** (60 mg, 0.302 mmol) with 2-hydroxy-4-methoxybenzaldehyde (38 mg, 0.251 mmol) followed by addition of NaCNBH₃ (57 mg, 0.906 mmol) afforded imine **91**; yield 58 mg (7%). Reaction of imine **91** (58 mg, 0.178 mmol) with PTSA (31 mg, 0.178 mmol) and NaBH₄ (27 mg, 0.712 mmol) in MeOH (2 mL) afforded amine **62**; 21 mg (yield 35%); ¹H NMR (CDCl₃, 400 MHz) δ (ppm) 0.94-0.99 (m, 15H, 5xCH₃), 1.30-1.44 (m, 10H, 5xCH₂), 1.63-1.71 (m, 2H, 2xCH), 3.76 (br s, 5H, CH₂N, OCH₃), 6.35 (dd, *J* = 8, 2.4 Hz, 1H, phenyl), 6.43 (d, *J* = 2 Hz, 1H, phenyl), 6.85 (d, *J* = 8 Hz, 1H, phenyl); ¹³C NMR (CDCl₃, 50 MHz) δ (ppm) 14.3 (CH₃, n-Bu), 23.4 (CH₂CH₃, n-Bu), 23.6 (2xCH), 25.4 (i-Bu, 2xCH₃), 25.8 (CH₂CH₂CH₃, n-Bu), 36.7 (CH₂CNH), 44.7 (2xCH₂, i-Bu), 44.8 (CH₂NH), 55.4 (OCH₃), 59.1 (CNH), 102.2 (2-phenyl CH), 105.0 (5-phenyl CH), 115.8 (1-phenyl C), 128.8 (6-phenyl CH); HRMS (*m/z*): [M + H⁺] calcd for C₂₁H₃₇NO₂ 335.2824, experimental 335.2832.

5.5.3 Cells and viruses

Madin-Darby canine kidney (MDCK) cells (Cat.no. RIE 328, Friedrich-Loeffler Institute, Riems, Germany) were propagated as monolayer in Eagle's minimum essential medium (EMEM) supplemented with 10% fetal bovine serum, 1% non-essential amino acids (NEAA), 1 mM sodium pyruvate and 2 mM L-glutamine. Amantadine-sensitive Udorn/72, amantadine-resistant WSN/33-M2-WT (with am N31 in M2) and its variant with N31S amino acid substitution in the M2 ion channel were used in this study. Briefly for the generation of WSN/33-M2-N31S⁷⁵ the plasmid pHW187-M2-N31S was altered by site-directed mutagenesis PCR and afterwards used as part of a plasmid set for the recovery of A/WSN/33 virus.⁷⁶ WSN/33-variants were propagated on MDCK cells in serum-free EMEM supplemented with 2 mM L-glutamine, 2 μ g/mL trypsin, and 0.1% sodium bicarbonate (test medium). Virus containing supernatant was harvested after about 48 h of incubation at 37 °C when cytopathic effect became microscopically visible. Aliquots were stored at -80 °C until use. The M2 gene identity of all recombinant viruses was verified by sequencing.

5.5.4 CPE assay

Cytotoxicity and CPE inhibition studies were performed on two-day-old confluent monolayers of MDCK cells grown in 96-well plates as published.⁶² Cytotoxicity was analyzed 72 h after compound addition. In CPE inhibition assay, 50 μ l of a serial half-log dilution of compound in test medium (maximum concentration 100 μ M) and a constant multiplicity of infection of test virus in a volume of 50 μ L of the test medium were added to cells. Then, plates were incubated at 37 °C with 5% CO₂ for 48 h. Crystal violet staining and determination of the 50% cytotoxic (CC₅₀) and 50% inhibitory concentration (IC₅₀) was performed as described before.^{62,77} At least three independent assays were conducted.

5.5.5 MD simulations of M2TM-aminoadamantyl Complexes

5.5.5.1 Docking calculations

The ligands in their ammonium forms were built by means of Maestro 8.5⁷⁸ and were then minimized by means of Macromodel 9.6 and the MMFF94 force field^{79,80} implemented with Macromodel 9.6 using the CG method and a distance-dependent dielectric constant of 4.0 until a convergence value of 0.0001 kJ $\text{\AA}^{-1} \text{mol}^{-1}$ was reached. The ligands minimized in this manner were docked into the M2TM WT or M2TM S31N binding site. The M2TM WT-1 complex structure (PDB ID 2KQT^{6,8}) served as a model structure for M2TM WT with bound ligands. N- and C-termini of the M2TM model systems were capped by acetyl and methylamino groups. After applying the protein preparation module of Maestro, all hydrogens of the protein complex were minimized with the AMBER* force field by means of Maestro/Macromodel 9.6 using a distance-dependent dielectric constant of 4.0. The molecular mechanics minimizations were performed with a conjugate gradient (CG) method and a threshold value of 0.0001 kJ $\text{\AA}^{-1} \text{mol}^{-1}$ as the convergence criterion. The structures of the protein and ligand **1** were saved separately and were used for the subsequent docking calculations. Models of M2TM_{S31N}-aminoadamantyl Complexes were generated from M2TM_{WT} aminoadamantyl complexes by mutating amino acids S31 to N31 with Maestro⁷⁸ and preparing the structure as described above i.e. N- and C-termini of the M2TM peptides were capped by acetyl- and methylamino groups, respectively. This M2TM S31N (22-46) structure was superimposed with M2TM S31N (18-60) solved by solution NMR spectroscopy in DPC micelles (PDB: 2LY0)⁴³ in order to produce a complex between the M2TM S31N (22-46) and M2WJ332 for docking calculations. Thus, the structures of the M2TM S31N and ligand M2WJ332⁴³ were saved separately and were used for the subsequent docking calculations.

Docking poses of the aminoadamantane derivatives in the M2TM WT bound state were generated with GOLD 5.2,^{64,65,66} considering five water molecules located between ammonium group of **1** and H37 within the

M2TM_{WT} pore-binding site and applying the GoldScore implemented in the software.^{64,65,66} The option “toggle” was used to let the algorithm decide whether taking into account a water molecule or neglecting it based on an empirical desolvation penalty. The region of interest used by GOLD was defined to contain the atoms that were within ~15 Å of **1** binding site in the receptor structure. The “allow early termination” command was deactivated. For all the other parameters, GOLD default values were used. Ligands were submitted to 30 genetic algorithm runs. Ten docking poses were produced for each ligand which were visually inspected using the UCSF Chimera package.⁸¹ The docking pose of the ligand inside M2TM WT with the best GoldScore score was used for the subsequent MD simulations with M2TM WT. As regards the complexes between M2TM S31N and ligands consisting by an amantadine analogue connected with polar head, two docking poses were selected for MD simulation, one with polar head oriented towards the N-end as in the experimental solution NMR structure of complex with M2WJ332 (PDB: 2LY0)⁴³ and one with polar head oriented towards the C-end.

5.5.5.2 MD simulations

The M2TM WT complexes or M2TM S31N complexes were embedded in a DMPC lipid bilayer extending 10 Å beyond the solutes. Complex and ligand systems were solvated using the TIP3P⁸² water model. Na⁺ and Cl⁻ ions were placed in the water phase to neutralize the systems and to reach the experimental salt concentration of 0.150 M NaCl. Membrane creation and system solvation were conducted with the “System Builder” utility of Desmond.^{83,84} The M2TM_{WT}-**1** complex structure in the hydrated DMPC bilayer with ions included 18617 atoms.

The OPLS 2005 force field^{85,86,87} was used to model all protein and ligand interactions, and the TIP3P model⁸² was used for water. The particle mesh Ewald method (PME)^{88,89} was employed to calculate long-range electrostatic interactions with a grid spacing of 0.8 Å. Van der Waals and short range electrostatic interactions were smoothly truncated at 9.0 Å. The Nosé-Hoover thermostat⁹⁰ was utilized to maintain a constant temperature in all simulations, and the Martyna-Tobias-Klein method⁹⁰ was used to control the pressure. Periodic boundary conditions were applied (50×50×80)Å³. The equations of motion were integrated using the multistep RESPA integrator⁹¹ with an inner time step of 2 fs for bonded interactions and non-bonded interactions within a cutoff of 9 Å. An outer time step of 6.0 fs was used for non-bonded interactions beyond the cut-off.

Each system was equilibrated in MD simulations with a modification of the default protocol provided in Desmond, which consists of a series of restrained minimizations and MD simulations designed to relax the system, while not deviating substantially from the initial coordinates. First, two rounds of steepest descent minimization were performed with a maximum of 2000 steps with harmonic restraints of 50 kcal mol⁻¹ Å⁻² applied on all solute atoms, followed by 10000 steps of minimization without restraints. The first simulation

was run for 200 ps at a temperature of 10 K in the NVT (constant number of particles, volume, and temperature) ensemble with solute heavy atoms restrained with a force constant of $50 \text{ kcal mol}^{-1} \text{ \AA}^{-2}$. The temperature was then raised during a 200 ps MD simulation to 310 K in the NVT ensemble with the force constant retained. The temperature of 310 K was used in our MD simulations in order to ensure that the membrane state is above the melting temperature state of 297 K for DMPC lipids.⁹²

The heating was followed by equilibration runs. First, two stages of NPT equilibration (constant number of particles, pressure, and temperature) were performed, one with the heavy atoms of the system restrained for 1 ns and one for solvent and lipids for 10 ns, with a force constant of $10 \text{ kcal/mol/\AA}^2$ for the harmonic constraints, respectively. A NPT simulation followed with the C_α atoms restrained for 1 ns with a force constant of 2 kcal/mol/\AA^2 . The above-mentioned equilibration was followed by a 80 ns NPT simulation without restraints. Within this time, the total energy and the RMSD reached a plateau, and the systems were considered equilibrated.

5.6 References

- ¹ Wang, C.; Takeuchi, K.; Pinto, L. H.; Lamb, R. a. Ion Channel Activity of Influenza A Virus M2 Protein: Characterization of the Amantadine Block. *J. Virol.* **1993**, *67*, 5585–5594.
- ² Chizhnikov, I. V.; Geraghty, F. M.; Ogden, D. C.; Hayhurst, A.; Antoniou, M.; Hay, A. J. Selective Proton Permeability and PH Regulation of the Influenza Virus M2 Channel Expressed in Mouse Erythroleukaemia Cells. *J. Physiol.* **1996**, *494*, 329–336.
- ³ Hayden, F. G. Clinical Applications of Antiviral Agents for Chemoprophylaxis and Therapy of Respiratory Viral Infections. *Antiviral Res.* **1985**, *Suppl 1*, 229–239.
- ⁴ Wang, J.; Qiu, J. X.; Soto, C.; Degrado, W. F. Structural and Dynamic Mechanisms for the Function and Inhibition of the M2 Proton Channel from Influenza A Virus. *Curr. Opin. Struct. Biol.* **2011**, *21*, 68–80.
- ⁵ Hu, J.; Asbury, T.; Achuthan, S.; Li, C.; Bertram, R.; Quine, J. R.; Fu, R.; Cross, T. a. Backbone Structure of the Amantadine-Blocked Trans-Membrane Domain M2 Proton Channel from Influenza A Virus. *Biophys. J.* **2007**, *92*, 4335–4343.
- ⁶ Stouffer, A. L.; Acharya, R.; Salom, D.; Levine, A. S.; Di Costanzo, L.; Soto, C. S.; Tereshko, V.; Nanda, V.; Stayrook, S.; DeGrado, W. F. Structural Basis for the Function and Inhibition of an Influenza Virus Proton Channel. *Nature* **2008**, *451*, 596–599.
- ⁷ Cady, S. D.; Schmidt-Rohr, K.; Wang, J.; Soto, C. S.; DeGrado, W. F.; Hong, M. Structure of the Amantadine Binding Site of Influenza M2 Proton Channels in Lipid Bilayers. *Nature* **2010**, *463*, 689–U127.
- ⁸ Pielak, R. M.; Oxenoid, K.; Chou, J. J. Structural Investigation of Rimantadine Inhibition of the AM2-BM2 Chimera Channel of Influenza Viruses. *Structure* **2011**, *19*, 1655–1663.
- ⁹ Cady, S. D.; Wang, J.; Wu, Y.; Degrado, W. F.; Hong, M. Specific Binding of Adamantane Drugs and Direction of Their Polar Amines in the Pore of the Influenza M2 Transmembrane Domain in Lipid Bilayers and Dodecylphosphocholine Micelles Determined by NMR Spectroscopy. *J. Am. Chem. Soc.* **2011**, *133*, 4274–4284.
- ¹⁰ Wright, A. K.; Batsomboon, P.; Dai, J.; Hung, I.; Zhou, H. X.; Dudley, G. B.; Cross, T. A. Differential Binding of Rimantadine Enantiomers to Influenza A M2 Proton Channel. *J. Am. Chem. Soc.* **2016**, *138*, 1506–1509.
- ¹¹ Ma, C.; Polishchuk, a L.; Ohigashi, Y.; Stouffer, a L.; Schon, a; Magavern, E.; Jing, X.; Lear, J. D.; Freire, E.; Lamb, R. a; DeGrado, W. F.; Pinto, L. H. Identification of the Functional Core of the Influenza A Virus A/M2 Proton-Selective Ion Channel. *Proc Natl Acad Sci U S A* **2009**, *106*, 12283–12288.
- ¹² Luo, W.; Hong, M. Conformational Changes of an Ion Channel Detected through Water-Protein Interactions Using Solid-State NMR Spectroscopy. *J Am Chem Soc* **2010**, *132*, 2378–2384.
- ¹³ Gianti, E.; Carnevale, V.; Degrado, W. F.; Klein, M. L.; Fiorin, G. Hydrogen-Bonded Water Molecules in the M2 Channel of the Influenza a Virus Guide the Binding Preferences of Ammonium-Based Inhibitors. *J. Phys. Chem. B* **2015**, *119*, 1173–1183.

- ¹⁴ Gleed, M. L.; Ioannidis, H.; Kolocouris, A.; Busath, D. D. Resistance-Mutation N31 Effects on Drug Orientation and Channel Hydration in Amantadine-Bound Influenza A M2. *J. Phys. Chem. B* **2015**, *119*, 11548–11559.
- ¹⁵ Leonov, H.; Astrahan, P.; Krugliak, M.; Arkin, I. T. How Do Aminoadamantanes Block the Influenza M2 Channel, and How Does Resistance Develop? *J. Am. Chem. Soc.* **2011**, *133*, 9903–9911.
- ¹⁶ Yi, M.; Cross, T. a; Zhou, H.-X. Conformational Heterogeneity of the M2 Proton Channel and a Structural Model for Channel Activation. *Proc. Natl. Acad. Sci. U. S. A.* **2009**, *106*, 13311–13316.
- ¹⁷ Intharathep, P.; Laohpongspaisan, C.; Rungrotmongkol, T.; Loiruangsinsin, A.; Malaisree, M.; Decha, P.; Aruksakunwong, O.; Chuenpennit, K.; Kaiyawet, N.; Sompornpisut, P.; Pianwanit, S.; Hannongbua, S. How Amantadine and Rimantadine Inhibit Proton Transport in the M2 Protein Channel. *J. Mol. Graph. Model.* **2008**, *27*, 342–348.
- ¹⁸ Khurana, E.; Devane, R. H.; Dal Peraro, M.; Klein, M. L. Computational Study of Drug Binding to the Membrane-Bound Tetrameric M2 Peptide Bundle from Influenza A Virus. *Biochim. Biophys. Acta - Biomembr.* **2011**, *1808*, 530–537.
- ¹⁹ Gkeka, P.; Eleftheratos, S.; Kolocouris, A.; Cournia, Z. Free Energy Calculations Reveal the Origin of Binding Preference for Aminoadamantane Blockers of Influenza A/M2TM Pore. *J. Chem. Theory Comput.* **2013**, *9*, 1272–1281.
- ²⁰ Ioannidis, H.; Drakopoulos, A.; Tzitzoglaki, C.; Homeyer, N.; Kolarov, F.; Gkeka, P.; Freudenberger, K.; Liolios, C.; Gauglitz, G.; Cournia, Z.; Gohlke, H.; Kolocouris, A. Alchemical Free Energy Calculations and Isothermal Titration Calorimetry Measurements of Aminoadamantanes Bound to the Closed State of Influenza A/M2TM. *J. Chem. Inf. Model.* **2016**, *56*, 862–876.
- ²¹ Homeyer, N.; Stoll, F.; Hillisch, A.; Gohlke, H. Binding Free Energy Calculations for Lead Optimization: Assessment of Their Accuracy in an Industrial Drug Design Context. *J. Chem. Theory Comput.* **2014**, *10*, 3331–3344.
- ²² Astrahan, P.; Arkin, I. T. Resistance Characteristics of Influenza to Amino-Adamantyls. *Biochim. Biophys. Acta - Biomembr.* **2011**, *1808*, 547–553.
- ²³ Abed, Y.; Goyette, N.; Boivin, G. Generation and Characterization of Recombinant Influenza A H1N1 Viruses Harboring Amantadine Resistance Mutations Generation and Characterization of Recombinant Influenza A H1N1 Viruses Harboring Amantadine Resistance Mutations. **2005**, *49*, 556–559.
- ²⁴ Furuse, Y.; Suzuki, A.; Oshitani, H. Large-Scale Sequence Analysis of M Gene of Influenza A Viruses from Different Species: Mechanisms for Emergence and Spread of Amantadine Resistance. *Antimicrob. Agents Chemother.* **2009**, *53*, 4457–4463.
- ²⁵ Furuse, Y.; Suzuki, A.; Kamigaki, T.; Oshitani, H. Evolution of the M Gene of the Influenza A Virus in Different Host Species: Large-Scale Sequence Analysis. *Viol. J.* **2009**, *6*, 67.
- ²⁶ Bright, R. A.; Medina, M. J.; Xu, X.; Perez-Oronoz, G.; Wallis, T. R.; Davis, X. M.; Povinelli, L.; Cox, N. J.; Klimov, A. I. Incidence of Adamantane Resistance among Influenza A H3N2 Viruses Isolated Worldwide from 1994 to 2005: A Cause for Concern. *Lancet* **2005**, *366*, 1175–1181.

- ²⁷ Lan, Y.; Zhang, Y.; Dong, L.; Wang, D.; Huang, W.; Xin, L.; Yang, L.; Zhao, X.; Li, Z.; Wang, W.; Li, X.; Xu, C.; Yang, L.; Guo, J.; Wang, M.; Peng, Y.; Gao, Y.; Guo, Y.; Wen, L.; Jiang, T.; Shu, Y. A Comprehensive Surveillance of Adamantane Resistance among Human Influenza A Virus Isolated from Mainland China between 1956 and 2009. *Antivir. Ther.* **2010**, *15*, 853–859.
- ²⁸ Dong, G.; Peng, C.; Luo, J.; Wang, C.; Han, L.; Wu, B.; Ji, G.; He, H. Adamantane-Resistant Influenza A Viruses in the World 1902-2013 : Frequency and Distribution of M2 Gene Mutations. *PLoS One* **2015**, *10*, 1–20.
- ²⁹ Garcia, V.; Aris-Brosou, S. Comparative Dynamics and Distribution of Influenza Drug Resistance Acquisition to Protein M2 and Neuraminidase Inhibitors. *Mol. Biol. Evol.* **2014**, *31*, 355–363.
- ³⁰ Rey-Carrizo, M.; Barniol-Xicota, M.; Ma, C.; Frigolé-Vivas, M.; Torres, E.; Naesens, L.; Llabrés, S.; Juárez-Jiménez, J.; Luque, F. J.; Degrado, W. F.; Lamb, R. A.; Pinto, L. H.; Vázquez, S. Easily Accessible Polycyclic Amines That Inhibit the Wild-Type and Amantadine-Resistant Mutants of the M2 Channel of Influenza A Virus. *J. Med. Chem.* **2014**, *57*, 5738–5747.
- ³¹ Rey-Carrizo, M.; Gazzarrini, S.; Llabrés, S.; Frigolé-Vivas, M.; Juárez-Jiménez, J.; Font-Bardia, M.; Naesens, L.; Moroni, A.; Luque, F. J.; Vázquez, S. New Polycyclic Dual Inhibitors of the Wild Type and the V27A Mutant M2 Channel of the Influenza A Virus with Unexpected Binding Mode. *Eur. J. Med. Chem.* **2015**, *96*, 318–329.
- ³² Balannik, V.; Carnevale, V.; Fiorin, G.; Levine, B. G.; Lamb, R. A.; Klein, M. L.; DeGrado, W. F.; Pinto, L. H. Functional Studies and Modeling of Pore-Lining Residue Mutants of the Influenza A Virus M2 Ion Channel. *Biochemistry* **2010**, *49*, 696–708.
- ³³ Wang, J.; Ma, C.; Balannik, V.; Pinto, L. H.; Lamb, R. A.; Degrado, W. F. Exploring the Requirements for the Hydrophobic Scaffold and Polar Amine in Inhibitors of M2 from Influenza A Virus. *ACS Med. Chem. Lett.* **2011**, *2*, 307–312.
- ³⁴ Wang, J.; Ma, C.; Fiorin, G.; Carnevale, V.; Wang, T.; Hu, F.; Lamb, R. a; Pinto, L. H.; Hong, M.; Klein, M. L.; Degrado, W. F. Molecular Dynamics MD Simulation Directed Rational Design of Inhibitors Targeting Drug-Resistant Mutants of Influenza A Virus M2 Molecular Dynamics MD Simulation Directed Rational Design of Inhibitors Targeting Drug-Resistant Mutants of Influenza. *J. Am. Chem. Soc.* **2011**, 12834–12841.
- ³⁵ Aldrich, P. E.; Hermann, E. C.; Meier, W. E.; Paulshock, M.; Prichard, W. W.; Snyder, J. A.; Watts, J. C. Antiviral Agents. 2. Structure-Activity Relationships of Compounds Related to 1-Adamantanamine. *J. Med. Chem.* **1971**, *14*, 535–543.
- ³⁶ Kolocouris, N.; Foscolos, G. B.; Kolocouris, A.; Marakos, P.; Pouli, N.; Fytas, G.; Ikeda, S.; De Clercq, E. Synthesis and Antiviral Activity Evaluation of Some Aminoadamantane Derivatives. *J. Med. Chem.* **1994**, *37*.
- ³⁷ Kolocouris, N.; Kolocouris, A.; Foscolos, G. B.; Fytas, G.; Neyts, J.; Padalko, E.; Balzarini, J.; Snoeck, R.; Andrei, G.; De Clercq, E. Synthesis and Antiviral Activity Evaluation of Some New Aminoadamantane Derivatives. 2. *J. Med. Chem.* **1996**, *39*.
- ³⁸ Kolocouris, A.; Tzitzoglaki, C.; Johnson, F. B.; Zell, R.; Wright, A. K.; Cross, T. A.; Tietjen, I.; Fedida, D.; Busath, D. D. Aminoadamantanes with Persistent in Vitro Efficacy against H1N1 2009 Influenza A. *J. Med. Chem.* **2014**, *57*.

- ³⁹ Torres, E.; Fernández, R.; Miquet, S.; Font-Bardia, M.; Vanderlinden, E.; Naesens, L.; Vázquez, S. Synthesis and Anti-Influenza A Virus Activity of 2,2-Dialkylamantadines and Related Compounds. *ACS Med. Chem. Lett.* **2012**, *3*, 1065–1069.
- ⁴⁰ Zhao, X.; Li, C.; Zeng, S.; Hu, W. Discovery of Highly Potent Agents against Influenza A Virus. *Eur. J. Med. Chem.* **2011**, *46*, 52–57.
- ⁴¹ Zhao, X.; Jie, Y.; Rosenberg, M. R.; Wan, J.; Zeng, S.; Cui, W.; Xiao, Y.; Li, Z.; Tu, Z.; Casarotto, M. G.; Hu, W. Design and Synthesis of Pinanamine Derivatives as Anti-Influenza A M2 Ion Channel Inhibitors. *Antiviral Res.* **2012**, *96*, 91–99.
- ⁴² Dong, J.; Chen, S.; Li, R.; Cui, W.; Jiang, H.; Ling, Y.; Yang, Z.; Hu, W. Imidazole-Based Pinanamine Derivatives: Discovery of Dual Inhibitors of the Wild-Type and Drug-Resistant Mutant of the Influenza A Virus. *Eur. J. Med. Chem.* **2016**, *108*, 605–615.
- ⁴³ Wang, J.; Wu, Y.; Ma, C.; Fiorin, G.; Pinto, L. H.; Lamb, R. a.; Klein, M. L.; Degrado, W. F.; Wang, J. J.; Pinto, L. H.; Lamb, R. a.; Klein, M. L.; Degrado, W. F. Structure and Inhibition of the Drug-Resistant S31N Mutant of the M2 Ion Channel of Influenza A Virus. *Proc Natl Acad Sci U S A* **2013**, *110*, 1315–1320.
- ⁴⁴ Wang, J.; Ma, C.; Wang, J.; Jo, H.; Canturk, B.; Fiorin, G.; Pinto, L. H.; Lamb, R. A.; Klein, M. L.; DeGrado, W. F. Discovery of Novel Dual Inhibitors of the Wild-Type and the Most Prevalent Drug-Resistant Mutant, S31N, of the M2 Proton Channel from Influenza A Virus. *J. Med. Chem.* **2013**, *56*, 2804–2812.
- ⁴⁵ Wu, Y.; Canturk, B.; Jo, H.; Ma, C.; Gianti, E.; Klein, M. L.; Pinto, L. H.; Lamb, R. A.; Fiorin, G.; Wang, J.; Degrado, W. F. Flipping in the Pore: Discovery of Dual Inhibitors That Bind in Different Orientations to the Wild-Type versus the Amantadine-Resistant S31n Mutant of the Influenza a Virus M2 Proton Channel. *J. Am. Chem. Soc.* **2014**, *136*, 17987–17995.
- ⁴⁶ Li, F.; Ma, C.; Degrado, W. F.; Wang, J. Discovery of Highly Potent Inhibitors Targeting the Predominant Drug-Resistant S31N Mutant of the Influenza A Virus M2 Proton Channel. *J. Med. Chem.* **2016**, *59*, 1207–1216.
- ⁴⁷ Li, F.; Ma, C.; Hu, Y.; Wang, Y.; Wang, J. Discovery of Potent Antivirals against Amantadine-Resistant Influenza A Viruses by Targeting the M2-S31N Proton Channel. *ACS Infect. Dis.* **2016**, *2*, 726–733.
- ⁴⁸ Wang, J.; Li, F.; Ma, C. Recent Progress in Designing Inhibitors That Target the Drug-Resistant M2 Proton Channels from the Influenza A Viruses. *Biopolymers* **2015**, *104*, 291–309.
- ⁴⁹ Williams, J. K.; Tietze, D.; Wang, J.; Wu, Y.; Degrado, W. F.; Hong, M. Drug-Induced Conformational and Dynamical Changes of the S31N Mutant of the Influenza M2 Proton Channel Investigated by Solid-State NMR. *J. Am. Chem. Soc.* **2013**, *135*, 9885–9897.
- ⁵⁰ Alhadeff, R.; Assa, D.; Astrahan, P.; Krugliak, M.; Arkin, I. T. Computational and Experimental Analysis of Drug Binding to the Influenza M2 Channel. *Biochim. Biophys. Acta* **2014**, *1838*, 1068–1073.
- ⁵¹ Tzitzoglaki, C.; Wright, A.; Freudenberger, K.; Hoffmann, A.; Tietjen, I.; Stylianakis, I.; Kolarov, F.; Fedida, D.; Schmidtke, M.; Gauglitz, G.; Cross, T. A.; Kolocouris, A. Binding and Proton Blockage by Amantadine Variants of the Influenza M2WT and M2S31N Explained. *J. Med. Chem.* **2017**, *60*, 1716–1733.

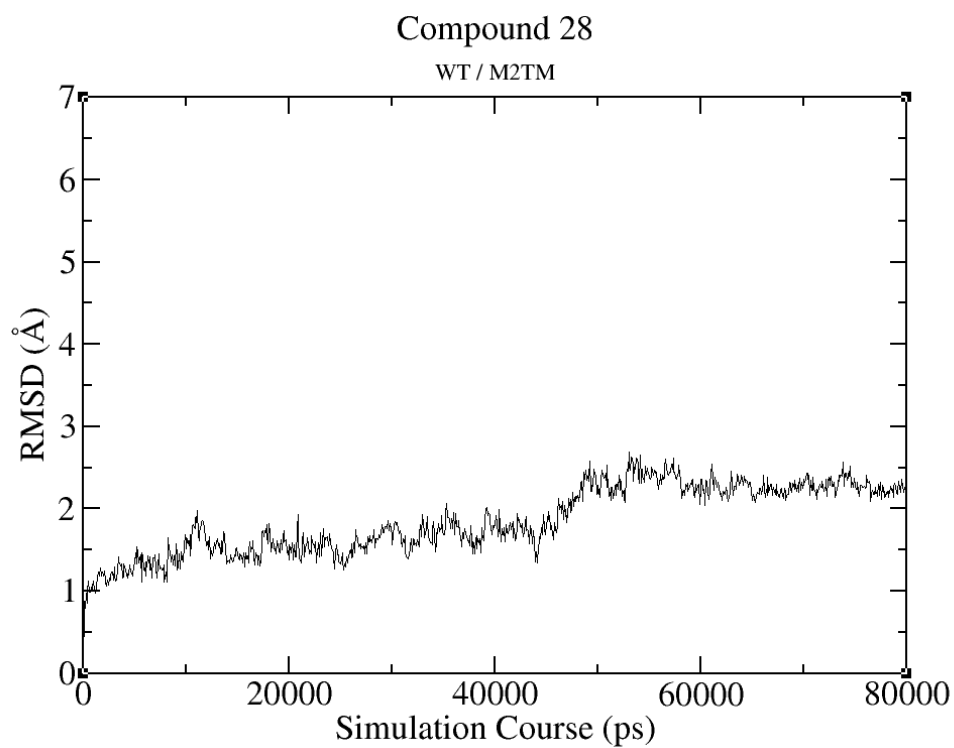
- ⁵² Kolocouris, N.; Foscolos, G. B.; Kolocouris, A.; Marakos, P.; Pouli, N.; Fytas, G.; Ikeda, S.; De Clercq, E. Synthesis and Antiviral Activity Evaluation of Some Aminoadamantane Derivatives. *J Med Chem* **1994**, *37*, 2896–2902.
- ⁵³ Drakopoulos, A.; Tzitzoglaki, C.; McGuire, K.; Hoffmann, A.; Konstantinidi, A.; Kolokouris, D.; Ma, C.; Freudenberger, K.; Hutterer, J.; Gauglitz, G.; Wang, J.; Schmidtke, M.; Busath, D. D.; Kolocouris, A. Unraveling the Binding, Proton Blockage, and Inhibition of Influenza M2 WT and S31N by Rimantadine Variants. *ACS Med. Chem. Lett.* **2018**, *9*.
- ⁵⁴ Fokina, N. A.; Tkachenko, B. A.; Merz, A.; Serafin, M.; Dahl, J. E. P.; Carlson, R. M. K.; Fokin, A. A.; Schreiner, P. R. Hydroxy Derivatives of Diamantane, Triamantane, and [121]Tetramantane: Selective Preparation of Bis-Apical Derivatives. *European J. Org. Chem.* **2007**, 4738–4745.
- ⁵⁵ Kovalev, V. V.; Rozov, A. K.; Shokova, E. A. Novel Approach to Trisubstituted Adamantanes. *Tetrahedron* **1996**, *52*, 3983–3990.
- ⁵⁶ Jirgensons, A.; Kauss, V.; Kalvinsh, I.; Gold, M. R. A Practical Synthesis of Tert-Alkylamines via the Ritter Reaction with Chloroacetonitrile. *Synthesis Stuttg.* **2000**, 1709–1712.
- ⁵⁷ Jasys, V. J.; Lombardo, F.; Appleton, T. A.; Bordner, J.; Ziliox, M.; Volkmann, R. A. Preparation of Fluoroadamantane Acids and Amines: Impact of Bridgehead Fluorine Substitution on the Solution- and Solid-State Properties of Functionalized Adamantanes. *J. Am. Chem. Soc.* **2000**, *122*, 466–473.
- ⁵⁸ Huc, I.; Rebek, J. Molecular Recognition of Adenine : Role of Geometry, Electronic Effects and Rotational Restrictions. *Tetrahedron Lett.* **1994**, *35*, 1035–1038.
- ⁵⁹ Whitmore, F. C.; George, R. S. Abnormal Grignard Reactions. X. Enolizing and Reducing Action of Grignard Reagents Upon Diisopropyl Ketone. *J. Am. Chem. Soc.* **1942**, *64*, 1239–1242.
- ⁶⁰ Salom, D.; Hill, B. R.; Lear, J. D.; DeGrado, W. F. PH-Dependent Tetramerization and Amantadine Binding of the Transmembrane Helix of M2 from the Influenza A Virus. *Biochemistry* **2000**, *39*, 14160–14170.
- ⁶¹ Vaultier, M.; Knouzi, N.; Carrié, R. Reduction d'azides En Amines Primaires Par Une Methode Generale Utilisant La Reaction de Staudinger. *Tetrahedron Lett.* **1983**, *24*, 763–764.
- ⁶² Schmidtke, M.; Schnittler, U.; Jahn, B.; Dahse, H.-M.; Stelzner, A. A Rapid Assay for Evaluation of Antiviral Activity against Coxsackie Virus B3, Influenza Virus A, and Herpes Simplex Virus Type 1. *J. Virol. Methods* **2001**, *95*, 133–143.
- ⁶³ Kolocouris, A.; Tzitzoglaki, C.; Johnson, F. B.; Zell, R.; Wright, A. K.; Cross, T. A.; Tietjen, I.; Fedida, D.; Busath, D. D. Aminoadamantanes with Persistent in Vitro Efficacy against H1N1 2009 Influenza A. *J. Med. Chem.* **2014**, *57*, 4629–4639.
- ⁶⁴ GOLD Suite, Version 5.2; Cambridge Crystallographic Data Centre: Cambridge, U. K. [Http://www.ccdc.cam.ac.uk](http://www.ccdc.cam.ac.uk). 5.
- ⁶⁵ Jones, G.; Willett, P.; Glen, R. C.; Leach, a R.; Taylor, R. Development and Validation of a Genetic Algorithm for Flexible Docking. *J. Mol. Biol.* **1997**, *267*, 727–748.

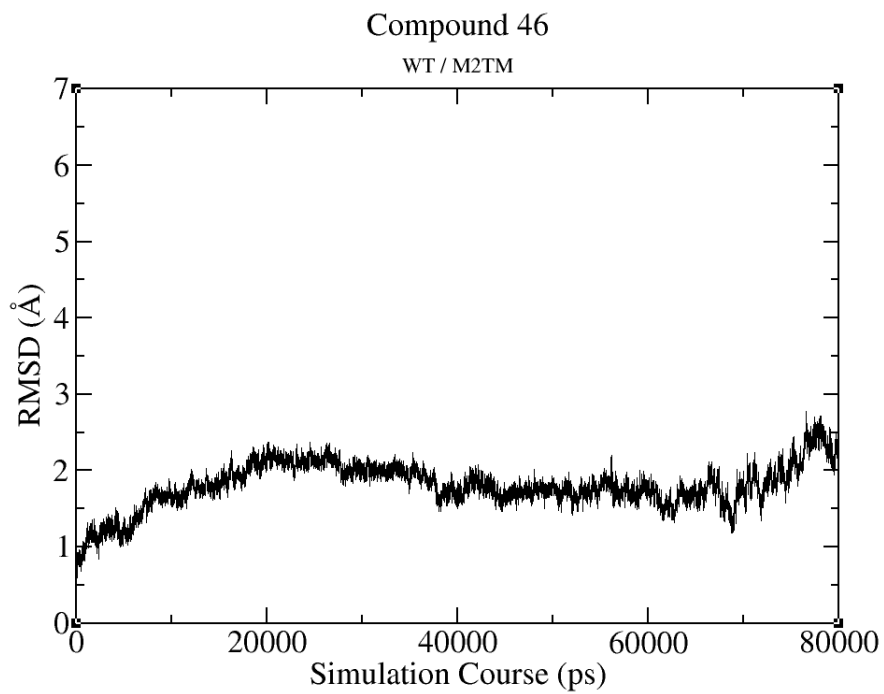
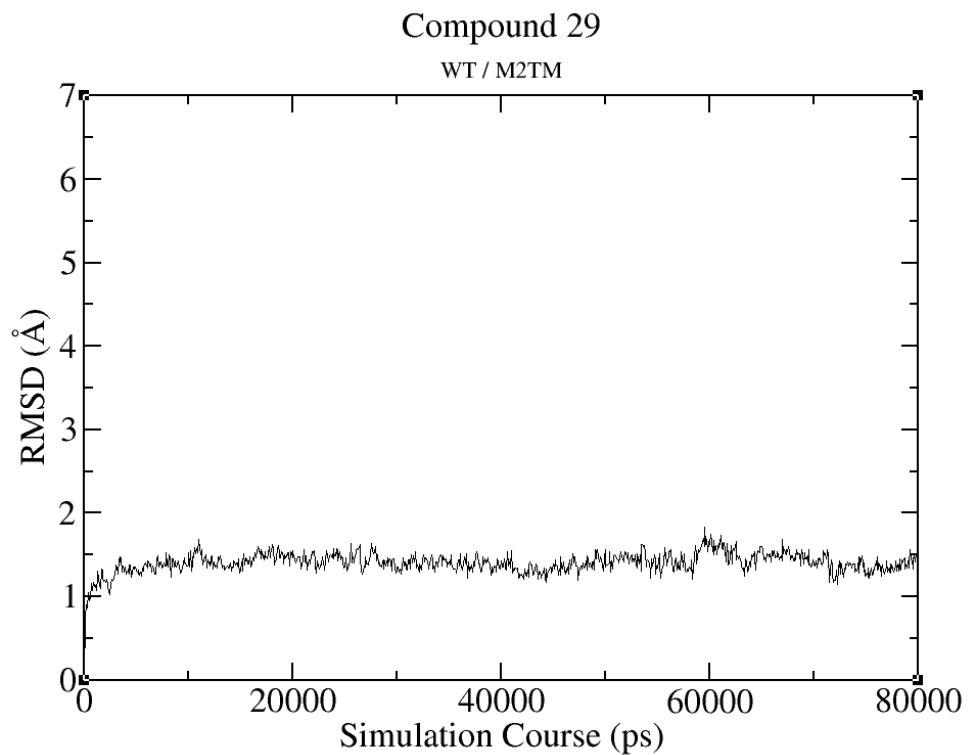
- ⁶⁶ Verdonk, M. L.; Chessari, G.; Cole, J. C.; Hartshorn, M. J.; Murray, C. W.; Nissink, J. W. M.; Taylor, R. D.; Taylor, R. Modeling Water Molecules in Protein-Ligand Docking Using GOLD. *J. Med. Chem.* **2005**, *48*, 6504–6515.
- ⁶⁷ Cristian, L.; Lear, J. D.; DeGrado, W. F. Use of Thiol-Disulfide Equilibria to Measure the Energetics of Assembly of Transmembrane Helices in Phospholipid Bilayers. *Proc. Natl. Acad. Sci.* **2003**, *100*, 14772–14777.
- ⁶⁸ Cady, S.; Wang, T.; Hong, M. Membrane-Dependent Effects of a Cytoplasmic Helix on the Structure and Drug Binding of the Influenza Virus M2 Protein. *J. Am. Chem. Soc.* **2011**, *133*, 11572–11579.
- ⁶⁹ Thomaston, J.; Konstantinidi, A.; Kolocouris, A.; DeGrado, W. Unpublished Results.
- ⁷⁰ Wang, J.; Ma, C.; Fiorin, G.; Carnevale, V.; Wang, T.; Hu, F.; Lamb, R. A.; Pinto, L. H.; Hong, M.; Klein, M. L.; DeGrado, W. F. Molecular Dynamics Simulation Directed Rational Design of Inhibitors Targeting Drug-Resistant Mutants of Influenza A Virus M2. *J. Am. Chem. Soc.* **2011**, *133*, 12834–12841.
- ⁷¹ Tzitzoglaki, C.; Wright, A.; Freudenberger, K.; Hoffmann, A.; Tietjen, I.; Stylianakis, I.; Kolarov, F.; Fedida, D.; Schmidtke, M.; Gauglitz, G.; Cross, T. A.; Kolocouris, A. Binding and Proton Blockage by Amantadine Variants of the Influenza M2_{WT} and M2_{S31N} Explained. *J. Med. Chem.* **2017**, *60*, 1716–1733.
- ⁷² Grohskopf, L. A.; Shay, D. K.; Shimabukuro, T. T.; Sokolow, L. Z.; Keitel, W. A.; Bresee, J. S.; Cox, N. J. Prevention and Control of Seasonal Influenza with Vaccines: Recommendations of the Advisory Committee on Immunization Practices - United States, 2013-2014. *Mmwr Recomm. Reports* **2013**, *62*, 1–43.
- ⁷³ Jin, H.; Chen, Z. Production of Live Attenuated Influenza Vaccines against Seasonal and Potential Pandemic Influenza Viruses. *Curr. Opin. Virol.* **2014**, *6*, 34–39.
- ⁷⁴ Koperniku, A.; Foscolos, A.-S.; Papanastasiou, I.; Foscolos, G. B.; Tsotinis, A.; Schols, D. 4-1-Adamantyl Phenylalkanamines with Potential Antiproliferative Activity. *Lett. Org. Chem.* **2016**, *13*, 171–176.
- ⁷⁵ Schade, D.; Kotthaus, J.; Riebling, L.; Kotthaus, J.; Müller-Fielitz, H.; Raasch, W.; Hoffmann, A.; Schmidtke, M.; Clement, B. Zanamivir Amidoxime- and N-Hydroxyguanidine-Based Prodrug Approaches to Tackle Poor Oral Bioavailability. *J. Pharm. Sci.* **2015**, *104*, 3208–3219.
- ⁷⁶ Hoffmann, E.; Neumann, G.; Kawaoka, Y.; Hobom, G.; Webster, R. G. A DNA Transfection System for Generation of Influenza A Virus from Eight Plasmids. *Proc. Natl. Acad. Sci.* **2000**, *97*, 6108–6113.
- ⁷⁷ Torres, E.; Duque, M. D.; Vanderlinden, E.; Ma, C.; Pinto, L. H.; Camps, P.; Froeyen, M.; Vázquez, S.; Naesens, L. Role of the Viral Hemagglutinin in the Anti-Influenza Virus Activity of Newly Synthesized Polycyclic Amine Compounds. *Antiviral Res.* **2013**, *99*, 281–291.
- ⁷⁸ Maestro, Version 8.5; Schrodinger, Inc.: New York, NY, 2008.
- ⁷⁹ Halgren, T. A. Merck Molecular Force Field. V. Extension of MMFF94 Using Experimental Data, Additional Computational Data, and Empirical Rules. *J. Comput. Chem.* **1996**, *17*, 616–641.
- ⁸⁰ Halgren, T. T. A. Merck Molecular Force Field. I. Basis, Form, Scope, Parameterization, and Performance of MMFF94. *J. Comput. Chem.* **1996**, *17*, 490–519.

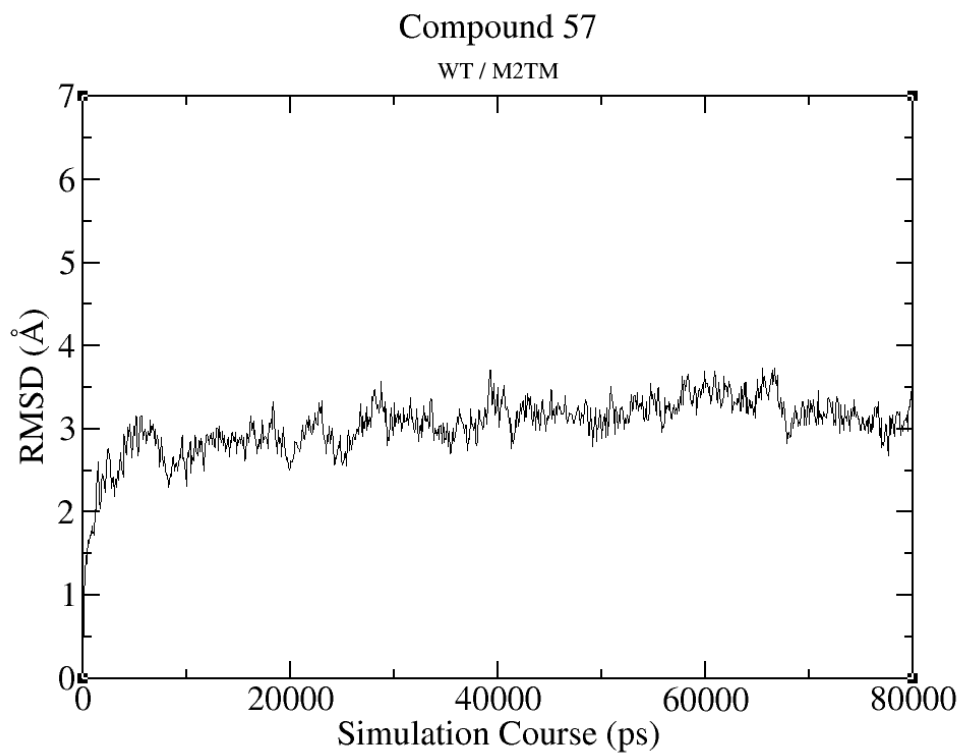
- ⁸¹Pettersen, E. F.; Goddard, T. D.; Huang, C. C.; Couch, G. S.; Greenblatt, D. M.; Meng, E. C.; Ferrin, T. E. UCSF Chimera - A Visualization System for Exploratory Research and Analysis. *J. Comput. Chem.* **2004**, *25*, 1605–1612.
- ⁸²Jorgensen, W. L.; Chandrasekhar, J.; Madura, J. D.; Impey, R. W.; Klein, M. L. Comparison of Simple Potential Functions for Simulating Liquid Water. *J. Chem. Phys.* **1983**, *79*, 926.
- ⁸³Desmond Molecular Dynamics System, Version 3.0, D.E. Shaw Research, New York, NY, 2011.Pdf.
- ⁸⁴Maestro-Desmond.Pdf.
- ⁸⁵Jorgensen, W. L.; Maxwell, D. S.; Tirado-Rives, J. Development and Testing of the OLPS All-Atom Force Field on Conformational Energetics and Properties of Organic Liquids. *J. Am. Chem. Soc.* **1996**, *118*, 11225–11236.
- ⁸⁶Kaminski, G. a; Friesner, R. a; Tirado-rives, J.; Jorgensen, W. L. Comparison with Accurate Quantum Chemical Calculations on Peptides †. *J. Phys. Chem. B* **2001**, *105*, 6474–6487.
- ⁸⁷Shivakumar, D.; Williams, J.; Wu, Y. J.; Damm, W.; Shelley, J.; Sherman, W. Prediction of Absolute Solvation Free Energies Using Molecular Dynamics Free Energy Perturbation and the OPLS Force Field. *J. Chem. Theory Comput.* **2010**, *6*, 1509–1519.
- ⁸⁸Darden, T.; York, D.; Pedersen, L. Particle Mesh Ewald: An N·log N Method for Ewald Sums in Large Systems. *J. Chem. Phys.* **1993**, *98*, 10089.
- ⁸⁹Essmann, U.; Perera, L.; Berkowitz, M. L.; Darden, T.; Lee, H.; Pedersen, L. G. A Smooth Particle Mesh Ewald Method. *J Chem Phys* **1995**, *103*, 8577–8593.
- ⁹⁰Martyna, G. J.; Tobias, D. J.; Klein, M. L. Constant Pressure Molecular Dynamics Algorithms. *J. Chem. Phys.* **1994**, *101*, 4177.
- ⁹¹Humphreys, D. D.; Friesner, R. a.; Berne, B. J. A Multiple-Time-Step Molecular Dynamics Algorithm for Macromolecules. *J. Phys. Chem.* **1994**, *98*, 6885–6892.
- ⁹²Koynova, R.; Caffrey, M. Phases and Phase Transitions of the Phosphatidylcholines. *Biochimica et Biophysica Acta - Reviews on Biomembranes*, 1998, *1376*, 91–145.

5.7 SUPPORTING INFORMATION

Figure S1. RMSD plots of compounds **28, 29, 40, 46, 58** in complex with M2TM WT.







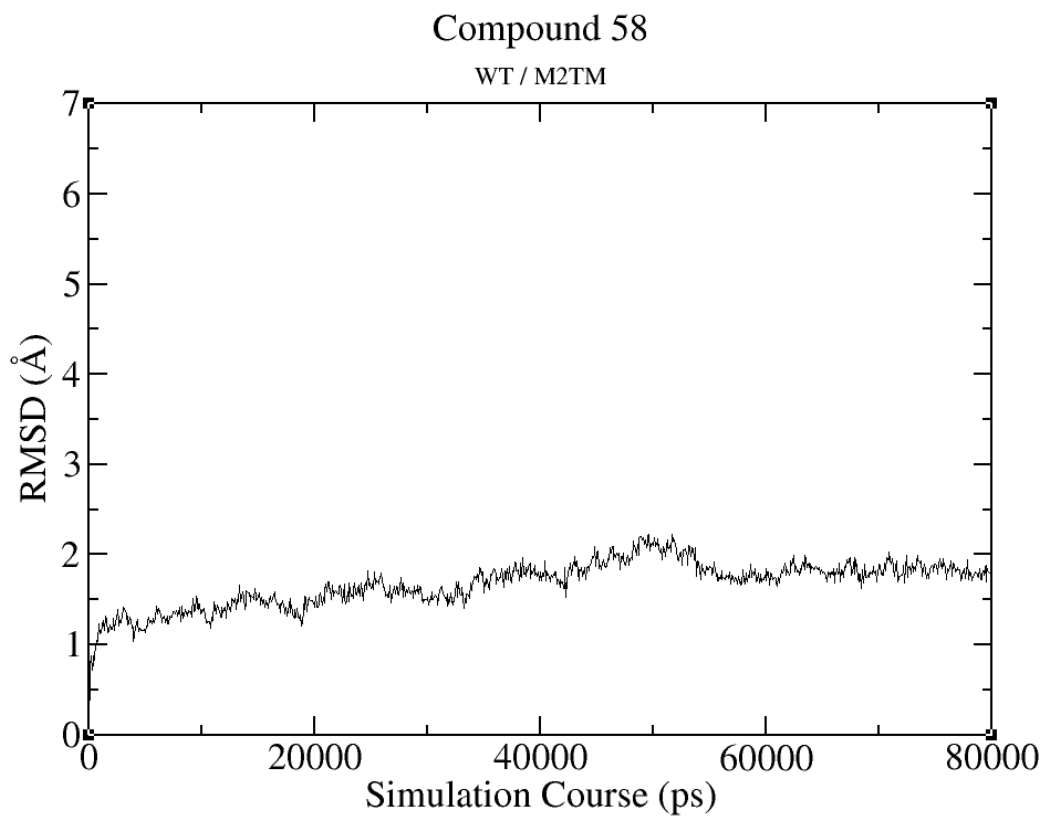
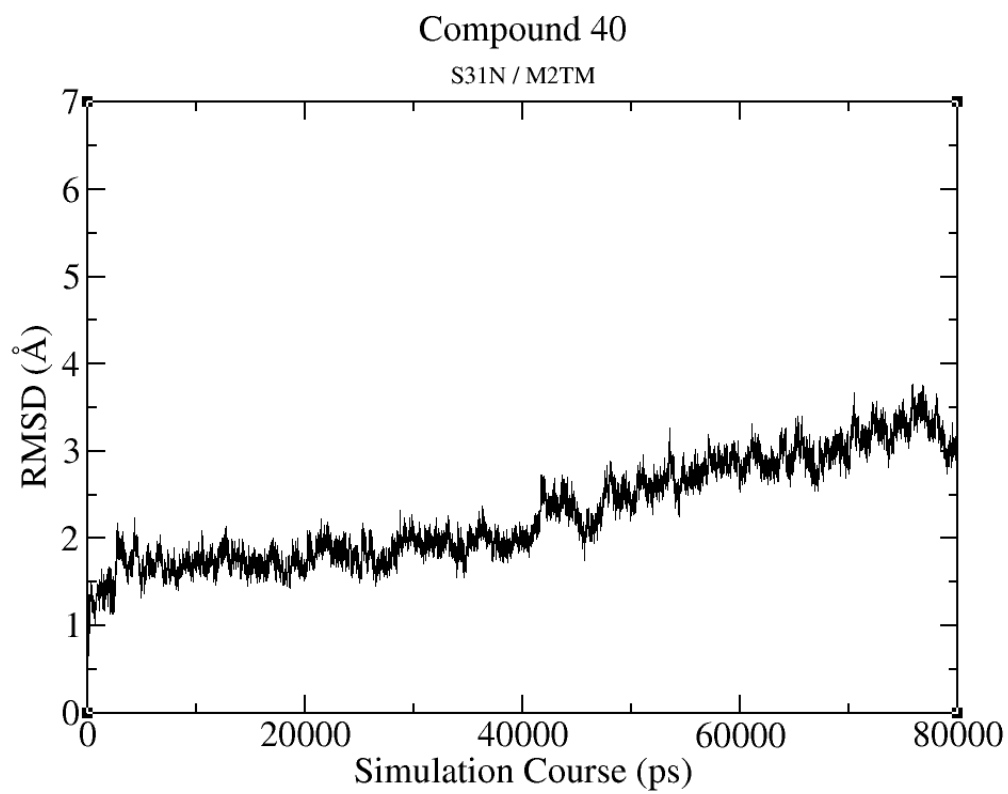
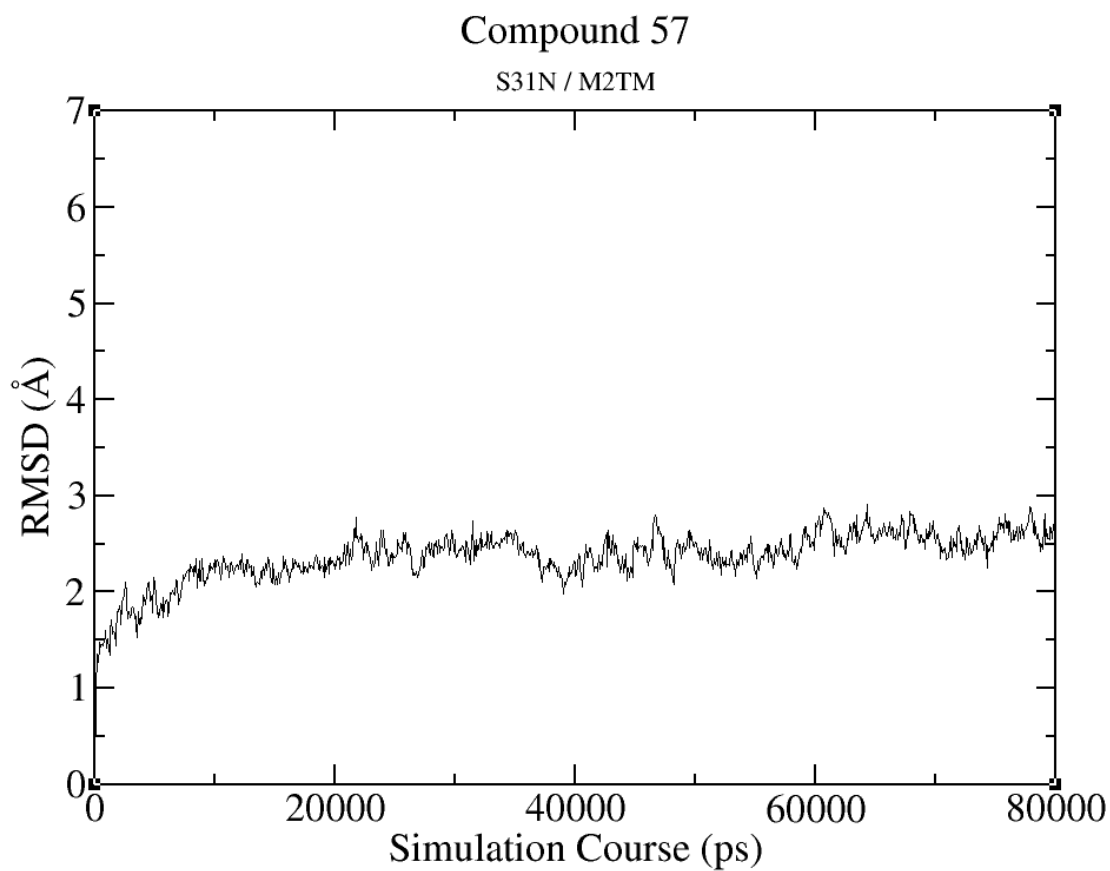
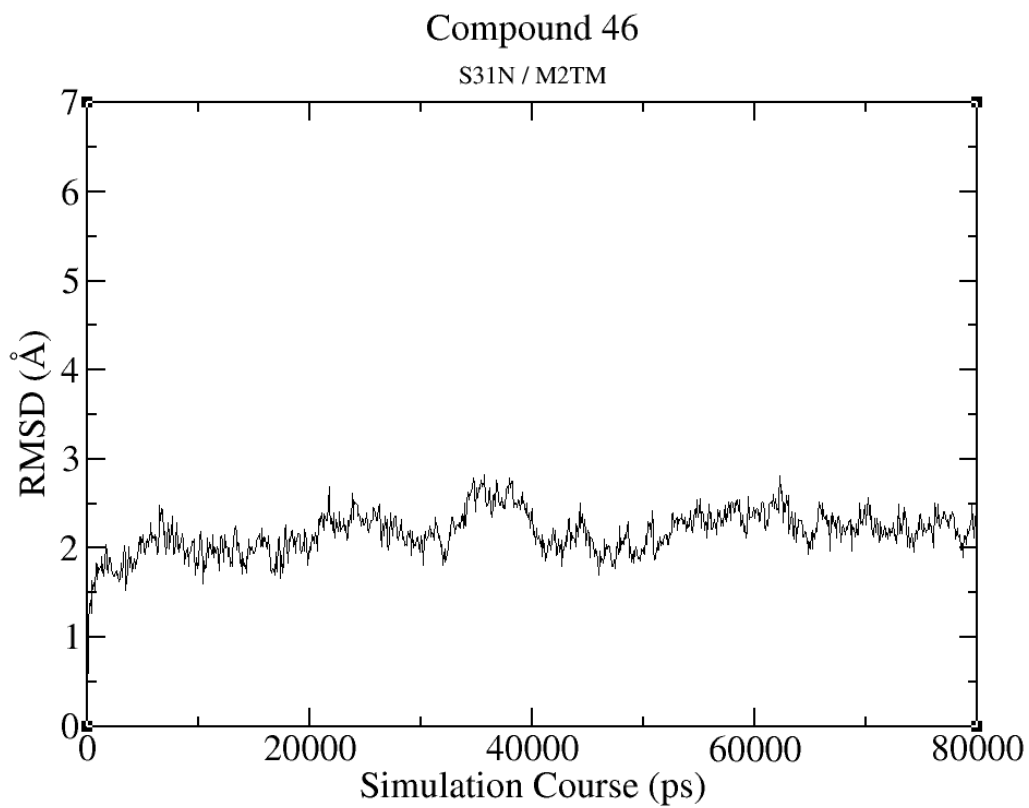
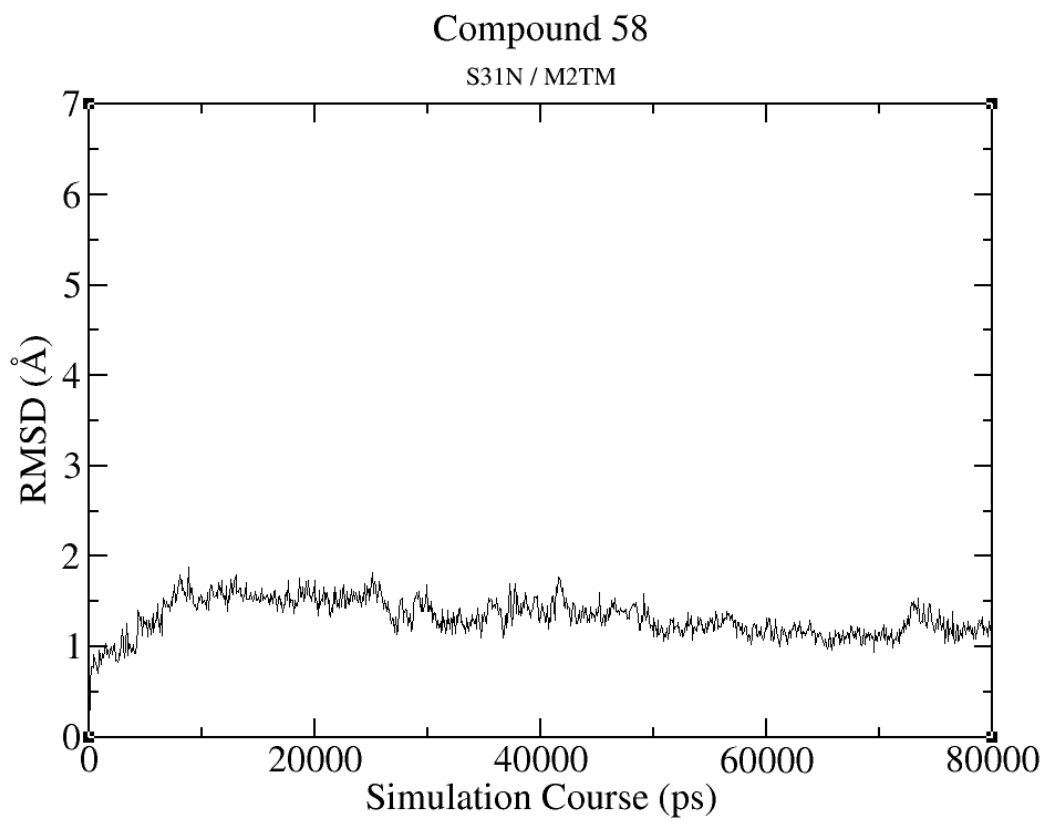
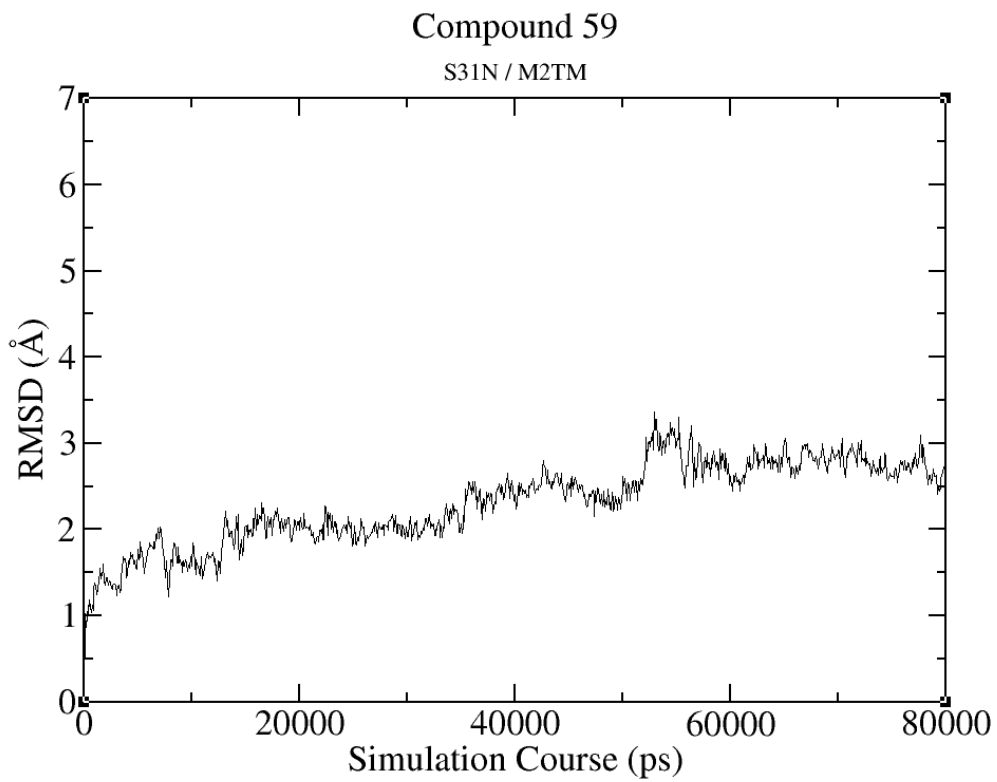


Figure S2. RMSD plots of compounds **40**, **46**, **57-59** in complex with M2TM S31N.









CHAPTER 6

Publications

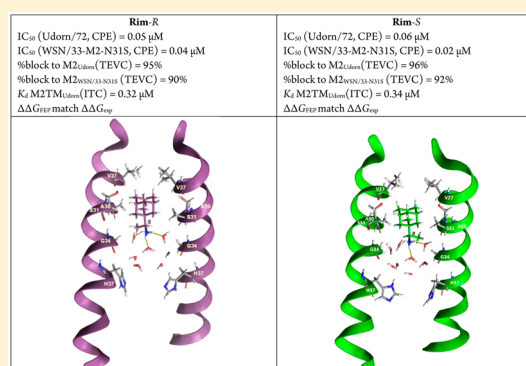
Affinity of Rimantadine Enantiomers against Influenza A/M2 Protein Revisited

Antonios Drakopoulos,[†] Christina Tzitzoglaki,[†] Chulong Ma,^{||} Kathrin Freudenberger,[‡] Anja Hoffmann,[§] Yanmei Hu,^{||} Günter Gauglitz,[‡] Michaela Schmidtke,[§] Jun Wang,^{*,||,§} and Antonios Kolocouris^{*,†,§}[†]Department of Pharmaceutical Chemistry, Faculty of Pharmacy, National and Kapodistrian University of Athens, Athens, Greece^{||}Department of Pharmacology and Toxicology, College of Pharmacy, University of Arizona, Tucson, Arizona 85721, United States[‡]Institut für Physikalische und Theoretische Chemie, Eberhard-Karls-Universität, D-72076 Tübingen, Germany[§]Department of Virology and Antiviral Therapy, Jena University Hospital, Hans Knoell Str. 2, D-07745 Jena, Germany

Supporting Information

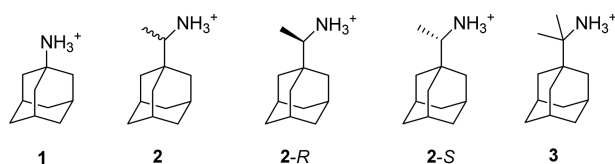
ABSTRACT: Recent findings from solid state NMR (ssNMR) studies suggested that the (*R*)-enantiomer of rimantadine binds to the full M2 protein with higher affinity than the (*S*)-enantiomer. Intrigued by these findings, we applied functional assays, such as antiviral assay and electrophysiology (EP), to evaluate the binding affinity of rimantadine enantiomers to the M2 protein channel. Unexpectedly, no significant difference was found between the two enantiomers. Our experimental data based on the full M2 protein function were further supported by alchemical free energy calculations and isothermal titration calorimetry (ITC) allowing an evaluation of the binding affinity of rimantadine enantiomers to the M2TM pore. Both enantiomers have similar channel blockage, affinity, and antiviral potency.

KEYWORDS: Rimantadine enantiomers, isothermal titration calorimetry, free energy perturbation, Bennett's acceptance ratio, electrophysiology, synthesis, antiviral assay, membrane protein, influenza M2 pore



Amantadine (**1**) and rimantadine (**2**) (Scheme 1) are channel blockers of proton transit by the influenza virus

Scheme 1. Structures of Studied Aminoadamantane Derivatives Amantadine (1), Rimantadine (2, 2-R, and 2-S), and Rimantadine Analogue 3



M2 proton channel^{1,2} and long used prophylactics and therapeutics against influenza A viruses.³ The primary binding site of **1** and **2** is the lumen of the transmembrane domain of a tetrameric M2 protein (M2TM: amino acids 22–46) that forms the proton transit path.⁴

Although **1** and **2** have been used as antivirals for decades, it was only after 2008 that high resolution structures from X-ray and ssNMR experiments unveiled the structures of M2TM in complex with **1** or **2**.^{5–9} According to these findings, the M2TM protein channel is blocked by **1** or **2** via a pore-binding mechanism.^{6–10} The adamantane cage in **1** or **2**, as well as in other aminoadamantane analogues,^{11–13} is tightly contacted on all sides by V27 and A30 side chains, producing a steric

occlusion of proton transit^{6–9} and thereby preventing the viral replication. The ssNMR results for **2** also demonstrated that the ammonium group of the drug is pointing toward the four H37 residues at the C-terminus.⁹ This orientation can be stabilized either through hydrogen bonds between the ammonium group of the aminoadamantane ligand and water molecules in the channel lumen which exist between the imidazoles of H37 and the ligand,¹³ and/or with A30 carbonyls in the vicinity,¹⁴ according to experimental^{9,14–16} and MD simulations data.^{13,17–22} Provided that M2TM is a minimal model for M2 binding,¹⁰ these high resolution structures can be used for the development of new ligands which may bind more effectively to the M2TM pore.

The effect of ligand's chirality in its binding with a chiral receptor is of outstanding significance and the characterization of protein–ligand interactions for each enantiomer separately may identify potential stereospecific binding interactions to the receptor. While rimantadine analogues are known antiviral drugs for more than four decades, the relative potency of rimantadine enantiomers has not been studied at the molecular level. The binding affinity of each enantiomer results from

Received: August 12, 2016

Accepted: January 13, 2017

chiral interactions with the binding area inside the 4-fold symmetric M2 protein. Based on differences in isotropic chemical shift changes measured using ssNMR and MD simulations results, it has been recently suggested that 2-R and 2-S have a strong but differential binding to full length M2, i.e., that 2-R binds more tightly than 2-S.²⁵ This was the first state of the art ssNMR study of the full M2 protein and analysis of the rimantadine enantiomers binding by ssNMR, but this conclusion appears to be puzzling because: (1) 2-R and 2-S have similar in vivo antiviral activity in protecting mice from lethal influenza;²⁴ (2) rimantadine was developed prior to the 1992 FDA guidance on the development of stereoisomers. It was approved as commercial drug in the US in 1993 containing both enantiomers. To solve the controversy between the in vitro binding assay, i.e., ssNMR results, and the in vivo efficacy results, we hereby characterize the binding affinity of the two rimantadine enantiomers and their antiviral efficacy using a consortium of in vitro and cellular assays and biophysical/computational studies.

Taken together, our results demonstrate that rimantadine enantiomers (2-R and 2-S) have equal potency. Since the controversy aroused from previous ssNMR studies of 2-R, 2-S bound to the full M2 protein, we first provided data including the antiviral activity of 2-R, 2-S against amantadine-sensitive influenza A virus strains and the blocking effect of the enantiomers against M2 using EP. Then we investigated the effect of the enantiomers to M2TM using biophysical techniques. More specifically, the antiviral potency of compounds 2-R, 2-S, and 3 against amantadine-sensitive A/Udorn/72 and A/WSN/33-M2-N31S viruses was measured. The blocking effect of 2-R, 2-S, and 3 against full length A/Udorn/72 M2 protein (M2_{Udorn/72}) and A/WSN/33-M2-N31S protein (M2_{WSN/33-N31S}) conductance was measured using EP via a two-electrode voltage clamp (TEVC) assay. Compound 3 is a nonchiral dimethyl analogue of rimantadine, and it was designed and synthesized as a probe to independently validate the biophysical assay results from 2-R and 2-S, as described below. The ITC binding affinities of 2-R, 2-S, and 3 against the M2TM_{Udorn/72} in its closed form at pH 8 were measured. Following up, we applied a free energy perturbation coupled with MD simulations (FEP/MD) scheme to calculate the relative free energies of binding between the rimantadine enantiomers (2-R and 2-S) as well as compound 3 to M2TM_{Udorn/72}. In particular, we calculated the relative free energies of binding for the alchemical transformations of 3 to 2-R and 3 to 2-S.

For the synthesis of primary *tert*-alkyl amine 3 (AdC-Me₂NH₂), the *tert*-alkyl alcohol 5 was prepared according to Scheme 2 from the Grignard reaction between 1-adamantane carbonyl chloride 4 and methylmagnesium iodide. Treatment of *tert*-alkyl alcohol 5 with NaN₃/CF₃CO₂H in dichloromethane afforded azide 6 in high yield, which was further subjected to reduction through LiAlH₄ to form *tert*-alkyl amine 3 in a good yield.

An antiviral assay was used^{25,26} to compare the antiviral activity of 1, 2, 2-R, 2-S, and 3 against two amantadine-sensitive influenza A strains, A/Udorn/72 (H3N2), and A/WSN/33-M2-N31S²⁷ (H1N1) in MDCK cells. All compounds showed submicromolar EC₅₀ values against both influenza strains, and there was no significant difference between the two rimantadine enantiomers 2-R and 2-S (Table 1).

The inhibitors were tested via TEVC assay using *X. laevis* frog oocytes microinjected with RNA expressing the M2

Scheme 2. Synthetic Scheme for the Preparation of *tert*-Alkyl Amine 3

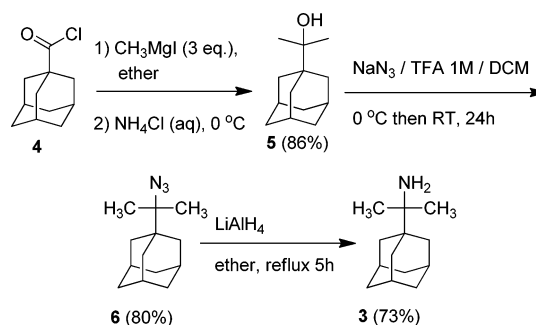


Table 1. Antiviral Activity of Compounds 1–3 against Influenza Virus A/Udorn/72 (H3N2) and A/WSN/33-M2-N31S (H1N1) in Madin–Darby Canine Kidney Cells

compd	IC ₅₀ (μM) ^a (A/Udorn/72)	IC ₅₀ (μM) ^a (A/WSN/33-M2-N31S)
1	0.33 ± 0.04	0.48 ± 0.05
2	0.05 ± 0.02	0.04 ± 0.02
2-R	0.05 ± 0.01	0.04 ± 0.01
2-S	0.06 ± 0.02	0.02 ± 0.01
3	0.04 ± 0.01	0.03 ± 0.02

^aMean and standard deviations of the 50% inhibitory concentration (IC₅₀) of at least three independent measures.

protein as in a previous report.²⁸ Specifically, the blocking effect of the aminoadamantane derivatives against M2 was investigated with electrophysiology experiments using M2_{Udorn/72} (Table 2). The potency of the inhibitors was expressed as the

Table 2. Block of Full-Length M2-Dependent Current by Adamantane Analogues^a

compd	M2 _{Udorn/72}		M2 _{WSN/33-N31S}	
	% block after 2 min	% block after 5 min	% block after 2 min	% block after 5 min
1	90 ± 2% (100 μM; 3)	95 ± 1% (100 μM; 3)		
2	96 ± 1% (100 μM; 3)	96 ± 1% (100 μM; 3)	84 ± 1% (100 μM; 3)	93 ± 0% (100 μM; 3)
2-R	93 ± 1% (100 μM; 3)	95 ± 1% (100 μM; 3)	71 ± 1% (100 μM; 3)	90 ± 1% (100 μM; 3)
2-S	95 ± 1% (100 μM; 3)	96 ± 1% (100 μM; 3)	78 ± 1% (100 μM; 4)	92 ± 0% (100 μM; 4)
3	90 ± 2% (100 μM; 3)	96 ± 1% (100 μM; 4)	56 ± 3% (100 μM; 3)	80 ± 2% (100 μM; 3)

^aFor each compound, percent block of pH-dependent M2 current at listed concentrations (± SEM). Parentheses show number of replicates.

inhibition percentage of the A/M2 current observed after 2 and 5 min of incubation with 100 μM compound. The electrophysiology experiments against M2_{Udorn/72} showed that 2-R and 2-S block the M2 channel equally to amantadine (about 90%) at a concentration of 100 μM. In addition, we also tested these aminoadamantane analogues in inhibiting another amantadine-sensitive M2 channel, M2_{WSN/33-N31S}, which contains the V28I mutation in M2TM sequence, with an electrophysiology assay. Again, no significant difference in channel blockage after 5 min was found among 2-R, 2-S, and 3. As discussed previously,²⁸ these measurements at 2 or 5 min are made prior to the establishment of equilibrium due to very slow on and off rates

Table 3. Binding Constant, Free Energy, Enthalpy, and Entropy of Binding Derived from ITC Measurements for M2TM_{Udorn/72}

ligand ^a	K_d^b	$\Delta G^{c,d}$	$\Delta H^{c,e}$	$-T\Delta S^{c,f}$
1	2.17 ± 0.52	-7.77 ± 0.14	-6.66 ± 0.50	-1.11 ± 0.52
2	0.51 ± 0.26	-8.64 ± 0.30	-7.60 ± 0.28	-1.04 ± 0.41
2-R ^g	0.32 ± 0.16	-8.97 ± 0.26	-7.54 ± 0.34	-1.42 ± 0.43
2-S ^g	0.34 ± 0.12	-8.88 ± 0.21	-7.73 ± 0.28	-1.15 ± 0.35
3	0.13 ± 0.12	-9.30 ± 0.43	-4.19 ± 0.28	-5.12 ± 0.51

^aSee Scheme 1. ^bBinding constant K_d in μM calculated from measured K_a in M^{-1} by $K_d = 1/K_a \times 10^{-6}$ and error in K_d in μM determined by $K_{d,\text{error}} = (K_{a,\text{error}}/K_a^2) \times 10^{-6}$ (ITC measurements were performed in triplicate for each ligand to calculate means and standard deviations). ^cIn kcal mol^{-1} .

^dFree energy of binding computed from K_d by $\Delta G = -RT \ln(K_d^{\text{ref}}/K_d)$ with $K_d^{\text{ref}} = 1 \text{ M}$ and $T = 300 \text{ K}$ and error in ΔG determined according to

$\Delta G_{\text{error}} = \sqrt{\left(\frac{RTK_{d,\text{error}}}{K_d}\right)^2}$ with $T = 300 \text{ K}$. ^eEnthalpy of binding and error in the enthalpy of binding calculated from measured binding enthalpy and

measured error by $\Delta H = \Delta H_{\text{measured}} (T/T_{\text{measured}})$ with $T = 300 \text{ K}$ and the temperature at which the ITC measurements were performed $T_{\text{measured}} =$

293.15 K. ^fEntropy of binding calculated by $\Delta S = (-\Delta G + \Delta H)/T$ and error in ΔS computed by the equation $\Delta S_{\text{error}} = \sqrt{\Delta G_{\text{error}}^2 + \Delta H_{\text{error}}^2}$.

^gThe purity of each enantiomer used was 90% for 2-R and 95% for 2-S; the enantiomeric excess (*ee*) of both 2-R and 2-S is 99% (Mosher's method); the purity of compound 3 used was >99%.

for entry of the drugs into the constricted M2 channel and the problems of maintaining cells at low pH for extended periods.

Table 3 includes thermodynamic parameters of binding against M2TM_{Udorn/72}. Binding affinities were determined by ITC²⁹ for M2TM-ligand systems in dodecylphosphocholine (DPC) micelles at pH 8, where M2TM fragments form stable tetramers.³⁰ ITC measurements yield the enthalpy of binding (ΔH) as well as the dissociation constant (K_d). From K_d , the binding free energy (ΔG) is calculated (Table 3). The estimation of the binding entropy is based on the difference between ΔG and ΔH . Binding constants of 1, 2-R, 2-S, and racemate 2 were measured in a previous work¹³ and were included in Table 1. The enantiomers 2-R and 2-S may have a different enthalpy of binding against M2TM protein since the two complexes formed are diastereomers.³¹ As depicted in Table 3, enantiomers 2-R and 2-S have the same K_d values against M2TM_{Udorn/72} ($K_d = 0.34$ and $0.32 \mu\text{M}$ respectively). These values are close to the $K_d = 0.51 \mu\text{M}$ of the racemic 2,¹³ considering the errors of the measurements and that the commercially available enantiomers have a lower chemical purity compared to racemic 2 (see Table 3, note g). An effect from the impurities on the ITC results of 2-R and 2-S cannot be excluded. However, we do not expect large changes in the measured K_d values for 2-R and 2-S, given also the very similar/identical affinity results of the two enantiomers from TEVC and antiviral assays. Compound 3, having two methyl groups instead of one methyl group in 2, has the smallest K_d ($0.13 \mu\text{M}$), i.e., the highest binding affinity of all studied amino-adamantane compounds, suggesting that polar and lipophilic characteristics are well balanced in its structure. All three compounds (2-R, 2-S, and 3) were more potent than amantadine (1).

We then analyzed the binding properties of 2-R and 2-S by performing alchemical free energy calculations^{13,32} using the Bennett acceptance ratio (BAR) method.^{33,34} The calculations for the alchemical transformations $3 \rightarrow 2\text{-R}$, $3 \rightarrow 2\text{-S}$ were run, and the results of the FEP/MD predictions were compared with binding affinities measured by ITC (Table 4). The computational predictions were set by employing a protocol successfully benchmarked by our group in order to match experimental conditions as closely as possible.¹³ M2TM_{Udorn/72} structure was simulated in the closed conformation found at high pH and after assigning a neutral form for all H37. M2TM_{Udorn/72}-ligand complexes were simulated in DMPC bilayers, which represent an optimal membrane mimetic system

Table 4. Relative Binding Free Energies for Pairs of Compounds Computed with the BAR Method for M2TM Embedded in a DMPC Bilayer or Derived from Experimental Binding Affinity Data in Table 3

transformation	M2TM _{Udorn/72}	
	$\Delta\Delta G_{\text{FEP}}^{a,b}$	$\Delta\Delta G_{\text{exp}}^{a,c}$
3 \rightarrow 2-R	0.62 ± 0.14	0.33 ± 0.50
3 \rightarrow 2-S	0.68 ± 0.15	0.42 ± 0.48

^aIn kcal mol^{-1} . ^bPropagation error calculated according to the bootstrap method.³² ^cDifference in binding free energy calculated from experimentally determined K_d values by $\Delta\Delta G = -RT \ln(K_d^A/K_d^B)$ with $T = 300 \text{ K}$ and error calculated from individual experimental errors by $\text{error}_{\Delta\Delta G} = \sqrt{(\text{error}_{\Delta G,A})^2 + (\text{error}_{\Delta G,B})^2}$.

for retaining proper M2TM structure compared to other glycerophospholipids.³⁵ We used an experimental structure (PDB ID 2KQT^{3,7}) determined at pH 7.5 in DMPC bilayers; the restraints of the apo-M2TM structure were originally measured by the Cross group.⁵ This M2TM_{Udorn/72} structure is already adapted to these environmental conditions, and thus only a short equilibration phase is required. The experimental relative binding free energy values ($\Delta\Delta G_{\text{exp}}$) for the transformations $3 \rightarrow 2\text{-R}$ and $3 \rightarrow 2\text{-S}$ were 0.33 and 0.42 kcal mol^{-1} (Table 4), favoring 3. The experimental relative binding free energy values were quite close to calculated values ($\Delta\Delta G_{\text{FEP}}$) of 0.62 and 0.68 kcal mol^{-1} , respectively (the accuracy of the calculations method is $\sim 1 \text{ kcal mol}^{-1}$).^{33,34} The calculations also predict the experimental finding by ITC that 2-R and 2-S have the same binding affinity against M2TM_{Udorn/72} (Table 3), which is consistent with the results from aforementioned antiviral and electrophysiology assays performed using full M2 protein (Tables 1 and 2). Thus, using the functional core of M2 (transmembrane domain) for binding studies is appropriate.

The simulated complexes of M2TM_{Udorn/72} with 2-R, 2-S, and 3 showed that the height of the ligands inside the pore differed only slightly, that is less than 0.3 Å toward the N-terminus relatively to 1 (Table S1), and the orientation of 2-R and 2-S in the pore differs only slightly, in accordance to their induced similar ssNMR chemical shifts for S31 and G34 when complexed with M2.²³ The center of mass between the four V27 and the adamantyl ring of the ligand (V27-Ad) varies between 4.0 and 4.5 Å on average (Table S1). For 2-R and 2-S the average tilt angle was measured $\sim 14^\circ$, in accordance to experimental ssNMR values,⁹ and for 3 the average tilt angle

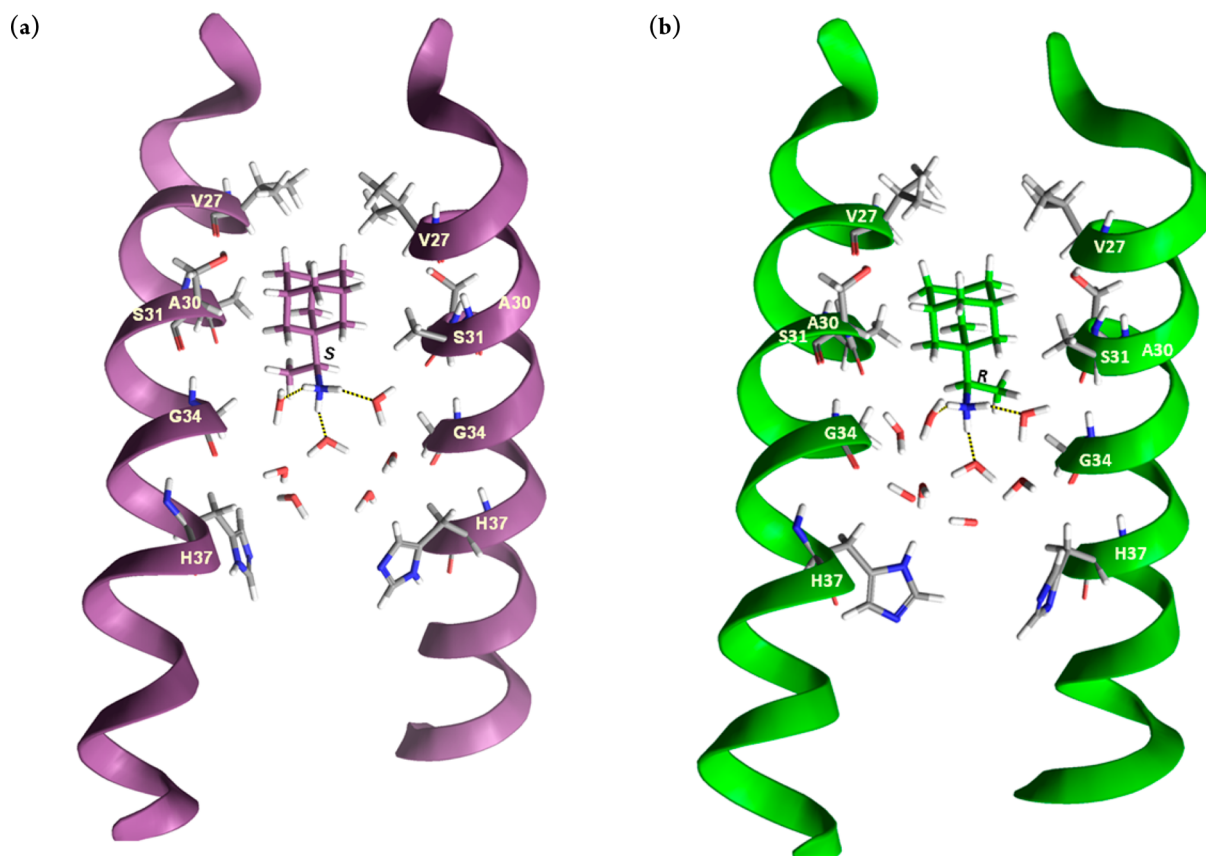


Figure 1. Representative replicas from the simulation (a) of 2-S and (b) of 2-R bound to M2TM_{Udom/72}. Seven and eight waters are shown between the ligand and H37 residues, respectively. Three hydrogen bonds between the ammonium group of the ligand and three water molecules are shown. Hydrogen bonding together with van der Waals interactions of the adamantane core with V27 and A30 stabilize the ligand inside the pore with its ammonium group oriented toward the C-terminus.

was measured $\sim 5^\circ$. The angle between the pore axis or the normal of the membrane and C–N bond vector was $\sim 11^\circ$ for **1** and close to 50° for 2-R, 2-S, and **3**. These angle values suggest that the ammonium group of all aminoadamantane compounds is oriented toward the C-terminus, in consistency with previous experimental findings^{6,7,9} and MD simulations^{13,32,36} (Table S1). The distance between the adamantyl ring and the center of mass between the four A30 (Ad-A30) for **1**–**3** was measured ~ 1 Å, and the distance CH₃(lig.)–G34Ca for 2-R, 2-S, and **3** was 2.9, 3.2 and 2 Å respectively, close to the REDOR measurements for 2-R, 2-S.²³ The adamantyl ring was embraced by the V27 and A30 side chains, which defined the binding site of the ligands. Compounds **1**, 2-R, 2-S, and **3** form hydrogen bonds (average of three hydrogen bonds) through the ammonium group with neighboring water molecules which are positioned between the ligand and H37 residues. In the area located below the adamantyl ring toward the N-terminus no waters were found,^{13,22,32,36} which is consistent with the proton blocking effect of **1** and other aminoadamantane derivatives.^{1,12,28} A snapshot from the simulation of ligands 2-R and 2-S is depicted in Figure 1. The CHCH₃ fragment, which includes the chiral carbon of 2-R, 2-S, fits into the cleft between G34 and A30, with the later being a chiral amino acid that can differentiate binding interactions between the two enantiomers. However, the distance CH₃(lig.)–A30CH₃, which is similar for both enantiomers (3.9 ± 0.3 and 3.5 ± 0.3 Å), suggests no difference in their van der Waals interactions. The measures suggest that hydrogen bonding interactions for 2-R, 2-S and

geometric measures, which reflect van der Waals contacts, were found to be similar for both enantiomers (see Table S1). These measures are consistent with the calculated relative binding affinities, which are in accordance to the ITC data and functional assays described previously.

Our results demonstrated no difference in the binding affinity between the two enantiomers, whereas the recent ssNMR study²³ concluded that 2-R is a stronger binder than 2-S. According to our best understanding, the authors in ref 23 made the following important observations in the ssNMR spectra regarding the relative binding of 2-R and 2-S. In the presence of 2-R or 2-S a new resonance (i.e., one that was not recorded in the spectrum of the apo-M2 protein) was observed for S31 at 120/64 ppm in the ¹⁵N/¹³Ca spectrum, which had strong intensity for both enantiomers. The G34 resonance had also a stronger intensity for both enantiomers compared to the spectrum of the apo-M2. The S31 and G34 resonance frequencies were similar for both 2-R and 2-S. These results provided an experimental evidence that both enantiomers bind strongly and the binding site and orientation of the drug in the pore are similar for the two enantiomers as mentioned in ref 23. However, the authors reported the appearance of an additional resonance of medium intensity for the 2-S enantiomer at 115/63 ppm close to the frequencies of the S31 resonance of the unbound M2 state at $\sim 114/62$ ppm and suggested a weaker binding of 2-S. Possibly the results published by Wright et al.²³ are not in full agreement with those reported here as a

consequent of the different methodology they applied, i.e., ssNMR spectroscopy.

In conclusion, our results showed that rimantadine enantiomers (2-*R* and 2-*S*) bind equally well to the M2 proton channel and have equal channel blockage and antiviral activity against amantadine-sensitive M2 channels. This conclusion was supported by a consortium of techniques including antiviral assays, electrophysiology ITC, and FEP/MD. Our nonclinical results support the previous use of rimantadine as a racemic mixture drug for the prevention and treatment of influenza virus infection. Further correlation of these results with the pharmacokinetic and pharmacodynamic properties for each enantiomer in humans would confirm these findings. For example, although there are no significant differences in the concentration–time profiles and disposition of 2-*R* and 2-*S* and of the 3-hydroxyrimantadine metabolites,³⁷ large stereospecific differences in the disposition of their 4-hydroxyrimantadine metabolites are observed.³⁸ However, it should be noted that 3- and 4-hydroxy metabolites, both of which are found in rimantadine-treated patients, showed only modest inhibitory activity against influenza A virus, i.e., they are modestly active metabolites.³⁹

■ ASSOCIATED CONTENT

Supporting Information

The Supporting Information is available free of charge on the ACS Publications website at DOI: 10.1021/acsmchemlett.6b00311.

Supplementary material including computational and experimental protocols, as well as one table with measures from simulations, and references (PDF)

■ AUTHOR INFORMATION

Corresponding Authors

*Tel: (+301) 210-7274834. Fax: (+301) 210 727 4747. E-mail: ankol@pharm.uoa.gr.

*Tel: 520-626-1366. Fax: 520-626-0749. E-mail: junwang@pharmacy.arizona.edu.

ORCID

Jun Wang: 0000-0002-4845-4621

Antonios Kolocouris: 0000-0001-6110-1903

Present Address

(A.D.) Pharmaceutical and Medicinal Chemistry, Institute of Pharmacy and Food Chemistry, Julius-Maximilians-Universität Würzburg, Am Hubland, 97074 Würzburg, Germany.

Author Contributions

A.D. and C.T. contributed equally. This research includes part of the Master thesis of A.D. and part of the Ph.D. work of C.T. A.K. designed this research project. A.D. and C.T. both did FEP calculations and ligand synthesis. C.M. and Y.H. in J.W. group did the detailed EP experiments against the A/Udorn/72 and A/WSN/33-M2-N31S M2 and CPE assay testing against A/Udorn/72 virus. K.F. in G.G. group did the ITC measurements. A.H. in M.S. group performed CPE inhibitory assays with A/WSN/33-M2-N31S virus. A.K. wrote the manuscript, and J.W., M.S., A.H., and A.D. revised it.

Notes

The authors declare no competing financial interest.

■ ACKNOWLEDGMENTS

We are grateful to Chiesi Hellas for supporting this research and the Ph.D. work of C.T.; J.W. thanks the support from NIH AI119187 and the PhRMA Foundation 2015 Research Starter Grant in Pharmacology and Toxicology; A.H. and M.S. thank Andreas Sauerbrei for continuous kind support.

■ ABBREVIATIONS

M2TM, residues 22–46 of M2 protein comprising the transmembrane domain; CPE assay, cytopathic effect assay; ssNMR spectroscopy, solid state Nuclear Magnetic Resonance spectroscopy; DMPC, 1,2-dimyristoyl-*sn*-glycero-3-phosphocholine; FEP, free energy perturbation; MD, molecular dynamics; REDOR experiment, rotational echo double resonance experiment; ITC, isothermal titration calorimetry; EP, electrophysiology; TEVC assay, two-electrode voltage clamp assay; BAR, Bennett acceptance ratio; PDB, protein data bank; IC₅₀, 50% inhibitory concentration; *ee*, enantiomeric excess

■ REFERENCES

- (1) Wang, C.; Takeuchi, K.; Pinto, L. H.; Lamb, R. A. Ion channel activity of influenza A virus M2 protein: characterization of the amantadine block. *J. Virol.* **1993**, *67*, 5585–94.
- (2) Chizhnikov, I. V.; Geraghty, F. M.; Ogden, D. C.; Hayhurst, A.; Antoniou, M.; Hay, A. J. Selective proton permeability and pH regulation of the influenza virus M2 channel expressed in mouse erythrocyte cells. *J. Physiol.* **1996**, *494*, 329–36.
- (3) Hayden, F. G. Clinical applications of antiviral agents for chemoprophylaxis and therapy of respiratory viral infections. *Antiviral Res.* **1985**, *5* (Suppl 1), 229–39.
- (4) Wang, J.; Qiu, J. X.; Soto, C.; DeGrado, W. F. Structural and dynamic mechanisms for the function and inhibition of the M2 proton channel from influenza A virus. *Curr. Opin. Struct. Biol.* **2011**, *21*, 68–80.
- (5) Hu, J.; Asbury, T.; Achuthan, S.; Li, C.; Bertram, R.; Quine, J. R.; Fu, R.; Cross, T. A. Backbone structure of the amantadine-blocked trans-membrane domain M2 proton channel from Influenza A virus. *Biophys. J.* **2007**, *92*, 4335–43.
- (6) Stouffer, A. L.; Acharya, R.; Salom, D.; Levine, A. S.; Di Costanzo, L.; Soto, C. S.; Tereshko, V.; Nanda, V.; Stayrook, S.; DeGrado, W. F. Structural basis for the function and inhibition of an influenza virus proton channel. *Nature* **2008**, *451*, 596–9.
- (7) Cady, S. D.; Schmidt-Rohr, K.; Wang, J.; Soto, C. S.; DeGrado, W. F.; Hong, M. Structure of the amantadine binding site of influenza M2 proton channels in lipid bilayers. *Nature* **2010**, *463*, 689–92.
- (8) Pielak, R. M.; Oxenoid, K.; Chou, J. J. Structural investigation of rimantadine inhibition of the AM2-BM2 chimera channel of influenza viruses. *Structure* **2011**, *19*, 1655–1663.
- (9) Cady, S. D.; Wang, J.; Wu, Y.; DeGrado, W. F.; Hong, M. Specific binding of adamantane drugs and direction of their polar amines in the pore of the influenza M2 transmembrane domain in lipid bilayers and dodecylphosphocholine micelles determined by NMR spectroscopy. *J. Am. Chem. Soc.* **2011**, *133*, 4274–84.
- (10) Ma, C.; Polishchuk, A. L.; Ohigashi, Y.; Stouffer, A. L.; Schön, A.; Magavern, E.; Jing, X.; Lear, J. D.; Freire, E.; Lamb, R. A.; DeGrado, W. F.; Pinto, L. H. Identification of the functional core of the influenza A virus A/M2 proton-selective ion channel. *Proc. Natl. Acad. Sci. U. S. A.* **2009**, *106*, 12283–12288.
- (11) Kolocouris, N.; Foscolos, G. B.; Kolocouris, A.; Marakos, P.; Pouli, N.; Fytas, G.; Ikeda, S.; De Clercq, E. Synthesis and antiviral activity evaluation of some aminoadamantane derivatives. *J. Med. Chem.* **1994**, *37*, 2896–2902.
- (12) Kolocouris, A.; Tzitzoglaki, C.; Johnson, F. B.; Zell, R.; Wright, A. K.; Cross, T. A.; Tietjen, I.; Fedida, D.; Busath, D. D.

Aminoadamantanes with persistent in vitro efficacy against H1N1 (2009) influenza A. *J. Med. Chem.* **2014**, *57*, 4629–39.

(13) Ioannidis, H.; Drakopoulos, A.; Tzitzoglaki, C.; Homeyer, N.; Kolarov, F.; Gkeka, P.; Freudenberger, K.; Liolios, C.; Gauglitz, G.; Cournia, Z.; Gohlke, H.; Kolocouris, A. Alchemical free energy calculations and isothermal titration calorimetry measurements of aminoadamantanes bound to the closed state of influenza A/M2TM. *J. Chem. Inf. Model.* **2016**, *56*, 862–876.

(14) Andreas, L. B.; Barnes, A. B.; Corzilius, B.; Chou, J. J.; Miller, E. A.; Caporini, M.; Rosay, M.; Griffin, R. G. Dynamic nuclear polarization study of inhibitor binding to the M2(18–60) proton transporter from influenza A. *Biochemistry* **2013**, *52*, 2774–82.

(15) Yi, M.; Cross, T. A.; Zhou, H.-X. Conformational heterogeneity of the M2 proton channel and a structural model for channel activation. *Proc. Natl. Acad. Sci. U. S. A.* **2009**, *106*, 13311–13316.

(16) Luo, W.; Hong, M. Conformational changes of an ion channel detected through water-protein interactions using solid-state NMR spectroscopy. *J. Am. Chem. Soc.* **2010**, *132*, 2378–84.

(17) Intharathep, P.; Laothongpaysan, C.; Rungrotmongkol, T.; Loisuangsinsin, A.; Malaisree, M.; Decha, P.; Aruksakunwong, O.; Chuenpennit, K.; Kaiyawet, N.; Sompornpisut, P.; Pianwanit, S.; Hannongbua, S. How amantadine and rimantadine inhibit proton transport in the M2 protein channel. *J. Mol. Graphics Modell.* **2008**, *27*, 342–348.

(18) Khurana, E.; Devane, R. H.; Dal Peraro, M.; Klein, M. L. Computational study of drug binding to the membrane-bound tetrameric M2 peptide bundle from influenza A virus. *Biochim. Biophys. Acta, Biomembr.* **2011**, *1808*, 530–537.

(19) Leonov, H.; Astrahan, P.; Krugliak, M.; Arkin, I. T. How Do aminoadamantanes block the influenza M2 channel, and how does resistance develop? *J. Am. Chem. Soc.* **2011**, *133*, 9903–9911.

(20) Gianti, E.; Carnevale, V.; DeGrado, W. F.; Klein, M. L.; Fiorin, G. Hydrogen-bonded water molecules in the M2 channel of the influenza A virus guide the binding preferences of ammonium-based inhibitors. *J. Phys. Chem. B* **2015**, *119*, 1173–83.

(21) Wang, J.; Ma, C.; Fiorin, G.; Carnevale, V.; Wang, T.; Hu, F.; Lamb, R. A.; Pinto, L. H.; Hong, M.; Klein, M. L.; DeGrado, W. F. Molecular dynamics simulation directed rational design of inhibitors targeting drug-resistant mutants of influenza A virus M2. *J. Am. Chem. Soc.* **2011**, *133*, 12834–12841.

(22) Gleed, M. L.; Ioannidis, H.; Kolocouris, A.; Busath, D. D. Resistance-mutation (N31) effects on drug orientation and channel hydration in amantadine-bound influenza A M2. *J. Phys. Chem. B* **2015**, *119*, 11548–59.

(23) Wright, A. K.; Batsomboon, P.; Dai, J.; Hung, I.; Zhou, H.-X.; Dudley, G. B.; Cross, T. A. Differential binding of rimantadine enantiomers to influenza A M2 proton channel. *J. Am. Chem. Soc.* **2016**, *138*, 1506–1509.

(24) Aldrich, P. E.; Hermann, E. C.; Meier, W. E.; Paulshock, M.; Prichard, W. W.; Snyder, J. A.; Watts, J. C. Antiviral agents. 2. Structure-activity relationships of compounds related to 1-adamantanamine. *J. Med. Chem.* **1971**, *14*, 535–543.

(25) Torres, E.; Duque, M. D.; Vanderlinden, E.; Ma, C.; Pinto, L. H.; Camps, P.; Froeyen, M.; Vázquez, S.; Naesens, L. Role of the viral hemagglutinin in the anti-influenza virus activity of newly synthesized polycyclic amine compounds. *Antiviral Res.* **2013**, *99*, 281.

(26) Schmidtke, M.; Schnittler, U.; Jahn, B.; Dahse, H.-M.; Stelzner, A. A rapid assay for evaluation of antiviral activity against coxsackie virus B3, influenza virus A, and herpes simplex virus type 1. *J. Virol. Methods* **2001**, *95*, 133–143.

(27) Schade, D.; Kotthaus, J.; Riebling, L.; Kotthaus, J.; Müller-Fielitz, H.; Raasch, W.; Hoffmann, A.; Schmidtke, M.; Clement, B. Zanamivir amidoxime- and N-hydroxyguanidine-based prodrug approaches to tackle poor oral bioavailability. *J. Pharm. Sci.* **2015**, *104*, 3208–3219.

(28) Balannik, V.; Wang, J.; Ohigashi, Y.; Jing, X.; Magavern, E.; Lamb, R. A.; DeGrado, W. F.; Pinto, L. H. Design and pharmacological characterization of inhibitors of amantadine-resistant mutants of the M2 ion channel of influenza A virus. *Biochemistry* **2009**, *48*, 11872.

(29) Chaires, J. B. Calorimetry and thermodynamics in drug design. *Annu. Rev. Biophys.* **2008**, *37*, 135–151.

(30) Salom, D.; Hill, B. R.; Lear, J. D.; DeGrado, W. F. pH-Dependent tetramerization and amantadine binding of the transmembrane helix of M2 from the influenza A virus. *Biochemistry* **2000**, *39*, 14160–14170.

(31) Fokkens, J.; Klebe, G. A simple protocol to estimate differences in protein binding affinity for enantiomers without prior resolution of racemates. *Angew. Chem., Int. Ed.* **2006**, *45*, 985–989.

(32) Gkeka, P.; Eleftheratos, S.; Kolocouris, A.; Cournia, Z. Free energy calculations reveal the origin of binding preference for aminoadamantane blockers of influenza A/M2TM pore. *J. Chem. Theory Comput.* **2013**, *9*, 1272–1281.

(33) Bennett, C. H. Efficient estimation of free energy differences from Monte Carlo data. *J. Comput. Phys.* **1976**, *22*, 245–268.

(34) Chipot, C.; Pohorille, A., Eds. *Free Energy Calculations. Theory and Applications in Chemistry and Biology*; Springer Verlag: Berlin, NY, 2007.

(35) Cady, S.; Wang, T.; Hong, M. Membrane-dependent effects of a cytoplasmic helix on the structure and drug binding of the influenza virus M2 Protein. *J. Am. Chem. Soc.* **2011**, *133*, 11572–11579.

(36) Wang, J.; Ma, C.; Fiorin, G.; Carnevale, V.; Wang, T.; Hu, F.; Lamb, R. A.; Pinto, L. H.; Hong, M.; Klein, M. L.; DeGrado, W. F. Molecular dynamics simulation directed rational design of inhibitors targeting drug-resistant mutants of influenza A virus M2. *J. Am. Chem. Soc.* **2011**, *133*, 12834–12841.

(37) Miwa, B. J.; Choma, N.; Brown, S. Y.; Keigher, N.; Garland, W.; Fukuda, E. K. Quantitation of the enantiomers of rimantadine in human plasma and urine by gas chromatography-mass spectrometry. *J. Chromatogr., Biomed. Appl.* **1988**, *431*, 343–352.

(38) Choma, N.; Davis, P. P.; Edorn, R. W.; Fukuda, E. K. Quantitation of the enantiomers of rimantadine and its hydroxylated metabolites in human plasma by gas chromatography/mass spectrometry. *Biomed. Chromatogr.* **1992**, *6*, 12–15.

(39) Manchand, P. S.; Cerutti, R. L.; Martin, J. A.; Hill, C. H.; Merrett, E. K.; Keech, E.; Belshe, R. B.; Connell, E. V.; Sim, I. S. Synthesis and antiviral activity of metabolite of rimantadine. *J. Med. Chem.* **1990**, *33*, 1992–1995.

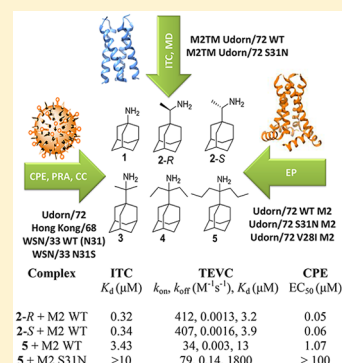
Unraveling the Binding, Proton Blockage, and Inhibition of Influenza M2 WT and S31N by Rimantadine Variants

Antonios Drakopoulos,[†] Christina Tzitzoglaki,[†] Kelly McGuire,[‡] Anja Hoffmann,[§] Athina Konstantinidi,[†] Dimitrios Kolokouris,[†] Chunlong Ma,^{||} Kathrin Freudenberg,[⊥] Johanna Hutterer,[⊥] Günter Gauglitz,[⊥] Jun Wang,^{||} Michaela Schmidtke,[§] David D. Busath,[‡] and Antonios Kolocouris^{*,†,||}[†]Department of Pharmaceutical Chemistry, Faculty of Pharmacy, National and Kapodistrian University of Athens, Panepistimiopolis-Zografou 15771, Greece[‡]Department of Physiology and Developmental Biology, Brigham Young University, Provo, Utah 84602, United States[§]Department of Medicinal Microbiology, Section Experimental Virology, Jena University Hospital, Hans Knoell Str. 2, D-07745 Jena, Germany^{||}Department of Pharmacology and Toxicology, College of Pharmacy, University of Arizona, Tucson, Arizona 85721, United States[⊥]Institut für Physikalische und Theoretische Chemie, Eberhard-Karls-Universität Tübingen, 72074 Tübingen, Germany

Supporting Information

ABSTRACT: Recently, the binding kinetics of a ligand–target interaction, such as the residence time of a small molecule on its protein target, are seen as increasingly important for drug efficacy. Here, we investigate these concepts to explain binding and proton blockage of rimantadine variants bearing progressively larger alkyl groups to influenza A virus M2 wild type (WT) and M2 S31N protein proton channel. We showed that resistance of M2 S31N to rimantadine analogues compared to M2 WT resulted from their higher k_{off} rates compared to the k_{on} rates according to electrophysiology (EP) measurements. This is due to the fact that, in M2 S31N, the loss of the V27 pocket for the adamantyl cage resulted in low residence time inside the M2 pore. Both rimantadine enantiomers have similar channel blockage and binding k_{on} and k_{off} against M2 WT. To compare the potency between the rimantadine variants against M2, we applied approaches using different mimicry of M2, i.e., isothermal titration calorimetry and molecular dynamics simulation, EP, and antiviral assays. It was also shown that a small change in an amino acid at site 28 of M2 WT, which does not line the pore, seriously affects M2 WT blockage kinetics.

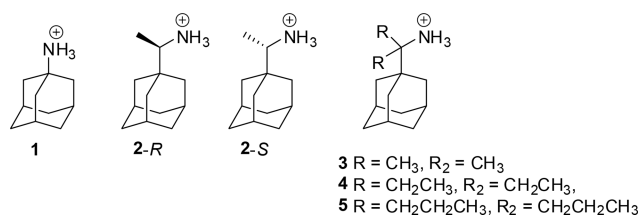
KEYWORDS: Influenza M2, S31N mutation, rimantadine, rimantadine enantiomers, isothermal titration calorimetry, electrophysiology, binding kinetics, synthesis, antiviral assay, molecular dynamic simulations



Novel approaches are necessary in early drug discovery for optimal drug design and improved therapy. Recently, the kinetics of a ligand–target interaction, such as the residence time of a small molecule on its protein target, are seen as increasingly important for *in vivo* efficacy and safety.¹

The antiviral agents amantadine (**1**) and rimantadine (**2**) (Scheme 1) are well-established to be blockers of proton transport by the influenza A virus (IAV).^{2,3} The primary binding site of **1** and **2** is the transmembrane domain lumen (TM, amino

Scheme 1. Structures of Aminoadamantane Derivatives 1–5



acids 22–46) in the four-helix bundle of tetrameric M2, which forms the proton transport path.² Since 2008, high-resolution structures have become available for complexes of M2TM wild type (WT) with **1** or **2** (Figure S1).^{4–9}

Compounds **1** and **2** are effective prophylactics and therapeutics against IAVs, provided they contain the M2TM WT such as A/Udorn/72 H3N2 (Udorn) and A/Hong Kong/68 H3N2 (HK), but not those containing M2 S31N such as A/WSN/33 H1N1 (WSN) (Figure S2). Since 2005, the amantadine (**1**)-insensitive Ser-to-Asn mutation at position 31 in M2 (S31N) has become globally prevalent, abrogating the clinical usefulness of **1**.¹⁰

Compound **2** is ranked among the best binders to M2TM WT^{11,12} and most potent anti-IAV agents among the aminoadamantane derivatives.^{13,14} Thus, the synthesis of symmetrical

Received: November 3, 2017

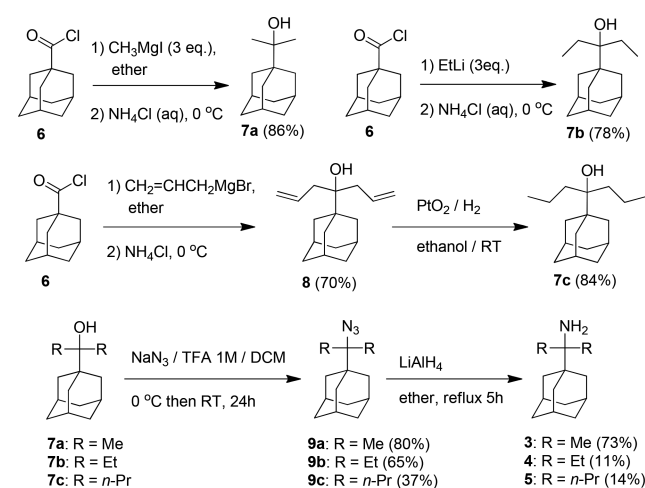
Accepted: January 29, 2018

Published: January 29, 2018

analogues of **2** with the addition of two methyl (**3**), ethyl (**4**), and *n*-propyl (**5**) groups on the carbon bridge was accomplished (Scheme 1) aiming at filling progressively from **3** to **5** the extra space between the ligand and the walls in M2 WT or M2 S31N with a few alkyl groups. Binding affinities of **1**, **2**, **2-R**, **2-S**, and **3–5** were measured by ITC against the M2TM WT and its S31N variant in their closed form at pH 8. Furthermore, we measured the antiviral activity of the rimantadine analogues against IAV strains and the blocking effect of the compounds against full length Udorn M2, Udorn M2 S31N, and Udorn M2 V281 using electrophysiology (EP), and the kinetics of binding were compared. Molecular dynamics (MD) simulations of ligand binding to M2TM WT and its S31N variant in their closed form were performed for investigation of the binding mode interactions.

For the synthesis of primary *tert*-alkyl amines **3–5**, the raw *tert*-alkyl alcohols **7a–c** were prepared according to Scheme 2 from

Scheme 2. Synthetic Scheme for the Preparation of Compounds **3–5**



the reaction between 1-adamantanecarbonyl chloride **6** and an organometallic reagent (see Supporting Information). It was reported that the reaction of 1-adamantanecarbonyl chloride with ethyl magnesium bromide and titanium tetrakisopropoxide afforded **4** in 52% yield.¹⁵ We tested twice this procedure with 1-

adamantanecarbonitrile and methylmagnesium bromide yielding in our hands **3** with only 10% yield, which is lower than the ~50% yield starting from **6** or 1-adamantanecarboxylic acid (Scheme 2).

Table 1 includes thermodynamic parameters of binding against M2TM WT and M2TM S31N. Binding affinities were determined by ITC for M2TM–ligand systems in dodecylphosphocholine (DPC) micelles at pH 8, where M2TM fragments form stable tetramers (see also Supporting Information).¹⁶ Compound **1** has a K_d of $2.17\ \mu\text{M}$. As depicted in Table 1, enantiomers **2-R** and **2-S** have the same K_d values¹⁷ against M2TM WT ($K_d = 0.34$ and $0.32\ \mu\text{M}$, respectively). Compound **3**, having two methyl groups instead of one methyl group in **2**, has the smallest $K_d = 0.13\ \mu\text{M}$, i.e., the highest binding affinity of all studied aminoadamantane compounds, suggesting that polar and lipophilic characteristics are well balanced in its structure. The diethyl derivative **4** and dipropyl derivative **5** exhibit lower binding affinities against M2TM WT ($K_d = 4.59$ and $3.43\ \mu\text{M}$, respectively). A balance between enthalpy and entropy determines the free energy of binding as shown in Table 1. The entropy presumably changes significantly from **1**, **2** to **3**, **4** on binding because the ordered clathrate water surrounding the ligand is dispersed as the ligand enters the water-poor channel cavity. This is more prominent for **3** and **4**, as expected due to their larger hydrophobic surfaces. Presumably, it would have gone up even more for **5**, but this clathrate effect was probably countered by a reduced ligand entropy in the channel due to restricted rotation inside the receptor binding area. Compounds **1–3** did not bind efficiently to M2TM S31N according to isothermal titration calorimetry (ITC) and previous surface plasmon resonance measurements for **1**,¹⁸ while **5**, with a larger adduct connected to adamantane, binds weakly to M2TM S31N compared to M2TM WT according to ITC.

The cytopathic effect (CPE) inhibition assay was used¹⁹ to compare the antiviral potency of **1–5** against HK, Udorn, WSN, and WSN M2 N31S (generated by reverse genetics from WSN) in MDCK cells (Table 2). The amino acid sequences of M2 WT in Udorn and HK are identical, not just in the TM region but in the full length protein. There was no potency against the amantadine-resistant WSN with the compound concentrations used. All compounds showed low micromolar activity against Udorn, HK, and WSN M2 N31S with **3** being the most potent agent exhibiting submicromolar potency. Inhibition of repli-

Table 1. Binding Constant, Free Energy, Enthalpy, and Entropy of Binding at 300 K Derived from ITC Measurements for M2TM WT (from Udorn, Upper Table) and the M2TM S31N (Lower Table)

ligand ^a	K_d^b	ΔG^c	ΔH^d	$-T\Delta S^e$
M2TM WT				
1	2.17 ± 0.52	-7.77 ± 0.14	-6.66 ± 0.50	-1.11 ± 0.52
2	0.51 ± 0.26	-8.64 ± 0.30	-7.60 ± 0.28	-1.04 ± 0.41
2-R	0.32 ± 0.16	-8.97 ± 0.26	-7.54 ± 0.34	-1.42 ± 0.43
2-S	0.34 ± 0.12	-8.88 ± 0.21	-7.73 ± 0.28	-1.15 ± 0.35
3	0.13 ± 0.12	-9.30 ± 0.43	-4.19 ± 0.28	-5.12 ± 0.51
4	4.59 ± 2.21	-7.33 ± 0.28	-3.29 ± 0.62	-4.03 ± 0.68
5	3.43 ± 1.05	-7.50 ± 0.18	-6.23 ± 0.45	-1.27 ± 0.48
M2TM S31N				
1–3	<i>f</i>	<i>f</i>	<i>f</i>	<i>f</i>
5	>10	<i>f</i>	<i>f</i>	<i>f</i>

^aSee Scheme 1. ^bBinding constant K_d in μM . ^cFree energy of binding in kcal mol^{-1} . ^dBinding enthalpy in kcal mol^{-1} . ^eEntropy of binding in kcal mol^{-1} . ^fValues could not be determined reliably due to the limitations of the methods in the area of very weak binding (see also SI for definition of quantities).

Table 2. Cytotoxicity (CC_{50}) and Antiviral Activity (EC_{50}) of Compounds 1–5 against IAVs HK, Udorn, WSN, and WSN M2 N31S in Madin–Darby Canine Kidney Cells

ligand	EC_{50} (μM) ^a				CC_{50} (μM) ^a
	HK		Udorn		
	WSN		WSN		
	M2 (V28; S31)	M2 (V28; S31)	M2 (I28; N31S)	M2 (I28; N31)	
1	ND ^c	0.78 ± 0.44	0.48 ± 0.05	>100	>100
2	0.05 ± 0.04	0.09 ± 0.03	0.04 ± 0.02	>100	>100
2-R	ND ^c	0.05 ± 0.01	0.04 ± 0.01	>100	>100
2-S	ND ^c	0.06 ± 0.02	0.02 ± 0.01	>100	>100
3	0.012 ± 0.003	0.01 ± 0.001	0.03 ± 0.02	>100	>100
4	0.46 ± 0.25	0.41 ± 0.23	1.01 ± 0.13	>100	>100
5	0.45 ± 0.34	1.07 ± 0.31 ^b	1.06 ± 0.23	>100	57.3 ± 11.3
Oseltamivir	0.002 ± 0.001	0.001	0.02 ± 0.01	0.03 ± 0.01	>100

^aMean and standard deviations of the 50% inhibitory concentration (EC_{50}) and the 50% cytotoxic concentration (CC_{50}) of at least three independent assays. ^bInhibition of plaque size without reduction of plaque number. ^cND: Not determined.

cation of Udorn was further confirmed with plaque-reduction assay (results not shown). It is of note that **5** only reduced the plaque size but not the number of plaques. The cytotoxicity data (Table 2) showed that **1**–**4** are nontoxic with CC_{50} values >100 μM , but **5** is mildly toxic with $CC_{50} \approx 57 \mu\text{M}$.

The EC_{50} values for **1**–**5** (Table 2) prioritize the same derivative for M2 WT virus inhibition, i.e., **3**, in agreement with the results from the K_d values from ITC experiments based on M2TM WT binding (Table 1). Compound **3** is almost equal in structure with rimantadine (**2**) without having a chiral center. Compound **3** has also a promising selectivity index based on the *in vitro* cytotoxicity data.

The inhibitors were tested with a two-electrode voltage clamp (TEVC) assay using *X. laevis* frog oocytes microinjected with RNA expressing the M2 protein as in previous reports.^{13,17} The blocking effect of the aminoadamantane derivatives against M2 was investigated with EP experiments using Udorn M2 and Udorn M2 S31N. Because WSN has the V28I substitution in M2, Udorn M2 V28I was generated and studied in parallel to examine whether small changes in WSN in the side chains of amino acids that do not line the pore (Figure S2) affect aminoadamantane blocking properties. The blocking effect of the inhibitors was expressed as the inhibition percentage of the M2 current observed after 2, 5, and/or 10 min of incubation with 100 μM compound (Tables 3 and S1).

After 5 min, **3** and **4** block Udorn M2 and Udorn M2 V28I as well as **1** (about 90% and 80%, respectively). Generally, after 2 and 5 min, the percentage of current inhibition was progressively increased for **3** and **4**. It is noteworthy that **5** against Udorn M2 exhibited 27% blocking at 2 min, 38% at 5 min, and 61% at 10 min (Table 3). The IC_{50} values of **3** and **4** for Udorn M2 and Udorn M2 V28I were reduced from 2 to 5 min time points (Tables 3 and S1). These measurements at 2, 5, or 10 min are made prior to the establishment of equilibrium²¹ due to very slow on- and off-rates for entry (see the k_{on} and k_{off} rate values in Tables 3 and 4), especially of the bulky ligands like **5**, together with the difficulty of maintaining cells at low pH for extended periods. Thus, the very slow binding of **5** (Table 3) should not be viewed as inconsistent with the high antiviral potency (submicromolar EC_{50}) against WT (V28; S31) viruses (Table 2), the latter representing much longer exposure times than EP experiments.

In a very recent paper,²⁰ the authors showed that when $K_d(\text{TEVC}) = k_{\text{off}}/k_{\text{on}}$ was smaller than a threshold, an *in vitro* antiviral activity was exhibited. For amantadine (**1**), $k_{\text{off}}/k_{\text{on}} =$

Table 3. Block^a of Inward Currents in Oocytes^b Transfected with Full-Length Udorn M2 by Selected Compounds

ligand	Udorn M2 ^{a,b}				
	% block (2 min)	% block (5 min)	% block (10 min)	IC_{50} (2 min) (μM)	IC_{50} (5 min) (μM)
1	90 ± 2	95 ± 1	ND ^c	12.5	4.7
2	96 ± 1	96 ± 1	ND ^c	10.8	ND ^c
2-R	95 ± 1	96 ± 1	ND ^c	ND ^c	ND ^c
2-S	93 ± 1	95 ± 1	ND ^c	ND ^c	ND ^c
3	90 ± 2	96 ± 1	ND ^c	9.3	4.0
4	78 ± 2	91 ± 1	ND ^c	24.3	13.2
5	27 ± 1.2	38 ± 1.6	61 ± 2.3	ND ^c	ND ^c
ligand	k_{on} ($\text{M}^{-1} \text{s}^{-1}$)	k_{off} (s^{-1})	K_d (μM) ^d		
1	327	0.003	9		
2	416	0.003	7		
2-R	412	0.0013	3.2		
2-S	407	0.0016	3.9		
3	230	0.003	13		
4	ND ^c	ND ^c	ND ^c		
5	34	0.003	88		

^aFor each compound, percent block of pH-dependent M2 current at listed concentrations ($\pm\text{SEM}$) and IC_{50} (μM) are shown. ^bThree replicates were used for measurements at 100 μM . ^cND: Not determined. ^d K_d (TEVC) = $k_{\text{off}}/k_{\text{on}}$.

10^{-6} M (1 μM) was measured against M2 WT, which correlates with good *in vitro* antiviral potency. When $k_{\text{off}}/k_{\text{on}} \sim 100 \mu\text{M}$ or higher, antiviral potency was not observed even for quick binders. For example, 4-(2-adamantyl)piperidine (compound **3** in ref 20), although a quick blocker against Udorn M2 and the amantadine resistant Udorn M2 V27A, was ineffective against the corresponding influenza A strains. The authors also showed that 2-(1-adamantyl)piperidine (compound **8** in ref 20) was a slow binder against Udorn M2 (48% at 2 min, but 90% at 6 min) but still has good antiviral efficacy, possibly because, although k_{on} is low, k_{off} is really low. This is the case with compound **5** against Udorn M2 WT in the present study (see Table 3). It has a reduced onset of block compared to **1**, **2**, and **3**, but also has a low dissociation rate constant, so it still has micromolar efficacy against infections of cell cultures by viral strains with M2 WT.

In studies focusing on the development of aminoadamantane ligands against IAV, derivatives are often initially tested in TEVC assays at 100 μM concentration at 2 min, and only the most potent compounds are then tested using whole cell assays.²¹ If the same procedure had been applied here, **5** would not have

Table 4. Block of Full-Length Udmr M2 S31N-Dependent Current 2 by Selected Compounds^{a,b}

ligand	Udmr M2 S31N					
	% block after 2 min	% block after 5 min	% block after 10 min	k_{on} ($\text{M}^{-1} \text{s}^{-1}$)	k_{off} (s^{-1})	K_{d} ^c
1	35 ± 2	36 ± 1	36.3 ± 1	143	0.03	210 μM
2 ^c	1.0 ± 0.2	1.5 ± 0.4	ND ^d	22	0.9	>10 mM
3	21 ± 2	30 ± 3	33 ± 1	18	0.008	444 μM
5	7.0 ± 0.4	7.6 ± 0.2	8.0 ± 0.4	79	0.14	1.8 mM

^aFor each compound, percent block of pH-dependent M2 current at listed concentrations (\pm SEM) and IC_{50} (μM) are shown. ^bThree replicates were used for measurements at 100 μM . ^cRacemic. ^dND: Not determined. ^e $K_{\text{d}} = k_{\text{off}}/k_{\text{on}}$.

been tested, even though it proved to be a low micromolar inhibitor according to K_{d} values from ITC experiments with M2TM WT (Table 1) and CPE assay (Table 2) results. Thus, TEVC percent block for 100 μM at 2 min in MDCK cells underestimated the potential of 5. Similarly 4 would not have been tested based on percent block at 2 min in TEVC with Udmr M2 V28I (Table S1). Slow block could be associated with tight block, and this phenomenon should not be overlooked in short-lasting experiments. The results suggested that TEVC results, when used for compound filtering, need careful interpretation for compounds having low association rate constant for binding to the full length M2, which also depends on the M2 pore. In this regard, ITC measurements represent an important additional tool for clarifying the binding energies of novel derivatives to M2TM given their capacity for sufficient relaxations of equilibrium between titration injections. Nevertheless, it is clear from the ITC, CPE (all strains with M2 WT), that 5 (and 4 where tested) are \sim 10-fold less active than 3.

For Udmr M2 V28I, the percentage of current inhibition is lower; compounds 3 and 4 inhibit Udmr M2 more rapidly than Udmr M2 V28I (Table S1). A small change in an amino acid at site 28 (V28I) of M2, which does not line the pore, seriously affects M2 blockage kinetics. The inhibition of 3 and 4 on both Udmr M2 and Udmr M2 V28I are irreversible in our experimental time frame, as was also observed for 1 with both proteins (data not shown).

After the aforementioned results highlighted the importance of k_{on} , k_{off} values on ligand behavior, we were intrigued to further investigate the block of rimantadine enantiomers against Udmr M2 WT protein in EP, considering the differences in resonances seen in ssNMR studies of 2-R or 2-S bound to the full-length Udmr M2 protein.²² We previously showed¹⁷ that 2-R and 2-S showed similar channel blockage against Udmr M2 WT when tested in EP at 100 μM at the 2- or 5 min time point, and this result is consistent with that from ITC measurements (see ref 17 and Table 1) and antiviral assays (see ref 17 and Table 2). In our present work we seek to further investigate the binding kinetics 2-R, 2-S by measuring the respective k_{on} , k_{off} , K_{d} (TEVC) values. The EP measurements showed a $k_{\text{off}} = 0.0013 \text{ s}^{-1}$ for 2-R and a $k_{\text{off}} = 0.0016 \text{ s}^{-1}$ for 2-S (Table 3), i.e., the two enantiomers had very similar binding kinetics. Thus, 2-R has a bit longer residence time inside the receptor than 2-S, as reflected by its slightly lower k_{off} and K_{d} values (2.4 vs 3.2 μM). In ref 22, the first ssNMR study of the full length M2 in complex with rimantadine enantiomers was published. Compound 2-R was argued to have a higher affinity than 2-S based on differences in peak intensities and position restrained MD simulations. The results published in ref 22 are in qualitative agreement with those reported here, but not in quantitative agreement, as here we see no statistically significant (ITC and EC_{50}) or meaningful (EP) difference. Perhaps this is a consequence of the different methodologies applied, i.e., EP vs ssNMR spectroscopy. Chemical shifts

differences and peak intensities do not provide an accurate quantitative estimate of binding affinity values. The EP results, antiviral assays, and ITC results showed clearly that the two rimantadine enantiomers have similar binding free energies, channel blockage, k_{on} and k_{off} rate constants, and antiviral potencies. We conclude that they form equally stable complexes and have the same residence time inside M2 WT.

The compounds did not bind to Udmr M2TM S31N according to ITC and did not exhibit antiviral potency against WSN virus, which contains both the S31N and the V28I mutations. We showed that a valuable parameter to explain the resistance of M2 S31N viruses to rimantadine analogues compared to M2 WT is a higher k_{off} rate (i.e., a smaller residence time inside M2 S31N). According to our previous results, this is due to the fact that, in M2 S31N, the loss of the V27 pocket for the adamantyl cage¹¹ resulted in low residence time inside M2TM and a lack of antiviral potency; but for 5, the sizable adducts resulted in a weak binding, which is albeit not sufficient for antiviral potency.¹¹ It is the high dissociation rate constants that render aminoadamantanes useless against S31N viruses like WSN leading to K_{d} (TEVC) in the millimolar range compared to the micromolar range for M2 WT binding.

In the S31N variants, TEVC (Table 4) shows very high exit rate constants, especially for 2 (0.9 s^{-1}) and 5 (0.14 s^{-1}), consistent with the unmeasurably high K_{d} in ITC (Table 1, lower) and EC_{50} in CPE (Table 2, WSN). Interestingly, in these two cases, 2 and 5 have low % block of inward currents at 2, 5, and 10 min in Udmr M2 S31N (Table 4), and somewhat similar k_{on} rates to 1 and 3, albeit lower compared to M2 WT, (Table 3), demonstrating that mutations can have complex, ligand-dependent effects on entry and exit rates.

M2TM WT complexes were simulated using an experimental structure of M2TM WT (PDB ID 2KQT^{4,8}) determined at pH 7.5 in the presence of 1 (see ref 11 for details). No significant differences in measures were detected between trajectories with production times of 4 and 80 ns (Tables S2 and S3). To ensure that the measures were meaningful, the equilibration of the membranes was tested. To verify this, the average area per lipid headgroup was measured in the simulation of the different lipids and compared with experimental results.²³ The calculated values approached the experimental ones of pure lipid bilayers (see Figure S4 and Table S5). The center of mass between the four V27 residues and the adamantane cage of the ligand stabilized as explained in Figure 1 varies between 4.1 and 4.5 Å on average (Tables S2 and S3). Hydrogen bond interactions for 2-R and 2-S and geometric measures, which reflect van der Waals contacts, were found to be similar for the two enantiomers, suggesting equal binding interactions as previously discussed (Figure S3).¹⁷ In diethyl and di-*n*-propyl derivatives (4 and 5), the alkyl groups seem to better fill the space between the ligand and the pore walls; but in these cases, restricted motion and the resulting entropy cost of binding may be significant and decrease the

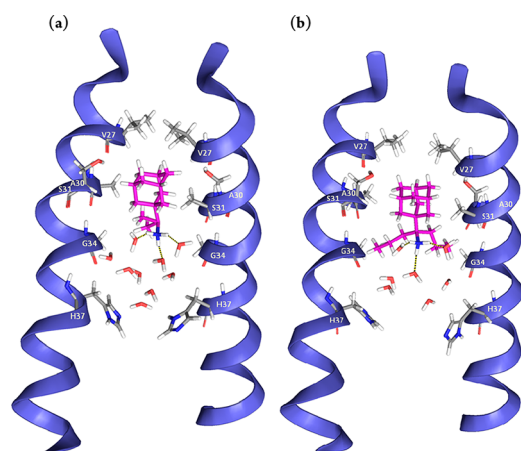


Figure 1. Representative snapshots from the simulation of ligands 3 (a) and 5 (b) bound to M2TM WT. Nine and seven water molecules are shown between the ligand and H37 residues for 3 and 5, respectively. Three hydrogen bonds between the ammonium group of the ligand and three water molecules are shown. Hydrogen bonding with water molecules and van der Waals interactions of the adamantane core with V27 and A30 side chains stabilize the ligand inside the pore with its ammonium group oriented towards the C-terminus of the channel.

binding affinities compared to 3 (Tables 1–3 and S1). Configurations from the simulations of ligands 3 and 5 are depicted in Figure 1. In all cases, in the region located above the adamantane core (i.e., toward the N-terminus) no water molecules were found, which is consistent with the proton blocking effect of the aminoadamantane derivatives.^{2,11,22,24}

The MD simulations of the complex of 3 or 5 with M2TM S31N showed that the ligand cannot bind tightly to M2TM S31N because significant favorable van der Waals interactions are missing (Figure 2). The S31N mutation of M2TM results in a shift of the hydrophobic adamantyl ring toward the C-terminus, due to the enhanced repulsive forces of the asparagine amide side chains to the adamantyl ring and attraction to water molecules. As a consequence, the stabilizing hydrophobic interactions of the

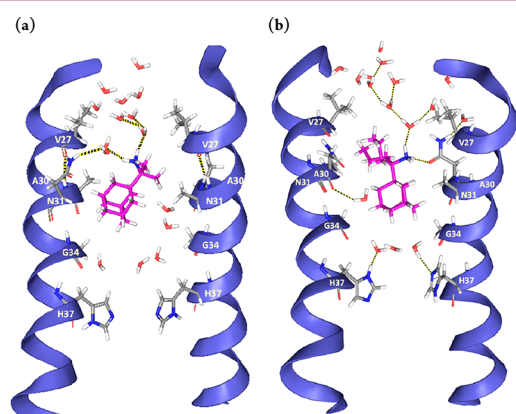


Figure 2. Representative snapshots from the simulations of ligand 3 (a) and 5 (b) bound to M2TM S31N. Five and three water molecules are shown between ligand 3 and 5, respectively, and the H37 residues and ten and twelve water molecules, respectively, between N31 and the mouth of the pore. The ammonium group of the ligand is oriented towards the N-terminus, where it forms hydrogen bonds with water molecules or the carbonyl group of the N31 amide side chain. The loss of the V27 pocket for the adamantyl cage would be expected to lead to weak binding of aminoadamantane ligands.

V27 isopropyl groups with the adamantyl ring that are present in the M2TM WT are lost in M2TM S31N.¹¹ The bulky Val27 and N31 side chains are oriented toward the N-terminus of the latter forming hydrogen bonding interactions with water molecules; the ammonium group of the ligands are also turned toward the N-terminus, allowing significant hydrogen bonding interactions with the polar N31 side chains and the nearby water molecules.¹¹ The hydrogen bonding interactions with N31 are consistent with our magic angle spinning (MAS) experimental data for spiro[pyrrolidine-2,2'-adamantane]–M2TM S31N complex. With the adamantane compound present, there was a chemical shift perturbation for N31 and G34 compared to the *apo* M2TM S31N.¹¹ In the M2TM WT, the adamantyl ring is well accommodated by the V27 and A30 side chains, and sizable adducts such as ligands 4 and 5 additionally fill the region between A30 and G34 (Figure 1); but in M2TM S31N, the adamantyl ring is between A30 and G34 (Figure 2), due to the lack of a favorable hydrophobic pocket. We have also found¹¹ an absence of chemical shift perturbations for V27 in M2TM S31N in presence of a bulky ligand, in comparison with the *apo* M2TM S31N, contrasting with the significant chemical shift changes at V27, S31, and G34 relative to the *apo* state reported when rimantadine is bound to M2TM WT.^{17,22}

Compound 5 has sizeable adducts in addition to the adamantyl ring that can fill the region between A30 and G34, and the interactions needed for binding are slightly improved, resulting in weak binding to M2TM S31N according to ITC compared to no binding for 1–3 (Table 1). This can be observed from the snapshot for the complex of 5 with M2TM S31N in Figure 2b. The results showed no binding of 1 and similar in size analogues to M2 S31N and M2TM S31N, and only possible weak binding for sizable adducts in the region between A30 and G34, which is reflected by the high k_{off} values. The last point is in agreement with the results from MAS and OS ssNMR spectra.¹¹

In summary, in this work, we compared the potency between the rimantadine analogues against M2 using four different M2 mimicry methods, i.e., ITC, MD simulations, EP, and antiviral assays. We investigated the binding kinetics of rimantadine analogues with M2 WT and M2 S31N and how they influenced the outcome of potency. We provided a kinetic perspective to explain rimantadine variant binding, proton transport blockage, and antiviral potency against influenza M2 WT and M2 S31N. According to this study, aminoadamantane variants bearing a polar head should exhibit a kinetic profile of small k_{off} rates (i.e., long residence time inside the M2 S31N protein channel pore) resulting in $K_{\text{d}} = k_{\text{off}}/k_{\text{on}}$ values at the low micromolar region, for them to exhibit inhibitory potency against M2 S31N protein.²⁵

■ ASSOCIATED CONTENT

Supporting Information

The Supporting Information is available free of charge on the ACS Publications website at DOI: 10.1021/acsmchemlett.7b00458.

Experimental and MD simulations additional material (PDF)

■ AUTHOR INFORMATION

Corresponding Author

*Tel: (+301) 210-7274834. Fax: (+301) 210 727 4747. E-mail: ankol@pharm.uoa.gr.

ORCID

Jun Wang: 0000-0002-4845-4621

Antonios Kolocouris: 0000-0001-6110-1903

Present Address

A.D.: Pharmaceutical and Medicinal Chemistry, Institute of Pharmacy and Food Chemistry, Julius-Maximilians-Universität Würzburg, Am Hubland, 97074 Würzburg, Germany.

Author Contributions

A.K. designed this research project. A.D. and C.T. contributed equally. A.D. and C.T. did ligand synthesis. C.T., A.D., Ath.K., and D.K. did the MD simulations. C.M. in J.W. group did the EP experiments against the Udorn M2 and WSN M2 N31S and the plague reduction assay against Udorn virus. K.M. in D.B. group did the EP experiments against the Udorn M2 and kinetic measurements. K.F. and J.H. in G.G. group did the ITC measurements. A.H. in the M.S. group performed CPE inhibitory assays with WSN M2 N31S and HK virus and plague reduction assay against Udorn virus as well as the cytotoxicity determinations. A.K. wrote the manuscript, and J.W., M.S., A.H., A.D., and D.B. revised it. This research includes part of the Master thesis work of A.D. and part of the Ph.D. work of C.T.

Notes

The authors declare no competing financial interest.

ACKNOWLEDGMENTS

We are grateful to Chiesi Hellas for supporting this research and the Ph.D. work of C.T.; J.W. thanks the support from NIH AI119187 and PhRMA Foundation 2015 Research Starter Grant in Pharmacology and Toxicology; A.H. and M.S. thank Andreas Sauerbrei for continuous kind support; A.K. and M.S. thank Professor Adolfo Garcia-Sastre group and the CEIRS program (NIAD Centers of Excellence for Influenza Research and Surveillance) for providing the Udorn virus.

REFERENCES

- (1) Ferruz, N.; De Fabritiis, G. Binding Kinetics in Drug Discovery. *Mol. Inf.* **2016**, *35*, 216–226.
- (2) Wang, C.; Takeuchi, K.; Pinto, L. H.; Lamb, R. A. Ion Channel Activity of Influenza A Virus M2 Protein: Characterization of the Amantadine Block. *J. Virol.* **1993**, *67*, 5585–5594.
- (3) Hayden, F. G. Clinical Applications of Antiviral Agents for Chemoprophylaxis and Therapy of Respiratory Viral Infections. *Antiviral Res.* **1985**, *5*, 229–239.
- (4) Hu, J.; Asbury, T.; Achuthan, S.; Li, C.; Bertram, R.; Quine, J. R.; Fu, R.; Cross, T. A. Backbone Structure of the Amantadine-Blocked Trans-Membrane Domain M2 Proton Channel from Influenza A Virus. *Biophys. J.* **2007**, *92*, 4335–4343.
- (5) Schnell, J. R.; Chou, J. J. Structure and Mechanism of the M2 Proton Channel of Influenza A Virus. *Nature* **2008**, *451*, 591–595.
- (6) Stouffer, A. L.; Acharya, R.; Salom, D.; Levine, A. S.; Di Costanzo, L.; Soto, C. S.; Tereshko, V.; Nanda, V.; Stayrook, S.; DeGrado, W. F. Structural Basis for the Function and Inhibition of an Influenza Virus Proton Channel. *Nature* **2008**, *451*, 596–599.
- (7) Cady, S. D.; Mishanina, T. V.; Hong, M. Structure of Amantadine-Bound M2 Transmembrane Peptide of Influenza A in Lipid Bilayers from Magic-Angle-Spinning Solid-State NMR: The Role of Ser31 in Amantadine Binding. *J. Mol. Biol.* **2009**, *385*, 1127–1141.
- (8) Cady, S. D.; Schmidt-Rohr, K.; Wang, J.; Soto, C. S.; DeGrado, W. F.; Hong, M. Structure of the Amantadine Binding Site of Influenza M2 Proton Channels in Lipid Bilayers. *Nature* **2010**, *463*, 689–692.
- (9) Cady, S. D.; Wang, J.; Wu, Y.; DeGrado, W. F.; Hong, M. Specific Binding of Adamantane Drugs and Direction of Their Polar Amines in the Pore of the Influenza M2 Transmembrane Domain in Lipid Bilayers and Dodecylphosphocholine Micelles Determined by NMR Spectroscopy. *J. Am. Chem. Soc.* **2011**, *133*, 4274–4284.
- (10) CDC. High Levels of Adamantane Resistance among Influenza A (H3N2) Viruses and Interim Guidelines for Use of Antiviral Agents–

United States, 2005–06 Influenza Season. *MMWR. Morb. Mortal. Wkly. Rep.* **2006**, *55*, 44–46.

(11) Tzitzoglaki, C.; Wright, A.; Freudenberger, K.; Hoffmann, A.; Tietjen, I.; Stylianakis, I.; Kolarov, F.; Fedida, D.; Schmidtke, M.; Gauglitz, G.; Cross, T. A.; Kolocouris, A. Binding and Proton Blockage by Amantadine Variants of the Influenza M2_{WT} and M2_{S31N} Explained. *J. Med. Chem.* **2017**, *60*, 1716–1733.

(12) Ioannidis, H.; Drakopoulos, A.; Tzitzoglaki, C.; Homeyer, N.; Kolarov, F.; Gkeka, P.; Freudenberger, K.; Liolios, C.; Gauglitz, G.; Cournia, Z.; Gohlke, H.; Kolocouris, A. Alchemical Free Energy Calculations and Isothermal Titration Calorimetry Measurements of Aminoadamantanes Bound to the Closed State of Influenza A/M2TM. *J. Chem. Inf. Model.* **2016**, *56*, 862–876.

(13) Kolocouris, A.; Tzitzoglaki, C.; Johnson, F. B.; Zell, R.; Wright, A. K.; Cross, T. A.; Tietjen, I.; Fedida, D.; Busath, D. D. Amino-adamantanes with Persistent in Vitro Efficacy against H1N1 (2009) Influenza A. *J. Med. Chem.* **2014**, *57*, 4629–4639.

(14) Kolocouris, N.; Foscolos, G. B.; Kolocouris, A.; Marakos, P.; Pouli, N.; Fytas, G.; Ikeda, S.; De Clercq, E. Synthesis and Antiviral Activity Evaluation of Some Aminoadamantane Derivatives. *J. Med. Chem.* **1994**, *37*, 2896–2902.

(15) Fan, Z.; Shu, S.; Ni, J.; Yao, Q.; Zhang, A. Ligand-Promoted Pd(II)-Catalyzed Functionalization of Unactivated C(sp³)-H Bond: Regio- and Stereoselective Synthesis of Arylated Rimantadine Derivatives. *ACS Catal.* **2016**, *6*, 769–774.

(16) Salom, D.; Hill, B. R.; Lear, J. D.; DeGrado, W. F. pH-Dependent Tetramerization and Amantadine Binding of the Transmembrane Helix of M2 from the Influenza A Virus. *Biochemistry* **2000**, *39*, 14160–14170.

(17) Drakopoulos, A.; Tzitzoglaki, C.; Ma, C.; Freudenberger, K.; Hoffmann, A.; Hu, Y.; Gauglitz, G.; Schmidtke, M.; Wang, J.; Kolocouris, A. Affinity of Rimantadine Enantiomers against Influenza A/M2 Protein Revisited. *ACS Med. Chem. Lett.* **2017**, *8*, 145–150.

(18) Rosenberg, M. R.; Casarotto, M. G. Coexistence of Two Adamantane Binding Sites in the Influenza A M2 Ion Channel. *Proc. Natl. Acad. Sci. U. S. A.* **2010**, *107*, 13866–13871.

(19) Schmidtke, M.; Schnittler, U.; Jahn, B.; Dahse, H.-M.; Stelzner, A. A Rapid Assay for Evaluation of Antiviral Activity against Coxsackie Virus B3, Influenza Virus A, and Herpes Simplex Virus Type 1. *J. Virol. Methods* **2001**, *95*, 133–143.

(20) Barniol-Xicota, M.; Gazzarrini, S.; Torres, E.; Hu, Y.; Wang, J.; Naesens, L.; Moroni, A.; Vázquez, S. Slow but Steady Wins the Race: Dissimilarities among New Dual Inhibitors of the Wild-Type and the V27A Mutant M2 Channels of Influenza A Virus. *J. Med. Chem.* **2017**, *60*, 3727–3738.

(21) Wang, J. J.; Wu, Y.; Ma, C.; Fiorin, G.; Pinto, L. H.; Lamb, R. A.; Klein, M. L.; DeGrado, W. F. Structure and Inhibition of the Drug-Resistant S31N Mutant of the M2 Ion Channel of Influenza A Virus. *Proc. Natl. Acad. Sci. U. S. A.* **2013**, *110*, 1315–1320.

(22) Wright, A. K.; Batsomboon, P.; Dai, J.; Hung, I.; Zhou, H. X.; Dudley, G. B.; Cross, T. A. Differential Binding of Rimantadine Enantiomers to Influenza A M2 Proton Channel. *J. Am. Chem. Soc.* **2016**, *138*, 1506–1509.

(23) Mori, T.; Ogushi, F.; Sugita, Y. Analysis of Lipid Surface Area in Protein-Membrane Systems Combining Voronoi Tessellation and Monte Carlo Integration Methods. *J. Comput. Chem.* **2012**, *33*, 286–293.

(24) Andreas, L. B.; Eddy, M. T.; Pielak, R. M.; Chou, J.; Griffin, R. G. Magic Angle Spinning NMR Investigation of Influenza A M2_{18–60}: Support for an Allosteric Mechanism of Inhibition. *J. Am. Chem. Soc.* **2010**, *132*, 10958–10960.

(25) Wang, Y.; Hu, Y.; Xu, S.; Zhang, Y.; Musharrafieh, R.; Hau, R.-K.; Ma, C.; Wang, J. In Vitro Pharmacokinetic Optimizations of AM2-S31N Channel Blockers Led to the Discovery of Slow-Binding Inhibitors with Potent Antiviral Activity against Drug-Resistant Influenza A Viruses. *J. Med. Chem.* **2018**, DOI: 10.1021/acs.jmedchem.7b01536.

Alchemical Free Energy Calculations and Isothermal Titration Calorimetry Measurements of Aminoadamantanes Bound to the Closed State of Influenza A/M2TM

Harris Ioannidis,^{†,□} Antonios Drakopoulos,^{†,◇} Christina Tzitzoglaki,[†] Nadine Homeyer,^{§,▲} Felix Kolarov,[‡] Paraskevi Gkeka,^{⊥,●} Kathrin Freudenberger,[‡] Christos Liolios,^{||,○} Günter Gauglitz,[‡] Zoe Cournia,^{*,△,⊥} Holger Gohlke,^{*,△,§} and Antonios Kolocouris^{*,△,†}

[†]Department of Pharmaceutical Chemistry, Faculty of Pharmacy, National and Kapodistrian University of Athens, 15771 Athens, Greece

[§]Mathematisch-Naturwissenschaftliche Fakultät, Institut für Pharmazeutische und Medizinische Chemie, Heinrich-Heine-Universität Düsseldorf, 40225 Düsseldorf, Germany

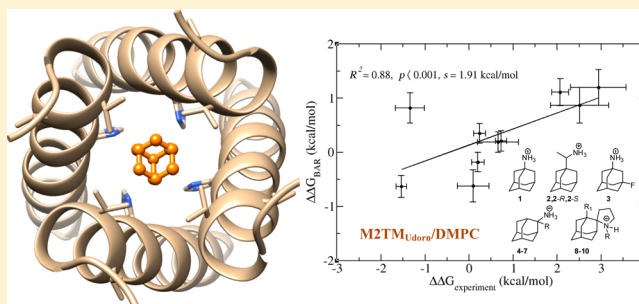
[‡]Institut für Physikalische und Theoretische Chemie, Eberhard-Karls-Universität, D-72076 Tübingen, Germany

[⊥]Biomedical Research Foundation, Academy of Athens, 11527 Athens, Greece

^{||}Demokritos, National Center for Scientific Research, 15310 Athens, Greece

Supporting Information

ABSTRACT: Adamantane derivatives, such as amantadine and rimantadine, have been reported to block the transmembrane domain (TM) of the M2 protein of influenza A virus (A/M2) but their clinical use has been discontinued due to evolved resistance in humans. Although experiments and simulations have provided adequate information about the binding interaction of amantadine or rimantadine to the M2 protein, methods for predicting binding affinities of whole series of M2 inhibitors have so far been scarcely applied. Such methods could assist in the development of novel potent inhibitors that overcome A/M2 resistance. Here we show that alchemical free energy calculations of ligand binding using the Bennett acceptance ratio (BAR) method are valuable for determining the relative binding potency of A/M2 inhibitors of the aminoadamantane type covering a binding affinity range of only ~ 2 kcal mol⁻¹. Their binding affinities measured by isothermal titration calorimetry (ITC) against the A/M2TM tetramer from the Udorn strain in its closed form at pH 8 were used as experimental probes. The binding constants of rimantadine enantiomers against M2TM_{Udorn} were measured for the first time and found to be equal. Two series of alchemical free energy calculations were performed using 1,2-dipalmitoyl-*sn*-glycero-3-phosphocholine (DPPC) and 1,2-dimyristoyl-*sn*-glycero-3-phosphocholine (DMPC) lipids to mimic the membrane environment. A fair correlation was found for DPPC that was significantly improved using DMPC, which resembles more closely the DPC lipids used in the ITC experiments. This demonstrates that binding free energy calculations by the BAR approach can be used to predict relative binding affinities of aminoadamantane derivatives toward M2TM with good accuracy.



1. INTRODUCTION

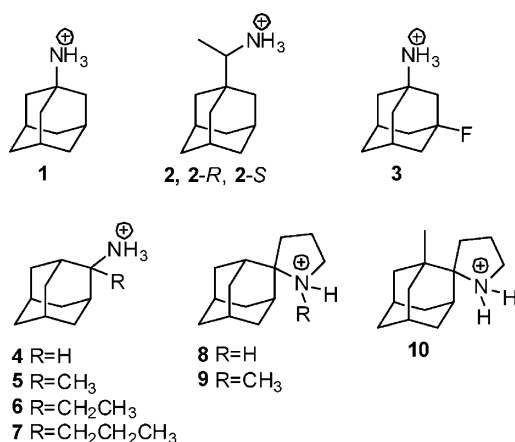
Amantadine (*Amt*, (1)) and rimantadine (2) (Scheme 1) are blockers of proton transport in the wildtype (WT) influenza A M2 proton channel^{1,2} and have been effective prophylactics and therapeutics against influenza A virus.³ The M2 protein of the influenza A virus has a short 97-residue sequence. It forms tetramers, and its transmembrane domain (A/M2TM, residues 22–46) comprises the pore of a proton channel that is activated by low pH in the viral endosome; the open state of the channel results when the imidazole rings of the four His37 residues, which line the inner part of the pore, are protonated.⁴ Its activation ultimately leads to the unpacking of the influenza viral genome and to pathogenesis.⁵ The TM domain of the M2

protein, which contains the proton-conducting residue, His37,⁴ and the channel-gating residue, Trp41,^{6,7} reproduces most of the electrophysiological, pharmacological, and biophysical features of the full-length M2 protein, such as low-pH activated proton conductivity, I-dependent sensitivity of the proton current, and tetramerization of the protein.^{8–11} Starting at the exterior of the virus, the N-terminal half of the M2TM sequence forms a water-filled pore lined by Val27, Ala30, Ser31, and Gly34. These sites are frequently mutated in I-resistant mutants.^{12,13} The pore is interrupted by His37 and Trp41,

Received: February 13, 2016

Published: April 22, 2016

Scheme 1. Structures of Aminoadamantane Derivatives 1–10 that Bind to A/M2TM



which project toward the center of the channel, while Asp44 defines its C-terminal end.⁹

The binding site of **1** and **2** is the lumen of the four-helix bundle of the M2TM. It was only after 2008 that high resolution structures (X-ray and solid-state NMR (ssNMR)) for the primary drug target domain, residues 26–37, have been unveiled at alkaline pH including complexes of M2TM with **1** or **2**.^{14–18} Assuming that M2TM can serve as a minimal model for M2 binding,^{8,9,11} these structures can be used for the development of novel inhibitors of A/M2. M2TM is blocked by **1** and **2** via a pore-binding mechanism. The adamantane cage in these molecules is tightly contacted on all sides by Val27 and Ala30 side chains, producing a steric occlusion of proton transport^{15–17} and thereby preventing a continuation of the viral life cycle. The ssNMR results also demonstrated that the ammonium group of **2** is pointing toward the four His37 residues (Figure 1).¹⁸ This orientation can be stabilized only through a network of hydrogen-bonds, mediated by water molecules in the channel lumen, with the imidazoles of His37, and possibly with Ala30 carbonyls in the vicinity.^{18–22} This is consistent with a lowering of the p*K*_a of the proton-sensing

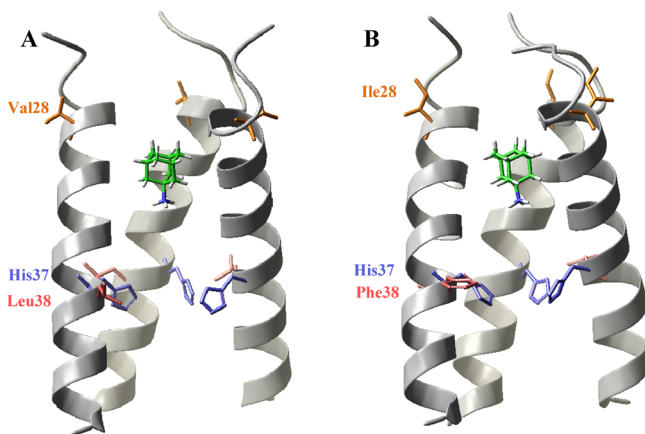


Figure 1. Structure of M2TM. Cartoon representation of M2TM_{Udom} (PDB entry: 2KQT¹⁶) (left, A) and M2TM_{Weybridge} (right, B). The figures show the critical residues His37 (blue), and residues Val28 (orange) and Leu38 (red) of M2TM_{Udom} (left, A) that are mutated in M2TM_{Weybridge} to Ile28 (orange) and Phe38 (red) (right, B), depicted as sticks. Side view of M2TM; one monomer of the tetramer was removed for better visibility; the N-terminal end is at the top.

His37 by ~3 log units compared with the first p*K*_a of histidine in apo M2TM. Thus, upon drug binding to M2TM, the p*K*_a of His37 drops from 8.2 to 5.4.^{14,23}

Resistance to **1** develops rapidly in vitro,^{24,25} in mice,²⁶ and in the clinical setting.²⁷ Since 2005,²⁸ 1/2-resistant mutants have become prevalent globally,^{29,30} abrogating clinical usefulness of **1** and **2**³¹ and consequently of other aminoadamantane derivatives.^{32–34} The main route of transmission of influenza viruses is from aquatic birds to other species.³⁵ These strains have small differences in the M2TM sequence, for example, M2TM of the avian “Weybridge” strain (M2TM_{Weybridge}) differs in only two amino acids, V28 → I28 and L38 → F38, from the human wildtype “Udom” strain (M2TM_{Udom}) (Figure 1, see the Materials and Methods section). Although these residues do not point into the pore, these mutations cause different sensitivities to binding of **1** and stability of the M2TM tetramer and its complex with **1**.^{36–38}

Computational prediction of the relative binding affinity of ligands for mutant M2TM is desirable for designing M2 inhibitors active against multiple influenza strains, which is considered important for combating influenza effectively. So far mainly molecular dynamics (MD) simulations and potential of mean force calculations for individual aminoadamantane compounds binding to the M2 protein have been conducted.^{20–22,39–50} Methods for predicting binding affinities of whole series of M2 inhibitors have so far been scarcely applied.^{51,52} However, such studies are an important prerequisite for rationally developing better ligands for M2. The binding properties of a series of aminoadamantane derivatives were measured for full length M2 at acidic pH.⁵³ The relative binding affinities of a subset of this series, i.e., of 11 aminoadamantane ligands with a range of binding affinities of about 3 orders of magnitude was studied recently by rigorous free energy calculations for M2TM in the low pH, open state.⁵¹ A high correlation was obtained between computed binding free energies and experimental binding affinities. In that work⁵¹ binding constants against full length M2 protein were used as experimental probes,⁵³ whereas simulations were performed for M2TM-aminoadamantane complexes with all His37 in the doubly protonated state. In a recent work,⁵² a very good correlation was obtained with the molecular mechanics Poisson–Boltzmann surface area (MM-PBSA) method using a smaller subset of the above-mentioned binding affinities measured against the M2 protein at acidic pH.⁵³ The six ligands selected for the calculation had a range of binding affinities of three orders of magnitude, and only compounds for which the relative change in the configurational entropy upon binding could be expected to be negligible were chosen.⁵² Most recently, we interpreted thermodynamic profiles of isothermal titration calorimetry (ITC) for aminoadamantane compounds binding to M2TM by MM-PBSA calculations and used this information for successfully and prospectively prioritizing aminoadamantane derivatives.⁵⁴

Here, we adjusted the conditions more properly compared to ref 51 for rigorous free energy calculations of M2TM–aminoadamantane complexes in order to predict accurate binding affinities against M2TM. For a direct comparison the affinities of 12 compounds (**1**, **2**, 2-*R*, 2-*S*, and **3**–**10**, Scheme 1) binding to M2TM_{Udom} and nine compounds (**1**–**9**) binding to M2TM_{Weybridge} under high pH conditions were determined by ITC (Table 1, Table S6). Measurements were performed at pH 8 because M2TM tetramers, in contrast to the full length M2 protein, are not stable at low pH (<6.5) conditions.^{10,37,38}

Table 1. Binding Constant, Free Energy, Enthalpy, and Entropy of Binding Derived from ITC Measurements for M2TM_{Udom}

ligand ^a	K_d^b	$\Delta G^{c,d}$	$\Delta H^{e,e}$	$T\Delta S^{c,f}$
1	2.17 ± 0.52	-7.77 ± 0.14	-6.66 ± 0.50	1.11 ± 0.52
2 ^g	0.51 ± 0.26	-8.64 ± 0.30	-7.60 ± 0.28	1.04 ± 0.41
2-R	0.34 ± 0.12	-8.88 ± 0.21	-7.73 ± 0.28	1.15 ± 0.35
2-S	0.32 ± 0.16	-8.97 ± 0.26	-7.54 ± 0.34	1.42 ± 0.43
3	6.33 ± 1.53	-7.14 ± 0.14	-3.60 ± 0.31	3.54 ± 0.34
4	1.60 ± 0.34	-7.96 ± 0.13	-7.03 ± 0.42	0.93 ± 0.44
5	0.89 ± 0.19	-8.31 ± 0.13	-6.79 ± 0.26	1.51 ± 0.29
6	0.62 ± 0.14	-8.52 ± 0.13	-7.14 ± 0.21	1.38 ± 0.25
7	0.63 ± 0.17	-8.53 ± 0.16	-7.62 ± 0.30	0.91 ± 0.34
8	0.36 ± 0.22	-8.90 ± 0.43	-5.02 ± 0.41	3.88 ± 0.60
9 ^h	0.93 ± 0.36	-8.28 ± 0.23	-3.82 ± 0.28	4.46 ± 0.36
10 ^g	1.30 ± 0.43	-8.08 ± 0.20	-5.08 ± 0.31	3.00 ± 0.37

^aSee Scheme 1. ^bBinding constant K_d in micromolar calculated from measured K_a in inverse molar by $K_d = 1/K_a \times 10^{-6}$, and error in K_d in micromolar determined by $K_{d,error} = (K_{a,error}/K_a^2) \times 10^{-6}$. ^cIn kilocalories per mole. ^dFree energy of binding computed from K_d by $\Delta G = -RT \ln(K_d^{ref}/K_d)$ with $K_d^{ref} = 1$ M and $T = 300$ K and error in ΔG determined according to $\Delta G_{error} = \sqrt{\left(\frac{RTK_{d,error}}{K_d}\right)^2}$ with $T = 300$ K. ^eEnthalpy of binding and error in the enthalpy of binding calculated from measured binding enthalpy and measured error by $\Delta H = \Delta H_{measured}(T/T_{measured})$ with $T = 300$ K and the temperature at which the ITC measurements were performed $T_{measured} = 293.15$ K. ^fEntropy of binding calculated by $\Delta S = (-\Delta G + \Delta H)/T$ and error in ΔS computed by the equation $\Delta S_{error} = \sqrt{\Delta G_{error}^2 + \Delta H_{error}^2}$. ^gRacemic mixture. ^hRacemic mixture resulted from the protonation of *N*-methyl spiro[pyrrolidine-2,2'-adamantane].

Furthermore, aminoadamantane compounds bind with higher affinity to full length M2 and M2TM at alkaline pH, when His37 is unprotonated and the M2TM channel is in the closed state, than at low pH, where the open state of M2TM is prevalent.^{1,10,38} We analyzed the binding properties of this set of compounds covering a binding affinity range of only ~2 kcal mol⁻¹ by MD simulations and alchemical free energy calculations with the BAR method.^{55–57} Rigorous free energy calculations have proven capable to predict relative binding free energies with an accuracy of ~1 kcal mol⁻¹ in optimal cases.^{58–63} When comparing the results to binding affinities determined by ITC, we found that the BAR method can yield good relative binding affinity rankings for aminoadamantane derivatives binding to M2TM.

2. MATERIALS AND METHODS

2.1. Experimental Work. **2.1.1. Peptide Synthesis and Compounds.** M2TM peptides corresponding to residues 22–46 of the Udom sequence of M2 (C-terminally amidated M2TM_{Udom}: SSDPLVVAASIIGILHLLWILDRL) were synthesized by standard Fmoc solid phase peptide synthesis using an aminomethyl polystyrene resin loaded with the amide linker and purified by reverse phase HPLC. A purification procedure previously described⁶⁴ and modified was used.⁶⁵ The final peptide purity was 98%. **1** was purchased from Merck, and **2** from Alfa chemicals (>99% purity). Enantiomers of **2** were purchased from Enamine; **2-S** has 95% chemical purity and **2-R** has 90% chemical purity, and the enantiomeric excess of each enantiomer sample is 99%. The details of the synthesis of compound **3** can be found in ref 65. Details for the synthesis of compounds **4–7** and **8**, **9** can be found in refs 34 and 32, respectively. Details for the synthesis of compound **10** will be published elsewhere.

2.1.2. ITC Measurements. Binding affinities of aminoadamantane derivatives (Scheme 1) for M2TM_{Udom} were determined by ITC experiments for M2TM-ligand systems in dodecylphosphocholine (DPC) micelles at pH 8.

All measurements were performed in triplicate with a TAM 2277 (TA Instruments) at pH 8 and 20 °C in a buffer of 50 mM NaH₂PO₄ and 100 mM NaCl. The peptide and the aminoadamantane derivative were dissolved in a freshly prepared DPC solution with a concentration of 13 mmol L⁻¹. Concentrations of the peptide and the ligands and the volumes used for the measurements are listed in Table S1. If not specified otherwise, measurements were conducted using 2 mL of 125 μM peptide (corresponding to 31.25 μM M2TM tetramer) (see also Table S1 in the Supporting Information (SI)). A concentration of 1.1 mM of the ligand was used for the titrant, of which 7.6 μL (equivalent to 8.4 nmol) were dispensed in the peptide/DPC solution with each injection. The time interval between two injections was set to at least 6 min.

Synthetic M2TM (residues 22–46) was reconstituted at a 1:57 monomer/lipid ratio—which guarantees the quantitative formation of M2TM tetramers—^{10,37,38} in DPC micelles at pH 8 by dissolving and sonicating 225 nmol of M2TM with the 57-fold amount of DPC in the aforementioned buffer system. Solutions of ligands **1**, **2**, **2-R**, **2-S**, and **3–10** (Scheme 1) in the buffer were titrated into the calorimetric cell at 20 °C. The heat evolved was obtained from the integral of the calorimetric signal. The heat associated with the binding of the ligand to M2TM was derived by subtracting the heat of dilution from the heat of reaction.^{66,67} Data evaluation was carried out with Digitam for Windows v4.1.

Affinity constants were calculated by nonlinear regression of the measured heat per injection using Origin 8.0⁶⁸ and are included in Table 1. For the calculation, the concentration of the peptide was kept variable because the M2TM tetramer formation is not complete. Data of three independent measurements were used, whereby all measurements were performed with the same experimental conditions using one stock solution. Data evaluation was done by plotting the measured heat per amount of substance against the molar ratio of titrant to peptide tetramer. The resulting titration curve was fitted using a global fit including the data of three independent measurements. The measured binding affinity of **1** was

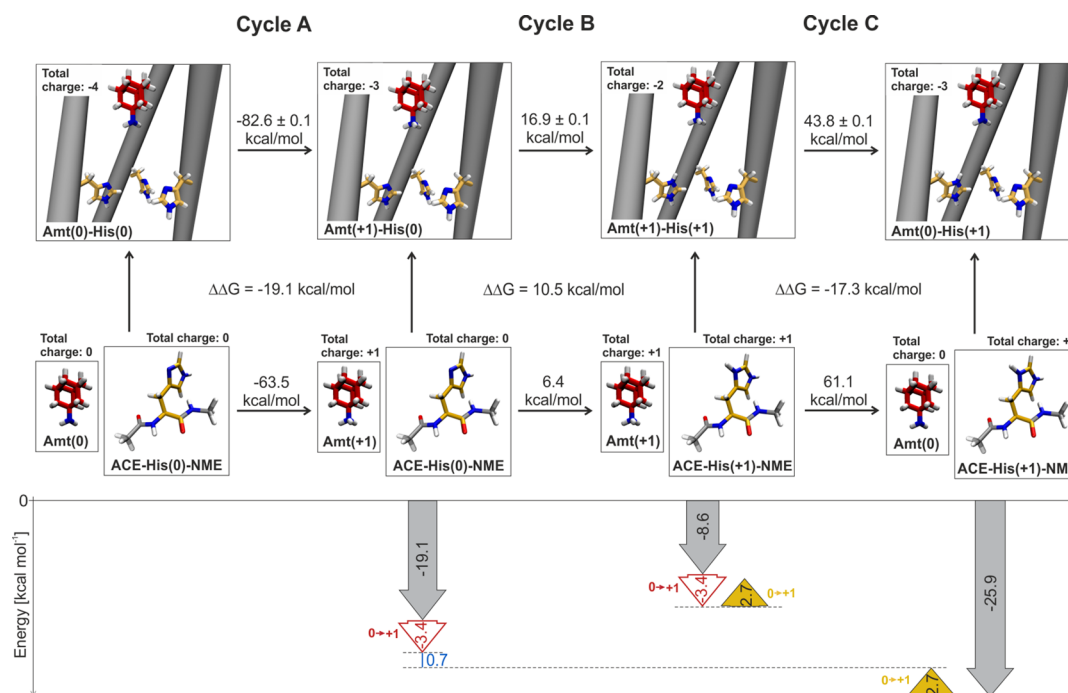


Figure 2. Thermodynamic cycle employed for studying the preferred protonation states of His37 and *Amt*. Free energy differences were calculated by single point perturbation calculations based on changes in electrostatic energies, using the Poisson–Boltzmann approach for estimating the polar part of the solvation free energy. ΔG values for the protonation of His37 are mean values obtained by averaging over ΔG values calculated for the protonation of each His37 residue of the M2TM homotetramer. Errors in ΔG have been determined as described in ref 54. Errors for the transformations of histidine and amantadine in solution (lower arm of the thermodynamic cycle) are <0.01 kcal mol⁻¹. Subcycles reflect the protonation of *Amt* in M2TM with neutral His37 (Cycle A), the protonation of one His37 residue in M2TM with a bound positively charged *Amt* (Cycle B), and the deprotonation of the positively charged *Amt* in M2TM with one protonated His37 (Cycle C). For each subcycle, $\Delta\Delta G$ was calculated as the difference of ΔG values associated with the upper transformation minus those of the lower one. A negative $\Delta\Delta G$ indicates that the right vertical transformation of each cycle is more favorable than the left one. For clarity one monomer of the M2TM tetramer is not shown in the schematic depiction of the M2TM-*Amt* complex states; for each state the total charge of the system is given. Changes in free energy relative to the *Amt*(0)-His(0) state are shown as arrow diagram below the thermodynamic cycle. All free energies are given in kilocalories per mole. The free energies that are associated with the protonation of histidine and *Amt* in solution at pH 8 are depicted by red and yellow arrows. The overall free energy difference between the most favorable states, *Amt*(+1)-His(0) and *Amt*(0)-His(+1), of 0.7 kcal mol⁻¹ is highlighted in blue.

2.17 ± 0.52 μ M and is comparable with the value of 12 μ M measured using analytical ultracentrifugation,³⁸ and the value of 9 ± 2 μ M derived based on kinetic studies in electrophysiological experiment.¹

ITC is a widely used method in drug discovery, especially in quantitative structure–activity-relationship studies.^{69,70} However, there are some inherent limitations with respect to the overall applicability of this method. Since warmth released or consumed by an interaction is detected, the method fails measuring interactions that are almost exclusively driven by entropy. The bigger the change of enthalpy during an interaction, the easier this interaction can be measured with ITC. A further limitation is set by the affinity of the interaction. The product of dissociation constant and receptor concentration (called Wiseman constant) determines the slope of the resulting titration curve and should be optimally between 10 and 100.⁷¹ For very high affinity interactions, one needs to dilute the system. For low affinity interactions (i.e., K_d values in the range of 10 μ M) a very high quantity of the receptor is needed, and this is accompanied by difficulties due to limitations such as availability, cost, solubility, or stability. For the M2TM peptide investigated in this study, the solubility in the DPC micelles limits the possible concentration. Consequently, affinity constants of low affinity binders (e.g., ligand 3) possess relatively large errors. The procedure for the peptide synthesis, the experimental details for determining binding

constants for the Weybridge complexes, and the affinity constants for M2TM_{Weybridge} of compounds 1–9 have been reported in another publication⁵⁴ (affinity constants for M2TM_{Weybridge} are included in Table S6).

2.2. Computational Methods. **2.2.1. Identification of Preferred Protonation States of Amantadine and His37.** For determining the most likely protonation states of *Amt* (1) and His37 when bound to M2TM_{Udown}, we performed MD simulations and relative free energy calculations as detailed somewhere else for M2TM_{Weybridge}.⁵⁴ Assuming that the shift in proton affinity [$\Delta\Delta G$; eq 1] is due solely to altered electrostatic interactions, the relative free energies between different protonation states of *Amt* and His37 in the complex as well as of *Amt* and a histidine with acetyl- and *N*-methylamino blocking groups (ACE-His-NME) in solution (Figure 2) were computed according to a single step, free energy perturbation approach described by Rod et al.⁷² Ensembles were generated by extracting structures from MD simulations of M2TM_{Udown}-*Amt*, ACE-His-NME, and *Amt* in solution. M2TM_{Udown}-*Amt*, ACE-His-NME, and *Amt* in solution were simulated with *Amt* in the protonated, singly positively charged state and with all His residues in the Ne2-protonated, neutral state. The protonation states of the other residues were set according to the default settings in the LEaP program of the Amber12 program package, i.e. Asp was negatively charged, and Lys and Arg carried a positive charge. The simulations were

performed with Amber12⁷³ as described in ref 54. In brief, the systems were optimized by a thorough minimization procedure involving 2500 steps steepest-descent and 7500 steps conjugate gradient minimization in the presence of a harmonic restraint with a force constant of 5 kcal mol⁻¹ Å⁻². It followed a heating phase in which the temperature of the systems was raised to 303 K applying Langevin dynamics in the presence of a harmonic restraint with a force constant of 10 kcal mol⁻¹ Å⁻² on all protein, peptide, and *Amt* atoms. The heating was performed in two consecutive steps: first, the temperature was raised to 100 K in a short NVT simulation; then, the systems were heated from 100 to 300 K in a 100 ps NPT simulation with isotropic pressure scaling to $p = 1$ bar in intervals of 1 ps (*Amt* and ACE-His-NME) or in a 100 ps NPT γ simulation with $\gamma = 10$ dyn cm⁻¹ and semi-isotropic pressure scaling to $p = 1$ bar in intervals of 1 ps (M2TM_{U_{down}}-*Amt*). Finally, the systems were freely equilibrated without restraints in a 1 ns NPT or NPT γ simulation, respectively ($p = 1$ bar, $T = 303$ K, $\gamma = 10$ dyn cm⁻¹). Production simulations were performed for 30 ns (*Amt* and ACE-His-NME) or 50 ns (M2TM_{U_{down}}-*Amt*) using the same settings as in the final equilibration step. Bonds to hydrogen atoms were constrained employing the SHAKE algorithm,⁷⁴ and the equations of motion were integrated in time steps of 2 fs. An 8 Å cutoff was used for truncating short-range nonbonding interactions, and long-range electrostatic interactions were treated by the particle-mesh Ewald summation method.^{75,76} 1500 snapshots were extracted in 20 ps steps from the 20–50 ns interval of the M2TM_{U_{down}}-*Amt* MD simulation (i.e., the *Amt*(+1)-His(0) state) as well as from the 0–30 ns interval of the simulations of ACE-His(0)-NME and *Amt*(+1) in solution. Free energy differences (ΔG) between two states were calculated by the Zwanzig equation^{77,78} averaging over the structural ensembles, and the difference in free energy with respect to the shift in the proton affinity ($\Delta\Delta G$) was calculated according to eq 1.

$$\Delta\Delta G = \Delta G_{\text{protonation state A} \rightarrow \text{B}}^{\text{bound}} - \Delta G_{\text{protonation state A} \rightarrow \text{B}}^{\text{unbound}} \quad (1)$$

To do this, all water molecules and ions were removed from the ensemble structures prior to single point energy calculations with the *mm_pbsa.pl* module of Amber12.⁷³ Total energies of the systems were estimated as the sum of the electrostatic energies of the molecules in gas phase and the polar part of their solvation free energy applying a Poisson–Boltzmann (PB) approach^{79,80} using an ionic strength of 100 mM for the implicit solvent and Parse radii.⁸¹ Structures of the states for which no snapshots were extracted from the simulations, i.e., *Amt*(+1)-His(+1), *Amt*(0)-His(+1), and *Amt*(0)-His(0) as well as *Amt*(0) and ACE-His(+1)-NME were created by post-processing of the M2TM_{U_{down}}-*Amt* trajectory adapting the charges and adding or deleting hydrogens at the respective sites accordingly. ΔG values for transformations involving His37 of the M2TM tetramer were calculated as mean values over the ΔG values obtained for changing His37 one-by-one in the four chains. The uncertainties in eq 1 were calculated as described in ref 54.

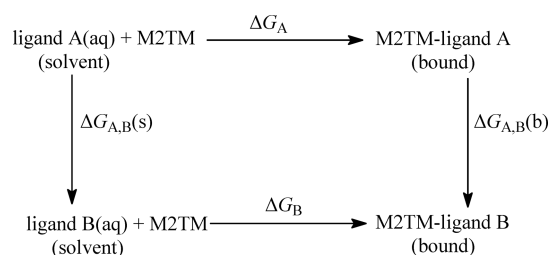
For the preferred protonation state of *Amt* and histidine at the given pH, the free energy associated with protonating *Amt* and histidine at pH 8 was calculated by eq 2

$$\Delta G = 2.303RT(\text{pH} - \text{p}K_{\text{a,model}}) \quad (2)$$

with $T = 300$ K. For *Amt* and histidine in solution, $\text{p}K_{\text{a,model}}$ values of 10.5 and 6.0 were considered, respectively.^{10,82}

2.2.2. Free Energy Calculations by the BAR Approach of M2TM-Amantadine Derivatives in Lipid Bilayers. Relative binding free energies for aminoadamantane derivatives (Scheme 1) bound to M2TM were computed following the BAR approach⁵⁵ and applying a thermodynamic cycle (Scheme 2). Alchemical free energy calculations were carried out for

Scheme 2. Thermodynamic Cycle for the Calculation of Relative Free Energies of Binding Applied to Alchemical Transformations of Aminoadamantane Derivatives 1–10 (Scheme 1)^a



^a ΔG_A , ΔG_B are the free energies of transfer of A and B from the aqueous phase (unbound state) to the bound state, respectively. $\Delta G_{A,B}(s)$ and $\Delta G_{A,B}(b)$ are the free energy differences of the mutation of A into B in aqueous solution, and bound to the protein, respectively.

M2TM_{U_{down}}-ligand and M2TM_{Weybridge}-ligand complexes under periodic boundary conditions with Desmond^{83–85} using the settings and the simulation protocol described above and also in ref 51. The structures for the simulations of the aminoadamantane compounds in solution were generated and minimized in Maestro⁸⁶ using the MMFF94 force field implemented with Macromodel 9.6.^{87,88} The M2TM_{U_{down}}-1 complex structure (PDB ID 2KQT¹⁶) served as a model structure for M2TM_{U_{down}} with bound ligands 1–10 (Scheme 1) in DMPC or DPPC. We chose this structure because it was determined at pH 7.5 and in DMPC vesicles,¹⁶ i.e., under conditions that closely resemble the conditions we applied in our simulations to model high pH and a DMPC or DPPC lipid bilayer system. Consequently, this M2TM structure should already be adapted to these environmental conditions, such that no large structural changes are to be expected during MD simulations, and only a short equilibration phase should be required. For M2TM_{Weybridge} with bound ligands, a model structure was generated from M2TM_{U_{down}} (from PDB ID 2KQT¹⁶) by mutating amino acids V28 to I28 and L38 to F38 with Maestro.⁸⁶

N- and C-termini of the M2TM model systems were capped by acetyl and methylamino groups after applying the protein preparation module of Maestro. The structures of the protein and 1 were saved separately and were used for the subsequent docking calculations. The ligands in their ammonium forms were built by means of Maestro 8.5 and were then minimized by means of Macromodel 9.6 and the MMFFs force field using the conjugate gradient (CG) method and a distance-dependent dielectric constant of 4.0 until a convergence value of 0.0001 kJ Å⁻¹ mol⁻¹ was reached. Docking poses of aminoadamantane derivatives in the M2TM bound state were generated by docking the prepared compound structures into the pore binding site of the M2TM. The M2TM-1 complex structure after 80 ns of MD simulations of M2TM_{U_{down}}-*Amt* and M2TM_{Weybridge}-*Amt*, respectively, was used as a template structure. Docking was performed with GOLD 5.2^{89,90} using

Table 2. Relative Binding Free Energies for Pairs of Compounds Computed by the BAR Method for M2TM Embedded in a DPPC Bilayer or Derived from the Experimental Binding Affinity Data in Tables 1 and S6.⁵⁴

transformation	M2TM _{Udom}		transformation	M2TM _{Weybridge}	
	$\Delta\Delta G_{\text{FEP}}^{a,b}$	$\Delta\Delta G_{\text{exp}}^{a,c}$		$\Delta\Delta G_{\text{FEP}}^{a,b}$	$\Delta\Delta G_{\text{exp}}^{a,c}$
2-R → 1	1.21 ± 0.51 ^f	1.11 ± 0.25	2-R → 1	-0.72 ^d	<i>e</i>
2-S → 1	1.16 ^d	1.20 ± 0.33	2-S → 1	0.24 ^{d,f}	<i>e</i>
2 → 1	1.19 ^g	0.87 ± 0.33 ^f	2 → 1	-0.24 ^g	0.84 ± 0.36 ^f
3 → 1	-1.58 ± 0.14	-0.63 ± 0.20	3 → 1	-1.36 ± 0.13	-1.17 ± 0.29
4 → 1	-0.20 ± 0.66	0.19 ± 0.19	4 → 1	1.11 ± 0.65	0.47 ± 0.32
5 → 4	0.68 ± 0.21	0.35 ± 0.18	5 → 4	0.41 ± 0.17	0.29 ± 0.38
6 → 5	0.17 ± 0.20	0.21 ± 0.19	6 → 5	-0.34 ± 0.22	-0.05 ± 0.42
7 → 6	0.47 ± 0.14	-0.18 ± 0.18	7 → 6	0.24 ± 0.14	-1.27 ± 0.37
9-R → 8	-0.71 ± 0.38 ^f	<i>e</i>	9-R → 8	-1.17 ± 0.39 ^f	<i>e</i>
9-S → 8	2.27 ± 0.40	<i>e</i>	9-S → 8	-1.70 ± 0.40	<i>e</i>
9 → 8	0.78 ± 0.55 ^g	-0.62 ± 0.30 ^f	9 → 8	-1.44 ± 0.56 ^g	-0.57 ± 0.27 ^f
10-R → 8	-2.87 ± 0.21	<i>e</i>	10-R → 8	-2.70 ± 0.20	<i>e</i>
10-S → 8	-1.30 ± 0.23	<i>e</i>	10-S → 8	-1.57 ± 0.16	<i>e</i>
10 → 8	-2.09 ± 0.31 ^g	-0.82 ± 0.28 ^f	10 → 8	-2.14 ± 0.25 ^g	<i>h</i>

^aIn kilocalories per mole. ^bPropagation error calculated according to the bootstrap method. ^cDifference in binding free energy calculated from experimentally determined K_d values by $\Delta\Delta G = -RT \ln(K_d^A/K_d^B)$ with $T = 300$ K and error calculated from individual experimental errors by $\text{error}_{\Delta\Delta G} = \sqrt{(\text{error}_{\Delta G,A})^2 + (\text{error}_{\Delta G,B})^2}$. ^dError in $\Delta\Delta G_{\text{FEP}}$ not known. ^eThe enantiomers were not available and were not measured with ITC. The racemic mixture was measured instead. ^fThis value corresponds to a free energy difference of binding between the racemic mixture of compound 9 or 10 and compound 8. ^gMean of the computed free energy values for the transformations including the corresponding R and S enantiomers. ^hNot determined.

the ASP scoring function,^{91,92} after deletion of **1**, and considering six water molecules located within the M2TM pore-binding site between the ligand and His37. The option “toggle” was used to let the algorithm decide whether taking into account a water molecule or neglecting it based on an empirical desolvation penalty. The region of interest used by GOLD was defined to contain the atoms that were within ~15 Å of the ligand binding site in the receptor structure. The “allow early termination” command was deactivated. For all the other parameters, GOLD default values were used. Ligands were submitted to 30 genetic algorithm runs. Ten docking poses were produced for each ligand and were visually inspected using the UCSF Chimera package.⁹³ The pose with the best score was used in FEP/MD simulations.

The M2TM complexes were embedded in either a DPPC or a DMPC lipid bilayer extending 10 Å beyond the solutes. Complex and ligand systems were solvated using the TIP3P⁹⁴ water model. Na⁺ and Cl⁻ ions were placed in the water phase to neutralize the systems and to reach the experimental salt concentration of 0.150 M NaCl. Membrane creation and system solvation were conducted with the “System Builder” utility of Desmond.^{83–85}

The OPLS 2005 force field^{95–98} was used to model all protein and ligand interactions, and the TIP3P model⁹⁴ was used for water. The particle mesh Ewald method (PME)^{75,76} was employed to calculate long-range electrostatic interactions with a grid spacing of 0.8 Å. van der Waals and short-range electrostatic interactions were smoothly truncated at 9.0 Å. The Nosé–Hoover thermostat⁹⁹ was utilized to maintain a constant temperature in all simulations, and the Martyna–Tobias–Klein method¹⁰⁰ was used to control the pressure. The equations of motion were integrated using the multistep RESPA integrator⁹⁹ with an inner time step of 2 fs for bonded interactions and nonbonded interactions within a cutoff of 9 Å. An outer time step of 6.0 fs was used for nonbonded interactions beyond the cutoff. Periodic boundary conditions were applied.

Each system was equilibrated in MD simulations with a modification of the default protocol provided in Desmond, which consists of a series of restrained minimizations and molecular dynamics simulations designed to relax the system, while not deviating substantially from the initial coordinates. First, two rounds of steepest descent minimization were performed with a maximum of 2000 steps with harmonic restraints of 50 kcal mol⁻¹ Å⁻² applied on all solute atoms, followed by 10 000 steps of minimization without restraints. A series of four MD simulations was performed. The first simulation was run for 12 ps at a temperature of 10 K in the NVT (constant number of particles, volume, and temperature) ensemble with solute heavy atoms restrained with a force constant of 50 kcal mol⁻¹ Å⁻², followed by an identical simulation in the NPT ensemble. The temperature was then raised during a 25 ps simulation to 310 K (DMPC systems) or 325 K (DPPC systems) in the NPT ensemble with the force constant retained. The temperatures of 310 and 325 K were used in the MD simulations in order to ensure that the membrane state is above the melting temperature state of 297 K for DMPC lipids and 314 K for DPPC lipids, respectively.¹⁰¹ Then an unrestrained NPT production simulation at 310 K (DMPC systems) and 325 K (DPPC systems)¹⁰¹ followed saving snapshots in intervals of 4 ps.

Production simulations at each λ value were run for 4 or 6 ns for compounds without and with a cyclic group, respectively. A λ schedule comprising 12 windows was used (see Table S1 in ref S1). Simulations were run for the transformations listed in Tables 2 and 3. Usually one step of alchemical transformations was conducted in order to reach the target ligand structure from the starting one. However, for transformations 4 → 1 and 2-R or 2-S → 1, two step alchemical simulations were performed (Figure S1) to ensure that the configurational ensembles between the end states are sufficiently sampled and, thus, the convergence of the simulation. The complex systems were stable in the alchemical free energy simulations as indicated by an RMSD of the protein heavy atoms ≤2.2 Å such

Table 3. Relative Binding Free Energies for Pairs of Compounds Computed by the BAR Method for M2TM Embedded in a DMPC Bilayer or Derived from Experimental Binding Affinity Data in Table 1

transformation	M2TM _{Udom} $\Delta\Delta G_{\text{FEF}}^{a,b}$	$\Delta\Delta G_{\text{exp}}^{a,c}$
2-R → 1	2.07 ± 0.19	1.11 ± 0.25
2-S → 1	2.94 ± 0.63	1.20 ± 0.33
2 → 1	2.51 ± 0.66 ^f	0.87 ± 0.33 ^e
3 → 1	-1.54 ± 0.12	-0.63 ± 0.20
4 → 1	0.66 ± 0.46	0.19 ± 0.19
5 → 4	0.24 ± 0.14	0.35 ± 0.18
6 → 5	0.73 ± 0.13	0.21 ± 0.19
7 → 6	0.20 ± 0.14	-0.18 ± 0.18
9-R → 8	-0.90 ± 0.36	<i>d</i>
9-S → 8	1.07 ± 0.36	<i>d</i>
9 → 8	0.09 ± 0.36 ^f	-0.62 ± 0.30 ^e
10-R → 8	-1.24 ± 0.22	<i>d</i>
10-S → 8	-1.44 ± 0.24	<i>d</i>
10 → 8	-1.34 ± 0.33	-0.82 ± 0.28 ^e

^aIn kilocalories per mole. ^bPropagation error calculated according to the bootstrap method. ^cDifference in binding free energy calculated from experimentally determined K_d values by $\Delta\Delta G = -RT \ln(K_d^A/K_d^B)$ with $T = 300$ K and error calculated from individual experimental errors by $\text{error}_{\Delta\Delta G} = \sqrt{(\text{error}_{\Delta G,A}^2 + \text{error}_{\Delta G,B}^2)}$. ^dThe enantiomers were not available and were not measured with ITC. The racemic mixture was measured instead. ^eThis value corresponds to a free energy difference of binding between the racemic mixture of compound 9 or 10 and compound 8. ^fMean of the computed free energy values for the transformations including the corresponding R and S enantiomers.

that the sampled structures could be used for computing relative binding free energies. Free energy differences ΔG were calculated by the BAR method⁵⁵ and checked for convergence by computing ΔG based on increasing time intervals of the alchemical free energy simulations.⁵¹ Relative binding free energies between pairs of ligands $\Delta\Delta G_{\text{ligand A} \rightarrow \text{B}}$ were calculated according to eq 3 based on ΔG obtained for the transformations of the ligands in the bound and the solvated state, respectively, $\Delta G_{\text{A,B}}(\text{b})$ and $\Delta G_{\text{A,B}}(\text{s})$ (see the thermodynamic cycle in Scheme 2).

$$\Delta\Delta G_{\text{ligand A} \rightarrow \text{B}} = \Delta G_{\text{A,B}}(\text{b}) - \Delta G_{\text{A,B}}(\text{s}) \quad (3)$$

Errors in the computed relative binding free energies were estimated using block bootstrapping¹⁰² as described in ref 51. The predictive index was calculated according to ref. 103.

For structural analyses, snapshots of the different systems were created with VMD¹⁰⁴ or Maestro.⁸⁶ Trajectories were analyzed with Maestro, Gromacs,^{105,106} and VMD.¹⁰⁴ For the calculation of hydrogen bonds, a cutoff angle of 30° deviation from 180° between the donor-hydrogen-acceptor atoms and a cutoff distance of 3.5 Å between the donor and acceptor atoms were applied.

3. RESULTS AND DISCUSSION

3.1. Identification of Preferred Protonation States of Amt and His37. We determined the energetically most favorable protonation states of Amt (1) and His37 in the M2TM_{Udom}-Amt system for pH 8 by a single-step perturbation approach that is similar to the approach described by Rod and Brooks.⁷² In this approach, it is assumed that the shift in proton

affinity [$\Delta\Delta G$; eq 1] is caused exclusively by altered electrostatic interactions. The change in free energy associated with the change in these interactions was determined both for the (de)protonation of His37 and Amt in the complex bound state (upper arm of the thermodynamic cycle in Figure 2) and for the (de)protonation of histidine and Amt in solution (lower arm of the thermodynamic cycle in Figure 2). For the complex form (upper arm of the thermodynamic cycle) only the Amt(+1)-His(0) state was simulated. The respective MD trajectory was used as reference to generate the states Amt(0)-His(0), Amt(+1)-His(+1), and Amt(0)-His(+1) by adding or removing hydrogen atoms at the respective sites and adapting the charges accordingly. To determine the change in the electrostatic interactions, gas-phase electrostatics and the polar part of the solvation free energy were calculated after all explicit water molecules and ions had been removed and protons had been deleted or added to reach the respective perturbed states. As pointed out in ref 54, where this calculation approach has already been used successfully on the M2TM_{Weybridge}-Amt system, the single step perturbation approach should give reasonable estimates of the pK_a shift within the accuracy of the force fields if (a) the proton added or deleted points into the solvent and (b) the reorganization of the M2TM channel due to a change in the protonation state is small. As a result of these two factors the perturbed state should sample regions of configuration space that overlap with those of the original one,^{55,56} due to the small changes associated with the protonation of Amt and histidine. Overall, qualitative results of the computed shifts are sufficient as detailed next.

The computed shifts reveal that the Amt(+1)-His(0) state is more favorable than the Amt(0)-His(0) state (cycle A in Figure 2). Phrased differently, the already high pK_a value of Amt of 10.5¹⁰ in solution is shifted to an even higher value in the M2TM environment with uncharged His37. To probe to what extent a protonation of His37 influences the proton affinity of Amt, we also analyzed the Amt(+1)-His(+1) and Amt(0)-His(+1) states, where a proton was added to one of the four His37 residues. The first state is much more unfavorable than the Amt(+1)-His(0) state (cycle B in Figure 2), not unexpected due to the close proximity of two like charges. The quantitatively rather large shift in proton affinity observed in cycle B may be attributed to our setup, which does not allow to take into account that the proton on His37 delocalizes between the four histidines of the M2TM tetramer.^{7,23} The Amt(0)-His(+1) state is again preferred relative to the Amt(+1)-His(+1) state (cycle C in Figure 2). Finally, taking cycles B and C together (Figure 2) shows that the Amt(0)-His(+1) state is by 0.7 kcal mol⁻¹ more favorable than the Amt(+1)-His(0) state. Taking the error in the calculations into account, which can be expected to be in the range of one pK_a unit, i.e. ~1.4 kcal mol⁻¹ at 300 K, the Amt(0)-His(+1) and Amt(+1)-His(0) states are equally likely.¹⁰⁷ The fact that the Amt(+1)-His(0) state is among the most favorable states compares favorably with experimental findings according to which the pK_a of histidine in solution of ~6⁸² drops to a value of ~5.4 for His37 of M2TM upon binding of Amt.¹⁴ Hence, at pH 8, Amt exists to a considerable extent in the protonated form in both solution and when bound to M2TM, whereas the four His37 of M2TM can be neutral under both conditions.

3.2. Isothermal Titration Calorimetry of Amino-adamantane Compounds Binding to M2TM_{Udom}. As reference values we measured binding affinities of the

aminoadamantane compounds **1**, **2**, **2-R**, **2-S**, and **3–10** in Scheme 1 toward M2TM_{Udom} by ITC (Table 1). The binding affinities of compounds **1–9** toward M2TM_{Weybridge} were measured by ITC in another work⁵⁴ and are included in Table S6. The measurements were conducted at pH 8 because previous findings indicated that **1** binds with high affinity to M2TM at high pH where all His37 residues are in the neutral form.¹⁰ Furthermore, M2TM tetramers are not stable in dodecylphosphocholine micelles at pH 5–6 and, thus, cannot bind aminoadamantane compounds to a sufficient extent under these conditions.^{10,65} ITC measurements yield the enthalpy of binding (ΔH) as well as the dissociation constant (K_d). From K_d , the binding free energy (ΔG) is calculated (Table 1). The binding entropy is obtained as the difference between ΔG and ΔH . Compounds **2**, **9**, and **10** are chiral whereas all other compounds, i.e., **1** and **3–8**, are achiral. Compound **2** was measured as a racemic mixture but also samples of the enantiomers **2-R** and **2-S** (which are commercially available) were measured. Compounds **9** and **10** were measured as racemic mixtures. Compound **9** exists in solution as a mixture of enantiomeric ammonium salts that are in equilibrium. The corresponding amines are conformational enantiomers, which are interconverted through ring and nitrogen inversion, and after protonation form the enantiomeric ammonium salts **9-R** and **9-S**.¹⁰⁸ Enantiomers may have a different enthalpy of binding against a protein since the two complexes formed are diastereomers.¹⁰⁹ It has been suggested through in silico prediction that enantiomers of compound **2** bind with different affinity to the M2 protein.¹¹⁰ As depicted in Table 1, including thermodynamic parameters of binding against M2TM_{Udom}, enantiomers **2-R** and **2-S** bind with the same affinity against M2TM_{Udom} ($K_d = 0.34, 0.32 \mu\text{M}$ respectively); for the racemic mixture **2** a $K_d = 0.51 \mu\text{M}$ was measured, which is close to the K_d 's of the enantiomers considering the experimental errors (see Table 1) and the lower chemical purity of the commercial enantiomers (90% for **2-R** and 95% for **2-S**) compared to racemic **2** (see the Materials and Methods section). It cannot be excluded that the impurities affect the ITC results, although we expect only small deviations from the measured K_d 's. It has been reported that the biological activity of **2-R** and **2-S** in vivo against influenza A virus is the same¹¹¹ but it has just been suggested that **2-R** and **2-S** affect different isotropic chemical shift changes when bound to the full M2 protein measured using ssNMR.¹¹² Spiro[pyrrolidine-2,2'-adamantane] (**8**) and the enantiomers of **2** have the smallest K_d 's (0.36, 0.34, and 0.32 μM , respectively) against M2TM_{Udom}, i.e., the highest binding affinities, of all studied aminoadamantane compounds. Compound **2** has the smallest K_d against M2TM_{Weybridge} ($K_d = 0.18 \mu\text{M}$), and **8** ($K_d = 0.38 \mu\text{M}$) is among the strongest binders⁵⁴ there (see Table S6). Compound **3** has the lowest binding affinity against M2TM_{Udom} ($K_d = 6.33 \mu\text{M}$) and against M2TM_{Weybridge} ($K_d = 5.32 \mu\text{M}$), which shows that the fluorine introduced into the adamantane core at position 3 is most unfavorable. Compared to compound **1**, the presence of a fluorine atom in compound **3** leads to a reduction of the enthalpy of binding while the entropic term is increased. Compared to **1**, in compound **4** the entropic term is reduced likely because **4** has a higher rotational entropy in the unbound state due to its lower symmetry. For **5–7**, it can be observed that the enthalpy of binding progressively increases with increasing size of the *n*-alkyl adduct; the entropy of binding generally progressively decreases with increasing size of the *n*-alkyl adduct most likely because of the restricted rotation in

the bound state. Entropy again increases when the carbon adduct is restricted to a ring in the spiroyrrolidine **8**. The thermodynamic values in Table 1 suggest that **2** and **8** have equal binding affinities as a compromise between enthalpy and entropy of binding; in **2** the enthalpic term is higher than in **8**, whereas in **8** the entropic term is higher than in **2**.

3.3. Ligand Ranking by the BAR Approach. If the correct ranking of relative affinities of structurally similar drug candidates against a receptor can be realized, costs and efforts can be saved during the process of lead optimization.^{113–115} It has been reported that BAR, which provides a maximum-likelihood estimator of the free-energy change, decreases the variance of the determined free energies using the simulation data more efficiently, thus providing a minimum uncertainty estimate of free energy differences between two thermodynamic states.^{55–57,116,117} Here we investigated whether aminoadamantane ligands binding to M2TM_{Udom} and M2TM_{Weybridge} under high pH conditions can be correctly ranked by alchemical perturbation calculations with the BAR approach. The binding affinities of the aminoadamantane compounds **1**, **2**, **2-R**, **2-S**, and **3–10** in Scheme 1 for M2TM_{Udom} (Table 1) and of compounds **1–9** for M2TM_{Weybridge}⁵⁴ (Table S6) were measured by ITC and used as reference values. It should be emphasized that the calculations performed in this work aim at the prediction of relative free energies of binding corresponding to binding constants covering a narrow range of about 1 order of magnitude, related to free energies covering a range of ~ 2 kcal mol⁻¹. The results from this investigation can be used as a benchmark to compare other methods' accuracies in the future.¹¹⁴

Appropriate adjustments were applied to binding free energy calculations in order to match experimental conditions as closely as possible, i.e., by using a M2TM structure in the closed conformation found at high pH and assigning a neutral form for all His37.¹¹⁸ M2TM-ligand complexes were simulated in phospholipid bilayers.¹¹⁹ The bilayer composition used in the MD simulations might have an effect on the computed binding free energies.¹²⁰ It has been reported that the conformation and dynamics of M2TM are influenced by the length of the acyl chains of the phospholipids,^{9,121} and it has been shown that DMPC represents a better membrane mimetic system for retaining proper M2TM structure compared to other glycerophospholipids.¹²² In addition to free energy calculations with a DMPC bilayer system, also calculations with a DPPC bilayer were conducted for M2TM_{Udom} for comparison.

3.3.1. Analysis of the MD Trajectories of M2TM-Ligand Complexes. Both possible enantiomers of aminoadamantane compounds **2**, **9**, and **10** were considered in the calculations. All M2TM-ligand complexes were stable, and the M2TM tetramer did not show any significant conformational changes in the course of the simulation as demonstrated by RMSDs $\leq 2.2 \text{ \AA}$ for M2TM α -carbons with respect to the initial structure¹⁶ (Tables S2–S4 in the SI). Consistent with experimental findings^{16,18} and previous observations,^{51,54} all aminoadamantane compounds pointed with their ammonium groups toward the C-terminal end as verified by angles $< 55^\circ$ (Tables S2–S4) between the vector along the C–N bond of the ligands and the normal of the membrane. The ammonium group of the ligands forms hydrogen bonds with water molecules located in the area between the ligands and His37 residues, while the adamantane core is embraced by Val27 and Ala30 side chains (see Figure 3). The distance between the center of mass of Val27 and the

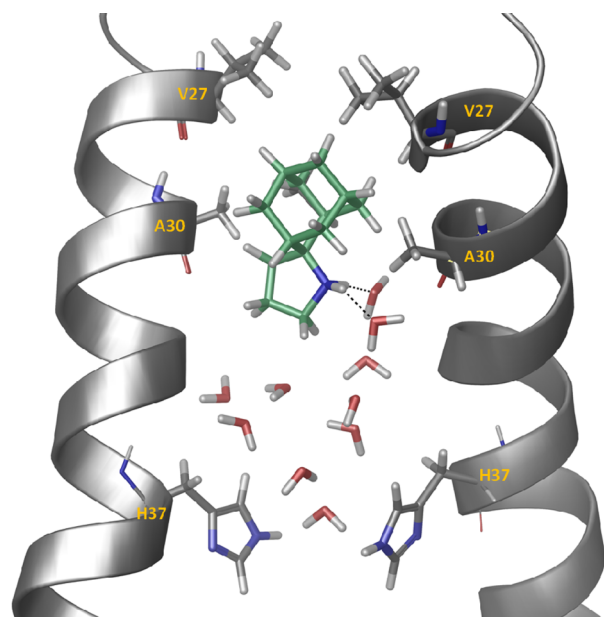


Figure 3. Representative snapshot from the simulation of ligand **8** bound to A/M2TM. Ten waters are shown between the ligand and His37 residues. Two hydrogen bonds between the ammonium group of the ligand and two water molecules are shown. Hydrogen bonding together with van der Waals interactions of the adamantane core with Val27 and Ala30 stabilize the ligand inside the pore with its ammonium group oriented toward the C-end.

adamantane core of the ligand (V27-Ad) varies between 4.0 and 4.5 Å on average, and the distance between the center of mass of Ala30 and the adamantane core of the ligand (A30-Ad) varies between 0.8 and 1.4 Å on average (Tables S2–S4). The position of the adamantane core of the ligands inside the pore differs only slightly, i.e., 0.2–0.6 Å toward the N- or C-terminal end relative to **1**. A close-up view of a snapshot from the simulation of ligand **8** is depicted in Figure 3. As expected, hydrogen bonding is more efficient for primary ammonium groups (ligands **1–7** form on average 2–3 hydrogen bonds with neighboring water molecules) than secondary (ligands **8** and **10** form 1–2 hydrogen bonds on average) and tertiary ones (ligand **9** forms one hydrogen bond) (Tables S2–S4). The distance between the center of mass of Val27 and the ammonium nitrogen of the ligand (V27-N⁺) varies between 7.1 and 8.3 Å on average^{20–22} (Tables S2–S4), with ligand **2**'s ammonium nitrogen being most displaced to the C-terminal direction. These positions are consistent with the PMF minima found when methylammonium or adamantyl-ammonium is moving along the M2TM pore axis.^{20–22} In ligands having a carbon substituent the molecule is rotated in order for the symmetric M2TM pore to accommodate the increasing alkyl group. For example, the average angle between the pore axis and C–N bond vector increases from 19.7° for **4**, 31.9° for **5**, and 26.2° for **6** to 38.9° for **7** (calculations in DMPC), and from 25.3° for **4**, 34.8° for **5**, and 40.6° for **6** to 37.3° for **7** (calculations in DPPC) as the size of the alkyl chain is increasing (Tables S2–S4). A subtle balance between hydrogen bonding and hydrophobic interactions with pore key residues, such as Val27, Ala30, and Gly34, may influence the ligand tilt inside the pore. Also, the mobility of the ligands inside the pore is in line with expectations that ligands with the largest flexible substituents, e.g., compounds **5–7** with a 2-alkyl substituent, show the highest root-mean-square fluctuations (RMSFs)

(Tables S2–S4 in the SI). The closer distances between amino acid residues in the binding region at the N-terminal end for the Weybridge-**1** complex compared to the Udorn-**1** complex may suggest a tighter complex in the former case consistent with the lower K_d of **1** against the Weybridge tetramer (Table S5); similar findings have been previously reported.⁵⁴ In a previous study, in which the (+4) state of M2TM in complex with positively charged ligands was simulated, Cl[−] ions were found to interact with the ligands;⁵¹ in our MD simulations of M2TM-ligand systems, no Cl[−] ion came inside the pore as indicated by the average Cl–N distance (Tables S2–S4). Overall, the analyses of the trajectories of the M2TM ligand complexes verified that the systems were stable and did not show any unexpected behavior.

3.3.2. Alchemical Transformations Including Chiral Ligands. In all cases, the calculated free energy changes for the alchemical transformations including the achiral compounds **1**, **3**, and **4–8** are quite close to experimental values with the biggest deviations being ~ 1 kcal mol^{−1}, which is equal to the accuracy of the method. For the Udorn/DPPC complexes the calculated free energy values for the alchemical transformations **2-R** → **1** and **2-S** → **1** were almost coincident in agreement with the ITC results which demonstrate experimentally that **2-R** and **2-S** have the same binding affinity against M2TM_{Udorn} (Table 1). For Weybridge/DPPC and Udorn/DMPC the calculated value for the transformation **2-R** → **1** differ from that of **2-S** → **1** by 0.96 and 0.87 kcal mol^{−1} respectively, which is still lower than the expected accuracy of the method. Thus, the calculation results in all systems suggest that both enantiomers of **2** bind with the same affinity to the M2TM protein.

The calculated free energy changes for the alchemical transformations **9-R** → **8** and **9-S** → **8** differ by ~ 3 and 2 kcal mol^{−1} in the case of Udorn/DPPC and Udorn/DMPC, respectively. For Weybridge, the free energies for the changes **9-R** → **8** and **9-S** → **8** differ by ~ 0.5 kcal mol^{−1}. The free energies for the alchemical transformations **10-R** → **8** and **10-S** → **8** for Udorn/DPPC and Weybridge/DPPC differ by ~ 1.5 and 1.1 kcal mol^{−1}; the calculated values are almost coincident in the case of Udorn/DMPC system. Considering that the calculations for the changes **2-R** → **1** and **2-S** → **1** against Udorn/DMPC or Weybridge/DPPC result in differences of ~ 1 kcal mol^{−1} and that **2-R** and **2-S** have experimentally the same binding affinity, these calculated differences suggest similar binding affinities also for **10-R** and **10-S**.

Since the racemic mixture **9** was measured by ITC the difference in free energy for **9** → **8** is only available experimentally and should be compared with the calculated values for the alchemical transformations **9-R** → **8** and **9-S** → **8**. Similarly, the experimental difference in free energy for **10** → **8** should be compared with the calculated values for the changes **10-R** → **8** and **10-S** → **8**. When a racemic mixture having enantiomers with different K_d 's is measured by ITC, the titration curve generally includes two steps.¹⁰⁹ If the K_d 's of the two enantiomers are similar (i.e., less than 50-fold different) then the experiment gives a major sigmoidal titration curve in the first step that is determined by the average of the binding affinities of the racemate.¹⁰⁹ The second step is determined mainly by the binding constant of the stronger binder replacing the weak binder and is only indicated at the end of the curve (see Figure 1e in ref 109). In the case of the racemic mixtures of compounds **9** and **10**, the second step of the titration curve is barely visible suggesting small differences in affinity between

enantiomers as described above. The measurement of the K_d of the racemic mixture was based on the main sigmoidal titration curve, and the mean of the computed values $9-R \rightarrow 8$ and $9-S \rightarrow 8$ was used for comparison with the experimental relative free energy of binding for $9 \rightarrow 8$.^{109,123} Similarly, the mean of the free energy values for $10-R \rightarrow 8$ and $10-S \rightarrow 8$ was used for comparison with the experimental ITC free energy measured for the change $10 \rightarrow 8$ (Tables 2 and 3 bold values).

3.3.3. Accuracy of the Free Energy Calculations. When the computed relative binding free energies are compared to experimental binding affinities (Tables 2 and 3) the correlation coefficient found for aminoadamantanes binding to M2TM_{Udorn} with DPPC was $R^2 = 0.58$ (Figure 4A; $p < 0.05$). This is a fair correlation as the range spanned by relative binding free energies from experiment is only ~ 2 kcal mol⁻¹, which is close to the accuracy limits of rigorous free energy calculations.^{55–57} Taking into account the error in the experiments of < 0.43 kcal mol⁻¹ and statistical errors in the calculations of 0.10 – 0.66 kcal mol⁻¹, this correlation coefficient is close to, or in the case of the DMPC model system, well above (Figure 4B; $R^2 = 0.85$, $p < 0.001$) the optimal correlation coefficient that can be expected in such a case.¹²⁴ The predictive index (PI) of Pearlman,¹⁰³ a measure for the correctness of the relative ranking of ligands according to binding free energy, was satisfactory for both M2TM_{Udorn} with DPPC bilayer (PI = 0.68) and M2TM_{Udorn} with DMPC bilayer (PI = 0.74). Thus, the M2TM_{Udorn}/DMPC model system overall showed a better performance than the M2TM_{Udorn}/DPPC model system. This can possibly be attributed to the fact that DMPC acyl chains are shorter by two methylenes compared to DPPC and thus the DMPC lipids resemble more closely the DPC lipids used in the experiments. This emphasizes the importance to use models for binding free energy calculations that reproduce experimental conditions as closely as possible.

For M2TM_{Weybridge} in DPPC bilayers, a lower correlation ($R^2 = 0.24$, $p = 0.27$, Figure 4C) was found between seven experimental and computed relative binding free energies. This is not the result of a few outliers but due to overall more scattered data points. A PI = 0.1 indicates an almost random ranking of the compounds by relative binding affinity. Among various factors that can contribute to the deterioration of the correlation, the lack of an experimental structure and the use of a M2TM_{Weybridge} model structure created by mutating the M2TM_{Udorn} structure could lead to the inaccuracies. We did not perform further calculations using DMPC, and this data set can be considered a limiting case for M2TM-ligand systems beyond which the BAR method does not provide acceptable ligand rankings by relative binding free energies.

The root-mean-square deviations (RMSDs) between experimental and computed relative binding free energies of the two M2TM_{Udorn} data sets are 0.73 and 0.94 kcal mol⁻¹ with DPPC and DMPC respectively; these RMSDs are below chemical accuracy (1 kcal mol⁻¹)^{55–57} and about two times larger than the experimental errors. Obtaining such low RMSD values is considered optimal according to recent performance studies on rigorous binding free energy calculations.^{63,113,125}

Chemical accuracy of 1 kcal mol⁻¹ is considered to be the limit for a deviation of computed from experimental values. The most significant deviations of computed from experimental relative binding free energies were observed for the transformations $10 \rightarrow 8$ for M2TM_{Udorn}/DPPC (1.27 kcal mol⁻¹); $2 \rightarrow 1$ (1.08 kcal mol⁻¹) and $7 \rightarrow 6$ (1.51 kcal mol⁻¹) for M2TM_{Weybridge}/DPPC; $2-S \rightarrow 1$ for M2TM_{Udorn}/DMPC

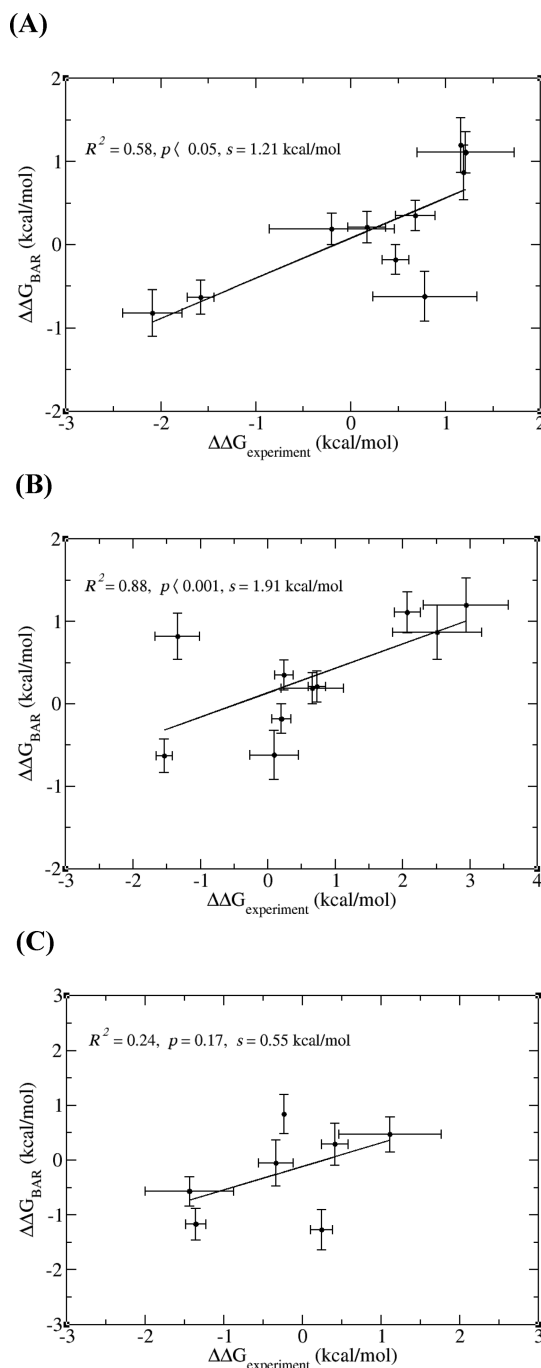


Figure 4. Relative binding free energies computed by the BAR approach ($\Delta\Delta G_{\text{BAR}}$) plotted against relative binding free energies derived from ITC data ($\Delta\Delta G_{\text{experiment}}$) for M2TM_{Udorn} embedded in a DPPC bilayer (A), M2TM_{Udorn} embedded in a DMPC bilayer (B), and M2TM_{Weybridge} embedded in a DPPC bilayer (C). The correlation lines obtained by a linear least-squares fit including all data points are shown (solid, black line). Maximal errors in $\Delta\Delta G_{\text{BAR}}$ and $\Delta\Delta G_{\text{experiment}}$ are shown as error bars along the vertical and horizontal axes, respectively. In each panel the squared correlation coefficient (R^2), the p value, and the slope (s) of the least-squares fit line is included.

(1.74 kcal mol⁻¹). All transformations between compounds involving linear alkyl chains, e.g., $7 \rightarrow 6$, generally resulted in small deviations, in agreement with previous findings.⁶³ Only in the case of M2TM_{Weybridge} was the $7 \rightarrow 6$ transformation among

those with a deviation >1 kcal mol⁻¹ from the experimental relative binding free energies.

The prediction of relative binding free energies for M2TM_{Udom} were highly satisfactory for the DMPC bilayer model system. This demonstrates that binding free energy calculations by the BAR approach can be used to predict relative binding affinities of aminoadamantane derivatives toward M2TM under high pH conditions with good accuracy. Thus, these calculations may help in the prediction of the potency of new inhibitors against WT influenza A virus prior to synthesis.

4. CONCLUSION

Influenza A viruses can be occasionally transmitted from wild birds to humans and may give rise to devastating pandemics. Adamantane derivatives such as compounds **1** and **2** are a main category of antivirals and also the main class of A/M2TM blockers. The structural basis of their interaction has been investigated through crystallographic, ssNMR, and simulation methods. Due to resistance of human influenza A viruses to **1** and **2**, there is an urgent need for novel A/M2TM inhibitors. Developing computational methods for predicting binding affinities of whole series of M2 aminoadamantane inhibitors could assist in the development of novel potent inhibitors that overcome A/M2 resistance. In a previous work a high correlation was obtained between computed FEP/MD binding free energies using the BAR method for a series of aminoadamantane ligands against M2TM in the low pH, open state.⁵¹ The relative binding affinities used as experimental probes were measured against full length M2 protein and the range of binding constants was about three orders.⁵³ In this work both simulations and experiments were applied using M2TM at high pH conditions. The affinities of aminoadamantane derivatives with subtle changes in structure binding to M2TM_{Udom} and M2TM_{Weybridge} under high pH conditions were determined by isothermal titration calorimetry (ITC). The effect of the ligand chirality was considered in the simulations, and the accuracy of the predictions was checked through measurement of the binding affinities of the enantiomers 2-*R*, 2-*S* and racemic mixture **2** against M2TM_{Udom}. The binding constants of rimantadine enantiomers against M2TM_{Udom} were measured for the first time and found to be equal although it has just been suggested that 2-*R* and 2-*S* affect different isotropic chemical shift changes when bound to the full M2 protein measured using ssNMR.¹¹² Two series of alchemical free energy calculations were performed using M2TM_{Udom} in DPPC and DMPC lipids to mimic the membrane environment. It was found that alchemical free energy calculations of ligand binding are valuable for determining the relative binding potency of A/M2 inhibitors of the aminoadamantane type against the M2TM_{Udom} tetramer covering a binding affinity range of only ~ 2 kcal mol⁻¹. A fair correlation ($R^2 = 0.58$, $p < 0.05$, $PI = 0.68$) was found for DPPC and a high correlation for DMPC ($R^2 = 0.88$, $p < 0.001$, $PI = 0.74$) between experimental and computed relative binding free energies. This result is most likely due to the fact that DMPC is structurally closer to DPC. For M2TM_{Weybridge} in DPPC bilayers, the calculations failed to provide a satisfying correlation, likely due to the lack of an experimental structure to model M2TM_{Weybridge} complexes.

■ ASSOCIATED CONTENT

Supporting Information

The Supporting Information is available free of charge on the ACS Publications website at DOI: 10.1021/acs.jcim.6b00079.

Computational and experimental protocols, as well as six tables and one figure showing experimental data or detailed computational analyses (PDF)

■ AUTHOR INFORMATION

Corresponding Authors

*Mailing address: Panepistimioupolis–Zografou, 15771 Athens, Greece. Phone: (+301) 210-7274834. Fax: (+301) 210 727 4747. E-Mail: ankol@pharm.uoa.gr (A.K.).

*Mailing address: Universitätsstr. 1, 40225 Düsseldorf, Germany. Phone: (+49) 211 81 13662. Fax: (+49) 211 81 13847. E-mail: gohlke@uni-duesseldorf.de (H.G.).

*Mailing address: Biomedical Research Foundation, Academy of Athens, 4 Soranou Ephessiou, 11527 Athens, Greece. E-Mail: zcournia@bioacademy.gr (Z.C.).

Present Addresses

□EaStCHEM School of Chemistry, University of Edinburgh, The King's Buildings, Edinburgh, EH9 3FJ, United Kingdom.

◇Pharmaceutical and Medicinal Chemistry, Institute of Pharmacy and Food Chemistry, Julius-Maximilians-Universität Würzburg, Am Hubland, 97074 Würzburg, Germany.

▲Drug Discovery Unit, Division of Biological Chemistry and Drug Discovery, School of Life Sciences, University of Dundee, Sir James Black Centre, DD1 5EH, United Kingdom.

●Sanofi R&D, LGCR, Structure Design and Informatics/Computer-aided Drug Design, 1 Avenue Pierre Brossolette, 91385, Chilly-Mazarin, France.

○Division of Radiopharmaceutical Chemistry, DKFZ Deutsches Krebsforschungszentrum, German Cancer Research Center, Im Neuenheimer Feld 280, 69121 Heidelberg, Germany.

Author Contributions

△Z.C., H.G., and A.K. share senior authorship.

Notes

The authors declare no competing financial interest.

■ ACKNOWLEDGMENTS

This research includes parts of the Master theses of H.I. (synthesis of peptides and FEP calculations using DPPC) and A.D. (FEP calculations using DMPC) and part of the Ph.D. work of C.T. (synthesis of ligand **10**, FEP calculations including enantiomeric forms). We are grateful to the Deutscher Akademischer Austauschdienst (DAAD) for funds to N.H. and H.G. (grant no.: 56538846), Chiesi Hellas for supporting the Ph.D. work of C.T., and the project IKYDA 2013 (a collaborative project between Greek State Scholarships Foundation and DAAD) which supported the exchange of researchers (H.I., A.D., C.T., N.H.) between the laboratories of A.K. and H.G.

■ REFERENCES

- (1) Wang, C.; Takeuchi, K.; Pinto, L. H.; Lamb, R. A. Ion Channel Activity of Influenza A Virus M2 Protein: Characterization of the Amantadine Block. *J. Virol.* **1993**, *67*, 5585–5594.
- (2) Chizhnikov, I. V.; Geraghty, F. M.; Ogden, D. C.; Hayhurst, A.; Antoniou, M.; Hay, A. J. Selective Proton Permeability and pH Regulation of The Influenza Virus M2 Channel Expressed In Mouse Erythroleukaemia Cells. *J. Physiol.* **1996**, *494*, 329–336.

- (3) Hayden, F. G. Clinical Applications of Antiviral Agents for Chemoprophylaxis and Therapy of Respiratory Viral Infections. *Antiviral Res.* **1985**, *5*, 229–239.
- (4) Wang, C.; Lamb, R. A.; Pinto, L. H. Activation of the M2 Ion Channel of Influenza Virus: a Role for the Transmembrane Domain Histidine Residue. *Biophys. J.* **1995**, *69*, 1363–1371.
- (5) Helenius, A. Unpacking the Incoming Influenza Virus. *Cell* **1992**, *69*, 577–578.
- (6) Tang, Y.; Zaitseva, F.; Lamb, R. A.; Pinto, L. H. The Gate of the Influenza Virus M2 Proton Channel is Formed by a Single Tryptophan Residue. *J. Biol. Chem.* **2002**, *277*, 39880–39886.
- (7) Hu, F.; Luo, W.; Hong, M. Mechanisms of Proton Conduction and Gating in Influenza M2 Proton Channels from Solid-State NMR. *Science* **2010**, *330*, 505–508.
- (8) Pinto, L. H.; Dieckmann, G. R.; Gandhi, C. S.; Papworth, C. G.; Braman, J.; Shaughnessy, M. A.; Lear, J. D.; Lamb, R. A.; DeGrado, W. F. A Functionally Defined Model for the M2 Proton Channel of Influenza A Virus Suggests a Mechanism for its Ion Selectivity. *Proc. Natl. Acad. Sci. U. S. A.* **1997**, *94*, 11301–11306.
- (9) Wang, J.; Qiu, J. X.; Soto, C.; DeGrado, W. F. Structural and Dynamic Mechanisms for the Function and Inhibition of the M2 Proton Channel from Influenza A Virus. *Curr. Opin. Struct. Biol.* **2011**, *21*, 68–80.
- (10) Salom, D.; Hill, B. R.; Lear, J. D.; DeGrado, W. F. pH-Dependent Tetramerization and Amantadine Binding of the Transmembrane Helix of M2 from the Influenza A Virus. *Biochemistry* **2000**, *39*, 14160–14170.
- (11) Ma, C.; Polishchuk, A. L.; Ohigashi, Y.; Stouffer, A. L.; Schön, A.; Magavern, E.; Jing, X.; Lear, J. D.; Freire, E.; Lamb, R. A.; DeGrado, W. F.; Pinto, L. H. Identification of the Functional Core of the Influenza A Virus A/M2 Proton-Selective Ion Channel. *Proc. Natl. Acad. Sci. U. S. A.* **2009**, *106*, 12283–12288.
- (12) Hay, A. J.; Wolstenholme, A. J.; Skehel, J. J.; Smith, M. H. The Molecular Basis of the Specific Anti-Influenza Action of Amantadine. *EMBO J.* **1985**, *4*, 3021–3024.
- (13) Balannik, V.; Carnevale, V.; Fiorin, G.; Levine, B. G.; Lamb, R. A.; Klein, M. L.; DeGrado, W. F.; Pinto, L. H. Functional Studies and Modeling of Pore-Lining Residue Mutants of the Influenza A Virus M2 Ion Channel. *Biochemistry* **2010**, *49*, 696–708.
- (14) Hu, J.; Fu, R.; Cross, T. A. The chemical and Dynamical Influence of the Anti-Viral Drug Amantadine on the M2 Proton Channel Transmembrane Domain. *Biophys. J.* **2007**, *93*, 276–283.
- (15) Stouffer, A. L.; Acharya, R.; Salom, D.; Levine, A. S.; Di Costanzo, L.; Soto, C. S.; Tereshko, V.; Nanda, V.; Stayrook, S.; DeGrado, W. F. Structural Basis for the Function and Inhibition of an Influenza Virus Proton Channel. *Nature* **2008**, *451*, 596–599.
- (16) Cady, S. D.; Schmidt-Rohr, K.; Wang, J.; Soto, C. S.; DeGrado, W. F.; Hong, M. Structure of the Amantadine Binding Site of Influenza M2 Proton Channels in Lipid Bilayers. *Nature* **2010**, *463*, 689–692.
- (17) Pielak, R. M.; Oxenoid, K.; Chou, J. J. Structural Investigation of Rimantadine Inhibition of the AM2-BM2 Chimera Channel of Influenza Viruses. *Structure* **2011**, *19*, 1655–1663.
- (18) Cady, S. D.; Wang, J.; Wu, Y.; DeGrado, W. F.; Hong, M. Specific Binding of Adamantane Drugs and Direction of their Polar Amines in the Pore of the Influenza M2 Transmembrane Domain in Lipid Bilayers and Dodecylphosphocholine Micelles Determined by NMR Spectroscopy. *J. Am. Chem. Soc.* **2011**, *133*, 4274–4284.
- (19) Luo, W.; Hong, M. Conformational Changes of an Ion Channel Detected through Water-Protein Interactions Using Solid-State NMR Spectroscopy. *J. Am. Chem. Soc.* **2010**, *132*, 2378–2384.
- (20) Gianti, E.; Carnevale, V.; DeGrado, W. F.; Klein, M. L.; Fiorin, G. Hydrogen-Bonded Water Molecules in the M2 Channel of the Influenza A Virus Guide the Binding Preferences of Ammonium-Based Inhibitors. *J. Phys. Chem. B* **2015**, *119*, 1173–1183.
- (21) Gleed, M. L.; Busath, D. D. Why Bound Amantadine Fails to Inhibit Proton Conductance According to Simulations of the Drug-Resistant Influenza A M2 (S31N). *J. Phys. Chem. B* **2015**, *119*, 1225–1231.
- (22) Gleed, M. L.; Ioannidis, H.; Kolocouris, A.; Busath, D. D. Resistance-Mutation (N31) Effects on Drug Orientation and Channel Hydration in Amantadine-Bound Influenza A M2. *J. Phys. Chem. B* **2015**, *119*, 11548–11559.
- (23) Hu, F.; Schmidt-Rohr, K.; Hong, M. NMR Detection of pH-Dependent Histidine-Water Proton Exchange Reveals the Conduction Mechanism of a Transmembrane Proton Channel. *J. Am. Chem. Soc.* **2012**, *134*, 3703–3713.
- (24) Cochran, K. W.; Maassab, H. F.; Tsunoda, A.; Berlin, B. S. Studies on the Antiviral Activity of Amantadine Hydrochloride. *Ann. N. Y. Acad. Sci.* **1965**, *130*, 432–439.
- (25) Appleyard, G. Amantadine-Resistance as a Genetic Marker for Influenza Viruses. *J. Gen. Virol.* **1977**, *36*, 249–255.
- (26) Oxford, J. S.; Potter, C. W.; Logan, I. S. Passage of Influenza Strains in the Presence of Amino-Adamantane. *Ann. N. Y. Acad. Sci.* **1970**, *173*, 300–313.
- (27) Hayden, F. G.; Sperber, S. J.; Belshe, R. B.; Clover, R. D.; Hay, A. J.; Pyke, S. Recovery of Drug-Resistant Influenza A Virus During Therapeutic Use of Rimantadine. *Antimicrob. Agents Chemother.* **1991**, *35*, 1741–1747.
- (28) Bright, R. A.; Medina, M. J.; Xu, X.; Perez-Orozco, G.; Wallis, T. R.; Davis, X. M.; Povinelli, L.; Cox, N. J.; Klimov, A. I. Incidence of Adamantane Resistance among Influenza A (H3N2) Viruses Isolated Worldwide from 1994 to 2005: A Cause for Concern. *Lancet* **2005**, *366*, 1175–1181.
- (29) Bright, R. A.; Shay, D. K.; Shu, B.; Cox, N. J.; Klimov, A. I. Adamantane Resistance Among Influenza A Viruses Isolated Early During the 2005–2006 Influenza Season in the United States. *J. Am. Med. Assoc.* **2006**, *295*, 891–894.
- (30) Lan, Y.; Zhang, Y.; Dong, L.; Wang, D.; Huang, W.; Xin, L.; Yang, L.; Zhao, X.; Li, Z.; Wang, W.; Li, X.; Xu, C.; Guo, J.; Wang, M.; Peng, Y.; Gao, Y.; Guo, Y.; Wen, L.; Jiang, T.; Shu, Y.; Yang, L. A Comprehensive Surveillance of Adamantane Resistance Among Human Influenza A Virus Isolated from Mainland China Between 1956 and 2009. *Antiviral Ther.* **2010**, *15*, 853–859.
- (31) High Levels of Adamantane Resistance Among Influenza A (H3N2) Viruses and Interim Guidelines for Use of Antiviral Agents—United States, 2005–06 Influenza Season. *MMWR Morb. Mortal Wkly Rep.* **2006**; Vol. 55, pp 44–46.
- (32) Kolocouris, N.; Foscolos, G. B.; Kolocouris, A.; Marakos, P.; Pouli, N.; Fytas, G.; Ikeda, S.; De Clercq, E. Synthesis and Antiviral Activity Evaluation of Some Aminoadamantane Derivatives. *J. Med. Chem.* **1994**, *37*, 2896–2902.
- (33) Stylianakis, I.; Kolocouris, A.; Kolocouris, N.; Fytas, G.; Foscolos, G. B.; Padalko, E.; Neyts, J.; De Clercq, E. Spiro[pyrrolidine-2,2'-adamantanes]: Synthesis, Anti-Influenza Virus Activity and Conformational Properties. *Bioorg. Med. Chem. Lett.* **2003**, *13*, 1699–1703.
- (34) Kolocouris, A.; Tzitzoglaki, C.; Johnson, F. B.; Zell, R.; Wright, A. K.; Cross, T. A.; Tietjen, I.; Fedida, D.; Busath, D. D. Aminoadamantanes with Persistent in Vitro Efficacy Against H1N1 (2009) Influenza A. *J. Med. Chem.* **2014**, *57*, 4629–4639.
- (35) Webster, R. G.; Bean, W. J.; Gorman, O. T.; Chambers, T. M.; Kawaoka, Y. Evolution and Ecology of Influenza A Viruses. *Microbiol. Rev.* **1992**, *56*, 152–179.
- (36) Astrahan, P.; Arkin, I. T. Resistance Characteristics of Influenza to Amino-Adamantyls. *Biochim. Biophys. Acta, Biomembr.* **2011**, *1808*, 547–553.
- (37) Stouffer, A. L.; Ma, C.; Cristian, L.; Ohigashi, Y.; Lamb, R. A.; Lear, J. D.; Pinto, L. H.; DeGrado, W. F. The Interplay of Functional Tuning, Drug Resistance, and Thermodynamic Stability in the Evolution of the M2 Proton Channel from the Influenza A Virus. *Structure* **2008**, *16*, 1067–1076.
- (38) Stouffer, A. L.; Nanda, V.; Lear, J. D.; DeGrado, W. F. Sequence Determinants of a Transmembrane Proton Channel: An Inverse Relationship between Stability and Function. *J. Mol. Biol.* **2005**, *347*, 169–179.

- (39) Yi, M.; Cross, T. A.; Zhou, H.-X. Conformational Heterogeneity of the M2 Proton Channel and a Structural Model for Channel Activation. *Proc. Natl. Acad. Sci. U. S. A.* **2009**, *106*, 13311–13316.
- (40) Khurana, E.; Devane, R. H.; Dal Peraro, M.; Klein, M. L. Computational Study of Drug Binding to the Membrane-Bound Tetrameric M2 Peptide Bundle from Influenza A Virus. *Biochim. Biophys. Acta, Biomembr.* **2011**, *1808*, 530–537.
- (41) Qin, G.; Yu, K.; Shi, T.; Luo, C.; Li, G.; Zhu, W.; Jiang, H. How Does Influenza Virus A Escape from Amantadine? *J. Phys. Chem. B* **2010**, *114*, 8487–8493.
- (42) Leonov, H.; Astrahan, P.; Krugliak, M.; Arkin, I. T. How Do Aminoadamantanes Block the Influenza M2 Channel, and How Does Resistance Develop? *J. Am. Chem. Soc.* **2011**, *133*, 9903–9911.
- (43) Alhadeff, R.; Assa, D.; Astrahan, P.; Krugliak, M.; Arkin, I. T. Computational and Experimental Analysis of Drug Binding to the Influenza M2 Channel. *Biochim. Biophys. Acta, Biomembr.* **2014**, *1838*, 1068–1073.
- (44) Gu, R.-X.; Liu, L. A.; Wei, D. Q.; Du, J. G.; Liu, L.; Liu, H. Free Energy Calculations on the two Drug Binding Sites in the M2 Proton Channel. *J. Am. Chem. Soc.* **2011**, *133*, 10817–10825.
- (45) Gu, R.-X.; Liu, L. A.; Wang, Y.-H.; Xu, Q.; Wei, D.-Q. Structural Comparison of the Wild-Type and Drug-Resistant Mutants of the Influenza A M2 Proton Channel by Molecular Dynamics Simulations. *J. Phys. Chem. B* **2013**, *117*, 6042–6051.
- (46) Wang, J.; Ma, C.; Fiorin, G.; Carnevale, V.; Wang, T.; Hu, F.; Lamb, R. A.; Pinto, L. H.; Hong, M.; Klein, M. L.; DeGrado, W. F. Molecular Dynamics Simulation Directed Rational Design of Inhibitors Targeting Drug-Resistant Mutants of Influenza A Virus M2. *J. Am. Chem. Soc.* **2011**, *133*, 12834–12841.
- (47) Wang, J.; Wu, Y.; Ma, C.; Fiorin, G.; Wang, J.; Pinto, L. H.; Lamb, R. A.; Klein, M. L.; DeGrado, W. F. Structure and Inhibition of the Drug-Resistant S31N Mutant of the M2 Ion Channel of Influenza A Virus. *Proc. Natl. Acad. Sci. U. S. A.* **2013**, *110*, 1315–1320.
- (48) Intharathap, P.; Laohpongspaisan, C.; Rungrotmongkol, T.; Loisuangsinsin, A.; Malaisree, M.; Decha, P.; Aruksakunwong, O.; Chuenpennit, K.; Kaiyawet, N.; Sompornpisut, P.; Pianwanit, S.; Hannongbua, S. How Amantadine and Rimantadine Inhibit Proton Transport in the M2 Protein Channel. *J. Mol. Graphics Modell.* **2008**, *27*, 342–348.
- (49) Intharathap, P.; Rungrotmongkol, T.; Decha, P.; Nunthaboot, N.; Kaiyawet, N.; Kerdcharoen, T.; Sompornpisut, P.; Hannongbua, S. Evaluating How Rimantadines Control the Proton Gating of the Influenza A M2-Proton Port via Allosteric Binding Outside of the M2-Channel: MD Simulations. *J. Enzyme Inhib. Med. Chem.* **2011**, *26*, 162–168.
- (50) Laohpongspaisan, C.; Rungrotmongkol, T.; Intharathap, P.; Malaisree, M.; Decha, P.; Aruksakunwong, O.; Sompornpisut, P.; Hannongbua, S. Why Amantadine Loses Its Function in Influenza M2Mutants: MD Simulations. *J. Chem. Inf. Model.* **2009**, *49*, 847–852.
- (51) Gkeka, P.; Eleftheratos, S.; Kolocouris, A.; Cournia, Z. Free Energy Calculations Reveal the Origin of Binding Preference for Aminoadamantane Blockers of Influenza A/M2TM Pore. *J. Chem. Theory Comput.* **2013**, *9*, 1272–1281.
- (52) Homeyer, N.; Gohlke, H. Extension of the Free Energy Workflow FEW Towards Implicit Solvent/Implicit Membrane MM-PBSA Calculations. *Biochim. Biophys. Acta, Gen. Subj.* **2015**, *1850*, 972–982.
- (53) Eleftheratos, S.; Spearpoint, P.; Ortore, G.; Kolocouris, A.; Martinelli, A.; Martin, S.; Hay, A. Interaction of Aminoadamantane Derivatives with the Influenza A Virus M2 Channel-Docking Using a Pore Blocking Model. *Bioorg. Med. Chem. Lett.* **2010**, *20*, 4182–4187.
- (54) Homeyer, N.; Ioannidis, H.; Kolarov, F.; Gauglitz, G.; Zikos, C.; Kolocouris, A.; Gohlke, H. Interpreting Thermodynamic Profiles of Aminoadamantane Compounds Inhibiting the M2 Proton Channel of Influenza A by Free Energy Calculations. *J. Chem. Inf. Model.* **2016**, *56*, 110–126.
- (55) Bennett, C. H. Efficient Estimation of Free Energy Differences from Monte Carlo Data. *J. Comput. Phys.* **1976**, *22*, 245–268.
- (56) Chipot, C.; Pohorille, A. *Free Energy Calculations. Theory and Applications in Chemistry and Biology*; Springer Verlag: Berlin, NY, 2007.
- (57) Pohorille, A.; Jarzynski, C.; Chipot, C. Good Practices in Free-Energy Calculations. *J. Phys. Chem. B* **2010**, *114*, 10235–10253.
- (58) Michel, J.; Essex, J. W. Prediction of Protein-Ligand Binding Affinity by Free Energy Simulations: Assumptions, Pitfalls and Expectations. *J. Comput.-Aided Mol. Des.* **2010**, *24*, 639–658.
- (59) Jorgensen, W. L. Efficient Drug Lead Discovery and Optimization. *Acc. Chem. Res.* **2009**, *42*, 724–733.
- (60) Acevedo, O.; Ambrose, Z.; Flaherty, P. T.; Aamer, H.; Jain, P.; Sambasivarao, S. V. Identification of HIV Inhibitors Guided by Free Energy Perturbation Calculations. *Curr. Pharm. Des.* **2012**, *18*, 1199–1216.
- (61) Baggett, A. W.; Cournia, Z.; Han, M. S.; Patargias, G.; Glass, A. C.; Liu, S. Y.; Nolen, B. J. Structural Characterization and Computer-Aided Optimization of a Small-Molecule Inhibitor of the Arp2/3 Complex, a Key Regulator of the Actin Cytoskeleton. *ChemMedChem* **2012**, *7*, 1286–1294.
- (62) Hare, A. A.; Leng, L.; Gandavadi, S.; Du, X.; Cournia, Z.; Bucala, R.; Jorgensen, W. L. Optimization of N-benzyl-benzoxazol-2-ones as Receptor Antagonists of Macrophage Migration Inhibitory Factor (MIF). *Bioorg. Med. Chem. Lett.* **2010**, *20*, 5811–5814.
- (63) Mikulskis, P.; Genheden, S.; Ryde, U. A Large-Scale Test of Free-Energy Simulation Estimates of Protein-Ligand Binding Affinities. *J. Chem. Inf. Model.* **2014**, *54*, 2794–2806.
- (64) Hansen, R. K.; Broadhurst, R. W.; Skelton, P. C.; Arkin, I. T. Hydrogen/Deuterium Exchange of Hydrophobic Peptides in Model Membranes by Electrospray Ionization Mass Spectrometry. *J. Am. Soc. Mass Spectrom.* **2002**, *13*, 1376–1387.
- (65) Kolocouris, A.; Zikos, C.; Broadhurst, R. W. ¹⁹F NMR Detection of the Complex Between Amantadine and the Receptor Portion of the Influenza A M2 Ion Channel in DPC Micelles. *Bioorg. Med. Chem. Lett.* **2007**, *17*, 3947–3952.
- (66) Wiseman, T.; Williston, S.; Brandts, J. F.; Lin, L. N. Rapid Measurement of Binding Constants and Heats of Binding Using a New Titration Calorimeter. *Anal. Biochem.* **1989**, *179*, 131–137.
- (67) Doyle, M. L. Characterization of Binding Interactions by Isothermal Titration Calorimetry. *Curr. Opin. Biotechnol.* **1997**, *8*, 31–35.
- (68) *Origin 8.1G SRI*, v8.1.13.88; OriginLab Corporation, Northampton, MA, USA, 2009.
- (69) Ladbury, J. E.; Klebe, G.; Freire, E. Adding Calorimetric Data to Decision Making in Lead Discovery: a Hot Tip. *Nat. Rev. Drug Discovery* **2010**, *9*, 23–27.
- (70) Chaires, J. B. Calorimetry and Thermodynamics in Drug Design. *Annu. Rev. Biophys.* **2008**, *37*, 135–151.
- (71) Perozzo, R.; Folkers, G.; Scapozza, L. Thermodynamics of Protein-Ligand Interactions: History, Presence, and Future Aspects. *J. Recept. Signal Transduction Res.* **2004**, *24*, 1–52.
- (72) Rod, T. H.; Brooks, C. L., III How Dihydrofolate Reductase Facilitates Protonation of Dihydrofolate. *J. Am. Chem. Soc.* **2003**, *125*, 8718–8719.
- (73) Case, D. A.; Darden, T. A.; Cheatham, T. E., III; Simmerling, C. L.; Wang, J.; Duke, R. E.; Luo, R.; Walker, R. C.; Zhang, W.; Merz, K. M.; Roberts, B.; Hayik, S.; Roitberg, A.; Seabra, G.; Swails, J.; Götz, A. W.; Kolossváry, I.; Wong, K. F.; Paesani, F.; Vanicek, J.; Wolf, R. M.; Liu, J.; Wu, X.; Brozell, S. R.; Steinbrecher, T.; Gohlke, H.; Cai, Q.; Ye, X.; Wang, J.; Hsieh, M.-J.; G, C.; Roe, D. R.; Mathews, D. H.; G, S. M.; Salomon-Ferrer, R.; Sagui, C.; Babin, V.; Luchko, T.; Gusarov, S.; Kovalenko, A.; Kollman, P. A. *Amber12*; University of California, San Francisco, 2012.
- (74) Ryckaert, J.-P.; Ciccotti, G.; Berendsen, H. J. C. Numerical Integration of the Cartesian Equations of Motion of a System With Constraints: Molecular Dynamics of n-Alkanes. *J. Comput. Phys.* **1977**, *23*, 327–341.
- (75) Darden, T.; York, D.; Pedersen, L. Particle Mesh Ewald: An N log(N) Method for Ewald Sums in Large Systems. *J. Chem. Phys.* **1993**, *98*, 10089–10092.

- (76) Essmann, U.; Perera, L.; Berkowitz, M. L.; Darden, T.; Lee, H.; Pedersen, L. G. A Smooth Particle Mesh Ewald Method. *J. Chem. Phys.* **1995**, *103*, 8577–8593.
- (77) Zwanzig, R. W. High-Temperature Equation of State by a Perturbation Method. I. Nonpolar Gases. *J. Chem. Phys.* **1954**, *22*, 1420–1426.
- (78) Brandsdal, B. O.; Österberg, F.; Almlöf, M.; Feierberg, I.; Luzhkov, V. B.; Åqvist, J. Free Energy Calculations and Ligand Binding. *Adv. Protein Chem.* **2003**, *66*, 123–158.
- (79) Gilson, M. K.; Sharp, K. A.; Honig, B. H. Calculating the Electrostatic Potential of Molecules in Solution: Method and Error Assessment. *J. Comput. Chem.* **1988**, *9*, 327–335.
- (80) Honig, B.; Nicholls, A. Classical Electrostatics in Biology and Chemistry. *Science* **1995**, *268*, 1144–1149.
- (81) Sitkoff, D.; Sharp, K. A.; Honig, B. Accurate Calculation of Hydration Free Energies Using Macroscopic Solvent Models. *J. Phys. Chem.* **1994**, *98*, 1978–1988.
- (82) Kuriyan, J.; Konforti, B.; Wemmer, D. *The Molecules of Life: Physical and Chemical Principles*; Garland Science, Taylor & Francis group, LLC: New York, NY, USA, 2013.
- (83) *Desmond Molecular Dynamics System*, version 3.0; D. E. Shaw Research: New York, NY, 2012.
- (84) Bowers, K. J.; Chow, E.; Xu, H.; Dror, R. O.; Eastwood, M. P.; Gregersen, B. A.; Klepeis, J. L.; Kolossvary, I.; Moraes, M. A.; Sacerdoti, F. D.; Salmon, J. K.; Shan, Y.; Shaw, D. E. Scalable Algorithms for Molecular Dynamics Simulations on Commodity Clusters. In *Proceedings of the ACM/IEEE Conference on Supercomputing (SC06)*, Tampa, Florida, 2006.
- (85) *Maestro-Desmond Interoperability Tools*, version 3.1; Schrodinger: New York, NY, 2012.
- (86) *Maestro*, version 8.5; Schrodinger, Inc.: New York, NY, 2008.
- (87) Halgren, T. A. Merck molecular force field. V. Extension of MMFF94 Using Experimental Data, Additional Computational Data, and Empirical Rules. *J. Comput. Chem.* **1996**, *17*, 616–641.
- (88) Halgren, T. A. MMFF VII. Characterization of MMFF94, MMFF94s, and Other Widely Available Force fields for Conformational Energies and for Intermolecular-Interaction Energies and Geometries. *J. Comput. Chem.* **1999**, *20*, 730–748.
- (89) Jones, G.; Willett, P.; Glen, R. C.; Leach, A. R.; Taylor, R. Development and Validation of a Genetic Algorithm for Flexible Docking. *J. Mol. Biol.* **1997**, *267*, 727–748.
- (90) Verdonk, M. L.; Chessari, G.; Cole, J. C.; Hartshorn, M. J.; Murray, C. W.; Nissink, J. W.; Taylor, R. D.; Taylor, R. Modeling Water Molecules in Protein-Ligand Docking Using GOLD. *J. Med. Chem.* **2005**, *48*, 6504–6515.
- (91) Korb, O.; Stützel, T.; Exner, T. E. Empirical Scoring Functions for Advanced Protein-Ligand Docking with PLANTS. *J. Chem. Inf. Model.* **2009**, *49*, 84–96.
- (92) Mooij, W. T.; Verdonk, M. L. General and Targeted Statistical Potentials for Protein-Ligand Interactions. *Proteins: Struct., Funct., Genet.* **2005**, *61*, 272–287.
- (93) Pettersen, E. F.; Goddard, T. D.; Huang, C. C.; Couch, G. S.; Greenblatt, D. M.; Meng, E. C.; Ferrin, T. E. UCSF Chimera—A Visualization System for Exploratory Research and Analysis. *J. Comput. Chem.* **2004**, *25*, 1605–1612.
- (94) Jorgensen, W. L.; Chandrasekhar, J.; Madura, J. D.; Impey, R. W.; Klein, M. L. Comparison of Simple Potential Functions for Simulating Liquid Water. *J. Chem. Phys.* **1983**, *79*, 926–935.
- (95) Jorgensen, W. L.; Maxwell, D. S.; Tirado-Rives, J. Development and Testing of the OPLS All-Atom Force Field on Conformational Energetics and Properties of Organic Liquids. *J. Am. Chem. Soc.* **1996**, *118*, 11225–11236.
- (96) Rizzo, R. C.; Jorgensen, W. L. OPLS All-Atom Model for Amines: Resolution of the Amine Hydration Problem. *J. Am. Chem. Soc.* **1999**, *121*, 4827–4836.
- (97) Kaminski, G.; Friesner, R. A.; Tirado-Rives, J.; Jorgensen, W. L. Evaluation and Reparametrization of the OPLS-AA Force Field for Proteins via Comparison with Accurate Quantum Chemical Calculations on Peptides. *J. Phys. Chem. B* **2001**, *105*, 6474–6487.
- (98) Shivakumar, D.; Williams, J.; Wu, Y.; Damm, W.; Shelley, J.; Sherman, W. Prediction of Absolute Solvation Free Energies using Molecular Dynamics Free Energy Perturbation and the OPLS Force Field. *J. Chem. Theory Comput.* **2010**, *6*, 1509–1519.
- (99) Martyna, G. J. T.; Klein, M. L.; Tobias, D. Constant-Pressure Molecular-Dynamics Algorithms. *J. Chem. Phys.* **1994**, *101*, 4177–4189.
- (100) Humphreys, D. D.; Friesner, R. A.; Berne, B. J. A Multiple-Time-Step Molecular-Dynamics Algorithm for Macromolecules. *J. Phys. Chem.* **1994**, *98*, 6885–6892.
- (101) Koynova, R.; Caffrey, M. Phases and Phase Transitions of the Phosphatidylcholines. *Biochim. Biophys. Acta, Rev. Biomembr.* **1998**, *1376*, 91–145.
- (102) Boyce, S. E.; Mobley, D. L.; Rocklin, G. J.; Graves, A. P.; Dill, K. A.; Shoichet, B. K. Predicting Ligand Binding Affinity with Alchemical Free Energy Methods in a Polar Model Binding Site. *J. Mol. Biol.* **2009**, *394*, 747–763.
- (103) Pearlman, D. A.; Charifson, P. S. Are Free Energy Calculations Useful in Practice? A Comparison With Rapid Scoring Functions for the p38 MAP Kinase Protein System. *J. Med. Chem.* **2001**, *44*, 3417–3423.
- (104) Humphrey, W.; Dalke, A.; Schulten, K. VMD: Visual Molecular Dynamics. *J. Mol. Graphics* **1996**, *14*, 33–38.
- (105) Berendsen, H. J. C.; van der Spoel, D.; van Drunen, R. GROMACS: A Message-Passing Parallel Molecular Dynamics Implementation. *Comput. Phys. Commun.* **1995**, *91*, 43–56.
- (106) Hess, B.; Kutzner, C.; van der Spoel, D.; Lindahl, E. GROMACS 4: Algorithms for Highly Efficient, Load-Balanced, and Scalable Molecular Simulation. *J. Chem. Theory Comput.* **2008**, *4*, 435–447.
- (107) Bas, D. C.; Rogers, D. M.; Jensen, J. H. Very Fast Prediction and Rationalization of pKa Values for Protein-Ligand Complexes. *Proteins: Struct., Funct., Genet.* **2008**, *73*, 765–783.
- (108) Kolocouris, A. The Effect of Spiroadamantane Substitution on the Conformational Preferences of *N*-Me Pyrrolidine and *N*-Me Piperidine: A Description Based on Dynamic NMR Spectroscopy and Ab Initio Correlated Calculations. *Tetrahedron* **2009**, *65*, 9428–9435.
- (109) Fokkens, J.; Klebe, G. A Simple Protocol To Estimate Differences in Protein Binding Affinity for Enantiomers without Prior Resolution of Racemates. *Angew. Chem., Int. Ed.* **2006**, *45*, 985–989.
- (110) Fujii, I.; Akimoto, T.; Watadani, T.; Nunomura, S.; Takahashi, Y. Optical separation of rimantadine and *in silico* prediction of chiral selectivity of M2 protein. *Acta Crystallogr., Sect. A: Found. Crystallogr.* **2008**, *A64*, C380.
- (111) Aldrich, P. E.; Hermann, E. C.; Meier, W. E.; Paulshock, M.; Prichard, W. W.; Snyder, J. A.; Watts, J. C. Antiviral Agents. 2. Structure-Activity Relationships of Compounds Related to 1-Adamantanamine. *J. Med. Chem.* **1971**, *14*, 535–543.
- (112) Wright, A. K.; Batsomboon, P.; Dai, J.; Hung, I.; Zhou, H.-X.; Dudley, G. B.; Cross, T. A. Differential Binding of Rimantadine Enantiomers to Influenza A M2 Proton Channel. *J. Am. Chem. Soc.* **2016**, *138*, 1506–1509.
- (113) Homeyer, N.; Stoll, F.; Hillisch, A.; Gohlke, H. Binding Free Energy Calculations for Lead Optimization: Assessment of their Accuracy in an Industrial Drug Design Context. *J. Chem. Theory Comput.* **2014**, *10*, 3331–3334.
- (114) Wang, L.; Wu, Y.; Deng, Y.; Kim, B.; Pierce, L.; Krilov, G.; Lupyan, D.; Robinson, S.; Dahlgren, M. K.; Greenwood, J.; Romero, D. L.; Masse, C.; Knight, J. L.; Steinbrecher, T.; Beuming, T.; Damm, W.; Harder, E.; Sherman, W.; Brewer, M.; Wester, R.; Murcko, M.; Frye, L.; Farid, R.; Lin, T.; Mobley, D. L.; Jorgensen, W. L.; Berne, B. J.; Friesner, R. A.; Abel, R. Accurate and Reliable Prediction of Relative Ligand Binding Potency in Prospective Drug Discovery by Way of a Modern Free Energy Calculation Protocol and Force Field. *J. Am. Chem. Soc.* **2015**, *137*, 2695–2703.
- (115) Caldwell, G. W. In Silico Tools Used for Compound Selection During Target-Based Drug Discovery and Development. *Expert Opin. Drug Discovery* **2015**, *10*, 901–923.

(116) Shirts, M. R.; Pande, V. S. Comparison of Efficiency and Bias of Free Energies Computed by Exponential Averaging, the Bennett Acceptance Ratio, and Thermodynamic Integration. *J. Chem. Phys.* **2005**, *122*, 144107.

(117) Shirts, M. R.; Chodera, J. D. Statistically Optimal Analysis of Samples from Multiple Equilibrium States. *J. Chem. Phys.* **2008**, *129*, 124105.

(118) Colvin, M. T.; Andreas, L. B.; Chou, J. J.; Griffin, B. G. Proton Association Constants of His 37 in the Influenza-A M2_{18–60} Dimer-of-Dimers. *Biochemistry* **2014**, *53*, 5987–5994.

(119) The use of micelles in the FEP calculations would have been prohibitively expensive in terms of computational time, and as it is not expected to have a significant effect on the protein's structure within the time scales of our simulations, a lipid bilayer was used instead; see, for example: Tieleman, D. P.; van der Spoel, D.; Berendsen, H. J. C. Molecular Dynamics Simulations of Dodecylphosphocholine Micelles at Three Different Aggregate Sizes: Micellar Structure and Chain Relaxation. *J. Phys. Chem. B* **2000**, *104*, 6380–6388.

(120) Cournia, Z.; Allen, T. W.; Andricioaei, I.; Antonny, B.; Baum, D.; Brannigan, G.; Buchete, N. V.; Deckman, J. T.; Delemotte, L.; Del Val, C.; Friedman, R.; Gkeka, P.; Hege, H. C.; Hénin, J.; Kasimova, M. A.; Kolocouris, A.; Klein, M. L.; Khalid, S.; Lemieux, M. J.; Lindow, N.; Roy, M.; Selent, J.; Tarek, M.; Tofoleanu, F.; Vanni, S.; Urban, S.; Wales, D. J.; Smith, J. C.; Bondar, A. N. Membrane Protein Structure, Function, and Dynamics: a Perspective from Experiments and Theory. *J. Membr. Biol.* **2015**, *248*, 611–640.

(121) Cristian, L.; Lear, J. D.; DeGrado, W. F. Use of Thiol-Disulfide Equilibria to Measure the Energetics of Assembly of Transmembrane Helices in Phospholipid Bilayers. *Proc. Natl. Acad. Sci. U. S. A.* **2003**, *100*, 14772–14777.

(122) Cady, S.; Wang, T.; Hong, M. Membrane-Dependent Effects of a Cytoplasmic Helix on the Structure and Drug Binding of the Influenza Virus M2 Protein. *J. Am. Chem. Soc.* **2011**, *133*, 11572–11579.

(123) Breu, B.; Silber, K.; Gohlke, H. Consensus Adaptation of Fields for Molecular Comparison (AFMoC) Models Incorporate Ligand and Receptor Conformational Variability into Tailor-made Scoring Functions. *J. Chem. Inf. Model.* **2007**, *47*, 2383–2400.

(124) Brown, S. P.; Muchmore, S. W.; Hajduk, P. J. Healthy Skepticism: Assessing Realistic Model Performance. *Drug Discovery Today* **2009**, *14*, 420–427.

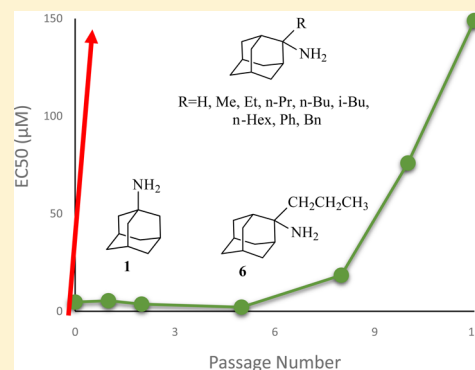
(125) Christ, C. D.; Fox, T. Accuracy Assessment and Automation of Free Energy Calculations for Drug Design. *J. Chem. Inf. Model.* **2014**, *54*, 108–120.

Aminoadamantanes with Persistent in Vitro Efficacy against H1N1 (2009) Influenza A

Antonios Kolocouris,^{*,†} Christina Tzitzoglaki,[†] F. Brent Johnson,[‡] Roland Zell,[§] Anna K. Wright,^{||} Timothy A. Cross,^{||} Ian Tietjen,[⊥] David Fedida,[⊥] and David D. Busath^{*,#}[†]Department of Pharmaceutical Chemistry, Faculty of Pharmacy, National and Kapodistrian University of Athens, Athens 15771, Greece[‡]Department of Microbiology and Molecular Biology, Brigham Young University, Provo, Utah 84602, United States[§]Department of Virology and Antiviral Therapy, Jena University Hospital, CMB Building, R. 443, Hans Knoell Strasse 2, D-07745 Jena, Germany^{||}Department of Chemistry and Biochemistry and National High Magnetic Field Laboratory, Florida State University, Tallahassee, Florida 32306, United States[⊥]Department of Anesthesiology, Pharmacology and Therapeutics, University of British Columbia, Vancouver, British Columbia, V6T 1Z3, Canada[#]Department of Physiology and Developmental Biology, Brigham Young University, Provo, Utah 84602, United States

Supporting Information

ABSTRACT: A series of 2-adamantanamines with alkyl adducts of various lengths were examined for efficacy against strains of influenza A including those having an S31N mutation in M2 proton channel that confer resistance to amantadine and rimantadine. The addition of as little as one CH₂ group to the methyl adduct of the amantadine/rimantadine analogue, 2-methyl-2-aminoadamantane, led to activity in vitro against two M2 S31N viruses A/Calif/07/2009 (H1N1) and A/PR/8/34 (H1N1) but not to a third A/WS/33 (H1N1). Solid state NMR of the transmembrane domain (TMD) with a site mutation corresponding to S31N shows evidence of drug binding. But electrophysiology using the full length S31N M2 protein in HEK cells showed no blockade. A wild type strain, A/Hong Kong/1/68 (H3N2) developed resistance to representative drugs within one passage with mutations in M2 TMD, but A/Calif/07/2009 S31N was slow (>8 passages) to develop resistance in vitro, and the resistant virus had no mutations in M2 TMD. The results indicate that 2-alkyl-2-aminoadamantane derivatives with sufficient adducts can persistently block p2009 influenza A in vitro through an alternative mechanism. The observations of an HA1 mutation, N160D, near the sialic acid binding site in both 6-resistant A/Calif/07/2009(H1N1) and the broadly resistant A/WS/33(H1N1) and of an HA1 mutation, I325S, in the 6-resistant virus at a cell-culture stable site suggest that the drugs tested here may block infection by direct binding near these critical sites for virus entry to the host cell.



INTRODUCTION

Since 2005,¹ the amantadine/rimantadine-insensitive S31N mutation has become prevalent globally,² abrogating clinical usefulness of amantadine **1** and rimantadine **2**³ and possibly previously developed M2 blocking compounds.⁴ If the replacement of Ser31 with the larger Asn in M2 S31N splay the helix bundle at the drug binding site,⁵ as suggested by solution state NMR studies,^{5d,6} then drugs larger than rimantadine might be expected to be effective blockers. However, initial attempts to identify larger adamantane-based compounds that block amantadine-resistant viruses were unsuccessful.⁷ Further efforts identified spiranamine analogues based on BL-1743⁸ that were effective against V27A and L26F mutants^{9a} but not against S31N, while other large templates could inhibit V27A^{9b-d} but not S31N. Subsequently, reports of

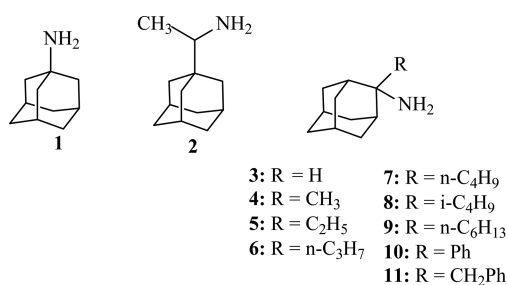
successful adamantane- and pinanamine-based M2 S31N blockers have appeared.^{6,10} The design of these molecules was not based on the enlargement of the amantadine WT-M2 binding site, and the structural analysis of one active compound, comprising an amantadine linked through a methylene bridge to an isoxazole having an aryl substituent, showed that its heterocyclic ring may be trapped by the V27 side chains at the mouth of the channel.⁶ Triggered by previous efforts aimed at adequately filling the empty expanded pore region due to the S31N mutation and to determine progressively the minimal variation of amantadine required to block influenza A (H1N1, M2 S31N), we evaluated drug

Received: January 16, 2014

Published: May 4, 2014

efficacy and mechanism for variations of amantadine **1** with alkyl adducts ranging from small to moderate and larger sizes (Scheme 1) as represented by the 2-alkyl-2-aminoadamantane

Scheme 1. Amantadine 1, Rimantadine 2, and 2-Alkyl-2-aminoadamantane Derivatives 3–11



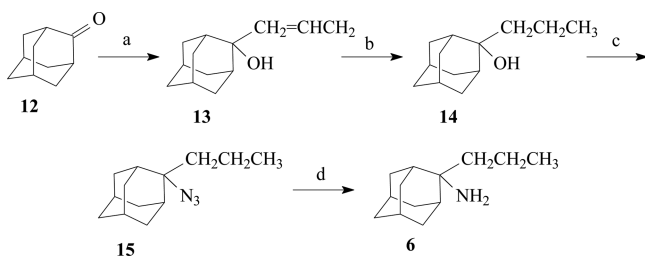
derivatives **3–11**, which are simpler than previously reported aminoadamantane derivatives active against S31N viruses^{10e} and the larger of which have increased volume compared to amantadine.

We found with **5** that the addition of as little as one CH₂ group to the methyl adduct of the amantadine/rimantadine analogue, 2-methyl-2-aminoadamantane **4** (Scheme 1), recovers activity in vitro against the amantadine-resistant A/Calif/07/2009. However, the mechanism of action is not M2-block but a second aminoadamantane target.

RESULTS AND DISCUSSION

Chemistry. Compounds **3–11** belong to the class of 2-alkyl-2-aminoadamantanes, which thus bear a substitution at adamantane C2 carbon. Compounds **3–6**^{4b} and **10**¹¹ were previously synthesized but resynthesized with slightly modified procedures in this work. Tertiary alcohol **13** was obtained by treating 2-adamantanone **12** with allylmagnesium bromide (Scheme 2). The unsaturated alcohol **13** was converted to the

Scheme 2. Preparation of 2-*n*-Propyl-2-aminoadamantane 6^a

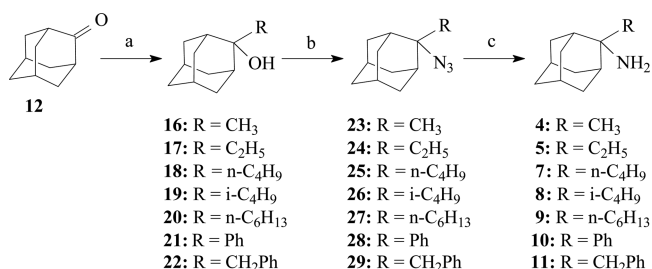


^aReagents and conditions: (a) CH₂=CHCH₂MgBr, ether, THF, rt, 2 h, then NH₄Cl/H₂O (quant); (b) H₂/PtO₂ (quant); (c) NaN₃, TFA, CH₂Cl₂, 0 °C, then rt (quant); (d) LiAlH₄, ether, rt, 5 h (74%).

n-propyl derivative **14** through catalytic hydrogenation over PtO₂. After experiments with tertiary alcohols in the adamantane series and an acyclic series (unpublished data), we concluded that the conversion of tertiary alcohols to the corresponding azides through NaN₃/H₂SO₄ (various concentrations)/CHCl₃^{4b,12} or NaN₃/TFA/CHCl₃¹¹ can result in unreacted alcohol and found that the transformation proceeds efficiently using NaN₃/TFA 1 M in CH₂Cl₂. The amine **6** was prepared by means of LiAlH₄ reduction of the azide **15** in refluxing ether.

The amines **4, 5, 7–11** were synthesized according to Scheme 3. Tertiary alcohols **16–22** were obtained by treating

Scheme 3. Preparation of 2-Alkyl-2-aminoadamantane Derivatives 4, 5, 7–11^a



^aReagents and conditions: (a) RLi, Ar, ether, THF, 0 °C, 2 h rt for **17–20** or RMgCl, ether, THF, 2 h rt for **16, 20, 21**, then NH₄Cl/H₂O (85–96%); (b) NaN₃, TFA, CH₂Cl₂, 0 °C, then rt (50–96%); (c) LiAlH₄, ether, rt, 5 h (23–65%).

2-adamantanone **12** with an organolithium (R = Et, *n*-Bu, *i*-Bu, *n*-hexyl) or organomagnesium reagent (R = Me,^{4b} Ph, or PhCH₂) (Scheme 3). While 2-methyl-2-adamantanol **16** was obtained after treating 2-adamantanone **12** with CH₃MgI, this is not an efficient method for the preparation of alcohols **17–22** because of the bulky 2-adamantanone **12** and the soft carbanion character of the Grignard reagent making the β-hydride transfer a competitive reaction to the alkyl addition and leading to a mixture of the desired tertiary alcohol with 2-adamantanol. The conversion of tertiary alcohols **16–22** to the corresponding azides **23–29** was accomplished efficiently through treatment with NaN₃/TFA 1 M in dichloromethane or dichloroethane for 24 h at room temperature. The primary *tert*-alkylamines **4, 5, 7–11** were prepared by means of LiAlH₄ reduction of the azides **23–29** in refluxing ether for 5 h.

Solid State NMR of the M2 TMD Tetramer. PISA wheel analysis gives a direct readout of helix tilt relative to the membrane normal for membrane proteins in uniformly oriented lipid bilayer preparations from solid state NMR PISEMA experiments.¹³ ¹⁵N anisotropic chemical shifts and ¹⁵N–¹H dipolar interactions observed in these spectra are very sensitive to the orientation of the peptide planes relative to the bilayer normal. Binding of compound **6** shifts the signals for three pertinent backbone amides that were isotopically labeled (Figure 1).

Binding of amantadine **1** to WT M2 TMD (A/Udorn/307/72 sequence) produces an 11° kink near G34 in each helix of the tetramer.^{5e} When drug-bound, the helix tilt for the N-terminal half (residues 22–34) is 31° and in the C-terminal half (residues 35–46) just 20°.¹⁴ Here, the S31N M2 TMD is labeled at two sites in the N-terminal half (residues V28 and A30) and one site in the C-terminal half (residue I42) of the TMD helix. The S31N data without drug suggest a helical tilt of approximately 36°, similar to that seen in the WT structure.⁵ The shifts in the anisotropic spin interactions upon drug binding demonstrate a significant change in the structure of the tetrameric complex. With compound **6**, there is a uniform tilt of ~33°. Thus, the **6**-induced changes in the resonance frequencies of these three sites indicate that the tilt angle for the entire TMD helix is decreased by 3° while maintaining a similar rotational orientation for the helices. Unlike the response of the WT to amantadine **1**, with **6** the S31N TMD helices do not appear to have kinked the helix at G34. Instead,

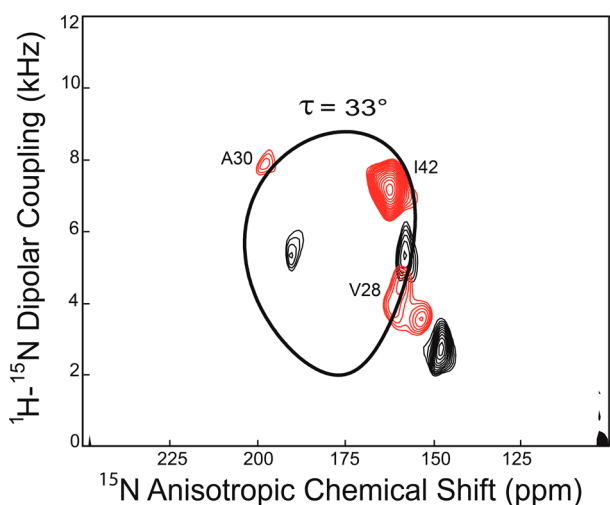


Figure 1. Superimposed PISEMA spectra of the S31N M2 transmembrane domain (residues 22–46), ^{15}N labeled at residues V28, A30, and I42, in dimyristoylphosphatidylcholine bilayers uniformly aligned on glass slides with (red) and without (black) compound **6**. Assignments were made based on the known structure and spectra of WT M2 TMD.¹⁵ The assignments with drug follow based on the rotational orientation of the helices.

the entire helix–helix interface changes with the $\sim 3^\circ$ reduction in tilt of the four helices. Similar results from ssNMR experiments and proteoliposome assays were obtained with two related aminoadamantanes that are not included in Scheme 1.

Electrophysiology Results Using Full-Length M2.

Representative compounds **3** and **6** were subsequently tested for block of proton currents through full-length M2 having the same amino acid sequence as A/California/07/2009 (*viz.*, S31N) using transiently transfected, voltage-clamped HEK cells¹⁶ and found not to block inward proton currents on the 3 min time scale with any improvement over amantadine **1** (Table 1, Figure S1 in Supporting Information). Prolonged exposure (30 min) yielded but little increase in net block over 3 min exposure for the two drugs. When the M2 protein was reverted to the S31 WT sequence (through an N31S mutation), inward proton currents in M2-transfected HEK cells were well blocked by **1**, **3**, and **6**. This electrophysiology result suggests (a) that these two drugs do not block the M2 S31N channel in full length A/Calif/07/2009 and must have a different target and (b) that biophysical models for the M2 protein should be based on the whole protein rather than segments. This conclusion supports other studies suggesting another target of aminoadamantane compounds.^{7,10e,g} Similar results were also obtained with a few other related aminoadamantanes not included in this work.

Biological Evaluation. (a) *Antiviral Evaluation.* EC_{50} values from dose–response tests against five strains of influenza A in Madin–Darby canine kidney (MDCK) cells were measured using a primary infection assay (Table 2). This assay detects block at the early stages of viral replication, from endocytotic uptake to protein synthesis.

All compounds except **1–5** display potent antiviral activity against the pandemic 2009 strain (arbitrarily designated as <24 μM based on the amantadine insensitivities observed here). It is striking that the addition of as little as one CH_2 group to the methyl adduct of the amantadine/rimantadine analogue, 2-methyl-2-aminoadamantane **4**, essentially recovers activity in vitro against this amantadine-resistant form of influenza A.

Likewise, the amantadine-resistant H1N1 strain from 1934 (second column), containing a double mutant M2 (T27 + N31), is highly sensitive to these compounds. But the drugs do not block all M2(S31N)-bearing or all H1N1 strains^{10e} as shown by the third column, which shows that the 1933 Wilson Smith H1N1 isolate is insensitive to most of these compounds. Furthermore, the M2 pore region (residues 22–46) of A/WS/33 and A/Calif/2009 are identical except for the L43T variation at the C-terminus (Supporting Information Table 1). These observations are consistent with the negative electrophysiology results for the A/Calif/2009/M2, further suggesting that the antiviral effects observed against the A/Calif/2009 strain are independent of M2 and that instead they attack a second target.^{7,10g} This second target is most likely present in A/Calif/07/2009 and probably in A/PR/8/34 but not in A/WS/33. Strains with WT M2 are very sensitive to these compounds (fourth and fifth columns), suggesting that, like amantadine, these drugs also block M2. However, from the structure–activity point of view, differences between the sequence and optimal efficacies vary, suggesting that nonbinding site residue differences in the M2 may alter efficacy. For instance **6** is the one of the most potent in the set against A2/Taiwan/1/64 H2N2 but the least potent of the set against A/Victoria/3/75 H3N2, even though both have WT-M2 amantadine-binding sites. They differ in only two residues, 13 and 56, neither of which is in the pore region (Supporting Information Table 1). This suggests that extra-pore residues may affect M2 block. On the other hand, **9** is the most effective from the set against all of the strains tested except A2/Taiwan/1/64, where it is among the least effective, which may suggest that the relative impacts of M2 block and any alternative mechanisms of action are also dependent on drug structure.

(b) *Resistance Experiments: Sequencing of Resistant Strains.* Resistance testing with semiweekly passages in MDCK cell cultures was performed for amantadine **1** against an amantadine-sensitive H3N2 virus and for compound **6** against amantadine-resistant H1N1 (2009) (Table 3).

In the amantadine–H3N2 system, drug resistance appeared after one passage in the presence of drug, with no detectable

Table 1. Proton Channel Block Measured in Transfected HEK Cells for Compounds Tested^a

compd	A/England/195/2009 (H1N1), ^b M2/N31		A/England/195/2009 (H1N1), M2/S31	
	% block after 3 min	% block after 30 min	% block after 3 min	IC_{50} , μM
1	14 \pm 2 (100 μM ; 26)	(N/A)	75 \pm 9 (10 μM ; 4)	1.6 \pm 2.7 (3)
3	13 \pm 3 (100 μM ; 2)	16 (100 μM ; 1)	95 \pm 8 (10 μM ; 2)	2.5 \pm 0.5 (2)
6	0 \pm 5 (100 μM ; 2)	9.4 \pm 10 (100 μM ; 3)	63 \pm 5 (10 μM ; 2)	7 \pm 2 (2)

^aFor each compound, % block of pH-dependent M2 current at 10 or 100 μM ($\pm\text{SEM}$) or the IC_{50} (μM) is shown. Number of replicates is shown in parentheses. ^bThe M2 sequence for this strain is identical to that of A/Calif/07/2009 M2.

Table 2. In Vitro Efficacy (EC_{50} , μM) of Scheme 1 Compounds against Initial MDCK Cell Infection^a

compd	A/Calif/07/09 (H1N1)	A/PR/8/34 (H1N1)	A/WS/33 (H1N1)	A2/Taiwan/1/64 (H2N2)	A/Victoria/3/75 (H3N2)
M2	S31N	V27T/S31N	S31N	WT	WT
1	240 ± 90 (13)	24 ± 3.5 (21)	24 ± 1.1 (21)	0.34 ± 0.01 (21)	2.8 ± 0.3 (16)
2	110 ± 40 (13)	3.3 ± 0.5 (2)	310 ± 140 (2)	1.6 ± 0.3 (2)	0.53 ± 0.07 (18)
3	150 ± 30 (20)	3.8 ± 1.0 (2)	110 ± 15 (2)	0.8 ± 0.3 (2)	3.3 ± 0.9 (2)
4	54 ± 2 (20)	0.4 ± 0.4 (2)	19 ± 4 (2)	0.5 ± 0.5 (2)	2.0 ± 0.4 (2)
5	25 ± 3 (21)	1.8 ± 0.9 (2)	23 ± 3 (2)	0.8 ± 0.3 (2)	2.0 ± 0.4 (2)
6	4.7 ± 0.9 (20)	0.5 ± 0.2 (2)	390 ± 8 (2)	<0.24 (2)	23 ± 8 (2)
7	8.5 ± 0.6 (20)	0.3 ± 0.3 (2)	355 ± 4 (2)	1.5 ± 0.3 (2)	4 ± 1 (2)
8	8.0 ± 0.3 (21)	0.3 ± 0.5 (2)	210 ± 40 (2)	0.4 ± 0.1 (2)	13 ± 2 (2)
9	0.13 ± 0.02 (2)	0.07 ± 0.09 (2)	13.0 ± 3.6 (2)	1.5 ± 0.3 (2)	1.1 ± 0.1 (2)
10	21 ± 2 (21)	<0.3 ± 0.5 (2)	86 ± 20 (2)	0.2 ± 0.2 (2)	8 ± 1 (21)
11	8.6 ± 0.8 (21)	1.2 ± 1.1 (2)	280 ± 150 (2)	0.2 ± 0.3 (2)	18 ± 2 (21)

^a $EC_{50} \pm$ its standard error (N) from miniplaque testing for dose–response or single-dose screens, using cultured MDCK cells, based on least-squares fitting of single-site binding curves. N is the number of assay counts fitted. Experiments with $N = 2$ are based on replicate 50 μM screens (except for 9, which were based on replicate 5 μM screens), with a single control ($N = 4$) for each virus. Row M2 gives variations from the WT amantadine-binding site (i.e., L26, V27, A30, S31, and G34) for the specific strain listed, WT if none. (See Tables S3, S4, and S5 for the M2 sequences of the isolates used here.) No microscopic evidence of cytotoxicity to MDCK cells was detected after an 18 h exposure at 50 μM except with compound 9, where a 5 μM dose was used instead. The EC_{50} values of amantadine 1 and rimantadine 2, known to be inactive against H1N1 (2009), and other cases where $EC_{50} \geq 24 \mu M$ are highlighted.

Table 3. Resistance Testing of Amantadine 1 and 2-*n*-Propyl-2-aminoadamantane 6^a

passage no.	$EC_{50} \pm SE$ (μM)	
	1 (5 μM), A/Victoria/3/75 (H3N2, M2 WT)	6 (5 μM), A/Calif/07/2009 (H1N1, M2 S31N)
0	2.77 ± 0.29	4.71 ± 0.92
1	inactive	5.4 ± 1.4
2	inactive	3.7 ± 0.5
5	ND	2.1 ± 1.6
8	ND	18.5 ± 1.0
10	ND	76 ± 9
12	ND	149 ± 115

^a $EC_{50} \pm SE$ (μM) ($N = 21$) after designated passage (incubation) stages. Drug concentration in medium as specified except that for 6, passages 1 and 2 were done in 10 μM . Inactive: no miniplaque reduction by 50 μM amantadine. ND: not done.

activity of amantadine 1 against the progeny from passage 1 or passage 2 at 50 μM but normal amantadine 1 activity against the original virus post hoc ($EC_{50} = 3.0 \pm 0.5 \mu M$; $N = 9$). In contrast, in the 6–H1N1 system, virus progeny produced in the presence of drug at passages 1–5 maintained full drug sensitivity ($EC_{50} = 2.1–5.4 \mu M$). Resistance to 6 developed steadily between passage 6 and passage 12, becoming significant after passage 10. Without any drug in the medium, the development of viral resistance to compound 6 was negligible; i.e., the EC_{50} retested at passage 0 was $4.7 \pm 0.7 \mu M$, at passage 10 was 3.0 ± 0.3 , and at passage 30 was $7.7 \pm 0.6 \mu M$. Resistance to amantadine develops rapidly in vitro,¹⁷ in mice,¹⁸ and in the clinical setting¹⁹ through a small set of mutations, primarily L26F, V27A, V27T, A30T, S31N, and G34E.²⁰ These are residues whose side chains are near the 4-fold symmetric amantadine binding site.⁵ No changes from the parent A/California/07/2009 were observed for the amino acid translation of the M-segment of the passage-12 6-resistant strain for residues sequenced, 10–73. Hence, resistance did not develop by selection of additional amantadine-resistance mutations in M2. Sequencing of segment 4 (HA gene), however, revealed three amino acid substitutions (Figure 2, Table S1) compared to the parental A/California/07/2009 sequence, i.e., N160D,

S187P, and I325S (numbering started after the 13-residue HA signal sequence).

To evaluate whether these mutations were merely due to adaptation to MDCK cell culture growth, we also sequenced the M (Tables S2 and S3) and HA segments (Table S1) from the parent virus after 30 passages in MDCK culture without drug. For the M segment of these drug-free controls, no changes were found in M1, while 2 of 5 plaques had an E14G

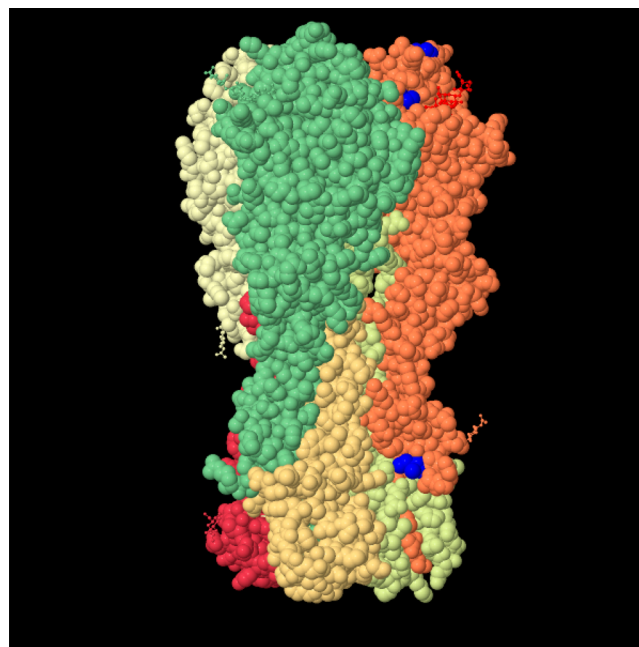


Figure 2. CPT structure of the HA trimer, produced by Gamblin et al. (1RVX, A/Puerto Rico/8/1934)²¹ with a bound NAG-GAL-SIA ligand as ball-and-stick (red) and with the two nearby 6-resistance sites highlighted in blue, residues 159 (above ligand) and 186 (left of ligand). The third 6-resistance site, 324, also in blue, is near the bottom of the structure. Because of a common insertion after residue 133 found in A/Calif/07/2009 (H1N1), these correspond to N160, S187, and I325, respectively, in the A/Calif/07/2009 6-resistant mutants.

substitution in M2, which is outside the transmembrane domain.

Substitution S187P, located near the N-terminus of the 190 sialic acid binding helix, is frequent in pandemic H1N1 and was observed previously by Torres et al. in resistance development using a related set of aminoadamantanes.^{10g} In the drug-free controls, 2 out of 5 plaques showed this mutation, as well as 1 of 4 previously sequenced isolates of A/California/07/2009 (KF00954, Table S1).

N160 is located on the tip of a nearby loop that is very close to the 190 helix, the region where sialic acid residues of the host cell receptor bind. Among 1750 HA sequences of pandemic H1N1 deposited in the GenBank only four sequences with D160 were observed. Substitution of N160 by an aspartic acid residue would modify the local charges and may thus affect receptor interactions. Interestingly, D160 is also observed in A/WS/33, which may account for the insensitivity of this strain to the compounds tested here (Table 1). However, in the drug-free controls, 1 of 5 plaques tested had this mutation (Table S1). Three other plaques had the G159E mutation, suggesting that an acidic group in that neighborhood is advantageous for the pandemic virus replication in MDCK culture. On the other hand that mutation is also present in our sample of the highly 6-sensitive A/PR/8/34 strain (Table S1), suggesting that if D160 is critical for drug inhibition, an acid group at position 159 is not sufficient for drug resistance. The possibility that N160D is important to escape from 6 cannot be ruled out.

S325 is close to the HA0 processing site at R331 and the corresponding residue, 324, was also found to be modified in the aminoadamantane resistance development study by Torres et al.^{10g} None of the 1750 HA sequences of pandemic H1N1 in GenBank has a serine at position 325. This substitution may affect maturation cleavage or pH stability of HA. Although it was pointed out^{10g} that a mutation to T at this site is found in one sequence of A/Puerto Rico/8/1934 and that this site may be polymorphic, we found seven sequences for that strain without the mutation and no I325T substitution was observed in our GenBank set of 1750 pandemic H1N1 strains. Furthermore, no instances of an I325 mutation were observed in the drug-free control virus plaques (Table S1). This suggests that drugs inhibit an important function at this site such as enzyme binding or cleavage.

To examine the resistance development pathways of the H3N2 M2 WT virus to these compounds in more detail, passaging experiments were carried out with plaque sequencing analysis in the presence of active compound 4 or 6 (Table 4). The WT virus rapidly develops resistance to both compounds through mutation at Ala30, especially to Thr, suggesting that these drugs block the M2 WT but do not block A30T. Conversely, the lack of sequence changes for M2(S31N)-bearing virus in the presence of compound 6 mentioned above indicates that M2(S31N)-bearing virus has a different escape route than M2(WT)-bearing virus. In the latter case changes inside the M2 pore confer resistance, while in the former no mutations were observed in the M2 channel amantadine binding site; therefore, some other change in the virus is implicated.

CONCLUSION

The addition of as little as one CH₂ group to the methyl adduct of the amantadine/rimantadine analogue, 2-methyl-2-aminoadamantane 4, has been discovered to largely recover activity in vitro against the amantadine-resistant 2009 H1N1 influenza A.

Table 4. Mutations Developing in Influenza A (M2 WT)^a after Passaging in Aminoadamantane Derivatives 4 and 6^b

passage no. ^d	plaque no.	compd ^c	
		4, 1 μg/mL	6, 5 μg/mL
2	1	WT	A30T
	2	WT	A30T
	3	WT	A30T
5	1	A30T	A30T
	2	A30V	A30T
	3	A30T	A30T

passage no. ^d	plaque no.	compd ^c	
		4, 2 μg/mL	6, 5 μg/mL
10	1	A30T	A30T
	2	A30T	A30T
	3	A30T	A30T

^aParent strain: A/Hong Kong/1/1968 (H3N2M2 WT). ^bSequences of resistant progeny of WT induced by compounds in the top row. MDCK cells were bathed in medium containing the concentrations specified. Three separate plaques were sampled and sequenced at passages 2, 5, and 10. ^cCompound number from Scheme 1. ^dPassage number.

The apparent simplicity of the synthetic schemes is a virtue of 2-alkyl-2-aminoadamantane derivatives. Resistance development in cell culture is markedly reduced for one representative compound 6 (R = *n*-Pr) compared to amantadine 1. These compounds found to be active against two of three S31N strains (A/Calif/07/009 and A/PR/8/34 but not A/WS/33) did not block M2, judging by the lack of transfected HEK cell current block and the lack of M2 changes in the 6-resistant A/Calif/07/2009, and therefore must have acted on a second target. The ssNMR study that confirmed that drugs with large alkyl adducts were sterically suited to fit in the amantadine binding site in M2 were done at effectively high drug concentrations and using truncated M2 protein (22–46) and do not indicate the potential of drugs to block the S31N variant of M2.

A few alternative candidate mechanisms of action for these drugs include pH buffering of the endosome, pH buffering of the viral interior, stabilization of hemagglutinin against acid activation, and mechanical stabilization at lipid–water interfaces against envelope–endosomal membrane fusion. The observations of an HA1 mutation, N160D, near the sialic acid binding site in both 6-resistant A/Calif/07/2009(H1N1) and the broadly resistant A/WS/33(H1N1) and of an HA1 mutation I325S in the 6-resistant virus at a cell-culture stable site suggest that the drugs tested here may block infection by direct binding near these critical sites. The region near residue 160 is critical for binding virus to the cell surface, and the region near residue 325 is critical for HA activation by proteolytic cleavage, both necessary for the virus entry into the host cell. It is also possible that the drugs neutralize the endosome and that these sites, individually or in combination, affect pH sensitivity of HA, as has been suggested in similar situations previously.^{7,10g} However, miniplaque assays with compounds 3–6 against influenza B/Russia/69 in MDCK cells and compound 6 against bovine parvovirus in bovine embryonic cells, respectively, both of which are chloroquine sensitive,^{22,23} showed no effect of 3–6 or 6, respectively, on virus growth with 50 μM drug in the medium (data not shown), suggesting that these compounds are less potent endosome neutralizers than chloroquine.

Further experiments are needed to explore these and other possibilities.

Continued outbreaks of amantadine-resistant viruses like H7N9 merit the urgency to develop new antivirals with persistent efficacy in global preparations for pandemic threats.²⁴ The new observation of persistent efficacy of these amantadine-like drugs via second targets, while retaining potency (albeit resistance vulnerable) to WT M2, makes this family of compounds intriguing starting points for further studies on resistance and mechanism of action against influenza A.

EXPERIMENTAL SECTION

(A) Chemistry. Melting points were determined using a Buchi capillary apparatus and are uncorrected. IR spectra were recorded on a Perkin-Elmer 833 spectrometer. ¹H and ¹³C NMR spectra were recorded on a Bruker DRX 400 and AC 200 spectrometer at 400 and 50 MHz, respectively, using CDCl₃ as solvent and TMS as internal standard. Carbon multiplicities were established by DEPT experiments. The 2D NMR techniques (HMQC and COSY) were used for the elucidation of the structures of intermediates and final products.

Microanalyses were carried out by the Service Central de Microanalyse (CNRS), France, and by the Microanalyses lab of the National Center for Scientific Research, Demokritos, Athens, Greece, and the results obtained had a maximum deviation of ±0.4% from the theoretical value. All tested synthesized compounds possess a purity above 95% as determined through elemental C, H, N analysis.

Full experimental details that were not given previously for compounds 4 and 5^{4b} are included in this paper.

2-Ethyltricyclo[3.3.1.1^{3,7}]decan-2-amine (5). 2-Ethyl-2-adamantanol 17 was obtained after treating a solution of 2-adamantanone 12 (500 mg, 3.34 mmol) in dry THF (10 mL, 30% solution w/v) with *n*-ethylolithium at 0 °C in a 3.7 molar excess (25 mL, 12.5 mmol, 0.5 M in benzene) and stirring the mixture overnight: yield 94%; ¹H NMR (CDCl₃, 400 MHz) δ 0.86 (t, *J* = 7 Hz, CH₂CH₃), 1.40–1.70 (m, 10 H, 1',3'-H, 4'eq, 9'eq-H, 6'-H, 8'eq,10'eq-H, CH₂CH₃), 1.75–1.83 (m, 2H, 5',7'-H), 1.94 (d, *J* = 12 Hz, 2H, 8'ax, 10'ax-H), 2.07 (d, *J* = 12 Hz, 2H, 4'ax, 9'ax-H); ¹³C NMR (CDCl₃, 50 MHz) δ 6.4 (CH₂CH₃), 27.4, 27.5 (5',7'-C), 30.6 (CH₂CH₃), 33.0 (8',10'-C), 34.6 (4',9'-C), 36.6 (1',3'-C), 38.5 (6'-C), 74.9 (2'-C).

To a stirred mixture of NaN₃ (0.195 g, 3.0 mmol) and dry dichloromethane (5 mL) at 0 °C, TFA (1.14 g, 10.0 mmol) was added. To the stirred mixture, a solution of 2-ethyl-2-adamantanol 17 (0.180 g, 1.0 mmol) in dry dichloromethane (5 mL) was added, and stirring was maintained at 0 °C for 4 h. The mixture was stirred at ambient temperature for 24 h and then was treated with NH₃ 12% (30 mL) at 0 °C. The organic phase was separated, and the aqueous phase was extracted twice with an equal volume of dichloromethane. The combined organic phase was washed with water and brine, dried (Na₂SO₄), and evaporated to afford oily 2-ethyl-2-adamantylazide 24: IR (Nujol) ν(N₃) 2100 cm⁻¹; yield 0.160 g (80%).

To a stirred suspension of LiAlH₄ (0.120 g, 0.78 mmol) in dry ether (10 mL) was added, dropwise at 0 °C, a solution of the 2-ethyl-2-adamantylazide 24 (0.160 g, 3.12 mmol) in dry ether (5 mL). The reaction mixture was refluxed for 5 h (TLC monitoring) and then hydrolyzed with water and NaOH (15%) and water under ice cooling. The inorganic precipitate was filtered off and washed with ether, and the filtrate was extracted with HCl (6%). The aqueous layer was made alkaline with solid Na₂CO₃, and the mixture was extracted with ether. The combined ether extracts were washed with water and brine and dried (Na₂SO₄). After evaporation of the solvent the oily amine 5 was obtained: yield 100 mg (71%); ¹H NMR (CDCl₃, 400 MHz) δ 0.85 (t, *J* = 7 Hz, 3H, CH₃), 1.55 (br s, 2H, 1',3'-H), 1.58–1.68 (m, 6H, 4'eq, 9'eq-H, 8'eq 6'-H), 1.78 (br s, 1H, 5'-H), 1.81 (br s, 1H, 7'-H), 1.93 (d, *J* = 12 Hz, 2H, 8'ax, 10'ax-H), 2.06 (d, *J* ≈ 12 Hz, 2H, 4'ax, 9'ax-H); ¹³C NMR (CDCl₃, 50 MHz) δ 6.5 (CH₂CH₃), 27.2, 27.6 (5',7'-C), 30.7 (CH₂CH₃), 33.0 (4',9'-C), 33.8 (8',10'-C), 36.6 (1',3'-C), 38.5 (6'-C), 74.9 (2'-C). Hydrochloride: mp >250 °C (EtOH–Et₂O).

Anal. Calcd for C₁₂H₂₂NCl: C, 66.80; H, 10.28; N, 6.49. Found: C, 66.93; H, 10.42; N, 6.87.

2-*n*-Propyltricyclo[3.3.1.1^{3,7}]decan-2-amine (6). Tertiary alcohol 13 was obtained after treating adamantanone 12 (1.0 g, 6.67 mmol) with CH₂CH=CH₂MgBr in 1:2 ratio (obtained from CH₂CH=CH₂Br (1.61 g, 13.3 mmol), 1.5 molar excess of Mg (486 mg, 20.01 mmol) in 20 mL of dry ether/g bromobenzene): yield 89%; ¹H NMR δ 1.52 (d, *J* = 12 Hz, 2H, 4'eq, 9'eq-H), 1.53–1.90 (m, 10H, adamantane-H), 2.15 (d, *J* = 12 Hz, 1H, 4'ax, 9'ax-H), 2.40 (d, *J* = 6 Hz, 2H, CH₂CH=CH₂), 5.05–5.15 (m, 2H, CH₂CH=CH₂), 5.75–6.0 (m, 1H, CH₂CH=CH₂). The unsaturated alcohol 13 (890 mg, 4.64 mmol) was hydrogenated under PtO₂ (45 mg) (catalyst was used in 1/20 percentage to the weight of the unsaturated compound) to afford the *n*-propyl analogue 14: yield, quant; ¹H NMR (CDCl₃, 400 MHz) δ 0.92 (t, *J* = 7 Hz, 3H, CH₃), 1.30–1.40 (m, 2H, CH₂CH₂CH₃), 1.52 (d, *J* = 12 Hz, 2H, 4'eq, 9'eq-H), 1.58–1.61 (m, 2H, CH₂CH₂CH₃), 1.68 (d, *J* = 12 Hz, 2H, 8'eq, 10'eq-H), 1.67 (br s, 2H, 6'-H), 1.68 (br s, 2H, 1', 3'-H), 1.79 (m, 2H, 5', 7'-H), 1.83 (d, *J* = 12 Hz, 2H, 8'ax, 10'ax-H), 2.16 (d, *J* = 12 Hz, 2H, 4'ax, 9'ax-H); ¹³C NMR (CDCl₃, 50 MHz) δ 14.9 (CH₃), 15.4 (CH₂CH₂CH₃), 27.4, 27.6 (5, 7-C), 33.1 (CH₂CH₂CH₃), 34.7 (4, 9-C), 37.1 (8, 10-C), 38.5 (1, 3-C), 40.9 (6-C), 75.2 (2-C).

The alcohol 14 (700 mg, 4.22 mmol) was added to a stirred mixture of H₂SO₄ 70% w/w (10 mL) and chloroform (25 mL) at 0 °C. Sodium azide was added in small portions at 0 °C, and the mixture was stirred for 48 h at ambient temperature. The mixture was poured into an ice–water mixture and was extracted with dichloromethane. The organic phase was washed with water, saturated NaHCO₃, and brine, dried (Na₂SO₄), and evaporated under vacuum at room temperature. The oily residue (650 mg) was flash-chromatographed on silical gel (35–70 μm) with hexane–AcOEt 5/1 as an eluent to give the pure azide 15: yield 530 mg (66%). The azide 15 was found to form quantitatively using TFA/CH₂Cl₂/NaN₃ system (1 mmol of alcohol 14 was treated with 10 mmol of TFA and 4 mmol of NaN₃ in 40 mL of CH₂Cl₂; see experimental procedure for ethyl- or 2-*n*-butyltricyclo[3.3.1.1^{3,7}]decan-2-azide 24 or 25): ¹H NMR (CDCl₃, 400 MHz) δ 0.96 (t, *J* = 7 Hz, 3H, CH₃), 1.42 (m, 2H, CH₂CH₂CH₃), 1.59 (d, *J* = 12 Hz, 2H, 4'eq, 9'eq-H), 1.68–2.03 (m, 12H, CH₂CH₂CH₃, adamantane-H), 2.10 (d, *J* = 12 Hz, 1H, 4'ax, 9'ax-H); ¹³C NMR (CDCl₃, 50 MHz) δ 14.7 (CH₃), 16.4 (CH₂CH₂CH₃), 27.2, 27.4 (5, 7-C), 33.8 (CH₂CH₂CH₃), 34.4 (4, 9-C), 37.9 (8, 10-C), 38.5 (1, 3-C), 40.0 (6-C), 69.7 (2-C).

To a stirred suspension of LiAlH₄ (390 mg, 10.3 mmol) in dry ether (20 mL) was added, dropwise at 0 °C, a solution of the azide 15 (490 mg, 2.57 mmol) in dry ether (10 mL). The reaction mixture was refluxed for 5 h (TLC monitoring) and then hydrolyzed with water and NaOH (15%) and water under ice cooling. The inorganic precipitate was filtered off and washed with ether, and the filtrate was extracted with HCl (6%). The aqueous layer was made alkaline with solid Na₂CO₃, and the mixture was extracted with ether. The combined ether extracts were washed with water and brine and dried (Na₂SO₄). After evaporation of the solvent the oily amine 6 was obtained: yield 350 mg (74%); ¹H NMR (CDCl₃, 400 MHz) δ 0.92 (t, *J* = 7 Hz, 3H, CH₃), 1.29–1.40 (m, 2H, CH₂CH₂CH₃), 1.52 (d, *J* = 12 Hz, 2H, 4'eq, 9'eq-H), 1.58–1.61 (m, 2H, CH₂CH₂CH₃), 1.67 (d, *J* = 12 Hz, 2H, 8'eq, 10'eq-H), 1.66 (br s, 2H, 6'-H), 1.68 (br s, 2H, 1', 3'-H), 1.78 (br s, 2H, 5', 7'-H), 1.83 (d, *J* = 12 Hz, 2H, 8'ax, 10'ax-H), 2.16 (d, *J* = 12 Hz, 1H, 4'ax, 9'ax-H). Hydrochloride: mp > 250 °C (EtOH–Et₂O). Anal. Calcd for C₁₃H₂₄NCl: C, 67.95; H, 10.53; N, 6.10. Found: C, 68.02; H, 10.63; N, 5.95.

2-*n*-Butyltricyclo[3.3.1.1^{3,7}]decan-2-amine (7). Tertiary alcohol 18 was obtained after treating a solution of adamantanone 12 (500 mg, 3.34 mmol) in dry THF (30% solution w/v) with 3 molar excess of *n*-butyllithium (6 mL, 10.02 mmol, 1.6 M in hexanes) at 0 °C and stirring the mixture overnight: yield 96%; ¹H NMR (CDCl₃, 400 MHz) δ 0.91 (t, *J* = 7 Hz, 3H, CH₃), 1.25–1.38 (m, 4H, CH₃CH₂CH₂CH₂), 1.54 (d, *J* = 12 Hz, 2H, 4'eq, 9'eq-H), 1.58–1.72 (m, 8H, 1', 3', 5', 7', 8'eq, 10'eq-H, CH₃CH₂CH₂CH₂), 1.78–1.90 (m, 4H, 8'ax, 10'ax-H, 5',7'-H), 2.16 (d, *J* = 12 Hz, 1H, 4'ax, 9'ax-H); ¹³C NMR (CDCl₃, 50 MHz) δ 14.3 (CH₃), 23.5

(CH₂CH₂CH₂CH₃), 24.4 (CH₂CH₂CH₂CH₃), 27.4, 27.6 (5',7'-C), 34.7 (4',9'-C), 33.1 (8',10'-C), 37.1 (1',3'-C), 38.2 (CH₂CH₂CH₂CH₃), 38.5 (6'-C), 75.2 (2'-C).

To a stirred mixture of NaN₃ (280 mg, 4.32 mmol) and dry dichloromethane (20 mL) at 0 °C, TFA (1.6 mg, 14.4 mmol) was added. To the stirred mixture, a solution of tertiary alcohol **18** (300 mg, 1.44 mmol) in dry dichloromethane (10 mL) was added, and stirring was maintained at 0 °C for 4 h. The mixture was stirred at ambient temperature for 24 h and then was treated with NH₃ 12% (30 mL) at 0 °C. The organic phase was separated, and the aqueous phase was extracted twice with an equal volume of dichloromethane. The combined organic phase was washed with water and brine, dried (Na₂SO₄), and evaporated to afford oily azide **25**: yield 96%; IR (Nujol) ν (N₃) 2088 cm⁻¹; ¹H NMR (CDCl₃, 400 MHz) δ 0.96 (t, *J* = 7 Hz, 3H, CH₃), 1.32–1.42 (m, 4H, CH₃CH₂CH₂CH₂), 1.62 (d, *J* = 12 Hz, 2H, 4'eq, 9'eq-H), 1.70–1.93 (m, 12H, adamantane-H, CH₃CH₂CH₂CH₂), 2.14 (d, *J* = 12 Hz, 2H, 4'ax, 9'ax-H); ¹³C NMR (CDCl₃, 50 MHz) δ 14.2 (CH₃), 23.3 (CH₂CH₂CH₂CH₃), 24.9 (CH₂CH₂CH₂CH₃), 27.2, 27.4 (5',7'-C), 33.8 (4',9'-C), 33.7 (8',10'-C), 34.4 (1',3'-C), 35.2 (CH₂CH₂CH₂CH₃), 38.5 (6'-C), 69.7 (2'-C).

To a stirred suspension of LiAlH₄ (163 mg, 4.29 mmol) in dry ether (15 mL) was added, dropwise at 0 °C, a solution of the azide **25** (250 mg, 1.07 mmol) in dry ether (10 mL). The reaction mixture was refluxed for 5 h (TLC monitoring) and then hydrolyzed with water and NaOH (15%) and water under ice cooling. The inorganic precipitate was filtered off and washed with ether, and the filtrate was extracted with HCl (6%). The aqueous layer was made alkaline with solid Na₂CO₃, and the mixture was extracted with ether. The combined ether extracts were washed with water and brine and dried (Na₂SO₄). After evaporation of the solvent the oily amine **7** was obtained: yield 50 mg (23%); ¹H NMR (CDCl₃, 400 MHz) δ 0.88 (t, *J* = 7 Hz, 3H, CH₃), 1.18–1.32 (m, 4H, CH₃CH₂CH₂CH₂), 1.45–1.65 (m, 10H, adamantane-H, CH₃CH₂CH₂CH₂), 1.77 (br s, 2H, 5',7'-H), 1.93 (d, *J* = 12 Hz, 2H, 8'ax, 10'ax-H), 2.03 (d, *J* = 12 Hz, 2H, 4'ax, 9'ax-H), 2.13 (br s, 2H, NH₂); ¹³C NMR (CDCl₃, 50 MHz) δ 14.3 (CH₃), 23.7 (CH₂CH₂CH₂CH₃), 24.6 (CH₂CH₂CH₂CH₃), 27.5, 27.8 (5',7'-C), 34.1 (4',9'-C), 33.2 (8',10'-C), 37.5 (1',3'-C), 38.6 (6'-C), 39.1 (CH₂CH₂CH₂CH₃), 54.5 (2'-C). Fumarate: mp 220 °C (EtOH–Et₂O). Anal. Calcd for C₁₈H₂₉NO₄: C, 66.86; H, 9.26; N, 4.32. Found: C, 66.91; H, 9.30; N, 4.29.

2-Isobutyltricyclo[3.3.1.1^{3,7}]decan-2-amine (8). Tertiary alcohol **19** was obtained after treating a solution of 2-adamantanone **12** (500 mg, 3.34 mmol) in dry THF (5 mL) with isobutyllithium (8 mL, 10.02 mmol, 1.6 M in hexanes) at 0 °C in a 1:3 ratio as before: yield 85%; ¹H NMR (CDCl₃, 400 MHz) δ 0.96 (d, *J* = 7 Hz, 6H, 2 x CH₃), 1.52 (d, *J* = 12 Hz, 2H, 4'eq, 9'eq-H), 1.57 (d, *J* = 6 Hz, 2H, CH₂CHMe₂), 1.66 (1',3',6'-H), 1.68–1.74 (m, 2H, 8'eq, 10'eq-H), 1.78 (br s, 2H, 5',7'-H), 1.76–1.87 (m, 1H, CH₂CHMe₂), 1.82 (d, *J* = 12 Hz, 2H, 8'ax, 10'ax-H), 2.16 (d, *J* = 12 Hz, 2H, 4'ax, 9'ax-H); ¹³C NMR (CDCl₃, 50 MHz) δ 23.2 (2 x CH₃), 25.3 (CH₂CHMe₂), 27.5 (5',7'-C), 35.1 (4',9'-C), 33.1 (8',10'-C), 37.6 (1',3'-C), 38.5 (6'-C), 46.5 (CH₂CHMe₂), 75.9 (2'-C). The corresponding azide **26** was prepared from the alcohol **19** (300 mg, 1.44 mmol) according to the same procedure followed for azide **25** using CH₂Cl₂ (30 mL)/NaN₃ (280 mg, 4.32 mmol)/TFA (1.6 mg, 14.4 mmol): yield 95%; IR (Nujol) ν (N₃) 2095 cm⁻¹; ¹³C NMR (CDCl₃, 50 MHz) 23.4 (2 x CH₃), 24.5 (CH₂CHMe₂), 27.3 (5',7'-C), 33.9 (4',9'-C), 33.6 (8',10'-C), 34.7 (1',3'-C), 38.5 (6'-C), 43.0 (CH₂CHMe₂), 69.7 (2'-C).

The corresponding oily amine **8** was prepared through LiAlH₄ (183 mg, 4.80 mmol) reduction of azide **26** (280 mg, 1.20 mmol) in refluxing ether for 5 h according to the same procedure followed for amine **7**: yield 65%; ¹H NMR (CDCl₃, 400 MHz) δ 0.94 (d, *J* = 7 Hz, 6H, 2 x CH₃), 1.49 (d, *J* = 6 Hz, 2H, CH₂CHMe₂), 1.52–1.65 (m, 2H, 1',3',6',4'eq,9'eq-H), 1.73–1.83 (m, 1H, CH₂CHMe₂), 1.75 (br s, 2H, 5',7'-H), 1.95 (d, *J* = 12 Hz, 2H, 8'ax, 10'ax-H), 2.05 (d, *J* = 12 Hz, 2H, 4'ax, 9'ax-H); ¹³C NMR (CDCl₃, 50 MHz) δ 23.4 (2 x CH₃), 25.7 (CH₂CHMe₂), 27.6 (5',7'-C), 34.3 (4',9'-C), 33.1 (8',10'-C), 38.0 (1',3'-C), 39.1 (6'-C), 47.4 (CH₂CHMe₂), 55.4 (2'-C). Fumarate: mp 225 °C (EtOH–Et₂O). Anal. Calcd for C₁₈H₂₉NO₄: C, 66.86; H, 9.26; N, 4.32. Found: C, 66.91; H, 9.30; N, 4.29.

2-*n*-Hexyltricyclo[3.3.1.1^{3,7}]decan-2-amine (9). Tertiary alcohol **20** was obtained after the reaction of *n*-hexyllithium with 2-adamantanone **12** (500 mg, 3.34 mmol) in dry THF (5 mL) with *n*-hexyllithium (4 mL, 10.02 mmol, 2.47 M in hexanes) at 0 °C in a 1:3 ratio as before: yield 97%; IR (Nujol) ν (OH) 3391 cm⁻¹; ¹H NMR (CDCl₃, 400 MHz) δ 0.87 (t, *J* = 7 Hz, 3H, CH₃), 1.24–1.33 (m, 8H, CH₂(CH₂)₄CH₃), 1.51–1.54 (d, *J* = 12 Hz, 2H, 4'eq, 9'eq-H), 1.60–1.64 (m, 2H, CH₂(CH₂)₄CH₃), 1.66–1.69 (m, 6H, 1',3',6', 5',7'-H), 1.78–1.81 (d, *J* = 11 Hz, 2H, 8'ax, 10'ax-H), 2.14–2.17 (d, *J* = 12 Hz, 2H, 4'ax, 9'ax-H); ¹³C NMR (CDCl₃, 50 MHz) δ 14.2 ((CH₂)₄CH₃), 22.1 ((CH₂)₄CH₃), 22.7 ((CH₂)₃CH₂CH₂CH₃), 27.4–27.6 (5',7'-C), 30.1 (CH₂CH₂CH₂(CH₂)₂CH₃), 32.0 (CH₂CH₂(CH₂)₃CH₃), 33.1 (4',9'-C), 34.7 (8',10'-C), 37.1 (1',3'-C), 38.4 (CH₂(CH₂)₄CH₃), 38.5 (6'-C), 75.1 (2'-C).

The corresponding azide **27** was prepared from the alcohol **20** (400 mg, 1.69 mmol) according to the same procedure followed for azide **25** using CH₂Cl₂ (30 mL)/NaN₃ (330 mg, 5.07 mmol)/TFA (1.9 mg, 16.9 mmol): yield 91%; IR (Nujol) ν (N₃) 2088 cm⁻¹; ¹³C NMR (CDCl₃, 50 MHz) δ 14.2 ((CH₂)₄CH₃), 22.6 ((CH₂)₄CH₂CH₃), 22.7 (CH₂)₃CH₂CH₂CH₃, 27.2–27.4 (5',7'-C), 29.9 (CH₂CH₂CH₂(CH₂)₂CH₃), 31.9 (CH₂CH₂(CH₂)₃CH₃), 33.7 (4',9'-C), 33.8 (8',10'-C), 34.4 (1',3'-C), 35.4 (CH₂(CH₂)₄CH₃), 38.5 (6'-C), 69.7 (2'-C).

The corresponding oily amine **9** was prepared through LiAlH₄ (233 mg, 6.13 mmol) reduction of azide **27** (400 mg, 1.53 mmol) in refluxing ether for 5 h according to the same procedure followed for amine **7**: yield 97%; ¹H NMR (CDCl₃, 400 MHz) δ 0.87 (t, *J* = 7 Hz, 3H, CH₃), 1.24–1.30 (m, 8H, CH₂(CH₂)₄CH₃), 1.51–1.56 (m, 4H, 4'eq, 9'eq-H, CH₂(CH₂)₄CH₃), 1.57–1.67 (m, 6H, 1', 3', 6', 8'eq, 10'eq-H), 1.79 (br s, 2H, 5',7'-H), 1.93 (d, *J* = 12 Hz, 2H, 8'ax, 10'ax-H), 2.04 (d, *J* = 12 Hz, 2H, 4'ax, 9'ax-H); ¹³C NMR (CDCl₃, 50 MHz) δ 14.2 (CH₃), 22.3 ((CH₂)₄CH₂CH₃), 22.8 ((CH₂)₃CH₂CH₂CH₃), 27.4–27.8 (5',7'-C), 30.3 (CH₂CH₂CH₂(CH₂)₂CH₃), 32.0 (CH₂CH₂(CH₂)₃CH₃), 33.1 (4',9'-C), 34.1 (8',10'-C), 37.4 (1',3'-C), 38.8 (CH₂(CH₂)₄CH₃), 39.1 (6'-C), 54.6 (2'-C). Fumarate: mp 225 °C (EtOH–Et₂O). Anal. Calcd for C₂₀H₃₃NO₄: C, 68.94; H, 9.46; N, 3.99. Found: C, 68.59; H, 9.55; N, 3.79.

2-Phenyltricyclo[3.3.1.1^{3,7}]decan-2-amine (10). Tertiary alcohol **21** was obtained after treating a solution of adamantanone **12** (500 mg, 3.34 mmol) in dry THF (30% solution w/v) with 2 molar excess PhMgBr (obtained from bromobenzene (1.05 g, 6.68 mmol) and 1.5 molar excess of Mg (240 mg, 10.02 mmol) in 20 mL of dry ether/g bromobenzene) and stirring the mixture overnight: yield 95%; ¹H NMR (CDCl₃, 400 MHz) δ 1.67–1.77 (m, 8H, adamantane-H), 1.89 (br s, 2H, 5',7'-H), 2.14 (s, 1H, OH), 2.40 (d, *J* = 12 Hz, 1H, 4'ax, 9'ax-H), 2.56 (br s, 2H, 1',3'-H), 7.20–7.60 (m, 5H, phenyl-H); ¹³C NMR (CDCl₃, 50 MHz) δ 27.0, 27.5 (5',7'-C), 33.1 (4',9'-C), 34.9 (8',10'-C), 35.7 (1',3'-C), 37.8 (6'-C), 75.8 (2'-C), 125.5, 127.1, 127.2, 128.8, 143.0 (Ph).

The corresponding azide **28** was prepared from alcohol **21** (300 mg, 1.31 mmol) according to the same procedure followed for azide **25** using CH₂Cl₂ (30 mL)/NaN₃ (256 mg, 3.94 mmol)/TFA (1.49 mg, 13.1 mmol): yield 95%; IR (Nujol) ν (N₃) 2098 cm⁻¹; ¹³C NMR (CDCl₃, 50 MHz) δ 26.8, 27.4 (5',7'-C), 33.1 (4',9'-C), 33.4 (8',10'-C), 34.1 (1',3'-C), 37.7 (6'-C), 70.3 (2'-C), 125.6, 127.3, 127.8, 128.9, 140.3 (Ph).

The corresponding oily amine **10** was prepared through LiAlH₄ (175 mg, 4.58 mmol) reduction of azide **28** (290 mg, 1.15 mmol) in refluxing ether for 5 h according to the same procedure followed for amine **7**: yield 55%; ¹H NMR (CDCl₃, 400 MHz) δ 1.53 (br s, 2H, 6'-H), 1.61–1.80 (m, 6H, adamantane-H), 1.90 (br s, 2H, 5',7'-H), 2.33 (d, *J* = 12 Hz, 1H, 4'ax, 9'ax-H), 2.45 (br s, 2H, 1',3'-H), 7.18–7.25 (m, 5H, phenyl-H); ¹³C NMR (CDCl₃, 50 MHz) δ 27.2, 27.6 (5',7'-C), 32.9 (4',9'-C), 34.6 (8',10'-C), 35.8 (1',3'-C), 38.2 (6'-C), 57.8 (2'-C), 125.2, 126.2, 128.8, 148.7 (Ph). Hydrochloride: mp > 265 °C (EtOH–Et₂O). Anal. Calcd for C₁₆H₂₂NCl: C, 72.85; H, 8.41; N, 5.31. Found: C, 72.81; H, 8.63; N, 5.29.

2-Benzyltricyclo[3.3.1.1^{3,7}]decan-2-amine (11). Tertiary alcohol **22** was obtained after treating a solution of adamantanone **12** (500

mg, 3.34 mmol) in dry THF (30% solution w/v) with 2-molar excess PhCH₂MgCl (obtained from PhCH₂Cl (846 mg, 6.68 mmol) and 1.5 molar excess of Mg (243 mg, 10.02 mmol) in 20 mL of dry ether/g bromobenzene) and stirring the mixture overnight: yield 95%; ¹H NMR (CDCl₃, 400 MHz) δ 1.51 (d, *J* = 12 Hz, 2H, 4'eq, 9'eq-H), 1.65 (br s, 1H, 6'-H), 1.69 (br s, 1H, 5',7'-H), 1.77 (d, *J* = 12 Hz, 2H, 8'eq, 10'eq-H), 1.78 (br s, 1H, 3'-H), 1.90 (br s, 1H, 1'-H), 2.07 (d, *J* = 12 Hz, 1H, 8'ax, 10'ax-H), 2.12 (d, *J* = 12 Hz, 1H, 4'ax, 9'ax-H), 2.97 (s, 2H, CH₂Ph), 7.10–7.32 (m, 5H, phenyl-H); ¹³C NMR (CDCl₃, 50 MHz) δ 27.4, 27.5 (5',7'-C), 33.1 (4',9'-C), 34.7 (8',10'-C), 36.9 (1',3'-C), 38.5 (6'-C), 43.9 (CH₂Ph), 74.7 (2'-C), 126.5, 128.3, 130.7, 137.4 (Ph).

The corresponding azide **29** was prepared from alcohol **22** (300 mg, 1.24 mmol) according to the same procedure followed for azide **25** using CH₂Cl₂ (30 mL)/NaN₃ (241 mg, 3.71 mmol)/TFA (1.41 mg, 12.4 mmol): yield 50%; IR (Nujol) ν(N₃) 2096 cm⁻¹; ¹³C NMR (CDCl₃, 50 MHz) δ 27.1, 27.4 (5',7'-C), 33.7 (4',9'-C), 33.8 (8',10'-C), 34.1 (1',3'-C), 38.4 (6'-C), 41.4 (CH₂Ph), 69.8 (2'-C), 126.7, 128.2, 130.3, 136.6 (Ph).

The corresponding oily amine **11** was prepared through LiAlH₄ (130 mg, 3.45 mmol) reduction of azide **29** (230 mg, 0.861 mmol) in refluxing ether for 5 h according to the same procedure followed for amine **7**: yield 45%; ¹H NMR (CDCl₃, 400 MHz) δ 1.61 (d, *J* = 12 Hz, 2H, 4'eq, 9'eq-H), 1.61 (br s, 1H, 6'-H), 1.73 (br s, 1H, 5',7'-H), 1.78 (d, *J* = 12 Hz, 2H, 8'eq, 10'eq-H), 1.87 (br s, 1H, 3'-H), 1.97 (br s, 1H, 1'-H), 2.09 (d, *J* = 12 Hz, 1H, 8'ax, 10'ax-H), 2.29 (d, *J* = 12 Hz, 1H, 4'ax, 9'ax-H), 2.97 (s, 2H, CH₂Ph), 7.10–7.32 (m, 5H, phenyl-H); ¹³C NMR (CDCl₃, 50 MHz) δ 27.6, 27.8 (5',7'-C), 33.2 (4',9'-C), 34.3 (8',10'-C), 37.3 (1',3'-C), 39.2 (6'-C), 44.2 (CH₂Ph), 55.1 (2'-C), 126.3, 128.1, 130.7, 138.4 (Ph). Fumarate: mp 205 °C (EtOH–Et₂O). Anal. Calcd for C₂₀H₃₃NO₄: C, 70.56; N, 3.92. Found: C, 70.99; N, 3.89.

(B) Biological Testing Methods. Cells and Media. Tissue used for preparation of virus stock cultures, virus infectivity titrations, and miniplaque drug assays were Madin–Darby canine kidney (MDCK) cells (ATCC CCL 34). The cell culture growth medium used was Dulbecco's modified Eagle medium (DMEM, Sigma-Aldrich) supplemented with 0.11% sodium bicarbonate, 5% Cosmic calf serum (Hyclone), 10 mM HEPES buffer, and 50 µg/mL gentamycin. For culture of virus stocks and virus infectivity assays, 0.125% bovine serum albumin (BSA, Sigma-Aldrich) was substituted for the Cosmic calf serum.

Virus. Influenza A virus, the 2009 pandemic strain (A/California/07/2009), was provided by Dr. Don Smee, Utah State University. Trypsin added to BSA-supplemented medium for virus activation was TPCK-treated bovine pancreas trypsin (Sigma-Aldrich). A virus stock culture (passage 1) was prepared in MDCK cells in a 150 cm² culture flask. The cells were plated in growth medium and incubated until the cell monolayer was at 90% confluency. The monolayer was washed with medium containing no serum, then renewed with BSA medium containing 2.5 µg/mL trypsin. The culture was infected with 1 mL of the virus inoculum obtained from Dr. Smee, then incubated at 33 °C. At 2 days postinfection the culture had reached complete cytopathic effect. Detached cells and cell debris were removed by low speed centrifugation (600g for 5 min). The supernate was aliquoted in 1 mL quantities, then frozen at –80 °C for storage. For virus titration, aliquots of the stock were thawed and dilution series were inoculated in MDCK cultures in shell vials and virus-infected cells were detected by immunofluorescence. Other virus strains were obtained from American Type Culture Collection (ATCC): influenza A (H3N2) Victoria/3/75 (ATCC VR-822), influenza A (H1N1) A/PR/8/34 (ATCC VR-95), influenza A (H1N1) A/WS/33 (ATCC VR-1520), and influenza A (H2N2) A2/Taiwan/1/64 (ATCC VR-480). Virus stock cultures were prepared in MDCK cells grown in BSA-supplemented media, processed, and stored as described above.

For resistance studies with A/Hong Kong/1/1968 (H3N2) (Table 4), Petri dishes with MDCK cells (Federal Research Institute for Animal Health, Greifswald-Insel Riems, catalog no. RIE328) were preincubated overnight in Eagle minimum essential medium (EMEM) supplemented with 10% fetal bovine serum, 100 U/mL penicillin, and

100 µg/mL streptomycin, and the assay compound at concentrations corresponding to 5–10× EC₅₀ was determined using the CPE assay.²⁵

Miniplaque Assay. In cell culture, miniplaques consist of single infected cells, double or multiple infected cells contiguously linked, that are observed microscopically and identified by immunofluorescence using FITC-labeled monoclonal antibody against viral protein. Antiviral activity of test drugs was detected in cultures exposed to drug by assessing inhibition of viral protein synthesis (virus replication) as measured by reduction in number of miniplaques. The tests were performed in MDCK cells. Cells were grown on 12 mm glass coverslips in shell vials (Sarstedt) to a cell density of 80–99% confluency in 1 mL of DMEM growth medium per vial. Prior to infection the cultures were washed with serumless media. The serumless medium was replaced with 1 mL per vial of DMEM containing BSA at a concentration of 0.125%. Test drugs at appropriate concentrations were added to the cultures and allowed to equilibrate with the media. Stock virus was thawed, and appropriate concentrations of virus (contained in BSA media) were then exposed to 1.0 µg/mL trypsin for 30 min at room temperature, then added to the cultures. Replicate cultures were included at each dilution step of test chemical. Control cultures containing no antiviral drug were included in each assay. The cultures were then incubated at 33 °C overnight. Cultures were washed with phosphate buffered saline (PBS) within the shell vials, fixed in –80 °C acetone, then stained with anti-influenza A, FITC-labeled monoclonal antibody (Millipore, Billerica, MA, USA). Possible drug toxicity in culture was assessed by microscopic observation of cytologic changes and cell multiplication rates. EC₅₀ determinations were carried out with a fluorescence microscope by counting miniplaques (clusters of infected cells) in confluent MDCK monolayers on a coverslip at drug concentrations of 50, 20, 10, 5 µM, and if necessary, 2 µM. From two to four replicate cultures were included at each drug concentration step. Plaque counts, *C(D)* (including controls and weighted by the standard error of the count for each concentration), were fitted, using the Levenberg–Marquardt algorithm (in KaleidaGraph from Synergy Software, Reading, PA, USA), to the sigmoidal function:

$$C(D) = \frac{C_0}{1 + \frac{D}{EC_{50}}}$$

with *D* being the drug concentration and *C*₀ and EC₅₀ being free parameters. The standard error of the EC₅₀, used as reported by the software, reflects the uncertainties due to variances in the counts at all concentrations, including the controls. The value of *C*₀ was constrained by the four independent controls. For the replicate screens, where the value of EC₅₀ was based only on the four controls and a pair of tests at a fixed concentration, the formal standard errors of the parameters may not adequately represent the uncertainty associated with extrapolating or interpolating the 50% reduction dose from the miniplaque reduction at the assay dose, which would probably be greater the greater the difference is between the assay dose and the EC₅₀. Nevertheless, in spite of this limitation, we found reproducibility of EC₅₀ values to be high (i.e., within factors of ~2) on several occasions where experiments were repeated, either screens repeated by screens or screens compared to complete dose–response curves.

Resistance Testing. For Table 4, cultured MDCK cells bathed in a concentration corresponding to approximately the EC₅₀ concentration were exposed to the usual quantities of virus for 3–4 days (5–7 virus replication cycles). After that time, the cultures developed cytopathic effects, and the cultures were terminated. The medium, containing virus, was then collected by low speed centrifugation. Dose–response tests utilizing the miniplaque technique were performed on the recovered virus for determination of the EC₅₀ against the potentially mutated virus. An increase in the EC₅₀ above the original value represents resistance development. A crude sequence on the passage-12 virus developed in **6** (see text) was carried out by extracting the virus directly with the RNAqueous kit (Life Technologies), transcribed with the Superscript III first-strand

synthesis kit (Life Technologies), amplified by PCR, and sequenced with an Applied Biosystems 3730xl DNA analyzer.

Resistance Test Plaque Sequencing. For the more detailed sequencing in (Supporting Information Table 1), MDCK cells were washed and incubated with influenza virus (multiplicity of infection is 1) for 1 h to allow virus adsorption. Then excessive virus was washed off and cells were incubated with EMEM supplemented with the assay compound for 3–4 days. If no cytopathic effect was visible, 0.5 mL of supernatant was centrifuged (2000 rpm) to remove cell detritus and transferred to Petri dishes with confluent MDCK monolayers (blind passage). Cells were incubated again up to 4 days in EMEM supplemented with the assay compound. If CPE was visible, 1 mL of supernatant was stored at $-80\text{ }^{\circ}\text{C}$ and 0.5 mL was passaged. Up to 10 passages were executed. For sequencing of resistant viruses, serial dilution (10-fold) of the stocks of the first, fourth, and ninth passages were used for plaque assays. Three to five arbitrarily selected plaques of each tested passage and compound were picked, amplified in MDCK cells (yielding second, fifth, and tenth passage virus) and used for RNA preparation as described.²⁶ Briefly, total RNA was prepared from virus-infected MDCK cells using the RNeasy Mini kit and Qiashredder kit (Qiagen, Hilden, Germany). Reverse transcription was conducted with a primer specific to the 3'-end of genomic RNA (5'-RGCRAAAGCAGG-3'), 20 units reverse transcriptase (Fermentas, St. Leon-Rot, Germany), and 5 μg of RNA in a final reaction volume of 20 μL . Specific oligonucleotide primers Bm-M-1 and Bm-M-1027R and Bm-HA-1 and Bm-HA-rev²⁷ were used for the amplification of the M and HA segments from cDNA. Amplified DNA fragments were analyzed by agarose gel electrophoresis and gel-extracted employing the QIAquick gel extraction kit (Qiagen, Hilden, Germany). Purified DNA fragments were sequenced by cycle sequencing using the CEQ DTCS quick start kit (Beckman Coulter, Krefeld, Germany) and analyzed on a CEQ8000 sequencer (Beckman Coulter, Krefeld, Germany).

Electrophysiology Methods. cDNA sequences encoding the full-length A/California/04/09 M2 protein containing an N-terminal FLAG-tag plus 3(Gly) repeat linker and either N31 or an S31 mutation were cloned into pcDNA3 and transiently co-transfected with a pcDNA3 vector encoding eGFP into TSA-201 cells using standard transfection protocols (Lipofectamine 2000, Life Technologies). Single GFP-positive transfected cells were then used for electrophysiological experiments.

Macroscopic ionic currents were recorded in the whole-cell configuration 24–48 h after transfection. Cells were perfused continuously at 3–5 mL/min with external (bath) solution containing the following (in mM): 150 NMG, 10 HEPES, 10 D-glucose, 2 CaCl₂, 1 MgCl₂ buffered at pH 7.4 with HCl. For low pH (5.5) solution, HEPES was replaced by MES. Solutions containing either K⁺ or Na⁺ were prepared by replacing NMG with the corresponding ion. Patch electrodes were pulled from thin-walled borosilicate glass (World Precision Instruments, Fl) and fire-polished before filling with standard pipet solution containing the following (in mM): 140 NMG, 10 EGTA, 10 MES, and 1 MgCl₂ buffered at pH 6.0 with HCl. Pipettes typically had a resistance of 3–5 M Ω . Voltage-clamp experiments were performed with an Axopatch 200B amplifier (Molecular Devices, CA) connected to a Digidata 1322A 16-bit digitizer. Data were acquired with the pCLAMP8.0 software (Molecular Devices, CA) sampled at 10 kHz and low-pass-filtered at 5 kHz. Cells were held at -40 mV . The standard voltage protocol consisted of a 100 ms pulse to -80 mV followed by a 300 ms ramp to $+40\text{ mV}$ and a 200 ms step to 0 mV before stepping back to -40 mV and repeated every 4 s. All experiments were performed at room temperature (20–22 $^{\circ}\text{C}$). All drugs were prepared as DMSO stocks (50 or 100 mM) and diluted with external solution to the desired concentration. To measure block of M2 currents by compounds, cells were recurrently treated with pH 7.4 and pH 5.5 solutions until stable, pH-dependent inward currents were reproducibly observed, followed by treatment with compound and concentration of interest at pH 5.5 for 2–30 min. At the end of each experiment, cells were then treated with 100 μM amantadine.

(C) Peptide Synthesis and Sample Preparation for Solid State NMR. S31N M2 TM (22–46) (A/Udm/307/72) with ¹⁵N labeled V28, A30, and I42 was synthesized using Fmoc (9-fluorenylmethoxycarbonyl) chemistry. Fmoc-^[15N]Val, fmoc-^[15N]Ala, and fmoc-^[15N]Ile were purchased from Cambridge Isotope Laboratory (Andover, MA). Solid-phase 0.25 mmol syntheses of M2 TMD were performed on an Applied Biosystems 430A peptide synthesizer as previously described.²⁸ The peptide was cleaved from the resin by the treatment with ice cold 95% TFA, 2.5% H₂O, 1.25% ethanedithiol, 1.25% thioanisole and precipitated from TFA using ice cold ether. Following centrifugation, the supernatant was discarded and the pellet was washed with cold ether again. The precipitated peptide was dried under vacuum. Peptide purity and identity were confirmed using ESI mass spectrometry (positive ion mode).

¹⁵N-V₂₈A₃₀I₄₂ S31N M2 TMD was co-dissolved in trifluoroethanol (TFE) with 1,2-dimyristoyl-*sn*-glycero-3-phosphocholine (DMPC) in a 1:30 molar ratio. The solvent was removed under a stream of nitrogen gas to yield a lipid film and then dried to remove residual organic solvent under vacuum for 12 h. Thoroughly dried lipid film was hydrated with 8 mL of 10 mM HEPES buffer at pH 7.5 to form multilamellar vesicles containing M2 TMD in tetrameric state. This suspension was bath sonicated, dialyzed against 2 L of HEPES 10 mM, pH 7.5, buffer for 1 day and centrifuged at 196000g to harvest unilamellar proteoliposomes. The pellet was resuspended in a 1 mL aliquot of the decanted supernatant containing compound 6, resulting in a 1:6 molar ratio of the M2 TMD tetramer to drug. Following overnight incubation at 37 $^{\circ}\text{C}$, the pellet was deposited on $5.7 \times 10\text{ mm}$ glass strips (Matsunami Trading, Osaka, Japan). The bulk of the water from the sample was removed during a 2-day period in a 98% relative humidity environment at 298 K. Rehydration of the slides, before stacking and sealing into a rectangular sample cell, generated 40–50% by weight water in the sample. The final sample composition is 1 mg of drug/60 mg of lipid/8 mg of peptide (mole ratio 1:20:0.7) with 40–50% hydration.

Solid State NMR Experiments. PISEMA spectra were acquired at 720 MHz utilizing a low-E ¹H/¹⁵N double resonance probe.^{28,29} Acquisition took place at 303 K, above the gel to liquid crystalline phase transition temperature of DMPC lipids. Experimental parameters included a 90° pulse of 5 μs and cross-polarization contact time of 1 ms, a 4 s recycle delay, and a SPINAL decoupling sequence.³⁰ Sixteen t_1 increments were obtained for the spectrum of ¹⁵N-V₂₈A₃₀I₄₂ S31N M2 TMD with compound 6, and nine t_1 increments were obtained for the sample without compound. Spectral processing was done with NMRPIPE³¹ and plotting with SPARKY. ¹⁵N chemical shifts were referenced to a concentrated solution of N₂H₈SO₄, defined as 26.8 ppm relative to liquid ammonia.

■ ASSOCIATED CONTENT

📄 Supporting Information

Plaque hemagglutinin-sequencing results, plaque M1-sequencing results, plaque M2-sequencing results, and representative diary plots from tSA-201 HEK cells. This material is available free of charge via the Internet at <http://pubs.acs.org>.

■ AUTHOR INFORMATION

Corresponding Authors

*A.K.: phone, 30-210-727-4834; e-mail, ankol@pharm.uoa.gr.

*D.D.B.: phone, 801-422-8753; e-mail, david_busath@byu.edu.

Author Contributions

A.K. and C.T. synthesized compounds. F.B.J. and R.Z. did dose–response and resistance tissue-culture testing. T.A.C. and A.K.W. did solid state NMR. I.T. and D.F. did electrophysiology tests. A.K. and D.D.B. conceived and supervised the project and wrote the paper with input from the coauthors.

Notes

The authors declare no competing financial interest.

ACKNOWLEDGMENTS

The authors thank Dr. Donald Smee for providing influenza A/California/07/2009 (H1N1) and Dr. Michaela Schmidtke for her collaboration and her valuable suggestions. D.D.B. thanks Curtis Evans, Steven Kearnes, Nathan Gay, Ben Nielsen, Trevor Anderson, Robert Childs, and Joseph Moulton. R.Z. thanks Birgit Jahn and Martina Müller, and D.F. thanks Daniel Kwan for technical assistance. The work is part of C.T.'s Master's thesis and was supported by grants from Chiesi Hellas (Project 10354, Special Account for Research Grants), the German Ministry for Education and Science (FluResearchNet, Grant 01 KI1006J), and NIH (Grants AI 23007 and AI 074805).

REFERENCES

- (1) Bright, R. A.; Medina, M. J.; Xu, X.; Perez-Orozco, G.; Wallis, T. R.; Davis, X. M.; Povinelli, L.; Cox, N. J.; Klimov, A. I. Incidence of adamantane resistance among influenza A (H3N2) viruses isolated worldwide from 1994 to 2005: a cause for concern. *Lancet* **2005**, *366*, 1175–1181.
- (2) (a) Bright, R. A.; Shay, D. K.; Shu, B.; Cox, N. J.; Klimov, A. I. Adamantane resistance among influenza A viruses isolated early during the 2005–2006 influenza season in the United States. *JAMA, J. Am. Med. Assoc.* **2006**, *295*, 891–894. (b) Lan, Y.; Zhang, Y.; Dong, L.; Wang, D.; Huang, W.; Xin, L.; Yang, L.; Zhao, X.; Li, Z.; Wang, W.; Li, X.; Xu, C.; Guo, J.; Wang, M.; Peng, Y.; Gao, Y.; Guo, Y.; Wen, L.; Jiang, T.; Shu, Y. A comprehensive surveillance of adamantane resistance among human influenza A virus isolated from mainland China between 1956 and 2009. *Antiviral Ther.* **2010**, *15*, 853–859.
- (3) High levels of adamantane resistance among influenza A (H3N2) viruses and interim guidelines for use of antiviral agents—United States, 2005–06 influenza season. *Morbidity Mortality Wkly. Rep.* **2006**, *55*, 44–46.
- (4) See, for examples, the following: (a) Kolocouris, N.; Foscolos, G. B.; Kolocouris, A.; Marakos, P.; Pouli, N.; Fytas, G.; Ikeda, S.; De Clercq, E. Synthesis and antiviral activity evaluation of some aminoadamantane derivatives. *J. Med. Chem.* **1994**, *37*, 2896–2902. (b) Kolocouris, A.; Spearpoint, P.; Martin, S. R.; Hay, A. J.; Lopez-Querol, M.; Sureda, F. X.; Padalko, E.; Neyts, J.; De Clercq, E. Comparisons of the influenza virus A M2 channel binding affinities, anti-influenza virus potencies and NMDA antagonistic activities of 2-alkyl-2-aminoadamantanes and analogues. *Bioorg. Med. Chem. Lett.* **2008**, *18*, 6156–6160.
- (5) (a) Stouffer, A. L.; Acharya, R.; Salom, D.; Levine, A. S.; Di Costanzo, L.; Soto, C. S.; Tereshko, V.; Nanda, V.; Stayrook, S.; DeGrado, W. F. Structural basis for the function and inhibition of an influenza virus proton channel. *Nature* **2008**, *451*, 596–599. (b) Cady, S. D.; Schmidt-Rohr, K.; Wang, J.; Soto, C. S.; DeGrado, W. F.; Hong, M. Structure of the amantadine binding site of influenza M2 proton channels in lipid bilayers. *Nature* **2010**, *463*, 689–692. (c) Cady, S. D.; Wang, J.; Wu, Y.; DeGrado, W. F.; Hong, M. Specific binding of adamantane drugs and direction of their polar amines in the pore of the influenza M2 transmembrane domain in lipid bilayers and dodecylphosphocholine micelles determined by NMR spectroscopy. *J. Am. Chem. Soc.* **2011**, *133*, 4274–4284. (d) Pielak, R. M.; Oxenoid, K.; Chou, J. J. Structural investigation of rimantadine inhibition of the AM2-BM2 chimera channel of influenza viruses. *Structure* **2011**, *19*, 1655–1663. (e) Hu, J.; Fu, R.; Cross, T. A. The chemical and dynamical influence of the anti-viral drug amantadine on the M2 proton channel transmembrane domain. *Biophys. J.* **2007**, *93*, 276–283.
- (6) Wang, J.; Wu, Y.; Ma, C.; Fiorin, G.; Pinto, L. H.; Lamb, R. A.; Klein, M. L.; DeGrado, W. F. Structure and inhibition of the drug-resistant S31N mutant of the M2 ion channel of influenza A virus. *Proc. Natl. Acad. Sci. U.S.A.* **2013**, *110*, 1315–1320.
- (7) Scholtissek, C.; Quack, G.; Klenk, H. D.; Webster, R. G. How to overcome resistance of influenza A viruses against adamantane derivatives. *Antiviral Res.* **1998**, *37*, 83–95.
- (8) Kurtz, S.; Luo, G.; Hahnenberger, K. M.; Brooks, C.; Gecha, O.; Ingalls, K.; Numata, K.; Krystal, M. Growth impairment resulting from expression of influenza virus M2 protein in *Saccharomyces cerevisiae*: identification of a novel inhibitor of influenza virus. *Antimicrob. Agents Chemother.* **1995**, *39*, 2204–2209.
- (9) (a) Balannik, V.; Wang, J.; Ohigashi, Y.; Jing, X.; Magavern, E.; Lamb, R. A.; DeGrado, W. F.; Pinto, L. H. Design and pharmacological characterization of inhibitors of amantadine-resistant mutants of the M2 ion channel of influenza A virus. *Biochemistry* **2009**, *49*, 696–708. (b) Duque, M. D.; Ma, C.; Torres, E.; Wang, J.; Naesens, L.; Juarez-Jimenez, J.; Camps, P.; Luque, F. J.; DeGrado, W. F.; Lamb, R. A.; Pinto, L. H.; Vazquez, S. Exploring the size limit of templates for inhibitors of the M2 ion channel of influenza A virus. *J. Med. Chem.* **2011**, *54*, 2646–2457. (c) Wang, J.; Ma, C.; Fiorin, G.; Carnevale, V.; Wang, T.; Hu, F.; Lamb, R. A.; Pinto, L. H.; Hong, M.; Klein, M. L.; DeGrado, W. F. Molecular dynamics simulation directed rational design of inhibitors targeting drug-resistant mutants of influenza A virus M2. *J. Am. Chem. Soc.* **2011**, *133*, 12834–12841. (d) Rey-Carrizo, M.; Torres, E.; Ma, M.; Barniol-Xicota, M.; Wang, J.; Wu, Y.; Naesens, L.; DeGrado, W. F.; Lamb, R. A.; Pinto, L. H.; Vázquez, S. 3-Azatetracyclo[5.2.1.1^{5,8}.0^{1,5}]undecane derivatives: from wild-type inhibitors of the M2 ion channel of influenza A virus to derivatives with potent activity against the V27A mutant. *J. Med. Chem.* **2013**, *56*, 9265–9274.
- (10) (a) Zhang, W. Heterodimers of histidine and amantadine as inhibitors for wild type and mutant M2 channels of influenza A. *Chin. J. Chem.* **2010**, *28*, 1417–1423. (b) Shibnev, V. A.; Garayev, T. M.; Finogenova, M. P.; Shevchenko, E. S.; Burtseva, E. I. New adamantane derivatives and ways of overcoming the resistance of influenza A viruses to rimantadine and amantadine. *Vopr. Virusol.* **2011**, *56*, 36–39. (c) Zhao, X.; Jie, Y.; Rosenberg, M. R.; Wan, J.; Zeng, S.; Cui, W.; Xiao, Y.; Li, Z.; Tu, Z.; Casarotto, M. G.; Hu, W. Design and synthesis of pinanamine derivatives as anti-influenza A M2 ion channel inhibitors. *Antiviral Res.* **2012**, *96*, 91–99. (d) Shibnev, V. A.; Garaev, T. M.; Finogenova, M. P.; Shevchenko, E. S.; Burtseva, E. I. New adamantane derivatives can overcome resistance of influenza A(H1N1)pdm2009 and A(H3N2) viruses to rimantadine. *Bull. Exp. Biol. Med.* **2012**, *153*, 233–235. (e) Torres, E.; Fernández, R.; Miquet, S. P.; Font-Bardia, M.; Vanderlinden, E.; Naesens, L.; Vázquez, S. Synthesis and anti-influenza A virus activity of 2,2-dialkylamantadines and related compounds. *ACS Med. Chem. Lett.* **2012**, *3*, 1065–1069. (f) Wang, J.; Ma, C.; Jo, H.; Canturk, B.; Fiorin, G.; Pinto, L. H.; Lamb, R. A.; Klein, M. L.; DeGrado, W. F. Discovery of novel dual inhibitors of wild-type and the most prevalent drug-resistant mutant, S31N, of M2 proton channel from influenza A virus. *J. Med. Chem.* **2013**, *56*, 2804–2812. (g) Torres, E.; Duque, M. D.; Vanderlinden, E.; Ma, C.; Pinto, L. H.; Camps, P.; Froeyen, M.; Vazquez, S.; Naesens, L. Role of the viral hemagglutinin in the anti-influenza virus activity of newly synthesized polycyclic amine compounds. *Antiviral Res.* **2013**, *99*, 281–291.
- (11) Kalir, A.; Balderman, D. *Org. Synth.* **1981**, *60*, 104–107.
- (12) Sasaki, T.; Eguchi, S.; Toi, N. Synthesis of adamantane derivatives. 47. Photochemical synthesis of 4-azahomoadamant-4-enes and further studies on their reactivity in some cycloadditions. *J. Org. Chem.* **1979**, *44*, 3711–3715.
- (13) Wang, J.; Denny, J.; Tian, C.; Kim, S.; Mo, Y.; Kovacs, F.; Song, Z.; Nishimura, K.; Gan, Z.; Fu, R.; Quine, J. R.; Cross, T. A. Imaging membrane protein helical wheels. *J. Magn. Reson.* **2000**, *144*, 162–167.
- (14) Hu, J.; Asbury, T.; Achuthan, S.; Li, C.; Bertram, R.; Quine, J. R.; Fu, R.; Cross, T. A. Backbone structure of the amantadine-blocked trans-membrane domain M2 proton channel from influenza A virus. *Biophys. J.* **2007**, *92*, 4335–4343.
- (15) Li, C.; Qin, H.; Gao, F. P.; Cross, T. A. Solid-state NMR characterization of conformational plasticity within the transmembrane domain of the influenza A M2 proton channel. *Biochim. Biophys. Acta* **2007**, *1768*, 3162–3170.

- (16) (a) Chizhnikov, I. V.; Geraghty, F. M.; Ogden, D. C.; Hayhurst, A.; Antoniou, M.; Hay, A. J. Selective proton permeability and pH regulation of the influenza virus M2 channel expressed in mouse erythroleukaemia cells. *J. Physiol.* **1996**, *494*, 329–336. (b) Balannik, V.; Carnevale, V.; Fiorin, G.; Levine, B. G.; Lamb, R. A.; Klein, M. L.; DeGrado, W. F.; L Pinto, L. H. Functional studies and modeling of pore-lining residue mutants of the influenza A virus M2 ion channel. *Biochemistry* **2010**, *49*, 696–708.
- (17) Appleyard, G. Amantadine-resistance as a genetic marker for influenza viruses. *J. Gen. Virol.* **1977**, *36*, 249–255.
- (18) Oxford, J. S.; Potter, C. W.; Logan, I. S. Passage of influenza strains in the presence of aminoadamantane. *Ann. N.Y. Acad. Sci.* **1970**, *173*, 300–313.
- (19) Hayden, F. G.; Sperber, S. J.; Belshe, R. B.; Clover, R. D.; Hay, A. J.; Pyke, S. Recovery of drug-resistant influenza A virus during therapeutic use of rimantadine. *Antimicrob. Agents Chemother.* **1991**, *35*, 1741–1747.
- (20) Hay, A. J.; Wolstenholme, A. J.; Skehel, J. J.; Smith, M. H. The molecular basis of the specific anti-influenza action of amantadine. *EMBO J.* **1985**, *4*, 3021–3024.
- (21) Gamblin, S. J.; Haire, L. F.; Russell, R. J.; Stevens, D. J.; Xiao, B.; Ha, Y.; Vasisht, N.; Steinhauer, D. A.; Daniels, R. S.; Elliot, A.; Wiley, D. C.; Skehel, J. J. The structure and receptor binding properties of the 1918 influenza hemagglutinin. *Science* **2004**, *303*, 1838–1842.
- (22) Shibata, M.; Aoki, H.; Tsurumi, T.; Sugiura, Y.; Nishiyama, Y.; Suzuki, S.; Maeno, K. Mechanism of uncoating of influenza B virus in MDCK cells: action of chloroquine. *J. Gen. Virol.* **1983**, *64*, 1149–1156.
- (23) Dudleemajil, E.; Lin, C. Y.; Dredge, D.; Murray, B. K.; Robison, R. A.; Johnson, F. B. Bovine parvovirus uses clathrin-mediated endocytosis for cell entry. *J. Gen. Virol.* **2010**, *91*, 3032–3041.
- (24) Kuehn, B. M. CDC: Use antivirals early, aggressively for H7N9 flu. *JAMA, J. Am. Med. Assoc.* **2013**, *309*, 2086.
- (25) Schmidtke, M.; Schnittler, U.; Jahn, B.; Dahse, H. M.; Stelzner, A. A rapid assay for evaluation of antiviral activity against coxsackievirus B3, influenza virus A, and herpes simplex virus type 1. *J. Virol. Methods* **2001**, *95*, 133–143.
- (26) Krumbholz, A.; Schmidtke, M.; Bergmann, S.; Motzke, S.; Bauer, K.; Stech, J.; Dürrwald, R.; Wutzler, P.; Zell, R. High prevalence of amantadine resistance among circulating European porcine influenza A viruses. *J. Gen. Virol.* **2009**, *90*, 900–908.
- (27) Hoffmann, E.; Stech, J.; Guan, Y.; Webster, R. G.; Perez, D. R. Universal primer set for the full-length amplification of all influenza A viruses. *Arch. Virol.* **2001**, *146*, 2275–2289.
- (28) Kovacs, F. A.; Cross, T. A. Transmembrane four-helix bundle of influenza A M2 protein channel: structural implications from helix tilt and orientation. *Biophys. J.* **1997**, *73*, 2511–2517.
- (29) Wu, C. H.; Ramamoorthy, A.; Opella, S. J. High-resolution heteronuclear dipolar solid-state NMR spectroscopy. *J. Magn. Reson.* **1994**, *109*, 270–272.
- (30) Fung, B. M.; Khitrin, A. K.; Ermolaev, K. An improved broadband decoupling sequence for liquid crystals and solids. *J. Magn. Reson.* **2000**, *142*, 97–101.
- (31) Delaglio, F.; Grzesiek, S.; Vuister, G. W.; Zhu, G.; Pfeifer, J.; Bax, A. NMRPipe: a multidimensional spectral processing system based on UNIX pipes. *J. Biomol. NMR* **1995**, *6*, 277–293.

Binding and Proton Blockage by Amantadine Variants of the Influenza M2_{WT} and M2_{S31N} Explained

Christina Tzitzoglaki,[†] Anna Wright,[‡] Kathrin Freudenberger,[§] Anja Hoffmann,^{||} Ian Tietjen,[⊥] Ioannis Stylianakis,[†] Felix Kolarov,[§] David Fedida,[⊥] Michaela Schmidtke,^{||} Günter Gauglitz,[§] Timothy A. Cross,^{‡,‡#} and Antonios Kolocouris^{*,†,†ID}

[†]Section of Pharmaceutical Chemistry, Department of Pharmacy, National and Kapodistrian University of Athens, Athens 157 71, Greece

[‡]Institute of Molecular Biophysics and National High Magnetic Field Laboratory, Florida State University, Tallahassee, Florida 32306, United States

[§]Institut für Physikalische und Theoretische Chemie, Eberhard-Karls Universität, Auf der Morgenstelle 18, D-72076 Tübingen, Germany

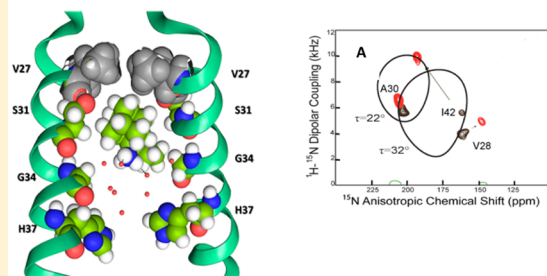
^{||}Department of Virology and Antiviral Therapy, Jena University Hospital, Hans Knoell Strasse 2, D-07745 Jena, Germany

[⊥]Department of Anesthesiology, Pharmacology and Therapeutics, University of British Columbia, Vancouver, British Columbia V6T 1Z3, Canada

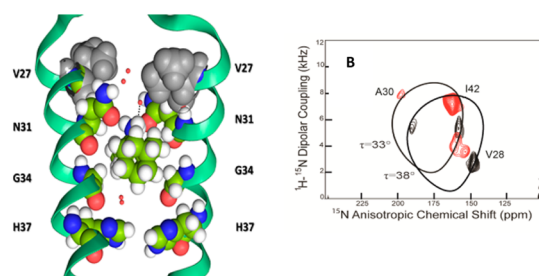
[#]Department of Chemistry and Biochemistry, Florida State University, Tallahassee, Florida 32306, United States

S Supporting Information

A Tight M2TM_{WT}-5 complex; strong C-terminus direction, V27 lipophilic pocket, 10° kink in C-terminus half



B Weak M2TM_{S31N}-5 complex; propensity for N-terminus direction, loss of V27 lipophilic pocket, uniform helical tilt



ABSTRACT: While aminoadamantanes are well-established inhibitors of the influenza A M2 proton channel, the mechanisms by which they are rendered ineffective against M2_{S31N} are unclear. Solid state NMR, isothermal titration calorimetry, electrophysiology, antiviral assays, and molecular dynamics simulations suggest stronger binding interactions for aminoadamantanes to M2_{WT} compared to negligible or weak binding to M2_{S31N}. This is due to reshaping of the M2 pore when N31 is present, which, in contrast to wild-type (WT), leads (A) to the loss of the V27 pocket for the adamantyl cage and to a predominant orientation of the ligand's ammonium group toward the N-terminus and (B) to the lack of a helical kink upon ligand binding. The kink, which reduces the tilt of the C-terminal helical domain relative to the bilayer normal, includes the W41 primary gate for proton conductance and may prevent the gate from opening, representing an alternative view for how these drugs prevent proton conductance.

1. INTRODUCTION

A proven vulnerability of influenza A infections is the blockage of the viral M2 proton channel. M2 is required for acidification of the virion interior during infection and neutralization of the trans-Golgi network during viral egress.¹ Amantadine (Amt, **1**; Scheme 1) is an established inhibitor of the influenza A/M2-mediated proton currents² and a licensed influenza A infection therapy.³ The primary binding site of **1** is located within the pore of the tetrameric M2 transmembrane (M2TM) domain that forms the transmembrane proton transit path.^{4,5} However, since 2005,⁶ the I-insensitive Ser-to-Asn mutation at position 31 in M2 (S31N) has become globally prevalent,⁷ abrogating

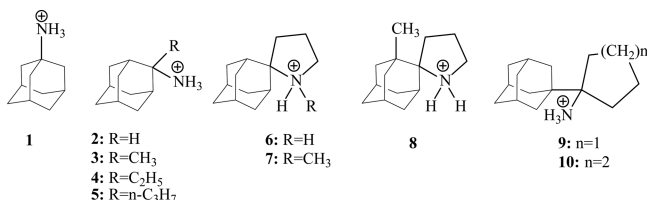
the clinical usefulness of **1**⁸ and possibly other previously reported M2 inhibitors.⁹ Thus, new agents are needed to combat drug-resistant forms of influenza.

Based on the experimental solid state NMR (ssNMR) structure of the complex M2TM-**1**,^{4a,5a,b} the replacement of S31 residues at the drug binding site with the more polar and bulky Asn side chains may induce the adamantyl ring to move deeper into the M2 pore, toward the C-terminus close to G34, where the pore of the helical bundle has its largest diameter,

Received: July 30, 2016

Published: January 20, 2017

Scheme 1. Aminoadamantane Derivatives 1–10



and drugs larger than **1** might be effective. We and the Vázquez group and the DeGrado group have searched for such larger drugs and found, for example, compounds **5**–**7**, which are active against A/California/07/2009 (H1N1) virus encoding S31N but not against WSN/33 also bearing the same mutation.^{10a–c} However, while a preliminary ssNMR experiment of the S31N M2TM domain complexed with compound **5** showed evidence of drug binding, electrophysiology (EP) studies showed no blockage for the full-length S31N M2 protein.^{10a} These studies therefore indicate that more detailed experimental investigation and modeling are needed to explain the mechanisms by which aminoadamantanes are rendered ineffective against M2_{S31N} in order to design effective drugs.

Recent molecular dynamics (MD) simulations showed that the ammonium group of **1** has a prevalent orientation toward the C-terminus of M2TM_{WT} (Udorn), with the adamantane hydrocarbon cage shifted slightly toward the N-terminus of the A30/S31 α sites,^{11–18} producing a region of the pore devoid of water^{17–19} consistent with blockage of proton transport and in agreement with ssNMR findings.^{5c,20,21} In contrast, MD simulations of **1** in M2TM_{S31N} from us and the Busath group^{17b} and rimantadine in M2TM_{S31N} from the Arkin group¹⁶ suggested that these compounds have a variable orientation, but with a propensity to have the ammonium group toward the N-terminus^{17b,22} of the M2TM_{S31N} pore (Figure 1). In this orientation water occupancy is not widely occluded in any configuration.¹⁷ These studies^{16,17b} presented a description of the potential of mean force (PMF) curves of amantadine and rimantadine in interaction with the M2TM_{S31N} pore, but the critical changes of the structure and interactions of the M2TM pore in contact with the drug due to S31N and leading to aminoadamantane resistance were not defined. In addition, no experimental evidence is presented to date for the binding of aminoadamantane ligands in M2TM_{S31N} pore. Nevertheless, the propensity of **1**'s amino group to orient toward the N-terminus was used by DeGrado and Wang for the successful design of **1**–polar head conjugates that were shown to be potent inhibitors of WSN/33 virus and proton conductance by M2_{S31N}.²³ A ssNMR analysis of a system including one of these compounds, a phenylisoxazole derivative linked with amantadine through a methylene bridge, with M2TM in membrane bilayers was realized by the Hong and DeGrado groups. The results showed that the compound's heterocyclic ring system may be trapped by the V27 side chains at the N-terminus of the M2TM pore²⁴ with the isoxazole group forming hydrogen bonds with the N31 amide side chains.

We are interested to investigate how subtle changes in amantadine structure are related with the binding affinity against M2TM variants. We previously used the molecular mechanics Poisson–Boltzmann surface area (MM/PBSA) to interpret thermodynamic profiles measured using isothermal titration calorimetry (ITC) for aminoadamantanes binding to the avian M2TM_{Weybridge} (M2TM_{Weybridge} has two different

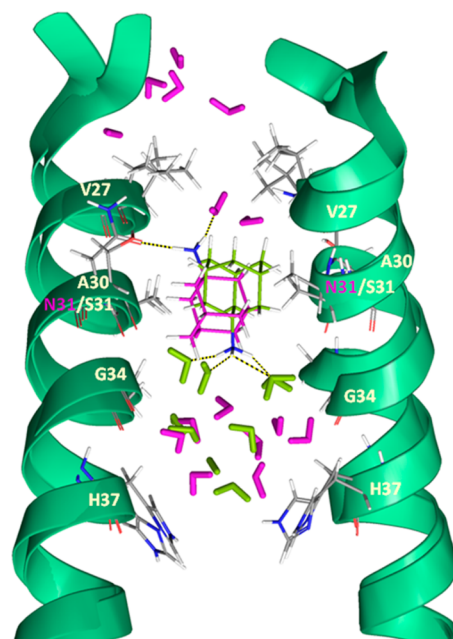


Figure 1. Amt (**1**) orients toward the protein C-terminus in M2TM_{WT} and toward the protein N-terminus in M2TM_{S31N}. Superposition of final snapshots and constant temperature and pressure molecular dynamics simulations at 310 K of **1** in complex with S31 or N31 M2 [PDB ID, 2KQT] in 150 mM NaCl, water, and DMPC lipid. Compound **1** and waters are shown in yellow-green and purple in WT and S31N, respectively. Two of four M2TM backbones are shown as green ribbons. In the S31 case, the ammonium group of **1** is projecting toward the C-terminus and hydrogen bonding with four water molecules. In the N31 case, the adamantane cage (purple) is lower, and the amantadine amine projects toward the N-terminus and hydrogen bonds with the one N31 side chain and a water molecule.

amino acids that do not line into the pore, i.e., V28 → I28 and L38 → F38 compared to M2TM_{WT}) in order to successfully prioritize aminoadamantane derivatives.²⁵ We also applied rigorous free energy binding calculations by the Bennett acceptance ratio (BAR) approach to accurately predict relative binding affinities of aminoadamantane derivatives toward M2TM_{WT} or M2TM_{Weybridge} measured by ITC or other methods, respectively.^{26,27}

Here we investigate the interaction of aminoadamantane derivatives (Scheme 1) with M2TM_{WT} and M2TM_{S31N} both through experiment and by MD simulations, with the aim of determining how the S31N mutation leads to the inability of **1** and other aminoadamantanes to block S31N M2 proton transport. First, we measured binding constants of selected aminoadamantane derivatives with ITC against M2TM_{WT} and M2TM_{S31N} in dodecylphosphocholine (DPC) micelles at alkaline pH. Second, we applied a series of MD simulations (80 ns trajectories) of the M2TM_{WT} and M2TM_{S31N} complexes with **1**–**10** (Scheme 1) to analyze in some detail how the polar N31 amide side chains affect binding of an aminoadamantane ligand inside the M2TM pore. To this end, we suggest that repulsive forces between N31 and the adamantane ring may influence the orientation and binding interactions of the ligand, the overall stability of the complexes, and the shape of M2TM. Third, we performed oriented sample (OS) and magic angle spinning (MAS) ssNMR experiments^{28–30} on representative M2TM–ligand complexes at alkaline pH using both M2TM_{WT} and M2TM_{S31N} sequences to characterize the structural

Table 1. Binding Constants and Other Thermodynamic Parameters Derived from ITC Measurements for Influenza A M2TM_{WT} and M2TM_{S31N}

ligand ^a	K _d ^b	M2TM _{WT}		
		ΔG ^{c,d}	ΔH ^{e,e}	TΔS ^f
1 ^g	2.17 ± 0.52	-32.51 ± 0.59	-27.87 ± 2.09	4.64 ± 2.18
2 ^g	1.60 ± 0.34	-33.30 ± 0.54	-29.41 ± 1.76	3.89 ± 1.84
3 ^g	0.89 ± 0.19	-34.77 ± 0.54	-28.41 ± 1.09	6.32 ± 1.21
4 ^g	0.62 ± 0.14	-35.65 ± 0.54	-29.87 ± 0.88	5.77 ± 1.05
5 ^g	0.63 ± 0.17	-36.43 ± 0.69	-32.62 ± 1.29	3.90 ± 1.45
6 ^g	0.36 ± 0.22	-38.11 ± 1.84	-21.49 ± 1.76	16.61 ± 2.57
7 ^g	0.93 ± 0.36	-34.64 ± 0.96	-15.98 ± 1.17	18.66 ± 1.51
8 ^g	1.30 ± 0.43	-33.81 ± 0.84	-21.25 ± 1.30	12.55 ± 1.55
9	14.61 ± 4.62	-27.77 ± 0.79	<i>h</i>	<i>h</i>
10	>10	<i>h</i>	<i>h</i>	<i>h</i>

ligand ^a	K _d ^b	M2TM _{S31N}		
		ΔG ^{c,d}	ΔH	TΔS
1–4	<i>i</i>			
5	>10	<i>h</i>	<i>h</i>	<i>h</i>
6	17.5 ± 8.5	-27.95 ± 1.24	<i>h</i>	<i>h</i>
9	15.8 ± 5.95	-28.22 ± 0.96	<i>h</i>	<i>h</i>
10	9.90 ± 4.99	-29.41 ± 1.29	<i>h</i>	<i>h</i>

^aSee Scheme 1. ^bBinding constant K_d in μM calculated from measured K_a in M⁻¹ by K_d = (1/K_a) × 10⁻³ and error in K_d in μM determined by K_{d,error} = (K_{a,error}/K_a²) × 10⁻⁶. ^cIn kJ mol⁻¹. ^dFree energy of binding computed from K_d by ΔG = -RT ln(K_d^{ref}/K_d) with K_d^{ref} = 1 M and T = 300 K, and error in ΔG determined according to

$$\Delta G_{\text{error}} = \sqrt{\left(\frac{RTK_{d,\text{error}}}{K_d}\right)^2}$$

with T = 300 K. ^eEnthalpy of binding and error in the enthalpy of binding calculated from measured binding enthalpy and measured error by ΔH = ΔH_{measured}(T/T_{measured}) with T = 300 K and the temperature at which the ITC measurements were performed T_{measured} = 293.15 K. ^fEntropy of binding calculated by ΔS = (-ΔG + ΔH)/T and error in ΔS computed by the equation

$$\Delta S_{\text{error}} = \sqrt{\Delta G_{\text{error}}^2 + \Delta H_{\text{error}}^2}$$

^gMeasured in ref 26. ^hValues could not be determined reliably due to the limitations of the methods in the area of very weak binding. ⁱNo detectable binding.

influence of compounds on the channel. Fourth, we selected and tested new synthetic derivatives with slightly larger or similarly sized adducts, such as **8** and **10**, compared to **5**–**7** and **9** for their abilities to bind M2TM_{S31N}. We realized EP experiments for selected compounds against both WT and S31N M2 proteins to test M2 channel blockage and additionally measured the antiviral potency of the compounds against the naturally amantadine-resistant H1N1 influenza strain A/WSN/1933 (WSN/33 with M2_{N31}) and its reverse genetics-generated amantadine-sensitive variant with the amino acid substitution N31S in M2 (WSN/33-M2-N31S) using cytopathic effect inhibition (CPE) assays.

2. RESULTS

2.1. Binding Affinities of Aminoadamantanes to M2TM by ITC. ITC measurements³¹ were determined for both M2TM_{WT} and M2TM_{S31N} tetramers at pH 8 corresponding to the closed state of the M2TM pore³² (Table 1). Binding data for compounds **1**–**8** to M2TM_{WT} measured in our previous work²⁶ were included in Table 1. Thus, as has been published recently²⁶ (see Tables 1 and S1) compounds **1**–**8** bind M2TM_{WT}. Compound **9** and the newly synthesized analogue **10**, which has a cyclohexane ring instead of the cyclopentane in **9**, bind M2TM_{WT} with at least an order of magnitude lower dissociation constant (K_d) than those for **1**–**8**,

possibly because their sizes do not enable them to fit well inside M2TM_{WT}. We noted in this work an example where techniques for measuring binding affinity against M2TM such as ITC correspond to the molecular recognition of ligand binding to M2TM and do not necessarily reflect functional inhibition of M2 proton currents or in vitro inhibition of influenza A virus. For example, **9** inhibits M2_{WT}-dependent currents as measured by electrophysiology with an IC₅₀ of 10 ± 2 μM (Table 4) and inhibited influenza A virus replication in infected cells with an IC₅₀ of 3.92 ± 2.22 μM (Table 5) while compound **10** was inactive. Nevertheless, ITC and related techniques such as surface plasmon resonance (SPR) and structural techniques such as ssNMR can provide useful insights for M2TM binding and trends in structure–activity relationships for the M2–aminoadamantane system. For example, compounds **1**–**4** did not bind efficiently to M2TM_{S31N} according to ITC and previous SPR measurements for **1**³³ while **5** and **6** with larger adducts connected to adamantane bind weakly to M2TM_{S31N} compared to M2TM_{WT} according to ITC (Table 1) and ssNMR. The K_d values of low-affinity binders (e.g., **5**, **6**, **9**, and **10**) against M2TM_{S31N}, and **9** against M2TM_{WT}, possess large errors due to the limitations of the ITC method (as explained in the Supporting Information). Subsequently comparison of the relative K_d values of compounds **5**, **6**, **9**, and **10** do not reflect relative binding affinity strength against M2TM_{S31N}.

Nevertheless, although the quantitation of the ITC results against M2TM_{S31N} is limited for this method, the measurements suggest that the K_d values of 5 and 6 against M2TM_{S31N} are much smaller compared to those of M2TM_{WT}, suggesting weaker binding to M2TM_{S31N} (Table 1). Narrower line widths and larger chemical shifts changes for 5 bound to M2TM_{WT} compared to M2TM_{S31N} were observed in the ssNMR spectra described below suggesting a reduction in dynamics for binding to M2TM_{WT} and a more specific binding site, which in turn causes a significant reduction in hydration due to drug-induced desolvation of the binding pocket.³¹

2.2. Solid State NMR of M2TM–Aminoadamantanes Complexes. **2.2.1. OS ssNMR Spectra.** Drug binding to the channel pore of M2TM_{WT} and M2TM_{S31N} was evaluated using OS ssNMR experiments. Spectral correlation observed in these data sets, between anisotropic ¹⁵N chemical shifts and ¹H–¹⁵N dipolar coupling values for selectively ¹⁵N-labeled backbone amide sites, gives rise to resonance patterns known as PISA (polarity index slant angle) wheels.^{34,35} The shape, size, and position of the PISA wheel for α -helical membrane proteins in uniformly oriented lipid bilayer preparations is determined by the helical tilt relative to the bilayer normal and is sensitive to drug-induced structural perturbations. Previous investigations by Cross and co-workers have reported dramatic changes in anisotropic chemical shifts and dipolar coupling values for M2TM_{WT} in the presence of 1.³⁶ PISA wheel analysis of M2TM_{WT} spectra in the *apo* state and in the presence of 1³⁶ or 5 correlates the shifts with a substantial reduction in the tilt angle for the C-terminal region of the M2TM_{WT} helix, following ligand binding. In contrast, M2TM_{S31N} in the presence of 5 results in a uniform $5 \pm 2^\circ$ decrease in the helical tilt imparting a change to the entire helix–helix interface.^{10a}

Here, to monitor changes in the resonance frequencies and to the resulting PISA wheel in the presence of other variants of 1, a ¹⁵N–V28,A30,I42 (VAI–M2TM) labeling scheme was used. Residues 28 and 30 are in the N-terminal domain of the M2TM helix and I42 in the C-terminal region, and hence the labels effectively sample both segments. Resonance frequencies for these sites are well-resolved allowing for a PISA wheel analysis of drug binding in the channel pore that induces small structural perturbations. The signals of these three pertinent and isotopically labeled backbone amides were shifted in nearly an identical fashion when 1 or 5 bind to the M2TM_{WT} (Figure 2). As before, changes suggest only a slight perturbation to the N-terminus and a much more significant structural perturbation to the C-terminus with a change in the tilt angle from 32° to just 22° , while the N-terminal tilt changes by only a degree or two (Table 2).^{4b,36} These results imply similar drug-induced structural perturbations to the TM configuration of WT M2 protein in the presence of 1 or 5.

For the binding studies to M2TM_{S31N}, no observable effect was detected for binding of 1, while 5 induces smaller changes compared to those induced by the binding of 1 or 5 to M2TM_{WT} based on the signals from the same three backbone amides (Figure 3). In addition, the linewidths are narrower when 5 is bound to M2TM_{WT} compared to M2TM_{S31N}, suggesting less dynamics in the WT complex implying a tighter complex.

There is a small difference in the structure of M2TM_{S31N} versus M2TM_{WT} without drugs in lipid bilayers (black resonances in Figure 2 versus Figure 3). The M2TM_{S31N} data suggest a helical tilt of approximately 38° , somewhat greater

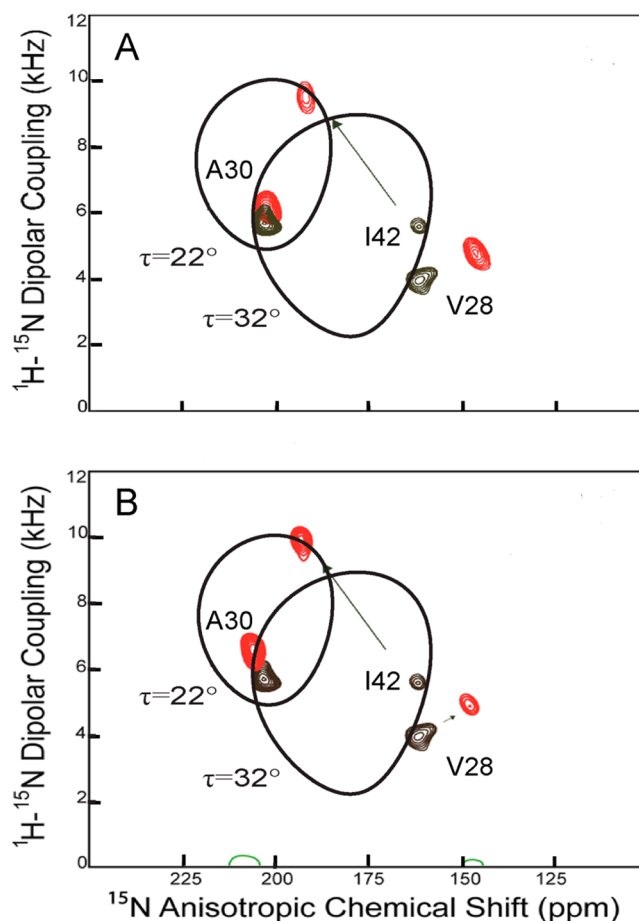


Figure 2. Superimposed PISEMA spectra of the M2TM_{WT} (residues 22–46), ¹⁵N-labeled at V28, A30, and I42, in DMPC lipid bilayers uniformly aligned on glass slides with (red) and without (black) compound 1 (A) and compound 5 (B). Assignments without drug were made based on the known structure and spectra of M2TM_{WT}.³⁶ Assignments with drug follow the rotational orientation of the helices. Changes in the resonance frequencies of the ¹⁵N-labeled backbone amide sites are indicated with black arrows. All spectra were collected at 720 MHz, pH 7.5, and 303 K. The molar ratio of lipid/protein was 30:1. PISA wheels are drawn for helix tilts of 22° and 32° for the N- and C-terminal residues, respectively, when the drugs are bound.

Table 2. Mean Helical Tilt Values Relative to the Bilayer Normal from MD Simulations of 1 and 5 in Complex with M2TM_{WT} in DMPC Bilayer

ligand ^a	helical tilt angle for N-terminus/C-terminus (deg)		
	MD simulations ^b	ssNMR expt ^c	2KQT ^{4a,5b}
1	$31 \pm 4.6/18 \pm 4.9$	$32 \pm 2/22 \pm 2$	30/19
5	$31 \pm 5.1/19 \pm 5.0$	$32 \pm 2/22 \pm 2$	

^aSee Scheme 1. ^bCalculated using Gromacs tools. ^cThis study.

than the helical tilt observed in the WT structure (32°) consistent with prior characterizations.^{4,36} While the binding of 1 to M2TM_{WT} produced a 10° kink near G34 in each helix of the tetramer,^{4b,36} the binding of 1 produced no such structural change for the 1-resistant M2TM_{S31N}. The shifts in the anisotropic resonance frequencies which resulted when 5 binds to M2TM_{S31N} demonstrates a significant change in helical tilt from 38° to 33° in the tetrameric complex (Table 3). Based on these resonances that sample the N- and C- regions of the TM helix, the structural change appears to be a uniform change in

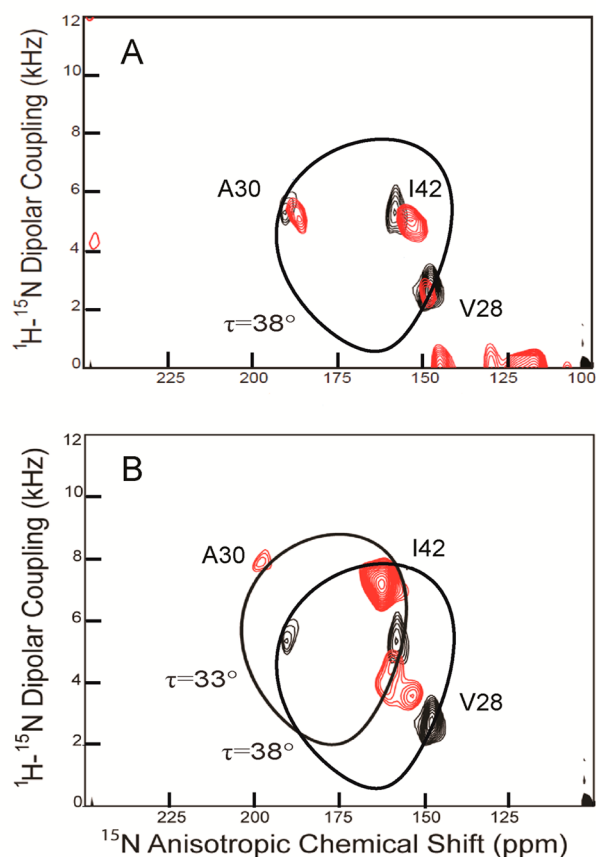


Figure 3. Superimposed PISEMA spectra of the M2TM_{S31N} ¹⁵N-labeled at residues V28, A30, and I42, in DMPC lipid bilayers uniformly aligned on glass slides with (red) and without (black) compound **1** (A) and compound **5** (B). Assignments without drug were made based on the known structure and spectra of M2TM_{WT}.³⁶ Assignments with drug follow the rotational orientation of the helices. Theoretical PISA wheel calculated for an ideal helix $[(\phi, \varphi)] = (-60^\circ, -45^\circ)$ with a 33° tilt angle relative to the bilayer normal is superimposed on M2TM_{S31N} resonance frequencies, which are shifted after compound **5** addition. All spectra were collected at 720 MHz, pH 7.5, and 303 K. The molar ratio of lipid/protein was 30:1.

Table 3. Mean Helical Tilt Values Relative to the Bilayer normal from MD Simulations of 5–8 in Complex with M2TM_{S31N} in DMPC Bilayer

ligand ^a	helical tilt angle (deg)	
	MD simulations ^b	expt ^{c,d}
1	34 ± 4	38 ± 1
5	31 ± 6	33 ± 1
6	28 ± 5	28 ± 1
7	33 ± 4	31 ± 1
8	31 ± 4	33 ± 1

^aSee Scheme 1. ^bCalculated using Gromacs tools. ^cThis study. ^dHelical tilt is uniform.

tilt. Consequently, the residues facing the pore remain the same, but the interactions between helices that provide the tetrameric stability may change substantially. Upon binding of **1** or **5** to M2TM_{WT} a kinked helix at G34 is produced but when adding these compounds to M2TM_{S31N} helices, are not kinked at G34. Instead, when **5** binds to M2TM_{S31N}, the entire helix–

helix interface changes with the $\sim 5^\circ$ reduction in tilt for each of the four helices.

The structurally similar aminoadamantanes **6–8** produced similar ssNMR results when added to M2TM_{S31N} (Figure 4) in

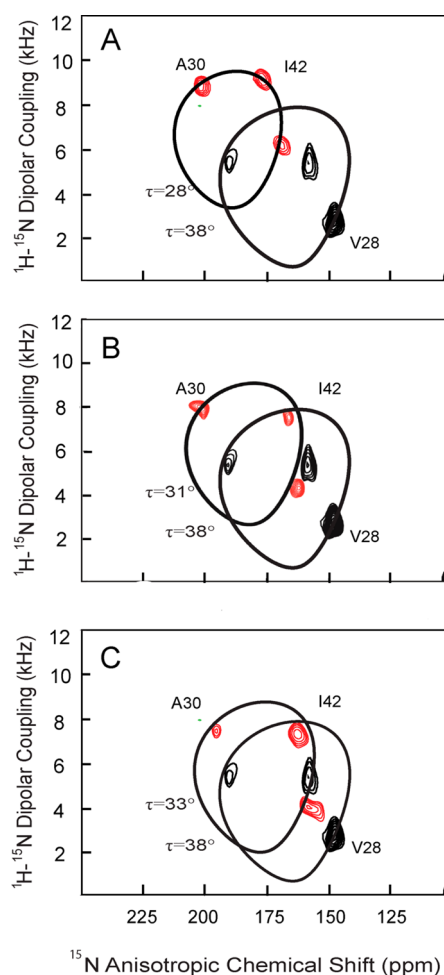


Figure 4. Superimposed PISEMA spectra of the M2TM_{S31N} (residues 22–46), ¹⁵N-labeled at residues V28, A30, and I42, in DMPC bilayers uniformly aligned on glass slides with (red) and without (black) **6**, **7**, and **8** (panels A–C, respectively). Assignments without drug were made based on the known structure and spectra of M2TM_{WT}.³⁶ Assignments with drug follow the rotational orientation of the helices. Theoretical PISA wheels calculated for an ideal helix $[(\phi, \varphi)] = (-60^\circ, -45^\circ)$ with varying tilt angles relative to the bilayer normal were superimposed on drug bound M2TM_{S31N} spectra (panels A–C). All spectra were collected at 720 MHz, pH 7.5, and 303 K. The molar ratio of lipid/protein was 30:1.

that the change in structure always reflected a uniform change in helical tilt. Compound **8** is a new derivative, which was synthesized to test the effect of C-methylation to binding compared to N-methylation in **6**. The measured helical tilt angles are 28° for **6**, 31° for **7**, and 33° for **8**, with the latter compound yielding results that are similar to those induced by **5** (Table 3). For **5–8**, there is no evidence for partial binding, since the unbound states are not observed in the spectra with drugs present. With **5**, V28 appears to have multiple resonances (Figure 3) clustered on an anisotropic chemical shift of 160 ppm and a dipolar interaction of 4 kHz. The structural differences would be small, i.e., no more than 1° change in the orientation of the V27–V28 peptide plane with respect to the

bilayer normal. This suggests that even with **5** on the time scale of 10–100 μ s there is no significant evidence for asymmetry in this tetrameric structure; i.e., there is no evidence from these three labeled sites that M2TM_{S31N} bound with different compounds **1** and **5–8** forms a dimer of dimer, as has been suggested for the S31N structure.^{37,38} If such structures are present, they must interconvert on a time scale faster than the difference in spectral frequencies in hertz. Furthermore, if this was occurring with significantly different structures, there would be a reduction in the width and height of the PISA wheel, which was not observed. The intensity of the resonances varies, again especially for **5**, suggesting that the compound may have competing binding interactions with the pore leading to heterogeneity in the frequencies, the weakening of the A30 resonance, and the small dispersion of the V28 resonances as described above. These dynamics are in sharp contrast to the intense resonance for I42 for M2TM_{S31N} bound with **5**. The uniformity of the resonance intensities that result from the interaction with heterocyclic compounds **6–8** may suggest less dynamics and more potent binders than **5** to M2TM_{S31N}.

2.2.2. MAS Spectra. To evaluate further the effect of **6** binding to M2TM_{S31N}, 2D N–C α correlation MAS ssNMR experiments were performed using uniformly ¹³C,¹⁵N-labeled V7, A30, S31, and G34 M2TM_{S31N} (¹³C,¹⁵N-VANG-labeled M2TM_{S31N}). The labeling used aims to explore the binding interactions of amantadine analogues into M2TM_{S31N} pore through measuring the effect of binding to the chemical shifts of V27, A30, G34, and N31. In M2TM_{WT} the binding area includes the expanded area including V27, A30 and also G34, S31.^{4a,5b} Spectra were obtained (Figure 5) for both the apo protein (blue) and for **6** bound (red) to the labeled M2TM_{S31N}. Addition of the drug to the M2TM_{S31N} sample resulted in chemical shift changes for N31 and G34 of 1.2 and 2.1 ppm, respectively; V27 and A30 resonances remain unchanged, suggesting that they are not involved in binding, while the

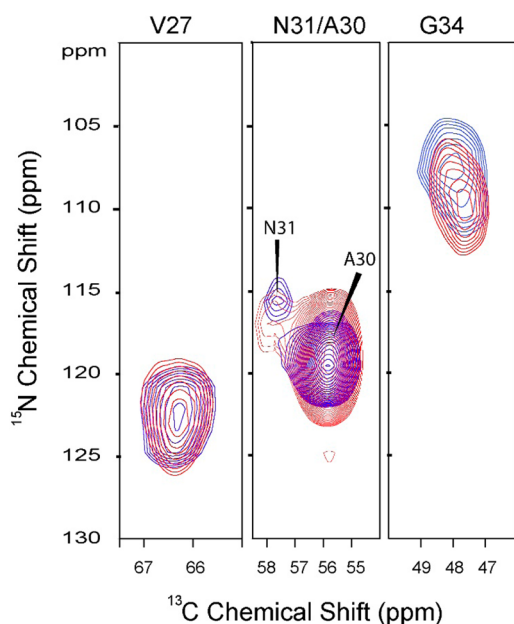


Figure 5. Superimposed 2D strip plots for ¹⁵N/¹³C (NCA) correlation spectra of ¹³C,¹⁵N–V₂₇A₃₀N₃₁G₃₄-labeled M2TM_{S31N} (residues 22–46) in DMPC lipid bilayers with (red) and without (blue) compound **6**. Spectra were collected at 600 MHz proton frequency, pH 7.5, 10 kHz spinning rate, and a calibrated temperature at sample of 263 K.

isotropic chemical shift perturbation of the N31 and G34 residues suggest the drug binding site for M2TM_{S31N} suggesting either direct hydrogen bonding with the backbone or indirect hydrogen bonding through water molecules.²¹ Significant ¹⁵N and/or ¹³C α chemical shift changes at V27, S31, and G34 have been reported when rimantadine is bound to M2TM_{WT}^{20,21} with S31 experiencing a dramatic 7 ppm shift relative to the apo state.²¹ Despite the observed chemical shift changes at residues N31 and G34 when **6** bound to the M2TM_{S31N}, cross-peak intensity was not increased as was observed for the WT full-length M2 in complex with rimantadine.²¹ This suggests that the conformational heterogeneity of M2TM_{S31N} was not increased for these residues in the presence of the drug. A reduction in dynamics which is in agreement with narrower line widths would be anticipated with a specific binding site or a significant reduction in hydration due to drug-induced desolvation of the binding pocket. The narrower line widths and increased anisotropic chemical shifts for the M2TM_{WT} and M2TM_{S31N} bound to **5** (Figures 2 and 3) illustrate reduced dynamics and weaker or less specific binding of the drug to the M2TM_{S31N}.

2.3. MD Simulations of M2TM–Aminoamantane Complexes.

2.3.1. Starting Structure of Protein–Ligand Complex.

MD simulations of the complexes between **1**, 2-alkyl-2-aminoamantanes **2–5**, and cyclic derivatives **6–10** with both M2TM_{WT} and M2TM_{S31N} provide insights for the binding interactions and possible structural changes in the binding area. All of the ligands' amino groups were considered to be protonated according to model calculations performed previously for ligands **1** and **6**.^{25,26} The structure of the complex M2TM_{WT}–**1** (PDB ID 2KQT^{4a,5b}) was used as a starting structure for the simulations of M2TM_{WT}–ligand complexes and of M2TM_{S31N}–ligand complexes. The PDB ID 2KQT^{4a,5b} structure was chosen since it was determined at pH 7.5 and DMPC planar bilayers and vesicles,^{4a,5b} i.e., similar conditions to those used in our simulations. Subsequently only small structural changes are to be expected in the M2TM structure during MD simulations of its complexes with ligands, and the equilibration phase should be short. It has been shown that the stability of the binding region for **1** in the M2TM tetramer is increased considerably when using DMPC compared to other lipids.^{39–42} In addition, 2KQT (see ref 5b) should be considered as the best structure of the amantadine bound state of M2TM since it utilized both isotropic chemical shift restraints and all of the orientational restraints of an earlier structure characterized by Cross and co-workers (see ref 4a). The structures of the M2TM_{S31N}–ligand (**1–10**) complexes were generated from M2TM_{WT} complexes by mutating S31 to N (see also Experimental Methods).

2.3.2. Complexes of Ligands with M2TM_{WT}. The MD simulations of the M2TM_{WT}–ligand complexes reached equilibration in less than 40 ns with the protein system having full flexibility. Snapshots of the simulation complexes with **5** and **6** are shown in Figure 6. The RMSDs values (Table S1) were ≤ 1.6 Å for M2TM C α -carbons with respect to the initial structure of the production period^{4a,5b} suggesting that M2TM_{WT}–ligand (**1–8**) complexes were very stable and the M2TM tetramer structure was considerably unchanged in the course of the simulation. The mean values of the N-terminal and the C-terminal helical tilt of M2TM_{WT} for the complexes with **1** and **5** from the corresponding MD trajectories were measured to be 31°, 18° and 31°, 19°, respectively, and are in very good agreement with the values of 32°, 22° and 32°, 22°

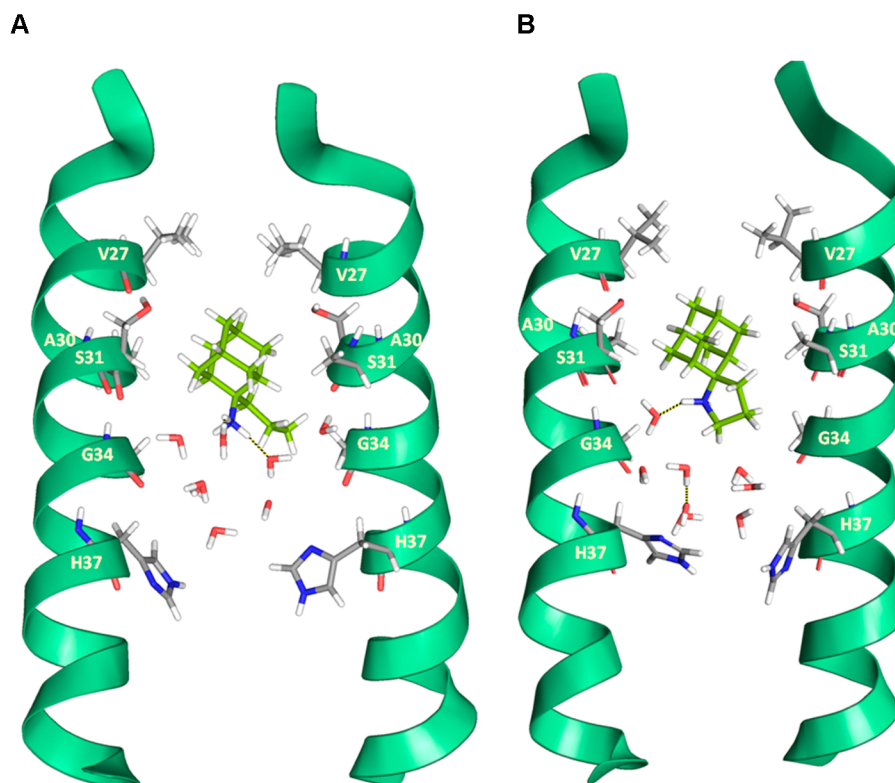


Figure 6. Snapshots from the simulation of ligands bound to M2TM_{WT}. Waters within 10 Å from the ligand are shown. (A) Compound 5 bound to M2TM_{WT}. Eight waters are shown between the ligand and H37 residues. Three hydrogen bonds between the secondary ammonium group of the ligand and three water molecules are shown (see Table S1). (B) Compound 6 bound to M2TM_{WT}. Eight waters are shown between the ligand and H37 residues. Two hydrogen bonds between the secondary ammonium group of the ligand and two water molecules are shown (see also Table S1). Hydrogen bonding together with van der Waals interactions of the adamantane core with V27 and A30 stabilize ligands 5 and 6 inside the pore with their ammonium group oriented toward the C-terminus.

determined by OS ssNMR (Table 2). As noted above, the starting structure 2KQT^{4a,5b} having helical domain tilt angles of 31°, 19° was determined in conditions similar to those used in our MD simulations by Cross and co-workers.^{4a} Even so these findings suggest that the ligand–M2TM_{WT} complex was successfully equilibrated and the conditions were well-adjusted to produce consistent results. Consistent with the experimental findings^{5b,c} and previous observations,^{25,26} the ammonium group of the aminoadamantane compounds was oriented toward the C-terminus with angles of <77° between the C–N bond of the ligand and the membrane’s normal (Table S1). The complexes of compounds 1–8 inside the M2TM lumen are stabilized through (a) formation of hydrogen bonds between their ammonium group and water molecules in the region between H37 residues and the ligand and (b) van der Waals interactions between the adamantyl group and a lipophilic pocket formed by V27 and A30 side chains (see Figure 6). This binding area is in accordance with (a) the ¹⁵N chemical shifts perturbations for V27, A30, and S31 in complexes between 1 or 3-azaspiro[5,5]undecane and M2TM_{WT} compared to the *apo* M2TM_{WT}³⁹ and (b) the measured distance of 4.5 Å between G34Ca and the methyl group of rimantadine from REDOR ssNMR experiments in studies of the full-length protein.²¹ In addition, for complexes of M2TM_{WT} with 1–8, the distance between the adamantyl ring of the ligand and the center of mass of the four V27 (V27–Ad) varies between 4 and 4.9 Å and the distance between the adamantyl ring of the ligand and the center of mass of the four A30 (A30–Ad) varies between 0.5 and 1.4 Å (Table S1). The

position of the adamantyl ring inside the lumen was similar for ligands 2–8 differing from 1 only by 0.2–0.6 Å. To account for the position of the ligands toward the C-end, we measured the distance between the center of mass of the four V27 and the ammonium nitrogen of the ligand (V27–N⁺) which varied between 7.1 and 7.8 Å (Table S1). According to the measures in Table S1 the hydrogen bonding ability is higher for the subset of ligands 1–5, 9, and 10 than for the subset 6, 8, or 7. Thus, 1–5, 9, and 10 can form on average three hydrogen bonds with neighboring water molecules; 6 and 8, two hydrogen bonds; and 7, one hydrogen bond, respectively (Table S1). This is what was expected since 1–5, 9, and 10 have a primary ammonium group, 6 and 8 have a secondary ammonium group, and 7 has a tertiary ammonium group. For ligands 3–8 which include a carbon substituent at the C-2 adamantane position the molecule is rotated in order to avoid repulsive van der Waals forces of the alkyl group with the symmetric M2TM pore. The average angle between the pore axis and the C–N bond vector was increased progressively according to the alkyl group size, i.e., from 13.5° for 1 to 25–35° for 2–8 (Table S1). Although all ligands 1–8 have a binding mode similar to that resulted in the OS ssNMR spectra of complexes including 1 and 5 (Figure 2), a subtle compromise between hydrogen bonding and hydrophobic interactions with key pore residues, such as V27, A30, affects the ligand tilt inside the pore and its different binding strength as shown by the ITC results (Table 1). The adamantyl ring is slightly toward the N-terminus compared to the A30/S31 C α , producing a region without water molecules.

The MD simulations suggest that the M2TM_{WT}–ligand complex stability is reduced when a sizeable adduct is attached to adamantane; i.e., the M2TM pore does not efficiently accommodate the large adducts of compounds **9** and **10**. This is in accordance with the weak or no binding respectively of these drugs according to the ITC results (Table 1). For example, the MD simulations showed that the stability of the complex is considerably reduced in the case of **10** where after 80 ns the ligand is shifted toward the N-terminus; the mean distances of the trajectory V27–Ad, A30–Ad, and V27–N⁺ were 3.5, 4.7, and 2.1 Å, respectively, suggesting a loosening of the M2TM-complex integrity at the N-terminus (a snapshot of the simulation complex with **10** is depicted in Figure S1).

2.3.3. Complexes of Ligands with M2TM_{S31N}. In the starting configuration of M2TM_{S31N}–aminoadamantane ligand complex the ammonium group points toward the C-terminus forming H-bonds with waters between the ligand and H37 residues as in the M2TM_{WT} pore. The MD simulations of the complexes between M2TM_{S31N} and **1–8** reach equilibration in less than 60 ns with the protein system having full flexibility. In complexes with M2TM_{S31N} the ligand is more mobile inside the pore having a propensity to orient its ammonium group toward the N-terminus, in contrast to M2TM_{WT}–ligand complexes where the ligand forms a stronger complex with the ammonium group having a tighter orientation toward the C-terminus. Thus, after a few nanoseconds of unrestrained dynamics the ligand moves toward the C-terminus by ~2 Å, probably because the adamantyl group is repelled by the polar N31 side chains resulting in the loss of the V27 lipophilic pocket, and the molecule rotates 180° through an attraction to the polar environment around N31. This finding is consistent with the narrower line widths and larger chemical shifts changes for M2TM_{WT} when bound with compound **5** compared to M2TM_{S31N} as observed in the ssNMR spectra suggesting a stronger binding interaction with M2TM_{WT}. In addition waters are transferred from the region between the ligand and H37 to the area around N31 where the drug's amine can interact with the carbonyls of the N31 amide groups and waters around the amide side chains. Snapshots of the MD simulation complexes of M2TM_{S31N} with **1**, **5**, **6**, and **10** are depicted in Figure 7. The MD runs showed that in complexes with **2–8** the ammonium group orientation turns toward the N-terminus and the drug keeps this orientation during the entire simulation period. While this change was observed for **1** after ~20 ns of production, the time needed for the aminoadamantane ligand to rotate toward the N-terminus may be increased for some larger adducts. For example, in the case of **5** the ligand's ammonium group keeps its orientation toward the C-terminus during the first 40 ns and then the molecule turns toward the N-terminus until the end of the 80 ns production time. While no significant conformational change was observed for M2TM_{S31N} tetramer in its complexes with **1–8** during the production period, the RMSDs for M2TM_{S31N} C α -carbons were ≤ 2.8 Å with respect to the initial structure of the production period,^{4a,5b} i.e., 1–1.5 Å higher than the RMSDs for M2TM_{WT} C α -carbons, suggesting less dynamics for M2TM_{WT} complexes (see Tables S1 and S2). The mean values of the helical tilt angles for the complexes of **1** and **5–8** with M2TM_{S31N} from the corresponding MD trajectories were measured to be ~34°, 31°, 28°, 33°, and 31° respectively, and are close to 38°, 33°, 28°, 31°, and 33° determined by OS ssNMR (Table 3). The uniformly tilted helical structure is a conversion from the initial kinked state in the 80 ns MD, where

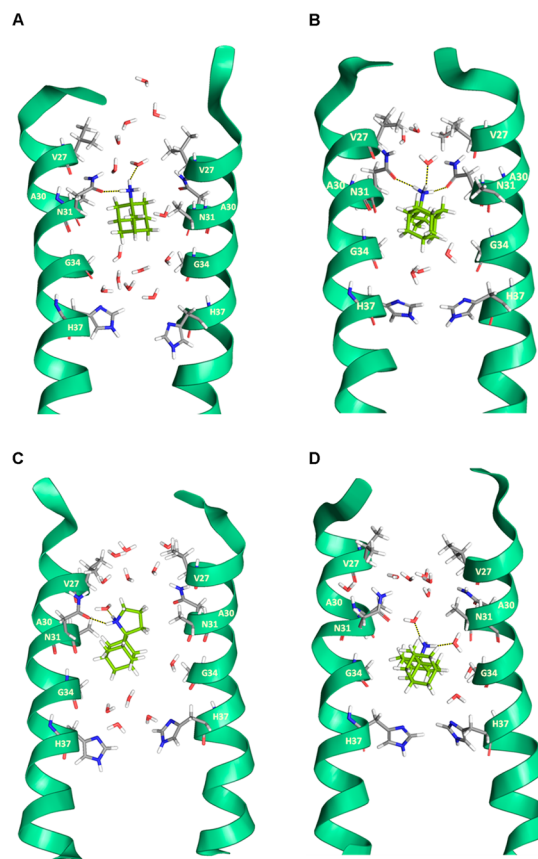


Figure 7. Snapshots from the simulation of various ligands bound to M2TM_{S31N}. Waters within 10 Å from the ligand are shown. Several waters are shown covering the region between the mouth of the ligand and H37 residues. Few waters may be found between the ligands and the wall of the pore, suggesting a relatively free passage through the lumen. (A) Compound **1** bound to M2TM_{S31N}. Seven waters are shown between the ligand and H37 residues and six waters between N31 and the mouth of the pore. In the depicted snapshot one hydrogen bond between the ammonium group of the ligand and one water, and one hydrogen bond between the ligand and the carbonyl group of N31 amide side chain, are shown (see also Table S2). No efficient van der Waals interactions can be formed for the adamantane core in the region close to A30, and the ligand cannot be stabilized inside the pore. (B) Compound **5** bound to M2TM_{S31N}. Three waters are shown between the ligand and the region close to H37 residues and three waters between N31 and the mouth of the pore. One water is shown between the ligand and the wall of the pore. One hydrogen bond between the ammonium group of the ligand and one water and two hydrogen bonds between the ligand and the carbonyl groups of two N31 amide side chain are shown (see also Table S2). (C) Compound **6** bound to M2TM_{S31N}. Four waters are shown between the ligand and H37 residues and seven waters between N31 and the mouth of the pore. Two hydrogen bonds between the ammonium group of the ligand and the carbonyl group of N31 amide side chain and one water are shown (see also Table S2). One water is shown between the ligand and the wall of the pore. (D) Compound **10** bound to M2TM_{S31N}. Two waters are shown in the region between the ligand and H37 residues and six waters between N31 and the mouth of the pore. One water is shown between the ligand and the wall of the pore. Two hydrogen bonds between the ammonium group of the ligand and two waters are shown (see also Table S2). Hydrogen bonding together with weak van der Waals interactions between the adamantane core and the cleft between A30 and G34 can moderately stabilize ligands **5**, **6**, and **10** inside the pore with their ammonium group oriented toward the N-terminus.

Table 4. Block of Full-Length M2-Dependent Currents by Selected Compounds in Transfected HEK Cells^a

compd	A/California/07/2009 (H1N1) M2: N31		A/California/09/2009 (H1N1) M2: S31	
	% block after 3 min	% block after 30 min	% block after 3 min	IC ₅₀
1 ^b	14 ± 2 (100 μM; 26)	N.A. ^c	75 ± 9 (10 μM; 4)	2 ± 3 μM (3)
2 ^b	13 ± 3 (100 μM; 2)	16 (100 μM; 1)	95 ± 8 (10 μM; 2)	2 ± 1 μM (2)
5 ^b	0 ± 5 (100 μM; 2)	9 ± 10 (100 μM; 3)	63 ± 5 (10 μM; 2)	7 ± 2 μM (2)
6	4 ± 3 (100 μM; 2)	5 ± 4 (100 μM; 2)	66 ± 6 (10 μM; 3)	5 ± 2 μM (3)
9	4 ± 4 (100 μM; 2)	4 ± 10 (100 μM; 4)	46 ± 2 (10 μM; 2)	10 ± 2 μM (2)

^aFor each compound, the percent block of pH-dependent M2 current at listed concentration (±sem) and/or IC₅₀ (μM) is shown. Parentheses show number of replicates. ^bData were also reported in ref 10a. ^cN.A., not active.

Table 5. Antiviral Activity of Compounds 1–10 against Influenza Virus A/WSN/33 (H1N1) Variants in Madin–Darby Canine Kidney Cells

compd	IC ₅₀ (μM) ^a		CC ₅₀ (μM) ^b
	A/WSN/33-M2-N31S	A/WSN/33-M2-N31	
1	0.27 ± 0.16	N.A. ^c	>100 ^d
2	0.42 ± 0.46	N.A.	70.50 ± 25.31
3	0.33 ± 0.10	N.A.	25.63 ± 7.65
4	0.34 ± 0.26	N.A.	>100
5	0.34 ± 0.10	N.A.	>100
6	0.34 ± 0.08	N.A.	>100
7	0.90 ± 0.29	N.A.	>100
8	6.12 ± 2.59	N.A.	>100
9	4.34 ± 2.94	N.A.	>100
10	N.A.	N.A.	>100
Oseltamivir	0.02 ± 0.01	0.02 ± 0.01	not determined

^aMean and standard deviations of the 50% inhibitory concentration (IC₅₀) of at least three independent measures. ^bMean and standard deviations of the 50% cytotoxic concentration (CC₅₀) of at least three independent measures. ^cN.A., not active. Maximum concentration tested, 100 μM. ^dExact value published in ref 46.

the starting structure reflects a homology model of 2KQT.^{4a,5b} Here the major finding is the lack of kinked helices in M2TM_{S31N} compared to the OS ssNMR structure when 1 binds M2TM_{WT} suggesting that the MD simulations describe well the ligand–M2TM_{S31N} structure.

For most of the ligands 1–8 the mean angle between the C–N bond vector and the normal of the membrane is >140° for more than 40 ns of the simulation reflecting the propensity of the ammonium group to orient toward the N-terminus (Table S2). The distance between the center of mass of the four V27 and the adamantyl ring of the ligands 1–8 (V27–Ad) was longer than in complexes with the M2TM_{WT}, which is consistent with an orientation of the ammonium group toward the N-terminus. On average, the adamantyl ring in M2TM_{S31N} was found to be ~1–2 Å toward the C-terminus compared to the M2TM_{WT} complexes. Accordingly, the distance between the center of mass of the four V27 and the ligand's ammonium group nitrogen in M2TM_{S31N} complexes was shorter by 3–3.5 Å compared to M2TM_{WT} complexes. In addition, especially for the ligands with sizeable adducts (for example, 5–8), the adamantyl ring is positioned toward the C-terminus close to G34 (see distances A30–Ad and G34–Ad in Table S2), whereas, in the M2TM_{WT} complexes, the adamantyl ring is shifted toward the N-terminus embraced by V27 and A30. The sum of the H-bonds between the ammonium groups of the ligands and waters and between the ammonium groups and the N31 side chain amides was on average three hydrogen bonds for the primary ammonium groups (ligands 1–5), two hydrogen bonds for secondary (ligands 6 and 8), and one hydrogen bond for tertiary ones (ligand 7) (Table S2). Compounds 9 and 10 form three hydrogen bonds only with

water molecules in the vicinity of N31 close to the wall of the pore, possibly because the ammonium group is sterically crowded between the adamantyl and cycloalkane rings and cannot reach the side chains' carbonyls of N31 (Table S2). In compound 10, due to the large hydrocarbon framework, the adamantyl ring moves more than in any other compound toward the C-terminus, i.e., the distance between the center of mass of the four V27 to the adamantyl cage was 3.7–2.3 Å longer than 1–8 to fit inside the pore close to G34, and the distance between the center of mass of the four G34 to the adamantyl cage was 2.7 Å (see Figure 7).

2.3.4. Electrophysiology Results of Aminoadamantanes Blockage Using Full-Length M2. Compound 1, its isomer 2, and three compounds with sizeable adducts (5, 6, and 9) were assessed for their ability to inhibit low-pH-dependent proton currents induced by full-length M2 protein (A/California/07/2009 with M2_{N31}) in transiently transfected, voltage clamped HEK cells (Table 4).^{10a,43} Data for compounds 1, 2, and 5 were reported previously.^{10a} It was found that none of these compounds blocked inward proton currents better than 1, either following a standard 3 min exposure to compound or after prolonged exposure for 30 min. These EP-based results indicated that the compounds were unable to block the full-length M2 channel encoding N31. However, when this M2 protein was modified to encode the I-sensitive S31 sequence (through an N31S mutation), all compounds inhibited proton currents with IC₅₀s of 10 μM or less (Table 4); by increasing the adduct size, the blocking effect of inward proton currents is reduced.

2.3.5. In Vitro Testing of Aminoadamantanes against Influenza A Virus. The antiviral potencies of compounds 1–10

were measured against WSN/33 (H1N1) bearing the N31 M2 mutation and its amantadine-sensitive variant WSN/33-M2-N31S⁴⁴ in MDCK cells with CPE inhibitory assay.^{45,46} Compounds 1–9 showed sub-micromolar IC₅₀ values against WSN/33-M2-N31S but were inactive against WSN/33 (Table 5). Compound 10 was inactive against both strains. The selectivity indices (CC₅₀/IC₅₀) of compounds 4–7 were comparable to 1. The inhibition efficiency showed stringent head-ammonium-group requirements for inhibition of amantadine-sensitive influenza A viruses—a result consistent with ITC and EP results.

3. DISCUSSION

3.1. Unraveling the Binding Differences for Aminoadamantanes to M2TM_{S31N} and M2TM_{WT}. Based on the MD simulations results and experimental findings, the molecular basis for weak binding and the inability of aminoadamantanes to effectively block M2_{S31N} is described. The results of the experimental data from ssNMR and ITC experiments directly correlate with the MD simulation results showing that aminoadamantane derivatives are weaker binders in the pore of M2TM_{S31N} compared to M2TM_{WT} and that 5–8 are stronger binders compared to 1–4 against M2TM_{S31N}.

The S31N mutation of M2TM results in a shift of the hydrophobic adamantyl ring toward the C-terminus thereby losing the stabilizing hydrophobic interactions of the four V27 isopropyl groups with the adamantyl ring that are present in M2TM_{WT} complexes. The bulky N31 side chains block contacts between adamantyl ring and the V27 side chains, and the ammonium group of the ligands is also turned toward the N-terminus to form significant hydrogen bonding interactions with the polar N31 side chains and surrounding waters. This ammonium group orientational preference of amantadine and rimantadine has been previously noted in MD simulations by us, the Busath group,^{17b} the Arkin group,¹⁶ and noted by DeGrado and co-workers.^{23b–d,24} The hydrogen bonding interactions with N31 are consistent with the MAS experimental data performed with compound 6 showing a chemical shift perturbation for N31 and G34 compared to the *apo* M2TM_{S31N}. Distance measurements from ssNMR experiments showed the preference for the ammonium group of the aminoadamantane drugs orienting toward the C-terminus in M2TM_{WT}^{5c} and toward the N-terminus in a complex of M2TM_{S31N} with a conjugate of 1 having a phenylisoxazole polar head.²⁴ In this class of conjugates,²³ additional van der Waals interactions with the N-terminus stabilizes the ligand resulting in potential anti-influenza drugs. Here, where the aminoadamantane ligands, such as 1–8, are hydrogen-bonded with the polar N31 environment, favorable van der Waals and hydrophobic interactions such as those in M2TM_{WT} are missing. In M2TM_{WT} the adamantyl ring is well-accommodated by the V27 and A30 side chains and sizeable adducts such as in ligands 5–8 additionally fill the region between A30 and G34 (Figure 6), but in M2TM_{S31N} the adamantyl ring is close to A30 and in the vicinity of G34 (Figure 7) lacking a favorable hydrophobic pocket (Tables S1 and S2). This is consistent with the absence of chemical shift perturbations for V27 in the NCA MAS spectrum of 6 bound to M2TM_{S31N} relative to the *apo* M2TM_{S31N} compared to the significant chemical shift changes at V27, S31, and G34 which have been reported when rimantadine is bound to M2TM_{WT} relative to the *apo* state.^{20,21} These structural differences can be clearly observed in Figures 6 and 7. The lack of favorable van der Waals

interactions results in less stable complexes and a weaker binding for aminoadamantane ligands consistent with the much smaller K_d values of 5 and 6 measured by ITC against M2TM_{S31N} compared to M2TM_{WT} (Table 1). In addition, line widths are narrower for the M2TM_{WT} complex with 5 compared to the M2TM_{S31N} complex suggesting less dynamics consistent with stronger interactions for the aminoadamantane derivatives in complexes with M2TM_{WT}. The RMSDs for M2TM C α -carbons are 1.0–1.5 Å higher for the trajectories of M2TM_{S31N} compared to M2TM_{WT} complexes further suggesting more dynamics and weaker interactions in the S31N complexes.

It should be noted that trajectories sampled in the MD simulations of ligands in the pore were of 80 ns length; i.e., they are much shorter than the microsecond to millisecond time scales sampled by ssNMR. The MD runs of the complexes of 1–4 with M2TM_{S31N} showed qualitatively that these molecules cannot bind M2TM_{S31N} because significant favorable van der Waals interactions are missing. This can be observed from the snapshot for the complex of 1 with M2TM_{S31N} in Figure 7. Molecules 5–8 with sizeable adducts of the adamantyl ring fill slightly more effectively the region between A30 and G34, and the interactions needed for binding are slightly improved resulting in weak binding to M2TM_{S31N} as compared to no binding for 1–4. This can be observed from snapshots for complexes of 5 and 6 with M2TM_{S31N} in Figure 7. Indeed, 1 did not bind as documented by the OS ssNMR spectra (Figure 3), but larger adducts such as those present in compounds 5–8 appear to stabilize weak binding of the drug in the region between A30 and G34 (see Figure 7), and this is in accordance with the results from OS ssNMR spectra for weak binding of compounds 5–8 (Figures 3 and 4) to M2TM_{S31N}. In addition, we were not able to detect any binding for 1–4 with M2TM_{S31N} using ITC while we obtained approximate binding constants for 5, 6, 9, and 10 (Table 1). NMR data were not obtained for 9 and 10 because they produced disordered lipid bilayers. Thus, the results from the combination of simulations and experiments showed that 1 (and similarly 2–4) did not bind M2TM_{S31N} contrary to the weak binding for 1 previously suggested from short simulations,^{17b} but 5–8 having sizeable adducts display weak binding.

While binding strength of aminoadamantanes against M2TM_{S31N} was not very sensitive to modification of the adduct, the M2TM_{WT}–aminoadamantane complex stability was found to be very sensitive to the adduct size, as shown by the ITC and MD simulation results especially when considering that 9 and 10 produce unstable complexes with M2TM_{WT}. The MD simulations clearly show that 10 moves considerably toward the N-terminus of the pore losing specific binding interactions. Ligands 9 and 10 cause a dramatic reduction in affinity for M2TM_{WT} compared to 1–8 but did not affect M2TM_{S31N} affinity, which seems to be similar to those of 5 and 6. The forces that cause the rotation of the adamantyl ring in the M2 pore appear to be inherent in the shared amine group and are not greatly perturbed by the other ligand variations as characterized by MD and OS ssNMR for adducts 1–4 and 5–8 against M2TM_{S31N}. Taken together, the results from the combination of MD simulations, ITC, and OS ssNMR showed no binding for 1 and similar in size analogues and only weak binding for sizeable adducts. The binding is more specific as showed by the more stringent head-ammonium-group requirements in the binding pocket of M2TM_{WT} than in the

M2TM_{S31N} according to the ITC but also as showed by the EP experiments and antiviral assay results.

3.2. Changes in C-Terminus Structure–Function of M2TM_{S31N} and M2TM_{WT} Induced by V27 Interactions with the Adamantyl Cage of Amantadine Variants. EP experiments indicate that the aminoadamantanes block the S31 but not the N31 full-length M2 protein. Notably, while the secondary gate formed by the V27 residues in the M2TM_{WT}¹¹ has the potential to limit water access to the pore, the hydrophilic asparagine side chains make this environment less hydrophobic and diminish the effectiveness of the V27 gate in the M2TM_{S31N} pore. The waters are observed above and below the ligand and in a few snapshots between the ligand and the wall of the pore suggesting a relatively free passage through the M2TM_{S31N} lumen despite the presence of the ligand.^{12,17,18} (see the snapshots from the simulation of the complexes of M2TM_{S31N} with **1**, **6**, and **10** in Figure 7).

Furthermore, it is suggested that the 10° helical kink that reduces the tilt of the C-terminal portion of the transmembrane helix in the WT is likely induced by the formation of a strong binding pocket for the aminoadamantanes. This hydrophobic pocket formed by the V27 aliphatic side chains coupled with the aliphatic adamantyl cage of the aminoadamantanes may prevent the W41 gate from opening further, defeating proton conductance. In contrast the aminoadamantanes in M2TM_{S31N} included a loss of V27 lipophilic pocket and have their amino group drawn toward the N-terminus by the asparagine side chains resulting in the presence of multiple water molecules in this region. In addition the weak binding of the aminoadamantanes results in no perturbation of the helical tilt and the W41 gate can function normally.

4. CONCLUSIONS

This work represents a study of the binding of amantadine variants against the proton channel formed by the tetrameric structure of the influenza A M2 protein. Significantly, we focus on aminoadamantane variants of **1** binding to M2TM_{S31N} compared to M2TM_{WT} aiming at investigating why these variants are ineffective in blocking proton conductance of the M2_{S31N} channel. The results of this effort are based on a combination of experimental techniques and MD simulations both performed in liquid crystalline lipid bilayer environments. Aminoadamantane derivatives are known to be blockers of the M2_{WT} protein. They are known to bind in the pore and are presumed to block proton access to the H37 tetrad that is known to shuttle protons through aqueous pore into the viral interior.⁴⁷ There are two gates that can inhibit conductance, the V27 tetrad, known as the secondary gate at the external entrance to the pore, and the W41 tetrad near the exit of the pore into the viral interior, known as the primary gate. These aminoadamantane derivatives were weaker binders to M2TM_{S31N} compared to M2TM_{WT} as observed by a reduced influence on the protein structure and by reduced amplitude of the channel dynamics as observed by both the MD and experimental data. Moreover, these aminoadamantane derivatives were ineffective against M2_{S31N} while blocking M2_{WT} protein. We suggest that **1** and the similar sized analogues **2–4** lack binding affinity and the larger sized analogues **5–8** showed weak binding affinity to M2TM_{S31N} because of a lack of effective hydrophobic interactions as a result of reshaping of the cavity when N31 is present which included loss of the V27 lipophilic pocket. In contrast V27 interactions are present with **1–8** in M2TM_{WT} pore and these ligands are effective binders to

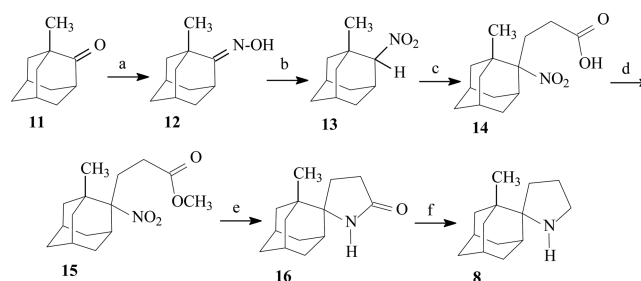
M2TM_{WT}. All ligands **1–8** have a tight binding for M2TM_{WT}, and the binding is more specific as showed by the more stringent head-ammonium-group requirements in the binding pocket of M2TM_{WT} than in the M2TM_{S31N} according to the ITC, EP, and CPE results. The weak binding of **5–8** to M2TM_{S31N} was significant enough to induce observable changes in the helix tilt angles characterized by the experimental data and by the MD simulations.

It is interesting to note that the blockage of M2TM_{WT} by both **1** and **5** involved a 10° kink in the TM helix and a very significant change in the helix orientation in the C-terminal half of the TM. This is likely due to the V27 side chains—adamantane hydrophobic interactions that are not possible in M2TM_{S31N}. While aminoadamantane ligand binding causes a kink in the C-terminal half of M2TM_{WT} and a blockage for proton conductance by the M2 channel, aminoadamantane ligand interactions with M2TM_{S31N} did not result in a helix kink in the TM helix and proton conductance was not blocked. While the helix kink has been associated with blockage and potential disabling of the opening of the W41 gate in M2TM_{WT} previously,⁴⁸ here, the explanation for the helix kink in the M2TM_{WT} and its absence in M2TM_{S31N} has been suggested to be induced by the V27 interactions with the adamantyl cage in M2TM_{WT} and the absence of such significant interactions in M2TM_{S31N}.

5. EXPERIMENTAL METHODS

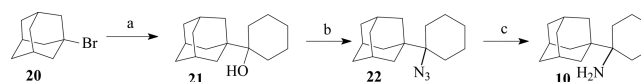
5.1. Synthesis of Aminoadamantane Ligands. The procedures applied for the synthesis of the new derivatives **8** and **10** are depicted in Schemes 2 and 3. The description of synthetic procedures for **8** and

Scheme 2. Synthesis of 1'-Methylspiro[pyrrolidine-2,2'-adamantane] (**8**)^a



^aReagents and conditions: (a) H₂NOH·HCl, Na₂CO₃ 90 °C, 40 min (93%). (b) (i) NBS, NaHCO₃, dioxane/water, 10 °C, 40 min; (ii) HNO₃, pentane, 0 °C, 15 min; (iii) NaBH₄, MeOH/H₂O. (c) (i) CH₂=CHCO₂Et, Triton-B, *t*-BuOH, 70 °C, 8 h; (ii) 1 N NaOH, 3:1 EtOH–H₂O, 70 °C, 8 h (89%). (d) MeOH/HCl(g), 60 °C, 4 h, and then overnight at room temperature (r.t.) (79%). (e) H₂/Ni-Raney, EtOH, 50 psi, r.t., 24 h (84%). (f) LiAlH₄, THF, reflux, 48 h (60%).

Scheme 3. Synthesis of 1-(1-Adamantyl)cyclohexanamine (**10**)^a



^aReagents and conditions: (a) Li, dry THF, cyclohexanone, sonication, 0 °C, 5 h (70%); (b) NaN₃, TFA, CH₂Cl₂, 0 °C, 5 h, then r.t. 24 h (35%). (c) LiAlH₄, dry ether, reflux, 5 h, then H₂O, NaOH 10% (65%).

10, experimental details, and compound characterization can be found in the [Supporting Information](#). All compounds' purity was $\geq 95\%$ as determined by elemental analysis (see [Supporting Information](#)).

5.2. M2TM Peptide Synthesis. M2TM_{WT} peptides corresponding to residues 22–46 of the Udorn (A/Udorn/307/72) sequence of M2 (C-terminally amidated SSDPLVVAASIIGILHLILWILDRL) and of the S31N mutant peptide (C-terminally amidated SSDPLVVAANIIGILHLILWILDRL) were synthesized in A.K.'s lab by standard Fmoc (9-fluorenylmethoxycarbonyl) solid phase peptide synthesis using an aminomethyl polystyrene resin loaded with the amide linker as previously described (ref 50). Additional quantities of these needed peptides were purchased from Centic Biotec, Heidelberg, Germany. For ssNMR experiments M2TM_{WT} and M2TM_{S31N} (22–46) peptides with ¹⁵N labeled at V28, A30, and I42 and M2TM_{S31N} (22–46) peptides with ¹³C, ¹⁵N labeled at structurally important residues V27, A30^{4a,5b} and N31, G34 (¹³C,¹⁵N-VANG) were synthesized using Fmoc chemistry. Fmoc-[¹⁵N]-Val, Fmoc-[¹⁵N]-Ala, Fmoc-[¹⁵N]-Ile, and Fmoc-[¹³C,¹⁵N]-Val, Fmoc-[¹³C,¹⁵N]-Ala, Fmoc-[¹³C,¹⁵N]-Ser, and Fmoc-[¹³C,¹⁵N]-Gly were purchased from Cambridge Isotope Laboratory (Andover, MA, USA). Solid phase syntheses of M2TM peptides (0.25 mmol) were performed on an Applied Biosystems 430A peptide synthesizer as previously described.⁴⁹ The peptides were cleaved from the resin by the treatment with ice cold 95% TFA, 2.5% H₂O, 1.25% ethanedithiol, and 1.25% thioanisole and precipitated from TFA using ice cold ether. Following centrifugation, the supernatant was discarded and the pellet was washed with cold ether again. The precipitated peptide was dried under vacuum. We used a purification procedure using reverse phase HPLC experiments for the peptides before their being used for the ITC or ssNMR experiments, as previously described⁵¹ and modified.⁵⁰ Peptide purity and identity was confirmed using ESI mass spectrometry (positive ion mode). The final peptide purity was 98%.

5.3. ITC Measurements of Aminoadamantane Ligands Binding to M2TM. Binding affinities of the aminoadamantane derivatives 1–5, 6, 9, and 10 for M2TM_{S31N} were measured by ITC experiments^{52,53} in DPC micelles at pH 8. Compounds 7 and 8 were not measured. M2TM fragments form stable tetramers at this pH, in contrast to low-pH (<6.5) conditions.⁵⁴ Experimental data indicate that 1 binds with higher affinity at alkaline pH to M2TM_{WT}, where the pore of the M2 channel is in the closed state, than at low pH, where the open state of M2TM_{WT} is prevalent.^{54a,2a}

All measurements were performed with a TAM 2277 (TA Instruments) at pH 8 and 20 °C in a buffer of 50 mM NaH₂PO₄ and 100 mM NaCl. The peptide and the aminoadamantane derivative were dissolved in a freshly prepared DPC solution with a concentration of 13 mmol L⁻¹. Measurements against M2TM_{WT} were conducted using 2 mL of 125 μ M peptide (corresponding to 31.25 μ M M2TM_{WT} tetramer) as has been described previously.²⁶ For the low-affinity ligands 9 and 10 a 250 μ M peptide concentration was used. For M2TM_{S31N} measurements the concentration of the peptide used was 167 μ M, which was increased to 500 μ M when 5 was tested in order to get a curve adequate for measurements. A concentration of 1.1 mM of the ligand was used for the titrant, of which 7.6 μ L (equivalent to 8.4 nmol) was dispensed in the peptide/DPC solution with each injection. The time interval between two injections was set to at least 6 min. The first injection was not used due to dilution effects.

Synthetic M2TM_{S31N} (residues 22–46) was reconstituted in DPC micelles at pH 8 at a 1:40 monomer/DPC ratio—which guarantees the quantitative formation of M2TM tetramers⁵⁴—by dissolving and sonicating 334 nmol of M2TM with the 40-fold amount of DPC in the aforementioned buffer system (for M2TM_{WT} a 1:26 ratio was applied for the measurements of ligands 9 and 10 compared to 1:57 applied previously²⁶). Solutions of the ligands in the buffer were titrated into the calorimetric cell at 20 °C. The released heat of binding was derived by subtracting the heat of dilution from the heat of reaction.^{55,56}

Describing in more detail, to determine the heat of dilution, ligand and receptor (M2TM) were dissolved in buffer containing DPC. Two reference experiments were carried out: (a) Ligand was titrated into the buffer containing DPC, and (b) receptor was titrated into buffer

containing DPC. The obtained signals showed that the released heat of each injection is very small and stays constant during the experiment. No interaction is detected between ligand and DPC containing buffer or receptor and DPC containing buffer, respectively. The released heat is the heat of dilution, which occurs when the two solutions are mixed. The heat of dilution was estimated for each titration experiment individually. At the end of each measurement, the receptor is titrated with the ligand being in an excess (the ratio for ligand/receptor after 19 injections is 2:1). If all binding sites are saturated, ligand cannot bind to the receptor anymore. The released heat is then equivalent to the heat of dilution. As mentioned, the heat of dilution is calculated as an average from the last five titration steps, when the heat is constant. This heat is taken into account as a Q correction. It is subtracted from all titration steps in this measurement.

Data evaluation, including the integration of the peaks, was carried out with Digitam for Windows v4.1. The measured heat per amount of substance against the molar ratio of titrant to peptide tetramer was plotted, and the affinity constants were calculated by nonlinear regression of the measured heat per injection using Origin 8.0⁵⁷ and have been included in [Table 1](#). Compounds 1–8 have been measured against M2TM_{WT} in a previous work (see footnote g in [Table 1](#)).²⁶ For the calculation, the concentration of the peptide was kept variable because the M2TM tetramer formation was not complete. The fit function involves three parameters. One of them is a factor for the correction of the peptide concentration (the difference between the concentration, which has been weighted in, and the active concentration). The cell volume is fixed at 2 mL. The concentration of the ligand in the solution is known, because pure substance was weighted in and the stoichiometry of the binding of ligand to receptor was assumed to be 1:1. If these quantities are set, the concentration of active receptor is obtained by fitting the measured data points. From the calculations, it can be seen that the concentration of active receptor is lower than the concentration of receptor that has been weighted in. The binding affinity of 1 measured against M2TM_{WT} in a previous work²⁶ was $2.17 \pm 0.52 \mu\text{M}$ and is comparable with the value of 12 μM measured using analytical ultracentrifugation^{54c} and the value of $9 \pm 2 \mu\text{M}$ derived based on kinetic studies in electrophysiological experiments.^{2a} For the M2TM peptide investigated in this study, the solubility in the DPC micelles limits the concentration of M2TM that can be tested. Consequently, affinity constants of low-affinity binders, e.g., aminoadamantanes against M2TM_{S31N} and 9 and 10 against M2TM_{WT}, possess relatively large errors.

5.4. Sample Preparation for Solid State NMR Spectroscopy. ¹⁵N-V₂₈A₃₀I₄₂ M2TM_{WT} or M2TM_{S31N} was codissolved in trifluoroethanol (TFE) with DMPC in a 1:30 molar ratio. (The molar ratio of one protein tetramer to 120 DMPC lipids was used. The molecular weight of the M2TM_{WT} peptide is MW = 2729 g/mol and that of the lipid is MW = 678 g/mol.) The solvent was removed under a stream of nitrogen gas to yield a lipid film and then dried to remove residual organic solvent under vacuum for 12 h. Thoroughly dried lipid film was hydrated with 10 mM HEPES buffer at pH 7.5 to form multilamellar vesicles containing M2TM in the tetrameric state. This suspension was bath sonicated, dialyzed against 2 L of 10 mM HEPES pH 7.5 buffer for 1 day, and centrifuged at 196000g to harvest unilamellar proteoliposomes. The pellet was resuspended in a 1 mL aliquot of the decanted supernatant containing the ligand, resulting in a 1:6 molar ratio of the M2TM tetramer to drug. Typically a preparation for solid state NMR would include 5 mg of protein and 37 mg of DMPC. For samples that included drug the molar ratio of drug to tetramer was 6:1. For 1 with a molecular weight of MW = 187.5 g/mol that would mean the addition 0.52 mg for a 5 mg protein sample. (There is sufficient evidence in the literature to demonstrate that M2 structure is not perturbed by drug concentration. The most obvious example in this work is the absence of structural changes in the S31N spectra in the presence of 1.) Following overnight incubation at 37 °C, the pellet was deposited on 5.7 × 10 mm glass strips (Matsunami Trading, Osaka, Japan). The bulk of the water from the sample was removed during a 2 day period in a 98% relative humidity environment at 298 K. Rehydration of the slides, before stacking and sealing into a rectangular sample cell, increased the sample weight by 40–50%.

Compounds **1** and **5** were used for ssNMR experiments against M2TM_{WT}; compounds **1** and **5–8** were used for ssNMR experiments against M2TM_{S31N}; compounds **9** and **10** produce disordered lipid bilayers according to the ³¹P spectra (not shown).

5.5. Solid State NMR Experiments of M2TM–Amino-Adamantane Complexes. **5.5.1. OS ssNMR Spectra.** PISEMA²⁸ and SAMPI4^{29,30} spectra were acquired at 720 MHz utilizing a low-*E* ¹H/¹⁵N double resonance probe.⁵⁸ Acquisition took place at 303 K, above the gel to liquid crystalline phase transition temperature of DMPC lipids. Experimental parameters included a 90° pulse of 5 μs and cross-polarization contact time of 0.8–1 ms, a 4 s recycle delay, and a SPINAL decoupling sequence.⁵⁸ For the spectrum of ¹⁵N–V₂₈A₃₀I₄₂ M2TM_{WT} with compounds **1** and **5**, 32 *t*₁ increments were obtained, and nine *t*₁, for the sample of ¹⁵N–V₂₈A₃₀I₄₂ M2TM_{WT} without drug; 16–28 *t*₁ increments were obtained for the spectrum of ¹⁵N–V₂₈A₃₀I₄₂ M2TM_{S31N} with compounds **1** and **5–8**, and nine *t*₁ increments, for the sample of ¹⁵N–V₂₈A₃₀I₄₂ M2TM_{S31N} without drug. Spectral processing was done with NMRPIPE⁵⁹ and plotting with SPARKY. ¹⁵N chemical shifts were referenced to a concentrated solution of N₂H₈SO₄, defined as 26.8 ppm relative to liquid ammonia.

5.5.2. NCA MAS Spectra. ¹⁵N–¹³Cα correlation experiments were performed on a Bruker Avance 600 MHz NMR spectrometer with an NHMFL 3.2 mm low-*E*-field triple resonance probe.^{60,61} The ¹³C chemical shifts were referenced using the published chemical shifts of adamantane relative to DSS⁶², and ¹⁵N chemical shifts were calculated with IUPAC relative frequency ratios between the DSS (¹³C) and liquid ammonia (¹⁵N).^{63,64} Spectra were acquired at MAS frequency of 10–12 kHz and a calibrated sample temperature of –10 °C. Thirty points were collected in the ¹⁵N dimension for an acquisition time of 5–6.25 ms, while in the direct dimension the acquisition time was 10.2 ms. In all experiments, 92 kHz of proton decoupling was used. To get one bond ¹⁵N–¹³C correlation, a mixing time of 5 ms was used. Spectra were processed with Topspin.

5.6. MD Simulations of M2TM–AminoAdamantane Complexes. **5.6.1. Docking Calculations.** The ligands in their ammonium forms were built by means of Maestro 8.5⁶⁵ and were then minimized by means of MacroModel 9.6 and the MMFF94 force field⁶⁶ implemented with MacroModel 9.6 using the CG method and a distance-dependent dielectric constant of 4.0 until a convergence value of 0.0001 kJ Å^{–1} mol^{–1} was reached. The M2TM_{WT}–**1** complex structure (PDB ID 2KQT^{4a,5b}) served as a model structure for M2TM_{WT} with bound ligands. N- and C-termini of the M2TM model systems were capped by acetyl and methylamino groups. After applying the protein preparation module of Maestro, all hydrogens of the protein complex were minimized with the AMBER* force field by means of Maestro/MacroModel 9.6 using a distance-dependent dielectric constant of 4.0. The molecular mechanics minimizations were performed with a conjugate gradient (CG) method and a threshold value of 0.0001 kJ Å^{–1} mol^{–1} as the convergence criterion. The structures of the protein and ligand **1** were saved separately and were used for the subsequent docking calculations. The ligands minimized in this manner were docked into the M2TM_{WT} binding site. Docking poses of the aminoAdamantane derivatives **1–10** in the M2TM_{WT} bound state were generated with GOLD 5.2^{67,68} considering five water molecules located between the ammonium group of **1** and H37 within the M2TM_{WT} pore-binding site and applying the ChemPLP implemented in the software.^{69,70} The option “toggle” was used to let the algorithm decide whether to take into account a water molecule or neglect it based on an empirical desolvation penalty. The region of interest used by GOLD was defined to contain the atoms that were within ~15 Å of the **1** binding site in the receptor structure. The “allow early termination” command was deactivated. For all of the other parameters, GOLD default values were used. Ligands were submitted to 30 genetic algorithm runs. Ten docking poses were produced for each ligand which were visually inspected using the UCSF Chimera package.⁷¹ The docking pose with the best ChemPLP score was used for the subsequent MD simulations with M2TM_{WT} and M2TM_{S31N} structures created as described below.

5.6.2. MD Simulations. Models of M2TM_{S31N}–aminoAdamantane complexes were generated from M2TM_{WT} aminoAdamantane

complexes by mutating amino acids S31–N31 with Maestro.⁶⁵ For N31, the side chain rotamers may have χ₁ angles of –160° or –80° corresponding to N31 side chains placed at the interface between helices or inside the lumen, respectively. Structures of M2TM_{S31N}(18–60) in DPC micelles solved by solution NMR spectroscopy show residue 31 in the helix–helix interface⁷² while MAS ssNMR studies in 1,2-diphytanoyl-*sn*-glycero-3-phosphocholine (DPhPC) bilayers showed the side chain of the N31 residue oriented toward the pore in two helices and toward an adjacent helix in the other two, with neighboring N31 side chains close enough to form polar contacts.³⁷ A just-released X-ray structure shows that N31 residues are oriented into the channel pore forming a hydrogen-bonding network,⁷³ and it was suggested that this may prevent drug from entering the channel. Preliminary OS ssNMR results in liquid crystalline lipid bilayers confirm that all four of the M2_{S31N} N31 residues are oriented toward the pore. Simulations of M2TM_{S31N}–ligands were run (a) with N31 side chains placed at the interface between helices⁷² (χ₁ angle is –80°) to avoid a biased starting conformer in which N31 repels adamantane and (b) with N31 pointing toward the pore in two helices (χ₁ angle is ~–160°) and toward an adjacent helix in the other two³⁷ (χ₁ angle is ~–80°). For comparison reasons a few MD simulations with **1**, **5**, and **6** were also performed with the starting structure of M2TM_{S31N} having N31 residues pointing into the center of the channel pore (χ₁ angle is –160°).⁷³ It should be mentioned that when the starting structure has all four N31 side chains placed at the interface between helices, after a few nanoseconds of simulation the side chains of at least two N31 residues change orientation pointing inside the pore lumen. This was also observed with the *apo* protein M2TM_{S31N} after a few nanoseconds. Configurations with different N31 rotamers produced MD trajectories with similar behavior for aminoAdamantane ligands. MD simulations were run in triplicate or more for **1**, **2**, **5**, and **6** to test the reproducibility of the behavior of the system.

The M2TM_{WT} complexes or M2TM_{S31N} complexes were embedded in a DMPC lipid bilayer extending 10 Å beyond the solutes. Complex and ligand systems were solvated using the TIP3P⁷⁴ water model. Na⁺ and Cl[–] ions were placed in the water phase to neutralize the systems and to reach the experimental salt concentration of 0.150 M NaCl. Membrane creation and system solvation were conducted with the “System Builder” utility of Desmond.^{75,76} The M2TM_{WT}–**1** complex structure in the hydrated DMPC bilayer with ions included 18617 atoms.

The OPLS 2005 force field^{77–79} was used to model all protein and ligand interactions, and the TIP3P model⁷⁴ was used for water. The particle mesh Ewald method (PME)^{80,81} was employed to calculate long-range electrostatic interactions with a grid spacing of 0.8 Å; van der Waals and short-range electrostatic interactions were smoothly truncated at 9.0 Å. The Nosé–Hoover thermostat⁸² was utilized to maintain a constant temperature in all simulations, and the Martyna–Tobias–Klein method⁸² was used to control the pressure. Periodic boundary conditions were applied (50 × 50 × 80 Å³). The equations of motion were integrated using the multistep RESPA integrator⁸³ with an inner time step of 2 fs for bonded interactions and nonbonded interactions within a cutoff of 9 Å. An outer time step of 6.0 fs was used for nonbonded interactions beyond the cutoff.

Each system was equilibrated in MD simulations with a modification of the default protocol provided in Desmond, which consists of a series of restrained minimizations and MD simulations designed to relax the system, while not deviating substantially from the initial coordinates. First, two rounds of steepest descent minimization were performed with a maximum of 2000 steps with harmonic restraints of 50 kcal mol^{–1} Å^{–2} applied on all solute atoms, followed by 10000 steps of minimization without restraints. The first simulation was run for 200 ps at a temperature of 10 K in the NVT (constant number of particles, volume, and temperature) ensemble with solute heavy atoms restrained with a force constant of 50 kcal mol^{–1} Å^{–2}. The temperature was then raised during a 200 ps MD simulation to 310 K in the NVT ensemble with the force constant retained. The temperature of 310 K was used in our MD simulations in order to ensure that the membrane state was above the melting temperature state of 297 K for DMPC lipids.⁸⁴

The heating was followed by equilibration runs. First, two stages of NPT equilibration (constant number of particles, pressure, and temperature) were performed, one with the heavy atoms of the system restrained for 1 ns with a force constant of 10 kcal mol⁻¹ Å⁻² for the harmonic constraints and one with the heavy atoms of the protein–ligand complex restrained for 1 ns with a force constant of 2 kcal mol⁻¹ Å⁻² for the harmonic constraints to equilibrate solvent and lipids. A NPT simulation followed with the C α atoms restrained for 1 ns with a force constant of 2 kcal mol⁻¹ Å⁻². The above-mentioned equilibration was followed by an 80 ns NPT simulation without restraints. Within this time, the total energy and the RMSD reached a plateau, and the systems were considered equilibrated (see RMSD plots in the Supporting Information).

5.7. Electrophysiology Experiments of M2 Blockage by Aminoadamantanes. Electrophysiology was performed as previously described.^{10a} pcDNA3 vectors encoding the full-length A/California/07/2009 (H1N1) M2 protein containing either an N31 or an S31 mutation was cotransfected with a pcDNA3 vector encoding eGFP into TSA-201 (HEK parental) cells using standard transfection protocols (Lipofectamine 2000, Life Technologies). This construct was previously annotated as A/England/195/2009 (H1N1)^{10a} but is identical in amino acid sequence to A/California/07/2009 (H1N1). Macroscopic ionic currents were recorded in the whole-cell configuration from GFP-positive cells 24–48 h after transfection. Cells were perfused continuously at 3–5 mL min⁻¹ with external (bath) solution containing (mM) 150 NMG, 10 HEPES, 10 D-glucose, 2 CaCl₂, and 1 MgCl₂ buffered at pH 7.4 with HCl. For low-pH (pH = 5.5) solution, HEPES was replaced by MES. Patch electrodes were pulled from thin-walled borosilicate glass (World Precision Instruments, Sarasota, FL, USA) and fire-polished before filling with standard pipet solution containing (mM) 140 NMG, 10 EGTA, 10 MES, and 1 MgCl₂ buffered at pH 6.0 with HCl. Voltage–clamp experiments were performed with an Axopatch 200B amplifier (Molecular Devices, Sunnyvale, CA, USA) connected to a Digidata 1322A 16-bit digitizer. Data were acquired with the pCLAMP8.0 software (Molecular Devices, CA) sampled at 10 kHz and low-pass-filtered at 5 kHz. Cells were held at –40 mV. The voltage protocol consisted of a 100 ms pulse to –80 mV followed by a 300 ms ramp to +40 mV and a 200 ms step to 0 mV before stepping back to –40 mV, which was repeated every 4 s. All drugs were prepared as DMSO stocks (50 or 100 mM) and diluted with external solution to desired concentrations. To measure a block of M2 currents by compounds, cells were recurrently treated with pH 7.4 and pH 5.5 solutions until stable and pH-dependent inward currents were reproducibly observed, followed by treatment with compound at pH 5.5 for 2–30 min. At the end of each experiment, cells were treated with a 100 μ M solution of 1.

5.8. Cells and Viruses. Madin–Darby canine kidney (MDCK) cells (Cat. No. RIE 328, Friedrich-Loeffler Institute, Riems, Germany) were propagated as monolayer in Eagle's minimum essential medium (EMEM) supplemented with 10% fetal bovine serum, 1% nonessential amino acids (NEAA), 1 mM sodium pyruvate, and 2 mM L-glutamine. Amantadine-resistant WSN/33 (with N31 in M2) and its amantadine-sensitive variant WSN/33-M2-N31S⁴⁴ were used in this study. For the generation of WSN/33-M2-N31S⁴⁴ the plasmid pHW187-M2-N31 was altered by site-directed mutagenesis PCR and afterward used as part of a plasmid set for virus recovery.⁴⁴ Both WSN/33-variants were propagated on MDCK cells in serum-free EMEM supplemented with 2 mM L-glutamine, 2 μ g/mL trypsin, and 0.1% sodium bicarbonate (test medium). Virus containing supernatant was harvested after about 48 h of incubation at 37 °C when cytopathic effect became microscopically visible. Aliquots were stored at –80 °C until use. The M2 gene identity of all recombinant viruses was verified by sequencing.

5.9. CPE Inhibition Assay of Influenza A Viruses by Aminoadamantanes. Cytotoxicity and CPE inhibition studies were performed on two-day-old confluent monolayers of MDCK cells grown in 96-well plates as published.⁴⁶ Cytotoxicity was analyzed 72 h after compound addition (2-fold or half-log dilutions; at least two parallels per concentration; maximum concentration, 100 μ M). In CPE inhibition assay, 50 μ L of 2-fold compound dilutions in test

medium and a constant multiplicity of infection of test virus (0.045 for WSN/33 and 0.04 for WSN/33-M2-N31S) in a volume of 50 μ L of the test medium were added to cells. Then, plates were incubated at 37 °C with 5% CO₂ for 48 h until the untreated, infected control showed maximum cytopathic effect. Crystal violet staining and optical density determination were performed as described before to determine the percentage of antiviral activity of the tests compounds.^{45,46} After log transformation of compound concentrations, linear regression was used to determine the 50% cytotoxic (CC₅₀) and the 50% inhibitory concentration (IC₅₀) (Table 5). At least three independent assays were conducted to calculate the mean CC₅₀ as well as IC₅₀s and their standard deviations.

■ ASSOCIATED CONTENT

📄 Supporting Information

The Supporting Information is available free of charge on the ACS Publications website at DOI: 10.1021/acs.jmedchem.6b01115.

Experimental details for synthetic procedures of compounds 8 and 10, information for ITC method limitations, tables of structural and dynamic measures, snapshots of additional MD runs, RMSD plots from MD runs, and relevant references (PDF)

Molecular formula strings (CSV)

■ AUTHOR INFORMATION

Corresponding Author

*Phone: (+301) 210 727 4834, Fax: (+301) 210 727 4747; E-mail: ankol@pharm.uoa.gr.

ORCID

Antonios Kolocouris: 0000-0001-6110-1903

Author Contributions

A.K. designed this research project. C.T. and A.W. contributed equally to this work. C.T. in A.K.'s group performed the MD simulations and did the synthesis of the M2TM_{S31N} peptide and of the new ligands 8 and 10 as part of her Ph.D. work. I.S. in A.K.'s group contributed in synthesis of compound 8. A.W. in T.A.C.'s group synthesized the labeled M2TM_{S31N} peptides and did the ssNMR experiments work. K.F. and F.K. in G.G.'s group did the ITC measurements. I.T. in D.F.'s group did the EP experiments. A.H. in M.S.'s group performed CPE inhibitory assays with A/WSN/33 and A/WSN/33-M2-N31S viruses. A.K. wrote the manuscript, and T.A.C. revised it.

Notes

The authors declare no competing financial interest.

■ ACKNOWLEDGMENTS

The NMR experiments were performed at the National High Magnetic Field Laboratory, which is supported by a National Science Foundation Cooperative Agreement (Grant DMR-1157490) with the State of Florida and under the proposal P08373 (National High Magnetic Field Laboratory with T.C. as PI and A.K. as one of the collaborators). A.K. thanks Chiesi Hellas for supporting the Ph.D. research of C.T. A.K. and C.T. thank S.A.R.G. of National and Kapodistrian University of Athens for a travel grant to participate in and present a poster including part of this work at EFMC-ISMIC 2016 at Manchester. A.K. also thanks Harris Ioannidis and Antonios Drakopoulos (previous M.Sc. students) for running a few preliminary MD runs. This work was in part supported by NIH Grant AI023007 and a Grand Challenges Stars in Global Health

grant to I.T. and D.F. D.F. thanks Daniel Kwan for technical assistance.

■ ABBREVIATIONS USED

BAR, Bennett acceptance ratio; CPE, cytopathic effect; DMPC, 1,2-dimyristoyl-*sn*-glycero-3-phosphocholine; DPhPC, 1,2-diphytanoyl-*sn*-glycero-3-phosphocholine; EP, electrophysiology; HEK, human embryonic kidney; ITC, isothermal titration calorimetry; M2TM, M2 transmembrane domain; MAS, magic angle spinning; MD, molecular dynamics; MM/PBSA, molecular mechanics Poisson–Boltzmann surface area; NCA, ^{15}N – $^{13}\text{C}\alpha$; OS, oriented sample; PMF, potential of mean force; ssNMR, solid state NMR; WT, wild-type

■ REFERENCES

- (1) Helenius, A. Unpacking the incoming influenza virus. *Cell* **1992**, *69*, 577–578.
- (2) (a) Wang, C.; Takeuchi, K.; Pinto, L. H.; Lamb, R. A. Ion channel activity of influenza A virus M2 protein: characterization of the amantadine block. *J. Virol.* **1993**, *67*, 5585–5594. (b) Chizhmakov, I. V.; Geraghty, F. M.; Ogden, D. C.; Hayhurst, A.; Antoniou, M.; Hay, A. J. Selective proton permeability and pH regulation of the influenza virus M2 channel expressed in mouse erythroleukaemia cells. *J. Physiol.* **1996**, *494*, 329–336.
- (3) Hayden, F. G. Clinical applications of antiviral agents for chemoprophylaxis and therapy of respiratory viral infections. *Antiviral Res.* **1985**, *5*, 229–239.
- (4) (a) Hu, J.; Asbury, T.; Achuthan, S.; Li, C.; Bertram, R.; Quine, J. R.; Fu, R.; Cross, T. A. Backbone structure of the amantadine-blocked trans-membrane domain M2 proton channel from influenza A virus. *Biophys. J.* **2007**, *92*, 4335–4343. (b) Hu, J.; Fu, R.; Cross, T. A. The chemical and dynamical influence of the anti-viral drug amantadine on the M2 proton channel transmembrane domain. *Biophys. J.* **2007**, *93*, 276–283.
- (5) (a) Stouffer, A. L.; Acharya, R.; Salom, D.; Levine, A. S.; Di Costanzo, L.; Soto, C. S.; Tereshko, V.; Nanda, V.; Stayrook, S.; DeGrado, W. F. Structural basis for the function and inhibition of an influenza virus proton channel. *Nature* **2008**, *451*, 596–599. (b) Cady, S. D.; Schmidt-Rohr, K.; Wang, J.; Soto, C. S.; DeGrado, W. F.; Hong, M. Structure of the amantadine binding site of influenza M2 proton channels in lipid bilayers. *Nature* **2010**, *463*, 689–692. (c) Cady, S. D.; Wang, J.; Wu, Y.; DeGrado, W. F.; Hong, M. Specific binding of adamantane drugs and direction of their polar amines in the pore of the influenza M2 transmembrane domain in lipid bilayers and dodecylphosphocholine micelles determined by NMR spectroscopy. *J. Am. Chem. Soc.* **2011**, *133*, 4274–4284. (d) Jing, X.; Ma, C.; Ohigashi, Y.; Oliveira, F. A.; Jardetzky, T. S.; Pinto, L. H.; Lamb, R. A. Functional studies indicate amantadine binds to the pore of the influenza A virus M2 proton-selective ion channel. *Proc. Natl. Acad. Sci. U. S. A.* **2008**, *105*, 10967–10972. (e) Pielak, R. M.; Oxenoid, K.; Chou, J. J. Structural investigation of rimantadine inhibition of the AM2-BM2 chimera channel of influenza viruses. *Structure* **2011**, *19*, 1655–1663.
- (6) Bright, R. A.; Medina, M. J.; Xu, X.; Perez-Orozco, G.; Wallis, T. R.; Davis, X. M.; Povinelli, L.; Cox, N. J.; Klimov, A. I. Incidence of adamantane resistance among influenza A (H3N2) viruses isolated worldwide from 1994 to 2005: a cause for concern. *Lancet* **2005**, *366*, 1175–1181.
- (7) (a) Bright, R. A.; Shay, D. K.; Shu, B.; Cox, N. J.; Klimov, A. I. Adamantane resistance among influenza A viruses isolated early during the 2005–2006 influenza season in the United States. *J. Am. Med. Assoc.* **2006**, *295*, 891–894. (b) Lan, Y.; Zhang, Y.; Dong, L.; Wang, D.; Huang, W.; Xin, L.; Yang, L.; Zhao, X.; Li, Z.; Wang, W.; Li, X.; Xu, C.; Yang, L.; Guo, J.; Wang, M.; Peng, Y.; Gao, Y.; Guo, Y.; Wen, L.; Jiang, T.; Shu, Y. A comprehensive surveillance of adamantane resistance among human influenza A virus isolated from mainland China between 1956 and 2009. *Antiviral Ther.* **2010**, *15*, 853–859.
- (8) High Levels of Adamantane Resistance Among Influenza A (H3N2) Viruses and Interim Guidelines for Use of Antiviral Agents—United States, 2005–06 Influenza Season. *MMWR Morb. Mortal. Wkly. Rep.* **2006**, *55*, 44–46.
- (9) See for example: (a) Kolocouris, N.; Foscolos, G. B.; Kolocouris, A.; Marakos, P.; Pouli, N.; Fytas, G.; Ikeda, S.; De Clercq, E. Synthesis and antiviral activity evaluation of some aminoadamantane derivatives. *J. Med. Chem.* **1994**, *37*, 2896–2902. (b) Kolocouris, N.; Kolocouris, A.; Foscolos, G. B.; Fytas, G.; Neyts, J.; Padalko, E.; Balzarini, J.; Snoeck, R.; Andrei, G.; De Clercq, E. Synthesis and antiviral activity evaluation of some new aminoadamantane derivatives. *2. J. Med. Chem.* **1996**, *39*, 3307–3318. (c) Kolocouris, A.; Spearpoint, P.; Martin, S. R.; Hay, A. J.; Lopez-Querol, M.; Sureda, F. X.; Padalko, E.; Neyts, J.; De Clercq, E. Comparisons of the influenza virus A M2 channel binding affinities, anti-influenza virus potencies and NMDA antagonistic activities of 2-alkyl-2-aminoadamantanes and analogues. *Bioorg. Med. Chem. Lett.* **2008**, *18*, 6156–6160.
- (10) (a) Kolocouris, A.; Tzitzoglaki, C.; Johnson, F. B.; Zell, R.; Wright, A. K.; Cross, T. A.; Tietjen, I.; Fedida, D.; Busath, D. D. Aminoadamantanes with persistent in vitro efficacy against H1N1 (2009) influenza A. *J. Med. Chem.* **2014**, *57*, 4629–4639. (b) Torres, E.; Fernández, R.; Miquet, S. P.; Font-Bardia, M.; Vanderlinden, E.; Naesens, L.; Vázquez, S. Synthesis and anti-influenza A virus activity of 2,2-dialkylamantadines and related compounds. *ACS Med. Chem. Lett.* **2012**, *3*, 1065–1069. (c) Torres, E.; Duque, M. D.; Vanderlinden, E.; Ma, C.; Pinto, L. H.; Camps, P.; Froeyen, M.; Vazquez, S.; Naesens, L. Role of the viral hemagglutinin in the anti-influenza virus activity of newly synthesized polycyclic amine compounds. *Antiviral Res.* **2013**, *99*, 281–291. (d) Wang, J.; Ma, C.; Balannik, V.; Pinto, L. H.; Lamb, R. A.; DeGrado, W. F. Exploring the requirements for the hydrophobic scaffold and polar amine in inhibitors of M2 from influenza A virus. *ACS Med. Chem. Lett.* **2011**, *2*, 307–312.
- (11) Yi, M.; Cross, T. A.; Zhou, H.-X. A secondary gate as a mechanism for inhibition of the M2 proton channel by amantadine. *J. Phys. Chem. B* **2008**, *112*, 7977–7979.
- (12) Laohpongpaian, C.; Rungrotmongkol, T.; Intharathep, P.; Malaisree, M.; Decha, P.; Aruksakunwong, O.; Sompornpisut, P.; Hannongbua, S. Why amantadine loses its function in influenza M2 mutants: MD Simulations. *J. Chem. Inf. Model.* **2009**, *49*, 847–852.
- (13) Khurana, E.; Devane, R. H.; Dal Peraro, M.; Klein, M. L. Computational study of drug binding to the membrane-bound tetrameric M2 peptide bundle from influenza A virus. *Biochim. Biophys. Acta, Biomembr.* **2011**, *1808*, 530–537.
- (14) Wang, J.; Ma, C.; Fiorin, G.; Carnevale, V.; Wang, T.; Hu, F.; Lamb, R. A.; Pinto, L. H.; Hong, M.; Klein, M. L.; DeGrado, W. F. Molecular dynamics simulation directed rational design of inhibitors targeting drug-resistant mutants of influenza A virus M2. *J. Am. Chem. Soc.* **2011**, *133*, 12834–12841.
- (15) Gu, R.-X.; Liu, L. A.; Wang, Y.-H.; Xu, Q.; Wei, D.-Q. Structural comparison of the wild-type and drug-resistant mutants of the influenza A M2 proton channel by molecular dynamics simulations. *J. Phys. Chem. B* **2013**, *117*, 6042–6051.
- (16) Alhadeff, R.; Assa, D.; Astrahan, P.; Krugliak, M.; Arkin, I. T. Computational and experimental analysis of drug binding to the influenza M2 channel. *Biochim. Biophys. Acta, Biomembr.* **2014**, *1838*, 1068–1073.
- (17) (a) Gleed, M. L.; Busath, D. D. Why bound amantadine fails to inhibit proton conductance according to simulations of the drug-resistant influenza A M2 (S31N). *J. Phys. Chem. B* **2015**, *119*, 1225–12231. (b) Gleed, M. L.; Ioannidis, H.; Kolocouris, A.; Busath, D. D. Resistance-mutation (N31) effects on drug orientation and channel hydration in amantadine-bound influenza A M2. *J. Phys. Chem. B* **2015**, *119*, 11548–11559.
- (18) Llabres, S.; Juarez-Jimenez, J.; Masetti, M.; Leiva, R.; Vazquez, S.; Gazzarrini, S.; Moroni, A.; Cavalli, A.; Luque, F. J. Mechanism of the pseudoirreversible binding of amantadine to the M2 proton channel. *J. Am. Chem. Soc.* **2016**, *138*, 15345–15358.
- (19) Gianti, E.; Carnevale, V.; DeGrado, W. F.; Klein, M. L.; Fiorin, G. Hydrogen-bonded water molecules in the M2 channel of the

influenza A virus guide the binding preferences of ammonium-based inhibitors. *J. Phys. Chem. B* **2015**, *119*, 1173–1183.

(20) (a) Andreas, L. B.; Barnes, A. B.; Corzilius, B.; Chou, J. J.; Miller, E. A.; Caporini, M.; Rosay, M.; Griffin, R. G. Dynamic nuclear polarization study of inhibitor binding to the M2_{18–60} proton transporter from influenza A. *Biochemistry* **2013**, *52*, 2774–2782.

(b) Andreas, L. B.; Eddy, M. T.; Pielak, R. M.; Chou, J.; Griffin, R. G. Magic angle spinning NMR investigation of influenza A M2(18–60): support for an allosteric mechanism of inhibition. *J. Am. Chem. Soc.* **2010**, *132*, 10958–10960.

(21) Wright, A. K.; Batsomboon, P.; Dai, J.; Hung, I.; Zhou, H.-X.; Dudley, G. B.; Cross, T. A. Differential binding of rimantadine enantiomers to influenza A M2 proton channel. *J. Am. Chem. Soc.* **2016**, *138*, 1506–1509.

(22) Rey-Carrizo, M.; Barniol-Xicota, M.; Ma, C.; Frigolé-Vivas, M.; Torres, E.; Naesens, L.; Lladrés, S.; Juárez-Jiménez, J.; Luque, F. J.; DeGrado, W. F.; Lamb, R. A.; Pinto, L. H.; Vázquez, S. Easily Accessible Polycyclic Amines that Inhibit the Wild-Type and Amantadine-Resistant Mutants of the M2 Channel of Influenza A Virus. *J. Med. Chem.* **2014**, *57*, 5738–5747.

(23) (a) Zhao, X.; Jie, Y.; Rosenberg, M. R.; Wan, J.; Zeng, S.; Cui, W.; Xiao, Y.; Li, Z.; Tu, Z.; Casarotto, M. G.; Hu, W. Design and synthesis of pinanamine derivatives as anti-influenza A M2 ion channel inhibitors. *Antiviral Res.* **2012**, *96*, 91–99. (b) Wang, J.; Wu, Y.; Ma, C.; Fiorin, G.; Wang, J.; Pinto, L. H.; Lamb, R. A.; Klein, M. L.; DeGrado, W. F. Structure and inhibition of the drug-resistant S31N mutant of the M2 ion channel of influenza A virus. *Proc. Natl. Acad. Sci. U. S. A.* **2013**, *110*, 1315–1320. (c) Wang, J.; Ma, C.; Wang, J.; Jo, H.; Canturk, B.; Fiorin, G.; Pinto, L. H.; Lamb, R. A.; Klein, M. L.; DeGrado, W. F. Discovery of novel dual inhibitors of wild-type and the most prevalent drug-resistant mutant, S31N, of M2 proton channel from influenza A virus. *J. Med. Chem.* **2013**, *56*, 2804–2812. (d) Wu, Y.; Canturk, B.; Jo, H.; Ma, C.; Gianti, E.; Klein, M. L.; Pinto, L. H.; Lamb, R. A.; Fiorin, G.; Wang, J.; DeGrado, W. F. Flipping in the pore: Discovery of dual inhibitors that bind in different orientations to the wild-type versus the amantadine-resistant S31N mutant of the influenza A virus M2 proton channel. *J. Am. Chem. Soc.* **2014**, *136*, 17987–17995.

(24) Williams, J. K.; Tietze, D.; Wang, J.; Wu, Y.; DeGrado, W. F.; Hong, M. Drug-induced conformational and dynamical changes of the S31N mutant of the influenza M2 proton channel investigated by solid-state NMR. *J. Am. Chem. Soc.* **2013**, *135*, 9885–9897.

(25) Homeyer, N.; Ioannidis, H.; Kolarov, F.; Gauglitz, G.; Zikos, C.; Kolocouris, A.; Gohlke, H. Interpreting thermodynamic profiles of aminoadamantane compounds inhibiting the M2 proton channel of influenza A by free energy calculations. *J. Chem. Inf. Model.* **2016**, *56*, 110–126.

(26) Ioannidis, H.; Drakopoulos, A.; Tzitzoglaki, C.; Homeyer, N.; Kolarov, F.; Gkeka, P.; Freudenberger, K.; Liolios, C.; Gauglitz, G.; Cournia, Z.; Gohlke, H.; Kolocouris, A. Alchemical free energy calculations and isothermal titration calorimetry measurements of aminoadamantanes bound to the closed state of influenza A/M2TM. *J. Chem. Inf. Model.* **2016**, *56*, 862–876.

(27) Gkeka, P.; Eleftheratos, S.; Kolocouris, A.; Cournia, Z. Free energy calculations reveal the origin of binding preference for aminoadamantane blockers of influenza A/M2TM pore. *J. Chem. Theory Comput.* **2013**, *9*, 1272–1281.

(28) (a) Wu, C. H.; Ramamoorthy, A.; Opella, S. J. High-resolution heteronuclear dipolar solid-state NMR spectroscopy. *J. Magn. Reson., Ser. A* **1994**, *109*, 270–272. (b) Ahuja, S.; Jahr, N.; Im, S.-C.; Vivekanandan, S.; Popovych, N.; Le Clair, S. V.; Huang, R.; Soong, R.; Xu, J.; Yamamoto, K.; Nanga, R. P.; Bridges, A.; Waskell, L.; Ramamoorthy, A. A model of the membrane-bound cytochrome b5-cytochrome P450 complex from NMR and mutagenesis data. *J. Biol. Chem.* **2013**, *288*, 22080–22095.

(29) Nevzorov, A. A.; Opella, S. J. Selective averaging for high-resolution solid-state NMR spectroscopy of aligned samples. *J. Magn. Reson.* **2007**, *185*, 59–70.

(30) De Simone, A.; Mote, K. R.; Veglia, G. Structural dynamics and conformational equilibria of SERCA regulatory proteins in membranes by solid-state NMR restrained simulations. *Biophys. J.* **2014**, *106*, 2566–2576.

(31) Rühmann, E. H.; Rupp, M.; Betz, M.; Heine, A.; Klebe, G. Boosting affinity by correct ligand preorganization for the S2 pocket of thrombin: a study by isothermal titration calorimetry, molecular dynamics, and high-resolution crystal structures. *ChemMedChem* **2016**, *11*, 309–319.

(32) Ma, C.; Polishchuk, A. L.; Ohigashi, Y.; Stouffer, A. L.; Schon, A.; Magavern, E.; Jing, X.; Lear, J. D.; Freire, E.; Lamb, R. A.; DeGrado, W. F.; Pinto, L. H. Identification of the functional core of the influenza A virus A/M2 proton-selective ion channel. *Proc. Natl. Acad. Sci. U. S. A.* **2009**, *106*, 12283–12288.

(33) Rosenberg, M. R.; Casarotto, M. G. Coexistence of two adamantane binding sites in the influenza A M2 ion channel. *Proc. Natl. Acad. Sci. U. S. A.* **2010**, *107*, 13866–13871.

(34) Marassi, F. M.; Opella, S. J. A solid-state NMR index of helical membrane protein structure and topology. *J. Magn. Reson.* **2000**, *144*, 150–155.

(35) Wang, J.; Denny, J.; Tian, C.; Kim, S.; Mo, Y.; Kovacs, F.; Song, Z.; Nishimura, K.; Gan, Z.; Fu, R.; Quine, J. R.; Cross, T. A. Imaging membrane protein helical wheels. *J. Magn. Reson.* **2000**, *144*, 162–167.

(36) Li, C.; Qin, H.; Gao, F. P.; Cross, T. A. Solid-state NMR characterization of conformational plasticity within the transmembrane domain of the influenza A M2 proton channel. *Biochim. Biophys. Acta, Biomembr.* **2007**, *1768*, 3162–3170.

(37) Andreas, L. B.; Eddy, M. T.; Chou, J. J.; Griffin, R. G. Magic-angle-spinning NMR of the drug resistant S31N M2 proton transporter from influenza A. *J. Am. Chem. Soc.* **2012**, *134*, 7215–7218.

(38) Andreas, L. B.; Reese, M.; Eddy, M. T.; Gelev, V.; Ni, Q.-Z.; Miller, E. A.; Emsley, L.; Pintacuda, G.; Chou, J. J.; Griffin, R. G. Structure and mechanism of the influenza A M2_{18–60} dimer of dimers. *J. Am. Chem. Soc.* **2015**, *137*, 14877–14886.

(39) (a) Cady, S. D.; Luo, W. B.; Hu, F.; Hong, M. Structure and function of the influenza M2 proton channel. *Biochemistry* **2009**, *48*, 7356–7364. (b) Cady, S. D.; Hong, M. Effects of amantadine binding on the dynamics of bilayer-bound influenza A M2 transmembrane peptide studied by NMR relaxation. *J. Biomol. NMR* **2009**, *45*, 185–196. (c) Hu, F.; Luo, W.; Cady, S. D.; Hong, M. Conformational plasticity of the influenza A M2 transmembrane helix in lipid bilayers under varying pH, drug binding and membrane thickness. *Biochim. Biophys. Acta, Biomembr.* **2011**, *1808*, 415–423.

(40) Cristian, L.; Lear, J. D.; DeGrado, W. F. Use of thiol-disulfide equilibria to measure the energetics of assembly of transmembrane helices in phospholipid bilayers. *Proc. Natl. Acad. Sci. U. S. A.* **2003**, *100*, 14772–14777.

(41) Cady, S.; Wang, T.; Hong, M. Membrane-dependent effects of a cytoplasmic helix on the structure and drug binding of the influenza virus M2 protein. *J. Am. Chem. Soc.* **2011**, *133*, 11572–11579.

(42) Saotome, K.; Duong-Ly, K.; Howard, K. P. Influenza A M2 protein conformation depends on choice of model membrane. *Biopolymers* **2015**, *104*, 405–411.

(43) (a) Chizhnikov, I. V.; Geraghty, F. M.; Ogden, D. C.; Hayhurst, A.; Antoniou, M.; Hay, A. J. Selective proton permeability and pH regulation of the influenza virus M2 channel expressed in mouse erythroleukaemia cells. *J. Physiol.* **1996**, *494*, 329–336. (b) Balannik, V.; Carnevale, V.; Fiorin, G.; Levine, B. G.; Lamb, R. A.; Klein, M. L.; DeGrado, W. F.; Pinto, L. H. Functional studies and modeling of pore-lining residue mutants of the influenza A virus M2 ion channel. *Biochemistry* **2010**, *49*, 696–708. (c) Duque, M. D.; Ma, C.; Torres, E.; Wang, J.; Naesens, L.; Juárez-Jiménez, J.; Camps, P.; Luque, F. J.; DeGrado, W. F.; Lamb, R. A.; Pinto, L. H.; Vázquez, S. Exploring the size limit of templates for inhibitors of the M2 ion channel of influenza A virus. *J. Med. Chem.* **2011**, *54*, 2646–2457.

(44) Schade, D.; Kotthaus, J.; Riebling, L.; Kotthaus, J.; Müller-Fielitz, H.; Raasch, W.; Hoffmann, A.; Schmidtke, M.; Clement, B. Zanamivir Amidoxime- and N-Hydroxyguanidine-Based Prodrug

Approaches to Tackle Poor Oral Bioavailability. *J. Pharm. Sci.* **2015**, *104*, 3208–3219.

(45) Torres, E.; Duque, M. D.; Vanderlinden, E.; Ma, C.; Pinto, L. H.; Camps, P.; Froeyen, M.; Vázquez, S.; Naesens, L. Role of the viral hemagglutinin in the anti-influenza virus activity of newly synthesized polycyclic amine compounds. *Antiviral Res.* **2013**, *99*, 281.

(46) Schmidtke, M.; Schnittler, U.; Jahn, B.; Dahse, H.-M.; Stelzner, A. A rapid assay for evaluation of antiviral activity against coxsackie virus B3, influenza virus A, and herpes simplex virus type 1. *J. Virol. Methods* **2001**, *95*, 133–143.

(47) Miao, Y.; Fu, R.; Zhou, H. X.; Cross, T. A. Dynamic short hydrogen bonds in histidine tetrad of full-length M2 proton channel reveal tetrameric structural heterogeneity and functional mechanism. *Structure* **2015**, *23*, 2300–2308.

(48) Yi, M.; Cross, T. A.; Zhou, H. X. Conformational heterogeneity of the M2 proton channel and a structural model for channel activation. *Proc. Natl. Acad. Sci. U. S. A.* **2009**, *106*, 13311–13316.

(49) Kovacs, F. A.; Cross, T. A. Transmembrane four-helix bundle of influenza A M2 protein channel: structural implications from helix tilt and orientation. *Biophys. J.* **1997**, *73*, 2511–2517.

(50) Kolocouris, A.; Zikos, C.; Broadhurst, R. W. ¹⁹F NMR detection of the complex between amantadine and the receptor portion of the influenza A M2 ion channel in DPC micelles. *Bioorg. Med. Chem. Lett.* **2007**, *17*, 3947–3952.

(51) Hansen, R. K.; Broadhurst, R. W.; Skelton, P. C.; Arkin, I. T. Hydrogen/deuterium exchange of hydrophobic peptides in model membranes by electrospray ionization mass spectrometry. *J. Am. Soc. Mass Spectrom.* **2002**, *13*, 1376–87.

(52) Ladbury, J. E.; Klebe, G.; Freire, E. Adding calorimetric data to decision making in lead discovery: a hot tip. *Nat. Rev. Drug Discovery* **2010**, *9*, 23–27.

(53) Perozzo, R.; Folkers, G.; Scapozza, L. Thermodynamics of protein-ligand interactions: history, presence, and future aspects. *J. Recept. Signal Transduction Res.* **2004**, *24*, 1–52.

(54) (a) Salom, D.; Hill, B. R.; Lear, J. D.; DeGrado, W. F. pH-dependent tetramerization and amantadine binding of the transmembrane helix of M2 from the influenza A virus. *Biochemistry* **2000**, *39*, 14160–14170. (b) Stouffer, A. L.; Ma, C.; Cristian, L.; Ohigashi, Y.; Lamb, R. A.; Lear, J. D.; Pinto, L. H.; DeGrado, W. F. The interplay of functional tuning, drug resistance, and thermodynamic stability in the evolution of the M2 proton channel from the influenza A virus. *Structure* **2008**, *16*, 1067–1076. (c) Stouffer, A. L.; Nanda, V.; Lear, J. D.; DeGrado, W. F. Sequence determinants of a transmembrane proton channel: an inverse relationship between stability and function. *J. Mol. Biol.* **2005**, *347*, 169–179.

(55) Wiseman, T.; Williston, S.; Brandts, J. F.; Lin, L.-N. Rapid measurement of binding constants and heats of binding using a new titration calorimeter. *Anal. Biochem.* **1989**, *179*, 131–137.

(56) Doyle, M. L. Characterization of binding interactions by isothermal titration calorimetry. *Curr. Opin. Biotechnol.* **1997**, *8*, 31–35.

(57) *Origin 8.1G SRI*, v8.1.13.88; OriginLab, Northampton, MA, USA, 2009.

(58) Fung, B. M.; Khitrin, A. K.; Ermolaev, K. An improved broadband decoupling sequence for liquid crystals and solids. *J. Magn. Reson.* **2000**, *142*, 97–101.

(59) Delaglio, F.; Grzesiek, S.; Vuister, G. W.; Zhu, G.; Pfeifer, J.; Bax, A. NMRPipe: a multidimensional spectral processing system based on UNIX pipes. *J. Biomol. NMR* **1995**, *6*, 277–293.

(60) Gor'kov, P. L.; Chekmenev, E. Y.; Li, C.; Cotten, M.; Buffy, J. J.; Traaseth, N. J.; Veglia, G.; Brey, W. W. Using low-E resonators to reduce RF heating in biological samples for static solid-state NMR up to 900 MHz. *J. Magn. Reson.* **2007**, *185*, 77–93.

(61) McNeill, S. A.; Gor'kov, P. L.; Shetty, K.; Brey, W. W.; Long, J. R. A low-E magic angle spinning probe for biological solid state NMR at 750 MHz. *J. Magn. Reson.* **2009**, *197*, 135–144.

(62) Morcombe, C. R.; Zilm, K. W. Chemical shift referencing in MAS solid state NMR. *J. Magn. Reson.* **2003**, *162*, 479–486.

(63) Markley, J. L.; Bax, A.; Arata, Y.; Hilbers, C. W.; Kaptein, R.; Sykes, B. D.; Wright, P. E.; Wüthrich, K. Recommendations for the presentation of NMR structures of proteins and nucleic acids. *J. Mol. Biol.* **1998**, *280*, 933–952.

(64) Harris, R. K.; Becker, E. D.; Cabral de Menezes, S. M.; Goodfellow, R.; Granger, P. NMR nomenclature: nuclear spin properties and conventions for chemical shifts. IUPAC recommendations 2001. *Solid State Nucl. Magn. Reson.* **2002**, *22*, 458–483.

(65) *Maestro*, version 8.5; Schrodinger: New York, NY, USA, 2008.

(66) (a) Halgren, T. A. Merck molecular force field. V. Extension of MMFF94 using experimental data, additional computational data, and empirical rules. *J. Comput. Chem.* **1996**, *17*, 616–641. (b) Halgren, T. A. MMFF VII. Characterization of MMFF94, MMFF94s, and other widely available force fields for conformational energies and for intermolecular-interaction energies and geometries. *J. Comput. Chem.* **1999**, *20*, 730–748.

(67) Jones, G.; Willett, P.; Glen, R. C.; Leach, A. R.; Taylor, R. Development and validation of a genetic algorithm for flexible docking. *J. Mol. Biol.* **1997**, *267*, 727–748.

(68) Verdonk, M. L.; Chessari, G.; Cole, J. C.; Hartshorn, M. J.; Murray, C. W.; Nissink, J. W.; Taylor, R. D.; Taylor, R. Modeling water molecules in protein-ligand docking using GOLD. *J. Med. Chem.* **2005**, *48*, 6504–6515. (c) Korb, O.; Stütze, T.; Exner, T. E. Empirical scoring functions for advanced protein-ligand docking with PLANTS. *J. Chem. Inf. Model.* **2009**, *49*, 84–96.

(69) Mooij, W. T.; Verdonk, M. L. General and targeted statistical potentials for protein-ligand interactions. *Proteins: Struct., Funct., Genet.* **2005**, *61*, 272–287.

(70) Korb, O.; Stütze, T.; Exner, T. E. Empirical scoring functions for advanced protein-ligand docking with PLANTS. *J. Chem. Inf. Model.* **2009**, *49*, 84–96.

(71) Pettersen, E. F.; Goddard, T. D.; Huang, C. C.; Couch, G. S.; Greenblatt, D. M.; Meng, E. C.; Ferrin, T. E. UCSF Chimera—a visualization system for exploratory research and analysis. *J. Comput. Chem.* **2004**, *25*, 1605–1612.

(72) Pielak, R. M.; Schnell, J. R.; Chou, J. J. Mechanism of drug inhibition and drug resistance of influenza A M2 channel. *Proc. Natl. Acad. Sci. U. S. A.* **2009**, *106*, 7379–7384.

(73) Thomaston, J. L.; DeGrado, W. F. Crystal structure of the drug-resistant S31N influenza M2 proton channel. *Protein Sci.* **2016**, *25*, 1551–1554.

(74) Jorgensen, W. L.; Chandrasekhar, J.; Madura, J. D.; Impey, R. W.; Klein, M. L. Comparison of simple potential functions for simulating liquid water. *J. Chem. Phys.* **1983**, *79*, 926–935.

(75) (a) *Desmond Molecular Dynamics System*, version 3.0; D. E. Shaw Research: New York, NY, USA, 2011. (b) *Desmond Molecular Dynamics System*, version 3.1; D. E. Shaw Research: New York, NY, USA, 2012. (c) Bowers, K. J.; Chow, E.; Xu, H.; Dror, R. O.; Eastwood, M. P.; Gregersen, B. A.; Klepeis, J. L.; Kolossvary, I.; Moraes, M. A.; Sacerdoti, F. D.; Salmon, J. K.; Shan, Y.; Shaw, D. E. Scalable algorithms for molecular dynamics simulations on commodity clusters. In *Proceedings of the 2006 ACM/IEEE Conference on Supercomputing (SC'06)*, article 84, Tampa, FL, USA; Association for Computing Machinery: New York, NY, USA, 2006; DOI: 10.1145/1188455.1188544

(76) *Maestro-Desmond Interoperability Tools*, version 3.1; Schrodinger: New York, NY, USA, 2012.

(77) (a) Jorgensen, W. L.; Maxwell, D. S.; Tirado-Rives, J. Development and testing of the OPLS all-atom force field on conformational energetics and properties of organic liquids. *J. Am. Chem. Soc.* **1996**, *118*, 11225–11236. (b) Rizzo, R. C.; Jorgensen, W. L. OPLS all-atom model for amines: resolution of the amine hydration problem. *J. Am. Chem. Soc.* **1999**, *121*, 4827–4836.

(78) Kaminski, G.; Friesner, R. A.; Tirado-Rives, J.; Jorgensen, W. L. Evaluation and reparametrization of the OPLS-AA force field for proteins via comparison with accurate quantum chemical calculations on peptides. *J. Phys. Chem. B* **2001**, *105*, 6474–6487.

(79) Shivakumar, D.; Williams, J.; Wu, Y.; Damm, W.; Shelley, J.; Sherman, W. Prediction of absolute solvation free energies using

molecular dynamics free energy perturbation and the OPLS force field.

J. Chem. Theory Comput. **2010**, *6*, 1509–1519.

(80) Darden, T.; York, D.; Pedersen, L. Particle mesh Ewald: an $N \log(N)$ method for Ewald sums in large systems. *J. Chem. Phys.* **1993**, *98*, 10089–10092.

(81) Essmann, U.; Perera, L.; Berkowitz, M. L.; Darden, T.; Lee, H.; Pedersen, L. G. A Smooth particle mesh Ewald method. *J. Chem. Phys.* **1995**, *103*, 8577–8593.

(82) Martyna, G. J. T.; Tobias, D. J.; Klein, M. L. Constant pressure molecular-dynamics algorithms. *J. Chem. Phys.* **1994**, *101*, 4177–4189.

(83) Humphreys, D. D.; Friesner, R. A.; Berne, B. J. A multiple-time-step molecular-dynamics algorithm for macromolecules. *J. Phys. Chem.* **1994**, *98*, 6885–6892.

(84) Koynova, R.; Caffrey, M. Phases and phase transitions of the phosphatidylcholines. *Biochim. Biophys. Acta, Rev. Biomembr.* **1998**, *1376*, 91–145.